

# **Physical Modelling Of Thermal Load on an Energy Pile**

Martina Onyeche Ananaba

Submitted in accordance with the requirements for the degree of  
Doctor of Philosophy

University of Leeds  
Institute of Resilient Infrastructure  
School of Civil Engineering

May, 2018

The candidate confirms that the work submitted is her own and that appropriate credit has been given where reference has been made to the work of others.

This copy has been supplied on the understanding that it is copyright material and that no quotation from the thesis may be published without proper acknowledgement.

The right of Martina Onyeche Ananaba to be identified as Author of this work has been asserted by her in accordance with the Copyright, Designs and Patents Act 1988.

## Acknowledgements

I express my sincere gratitude to Prof B G Clarke from whose wealth of experience and generosity I immensely benefitted and for giving me the unique opportunity to conduct this research under his supervision. I am particularly grateful for his dedication, guidance, insight and critical reviews which helped towards my development as an independent researcher. I also sincerely thank my second supervisor Dr B R Hughes for his kind encouragement, helpfulness, and willingness to share his experience and that of his research team.

I deeply appreciate my dear husband Nnamdi and wonderful sons Ikechukwu and Obinna for their love, understanding, generosity, sacrifices and support throughout the study period. Thanks for believing in me! I am very grateful to my parents Chief & Mrs Adaji, my parents-in-law Prof & Mrs Ananaba and all my worthy brothers and sisters, for their love, support, guidance, sacrifices and encouragement. Very special thanks to my father-in-law and mentor Prof S E Ananaba, for ensuring the success of this project!

I also extend my appreciation to the technical staff of the Civil Engineering Soil Laboratory, particularly to Mr Michael Marsden and Mr Marvin Wilman, for their kind assistance, support, and making the lab a cheerful work place. Big thanks to Marcia Martell for being so kind and helpful. I also acknowledge the technical assistance of Mr Graham Brown and Mr Steve Caddick for fabricating the test rig and Mr Robert Guest (Mechanical Engineering Workshop), Mr Pete Flatt (Casting Workshop), and Mr Tarsem Hunjan and his team (Engineering Electrical Workshop).

My sincere gratitude to Fr. Peter Kravos, Fr. Michael Kryschiwskyj (of blessed memory) and their parishioners for their friendship and pastoral support.

Many thanks and appreciation to my dear friends and all those who mentored and supported me in various ways during this period; Gloria, Nsikanabasi, Sandhya, Chisom, Carmellina, Aisha, Aunty Ije, Chindo, Ifeoma, Sabina, Abigail, Eliza, Tonia to mention but a few.

I am grateful to all my colleagues in the postgraduate research office 3.16. Thanks for your peerless support, friendship and assistance, Richard Wood, Azael, Teju, Adeolu, Oladipo Anie, David, Rosemary, Musa, Carolina, Ikpe, Caterina, Godwin, Dorian, Cigdem, Zaim, Manal.

I wish to acknowledge the Niger Delta Development Commission of Nigeria for their financial support, and the Management of National steel Raw Materials Exploration Agency, Nigeria for granting me leave to study.

To God be all the praise for his endless mercies!

## **Abstract**

Ground Source Heat Pumps (GSHPs) are a clean technology directed towards reducing dependence on the use of fossil fuels for heating and cooling of buildings by using the ground as a heat source or sink. Energy piles are one type of component GSHP that uses a closed loop system in foundation piles to transfer heat from the ground to a building or vice versa. The piles provide structural support while exchanging heat with the surrounding soil, but the thermal behaviour of the soil surrounding thermal piles and the effect of cyclic heating and cooling on the soil properties is not fully understood.

This research was aimed at addressing the aspect of inadequate geotechnical input in energy pile design by focusing on the factors that govern heat flow within soils around an energy pile. The relationships between soil type, water content, temperature, overburden pressure, time and thermal cycles were investigated.

A novel experimental test rig and laboratory procedures for operating it, were designed and developed to study heat dissipation radially by conduction from a linear heat source within a soil mass modelled to depict a scenario typical to that of an energy pile exchanging heat with the surrounding soil while being subjected to overburden pressure, to simulate practical use of energy piles in an office building. From tests conducted on soil samples in the rig, the results demonstrate a reliable system. An energy pile will perform suitably for cooling an office building, while continuous use of the ground as a heat sink will eventually lead to decreased water content and increased shear strength around the pile. The soil thermal diffusivity is mainly influenced by the soil composition. These and the other findings will be of interest to designers and other researchers as they are of practical importance in energy pile applications.

## Table of Contents

<b>Acknowledgements</b> .....	<b>ii</b>
<b>Abstract</b> .....	<b>iii</b>
<b>Table of Contents</b> .....	<b>iv</b>
<b>List of Tables</b> .....	<b>x</b>
<b>List of Figures</b> .....	<b>xiii</b>
<b>List of Abbreviations</b> .....	<b>xxviii</b>
<b>Chapter 1 Introduction</b> .....	<b>1</b>
1.1 Background .....	1
1.2 Climate Change .....	1
1.3 Energy Demands of Buildings .....	3
1.4 Renewable Energy Sources .....	4
1.5 Geothermal Energy .....	5
1.6 Earth Energy Systems/Ground Source Heat Pumps .....	6
1.6.1 Open Loop System .....	8
1.6.2 Closed Loop System .....	9
1.6.3 Energy Piles .....	9
1.7 Soil Heat Transfer .....	10
1.8 Overall Research Aim .....	11
1.8.1 Objectives .....	11
1.8.2 Benefit/Impact .....	11
1.9 Research Methodology .....	12
1.9.1 Critical Review of Literature .....	12
1.9.2 Design of Appropriate Experiment and Equipment/Test Rig .....	12
1.9.3 Test procedure .....	12
1.9.4 Interpretation and Presentation of Results .....	13
1.10 Thesis Outline .....	13
<b>Chapter 2 Literature Review</b> .....	<b>15</b>
2.1 Introduction .....	15
2.2 Renewable Energy Types .....	15
2.3 Low Grade Geothermal Energy .....	16
2.3.1 Heat Pumps .....	16
2.3.2 Ground Source Heat Pumps .....	18

2.3.3	Types of Ground Source Heat Pumps.....	18
2.4	Soil Heat Transfer and its Applications in GSHPs .....	19
2.4.1	Conduction.....	20
2.4.2	Convection .....	20
2.4.3	Radiation.....	20
2.5	Thermal Characteristics of Soils .....	20
2.5.1	Thermal Conductivity.....	21
2.5.2	Specific/Volumetric Heat Capacity.....	21
2.5.3	Thermal Diffusivity.....	21
2.6	The Role of Geotechnical and Thermal Properties of Soil in the Design Considerations for Energy Geo-structures.....	23
2.7	The Determination of the Thermal Properties of Soil .....	24
2.7.1	In-situ Thermal Response Testing.....	25
2.7.2	Dynamic Response Models and the Role of Thermal Diffusivity ....	27
2.8	Energy Piles.....	28
2.8.1	Uses of Energy Piles .....	29
2.8.2	Energy Pile Design.....	30
2.8.3	Coupling of Mechanical and Thermal Properties .....	32
2.9	Gaps in Knowledge .....	33
2.10	Overview of Research Questions .....	35
<b>Chapter 3 Experimental Methodology, Test Rig Design and Equipment.....</b>		<b>37</b>
3.1	Introduction .....	37
3.1.1	Soil type .....	38
3.1.2	Air and Water Content.....	39
3.1.3	Time to Equilibrium .....	39
3.1.4	Temperature .....	39
3.1.5	Pressure Applied.....	39
3.1.6	Heating and Cooling Cycles .....	40
3.1.7	Design Concept.....	40
3.2	Description of Test Rig Design .....	42
3.3	Design of Test Rig.....	43
3.3.1	Design Principles and Assumptions .....	46
3.3.2	Choice of Rig Material .....	47
3.3.3	The Diameter of the Cell .....	48
3.3.4	The effect of the cell wall.....	50
3.3.5	Ability to withstand Pressure Loading.....	55

3.3.6	Other Design Aspects .....	55
3.3.7	A summary of how the rig is set up.....	57
3.3.8	Additional Equipment .....	62
3.4	Commissioning of Rig .....	63
3.5	Results and Problems .....	64
3.6	Modifications to Rig Design after Preliminary Tests.....	66
3.6.1	Change to Design of Rigid Top Plate .....	68
3.6.2	Change in Cartridge Heater Design.....	69
3.6.3	Change to Cell Base Design .....	70
3.6.4	Change in Design of Cell Body.....	71
3.6.5	Change in Design of Perforated Bottom Plate .....	72
3.7	Description of Modified Test Rig.....	72
3.8	Assembling of the Rig .....	74
3.8.1	Task 1: Setting up the cell base and its components.....	74
3.8.2	Task 2: Setting up the cell body and its components.....	77
3.8.3	Task 3: Attaching the cell cover to the test chamber .....	80
3.9	Test set up .....	80
3.10	Summary of Features of the Rig that met Design Criteria.....	81
3.11	Conclusion .....	83
<b>Chapter 4 Test Procedure and Typical Results .....</b>		<b>84</b>
4.1	Introduction .....	84
4.2	Instrumentation and Leakage Testing of Rig and its Components.....	84
4.3	Typical Test Procedure .....	85
4.3.1	Sample Preparation .....	85
4.3.2	Consolidation Phase .....	91
4.3.3	Heating to Equilibrium and Cooling .....	94
4.3.4	Thermal Cycles .....	97
4.3.5	Soil Properties.....	98
4.4	Preliminary Tests .....	99
4.5	Typical Test Results.....	101
4.5.1	Heating to Equilibrium .....	101
4.5.2	Temperature Profile Contour plots.....	104
4.5.3	Variation of Temperature across layer of sample at one level .....	105
4.5.4	The Cooling Curve .....	107
4.5.5	Thermal Cycles .....	109

4.5.6	Analysis of Soil Properties after the Heating Tests carried out in both rig designs.....	110
4.6	Chapter Summary .....	112
<b>Chapter 5 Results obtained from Tests in the First Rig Design .....</b>		<b>113</b>
5.1	Introduction .....	113
5.2	Tests Carried out in Initial Rig Design .....	113
5.2.1	Objectives of Thermal Tests Carried out on Soil Samples.....	113
5.2.2	Other Tests .....	115
5.2.3	Sample No. 1 (Preliminary Tests on Kaolin Sample) .....	116
5.2.4	Sample No. 2 (Preliminary Tests on Kaolin Sample at 50kPa) ....	117
5.2.5	Sample No. 3 (Tests carried out on kaolin sample at 50kPa) .....	119
5.2.6	Sample No. 4 (Tests carried out on kaolin sample at 25kPa) .....	127
<b>Chapter 6 Results from Modified Rig Tests .....</b>		<b>137</b>
6.1	Introduction .....	137
6.2	Tests Carried out in Modified Rig .....	137
6.2.1	Objectives of Thermal Tests Carried out on Soil Samples.....	138
6.2.2	Tests carried out on Kaolin.....	138
6.2.3	Tests carried out on Kaolin and Sand Mixtures .....	170
6.2.4	Tests carried out on Sand .....	207
6.3	Conclusion .....	215
<b>Chapter 7 Discussion .....</b>		<b>216</b>
7.1	Introduction .....	216
7.2	Errors Associated with the Experimental Process .....	216
7.2.1	Sample Preparation .....	216
7.2.2	Water Content Determination.....	217
7.2.3	Temperature Measurements .....	217
7.2.4	Consolidation Pressure .....	219
7.2.5	Time / Duration of Test.....	219
7.2.6	Strength Tests.....	219
7.2.7	Impact of Errors on Results.....	219
7.3	Repeatability/Reproducibility of Tests.....	220
7.4	Validation of Experiment Results against Theory .....	221
7.4.1	Determination of Thermal Conductivity of Tested Samples .....	222
7.4.2	Comparing Measured Temperature Distribution Within Sample With Values Predicted From Theory.....	227
7.5	Discussion of Kaolin Sample at 100kPa .....	231



7.5.1	Heating To Steady State / Thermal Equilibrium .....	232
7.5.2	Cooling Of Sample .....	234
7.5.3	Temperature Variations within Sample in Thermal Equilibrium....	236
7.5.4	Temperature and Thermal Conductivity .....	237
7.5.5	Water Content and Thermal Conductivity .....	237
7.5.6	Water Content and shear strength across sample.....	238
7.5.7	Thermal Cyclic Loads.....	241
7.6	Effect of Soil Type/Composition on duration of heating to thermal equilibrium.....	243
7.7	Effect of Consolidation Pressure and Water Content on heat dissipation 246	
7.8	Discussion of the Determination and Prediction of Thermal Conductivity of the Samples and the influence of Water Content and Sample Composition on the Thermal Conductivity .....	253
7.9	Effect of Temperature (Power input).....	260
7.10	Thermal Cycles .....	262
7.11	Sample Properties Analyzed after Thermal Tests.....	269
7.12	Chapter Summary .....	271
<b>Chapter 8 Overall Conclusions and Recommendation for Further Work .....</b>		<b>274</b>
8.1	Introduction .....	274
8.2	Research Conclusions .....	274
8.2.1	Establishing the use of the ground as a low grade energy source 274	
8.2.2	Designing and developing of test rig to investigate the thermal behaviour of soil around a model energy pile .....	275
8.2.3	Developing of test procedure for carrying out experiments to study heat dissipation in soil and the effects of cooling of buildings over a typical diurnal cycle, and the Validation of results.....	275
8.2.4	Determining the effects of soil type, water content, temperature, overburden pressure, time and thermal cycles on the thermal performance of an energy pile.....	277
8.2.5	Studying the effects of thermal cyclic loading on an energy pile to determine what impact the thermal cycles have on the soil properties .....	278
8.3	Recommendations for Further Work.....	280

<b>References .....</b>	<b>281</b>
<b>Bibliography.....</b>	<b>288</b>
<b>Appendix .....</b>	<b>302</b>
<b>Drawings and Photos of Test Rig and Parts.....</b>	<b>302</b>

## List of Tables

Table 2.1: Summary of values of thermal conductivity and specific heat capacity of various soils (Clarke et al., 2008).....	22
Table 2.2: Summary of key parameters required for the design of energy geo-structures (Loveridge et al., 2017) .....	23
Table 3.1: Table showing additional equipment and their description .....	63
Table 5.1: Summary of samples prepared and tests carried out on each sample .....	114
Table 5.2: Temperature values at probe locations in equilibrium heating condition for kaolin at 50kPa and 5.4W power.....	121
Table 5.3: Table showing temperature variation for sample no.3 .....	122
Table 5.4: Temperature values after 8 hours thermal heating load and 16 hours cooling for day 1 and day 5 in kaolin at 50kPa and 5.4W power.	123
Table 5.5: The coefficients and regression values for sample No. 3 .....	126
Table 5.6: Temperature values at probe locations for thermal equilibrium for kaolin at 25kPa and 4.49W and 9.48W power.....	129
Table 5.7: Table showing temperature variation values at start of test on sample no.4.....	131
Table 5.8: Temperature values after 8 hours thermal heating load and 16 hours cooling in kaolin at 25kPa and 9.48W power.....	133
Table 5.9: The coefficients and regression values for sample No. 4 .....	136
Table 6.1: Detailed summary of samples and tests carried out on each sample .....	139
Table 6.2: Temperature values at probe locations in thermal equilibrium for kaolin test at 100kPa and power input of 17.03W .....	141
Table 6.3: Table showing temperature variation values at the start of test on kaolin at 100kPa.....	143
Table 6.4: Table showing temperature variation values at end of tests on sample no.5.....	144
Table 6.5: Temperature values at probe locations after thermal cyclic loads for 2, 4, 6, 8, 12, 14, 18 and 22 hours of heating and subsequent cooling within 24 hours.....	146
Table 6.6: The coefficients and regression values for sample No. 5 .....	149
Table 6.7: Temperature values at probe locations in thermal equilibrium for kaolin test at 200kPa and power input of 17.03W .....	150
Table 6.8: Table showing temperature variation values at start of tests on sample no.6.....	152
Table 6.9: Temperature values after 4, 8, 12, and 18 hours thermal heating load and subsequent cooling in sample no. 6 at 17.03W power.....	153
Table 6.10: The coefficients and regression values for the trend lines in Figure 6.19.....	155

<b>Table 6.11: Temperature values at probe locations in thermal equilibrium for sample no.7 tested at 0kPa and power input of 17.03W.....</b>	<b>157</b>
<b>Table 6.12: Table showing temperature variation values in sample no.7 at 0kPa .....</b>	<b>159</b>
<b>Table 6.13: Temperature values at probe locations after thermal cyclic loads for 8 &amp;12 hours of heating and subsequent cooling within 24 hours ...</b>	<b>160</b>
<b>Table 6.14: Table showing temperature variation values in sample no.7 at 25kPa .....</b>	<b>162</b>
<b>Table 6.15: Peak temperature values at thermal equilibrium and thermal cyclic loads in sample no. 7 at 25kPa .....</b>	<b>164</b>
<b>Table 6.16: Table showing temperature variation values in sample no.7 at 50kPa .....</b>	<b>166</b>
<b>Table 6.17: Peak temperature values at equilibrium condition and thermal cyclic loads in sample no. 7 at 50kPa.....</b>	<b>168</b>
<b>Table 6.18: The coefficients and regression values for the trend lines in Figure 6.35 and the validity range of water content. ....</b>	<b>170</b>
<b>Table 6.19: Table showing temperature variation values in sample no.8 at 25kPa .....</b>	<b>173</b>
<b>Table 6.20: Peak temperature values at equilibrium condition and thermal cyclic loads in sample no. 8 at 25kPa.....</b>	<b>175</b>
<b>Table 6.21: The coefficients and regression values for the trend lines in Figure 6.43 and the validity range of water content .....</b>	<b>177</b>
<b>Table 6.22: Temperature variation values in sample no.9 at 100kPa .....</b>	<b>180</b>
<b>Table 6.23: Peak temperature values at equilibrium condition and thermal cyclic loads in sample no. 9 at 100kPa.....</b>	<b>181</b>
<b>Table 6.24: The coefficients and regression values for the trend lines in Figure 6.51 and the validity range of water content .....</b>	<b>183</b>
<b>Table 6.25: Table showing temperature variation values in sample no.10 at 25kPa .....</b>	<b>186</b>
<b>Table 6.26: Peak temperature values at equilibrium condition and thermal cyclic loads in sample no. 10 at 25kPa.....</b>	<b>187</b>
<b>Table 6.27: Table showing temperature variation values in sample no.10 at 50kPa .....</b>	<b>190</b>
<b>Table 6.28: Peak temperature values at equilibrium condition and thermal cyclic loads in sample no. 10 at 50kPa.....</b>	<b>191</b>
<b>Table 6.29: Table showing temperature variation values in sample no.10 at 100kPa .....</b>	<b>193</b>
<b>Table 6.30: Peak temperature values at equilibrium condition and thermal cyclic loads in sample no. 10 at 100kPa.....</b>	<b>195</b>
<b>Table 6.31: Table showing temperature variation values in sample no.11 at 25kPa .....</b>	<b>198</b>

<b>Table 6.32: Peak temperature values at equilibrium condition and thermal cyclic loads in sample no. 11 at 25kPa.....</b>	<b>199</b>
<b>Table 6.33: Table showing temperature variation values in sample no.11 at 50kPa .....</b>	<b>202</b>
<b>Table 6.34: Peak temperature values at equilibrium condition and thermal cyclic loads in sample no. 11 at 50kPa.....</b>	<b>203</b>
<b>Table 6.35: Table showing temperature variation values in sample no.11 at 100kPa .....</b>	<b>205</b>
<b>Table 6.36: Peak temperature values at equilibrium condition and thermal cyclic loads in sample no. 11 at 100kPa.....</b>	<b>206</b>
<b>Table 6.37: Table showing temperature variation values in sample no.12 at 25kPa .....</b>	<b>209</b>
<b>Table 6.38: Peak temperature values at equilibrium condition and thermal cyclic loads in sample no. 12 at 25kPa.....</b>	<b>210</b>
<b>Table 6.39: Table showing temperature variation values in sample no.13 at 25kPa .....</b>	<b>213</b>
<b>Table 6.40: Peak temperature values at equilibrium condition and thermal cyclic loads in sample no. 13 at 25kPa.....</b>	<b>214</b>
<b>Table 7.1: Error margins for equipment used.....</b>	<b>217</b>
<b>Table 7.2: Summary of calculated values of thermal conductivity for the samples tested .....</b>	<b>225</b>
<b>Table 7.3: The coefficients and regression values for the trend lines in Figure 7.36 and the validity range of water content .....</b>	<b>241</b>
<b>Table 7.4: The composition of the samples .....</b>	<b>243</b>
<b>Table 7.5: The pressure applied during the tests .....</b>	<b>247</b>
<b>Table 7.6: Thermal conductivity of samples based on Fourier’s Law of heat conduction .....</b>	<b>253</b>
<b>Table 7.7: Effective thermal conductivity values of kaolin and sand based on Equation 7.2 .....</b>	<b>254</b>
<b>Table 7.8: Predicted mass thermal conductivity values of kaolin/sand samples based on Equation 7.2.....</b>	<b>255</b>
<b>Table 7.9: Effective thermal conductivity values of kaolin and sand based on Equation 7.3 .....</b>	<b>257</b>
<b>Table 7.10: Table showing the power inputs used in carrying out the tests ..</b>	<b>260</b>
<b>Table 7.11: Summary of maximum temperatures at 8 hours thermal load and at equilibrium, also showing percentage temperature of sample equilibrium is required for 8 hours thermal cycles.....</b>	<b>269</b>
<b>Table 7.12: Table showing details of soil properties analysed after thermal tests .....</b>	<b>270</b>

## List of Figures

Figure 1.1: Global GDP, energy demand and energy related carbon-dioxide emissions from years 2000 to 2017. Reproduced from (International Energy Agency, 2018).....	1
Figure 1.2: Overview of renewable energy sources. Reproduced from Ellabban et al. (2014).....	4
Figure 1.3: Geothermal heat from the Earth's core. Modified from Omer (2008) .....	5
Figure 1.4: Seasonal variation of the near-surface temperature profile (Busby, J. et al., 2009) .....	6
Figure 1.5: Relationship between surface air temperature and ground temperature in the UK (Preene and Powrie, 2009b).....	7
Figure 1.6: A ground source heat pump system using boreholes and piles (Clarke et al., 2008) .....	8
Figure 1.7: Open-loop system (Florides and Kalogirou, 2007) .....	8
Figure 1.8: Closed-loop ground energy system (Preene and Powrie, 2009b) ...	9
Figure 1.9: Energy pile system in heating and cooling operations (Abuel-Naga, H. et al., 2015a) .....	10
Figure 2.1: A typical temperature profile (Clarke et al, 2008).....	16
Figure 2.2: Schematic diagram of a heat pump, connected to a closed-loop borehole heat exchanger. The heat pump uses 1500 W electricity to extract 4267 W heat from the ground, yielding a grand total of 5.77 kW space heating and a COPH of 3.8 (Banks, 2008).....	17
Figure 2.3: The three main components of a geothermal heat pump system (Rybach, 2012).....	18
Figure 2.4: Schematic of a thermal response test, where T1 is the fluid input temperature and T2, the fluid output temperature. After (Rybach, 2012)	26
Figure 2.5: Typical energy pile arrangement after (Laloui et al., 2006) .....	28
Figure 2.6: Heating/cooling a small house with energy foundations (Brandl, 2006) .....	29
Figure 2.7: Number of installed GSHP units and energy provided for space heating in some European countries from 2000-2011 after (Bayer et al., 2012) .....	30
Figure 2.8: Absorber pipes fitted to the reinforcement cage of bored energy pile (Brandl, 2006) .....	31
Figure 2.9: Typical thermal pile construction details (Loveridge and Powrie, 2012) .....	31
Figure 2.10 : Absorber pipes entering a concrete slab (Brandl, 2006).....	32

Figure 2.11: Thermal effects on an energy pile ( $\Delta T$ , temperature variation; $P$ , mechanical load; $\delta_{th}$ , pile displacement induced by temperature variation; $\Delta\sigma_{th}$ , thermally induced stress; $c'$ , cohesion; and $\phi'$ , friction angle of the soil) Laloui and Di Donna (2011) .....	33
Figure 3.1: An energy pile exchanging heat with surrounding ground .....	38
Figure 3.2: Concept of Rig Design.....	40
Figure 3.3: Schematic diagram of Test Rig.....	42
Figure 3.4: Test Rig .....	43
Figure 3.5: Heat transport from soil to heat carrier fluid within the absorber pipe of an energy pile (Brandl, 2006).....	44
Figure 3.6: A long Cylindrical Layer .....	45
Figure 3.7: A section through a long cylindrical layer containing soil sample and heat source within the sample.....	48
Figure 3.8: Plot of $Q(W)$ vs $R_2/R_1$ for selecting appropriate diameters for the Heat Source and Test Rig.....	50
Figure 3.9: A section through a multi-layered cylinder filled with soil sample with a centrally placed heat source .....	51
Figure 3.10: Multi-layered Cylindrical Section filled with Soil Sample and showing the parameters being calculated .....	52
Figure 3.11: Plot of $T_1$ ( $^{\circ}C$ ) vs. $T_2$ ( $^{\circ}C$ ) where values for $T_2$ were obtained by changing the values of $T_1$ while keeping $T_3$ , $R_3$ , $R_1$ and $R_2$ constant .....	53
Figure 3.12: Plot of $R_1$ vs. $T_2$ ( $^{\circ}C$ ) where values of $T_2$ were obtained by changing the values of $R_1$ while keeping $T_3$ , $R_3$ , $T_1$ and $R_2$ constant .....	54
Figure 3.13: Plot of $R_2$ vs. $T_2$ ; where values of $T_2$ were obtained by changing the values of $R_2$ while keeping $T_3$ , $R_3$ , $T_1$ and $R_1$ constant.....	54
Figure 3.14: Cross-section of test rig showing the key elements .....	56
Figure 3.15: Cartridge heater and cartridge heater in copper pipe .....	57
Figure 3.16: Top view of cell base with O-ring attached .....	58
Figure 3.17: Bottom view of cell base showing fittings and copper pipe with heater .....	58
Figure 3.18: Perforated plate to be placed over cell base.....	59
Figure 3.19: Cylindrical cell body showing openings fitted with blanking plugs .....	59
Figure 3.20: Cylindrical cell body attached to cell base by threaded iron bars .....	60
Figure 3.21: Top view of cell before and after loading with sample.....	60
Figure 3.22: Showing top and bottom views of the piston (rigid plate) before and after it is placed over sample.....	61
Figure 3.23: Test rig being covered with cell cover fitted with flexible rubber diaphragm .....	62

Figure 3.24: Heating and cooling cycles in kaolin showing temperature variations at different radii as shown in the layout of probe positions...	65
Figure 3.25: Temperature variations across the sample compared to the theoretical variation .....	66
Figure 3.26: The initial rig design and the modifications made to improve its performance .....	67
Figure 3.27: Top piston and its parts .....	69
Figure 3.28: Cartridge heater .....	69
Figure 3.29: The initial and modified cell base designs.....	70
Figure 3.30: Top and bottom views of modified cell base .....	71
Figure 3.31: Modification of Cell body .....	71
Figure 3.32: Top view of initial and modified bottom plates.....	72
Figure 3.33: Diagrams of initial and modified rig designs .....	73
Figure 3.34: Assembling the cell base .....	75
Figure 3.35: Setting up of the cell base with O-rings and plugs.....	75
Figure 3.36: Installing the cartridge heater .....	76
Figure 3.37: Assembling the test rig showing the base plate with the cartridge heater in place and filter paper to allow excess pore pressures to dissipate as pore fluid is drained from the sample .....	76
Figure 3.38: Sealing the openings on the cell body for sample loading.....	77
Figure 3.39: Photograph showing (a) the cell body fitted into the already set-up cell base; and (b) the inside of the test chamber from top view .....	77
Figure 3.40: Top flange mounted on cell body .....	78
Figure 3.41: The test chamber (cell body and cell base) is bolted in place by threaded iron bars .....	78
Figure 3.42: Inside the test chamber loaded with sample.....	79
Figure 3.43: Top piston placed over sample.....	79
Figure 3.44: Attaching the cell cover to the test chamber .....	80
Figure 3.45: An overview of test set up in the modified rig .....	81
Figure 3.46: Temperature variations across the sample compared to the theoretical variation .....	82
Figure 4.1: The cartridge heater being tested on a small scale to establish its temperature response to power input .....	85
Figure 4.2: A mixing unit set up inside an extraction chamber for mixing samples .....	87
Figure 4.3: Photo showing kaolin sample mixing process where kaolin powder is being added to the distilled water in the mixer bowl .....	87
Figure 4.4: Photo showing (a) Well mixed kaolin sample ready for testing (b) Kaolin samples collected for determination of actual water content of prepared sample .....	88



<b>Figure 4.5: Photo showing sample mixture of three parts of kaolin to one part of sand in the test chamber.....</b>	<b>89</b>
<b>Figure 4.6: Photo showing sample mixture of one part of kaolin to one part of sand in test chamber .....</b>	<b>89</b>
<b>Figure 4.7: Photo showing sample mixture of one part of kaolin to one three parts of sand in test chamber .....</b>	<b>90</b>
<b>Figure 4.8: Photo showing process of loading test chamber with dry sand sample before testing.....</b>	<b>91</b>
<b>Figure 4.9: Photo showing the process of preparation of saturated sand sample where water is connected to the rig through the drainage tubing and the vacuum pump is connected to the rig to suck out air from the sample while drawing water into the sample.....</b>	<b>92</b>
<b>Figure 4.10: Photo showing drainage tubing connected at bottom of cell base to collect water expelled from sample during consolidation.....</b>	<b>93</b>
<b>Figure 4.11: Settlement dial-gauge set up to monitor progress of consolidation in sample .....</b>	<b>93</b>
<b>Figure 4.12: The blanking plugs are replaced with Swagelok gland for insertion of thermocouples.....</b>	<b>94</b>
<b>Figure 4.13: Drawing and photo of thermocouple arrangement within Test Chamber in relation to distance from heat source .....</b>	<b>95</b>
<b>Figure 4.14: Temperature profile within the test chamber is captured by inserting all the probes at uniform radial distances from the heater to the edge of the cell wall. ....</b>	<b>96</b>
<b>Figure 4.15: Temperature profile within the test chamber is captured by inserting all the probes from top to bottom at uniform distances from the heater to the edge of the cell wall. ....</b>	<b>97</b>
<b>Figure 4.16: Sketch of layout for sample analysis and testing at the end of the heating tests.....</b>	<b>98</b>
<b>Figure 4.17: Samples were collected for water content determination after the shear strength test carried out at every sample point .....</b>	<b>99</b>
<b>Figure 4.18: Arrangement of thermocouples within the test chamber to monitor temperature changes within the sample .....</b>	<b>100</b>
<b>Figure 4.19: The heating curves of kaolin sample to thermal equilibrium showing the variation in temperature with time at the various probe locations in the initial rig design.....</b>	<b>101</b>
<b>Figure 4.20: Layout of the probe arrangements for all the preliminary tests carried out in the modified rig design .....</b>	<b>103</b>
<b>Figure 4.21: The heating curves of kaolin sample to thermal equilibrium showing the variation in temperature with time at the various probe locations in the modified rig design .....</b>	<b>103</b>
<b>Figure 4.22: Temperature contour plot of the vertical temperature profiles at different radii across the sample in initial rig design.....</b>	<b>104</b>

<b>Figure 4.23: Temperature Contour plot of the vertical temperature profiles at different radii across the sample in modified rig.....</b>	<b>105</b>
<b>Figure 4.24: Range of average temperature measurements showing the variations from top to bottom of sample at each location across the sample layer, and also showing that the average temperature reduces with distance from the heater, in the initial rig design .....</b>	<b>106</b>
<b>Figure 4.25: Range of average temperature measurements showing the variations from top to bottom of sample at each location across the sample layer, and also showing that the average temperature reduces with distance from the heater, in the modified rig.....</b>	<b>106</b>
<b>Figure 4.26: Cooling curves of kaolin sample from equilibrium heating back to controlled room temperature showing the variation in temperature with time at the various probe locations in initial rig design.....</b>	<b>107</b>
<b>Figure 4.27: Cooling curves of kaolin sample from equilibrium heating back to controlled room temperature showing the variation in temperature with time at the various probe locations in modified rig.....</b>	<b>108</b>
<b>Figure 4.28: Five days thermal loading cycles consisting of 8 hours heating and 16 hours cooling in initial rig design.....</b>	<b>109</b>
<b>Figure 4.29: Two days of thermal loading cycles consisting of 8 hours heating and 16 hours cooling in modified rig.....</b>	<b>110</b>
<b>Figure 4.30: Shear strength against water content carried out on the sample at the end of the heating tests in the initial rig design at 25kPa.....</b>	<b>111</b>
<b>Figure 4.31: Shear strength against water content carried out on the sample at the end of the heating tests in the modified rig at 100kPa.....</b>	<b>111</b>
<b>Figure 5.1: Graph showing cartridge heater, thermocouple and room temperature changes during the small scale test .....</b>	<b>116</b>
<b>Figure 5.2: Graph of heating and cooling tests from second preliminary test .....</b>	<b>118</b>
<b>Figure 5.3: Layout of thermocouples within test chamber for tests carried out on sample no.3; kaolin at 50kPa .....</b>	<b>120</b>
<b>Figure 5.4: The variation of temperature with time across a sample of kaolin consolidated to 50kPa showing that thermal equilibrium was achieved after about 30hrs.....</b>	<b>120</b>
<b>Figure 5.5: The time to return to room temperature (test at 50kPa; sample no.3).....</b>	<b>121</b>
<b>Figure 5.6: Temperature variations across sample from outer wall of pipe containing the heater to edge of test chamber and from top to bottom of sample .....</b>	<b>122</b>
<b>Figure 5.7: The temperature variation across the sample during 8 hours heating and 16 hours cooling for five days on a kaolin sample at 50kPa and at 5.4W.....</b>	<b>123</b>
<b>Figure 5.8: Variation of shear strength with distance from heater in the four layers from top to bottom of the sample.....</b>	<b>124</b>

Figure 5.9: Variation of percentage water content with distance from heater in the four layers from top to bottom of the sample.....	125
Figure 5.10: The variation of shear strength with percentage water content in Sample No.3 at the end of the heating tests .....	125
Figure 5.11: Layout of thermocouples for tests carried out on kaolin sample at 25kPa .....	128
Figure 5.12: Kaolin Test at 25kPa at thermal equilibrium for power input of: 4.49W .....	128
Figure 5.13: Kaolin Test at 25kPa at thermal equilibrium for power input of 9.48W .....	129
Figure 5.14: Cooling curves for kaolin test at 25kPa from thermal equilibrium achieved at power input of 4.49W.....	130
Figure 5.15: Cooling curves for kaolin test at 25kPa from thermal equilibrium achieved at power input of: 9.48W.....	130
Figure 5.16: Temperature variations across sample and at four levels from top to bottom of sample at start of kaolin at 25kPa test.....	131
Figure 5.17: Contour plot of temperature variations across sample no.4 in heating equilibrium condition .....	132
Figure 5.18: Variation in temperature with time for thermal loading cycles of 8 hours heating and 16 cooling over five days on kaolin sample at 25kPa and 9.48W .....	133
Figure 5.19: Variation of shear strength with distance from heater in the four layers from top to bottom of the sample.....	134
Figure 5.20; Variation of percentage water content with distance from heater in the four layers from top to bottom of the sample.....	135
Figure 5.21: The variation of shear strength with percentage water content in kaolin sample tested at 25kPa at the end of the testing regime .....	135
Figure 6.1: Layout of thermocouples within the test chamber for tests on kaolin at 100kPa.....	140
Figure 6.2: The variation of temperature with time across a sample of kaolin consolidated to 50kPa showing that thermal equilibrium was achieved after about 29 hours.....	141
Figure 6.3: The time to return to room temperature (test at 100kPa) .....	142
Figure 6.4: Temperature variations across sample from heater to edge of test chamber and from top to bottom of sample at start of test on kaolin sample at 100kPa .....	142
Figure 6.5: Temperature variations across sample from heater to edge of test chamber and from top to bottom of sample at end of tests on sample no. 5 .....	143
Figure 6.6: Temperature contour plot showing temperature variations in sample no. 5 at the end of the testing period.....	144

<b>Figure 6.7: The temperature variation across the sample during 8 hours heating and 16 cooling for 14 days on kaolin sample at 100kPa and 17.03W .....</b>	<b>145</b>
<b>Figure 6.8: Variation of various thermal loads at peak temperatures across sample no. 5 from heater to edge of the test chamber.....</b>	<b>147</b>
<b>Figure 6.9: Variation of shear strength with distance from heater in the four layers from top to bottom of the sample .....</b>	<b>148</b>
<b>Figure 6.10: Variation of percentage water content with distance from heater in the four layers from top to bottom of the sample.....</b>	<b>148</b>
<b>Figure 6.11: The variation of shear strength with percentage water content in kaolin sample tested at 100kPa at the end of the testing regime .....</b>	<b>149</b>
<b>Figure 6.12: The variation of temperature with time across a kaolin sample consolidated to 200kPa showing that thermal equilibrium was achieved after about 48 hours.....</b>	<b>150</b>
<b>Figure 6.13: The time to return to room temperature for kaolin test at 200kPa .....</b>	<b>151</b>
<b>Figure 6.14: Temperature variations across sample from heater to edge of test chamber and from top to bottom of sample at start of test on kaolin sample at 200kPa .....</b>	<b>151</b>
<b>Figure 6.15: The temperature variation across the sample during thermal loading cycles of 12 hours heating and 12 cooling for three days on kaolin sample at 200kPa and 17.03W .....</b>	<b>152</b>
<b>Figure 6.16: Various thermal loads at peak temperatures when in thermal equilibrium, also showing the decrease in temperature across sample no. 6 away from the heater .....</b>	<b>153</b>
<b>Figure 6.17: Variation of shear strength with distance from heater in the three layers from top to bottom of the sample .....</b>	<b>154</b>
<b>Figure 6.18: Variation of percentage water content with distance from heater in the three layers from top to bottom of the sample .....</b>	<b>154</b>
<b>Figure 6.19: Plot of shear strength against water content carried out on kaolin sample tested at 200kPa at the end of the testing regime .....</b>	<b>155</b>
<b>Figure 6.20: Layout of thermocouples within test chamber for tests carried out on sample no. 7 .....</b>	<b>156</b>
<b>Figure 6.21: The variation of temperature with time across a sample of kaolin at 0kPa and power input of 17.03W showing thermal equilibrium was achieved after about 36 hours .....</b>	<b>157</b>
<b>Figure 6.22: Cooling curves for sample no. 7 at 0kPa showing the time to return to room temperature.....</b>	<b>158</b>
<b>Figure 6.23: Temperature variations across sample from heater to edge of test chamber and from top to bottom of sample at start of test on sample no. 7 at 0kPa .....</b>	<b>158</b>
<b>Figure 6.24: The temperature variation across sample during 8 and 12 hours heating and subsequent cooling on sample no. 7 at 0kPa and 17.03W</b>	<b>159</b>

Figure 6.25: The variation of temperature with time across a sample of kaolin consolidated to 25kPa showing that thermal equilibrium was achieved after about 40hrs.....	161
Figure 6.26: The time to return to room temperature for sample no. 7 at 25kPa .....	161
Figure 6.27: Temperature variations across sample from heater to edge of test chamber and from top to bottom of sample at start of test on sample no. 7 at 25kPa .....	162
Figure 6.28: The temperature variation across sample during 8 and 11.5 hours heating and subsequent cooling in sample no. 7 at 25kPa and 17.03W .....	163
Figure 6.29: The variation of temperature with time across a sample of kaolin consolidated to 50kPa showing that thermal equilibrium was achieved after about 38hours .....	165
Figure 6.30: The time to return to room temperature for sample no. 7 at 50kPa .....	165
Figure 6.31: Temperature variations across sample from heater to edge of test chamber and from top to bottom of sample at start of test on sample no. 7 at 50kPa .....	166
Figure 6.32: The temperature variation across sample during 8 and 12 hours heating and subsequent cooling in sample no. 7 at 50kPa and 17.03W .....	167
Figure 6.33: Variation of shear strength with distance from heater in the four layers from top to bottom of the sample .....	168
Figure 6.34: Variation of percentage water content with distance from heater in the four layers from top to bottom of the sample.....	169
Figure 6.35: Variation of shear strength with percentage water in sample no. 7 at the end of the tests carried out at 50kPa .....	169
Figure 6.36: Layout of thermocouples within test chamber for tests carried out on sample no. 8 .....	171
Figure 6.37: The variation of temperature with time across a sample of 75:25 Kaolin & sand consolidated to 25kPa showing that thermal equilibrium was achieved after about 26 hours.....	172
Figure 6.38: The time to return to room temperature for sample no. 8 at 25kPa .....	172
Figure 6.39: Temperature variations across sample from heater to edge of test chamber and from top to bottom of sample at end of test on sample no. 8 at 25kPa .....	173
Figure 6.40: Temperature variation across the sample during 8 hours heating and 16 hours cooling in sample no. 8 at 25kPa and 17.03W.....	174
Figure 6.41: Variation of shear strength with distance from heater in the four layers from top to bottom of the sample .....	175

Figure 6.42: Variation of percentage water content with distance from heater in the four layers from top to bottom of the sample.....	176
Figure 6.43: The variation of shear strength with percentage water content in sample no. 8 consolidated to 25kPa at the end of the testing regime...	176
Figure 6.44: Layout of thermocouples within test chamber for tests carried out on sample no. 9 .....	178
Figure 6.45: of the variation of temperature with time across sample no. 9 consolidated to 100kPa showing that thermal equilibrium was achieved after about 40 hours.....	178
Figure 6.46: The time to return to room temperature for sample no. 9 at 100kPa .....	179
Figure 6.47: Temperature variations across sample from heater to edge of test chamber and from top to bottom of sample at end of test on sample no. 9 at 100kPa .....	179
Figure 6.48: The temperature variation across the sample during 8 hours heating and 16 hours cooling in sample no. 9 at 100kPa and 17.03W ..	180
Figure 6.49: Variation of shear strength with distance from heater in the four layers from top to bottom of the sample .....	182
Figure 6.50: Variation of percentage water content with distance from heater in the four layers from top to bottom of the sample.....	182
Figure 6.51: Variation of shear strength with percentage water content carried out on 75:25 kaolin:sand sample tested at 100kPa at the end of the testing regime. ....	183
Figure 6.52: Layout of thermocouples within test chamber for tests carried out on sample no. 10 .....	184
Figure 6.53: The variation of temperature with time across sample no. 10 at 25kPa and power input of 17.03W showing thermal equilibrium was achieved after about 39 hours .....	185
Figure 6.54: Cooling curves for sample no. 10 at 25kPa showing the time to return to room temperature.....	185
Figure 6.55: Temperature variations across sample from heater to edge of test chamber and from top to bottom of sample at end of test on sample no. 10 at 25kPa .....	186
Figure 6.56: The temperature variation across the sample during thermal loading cycles of 8 hours heating and 16 hours cooling in sample no. 10 at 25kPa and 17.03W.....	187
Figure 6.57: Temperature variation with time across sample no. 10 consolidated to 50kPa showing that thermal equilibrium was achieved after about 42 hours.....	188
Figure 6.58: Time to return to room temperature for sample no. 10 at 50kPa .....	189

<b>Figure 6.59: Temperature variations across sample from heater to edge of test chamber and from top to bottom of sample at end of test on sample no. 10 at 50kPa .....</b>	<b>189</b>
<b>Figure 6.60: The temperature variation across the sample during thermal loading cycles of 8 hours heating and 16 hours cooling in sample no. 10 at 50kPa and 17.03W.....</b>	<b>190</b>
<b>Figure 6.61: Variation of temperature with time across sample no. 10 consolidated to 100kPa showing that thermal equilibrium was achieved after about 43 hours.....</b>	<b>192</b>
<b>Figure 6.62: The time to return to room temperature for sample no. 10 at 100kPa .....</b>	<b>192</b>
<b>Figure 6.63: Temperature variations across sample from heater to edge of test chamber and from top to bottom of sample at end of test on sample no. 10 at 100kPa .....</b>	<b>193</b>
<b>Figure 6.64: The temperature variation across the sample during thermal loading cycles of 8 hours heating and 16 hours cooling in sample no. 10 at 100kPa and 17.03W.....</b>	<b>194</b>
<b>Figure 6.65: Layout of thermocouples within test chamber for tests carried out on sample no. 11.....</b>	<b>196</b>
<b>Figure 6.66: The variation of temperature with time across sample no. 11 consolidated to 25kPa and power input of 17.03W showing thermal equilibrium was achieved after about 28 hours.....</b>	<b>197</b>
<b>Figure 6.67: Cooling curves for sample no. 11 consolidated to 25kPa showing the time to return to room temperature.....</b>	<b>197</b>
<b>Figure 6.68: Temperature variations across sample from heater to edge of test chamber and from top to bottom of sample at end of test on sample no. 11 at 25kPa .....</b>	<b>198</b>
<b>Figure 6.69: of the temperature variation across sample during 8 hours heating and 16 hours cooling in sample no. 11 at 25kPa and 17.03W ..</b>	<b>199</b>
<b>Figure 6.70: Temperature variation with time across sample no. 11 consolidated to 50kPa showing that thermal equilibrium was achieved after about 28 hours.....</b>	<b>200</b>
<b>Figure 6.71: Cooling curves for sample no. 11 at 50kPa showing time to return to room temperature .....</b>	<b>201</b>
<b>Figure 6.72: Temperature variations across sample from heater to edge of test chamber and from top to bottom of sample at end of test on sample no. 11 at 50kPa .....</b>	<b>201</b>
<b>Figure 6.73: Temperature variation across sample during 12 hours heating and 12 hours cooling in sample no. 11 at 50kPa and 17.03W.....</b>	<b>202</b>
<b>Figure 6.74: Variation of temperature with time across sample no. 11 at 100kPa in showing that thermal equilibrium was achieved after about 48 hours.....</b>	<b>204</b>
<b>Figure 6.75: Cooling curves for sample no. 11 at 100kPa showing the time to return to room temperature.....</b>	<b>204</b>

Figure 6.76: Temperature variations across sample from heater to edge of test chamber and from top to bottom of sample at end of test on sample no. 11 at 100kPa .....	205
Figure 6.77: Temperature variation across sample during 8 hours heating and 16 hours cooling in sample no. 11 at 100kPa and 17.03W .....	206
Figure 6.78: Layout of thermocouples within test chamber for tests carried out on sample no. 12 .....	207
Figure 6.79: Variation of temperature with time in sample no. 12 at 25kPa showing that thermal equilibrium was achieved after about 24 hours .....	208
Figure 6.80: Cooling curves for sample no. 12 at 25kPa showing time to return to room temperature .....	208
Figure 6.81: Temperature variations across sample from heater to edge of test chamber and from top to bottom of sample at end of test on sample no. 12 at 25kPa .....	209
Figure 6.82: Temperature variation across sample during thermal loading cycles of 8 hours heating and 16 hours cooling in sample no. 12 at 25kPa .....	210
Figure 6.83: Layout of thermocouples within test chamber for tests carried out on sample no13 .....	211
Figure 6.84: Variation of temperature with time in sample no. 13 at 25kPa showing that thermal equilibrium was achieved after about 24.5 hours .....	212
Figure 6.85: Cooling curves for sample no. 13 at 25kPa showing time to return to room temperature .....	212
Figure 6.86: Temperature variations across sample from heater to edge of test chamber and from top to bottom of sample at end of test on sample no. 13 at 25kPa .....	213
Figure 6.87: Temperature variation across sample during thermal loading cycles of 12 hours heating and 12 hours cooling in sample no. 13 at 25kPa .....	214
Figure 7.1: Variation of temperature with time from probes placed at two opposite sides of the test rig showing the similarity between the measurements.....	218
Figure 7.2: The fit of temperature measurements from opposite sides of the test rig.....	218
Figure 7.3: Test rig showing probe positions.....	219
Figure 7.4: Comparison between two tests on a kaolin sample subjected to 4 hours of heating and 20 hours of cooling .....	220
Figure 7.5: The fit of two tests carried out on a kaolin sample subjected to 4 hours of heating and 20 hours of cooling .....	221
Figure 7.6: Temperature contour profile of sample in equilibrium condition showing both radial and axial variations .....	222



Figure 7.7: Temperature profile measurements of sample within the test chamber at specified locations from top to bottom and at uniform distances from the heater to the edge of the cell wall while sample is in steady state .....	223
Figure 7.8: Radial and axial temperature variations within the sample in Fig 7.6.....	223
Figure 7.9: Range of average temperature measurements showing the variations from top to bottom of sample at each location and also showing that the average temperature reduces with distance from the heater, in the sample shown in Figure 7.6 .....	224
Figure 7.10: Water content variation from top to bottom and across sample in Figure 7.6, with respect to distance from heat source .....	224
Figure 7.11: The variation of thermal conductivity with percentage water content in kaolin samples .....	226
Figure 7.12: Comparing thermal conductivity values obtained from top, middle and bottom of sample with the average values.....	227
Figure 7.13: The fit of predicted and measured temperature distribution within kaolin sample with 84.5% water content, tested at 0kPa .....	228
Figure 7.14: The fit of predicted and measured temperature distribution within kaolin sample tested at 25kPa; 56.7% water content .....	228
Figure 7.15: The fit of predicted and measured temperature distribution within kaolin sample tested at 100kPa and 48% water content .....	229
Figure 7.16: The fit of predicted and measured temperature distribution within kaolin sample tested at 200kPa; 42% water content .....	229
Figure 7.17: The fit of predicted and measured temperature distribution within 75:25 kaolin:sand samples tested at 25kPa; 42.1% water content .....	229
Figure 7.18: The fit of predicted and measured temperature distribution within 75:25 kaolin:sand sample tested at 100kPa; 36.5% water content .....	230
Figure 7.19: The fit of predicted and measured temperature distribution within 50:50 kaolin:sand sample tested at 100kPa; 28% water content .....	230
Figure 7.20: The fit of predicted and measured temperature distribution within 25:75 kaolin:sand sample tested at 100kPa; 19.6% water content .....	230
Figure 7.21: The fit of predicted and measured temperature distribution within saturated sand sample tested at 25kPa.....	231
Figure 7.22: The fit of predicted and measured temperature distribution within dry sand sample tested at 25kPa.....	231
Figure 7.23: Layout of probes within kaolin sample during the heating test	232
Figure 7.24: Variation of temperature with time across kaolin sample consolidated at 100kPa being heated to steady state .....	232
Figure 7.25: Percentage of maximum temperature attained by sample against time of heating .....	234
Figure 7.26: Time for kaolin sample consolidated at 100kPa to cool back to controlled room temperature .....	235

Figure 7.27: Percentage of maximum temperature against time of cooling ..	235
Figure 7.28: Variations in average change in temperature at locations across sample of kaolin at 100kPa at both the start and end of thermal tests ..	236
Figure 7.29: Fit of variations in average change in temperature across sample at start and end of tests.....	236
Figure 7.30: Thermal conductivity values plotted against corresponding temperature values across the sample to show relationship .....	237
Figure 7.31: Thermal conductivity values plotted against corresponding water content values across the sample to show relationship.....	238
Figure 7.32: Variation in water content across the sample with respect to distance from the heater the range of average water content at each location indicating that the water content increases with distance from the heater.....	238
Figure 7.33: Variation of shear strength values with the sample .....	239
Figure 7.34: Range of variation in average shear strength values at each location showing that the average shear strength reduces with distance from the heat source.....	239
Figure 7.35: Relationship between the average shear strength values and corresponding water content values with respect to distance from the heat source.....	240
Figure 7.36: Shear strength values against corresponding water content values in top, middle and bottom of kaolin sample at 100kPa.....	240
Figure 7.37: Comparing temperature values from day 1 of 8 hours thermal load cycle with day 14 of the same thermal load.....	241
Figure 7.38: Comparing temperature values from day 1 of 16 hours cooling cycle with day 14 of the same cooling cycle.....	242
Figure 7.39: Thermal cyclic loading showing peak temperatures reached and corresponding cooling temperatures within a 24 hour period. ....	242
Figure 7.40: Heating curves of the different soils compositions with varying water contents, tested at same power input of 17.03W. The sample made up of just kaolin with no sand content took the longest time to reach equilibrium temperature and also had the highest equilibrium temperature of about 34°C. ....	244
Figure 7.41: Time to equilibrium of combination samples of kaolin and sand with respect to the percentage sand content.....	245
Figure 7.42: Maximum temperature attained relative to the percentage sand content of sample after 42 hours of heating .....	245
Figure 7.43: Cooling curves for the different soils compositions with varying water contents, after being heated at power input of 17.03W.....	246
Figure 7.44: Heating curves for kaolin samples at 84.5% water content at 0kPa, and 82% water content at start of test, and tested at the same power input of 17.03W but different consolidation pressures of 25, 100 and 200kPa .....	248

Figure 7.45: Cooling curves for the kaolin samples in Figure 7.44 .....	248
Figure 7.46: heating curves for kaolin:sand (75:25) samples with same water content at start of test, same power input of 17.03W but at different consolidation pressures of 25kPa and 100kPa.....	249
Figure 7.47: Cooling curves for the kaolin:sand (75:25) samples in Figure 7.46 .....	250
Figure 7.48: Heating curves for kaolin:sand (50:50) samples with same water content at start of test, same power input of 17.03W but different consolidation pressures of 25, 50 and 100kPa .....	250
Figure 7.49: Cooling curves for the kaolin:sand (50:50) samples in Figure 7.48 .....	251
Figure 7.50: Heating curves for kaolin:sand (25:75) samples with same water content at start of test, same power input of 17.03W but different consolidation pressures of 25, 50 and 100kPa .....	251
Figure 7.51: Cooling curves for the kaolin:sand (25:75) samples in Figure 7.50 .....	252
Figure 7.52: Thermal conductivity of sample as a function of both percentage sand content and percentage water content.....	252
Figure 7.53: Thermal conductivity in kaolin/sand samples showing an increase with increased sand content and a decrease with increased water content based on volume.....	256
Figure 7.54: Relationship between thermal conductivity and sand content at various levels of saturation based on volume .....	256
Figure 7.55: Thermal conductivity in kaolin/sand samples showing an increase with increased sand content and a decrease with increased water content based on mass .....	258
Figure 7.56: Relationship between thermal conductivity and sand content at various levels of saturation based on mass .....	259
Figure 7.57: Comparison of thermal conductivity values of determined from the heat transfer equation and those predicted based on the mass and volume of the sample constituents .....	259
Figure 7.58: Heating curves of the same soil type, kaolin at 82% water content and consolidation pressure but at different power inputs ranging from 4.49-17.05W .....	261
Figure 7.59: Spatial variation in temperature across the same kaolin sample at two different power inputs .....	261
Figure 7.60: Thermal loading cycles of 8 hours heating and 16 hours cooling in 75:25 kaolin:sand sample at 25kPa and 17.03W.....	263
Figure 7.61: 4, 8, 12 and 18 hours heating cycles on a kaolin sample tested over a 24 hour period to study to what degree cooling was established within time .....	263
Figure 7.62: Peak temperatures attained in kaolin samples of varying water contents with respect to duration of heating.....	264

<b>Figure 7.63: Peak temperatures attained in 75:25 kaolin:sand samples of varying water contents with respect to duration of heating .....</b>	<b>265</b>
<b>Figure 7.64: Peak temperatures attained in 50:50 kaolin:sand samples of varying water contents with respect to duration of heating .....</b>	<b>266</b>
<b>Figure 7.65: Peak temperatures attained in kaolin samples of varying water contents with respect to duration of heating .....</b>	<b>267</b>
<b>Figure 7.66: Peak temperatures attained in dry sand and saturated sand samples with respect to duration of heating.....</b>	<b>268</b>
<b>Figure 7.67: Spatial variation of shear strength and water content of four kaolin samples tested at 25, 50, 100 and 200kPa.....</b>	<b>270</b>
<b>Figure 7.68: Average water content in samples at end of tests plotted against normal load applied to samples during tests.....</b>	<b>271</b>

## List of Abbreviations

GDP	Gross Domestic Product
GSHP	Ground Source Heat Pumps
EES	Earth Energy Systems
BHE	Borehole Heat Exchanger
COP	Coefficient of performance
PPE	Personal Protective Equipment
$R_1, R_2$	Inner Radius, Outer Radius
L	Length
$k$	Thermal Conductivity
$T_1 - T_2$	Temperature Difference between boundaries
A	Cross Sectional Area
$Q$	Heat transfer rate
$S$	Shape factor
$K_{\text{wall}}$	Thermal conductivity of the cell wall
$K_{\text{soil}}$	Thermal conductivities of soil sample
WC	Water Content
$C_{\text{soil}}$	Heat capacity of soil
$C_p$	Specific heat capacity
$\rho$	Density
$\alpha$	Thermal diffusivity
V	Volume
$K_{\text{tmass}}$	Thermal conductivity of sample mass
$K_{\text{tkaoilin}}$	Thermal conductivity of kaolin
$K_{\text{tsand}}$	Thermal conductivity of sand
$K_{\text{twater}}$	Thermal conductivity of water

## Chapter 1 Introduction

### 1.1 Background

Population and Gross Domestic Product (GDP), which are identified as the key drivers of energy demand, have been on the increase; consequently the world's total energy consumption has also been on the increase recording a global rise of 2.5% in 2011 (British Petroleum, 2012); 1.8% in 2012 (Ellabban et al., 2014) and 2.1% in 2017 (International Energy Agency, 2018). Increased energy requirements has led to an increased demand for fossil fuels with resultant carbon-dioxide emissions and hence global warming. Figure 1.1 shows the increasing trend of GDP, carbon-dioxide emissions and energy demand by a growing population over the last seventeen years.

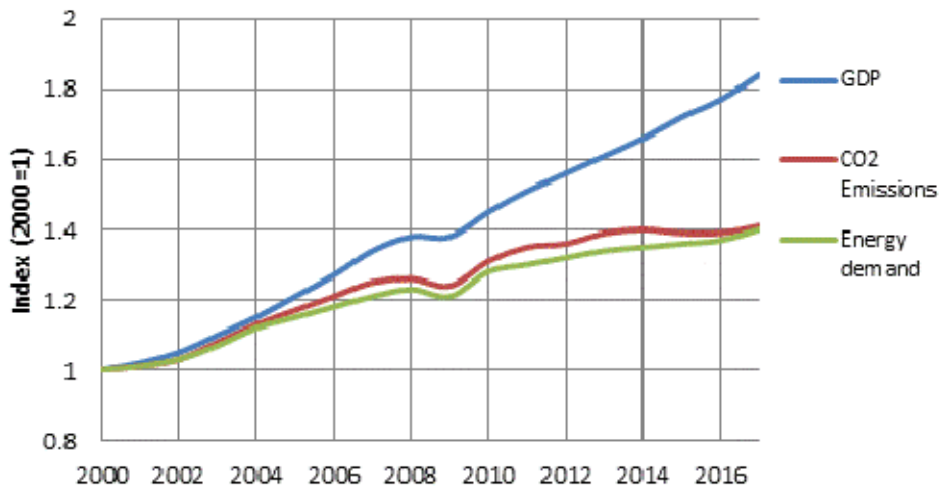


Figure 1.1: Global GDP, energy demand and energy related carbon-dioxide emissions from years 2000 to 2017. Reproduced from (International Energy Agency, 2018)

The global energy demand exceeds  $15 \times 10^{10}$  MWh/year, of which about 85% is attributed to fossil fuels while about 6% comes from renewable energy sources. Furthermore, approximately 33% of the world's total energy consumption is attributed to heating and air-conditioning systems (Kharseh et al., 2015).

### 1.2 Climate Change

The Framework Convention on Climate Change (UNFCCC), in its Article 1, defines climate change as: “a change of climate which is attributed directly or indirectly to human activity that alters the composition of the global atmosphere and which is in addition to natural climate variability observed over comparable time periods” (Field et

al., 2014). Although in some cases climate change has been used synonymously with the term “global warming”, scientists however, tend to use the term in the wider sense to also include natural changes in climate. According to Nathanail and Banks (2009), climate change is driven by an increased energy input into the global system resulting from heat trapping due to excess carbon dioxide, ozone layer depletion and increased solar energy radiation. The production of carbon dioxide emission is closely linked with climate change as it is one of the major greenhouse gases.

Climate change has been highlighted by key political figures in the United Kingdom as one of the largest threats to humankind and has risen on the political agenda. The Kyoto protocol which is an international agreement linked to the United Nations Framework Convention on Climate Change, adopted in Kyoto, Japan, on 11 December 1997 and entered into force on 16 February 2005, demonstrates a global consensus that is committed to reducing the carbon dioxide emissions. The Protocol, in setting internationally binding emission reduction targets, takes into consideration the fact that developed countries are in the lead for emitting higher levels of greenhouse gases, hence they face a heavier burden under the principle of "common but differentiated responsibilities" (United Nations Framework Convention on Climate Change, 2018).

A recent report by the International Energy Agency (2018) indicates a global increase in energy-related carbon-dioxide emissions of 1.4% in 2017. This, according to the report, is “a historic high of 32.5 Gigatonnes (Gt)”, which is said to be “a resumption of growth after three years of global emissions remaining flat”. It is of significant interest that the reported increase differed among countries, since some major economies registered a rise, it was a case of decline for others. The biggest decline is reported to be from the United States, which can be mainly attributed to their increased use of renewables.

With the international efforts are being made to reduce emissions, Brook et al. (2016) suggests additional actions such as reforms “that seek to secure ambitious abatement commitments and practical action”; thereby proposing that a ‘Low-Emissions Technology Commitment’ (LETC) be incorporated into the UNFCCC negotiations to ensure lasting benefits.

A focus on the use of renewable energy is suggested by Blum et al. (2010) as key approach to avoid additional carbon-dioxide emissions while also improving energy security and sustainability.

Towards “building a low-carbon economy” the UK government embraced “The Climate Change Act” of 2008, which commits it by law to reduce “greenhouse gas emissions by at least 80% of 1990 levels by 2050” (Committee on Climate Change, 2018). In

helping to achieve this target, Snape et al. (2016) reports that in 2010 the UK government introduced “two schemes that incentivise the adoption of domestic-scale renewable energy technologies (RETs), specifically the feed-in tariff (FiT) and the renewable heat incentive (RHI)”. These schemes encourage people who install RETs “a payback tariff based on the quantity (kWh) of renewable energy they can produce”, with expected contributions charted in the UK renewable energy roadmap.

In summary, climate change, which is attributed to the consumption of fossil fuels and their resultant emissions, will be greatly helped by a shift to renewable energy resources. The drive therefore, towards the reduction of carbon emissions and the need for reduced dependence on fossil fuels, which are non-renewable, has necessitated the development of clean technologies or renewable energy sources.

### **1.3 Energy Demands of Buildings**

Heating and cooling requirements of buildings vary according to their design, size, and the purpose for which the buildings are used. Traditional methods of heating and cooling of buildings result in depletion of fossil fuels and the emission of carbon dioxide and other gases into the atmosphere (CIBSE, 2004). With regard to heating and cooling energy requirements, “buildings are responsible for nearly 45% of the energy consumption in the UK and account for around half of the Nation’s carbon dioxide emissions” (The Institute of Refrigeration, 2012).

European Commission (2018) also attributes approximately 40% of energy consumption and 36% of carbon-dioxide emissions in the EU to buildings, and suggest that more effort towards the renovation of existing buildings could potentially result in significant energy savings, which according to them “could reduce the EU’s total energy consumption by 5-6% and lower CO<sub>2</sub> emissions by about 5%”. Similarly in the United States, residential buildings are said to be responsible for about 22% of the primary energy consumption and 17% of greenhouse gas (GHG) emissions, of which space heating and cooling contribute to more than half of this consumption (Lim et al., 2016).

In keeping with the current predictions in temperature increase, there arises a need, therefore, to find alternative means of heating and cooling buildings, which together account for a significant portion of total energy use (CIBSE, 2004). Towards achieving this goal, some buildings are already being designed to be passive such that they require ten times less heat energy than same building of standard design in Europe (Badescu et al., 2010). Consequently the use of alternative methods in heating and



cooling of buildings will significantly reduce the emission of carbon dioxide into the atmosphere.

## 1.4 Renewable Energy Sources

Ellabban et al. (2014) defines renewable energy as “energy sources that are continually replenished by nature and derived directly from the sun (such as thermal, photo-chemical, and photo-electric), indirectly from the sun (such as wind, hydropower, and photosynthetic energy stored in biomass), or from other natural movements and mechanisms of the environment (such as geothermal and tidal energy)”. They suggest that with the increasing concern for the protection of the environment from imminent extreme weather and climate impacts, a shift towards renewable energy can help in meeting both the goals of reducing greenhouse gas emissions, and also in providing energy.

Figure 1.2 presents an overview of common renewable energy sources which include hydropower, biomass, geothermal energy, solar energy, marine energy and wind energy.

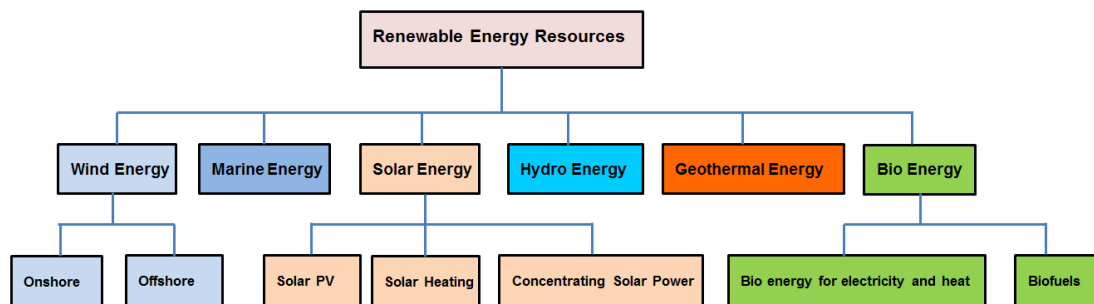


Figure 1.2: Overview of renewable energy sources. Reproduced from Ellabban et al. (2014)

Solar radiation from the sun is considered the principal or most significant source of the earth’s renewable energy which, by means of various technologies, can be converted into useful energy directly for different applications (Boyle, 2004). This includes the use of solar heating and cooling technologies to collect the sun’s thermal energy for use as heat source in providing hot water, space heating and cooling, and other uses for both individual and industrial applications (Ellabban et al., 2014).

Solar radiation which is absorbed by the earth’s surface is also stored in the ground due to its thermal properties and can be harnessed for use in heating and cooling of buildings achieved through the use of Ground Source Heat Pumps (Banks, 2008). While this can be classed as solar energy, it is more commonly referred to as ground

energy or geothermal energy. Geothermal energy includes low grade energy derived from solar radiation and high grade energy derived from the earth's core.

Biomass energy is energy from the sun that is stored in plants, animals, or their wastes, and recovered by burning them as fuel (Demirbas, 2005). Hydroelectric power plants which are location dependent, utilize potential energy from trapped water behind dams to produce energy to drive high-speed turbines for reliable electric power generation (Elliott, 2013).

## 1.5 Geothermal Energy

The temperature of the Earth's core estimated between 3000°C and 5000°C derives its source from the gradual breakdown of radioactive elements as well as intense gravitational forces acting on the rocks and minerals within the Earth (Omer, 2008). This is illustrated in Figure 1.3.

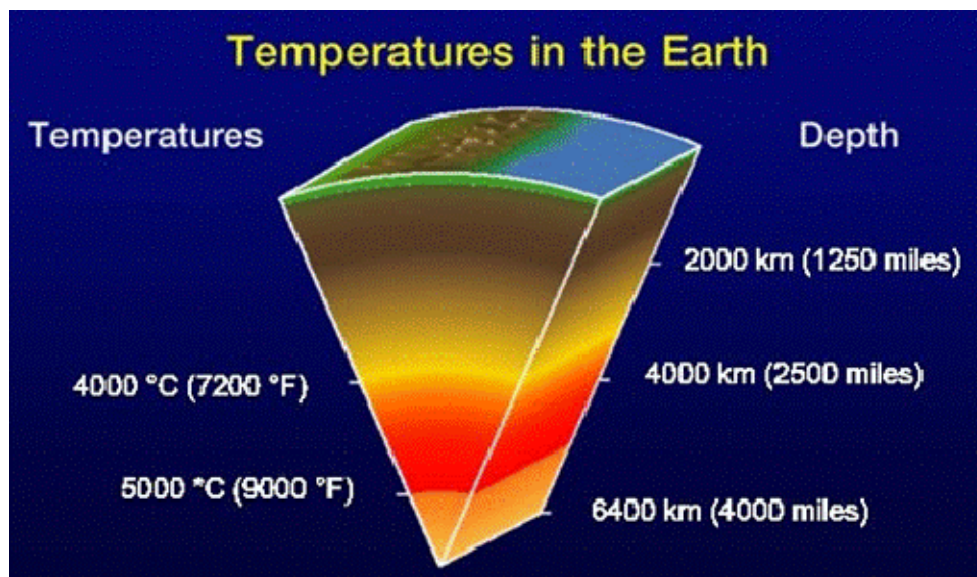


Figure 1.3: Geothermal heat from the Earth's core. Modified from Omer (2008)

According to Omer (2008), geothermal energy has been used since the 1920s to heat buildings up to commercial scales, and occurs naturally in certain geological regions in the form of geysers, hot springs and steam vents when groundwater makes contact with volcanically heated rocks through cracks or fractures.

High grade geothermal energy is usually harnessed by drilling to depths of a few thousand metres, or drilling wells into rocks of volcanic origin to extract hot water and steam (ETSU, 1994). The hot water or steam is transported via insulated pipes for district heating or superheated to drives turbines or electric generators.

Although high grade geothermal energy has the advantages of near zero emissions and little land space requirement for development unlike other energy sources, it suffers the drawback of not being strictly renewable, being capital intensive, and being restricted to specific geological zones.

The upper layers of the earth's surface have the capacity to store both solar energy from the surface and geothermal energy derived from the earth's core. Although the thermal capacity of the ground depends on the type of ground and the hydro-geological conditions, the temperature over the top 100-200m and below the zone of seasonal temperature variation is usually constant due to a combination of geothermal and solar energy and acts as a thermally stable mass in the absence of external influences (Preene and Powrie, 2009b). Figure 1.4 shows a typical ground temperature profile from the ground surface to 15m depth.

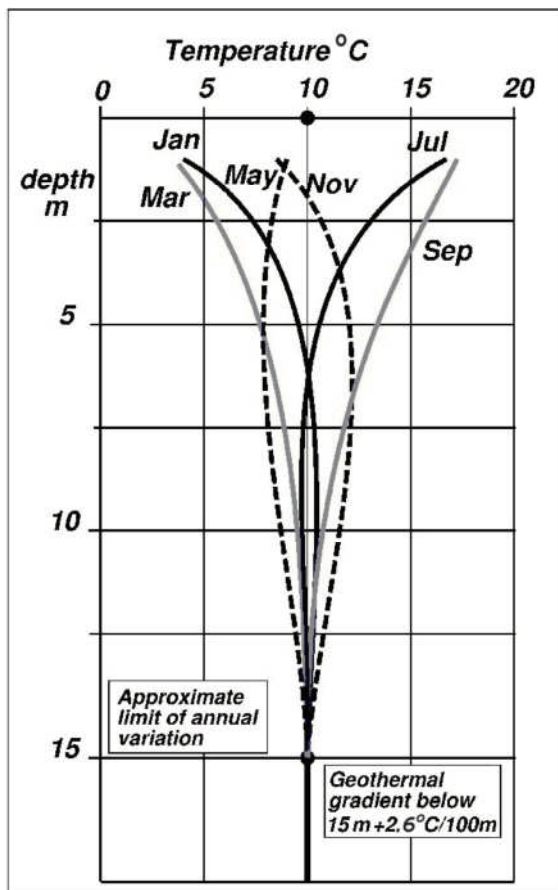


Figure 1.4: Seasonal variation of the near-surface temperature profile (Busby, J. et al., 2009)

## 1.6 Earth Energy Systems/Ground Source Heat Pumps

Rybach (2012) describes shallow geothermal resources as “the heat content of rocks in the top few 100m of the continental crust”. In order to take full advantage of this readily available, though low grade energy as opposed to geothermal energy which is

confined to regions with specific geological conditions, Ground or Earth Energy Systems (EESs) or Ground Source Heat Pumps (GSHPs) can be used to harness and efficiently transfer energy between a building and the ground by means of circulating fluids, thus using the ground as a heat source or sink (Banks, 2008). This system utilizes the temperature difference between the air and the ground for heat exchange through the use of a ground heat exchanger (Florides and Kalogirou, 2007).

The relationship between the surface air and ground temperatures is shown in Figure 1.5.

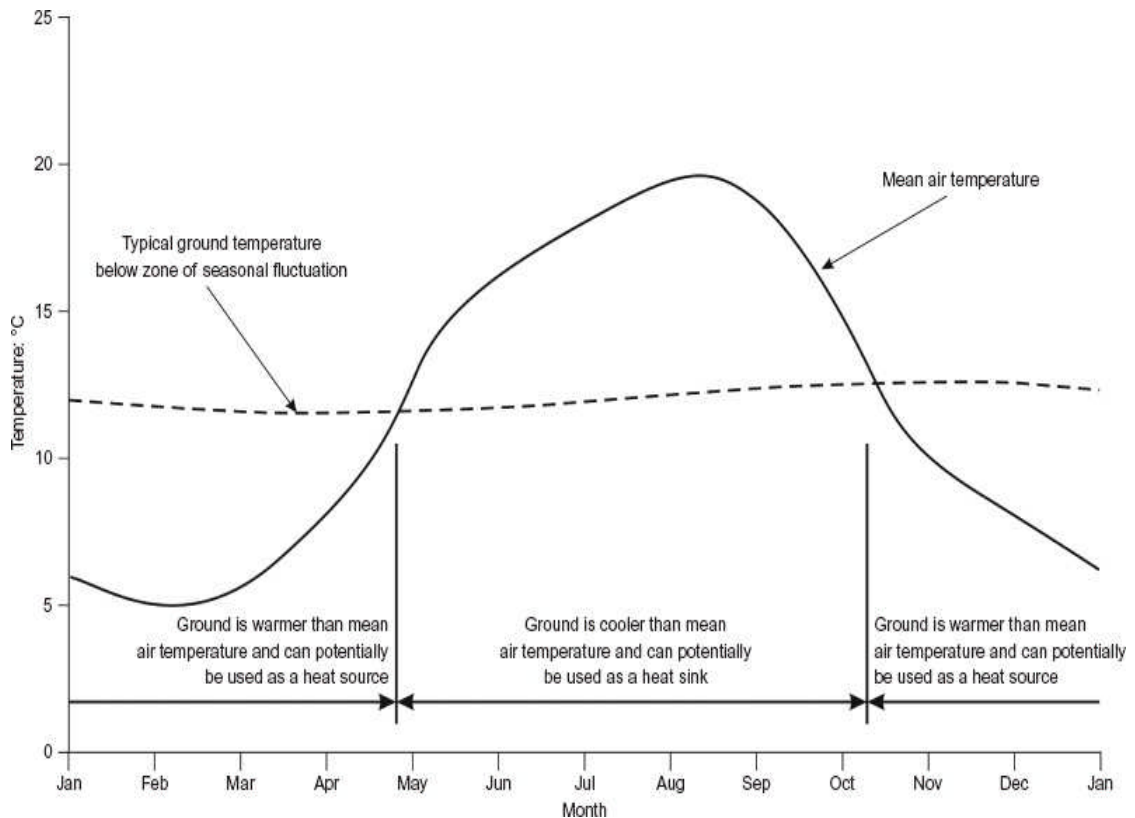


Figure 1.5: Relationship between surface air temperature and ground temperature in the UK (Preene and Powrie, 2009b)

According to Blum et al. (2010), GSHP systems commonly use electricity and sometimes gas to operate their heat pumps and “the ratio between output heat to supplied energy of GSHP is defined as the Coefficient of Performance (COP)”. Typical COP values for GSHPs lie between 3.0 and 5.0 (Glassley, 2010; Lim et al., 2016).

The design of GSHPs or EESs is based on three elements namely the source, the load and the heat transfer system; and operate through the use of series of buried pipes to transfer heat to and from the ground (the source) into a building (the load) making use of the ground as both heat source and sink as shown in Figure 1.6.

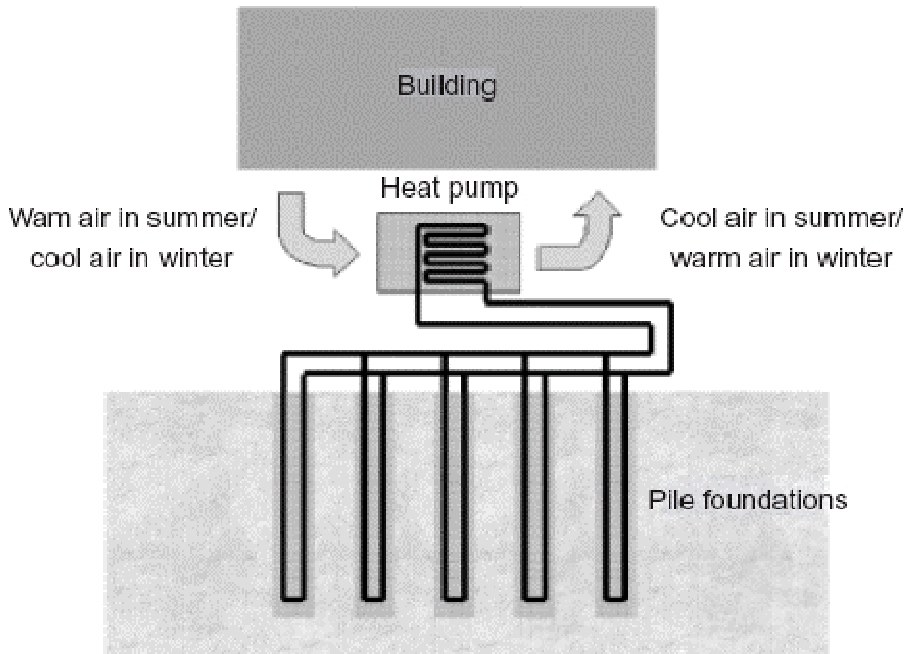


Figure 1.6: A ground source heat pump system using boreholes and piles (Clarke et al., 2008)

GSHPs can operate either as open loop system by circulating surface or underground water, or closed loop systems by circulating fluids within pipes while relying on heat transfer by conduction from the surrounding soil (CIBSE, 2005). The loops are usually made of very durable yet conductive materials such as high-density polyethylene and copper piping (Florides and Kalogirou, 2007).

### 1.6.1 Open Loop System

In open loop systems, groundwater is commonly used as the heating or cooling medium and usually requires both extraction and injection wells as shown in

Figure 1.7.

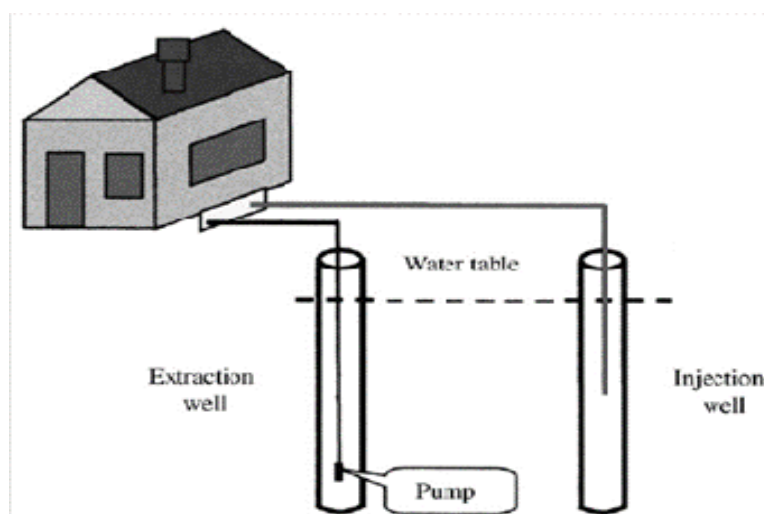


Figure 1.7: Open-loop system (Florides and Kalogirou, 2007)

### 1.6.2 Closed Loop System

In the closed loop system as shown in Figure 1.8, the heat exchangers which are buried underground can either be installed vertically, horizontally or obliquely, circulating a fluid which exchanges heat with the surrounding soil through the wall of the heat exchanger.

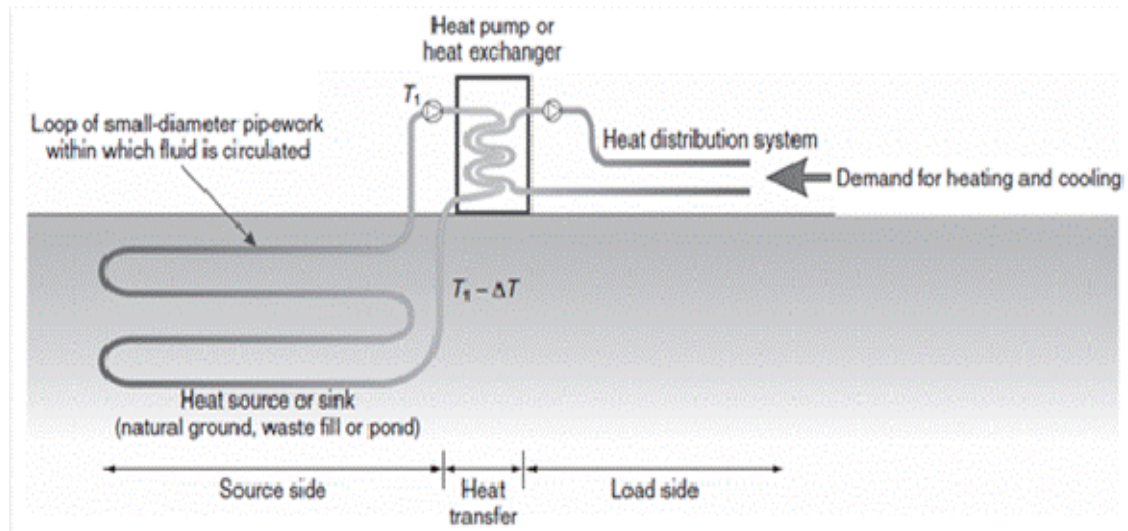


Figure 1.8: Closed-loop ground energy system (Preene and Powrie, 2009b)

In horizontal systems, pipes are buried in trenches with typical length of 35-60km per kW of heating or cooling capacity (Florides and Kalogirou, 2007), and requires considerable land space. Vertical systems which include vertical boreholes and energy piles require less surface area but are more expensive to install. Pipes are installed in boreholes of up to 20-300m depth and 10-15cm diameter which are then grouted.

### 1.6.3 Energy Piles

Energy piles are a form of closed-loop ground energy system and are also referred to as thermal piles or energy geo-structures which, while providing stability in buildings, also provide heating/cooling requirements by exchanging heat with the surrounding soil, as illustrated in Figure 1.9.

The use of energy piles for heat transfer takes advantage of structures primarily required for a building's stability; hence separate infrastructure is not necessary. According to Adam and Markiewicz (2009) foundation slabs, driven precast piles, bored piles and diaphragm walls have been used successfully for heating and cooling purposes, by installing fluid filled absorber pipes within the concrete elements.

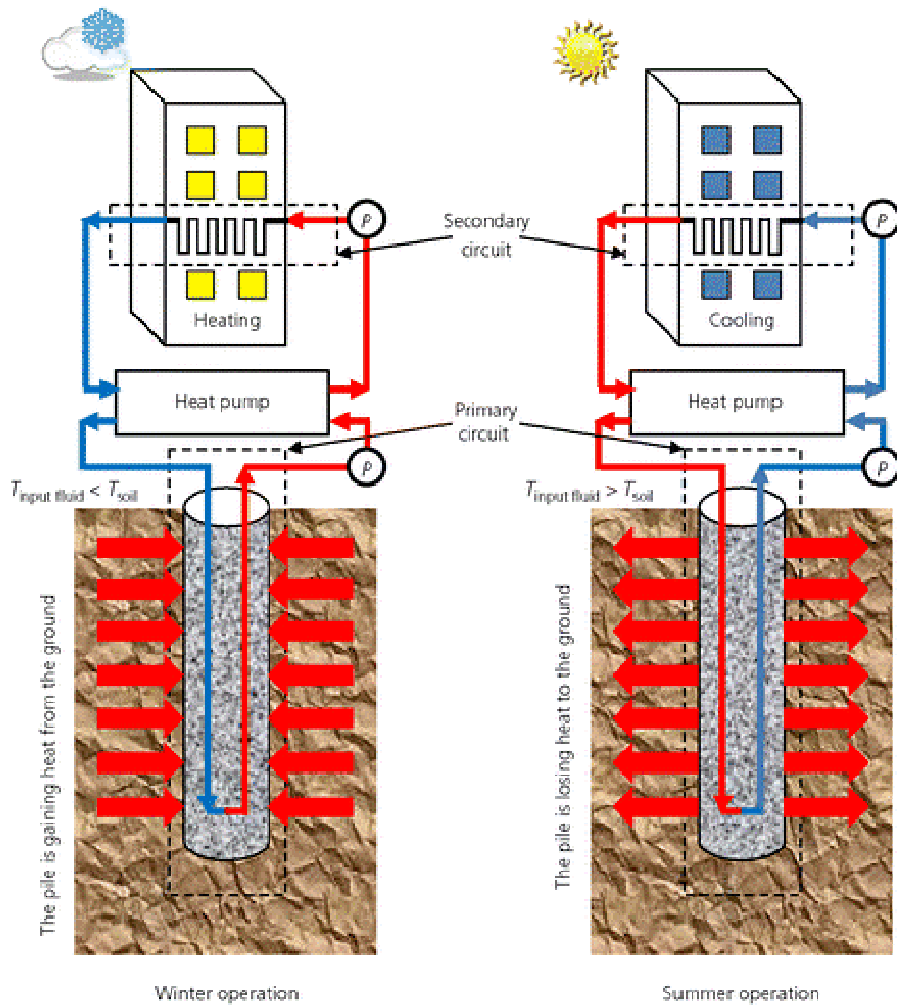


Figure 1.9: Energy pile system in heating and cooling operations (Abuel-Naga, H. et al., 2015a)

Energy geo-structures including basement slabs, diaphragm walls and tunnel linings have been used successfully in countries like Austria and Switzerland from the 1980s utilising the thermal properties of concrete for energy storage with proof of environmental and economic benefits (Brandl, 2006). An example of energy pile use in the United Kingdom is the One New Change Building in London which has 192 energy piles installed (Laloui and Di Donna, 2011).

## 1.7 Soil Heat Transfer

Heat transfer is simply defined as “thermal energy in transit due to a temperature difference” (Banks, 2008). Heat moves from a higher temperature region to a lower one and normally occurs via three mechanisms namely: Conduction, Convection and Radiation.

Properties that affect heat transfer mechanisms in soils include water content, porosity or density, mineral content and temperature (Gabrielsson et al., 2000; Mitchell and Soga, 2005). Heat transfer in the ground predominantly takes place through

conduction particularly in clays where convection is inhibited due to its low permeability (Thomas and Rees, 2009).

According to Busby, J. et al. (2009), thermal properties such as thermal conductivity which is the “capacity of a material to conduct or transmit heat” and thermal diffusivity which is “the rate at which heat is conducted through a medium”, mainly determine the rate of heat transfer between a heat exchanger and the ground.

## **1.8 Overall Research Aim**

The emphasis of this research is to assess how the conductive properties of the ground affect heat flowing from a line source (a simulated energy pile) and how it is affected by cyclic thermal loading.

This research aims to address the area of inadequate geotechnical input in energy pile design with a focus on the limited understanding of factors that govern heat flow within soils around an energy pile, by investigating the thermal behaviour of the soils around a simulated energy pile in a bid to establish a relationship between soil type, water content, temperature, overburden pressure, time and thermal cycles; and the performance of energy piles.

### **1.8.1 Objectives**

The research objectives undertaken in order to achieve the overall aims are:

- 1) Establish the use of the ground as a low grade energy source through a critical review of literature
- 2) Develop a piece of equipment/test rig to investigate the thermal behaviour of soil around a model energy pile
- 3) Develop a test procedure for running the experiments to investigate the effects of cooling of buildings over a typical diurnal cycle
- 4) Study the effects of cyclic heat loading on an energy pile to determine what impact the thermal cycles have on the soil properties
- 5) Determine the effects of soil type, water content, temperature, overburden pressure, time and thermal cycles on the thermal performance of an energy pile

### **1.8.2 Benefit/Impact**

The benefit of this research is to produce results based on investigations which will contribute to existing data on thermal behaviour of soils around an energy pile, to aid designers and other researchers in the field, thereby ensuring improved performance of energy piles.



The final results which include original analysis of correlations between thermal conditions and both thermal and mechanical properties will be of interest to designers and other researchers as they are of practical importance in energy pile applications.

## **1.9 Research Methodology**

The methodology adopted in achieving the aim and objectives of this research which involved the design and development of an experimental apparatus and laboratory procedures for investigating soil thermal behaviour, is described under the following headings of critical review of literature, design of experiment and test rig, test procedure and result analyses and interpretation.

### **1.9.1 Critical Review of Literature**

A critical review of existing literature was undertaken to gain understanding of the use of the ground as a low grade energy source, and how heat energy is stored and abstracted from the ground, and also to identify the factors that affect heat flow in the ground.

### **1.9.2 Design of Appropriate Experiment and Equipment/Test Rig**

An experiment was developed to simulate ground conditions by creating an axisymmetric problem similar to an installed energy pile. This allowed a linear heat source within a soil mass to be modelled to depict a scenario typical to that of an energy pile exchanging heat with the surrounding soil while being subjected to overburden pressure. The experimental model and test rig were designed to dissipate heat radially by conduction from a line source by optimising the radial distribution of temperature and the dimensions of the sample to minimise the effect of the boundary conditions. The test rig allowed a range of tests to be undertaken to simulate an energy pile under cyclic thermal loading based on a 24hr cycle to simulate an office environment

### **1.9.3 Test procedure**

Soils samples were prepared and thermal tests carried out in the fabricated test rig to investigate their thermal behaviour and to record changes in heat dissipation influenced by controlling/varying soil type, water content, pressure, temperature, time and thermal cycles. The test procedure involved the following steps:

- i. Sample preparation based on the soil types and their proportions in constituting the sample and the sample water content.

- ii. To determine the thermal capacity of samples in terms of time taken to achieve thermal equilibrium and time taken to cool back to controlled room temperature when a constant heat source was applied in a controlled room temperature at specific overburden pressure, water content, and power input.
- iii. To measure and record heat distribution within soil subject to varying cycles of thermal loading and unloading to simulate practical use of energy piles in an office environment
- iv. To monitor changes in heat flow influenced by soil water content, temperature, pressure and the power input to the system

#### **1.9.4 Interpretation and Presentation of Results**

The results obtained from the experiments were analysed and interpreted to show how soil water content, temperature, pressure, the power input to the system and cyclic thermal loading affected the performance of a simulated energy pile.

#### **1.10 Thesis Outline**

The outline of the thesis is briefly summarised in terms of the contents of the following chapters.

Chapter two critically explores the literature related to the topic area and identifies current development and gaps in knowledge necessitating this research.

Chapter three presents a detailed description of the experimental methodology and the processes undertaken in designing the test rig. It explains how each design parameter was chosen and the theory and assumptions behind their selection. The procedures in assembling and commissioning of the test rig are also covered in this chapter.

Chapter four describes the test procedure which encompasses sample preparation, loading the test rig and carrying out the tests. The test procedure is described in detail with typical results of the tests included.

The details of the results from all the tests carried out on various samples in the test rigs over the research period are presented in chapters five and six. Chapter five deals with the results from the original rig design while chapter six covers the results obtained from tests carried out in the modified rig.

The interpretation, discussion and validation of the results obtained from the experiments undertaken to investigate the thermal behaviour of the soil around a simulated energy pile, are covered in Chapter seven, while the research conclusions and recommendations are presented in Chapter eight.

Drawings and photographs of the test rig are included in the appendix.

## Chapter 2 Literature Review

### 2.1 Introduction

The justification for the adoption of renewable energy technologies to reduce carbon emissions while meeting the global energy demands was presented in Chapter 1. The heating and cooling demands of buildings were identified as mainly responsible for both energy consumption as well as being a major contributor to carbon-dioxide emissions. A shift of focus to the exploration and harnessing of renewable energy resources will therefore, be beneficial in the long-term in meeting energy demands while protecting the environment. One such technology is ground source heat pumps, particularly energy piles, to supplement the heating and cooling needs of the buildings, which will eventually lead to less dependence on fossil fuels and subsequently overall reduction of carbon-dioxide emissions.

This chapter discusses the key aspects of using this technology, the considerations of thermal properties necessary for its use, and finally the issues or problems currently hindering its optimum performance. These will lead to the identification of gaps in knowledge which address the need for the focus of this research.

### 2.2 Renewable Energy Types

The growth of renewable energy is enjoying a global boost especially due its advantage which Blum et al. (2010) identify as “avoiding of additional carbon-dioxide emissions while helping to enhance energy security and improve sustainability in preventing further carbon-dioxide emissions”. This is more so as renewable energy according to Ellabban et al. (2014) has the potential to meet and even exceed the global demands.

The common renewable energy resources include wind energy, marine energy, solar energy, hydro energy, biomass energy and geothermal energy and were described in Chapter 1.

Geothermal energy refers to energy extracted from the earth’s heat store originating from both radioactive decay of minerals and absorbed solar energy (Laloui and Di Donna, 2011). This cost effective and environmentally friendly source of energy can be utilized on both small and large scale for electrical power generation, direct use of heat; consisting of geothermal heat pump (GHP) technologies, or combined heat and power in cogeneration applications (Ellabban et al., 2014).

## 2.3 Low Grade Geothermal Energy

Unlike high grade geothermal energy resource which is derived from deep in the earth and associated with high temperatures, low grade or shallow geothermal energy refers to the use of the top 100m below the zone of seasonal influence (approximately 2m), and thermally stable, for the purpose of heating or cooling buildings by taking advantage of the temperature difference between the ground and the building. Figure 2.1 shows a typical temperature profile explaining how above approximately 100m, the ground temperature is mostly from surface temperatures particularly solar, and while below 100m, temperature sources are from the earth's core (Clarke et al., 2008).

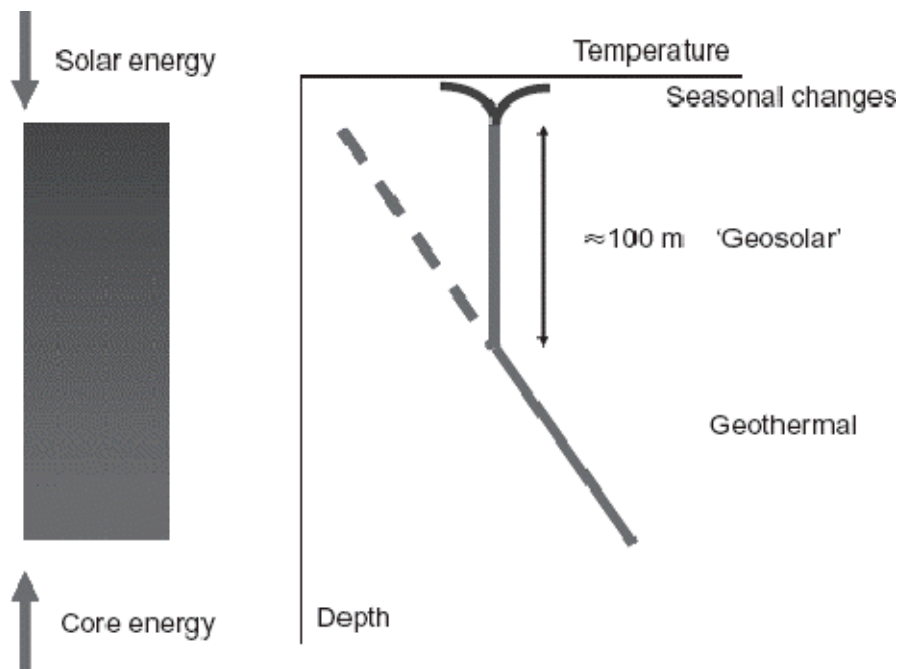


Figure 2.1: A typical temperature profile (Clarke et al, 2008)

The use of GSHPs for space heating and cooling is a renewable energy technology based on the Earth's relatively constant temperature at depths of 10-15m, and its difference in temperature from that of the air. Since they are associated with generally low temperatures of approximately 10-15°C in Europe and 20-25°C in the tropics, a heat pump is utilized to enhance its use (Abdelaziz and Ozudogru, 2016).

### 2.3.1 Heat Pumps

The invention of the heat pump by Peter Ritter von Rittinger an Austrian mining Engineer in 1855, was driven by environmental and economic considerations, which he justified two years later by showing an annual saving of 293,000m<sup>3</sup> of firewood if all Austrian saltworks used heat pump installations (Brandl, 2006).

A heat pump is simply described as “a device that pumps heat” and also “raises the temperature of the available heat from an unusable level to a usable one” (Banks,

2008). Similarly, Omer (2008) describes a heat pump as a mechanical device used for heating and cooling that operates on the principle of moving heat from a region of higher temperature to one of lower temperature. It is comprised of an evaporator, a compressor and a condenser as shown in Figure 2.2, and typically yields a higher useful heat output than that required to operate it.

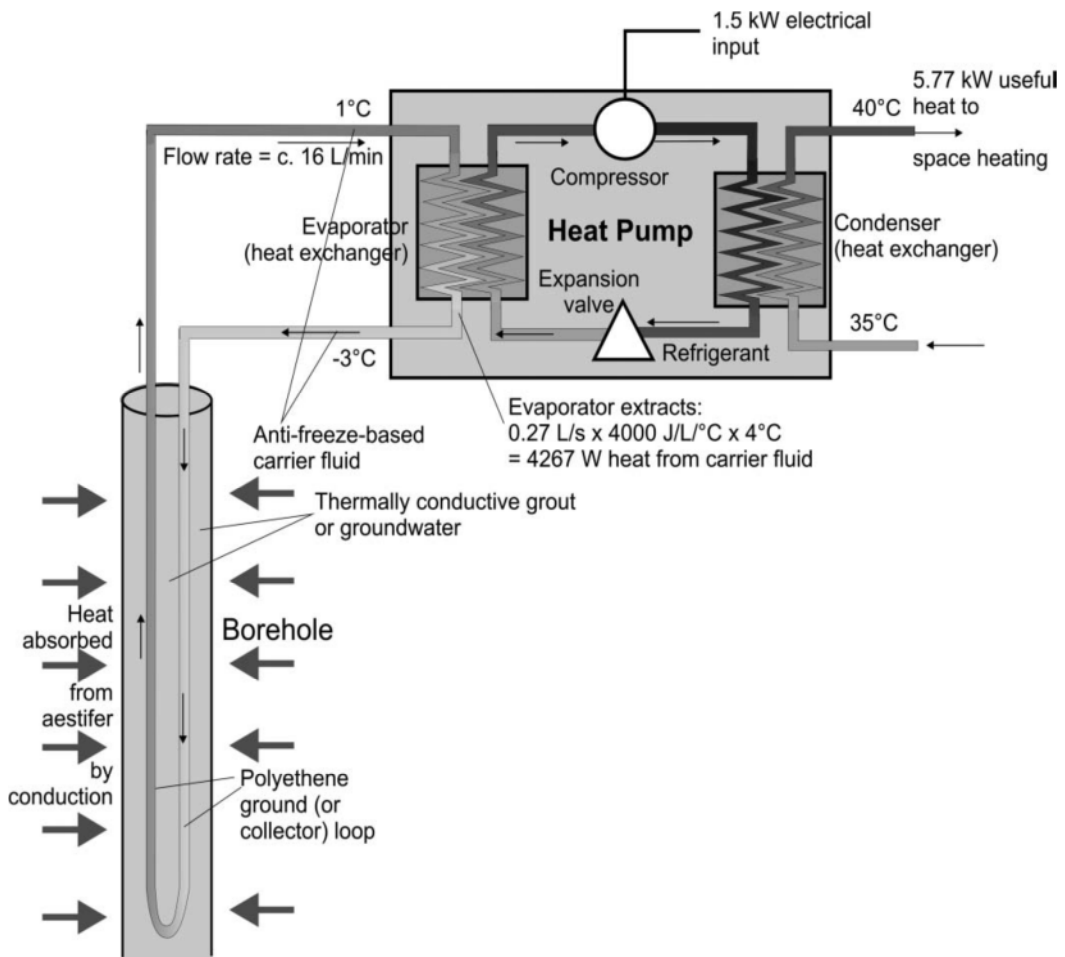


Figure 2.2: Schematic diagram of a heat pump, connected to a closed-loop borehole heat exchanger. The heat pump uses 1500 W electricity to extract 4267 W heat from the ground, yielding a grand total of 5.77 kW space heating and a COPH of 3.8 (Banks, 2008)

The coefficient of performance (COP) of a heat pump is a parameter defined (Rybach (2012) as the heat output divided by the electrical energy input for operation, both in kilowatts. A COP value of 4 means that four portions of usable energy are derived from one portion of electrical energy, and three portions of energy from the ground. A COP value of  $\geq 4$  is recommended for economic reasons (Brandl, 2006).

Heat pumps which also operate in reverse form typically gather heat from air, water or ground and concentrate it for inside use and can be grouped into three main types Air-to-air, Water source and Ground source according to the type of heat source and heat distribution medium (CIBSE, 2005).

### 2.3.2 Ground Source Heat Pumps

Ground Source Heat Pumps (GSHPs), are described by Rybach (2012) as “a decentral heating and/or cooling system that moves heat to or from the ground”, using “the Earth as a heat source (in the winter) or a heat sink (in the summer)”. These systems are also referred to as Geothermal Heat Pumps (GHPs), geo-exchange, earth-coupled, earth energy, or water-source heat pumps (HPs). GSHPs utilize renewable energy stored in the ground, through the use of pipes containing a fluid that exchanges its heat with its surroundings thus extracting and concentrating stored energy used for heating space in winter and cooling in summer (Faizal et al., 2016). They operate by simply moving heat around, and are accepted as unique technology in the heating and cooling of residential and commercial buildings (Omer, 2008).

GSHPs are composed of three basic parts, the heat storage or extraction part within the ground, the central heat pump, and the heat distributor within the building (Rybach, 2012). Figure 2.3 shows a schematic of these components.

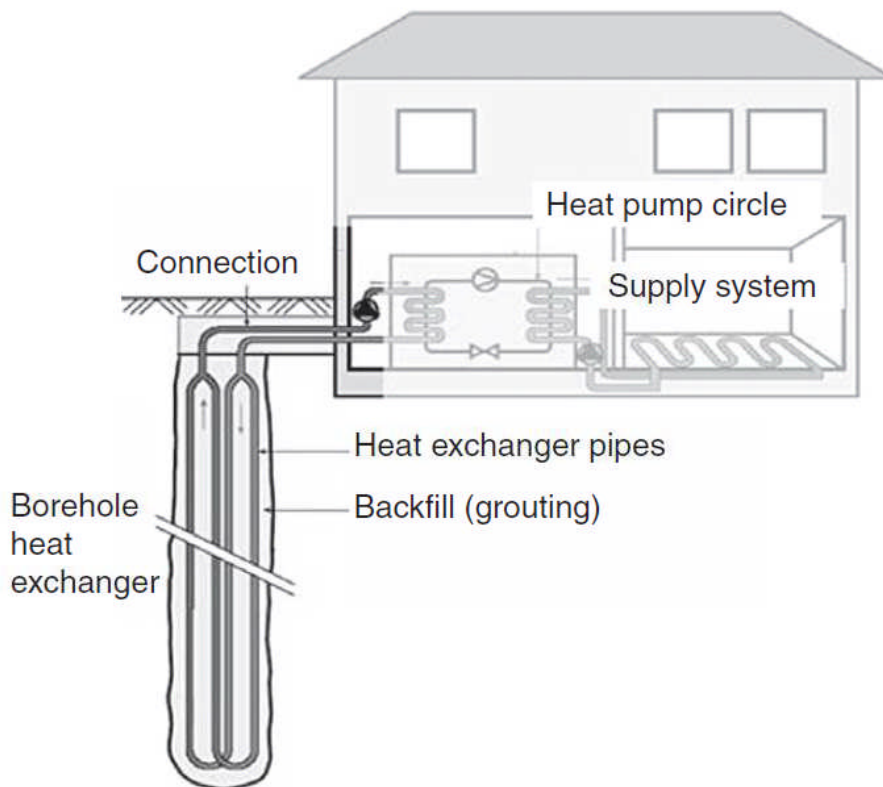


Figure 2.3: The three main components of a geothermal heat pump system (Rybach, 2012)

### 2.3.3 Types of Ground Source Heat Pumps

There are two main types of GSHPs, the ‘open loop’ and ‘closed loop’. In the open loop, water is pumped from bodies such as lakes, streams, pond and wells for heat exchange, after which it is returned to a discharge system or re-injection well. The closed loop systems involves the installation of plastic pipes, usually polyethylene,

either horizontally or vertically, through which a heat transfer fluid which could be water or an anti-freeze solution is circulated for heat exchange with the surrounding ground (Hemmingway and Long, 2012; Rybach, 2012). An energy pile is an example of the closed loop system.

Advantages of this technology as identified by (Laloui et al., 2006; Omer, 2008; Abuel-Naga, H. et al., 2015a) include:

- i. Clean and reliable energy source
- ii. Energy efficient with a Coefficient of Performance (COP), which is the ratio of heat output to electrical power consumption; of four versus a typical electric heater with COP of one
- iii. Environmentally friendly by reducing Green House Gas emissions by up to 66% compared with systems based on fossil fuels
- iv. Not being restricted to specific geologic regions
- v. Cost effective in the long term even though they cost more to install than conventional systems
- vi. Require electricity to power pump, but will typically deliver three to four times as much electrical energy as used
- vii. Are expected to perform reliably in excess of 20 years

The steady growth witnessed in the use of geothermal/ground source heat pump technology for heating and cooling of buildings, expressed through the increasing number of installations in the last 15 years, especially in countries like the United States, Denmark, and Sweden, clearly shows the prospective future of this technology (Blum et al., 2010).

## **2.4 Soil Heat Transfer and its Applications in GSHPs**

Heat transfer is simply defined as “thermal energy in transit due to a temperature difference” (Banks, 2008). Heat moves from a higher temperature region to a lower one and normally occurs via three mechanisms namely: Conduction, Convection and Radiation. Properties that affect heat transfer mechanisms in soils include water content, porosity or density, mineral content and temperature (Gabrielsson et al., 2000). Heat transfer in the ground predominantly takes place through conduction particularly in clays where convection can hardly take place due to its low permeability (Thomas and Rees, 2009). This research however, focuses on how the conductive properties of the ground affect heat flowing from a line source (a simulated energy pile) and how it is affected by cyclic thermal loading and other parameters.



### **2.4.1 Conduction**

Conduction describes energy transfer across a medium from its more energetic particles to the less energetic ones resulting from interactions between the particles (Çengel, 2005). According to Clarke et al. (2008), conduction occurs in all soils and depends on the thermal conductivity and specific heat capacity of the soil.

Glassley (2015), states that conduction takes place through the transfer of energy between atoms of a material leading to a change in their vibrational frequency, the rate which depends on the thermal conductivity and diffusivity of the material. Thus heat flow through a material depends on thermal conductivity and temperature gradient over a specified distance and can be expressed by Fourier's Law of heat conduction.

Since heat transfer through conduction requires a medium, it is the most dominant form of heat transfer in soils, although in some cases heat transfer by convection may take place.

### **2.4.2 Convection**

Convection describes the heat transfer between a solid surface and adjacent liquid or gas in motion thus involving a combination of conduction and fluid motion effects (Çengel, 2005). Convection may occur only in granular soils where hydraulic conductivity is significant enough to allow flow of water through the soil (Clarke et al., 2008).

Therefore where there is no bulk fluid motion, heat transfer takes place by conduction.

### **2.4.3 Radiation**

Radiation describes the energy emitted in form of electromagnetic waves resulting from changes in the electronic arrangements of the atoms that make up the matter, and does not require a medium (Çengel, 2005). According to Rees, S.W. et al. (2000), heat transfer in soil through radiation is negligible.

In conclusion therefore, conduction is the most important means of heat transfer in soils.

## **2.5 Thermal Characteristics of Soils**

Thermal or thermo-physical properties of soils are critical to heat transfer in soils and help to determine the soil's ability to perform effectively as a heat source or heat sink. For the purpose of this research, they include thermal conductivity, specific or volumetric heat capacity and thermal diffusivity. Knowledge of these properties in a particular site will aid in the design of a suitable and efficient GSHP for that site.

The thermal properties of the ground that determine rate at which heat is transferred from the ground to the heat exchanger are the thermal conductivity and thermal diffusivity (Busby, J. et al., 2009).

### 2.5.1 Thermal Conductivity

Thermal conductivity is defined by Rees, S.W. et al. (2000) as “the constant of proportionality that relates the rate at which heat is transferred by conduction to the temperature gradient in a material”. It is measured in Watts per metre Kelvin (W/m.K). This property determines how fast or slowly a material gains and loses heat or its ability to transfer heat by conduction (Banks, 2008). Thermal conductivity is also described by Busby, J. et al. (2009) as “the capacity of a material to conduct or transmit heat”. Thermal properties of soils are a function of soil water content, the degree of saturation determines the soil thermal conductivity (Thomas and Rees, 2009).

Thermal conductivity is critical to the successful performance of GSHPs as it determines how quickly heat exchange takes place between the heat transfer fluid in the pipes, and the surrounding soil, and also helps to determine the number of installations required to meet energy requirements of buildings (Suryatriyastuti et al., 2012).

### 2.5.2 Specific/Volumetric Heat Capacity

Specific or volumetric heat capacity is described by Banks (2008) as a material’s ability to store thermal energy or heat; that is the amount of heat locked up in the material for every degree Kelvin of temperature, and measured in Joules per Kelvin per kilogram. It can also be directly defined as “the amount of energy stored in a material per unit mass per unit change in temperature” (Rees, S.W. et al., 2000). This property will greatly determine the ability of the ground, based on its constituent minerals and properties to perform as a heat source or heat sink.

### 2.5.3 Thermal Diffusivity

Thermal diffusivity is the ratio of thermal conductivity to the heat capacity which is a measure of the ability of a material to conduct thermal energy relative to its ability to store it (Incropera, 2007a).

Busby, J. et al. (2009) describes thermal diffusivity as “the rate at which heat is conducted through a medium”, and relates thermal diffusivity to thermal conductivity, heat capacity and density via the equation:

$$\alpha = \lambda / C_p \rho \quad (2.1)$$

where:  $\alpha$  is thermal diffusivity ( $m^2/s$ ),  $\lambda$  is thermal conductivity (W/m.K),  $C_p$  is specific heat capacity (J/kg.K) and  $\rho$  is density ( $kg/m^3$ ).

Thermal diffusivity according to (Glassley, 2015), “provides a quantitative measure for evaluating how quickly a material will change temperature in comparison with its volumetric heat capacity”. “Materials with a high thermal diffusivity will quickly change temperature”. Both thermal conductivity and thermal diffusivity, according to Shiozawa and Campbell (1990) and Mitchell and Soga (2005) “depend on soil composition, bulk density, particle shape, and especially water content.

Table 2.1 presents a summary of thermal conductivity and specific heat capacity values of various soils.

Table 2.1: Summary of values of thermal conductivity and specific heat capacity of various soils (Clarke et al., 2008)

Soil type	Water content:%	Bulk density: Mg/m <sup>3</sup>	Dry density: Mg/m <sup>3</sup>	Thermal conductivity: W/m K	Specific heat capacity: J/kg K
BH C13 88	21.3	1920	1583	2.89	1520
Kaolin (sat.)	46.2	1730	1183	1.52	2362
Kaolin (dry)	0	1390	1390	0.25	800
Sandy CLAY	26.5	1890	1494	1.61	1696
Sandy CLAY	19.5	2100	1757	2.45	1459
Soft dark grey sandy gravelly CLAY	28.5	1912	1488	3.57	1764
Soft grey fine sandy CLAY	54.6	1650	1067	4.20	2646
Soft grey fine sandy CLAY	41.4	1741	1231	3.03	2200
Stiff dark grey sandy gravelly CLAY	10.1	2299	2088	3.69	1141
Stiff dark grey sandy gravelly CLAY	9.6	2369	2161	3.28	1125
Stiff grey-brown sandy gravelly CLAY	9	2352	2158	3.20	1104
Very soft grey fine sandy CLAY	46.2	1711	1170	3.51	2362
Grey slightly silty sandy GRAVEL	11.1	1983	1785	4.44	1175
Grout	166	1250	470	0.64	6412
Grout	199	1240	415	0.71	7528
Grey limestone (very hard)	0.4	2681	2670	2.30	814
Grey limestone (very hard)	0.1	2690	2687	2.54	803
Coarse SAND (dry)	0	1800	1800	0.25	800
Coarse SAND (sat.)	20.2	2080	1730	3.72	1483
Dark grey clayey fine sand/silt	28	1848	1444	4.26	1747
Fine SAND (dry)	0	1600	1600	0.15	800

Soil type	Water content:%	Bulk density: Mg/m <sup>3</sup>	Dry density: Mg/m <sup>3</sup>	Thermal conductivity: W/m K	Specific heat capacity: J/kg K
Fine SAND (sat.)	24.6	2010	1613	2.75	1632
Made ground (silty gravelly sand)	13.9	2182	1916	5.03	1270
Medium SAND (dry)	0	1700	1700	0.27	800
Medium SAND (sat.)	20.2	2080	1730	3.34	1483

## 2.6 The Role of Geotechnical and Thermal Properties of Soil in the Design Considerations for Energy Geo-structures

GSHPs can be installed at virtually any location (Rybach & Sanner 2000), but the type of system (open or closed loop), the choice of ground collector loop (horizontal or vertical) and the size of the loop all depend on local geological conditions (HEEBPP 2003; Sanner et al. 2003; Ondreka et al. 2007). Factors which affect the performance of the ground element of a GSHP system which are considered during their design and installation have been identified by Busby, J. et al. (2009) to include the temperature of the ground, thermal properties of the soil, groundwater levels and the ground conditions such as the geology/engineering geology aspects such as the rock strength, depth and thickness of deposits.

According to Loveridge et al. (2017), the design of energy geo-structures focuses on two main objectives. The first requires working out the energy output of the geo-structure within realistic temperature limits of the soil and heat pump, and relies on the thermal properties of the soil and concrete. The second objective is to ensure that geotechnical limit of the geo-structure is not exceeded due to temperature changes, and relies on its geotechnical properties and their thermal behaviour. Thus, the thermal and geotechnical properties of both the soil and concrete material of the heat pump are very important in the design considerations of an energy pile. Table 2.2 gives a summary of the key design parameters and their justifications.

Table 2.2: Summary of key parameters required for the design of energy geo-structures (Loveridge et al., 2017)

Design parameter	Required for	Comments
Soil thermal conductivity	Energy output	An average value is used in most design approaches, although real conditions are likely to be anisotropic and heterogeneous
Soil specific heat capacity	Energy output	
Undisturbed soil temperature	Energy output	Average value, or preferably a profile with depth
Groundwater flow rate (Darcy velocity)	Energy output	As a minimum, an indication is required of whether significant groundwater flow is to be expected at the site

Design parameter	Required for	Comments
Soil strength	Geotechnical design	In total or effective stress terms as appropriate; should include an estimate of whether likely to be significantly temperature dependent
Soil stiffness	Geotechnical design	For serviceability considerations
In situ stresses ( $K_0$ ) and pore water regime	Geotechnical design	'Apparent' pre-consolidation pressure can be affected by temperature
Stress history	Geotechnical design	
Over-consolidation ratio (OCR)	Geotechnical design	Determines the nature of the thermo-elastic (or thermo-plastic) response
Concrete thermal conductivity	Energy output	Often included within the thermal resistance parameter
Concrete specific heat	Energy output	For storage of heat within the concrete
Thermal resistance of heat exchanger	Energy output	A lumped parameter that includes the thermal properties and geometry of the heat exchanger
Concrete coefficient of thermal expansion	Geotechnical design	To determine the potential expansion of the geo-structure
Soil coefficient of thermal expansion	Geotechnical design	Expansion of soil relative to concrete may be important for soil structure interactions
Concrete limiting stress	Structural design	Additional stresses may develop owing to restraint of the geo-structure as it tries to expand on heating

## 2.7 The Determination of the Thermal Properties of Soil

In the wake of the EESs and their efficiency which largely depends on soil thermal properties, various tests have been developed to measure these properties. When the results of soil thermal tests from a particular site are incorporated into the design of a thermal pile along with other considerations such as thermal demands of a building, a more efficient system is produced.

Tests involving the measurement of soil thermal properties using different techniques and for various purposes have been going on for many years, the most common being in agriculture and climate change (International Workshop on Effects of Expected Climate Change on Soil Processes in the and Sub, 1990), nuclear waste disposal (Cui et al., 2009; Tang et al., 2008; Britto et al., 1989), pipeline laying, energy piles (Wood et al., 2009), energy geo-structures (Laloui and Di Donna, 2011), and high voltage cables (Di Donna and Laloui, 2015).

Test methods used for measuring soil thermal properties include the thermal response test which is carried out in-situ by introducing a defined heat load in a borehole heat exchanger and then measuring the resulting temperature changes in the circulating fluids (Sanner et al., 2003). Single and dual probe tests (Liu and Si, 2011), multi-needle probe thermal tests (Bristow et al., 2001). In addition to these, various studies carried out in a bid to better understand heat transfer mechanisms include in-situ tests

(Thomas and Rees, 2009; Wood et al., 2009; Bourne-Webb et al., 2009), numerical modelling (Brandl, 2006; Li et al., 2009; Rees, S.J., 2015; Fan et al., 2013), and laboratory tests (Burghignoli et al., 2000; Abuel-Naga, H.M. et al., 2007; Clarke et al., 2008; Kalantidou et al., 2012).

According to Loveridge et al. (2017), the determination of soil thermal properties can either be carried out through thermal steady state using Fourier's Law, or through transient temperature changes using diffusion equation. The measurement or determination of thermal conductivity values of soil samples in situ or in the laboratory according to Shiozawa and Campbell (1990) is either carried out under steady heat flow or unsteady or transient heat flow.

The method commonly involves the use of a heat probe containing an electrical heater and thermocouple by generating heat using a constant current through a heating wire, and determining the thermal conductivity by measuring the probe temperature change during the heating or consequent cooling phase. This method according to Shiozawa and Campbell (1990), was described by De Vries (1952) and Jackson and Taylor (1986) and is based on "a solution of the general heat conduction equation for a constant line heat source applied in a homogeneous isotropic medium of initially uniform temperature", and has acceptable accuracy where properly applied.

A theoretical method to calculate thermal conductivity from volume fraction and conductivities of solid, liquid and air phases was given by De Vries (1963), (Shiozawa and Campbell, 1990).

Clarke et al. (2008), describe the techniques used in measuring thermal conductivity as mostly comparative methods where a material of known conductivity is compared with that of the material being tested. They describe a laboratory method of directly determining thermal properties of samples obtained from site investigations. The test involves heating a cylindrical specimen from both ends to allow for axial heat flow, while measuring the temperature changes within the sample.

The needle probe method of determining soil thermal properties using transient heat flow involves inserting in a sample, a needle which contains a heating element and sensors, and then measuring temperature changes which are analysed using a line source approach. Another approach which is similar is to use the dual probe method which has a second monitoring point, with the added advantage of being able to determine thermal diffusivity and specific heat capacity from the measured temperature changes (Loveridge et al., 2017).

### **2.7.1 In-situ Thermal Response Testing**

Thermal response test (TRT) is a method used to determine the in situ ground thermal properties to aid the design of GSHP, and according to Sanner et al. (2003), is

achieved by putting a defined load into the borehole heat exchanger, and measuring the resulting temperature changes in the fluid circulated. According to Rybach (2012), “a standard TRT circulates a heated fluid in a test BHE and yields average values of thermal conductivity, thermal borehole resistance, and ground temperature over the BHE, by using a linear heat source model”.

The accurate determination of these thermal properties at any site is fundamental to appropriate design, costing and installation of a successful GSHP system, and prevents the use of estimated or generic values for key thermal properties (Hemmingway and Long, 2012).

Figure 2.4 shows a schematic diagram of a TRT.

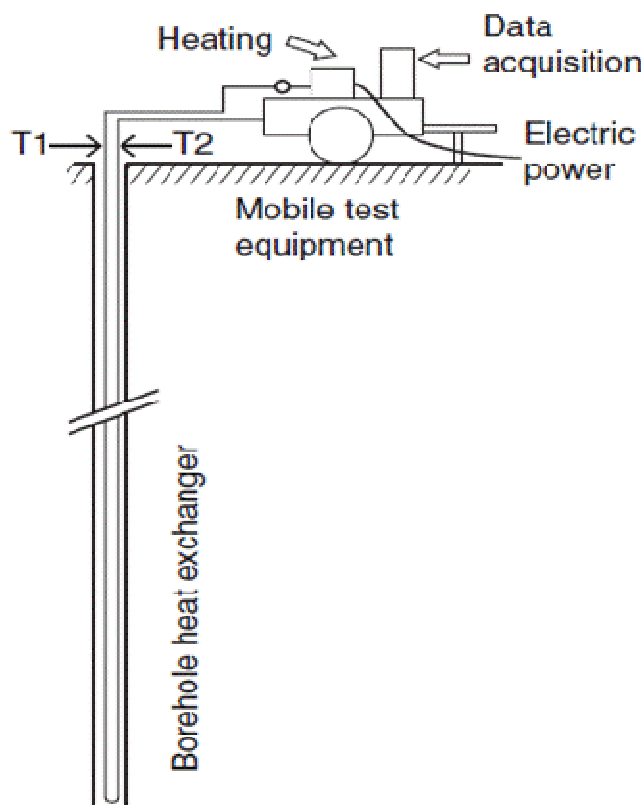


Figure 2.4: Schematic of a thermal response test, where T1 is the fluid input temperature and T2, the fluid output temperature. After (Rybach, 2012)

According to Sanner et al. (2008), although TRT also called Geothermal Response Test (GeRT) is open to possible sources of errors that are grouped as either under underground influence (usually from groundwater flow), or thermal influence, it is still a reliable method of determining actual site thermal properties for the correct designing of Borehole Heat Exchangers (BHEs) as opposed to use estimated or generic values for the design.

## 2.7.2 Dynamic Response Models and the Role of Thermal Diffusivity

Thermal diffusivity reflects the soil's ability to transfer heat and change temperature in response to heat supply or removal (Arkhangelskaya and Lukyashchenko, 2018) and is normally calculated directly from soil temperature distribution at depth and the thermal conductivity estimated from it after taking the soil parameters into consideration (Busby, Jon, 2016). The thermal diffusivity and conductivity are critical to the success of a GSHP performance, because whether functioning as a heat source or sink, the temperature distribution in the surrounding material according to Westaway (2016), "depends on its thermal diffusivity, whereas heat transfer also depends on its thermal conductivity". Apparent thermal diffusivity can be calculated from soil temperature data using a technique which according to (Busby, Jon, 2016), is based on "the decrease in amplitude and delay in temperature change (phase shift) with depth of a transmitted heat signal applied to the ground surface, the magnitudes of which are determined by thermal diffusivity".

To incorporate these thermal properties adequately into a high performance design with minimal installation costs, numerical/dynamic models are important as they give the advantage of simulating all possible aspects and parameters required to create a reliable and efficient system.

According to Zhang et al. (2018), the short-term ground temperature response is useful for determining energy consumption of a heat pump system for efficient operation, and thus requires the use of transient heat transfer. They also identify time scales, varying loads and thermal interactions between multiple boreholes, as major challenges to the optimal design of BHEs, thus justifying the need to develop accurate and efficient BHE models through the application of computational methods for ground dynamic thermal response.

One of the models in use is the Ground Loop Design program, which according to Mensah et al. (2017) "is composed of a building load, borehole design, and heat pump modules that enable the designer to perform a complete design of the ground loop heat exchanger".

In numerical modelling, Spitler et al. (2005) contribute that a design methodology should be able to adequately size the ground heat exchangers "with minimal user input and computational time", and also "have a simulation model that can predict hour-by-hour (or shorter time interval) responses of the ground loop heat exchanger to continuously changing building loads, as this approach allows the prediction of system energy consumption and electrical demand". A methodology which aids the temperature change around a borehole to be estimated was developed by Eskilson in 1987 using the g-function which according to Spitler et al. (2005) "allows the



calculation of the temperature change at the borehole wall in response to a step heat input for a time step”, and “the response to any arbitrary heat rejection/extraction profile can be determined by devolving the heat rejection/extraction profile into a series of step heat pulses, and superimposing the response to each step heat pulse”.

Another approach is the use of Dynamic Thermal Networks (DTN) which allows the simulation of complex three dimensional geometries required to solve building heat transfer problems. According to Fan et al. (2013) in the DTN approach “the time-dependent thermal processes are represented as a network to describe the relationship between boundary temperatures and heat fluxes”, and the “network includes a combination of admittive and transmittive heat paths and time-varying conductances that are characterized by a series of response factors”.

The development and use of thermal dynamic models contribute greatly to the development of optimal designs and realistic pricing of earth energy systems.

## 2.8 Energy Piles

Energy piles, also known as thermo-active piles, are pile foundations incorporated with heat exchangers to heat or cool buildings by taking advantage of the constant ground temperature to use it as a heat source/sink (Abdelaziz and Ozudogru, 2016). According to Loveridge and Powrie (2012), energy or thermal piles are “a specialist type of closed-loop ground energy system in which small diameter pipes are cast into the piled foundations of a building to allow circulation of a heat transfer fluid”. In further detail, Laloui and Di Donna (2011) describe energy piles as “a system of pipes installed within concrete structures, with a heat carrier fluid that circulates through it, can extract heat from the ground that is sufficient to satisfy the need for heat during the winter and can expel excess heat during the summer”, illustrated in figure 2.5.

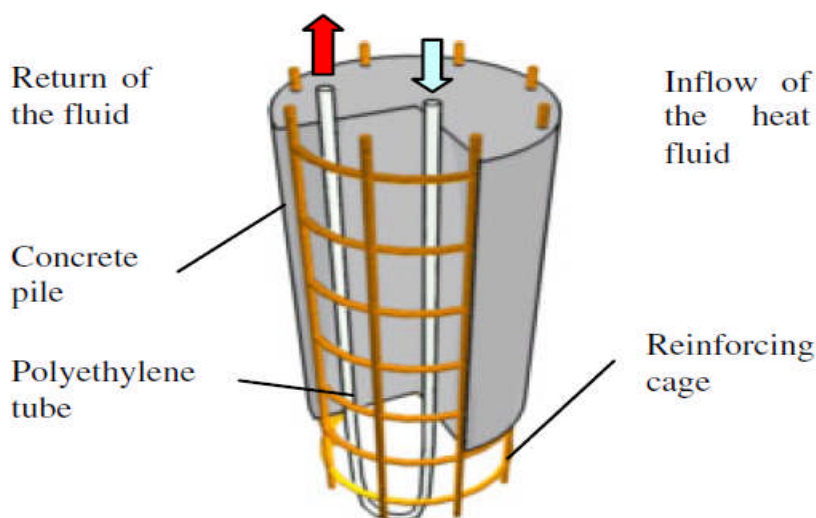


Figure 2.5: Typical energy pile arrangement after (Laloui et al., 2006)

Within the energy piles, the circulating heat carries fluids in a system of absorber pipes installed within their concrete structures, taking advantage of the relatively constant ground temperature at depths to provide heating in winter and cooling in summer by exchanging heat with the surrounding soil (Laloui and Di Donna, 2011). Figure 2.6 shows an illustration of energy piles installed in a small building.

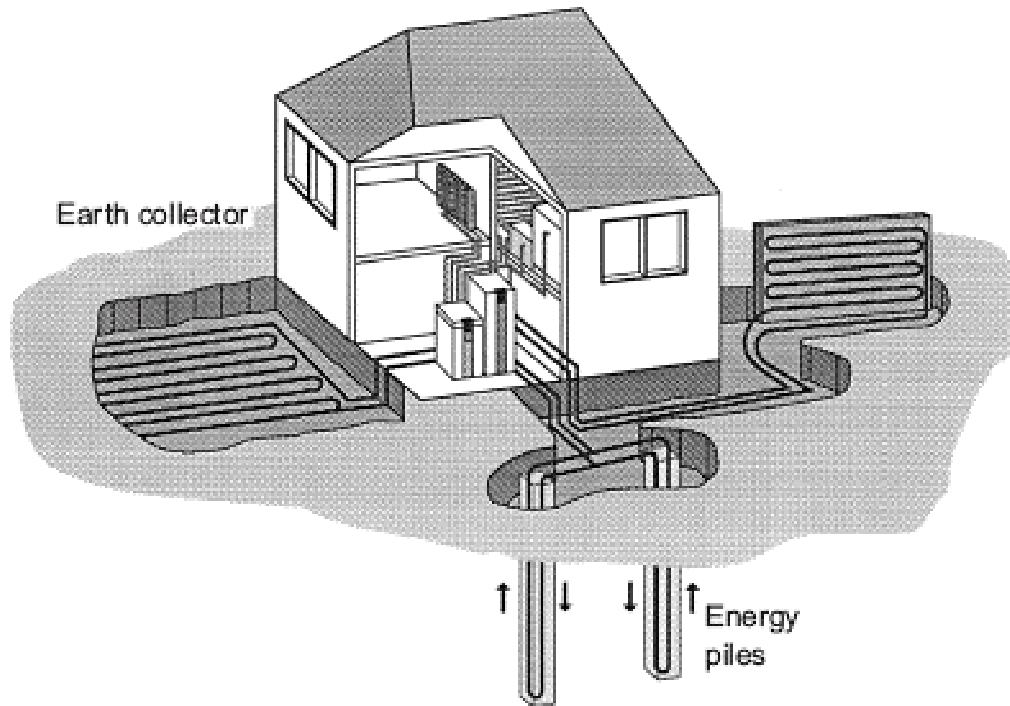


Figure 2.6: Heating/cooling a small house with energy foundations (Brandl, 2006)

Brandl (2006), considers energy piles to operate with higher heat transfer compared to the normal borehole heat exchangers owing to concrete having higher thermal conductivity than soil. An added advantage is the fact that there is no need for separate construction as the pile system is primarily required for structural reasons.

Growth has been recorded in the use of energy piles in the United Kingdom, also corresponding with carbon dioxide savings, which according to Laloui et al. (2006) can significantly reduce carbon dioxide emissions of buildings.

The acceptance of this technology and expected increase in installations requires a better understanding of how energy piles function.

### 2.8.1 Uses of Energy Piles

The use of energy foundations have been suggested to save up to two-thirds of the cost of conventional heating while also providing clean renewable energy (Brandl, 2006).

The key advantages associated with the use of GSHPs technology include a reduced dependence on fossil fuels for heating and cooling of buildings resulting in a significant reduction of CO<sub>2</sub> emissions of buildings. These advantages have resulted in a recorded increase in the popularity and use of GSHPs technology in the United Kingdom and other parts of Europe as shown in Figure 2.7.

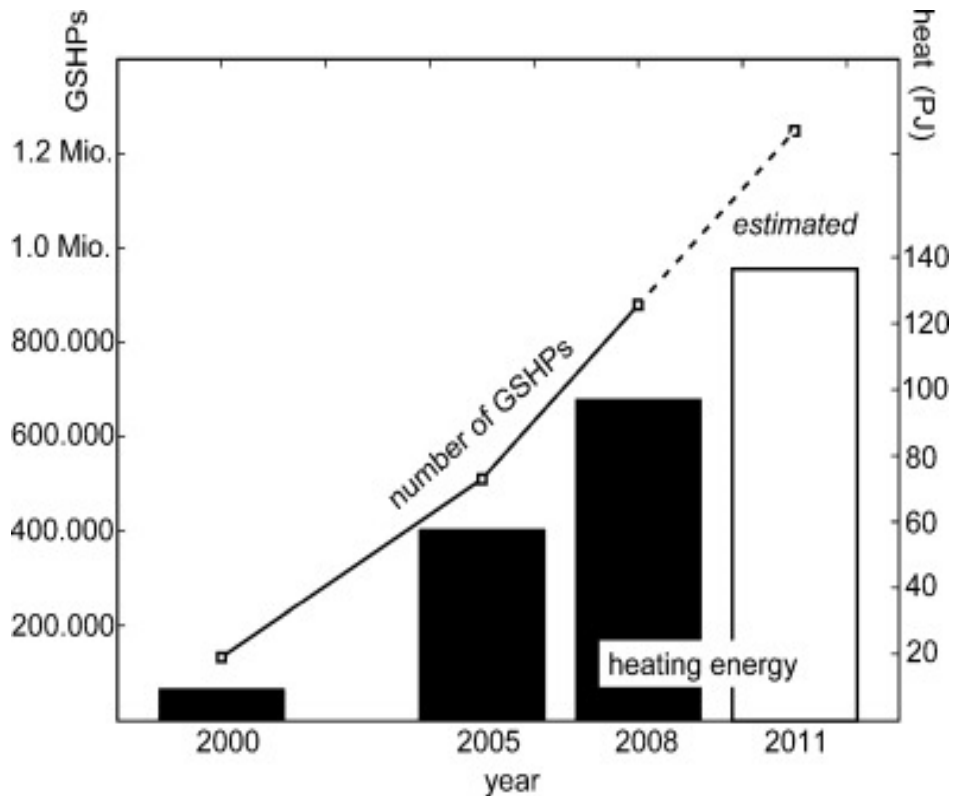


Figure 2.7: Number of installed GSHP units and energy provided for space heating in some European countries from 2000-2011 after (Bayer et al., 2012)

### 2.8.2 Energy Pile Design

The heat from energy piles is transferred into the ground mainly by conduction, therefore, the design of an energy pile takes advantage of the thermal properties of concrete which makes it suitable for use as a heat exchanger medium due to its high thermal conductivity compared with soil. Pipes made of high-density polyethylene plastic 20-25mm diameter, with wall thicknesses of 2.0-2.3mm through which a heat carrier fluid is circulated, are installed in the concrete. The pipes are placed to form coils or loops, and the heat transfer could be water, water mixed with antifreeze, or a saline solution (Brandl, 2006). Figure 2.8 shows pipes fitted to the reinforcement cage of a bored energy pile.

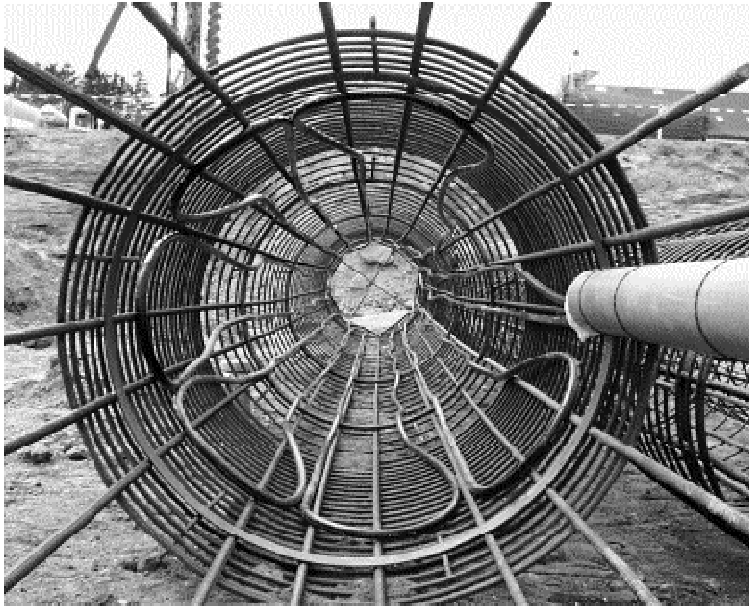


Figure 2.8: Absorber pipes fitted to the reinforcement cage of bored energy pile (Brandl, 2006)

According to Brandl (2006), it is more common to have the plastic piping fixed to the reinforcement cages of energy piles on site, even though it can also be fixed in the plant. During the pipe installation, the fluid inflow and outflow ends of the pipes are fixed with a locking valve and a manometer which allows for the pipe circuit to be pressurized to about 8 bar for both integrity check and to prevent the collapse of the wet concrete head during the installation process.

In rotary bored piles, the pipes are usually fixed to the pile cage, while in continuous flight auger (CFA) piles the pipe loops are plunged into the concrete centre as shown in Figure 2.9 (Loveridge and Powrie, 2012).

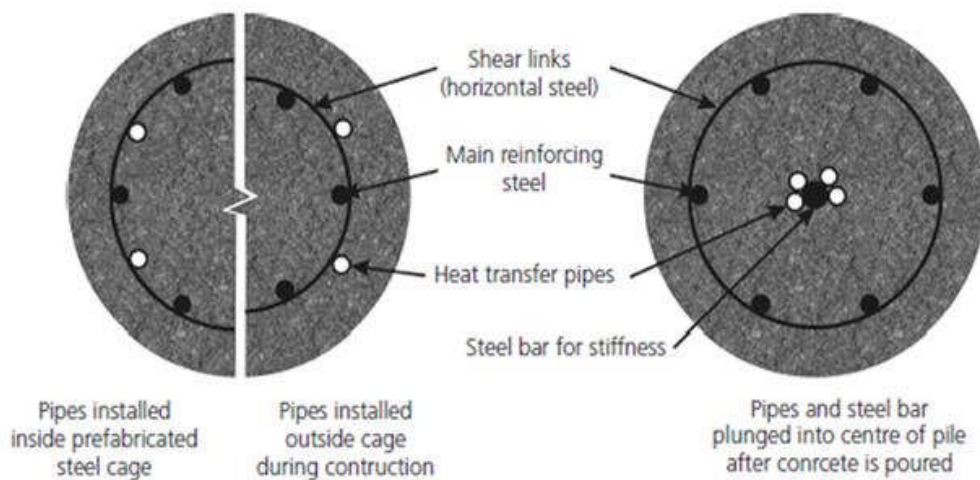


Figure 2.9: Typical thermal pile construction details (Loveridge and Powrie, 2012)

Brandl (2006) argues that the process of plunging the pipes into the wet concrete in the continuous flight auger may affect the final integrity of the absorber pipes and recommends the rotary bored technique for energy piles.

The heating and cooling process of a building using an energy pile, according to (Faizal et al., 2016), will require both a primary circuit within the foundation, and a secondary circuit installed in the building. The primary circuit of an energy pile consists of closed pipework through which a pumped heat-carrier fluid, usually glycol-water mixture found to prevent corrosion over time, exchanges energy with the ground. The secondary circuit on the other hand consists of pipework embedded in the floor and walls of the structure. A heat pump connected to both the primary and secondary circuits, typically raises the original temperature by up to 15-20°C to a higher usable temperature in the case of heating (Brandl, 2006). Figure 2.10 shows the layout of absorber pipes being installed in the concrete slab in the first floor of a building.



Figure 2.10 : Absorber pipes entering a concrete slab (Brandl, 2006)

### **2.8.3 Coupling of Mechanical and Thermal Properties**

Energy piles are required for both structural support and to meet the heating/cooling needs of buildings. However, temperature changes within the pile may induce stresses and strains capable of affecting the soil properties with respect to its bearing capacity that could eventually pose challenges to the structural integrity of the pile. Changes in temperature within saturated soils normally lead to resultant changes in effective stress and volume. As observed in clay, an increase in temperature will normally lead to pore pressure build up, and how fast or slowly it dissipates is a function of the soil's hydraulic conductivity. Temperature increase in soils could also lead to a reduction of shearing resistance leading to soil structure collapse and reduced void ratio. A

reduction in pore pressure on the other hand could result in soil structure being strengthened (Mitchell and Soga, 2005; Vieira et al., 2017).

Thus an understanding of the thermo-mechanical behaviour key to the long-term success of energy geo-structures and to achieve this, Laloui and Di Donna (2011), suggest the “couplings between the mechanical properties of the soil-foundation system, the temperature and the ground pore water, as well as the non-linear properties of the soil energy-storage system” to be given adequate consideration during its design Figure 2.11 shows mechanical and thermal stresses acting on an energy pile.

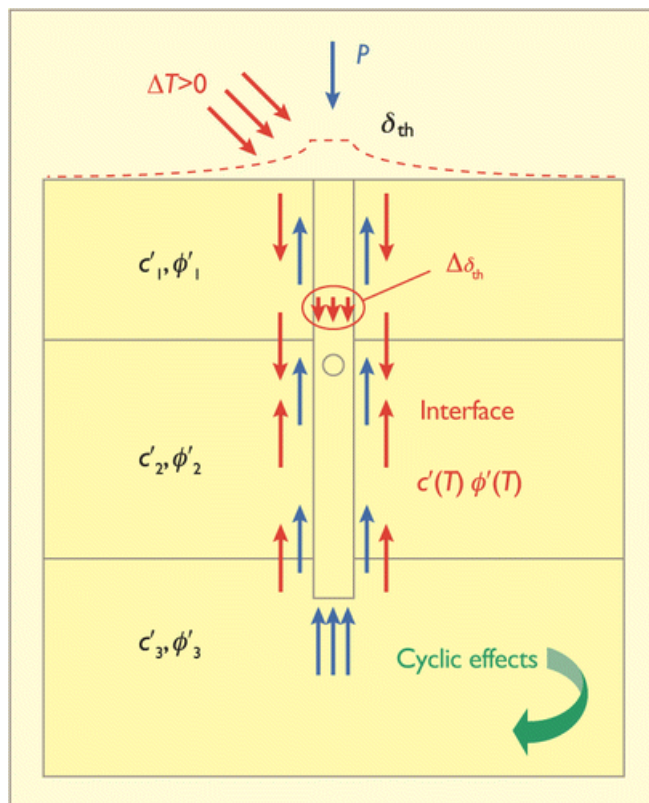


Figure 2.11: Thermal effects on an energy pile ( $\Delta T$ , temperature variation;  $P$ , mechanical load;  $\delta_{th}$ , pile displacement induced by temperature variation;  $\Delta \sigma_{th}$ , thermally induced stress;  $c'$ , cohesion; and  $\phi'$ , friction angle of the soil) Laloui and Di Donna (2011)

Models based on numerical analyses have been developed, capable of predicting the thermos-mechanical behaviour of energy geo-structures to better account for them in their design (Laloui and Di Donna, 2011; Suryatriyastuti et al., 2012; Bourne-Webb et al., 2009; Bourne-Webb et al., 2016)

## 2.9 Gaps in Knowledge

With the increased use of GSHPs technology, some concerns are also being raised about their reliability, efficiency and safety as identified from literature in terms of design, stability and long term performance.

While there are advantages associated with this technology, a major weakness identified from work done by (Rees, S.W. et al., 2000; Preene and Powrie, 2009b; Abuel-Naga, H. et al., 2015a), focuses on their designs which so far utilise inadequate data input from geotechnical engineers and hydro-geologists and the use of data on the key ground parameters such as initial ground temperature, thermal conductivity, and specific heat capacity only generically and from literature rather than from site-specific field or laboratory measurements. This weakness could result in systems with low Coefficient of Performance (COP) that may fail over the long term. The problem of “paucity of data on soil thermal properties required for the sizing of horizontal collector loops that is compounded by their seasonal dependence” was emphasized by Busby, Jon (2016).

In the study carried out by Laloui et al. (2006), limited knowledge in the area of thermal effects on the structural behaviour of foundations was identified as a major obstacle in the technology's industrial growth.

From a safety perspective, Brandl (2006), points out that a pile designed conventionally for stability may not have accounted for temperature induced stresses and strains within the pile, temperature induced changes in the soil properties and at the soil-pile interface, which may reduce its safety margin.

In addition to describing a method to determine thermal properties of soil samples, Clarke et al. (2008) also highlight the need for further investigations of the thermal characteristics of soils with emphasis on saturated and partially saturated soils for direct application in the installation of near surface horizontal loops (closed system) and also to build a database of knowledge.

Preene and Powrie (2009a), identified a possible danger as that of long-term changes in ground temperature with continued use of EESs, and suggest that to combat this effect, adequate geotechnical input from the early stage will result in more reliable and efficient designs.

Yu, X. et al. (2011), report a recorded increase of 0.5°C in soil temperature after operating a GSHP for a one year period. Though seemingly small for now, this increase could become significant over long periods of continuous usage, with possible negative impacts on the ground properties. Over an annual cycle, it is ideal that the energy extracted from the ground balances the energy put back into the ground to avoid changes in the mean ground temperature over the long term (Laloui and Di Donna, 2011). With more of these systems in use, it is important that over time the net heat input balances the heat extracted (an approach based on aquifer thermal energy storage, ATES) otherwise a change in the ground temperature will occur which over the long term may have negative resultant effects on the soil properties. As a

result of these concerns, Laloui and Di Donna (2011) point out gaps in the use of energy piles as limited understanding of their thermo-mechanical behaviour and inadequate geotechnical input in their design. A similar study by Darkwa et al. (2013) evaluating the thermal performance of a cooling dominated system was borne out of the concern regarding long term performance of GSHPs where thermal imbalance in the ground is created by higher rates of heat dissipation into the ground as against extraction rates where the cooling need is predominant.

It is reported that for investigations related to thermally driven volume change in soils, more focus is being placed on heating clays to high temperatures appropriate for nuclear waste disposal as opposed to studying the effect of smaller magnitudes of heating and cooling over long periods (Loveridge and Powrie, 2012). They expressed concern about temperature changes around the soil around a pile may result in soil volume change leading to potential changes in soil properties, and also suggest further investigation of long-term cyclic changes. Saggiu and Chakraborty (2015), pointed out that the “effect of cyclic heat flow in and out of the energy piles on the load carrying capacity of these piles and the resulting changes in soil stress–strain response are not well understood”, while suggesting the “need to understand and quantify the load transfer mechanism of energy piles under long term cyclic thermomechanical loading”.

Abuel-Naga, H. et al. (2015b), suggest further research work to thoroughly investigate the temperature effects on the soil-pile interaction to aid in validating the assumptions made in the available energy pile design methods.

In summary therefore, the gaps and concerns with the use of GSHPs technology were identified as follows:

- 1) Limited understanding of thermo-mechanical behaviour of energy piles
- 2) Possible temperature induced stresses and strains within pile, temperature induced changes in the soil properties and at soil-pile interface, which may reduce its safety margin.
- 3) Inadequate geotechnical input in energy pile design
- 4) Uncertainty about the effects of long-term cyclic loading on the thermal behaviour of soils

## **2.10 Overview of Research Questions**

In light of the challenges and gaps identified with the use of the GSHP technology, further research is required in the area of soil thermal behaviour in order to generate reliable data to aid in the design of more efficient and safer GSHPs and for other similar applications.



In conclusion therefore, this research aims to address the area of inadequate geotechnical input in energy pile design with a focus on the limited understanding of factors that govern heat flow within soils around an energy pile, by investigating the thermal behaviour of the soils around a simulated energy pile in a bid to establish a relationship between soil type, water content, temperature, overburden pressure, time and thermal cycles; and the performance of energy piles.

## **Chapter 3 Experimental Methodology, Test Rig Design and Equipment**

This chapter covers the description of the experimental methodology and the processes undertaken in designing the test rig. An explanation is given on how each design parameter was chosen and the theory and assumptions behind their selection. The procedures in assembling and commissioning the test rig are also covered in this chapter.

### **3.1 Introduction**

The ground is considered as a source of renewable energy due to its capacity to store both solar energy from the surface and geothermal energy from the earth's core and also its ability to act as a thermally stable mass at depths below the zone of seasonal temperature variations. It is utilized either as a heat source or sink through the use of Earth Energy Systems (EESs) which harness and efficiently transfer energy between a building and the ground by means of circulating fluids (Banks, 2008). This technology relies on heat transfer by conduction from the surrounding soil by circulating fluids within pipes when operating as a closed loop system (CIBSE, 2005).

An investigation of the thermal behaviour of the soil around a simulated energy pile under the influence of soil type, water content, temperature, pressure, time and thermal cycles was undertaken. To achieve this, an experiment was developed which allowed a linear heat source within a soil mass to be modelled to depict a scenario typical to that of an energy pile exchanging heat with the surrounding soil while being subjected to overburden pressure as depicted by Figure 3.1 on page 38.

Heat transfer by conduction is of primary importance in saturated clays as heat transfer by convection and radiation is limited because of the low permeability of clays and the fact they are saturated (Abuel-Naga, H. et al., 2015a; Abuel-Naga, H.M. et al., 2007). Thus the concept of the laboratory study of heat dissipation in the ground is based on the application of the principles of conduction heat transfer to the study of soil thermal behaviour under specific conditions of water content, overburden pressure, time (duration), cycles, and temperature difference; all acting as variables. These parameters were identified to find out how they impact heat dissipation in soil samples, in order to simulate an efficient earth energy system.

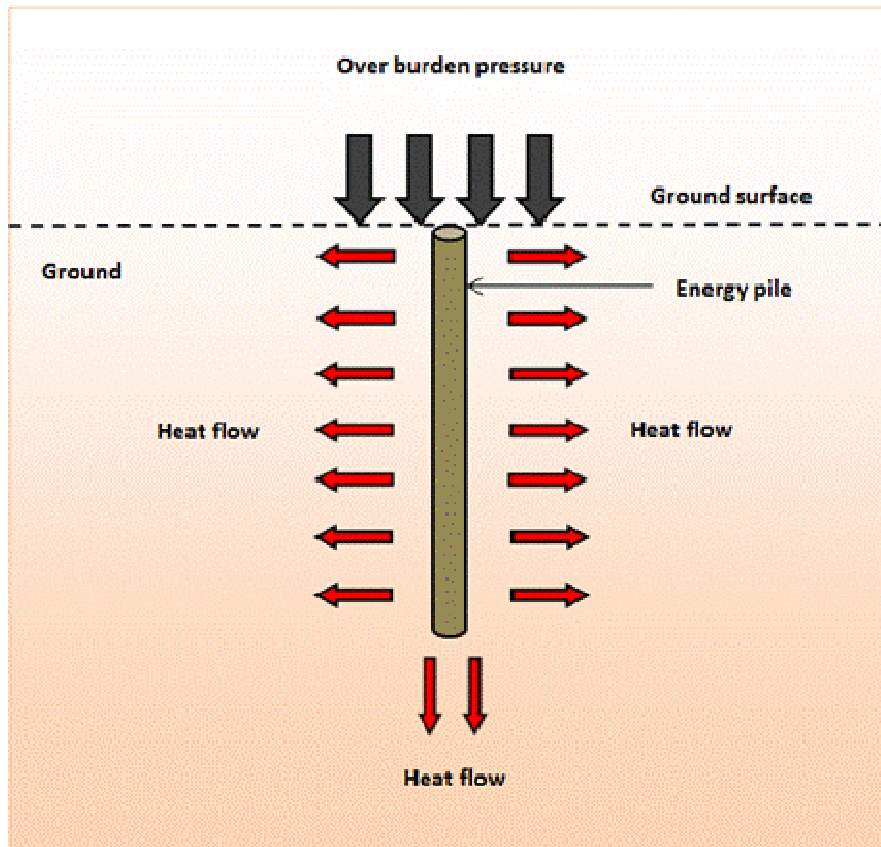


Figure 3.1: An energy pile exchanging heat with surrounding ground

The experimental model and test rig were designed to dissipate heat radially by conduction from a line source by optimising the radial distribution of temperature and the dimensions of the sample to minimise the effect of the boundary conditions (Incropera, 2007a; Mills, 1999).

### 3.1.1 Soil type

Soils are particulate materials that may contain rock (gravel and sand), clay minerals, water, air and organic matter depending on the composition. The composition and particle type of natural soils varies to the extent that there is no reference composition to determine typical soil properties. It is for this reason that soil behaviour is often studied using artificial soils (Mitchell and Soga, 2005). Three types of soils were studied – clay, sand and composite soil formed of clay and sand. The thermal properties of clay, sand, water and air are different therefore, the thermal properties of a soil will depend on the proportion of clay, sand, water and air within a sample. The heat capacity of a soil,  $C_{soil}$ , will depend on the mass specific heat,  $c$ , density,  $\rho$ , and volume,  $V$ , of its constituents:-

$$C_{soil} = (c\rho V)_{clay} + (c\rho V)_{sand} + (c\rho V)_{water} + (c\rho V)_{air} \quad (3.1)$$

Given the variation in the composition of natural soils, Equation 3.1 shows that the heat capacity of those soils will vary. Therefore, commercially available soil was used so that the composition of the samples could be controlled. Clay was represented by kaolin as it is often used to study the behaviour of fine grained soils. This was also the reason for using Leighton Buzzard sand. Composite soils were formed of mixtures of kaolin and sand in the proportions 75:25, 50:50 and 25:75.

### **3.1.2 Air and Water Content**

Equation 3.1 shows that the thermal properties of a soil will depend on the water and air content. Most natural soils in temperate climates below the level of seasonal water changes will be saturated. Therefore, saturated samples of clay and composite soils were used in these tests. In order to ensure saturation, samples were prepared as slurry and then consolidated to vary the water content. This is a further advantage of using commercially available soils as they are supplied dry.

It is more difficult to vary the water content of sand by consolidation. The density of sand can be varied by the method of preparing the sample. Loose sand is deposited rapidly with no further treatment; dense sand can be compacted or vibrated into place or deposited slowly allowing the grains to take up a dense configuration. In both cases, the sand was saturated by inundation.

### **3.1.3 Time to Equilibrium**

The thermal characteristics of soils can be assessed from either transient conditions as the soil is heated or cooled or steady state conditions. It was necessary to establish the time to steady state conditions in order to determine the soil thermal characteristics and assess whether steady state conditions are achieved in a typical daily thermal cycle. The time it took each sample type to attain the equilibrium conditions and to cool back to its initial temperature was studied to determine the time to equilibrium for heating and cooling for different soil compositions.

### **3.1.4 Temperature**

The sample temperature was controlled by the current and voltage (power) input to the test. Tests were carried out between 30°C and 40°C typical of site installations (Brandl, 2006), to study the influence temperature on heat dissipation in the soil samples being tested and to determine the effect of the thermal capacity of the ground on the performance of the energy pile.

### **3.1.5 Pressure Applied**

The test rig was built to allow for pressure to be applied to the top of a sample to simulate overburden pressure and vary the water content. Tests were carried out

within controlled ranges of overburden pressure from 0kPa to 200kPa to simulate depths from 0m to 40m below the ground surface in saturated soils. This means that the sample represented an element of soil within the depth of the energy pile.

### 3.1.6 Heating and Cooling Cycles

Samples were subjected to heating and cooling cycles to reflect heating load from a building. The cycles were based on 24 hours period consisting of 8 hours heating and 16 hours cooling simulating a typical office during its working day generating heat. Other heating and cooling cycle test durations within the 24 hour period were also carried out to study the thermal behaviour of the different soil composition under different thermal loads.

### 3.1.7 Design Concept

A linear heat source placed centrally in a cylindrical container filled with soil was used to represent the energy pile in the ground (Figure 3.2) and by insulating the top and bottom of the sample it is possible to simulate radial heat flow. The overburden pressure was simulated by applying a load to the surface of the soil sample which was insulated at the top and bottom. Drainage was permitted from the base of the sample.

The variation in temperature across a sample was monitored using thermal probes installed through glands in the wall of the cell.

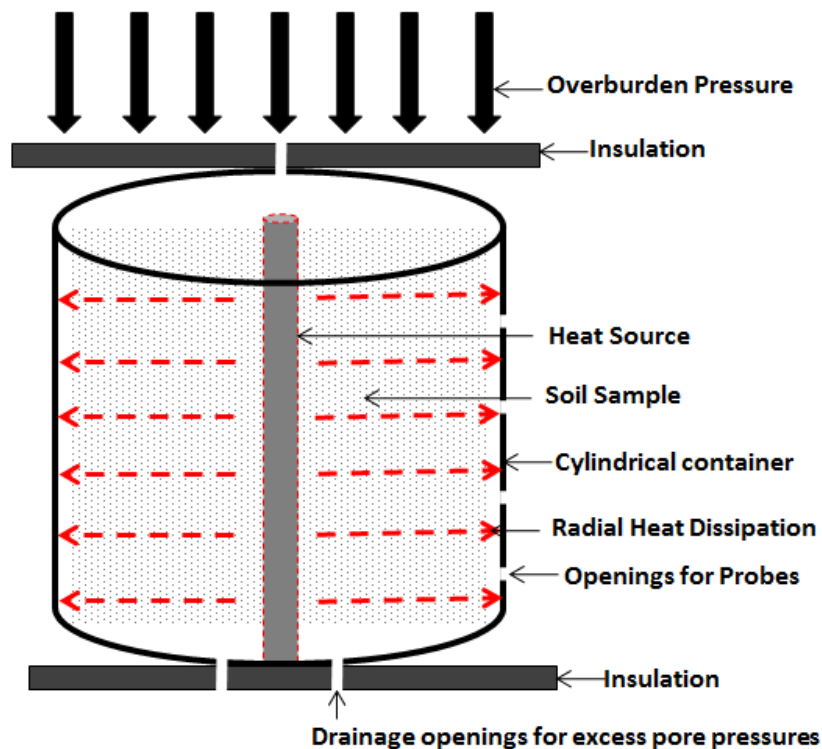


Figure 3.2: Concept of Rig Design

The variables during a test were:-

1. The soil composition
2. The overburden pressure (and hence the water content)
3. The temperature of the heat source
4. The time to apply the thermal load including the time to steady state (for heating and cooling) and the different loading cycles

Measurements taken during a test were:-

1. The vertical and radial temperature profiles
2. The final vertical and radial water content and soil strength

The emphasis of the tests was on the measurement of the following:

- 1) The time it takes a soil sample in the test rig to achieve steady state conditions when a constant heat source is applied from a central linear source, and the time it takes to cool back to its initial temperature. Steady state refers to temperatures that are constant with time; inferring that heat flow is also constant with time (Mills, 1999). The steady state condition in the sample was determined through the use of temperature probes to monitor its temperature changes. Thermal conductivity is defined by Rees, S.W. et al. (2000) as “the constant of proportionality that relates the rate at which heat is transferred by conduction to the temperature gradient in a material”. The data collected during an experiment could be used to determine the thermal properties of the sample.
- 2) The effects the cyclic thermal loading involved specified periods of heating and cooling, reflecting an office building’s daily heating and cooling loads, would have on the soil properties, determined from strength and water content tests carried out on sub samples collected after the experiment, and the ability of the soil to act as a heat sink.

Further details of the design and construction of the test rig, the commissioning of the rig, the experimental methodology, and the additional equipment required are provided in the rest of the chapter in the order listed below:

- i. Schematic diagram of Test Rig
- ii. Description and Design of Test Rig and Experiment
- iii. The Design of the Rig
- iv. Additional equipment required

### 3.2 Description of Test Rig Design

A test rig was designed to meet the principles set out in Section 3.1.7. The sample of soil to be tested (Figure 3.3) is within a cylindrical test chamber or cell body (7). There are openings fitted with glands down the sides of the chamber (9) to enable insertion of thermocouples (10) for monitoring temperature changes within the chamber.

A piston (5) placed on top of the sample is pressurised using a flexible membrane / rubber diaphragm (4) to simulate the overburden pressure on an element of soil at some depth below the ground surface. This was based on the Rowe cell (Head, 2006), a cell designed to consolidate large samples of soil.

The base of the cell (12) is fitted with a perforated plate (11) to allow excess pore water pressures to dissipate and drain out through openings in the cell base (13). The top and bottom plates are clamped to the body by long bolts (6), to provide a watertight seal.

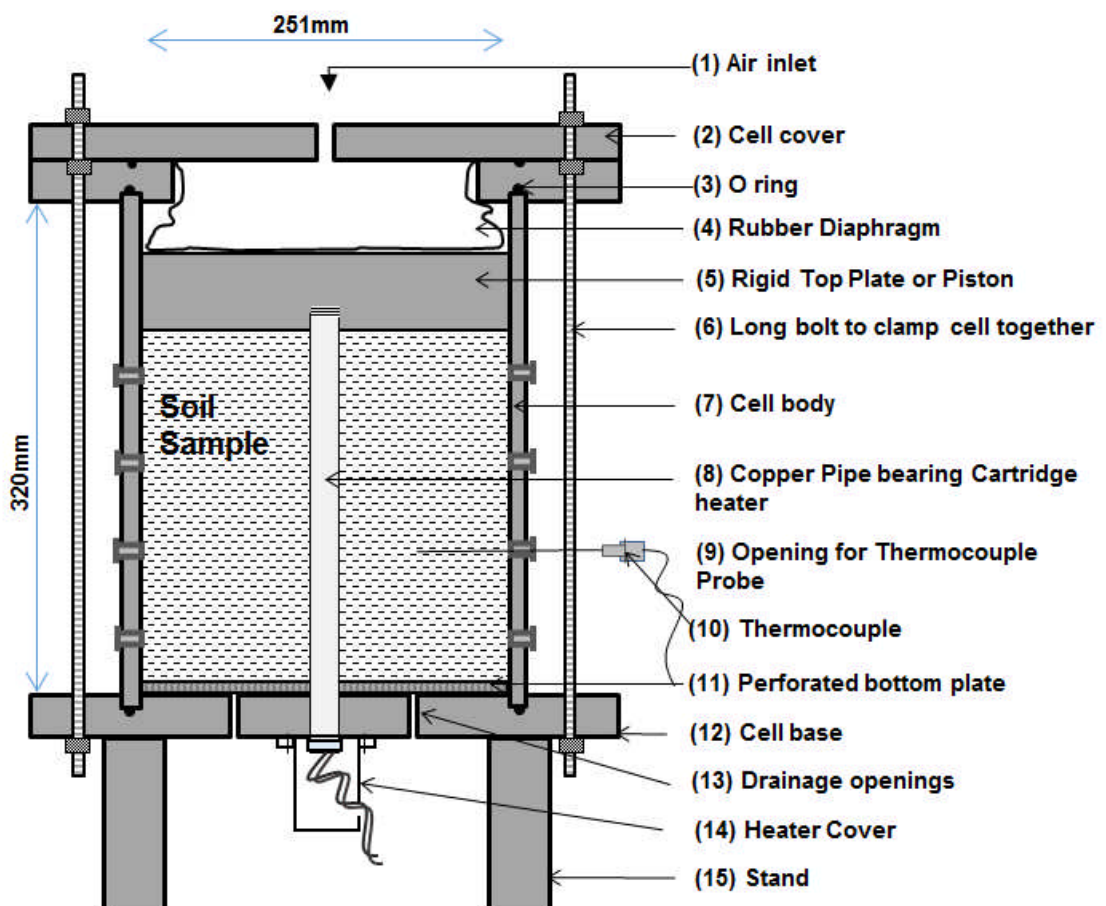


Figure 3.3: Schematic diagram of Test Rig

The heating element is inserted through the base of the cell into a copper pipe or tube (8) within the sample. The copper pipe is allowed to move down as the clay consolidates. To avoid heat loss to the surrounding, the end of the pipe projecting from the base plate moves within a cover (14) below the base of the cell. Drawings of the test rig and its parts are included in the Appendix.

Figure 3.4 displays a fully set up test rig in operation.



Figure 3.4: Test Rig

### 3.3 Design of Test Rig

This section briefly describes the processes involved in the design of the equipment. The selection of parameters for the design was based on the use of general heat transfer equations for conduction as this is the prime means of heat transfer in soils



(Thomas and Rees, 2009). Through the process of manual optimization, heat transfer equations were analysed to determine the geometry of the test rig.

A theoretical study was undertaken to select an experiment and test procedure and a test rig that would enable soil to be tested and data collected that corresponds to theory based on the thermal conductivity of soils. This property determines how fast or slowly a material gains and loses heat or its ability to transfer heat by conduction (Banks, 2008).

Figure 3.5 shows an energy pile exchanging heat with the surrounding soil.

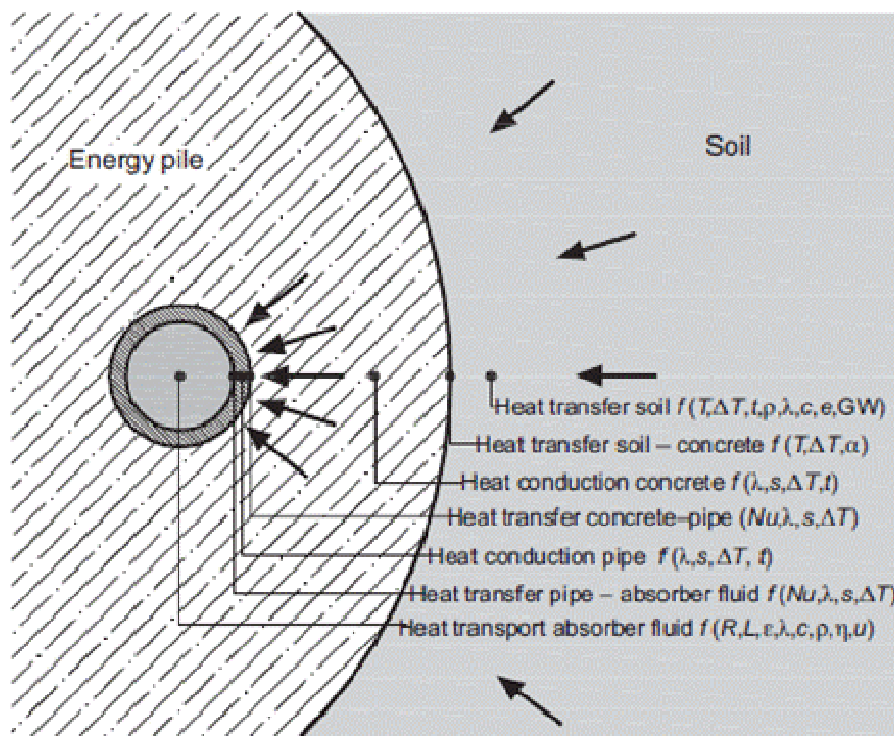


Figure 3.5: Heat transport from soil to heat carrier fluid within the absorber pipe of an energy pile (Brandl, 2006)

Conduction in cylinders is usually treated as a one-dimensional problem when temperature is a function of the radial coordinate (Mills, 1999). The model of the rig design was therefore, based on steady state one-dimensional heat conduction, with a centrally placed heat source radiating outwards.

To determine the appropriate geometry for the test chamber of the rig, the principle of heat transfer by conduction was applied to study the relationship between the geometry and variation of temperature due to radial heat flow. A tube of inner and outer radii  $R_1$  and  $R_2$ , length  $L$ , thermal conductivity  $k$ , with the two surfaces maintained at constant temperatures  $T_1$  and  $T_2$  as shown in Figure 3.6, is typically considered a one-dimensional problem (Mills, 1999).

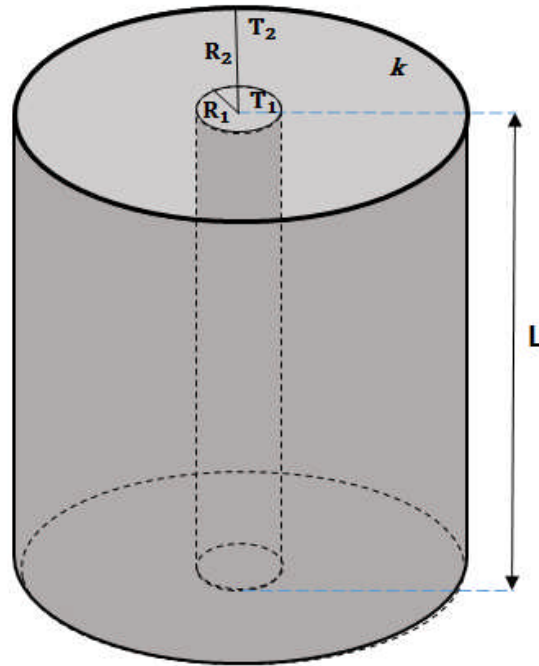


Figure 3.6: A long Cylindrical Layer

According to Janna (1988) Fourier's law of heat conduction for heat transfer through this layer can be expressed as

$$Q = -kA \frac{dT}{dR} \quad (3.2)$$

Where

Heat flux  $Q$  ( $W/m^2$ ) is the conduction heat transfer rate through the cylindrical layer and is constant in the radial direction

$k$  ( $W/m.K$ ) is the thermal conductivity of the material

$R$  is the radial direction in which the temperature varies

$T$  is the temperature at any radius  $R$

$A = 2\pi RL$  is heat transfer area at location  $R$  and varies in the direction of heat transfer.

Assuming thermal conductivity to be constant, and because radial conduction through a cylindrical wall is logarithmic, heat transfer rate can be further expressed as:

$$Q = \frac{2\pi Lk\Delta T}{\ln(R_2/R_1)} \quad (3.3)$$

The temperature difference between the boundaries is:  $T_1 - T_2 = \Delta T$  (3.4)

For a constant  $Q$ , Equation (3.2) can be re-arranged such that thermal resistance,  $R''$ , is expressed as:

$$R'' = \frac{\ln(R_2/R_1)}{2\pi Lk\Delta T} \quad (3.5)$$

Heat conduction problems may also be solved by using existing solutions reported in terms of a shape factor or steady-state dimensionless conduction heat rate and are specific to the geometry of the heat transfer problem (Incropera, 2007b). For a cylindrical shape, the steady heat transfer rate can be determined from the equation expressed below as:

$$Q = Sk(T_1 - T_2) \quad (3.6)$$

Where  $S$  = Shape factor

$T_1 - T_2$  = Temperature Difference between boundaries

The shape factor for a long cylindrical layer of length  $L$  is expressed as:

$$S = \frac{2\pi L}{\ln(R_2/R_1)} \quad (3.7)$$

(Janna, 1988)

### 3.3.1 Design Principles and Assumptions

As the experiment simulated an energy pile, a linear heat source, the design was based on the following principles:

- To create an axisymmetric problem similar to an installed energy pile to simulate the transfer of heat by conduction for an element of ground
- To ensure constant temperature boundaries to simulate the dissipation of heat from an energy source into ground at constant temperature remote from the pile
- To insulate the top and bottom of the rig in order to ensure heat flow is radial
- To allow temperature to be monitored across the sample to study the thermal behaviour of the soil
- To be able to simulate elements of the pile at different depths to study if thermal behaviour changes with depth.

All the calculations carried out for purpose of this research involving conduction heat transfer equations are based on the following assumptions:

- A single geological layer (thus constant properties such as thermal conductivity)
- Constant temperature at the internal and external boundaries
- Finite fixed boundary
- Single cylindrical heat source
  
- Heat transfer is radial by conduction

For the purpose of calculations to optimize the rig design, a typical thermal conductivity value of 1.8W/m.K for soil was used in the calculations (Banks, 2008), and a temperature difference of 20°C was also used in the calculations to determine appropriate parameters for the rig based on a room temperature of 20°C and a core temperature of 40°C.

### **3.3.2 Choice of Rig Material**

Conventional consolidation chambers are made of metal, often steel. Their purpose is to laterally restrain the soil to ensure one dimensional consolidation. In this experiment the cell wall is also an integral part of the heat transfer. Therefore, the thermal characteristics of the cell wall have to be taken into account. Further, the soil is to be consolidated therefore, the cell wall has to be able to provide the necessary lateral resistance to contain a soil sample subject to an overburden pressure, which, in these experiments will be a maximum of 200kPa.

The pile heats the soil with the temperature in the soil reducing from its maximum at the pile/soil interface to the ground temperature some distance from the pile, which, according to Equation (3.2) is infinity. In practical terms, the external boundary can be a finite distance from the pile because the variation in temperature is logarithmic and difference between the simulation and the theory would be small.

Thus the cell wall has to be strong enough to contain a sample subject to an overburden pressure and have thermal characteristics which are consistent with radial conduction. Various materials were considered before narrowing down the decision to steel and High Density Polyethylene (HDPE). An advantage HDPE has over steel is that its thermal conductivity (0.46W/m.K) is similar to that of soil. The thermal conductivity of steel (43W/m.K) is about one hundred times that of soil. This means that the temperature profile using HDPE will be little affected by the cell wall whereas, with steel there will be noticeable change in the temperature profile at the cell wall for a wall designed to resist the lateral stresses. The strength of steel (~400MPa) is sixteen times that of HDPE (~25MPa) which means that the cell wall thickness for HDPE will be greater than that for steel.

HDPE has three advantages over steel:-

1. It has a similar thermal conductivity to soil therefore, the temperature profile through the soil and cell wall will be similar to that of a soil sample with the same external diameter. This means that a smaller soil sample can be used if contained in a HDPE cell as opposed to a steel cell.
2. The wall thickness of a HDPE cell will be greater than that for a steel cell for the pressures to be applied. This increases the effective distance of the finite boundary of the sample.
3. The density of HDPE ( $\sim 1\text{Mg/m}^3$ ) is about an eighth of that of steel ( $\sim 8\text{Mg/m}^3$ ) making it easier to handle the test rig when assembling and disassembling the rig between tests.

### 3.3.3 The Diameter of the Cell

The soil was tested in a cylindrical container as shown in Figure 3.7

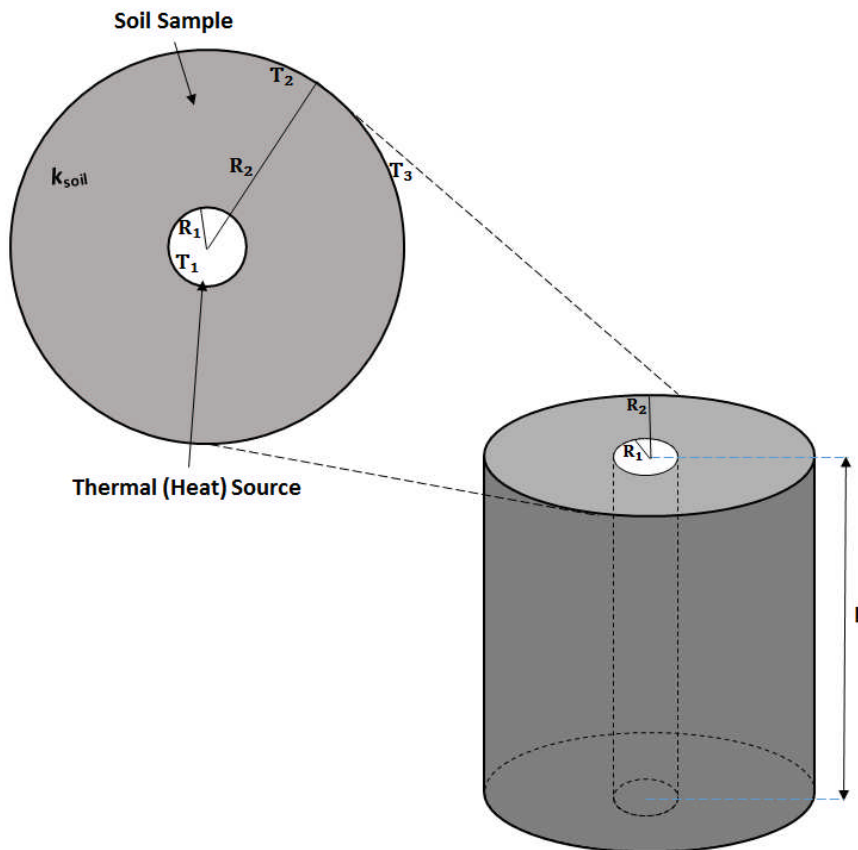


Figure 3.7: A section through a long cylindrical layer containing soil sample and heat source within the sample.

It was important that the cell diameter was of the right size relative to the diameter of the heat source to simulate radial conduction in an infinite soil mass yet be small enough to be able to assemble the rig. Since the soil and cell wall have similar thermal

properties, the initial calculations were based on a uniform cylinder of length,  $L$ , internal diameter,  $R_1$ , and external diameter,  $R_2$ .

The effect of cell/soil diameter on heat conduction was analysed using Eq. (3.5),

$$Q = Sk(T_1 - T_2)$$

Where  $S$  = Shape factor;  $S = \frac{2\pi L}{\ln(R_2/R_1)}$  (for a cylindrical layer)

$T_1 - T_2$  = Temperature Difference

$R_1$  = Radius of heat source

$R_2$  = distance from the centre of the heat source to the outer wall of the cell.

In the calculations, a temperature difference of 20°C was used based on a temperature at heat source of 40°C and controlled room temperature of 20°C.

It was proposed to use an HDPE tube which is supplied in standard sizes. 250mm was the nominal internal diameter since a Rowe cell piston was to be used to consolidate the sample. 262mm HDPE tube with a wall thickness of 11mm has a nominal internal diameter of 251mm which was deemed acceptable without further machining. This wall thickness is sufficient to withstand a working pressure of 800kPa; that is equivalent to a maximum overburden pressure of about 1600kPa.

It is impossible, experimentally, to ensure radial heat flow since some heat will be lost from the top and bottom of a sample. However, it is possible to ensure radial heat flow over a significant length of sample provided the sample is long enough. The top and base plates were made of HDPE providing similar thermal boundaries to the radial boundary. Therefore, heat loss from the top and bottom of the sample was inevitable. This is no different from an energy pile in which there will be heat will flow to the ground surface and to the soil below the pile. The coefficient of thermal conductivity, the length of the sample, and the internal and external temperatures are constant in a test. Therefore, the quantity of heat flow is a function of  $(R_2/R_1)$  as shown in Figure 3.8 on page 50.

In terms of pile capacity, the radial zone of influence of a pile is normally taken to be ten. The thermal zone of influence is much greater (Figure 3.8) since the power required to maintain the temperature difference increases as the volume of soil increases.

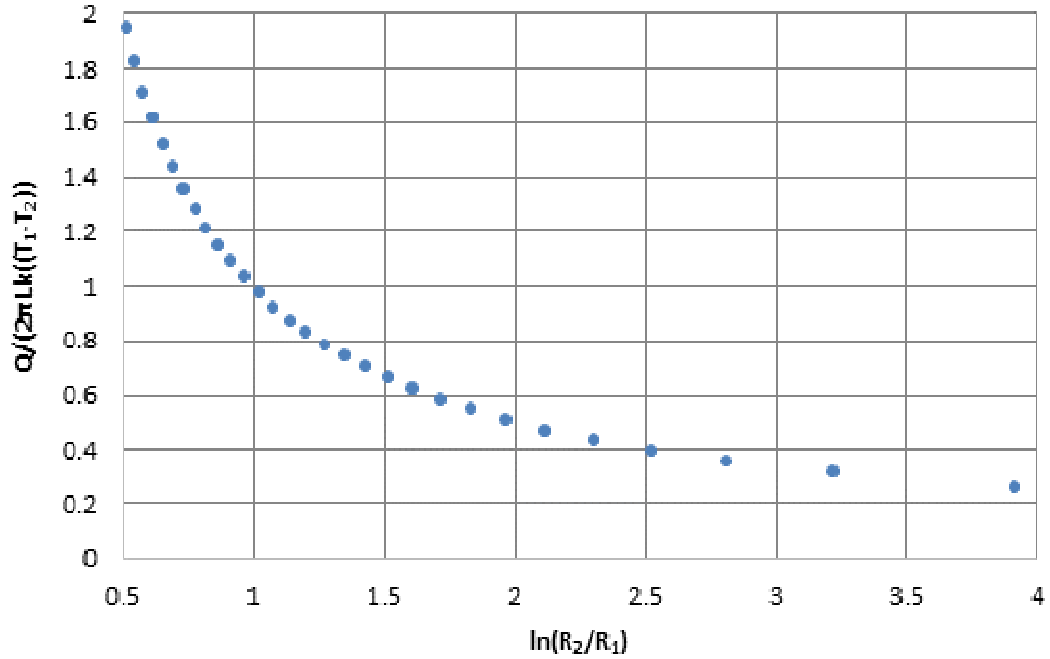


Figure 3.8: Plot of  $Q(W)$  vs  $R_2/R_1$  for selecting appropriate diameters for the Heat Source and Test Rig

The diameter of the cell was fixed by the dimensions of the Rowe cell and material chosen for the cell wall. A 12.7mm diameter cartridge heater was used as the heat source. The cartridge heater was inserted in a 15mm diameter copper tube to simulate the energy pile. This ratio ( $R_2/R_1$ ) is 16.74 which gives a value of  $[Q/(2\pi k(T_1 - T_2))]$  as 0.36 which exceeds the recommended ratio of ten and shows that the boundary will have little influence on the temperature profile in the soil.

### 3.3.4 The effect of the cell wall

Figure 3.9 on page 51, shows a multi-layered cylinder which models a centrally placed heat source in a cylindrical container filled with soil sample for radial heat dissipation.

Using Eq. (3.3),

$$Q = \frac{2\pi Lk\Delta T}{\ln(R_2/R_1)}$$

At the cell wall interface defined by  $R_2$ , the temperature is  $T_2$ . Thus:

$$Q_{soil} = \frac{2\pi Lk_{tsoil}(T_1 - T_2)}{\ln(R_2/R_1)} \quad (3.8)$$

And

$$Q_{wall} = \frac{2\pi Lk_{twall}(T_2 - T_3)}{\ln(R_3/R_2)} \quad (3.9)$$

It is assumed, at steady state, the flow of heat through the soil is the same as the flow of heat through the cell wall. Hence:

$$Q_{soil} = Q_{wall}$$

Therefore,

$$\frac{2\pi L k_{tsoil}(T_1 - T_2)}{\ln(R_2/R_1)} = \frac{2\pi L k_{twall}(T_2 - T_3)}{\ln(R_3/R_2)}$$

And

$$\frac{k_{tsoil}(T_1 - T_2)}{\ln(R_2/R_1)} = \frac{k_{twall}(T_2 - T_3)}{\ln(R_3/R_2)} \quad (3.10)$$

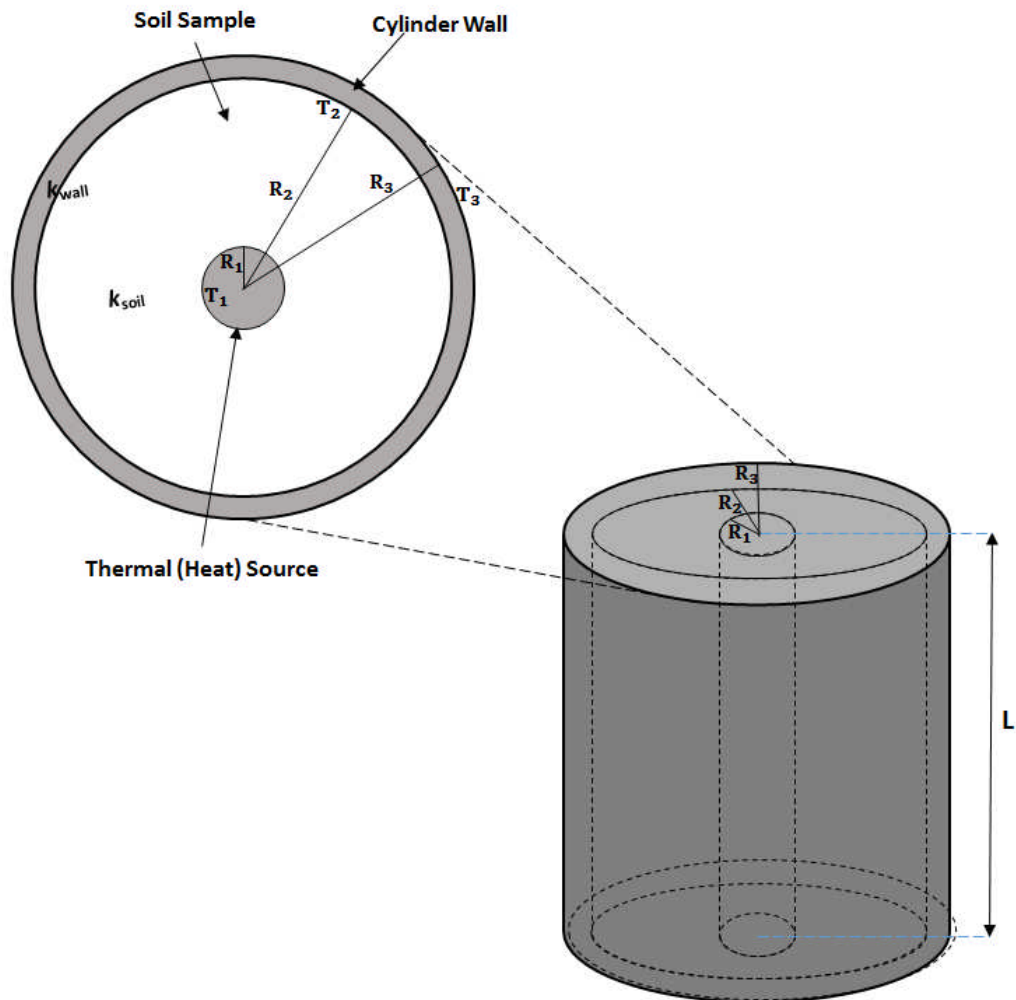


Figure 3.9: A section through a multi-layered cylinder filled with soil sample with a centrally placed heat source



Equation (3.10) was applied to study the influence of radial distances and cell wall thickness on temperature changes through heat conduction. The effect of wall thickness and the diameter of the heat source on the temperature at the soil/wall interface were considered.

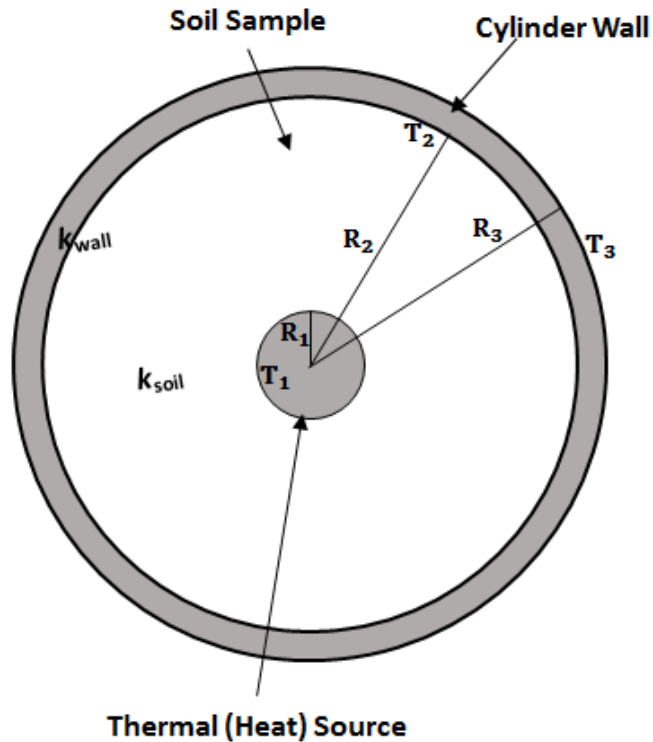


Figure 3.10: Multi-layered Cylindrical Section filled with Soil Sample and showing the parameters being calculated

Figure 3.10 is a cross-section of a multi-layered cylindrical pipe of an assumed thickness, filled with soil and with a centrally placed heat source. Heat dissipation is assumed to take place in the radial direction as stated earlier. Figure 3.10 is discussed as follows:

- $R_1$ ,  $R_2$  and  $R_3$  represent the radius of the heat source, distance from the centre of the heat source to the inner cell wall, and the distance from the centre of the heat source to the outside cell wall respectively.
- $T_1$ ,  $T_2$  and  $T_3$  are the temperature at the wall of the heat source, temperature at the inner cell wall and the temperature outside the cell wall (controlled room temperature).
- $k_{\text{wall}}$  and  $k_{\text{soil}}$  represent the thermal conductivities of the cell wall and soil sample respectively. Typical values of 0.46W/m.K and 1.8W/m.K were used in the calculations for both the cell wall material and soil sample respectively.

Figure 3.11 shows the variation of  $T_2$  with  $T_1$  for an external pressure of  $20^\circ\text{C}$  for 251mm diameter soil sample with an 11mm HDPE cell with an 11mm wall thickness. A temperature increase of  $10^\circ\text{C}$  at the heat source produced a temperature difference of approximately  $0.6^\circ\text{C}$  at the interface between the soil and the cylinder, while a  $20^\circ\text{C}$  increase produced a temperature difference of  $1.1^\circ\text{C}$  at the same location.

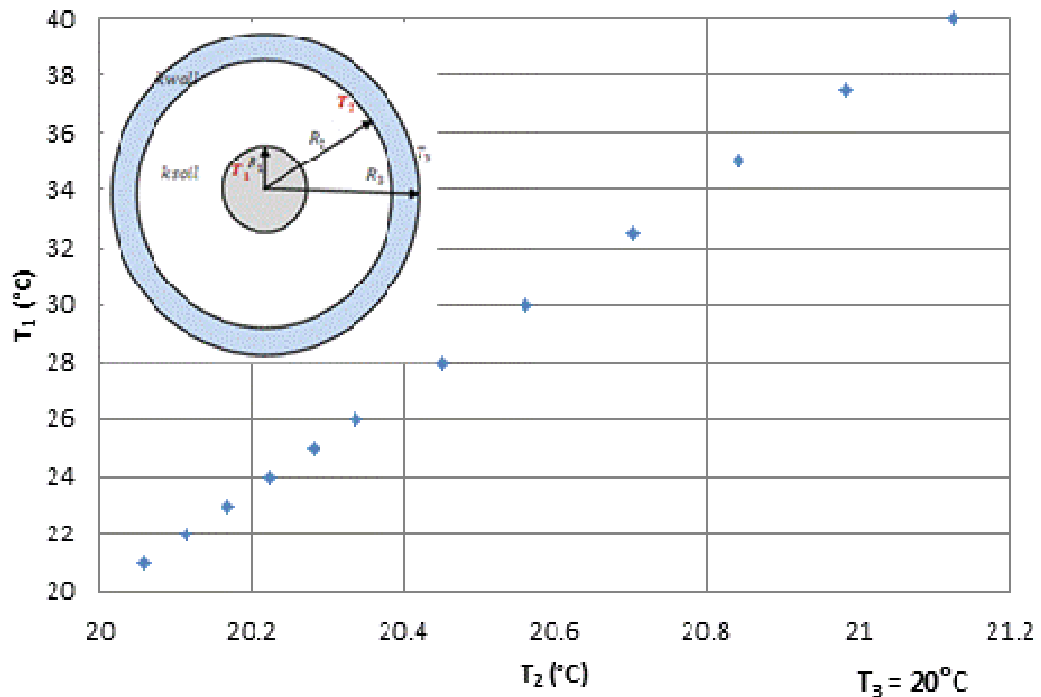


Figure 3.11: Plot of  $T_1$  ( $^\circ\text{C}$ ) vs.  $T_2$  ( $^\circ\text{C}$ ) where values for  $T_2$  were obtained by changing the values of  $T_1$  while keeping  $T_3$ ,  $R_3$ ,  $R_1$  and  $R_2$  constant

In the second instance, values were again generated for  $T_2$  (temperature at the inner cell wall) by changing values  $R_1$  (radius of the heat source), while keeping  $T_3$  (outside temperature),  $R_3$  (distance from the centre to the outside cell wall),  $T_1$  (source temperature),  $R_2$  (distance from the centre to the inner cell wall) all constant.

$T_2$  values obtained by changing the  $R_1$  values depict a relationship between the heat source radius ( $R_1$ ) and wall temperature ( $T_2$ ), are presented by the chart in Figure 3.12 on page 54.

It was observed that as the radius of the heat source ( $R_1$ ) was increased from 5mm to 10mm the inner wall temperature ( $T_2$ ) increased by only by  $0.3^\circ\text{C}$ . Increasing the radius further to 80mm only increased  $T_2$  by about  $1^\circ\text{C}$ .

Increased changes in  $T_2$  occur only as heater radius becomes greater than 90mm. Between 90mm and 100mm radius the increase in  $T_2$  is about  $1.8^\circ\text{C}$ , thus the gradual

heat flow within the sample which is desired for the experiment, requires keeping the heat source radius less than 80mm.

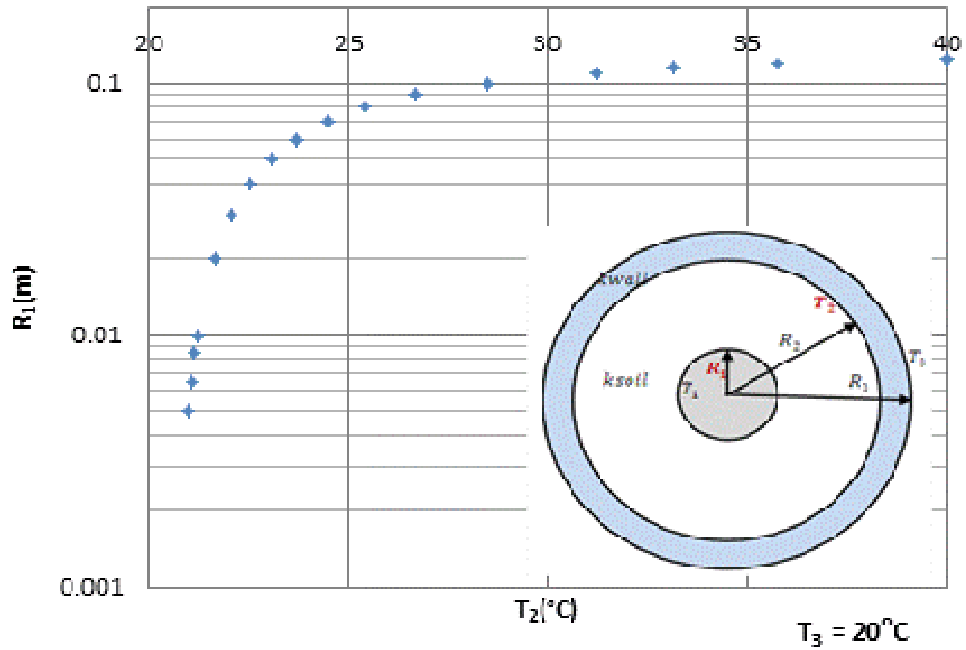


Figure 3.12: Plot of  $R_1$  vs.  $T_2$  ( $^{\circ}\text{C}$ ) where values of  $T_2$  were obtained by changing the values of  $R_1$  while keeping  $T_3$ ,  $R_3$ ,  $T_1$  and  $R_2$  constant

In the third and final instance, the relationship between  $R_2$  and  $T_2$  was studied (Figure 3.13).

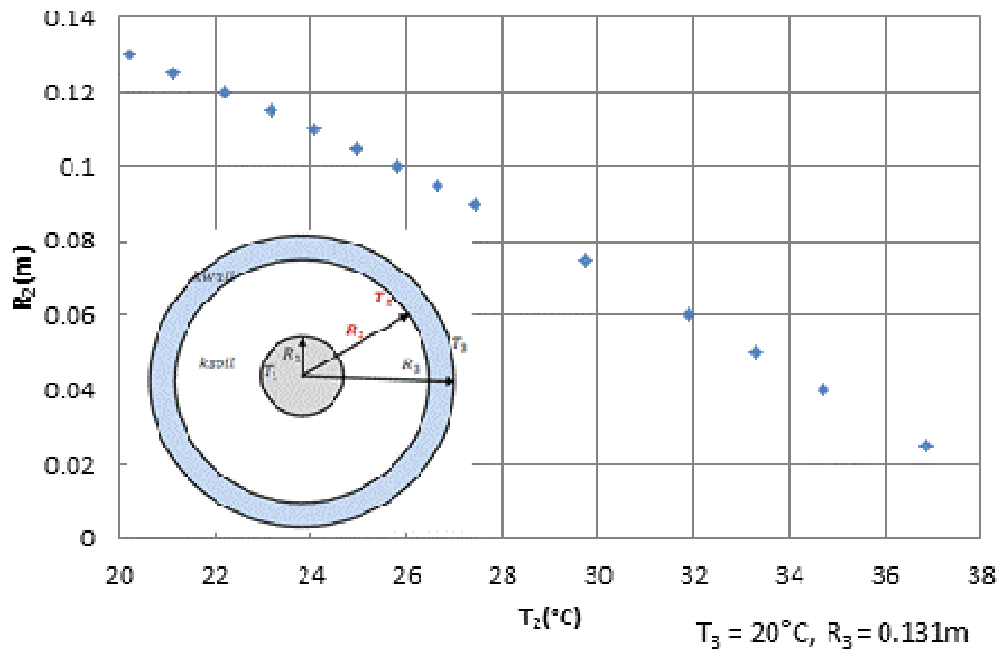


Figure 3.13: Plot of  $R_2$  vs.  $T_2$ ; where values of  $T_2$  were obtained by changing the values of  $R_2$  while keeping  $T_3$ ,  $R_3$ ,  $T_1$  and  $R_1$  constant

Values were generated for  $T_2$  (temperature at the inner cell wall) by changing values  $R_2$  (distance from the centre to the inner cell wall), while keeping  $T_3$  (outside temperature),  $R_3$  (distance from the centre to the outside cell wall),  $T_1$  (source temperature),  $R_1$  (radius of the heat source) all constant.

The prime purpose of the cell wall is to contain the soil. However, it also affects the heat flow and therefore, the temperature profile through the soil sample. HDPE was the chosen material for the cell because the thermal conductivities of soil and HDPE are similar thus increasing the effective volume of soil in the experiment. The tests were carried out in a constant temperature laboratory which, typically, meant a temperature of  $20^{\circ}\text{C} \pm 1.5^{\circ}\text{C}$ . Therefore, the cell wall had to act as an insulator to reduce the effect of the room temperature fluctuations on the soil. The standard HDPE pipe of 11mm thickness was tested based on the above criteria and therefore, found suitable for the purpose of the experiment.

### **3.3.5 Ability to withstand Pressure Loading**

A standard 251mm internal diameter HDPE pipe with 11mm cell wall thickness was used. The maximum pressure acting on the cell wall was due to the lateral stress in the soil. The operating pressure for this pipe is 640kPa. The maximum overburden pressure was 200kPa which gives an approximate lateral pressure of 100kPa. Therefore, the HDPE cell was acceptable.

### **3.3.6 Other Design Aspects**

Figure 3.14 on page 56, shows a fully labelled section of the rig used to highlight the design details that are referred to in the process. The cylindrical cell body (7) containing the sample, was clamped between the cell base (12) and the cell cover (2) with threaded bars (6). This technique ensured that the sample was properly sealed to prevent pore water leaking from a sample and to make the pressure system airtight.

The design of the cell cover was based on the Rowe consolidation cell (Head, 2006), with an attached flexible rubber diaphragm (4) and inlet (1) for air pressure to be uniformly distributed over the soil thereby simulating overburden pressure. The cell base was designed with outlet points (13) to serve as drainage for excess pore water during the consolidation stage when the sample to be pressurized.

Five 15mm round openings were made through the cell base. The central opening was for the heater and the others were for the purpose of investigating the location of heat sources in a concrete pile. This is not covered in this research therefore, they were plugged off during the experiment. The base required sturdy stands (15) to adequately support the weight of wet soil sample, the pressure load and other parts of the rig.

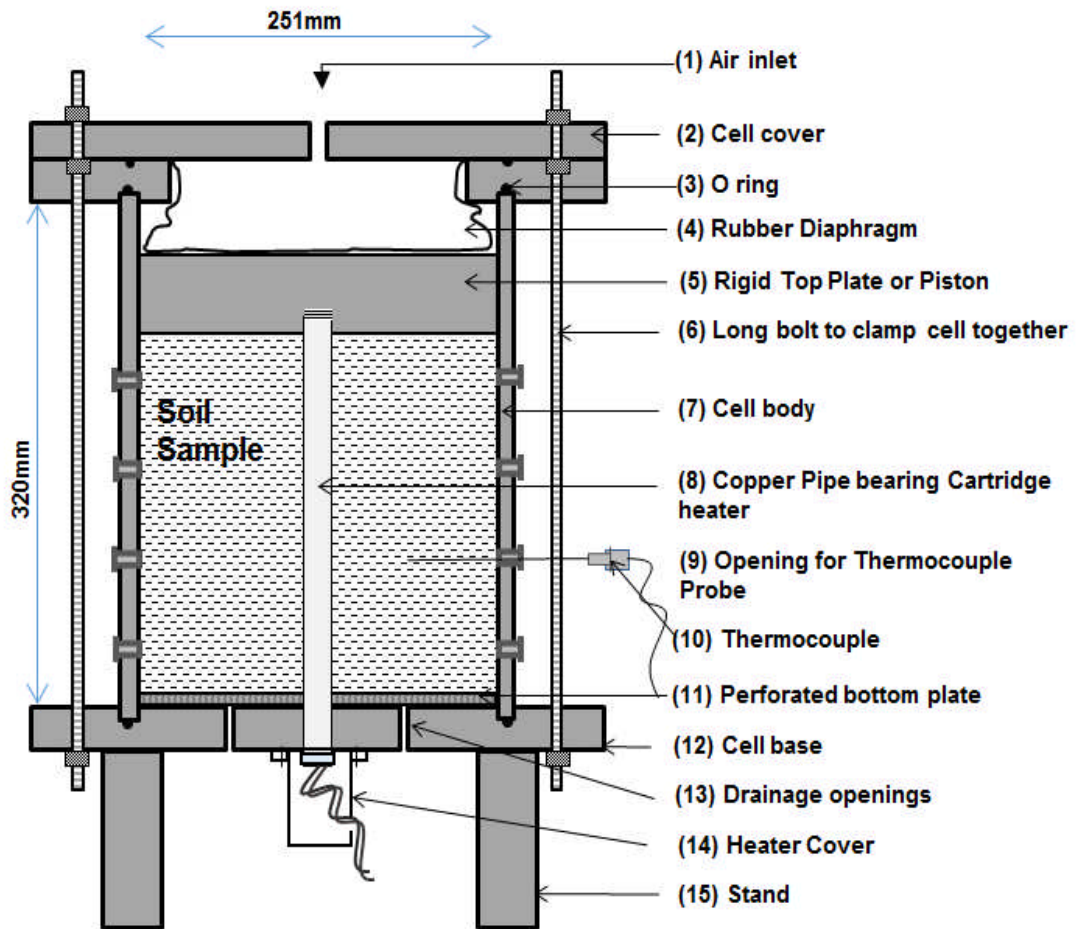


Figure 3.14: Cross-section of test rig showing the key elements

The stands were designed to be high enough to provide adequate clearance for the heater in a copper pipe (8) which was designed to be introduced through the bottom of the cell.

The copper pipe was designed to be fitted through the centre of the cell base to the cell body and threaded to the top rigid plate (5) so that the heater and copper pipe moved down as the sample was consolidated. Copper was selected as the material of choice due to its high thermal conductivity value of 401W/m.K (Incropera, 2007b), as the function of this pipe is to hold the heating element and conduct the heat to the surrounding soil. A heater cover (14) acted as an insulated casing for the heater. An opening by the side of the heater cover allows for the heater wiring to pass through.

Two rigid plates were designed for use within the cell body to keep the pipe in a fixed position and to keep the soil in place. The top plate (5) was designed to ensure uniform loading on top of the soil and has a threaded opening to secure the heater pipe in place. The thinner lower plate (11) has perforations to allow dissipation of excess pore water pressures.

Small openings (9) were made in the sides of the cell wall for thermocouples (10) to be inserted at various distances from the centre to measure the temperature changes within the soil sample.

Several O-rings (3) of varying sizes were placed at points where the rig parts are connected in order to ensure proper sealing.

### 3.3.7 A summary of how the rig is set up

The process of setting up the rig for use is described in the following steps and aided by the use of figures.

- i. The cartridge heater, A in Figure 3.15, is smeared all over with conductive gel to ensure uniform heat distribution within and along the pipe. When the heater is placed in the pipe, the gel helps to push out existing air in the pipe. The heater is then placed into the copper pipe, and firmly screwed together by means of its threaded base, B in Figure 3.15.



Figure 3.15: Cartridge heater and cartridge heater in copper pipe

- ii. The cell base is set up by fitting an O-ring into the groove of the cell base as shown in Figure 3.16. Openings 1 to 4 not in use during the experiment are blanked off with plugs.

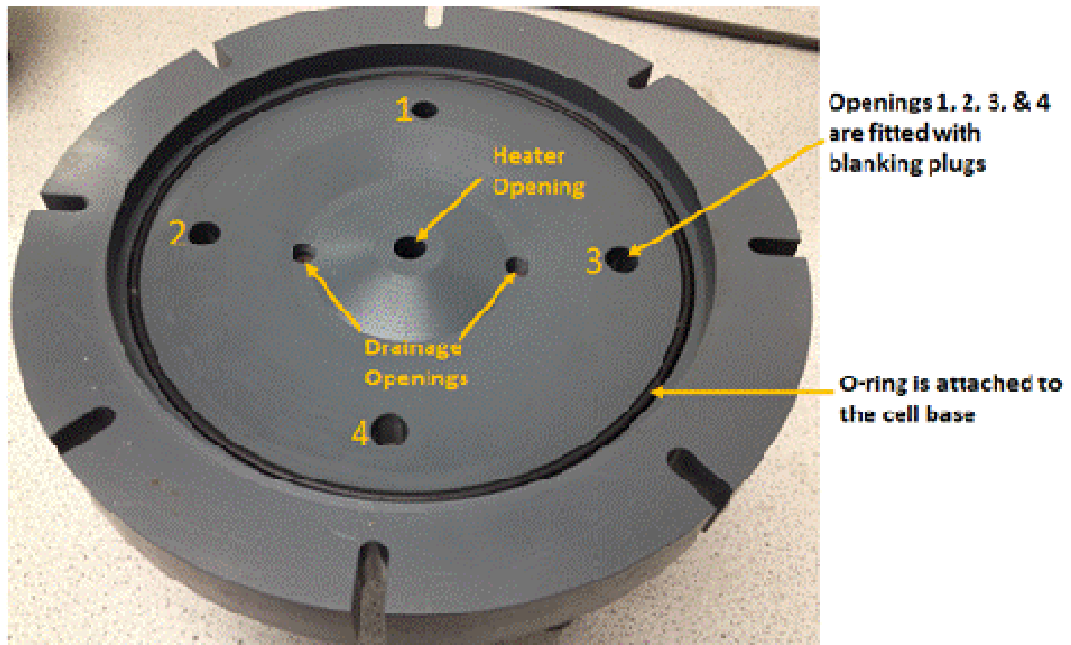


Figure 3.16: Top view of cell base with O-ring attached

- iii. From Figure 3.17; the stands are attached to the cell base from the bottom, drainage fittings are attached and the copper pipe bearing the heater firmly fitted through the central opening in the base. The heater cover is fitted over the base of the heater and under the cell base. The heater wires pass down through an opening on the side of the heater cover for that purpose.

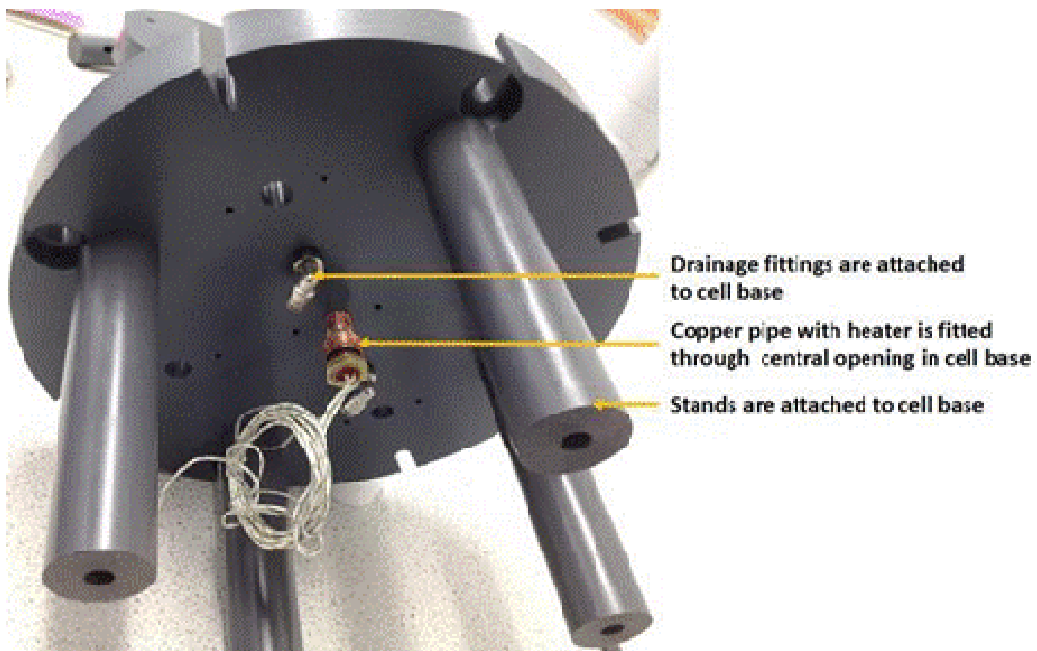


Figure 3.17: Bottom view of cell base showing fittings and copper pipe with heater

- iv. The perforated flat plate, A in Figure 3.18, is slid down the copper pipe and placed on the bottom of the base. Filter paper (B) cut to the shape and size of the perforated plate is placed over it to prevent blockage of drainage openings as shown in Figure 3.18. A layer of silicon grease is applied over the O-ring to help seal gaps around the cylindrical cell body to be placed over it.

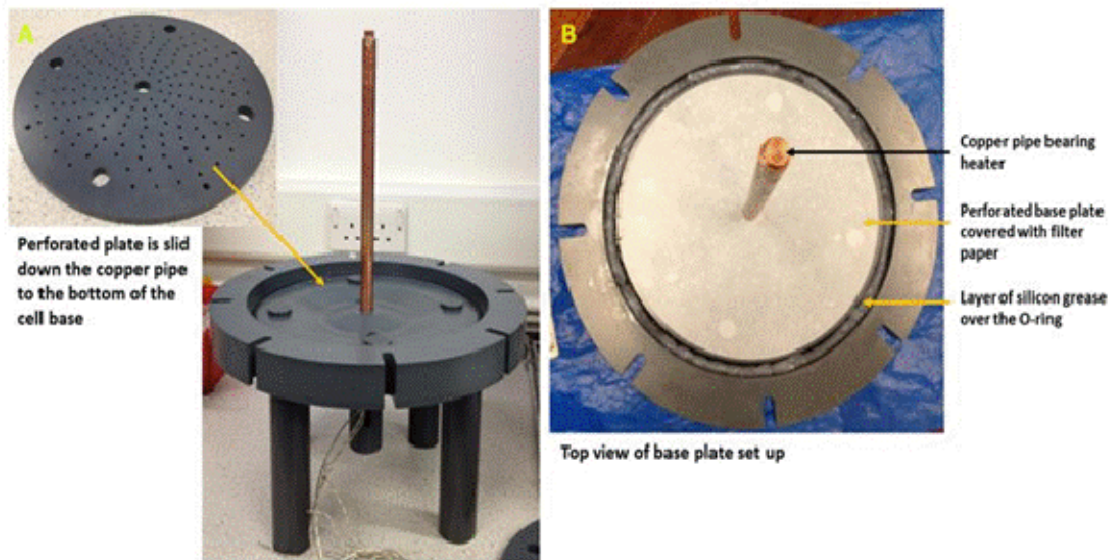


Figure 3.18: Perforated plate to be placed over cell base

- v. The openings on the sides of the cylindrical body are fitted with blanking plugs to ensure it does not leak when a sample is consolidated (Figure 3.19). The plugs are later replaced with Swagelok glands after consolidation of the sample.

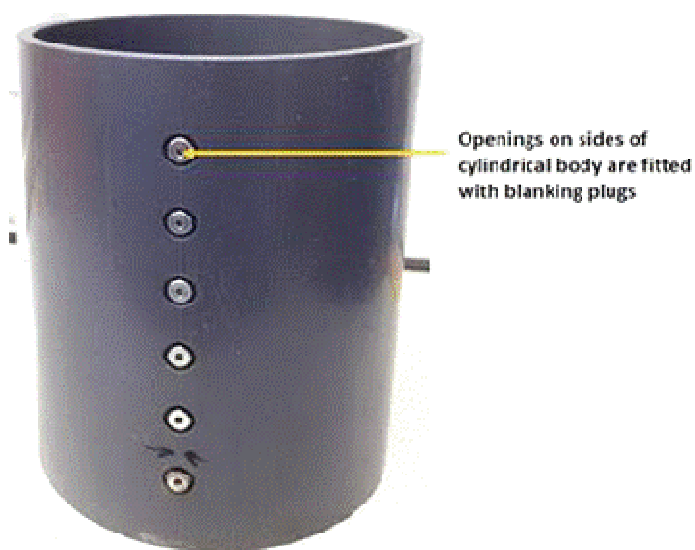


Figure 3.19: Cylindrical cell body showing openings fitted with blanking plugs



- vi. As shown in Figure 3.20, the cylindrical cell body is placed over the cell base where the silicon grease was applied to help hold it in place and seal off gaps. A top flange is placed over it enable the cell body and cell base to be clamped together by a set of threaded bars.

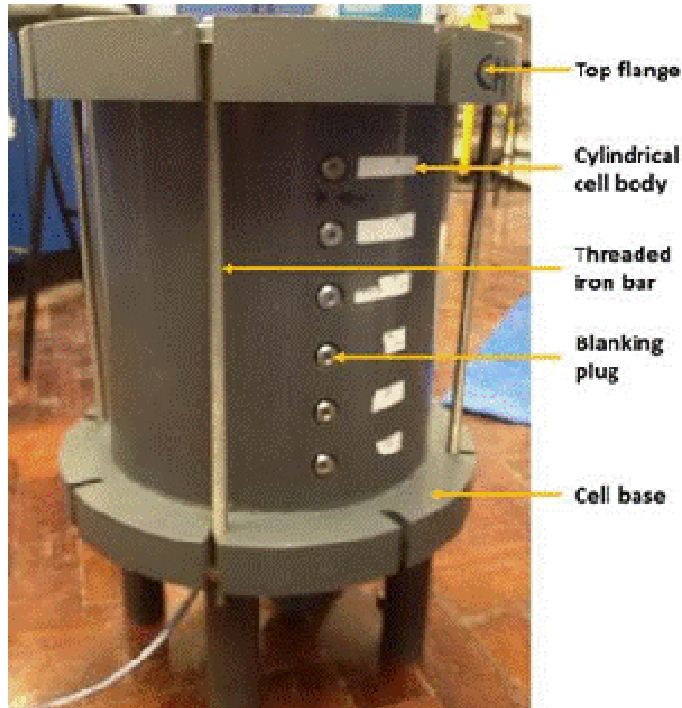


Figure 3.20: Cylindrical cell body attached to cell base by threaded iron bars

At this stage the soil slurry is carefully placed in the cell to eliminate air. Figure 3.21 shows a top view of the cell before and after loading with sample.

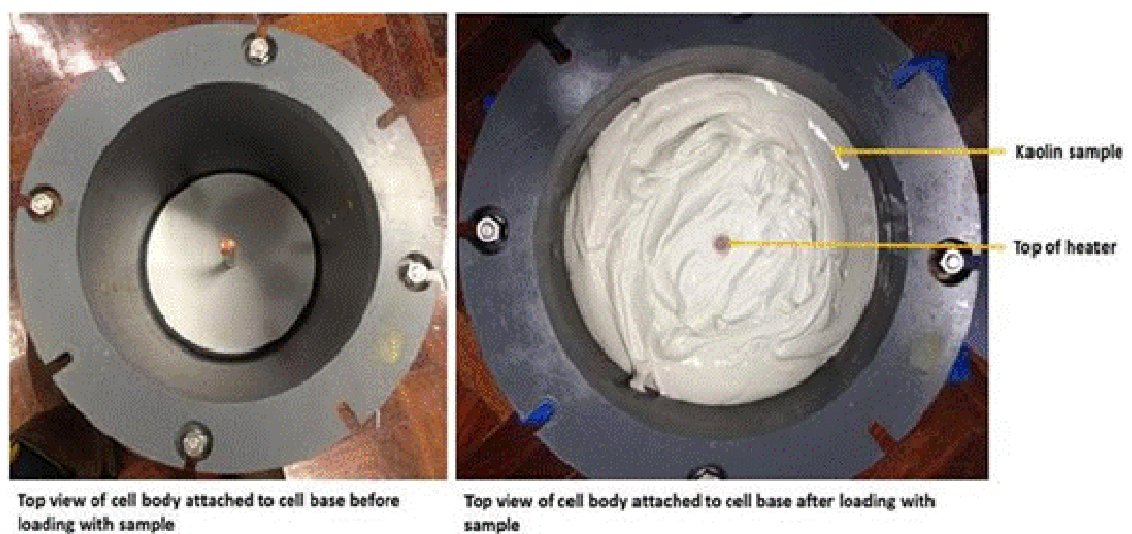


Figure 3.21: Top view of cell before and after loading with sample

- vii. The upper rigid plate is placed on the sample and screwed on to the top of the copper pipe to keep it in a fixed position, as shown in Figure 3.22. A layer of filter paper is placed between the sample and plate to prevent the soil sticking to the plate.

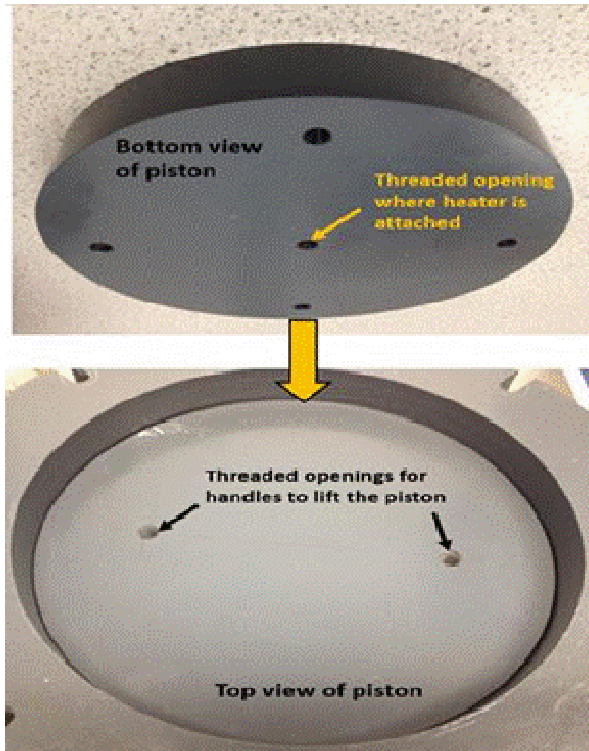


Figure 3.22: Showing top and bottom views of the piston (rigid plate) before and after it is placed over sample

- viii. The cell cover fitted with the flexible rubber diaphragm as shown in Figure 3.23 (page 62), is placed over the top flange and clamped to the cell base with another set of threaded iron bars. This concludes the setting up process.

After setting up the rig, an air pressure supply unit is connected through valves on the cell cover to introduce air pressure which is uniformly distributed over the sample by the rubber diaphragm.

When consolidation of the sample is over, power is supplied to the cartridge heater listed in Table 3.1, from a laboratory direct current power supply source. Thermocouples also listed in Table 3.1, are fitted through the Swagelok openings on the sides of the cell body at specific distances from the heat source to measure temperature changes across the sample. The thermocouples are connected to a data logger which is set to record the temperature changes at regular intervals. The data is

stored in the logger until retrieved using a laptop programmed with the appropriate data logger software.

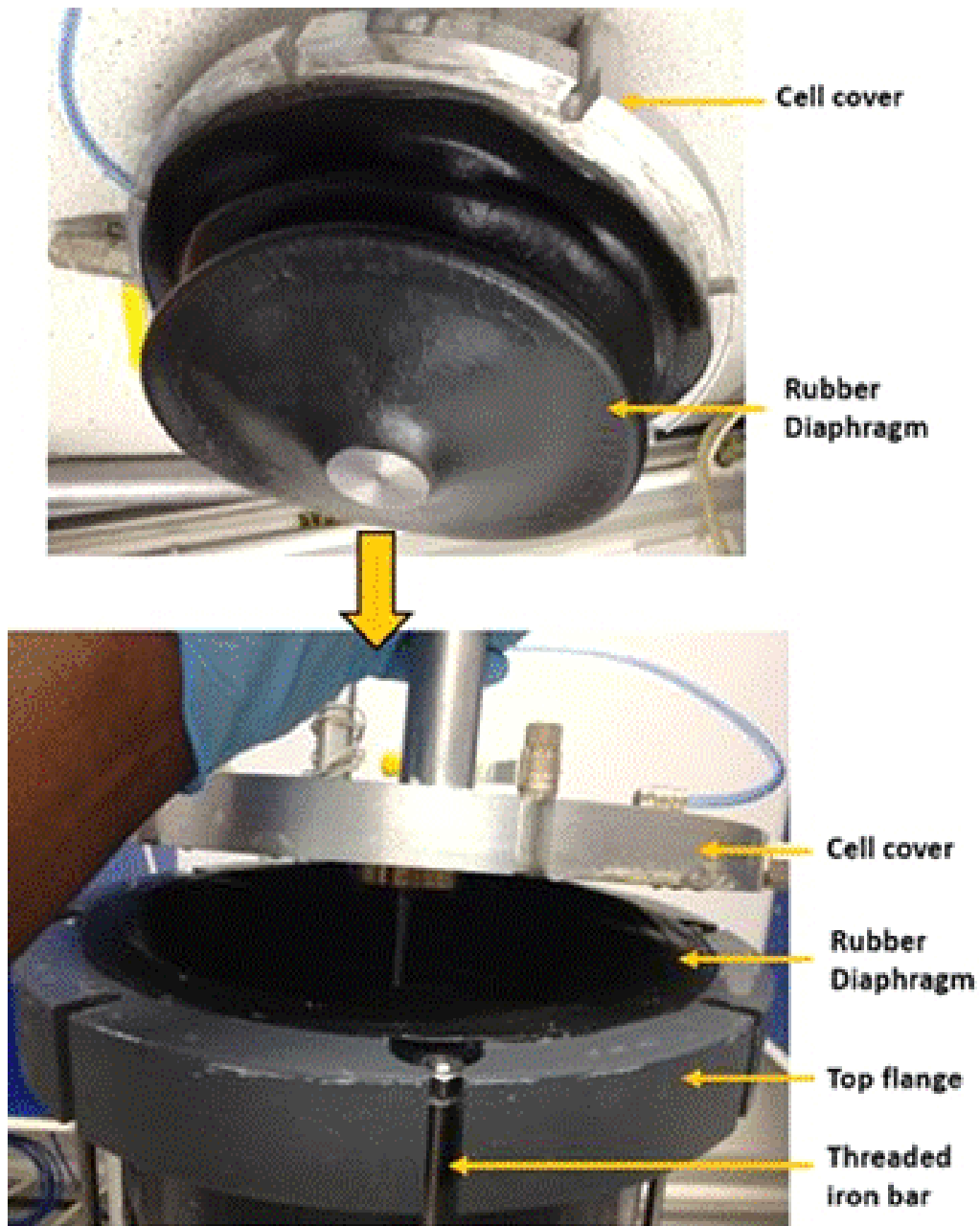
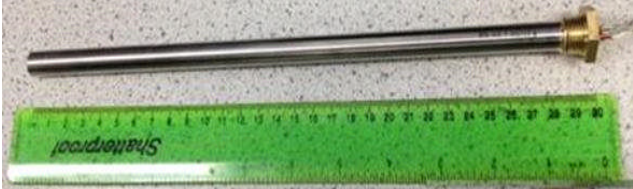



Figure 3.23: Test rig being covered with cell cover fitted with flexible rubber diaphragm

### 3.3.8 Additional Equipment

The equipment required for the experiment in addition to the test rig are; cartridge heater, Laboratory DC power supply, temperature sensor probes (thermistors/thermocouples), air pressure supply unit, a data logger and a computer. Specification details of the heater are included in the Appendix.

Table 3.1: Table showing additional equipment and their description

Equipment	Brief Description
Cartridge Heater	<p>A Chromalox DC heater half inch in diameter (12.7mm) and 300mm in length was designed and manufactured to run at 30V and 3A specifically to suit the purpose, with a maximum output temperature of 60°C.</p> 
Temperature Probes	<p>Thermocouples were required for measuring temperature changes in the sample and are connected to a data logger for the purpose of data monitoring and collection. K-type thermocouples of varying lengths were used. A photograph of the thermocouples is shown below.</p> 
Data logger	<p>The data logger CR800 series was used in conjunction with the thermocouples to record temperature data from tests run during the experiments.</p>
Air Pressure Supply Unit	<p>An air pressure supply unit installed in the laboratory was used as source of air pressure for the experiment.</p>
Computer	<p>A standard laptop installed with the data logger program was required to access the recorded data from the data logger.</p>
Lab DC Power Supply Unit	<p>A Laboratory Direct Current power supply was used as a source of constant power supply to the cartridge heater during the experiment. The Gwinstek GPS-3303 has a power supply range of 0-30Volts and 3Amperes.</p>

### 3.4 Commissioning of Rig

The rig was commissioned for use by carrying out leakage tests and a set of preliminary heating and cooling tests.

To carry out the leakage test, the rig was set up as described in the previous section and the cell body was filled with water. Slight leakage occurred from around the base of the cylinder which indicated the presence of a gap. Silicon grease was placed around the O-ring sealing the cell body to the base. This solved the leakage problem and allowed for heating tests to be conducted on kaolin samples as other parts of the rig worked according to design expectations.

The preliminary tests on kaolin involved loading the cell with saturated kaolin sample of known water content and introducing specific air pressure load through the top of the cell to the rubber diaphragm which distributes it evenly over the sample. On completion of the consolidation process, heat was introduced into the sample through the centrally placed cartridge heater and radial heat distribution is monitored across the sample.

### 3.5 Results and Problems

Figure 3.24 on page 65, shows a graphical representation of a typical heating and cooling test carried out on a kaolin sample with overburden pressure of 50kPa. The heating test run was for eight hours while the cooling took place for 16 hours, both within a 24 hour cycle. Temperature probes were inserted at specific distances across the cell as shown in the inset.

From the graph in Figure 3.24, it can be seen that within the eight hours heating period that the heater attained a temperature of approximately 35°C while the temperatures recorded by the probes just touching the outside wall of the copper pipe are 24°C and 27.8°C respectively. This significant temperature difference between the heater and outside wall of the pipe was not anticipated and was therefore, noted as an issue to be resolved. The use of heat transfer gel around the cartridge heater within the copper pipe to help in uniform heat conduction did not adequately resolve this problem.

Based on the sample in equilibrium heating condition, the variation of temperature across the sample, from the heater to the inner edge of the rig, is presented in Figure 3.25 on page 66.

In this figure, the temperature variations at the top and bottom layers of the sample are displayed alongside the theoretical temperature variation expected for the sample in heating equilibrium. The disparity in temperature between the top and bottom of the heater, and also the theoretical prediction, all point to non-uniform heating and therefore, the need to make modifications to the rig design.

Leakage was observed during the consolidation process. This occurred around the gap between the cell base and the copper pipe, where the water leaked onto the base

of the cartridge heater during consolidation. This could potentially affect the wiring of the heater over time and present an electrical hazard, and in addition affect the long-term performance of the rig.

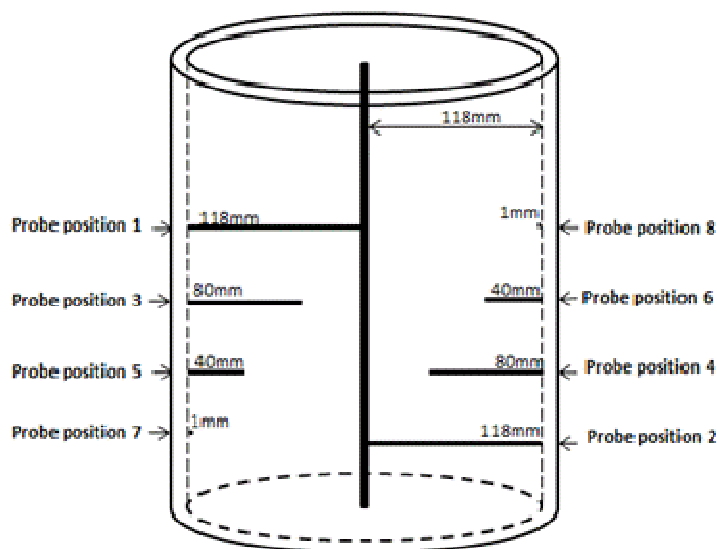
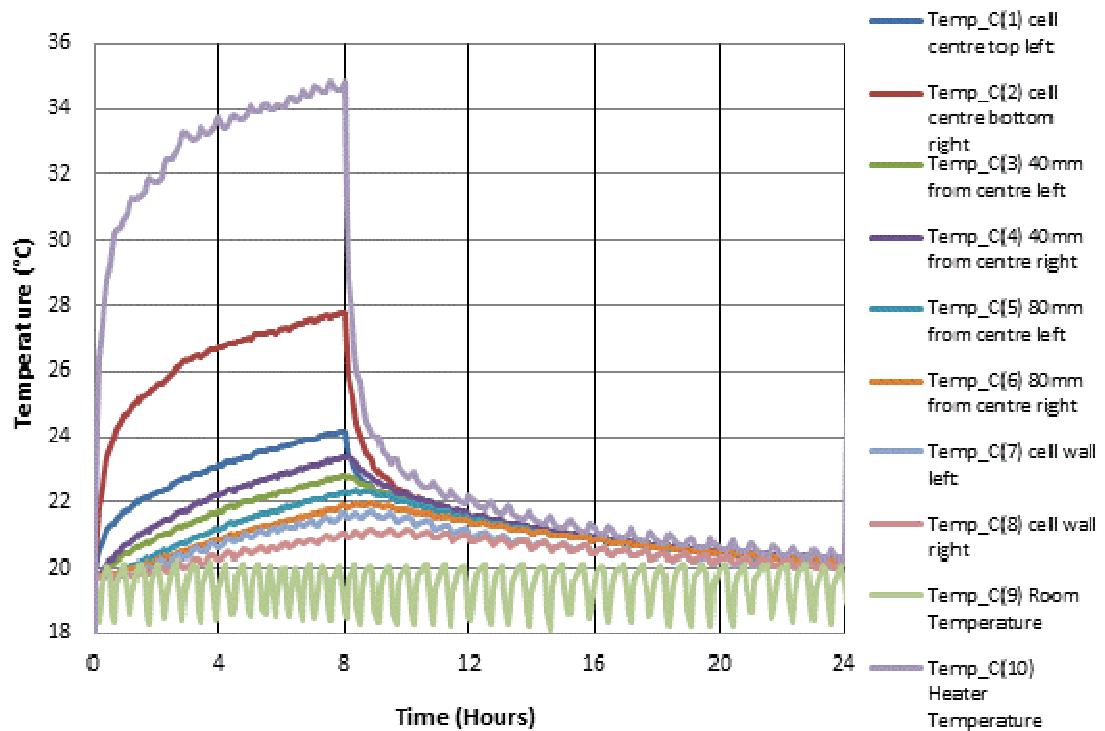


Figure 3.24: Heating and cooling cycles in kaolin showing temperature variations at different radii as shown in the layout of probe positions

While noting the leakage and temperature difference issues, observations were also made of a few changes that could potentially improve the performance of the rig. Therefore, based on challenges encountered and observations made during

preliminary tests carried out, modifications to the rig design were required for its optimum performance.

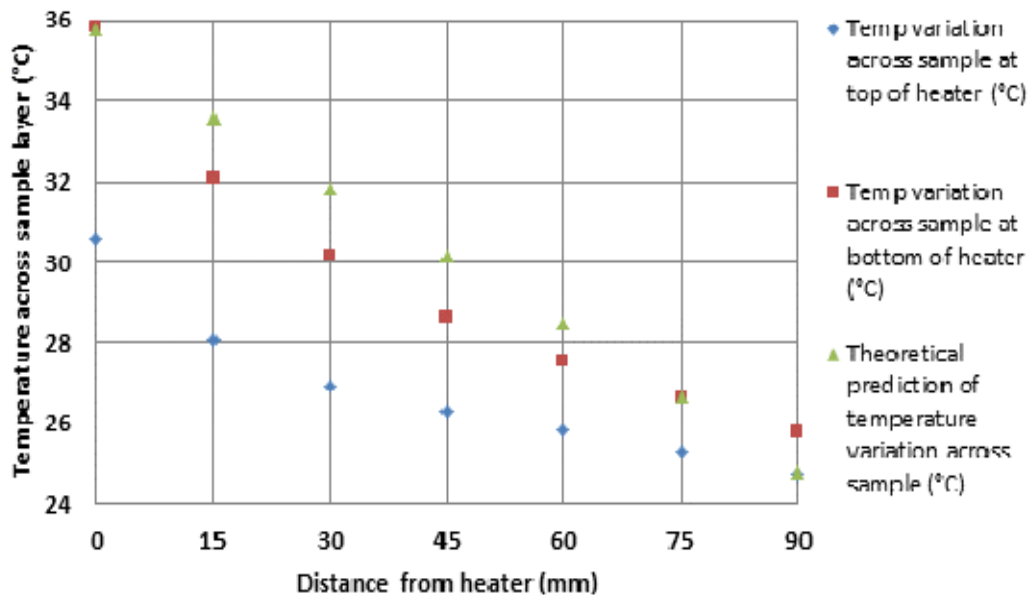


Figure 3.25: Temperature variations across the sample compared to the theoretical variation

### 3.6 Modifications to Rig Design after Preliminary Tests

Figure 3.26 on page 67, shows both the initial and modified rig designs and highlights the differences due to design change. The modifications made to the parts of the rig are first summarised and then in more detail in the following sections. Modifications made to address the issues found during the commissioning test led to changes to other parts of the rig.

The thickness of the piston was increased with a central hole to allow the cartridge heater to be fixed as the soil was consolidated. This change resolved the issues of possible heat loss from the length of heater below the cell and leakage from the base of the heater.

An increase in the length of the cell body was required in order to accommodate the thicker top plate (piston).

The design of the cartridge heater and its type of wiring was also modified to allow it be screwed directly to the base plate thus eliminating the need for the copper pipe and the use of a heat transfer gel to ensure heat distribution. This resulted in the added advantage of being able to measure heat flow directly from the source, while reducing the possibility of heat loss within the pipe due to trapped air.

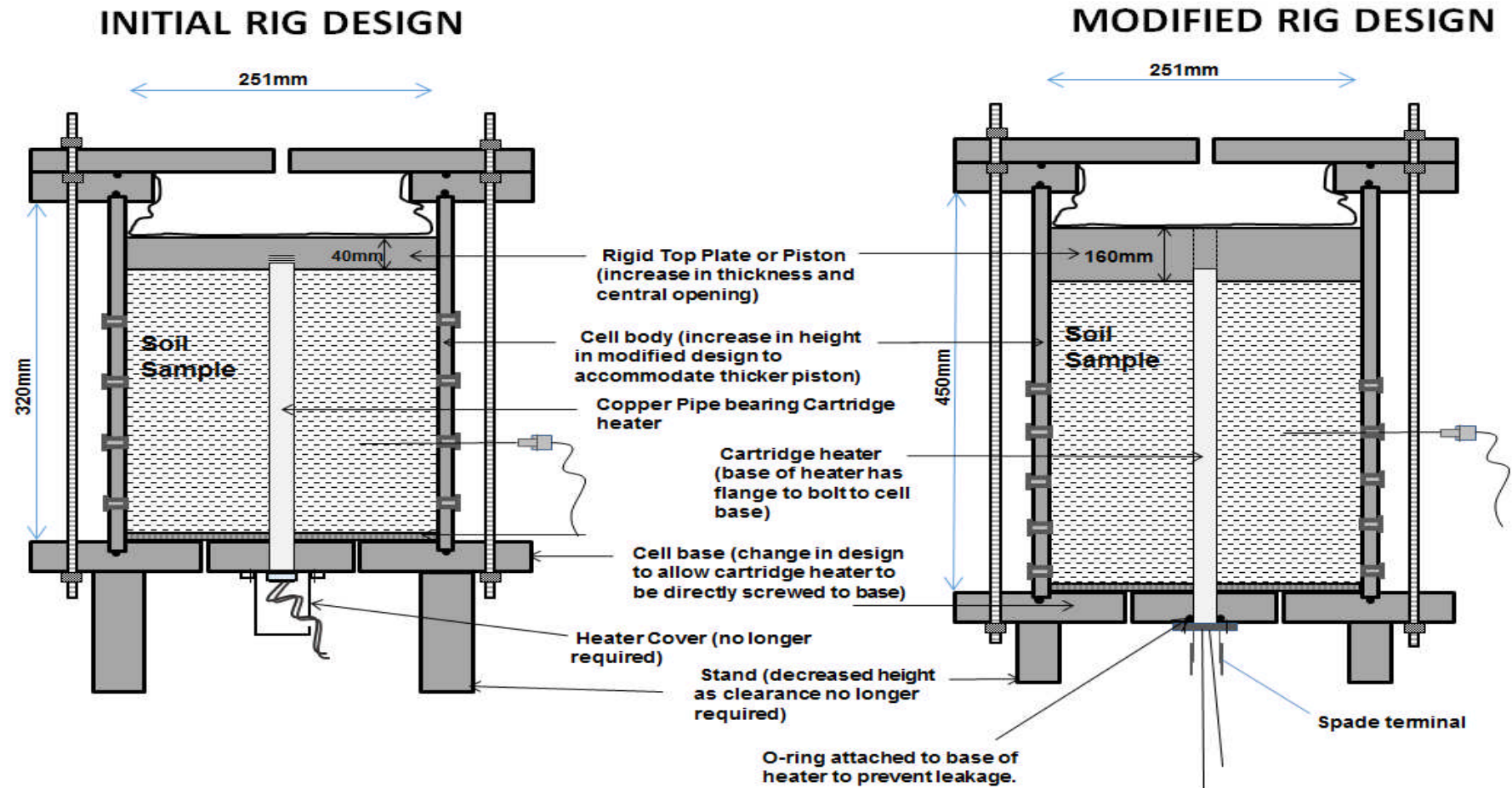


Figure 3.26: The initial rig design and the modifications made to improve its performance



During the modification to the cell base and piston, four extra heater openings were created at specified positions for the purpose of further testing to model different positions of energy piles in concrete and the effect of their interactions in future work. It is not part of this research as this research focused only on the central position modelling an energy pile in soil. The extra openings were plugged off while carrying out tests.

O-rings of different sizes were used in several places to prevent any possible leakages especially around the circumference of the base plate where the cell body is attached, and around the base of the cartridge heater as shown in Figure 3.26 on page 67.

The perforations made in the bottom plate were increased in a radial pattern to enhance better drainage of pore fluids during sample consolidation.

The modifications made to parts of the rig are described in more detail below.

### **3.6.1 Change to Design of Rigid Top Plate**

The thickness of the rigid top plate was increased from 40mm to 160mm to accommodate free upward movement of heater due to consolidation, as sample in the preliminary tests showed settlement of up to 97mm. The additional thickness was added to also prevent the rubber diaphragm from coming in direct contact with the heater to avoid damage.

The diameter of the piston was selected as 250mm to fit into the cell body with just enough room to limit friction between the cell wall and top plate as the soil consolidated.

Holes were drilled in the piston to align with the holes in the base plate. These holes were there to allow tests to be carried out with different locations of the heat source; to test the position of U-tubes in a concrete pile, for example. The holes were not used in these tests and therefore, were sealed with plugs.

The plugs were fitted with O-rings to ensure proper sealing as shown in Figure 3.27 on page 69.

Two threaded openings were made at the top of the piston to fit handles to aid in lifting the piston. Figure 3.27 (page 69), shows details of the piston and its attachments.

The piston also acts as an insulator to prevent heat loss from the cartridge heater.

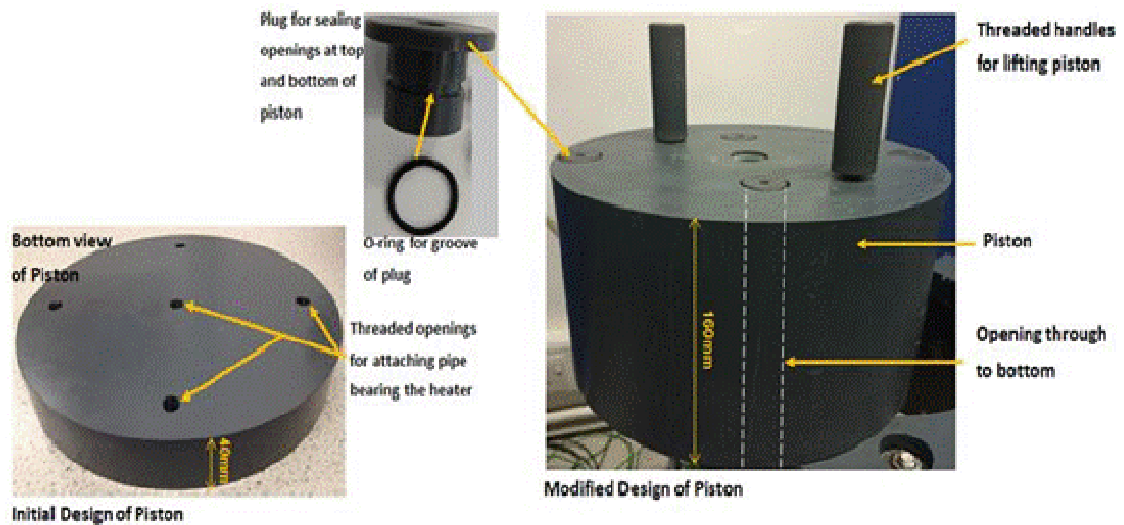


Figure 3.27: Top piston and its parts

### 3.6.2 Change in Cartridge Heater Design

The initial cartridge heater design which had a threaded base was changed to have a flange at the bottom to enable it to be screwed directly to the cell base. The heater is attached to the base of the rig by means of bolts fitted through a flange attached to its base. See Figure 3.28.

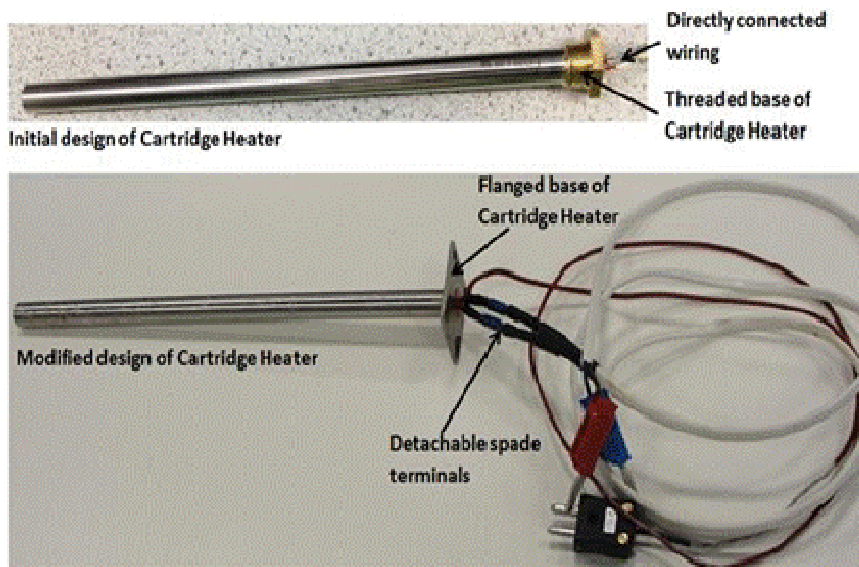


Figure 3.28: Cartridge heater

The wiring type was also changed from directly attached wires which were susceptible to damage, to detachable spade terminals. The heater is connected to the power source via 6.3mm spade terminals with 1000mm leads covered with protective sleeves. Its operational range is at 30 Volts and 90 Watts and runs on direct current.

The stainless steel cartridge heater was specially designed to fit the test rig according to specifications given to the manufacturer (Chromalox).

### 3.6.3 Change to Cell Base Design

The cell base supports the cell body. It sits on four legs to allow access to the base to attach drainage lines and electric cables.

The cell base has a central opening for the cartridge heater used in these experiments and four similar openings which were sealed with plugs for the purpose of these experiments but could be used in future similar investigations.

The cell base also has a groove around its circumference into which an O-ring of appropriate dimension is installed to ensure proper sealing when the cell body is clamped on securely. Figure 3.29 shows both the initial and modified cell base designs.

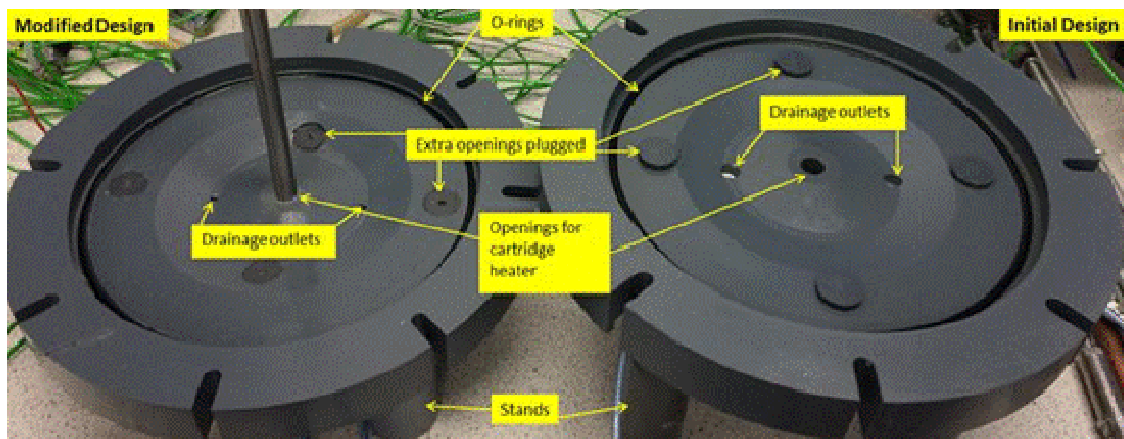


Figure 3.29: The initial and modified cell base designs

The main changes made to the cell base are:

- 1) The stands were re-designed to be shorter than the previous stands as the need for clearance required for heater movement was eliminated in the rig modification
- 2) The openings for the cartridge heater have grooves around their circumference for O-rings to ensure proper sealing and prevent leakage as shown in Figure 3.30 (page 71). There are also provisions made around the openings for bolts to secure the base of the cartridge heater
- 3) The positions of the openings made for the cartridge heater changed slightly from that of the initial design to enable the study of heater interactions based on distances from each other in future study

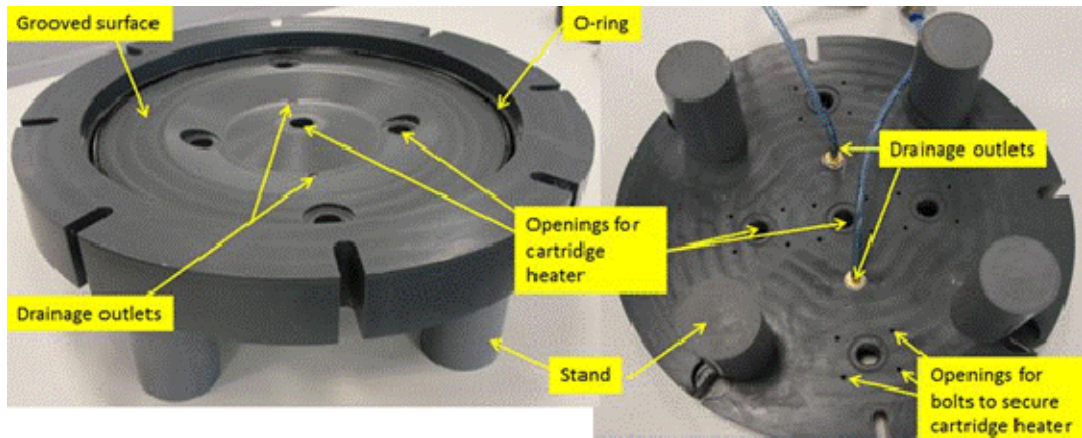


Figure 3.30: Top and bottom views of modified cell base

- 4) Plugs were fabricated in the same diameter as the heater to seal off the openings not in use during these experiments. As can be seen in Figure 3.29 (page 70), the surfaces around the openings are designed to flush with the top of the plugs unlike in the initial design where the plugs stood proud of its surrounding surface.
- 5) The cell base surface as shown in Figure 3.30 is grooved to allow easier drainage of pore pressures. Figure 3.30 also shows the top and bottom views of the cell base.

### 3.6.4 Change in Design of Cell Body

The cell body was designed with an additional increase in height of 130mm to accommodate the new top plate as shown in Figure 3.31.

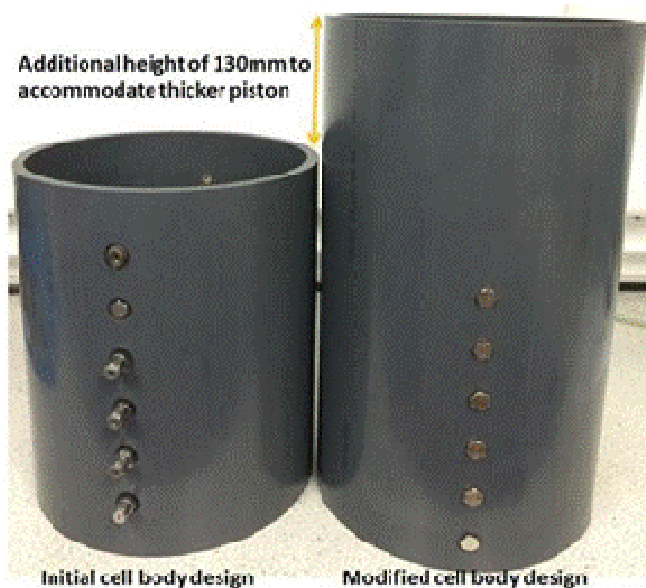


Figure 3.31: Modification of Cell body

The diameter and cell wall thickness remained the same. An additional probe opening was made in the modified cell wall to enable more probes to be inserted into the test chamber. In the initial design of the cell body, the lowest probe position was placed approximately 45mm from the base while in the modified cell body, it was placed 20mm from base.

### 3.6.5 Change in Design of Perforated Bottom Plate

Changes were made to the perforated bottom plate. Although both are of the same thickness (10mm), the positioning of the openings for the cartridge heater were changed to align them with those in the base and top plate.

In the modified design, additional perforations were made in the bottom plate in a more defined radial pattern to facilitate drainage of pore water pressures. The changes are shown in figure 3.32.

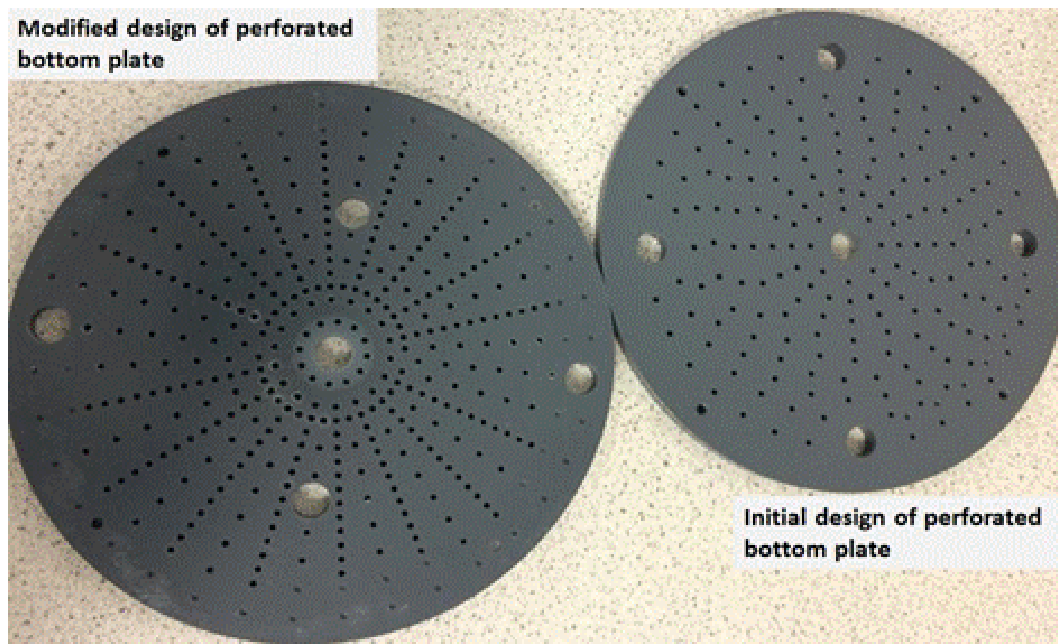
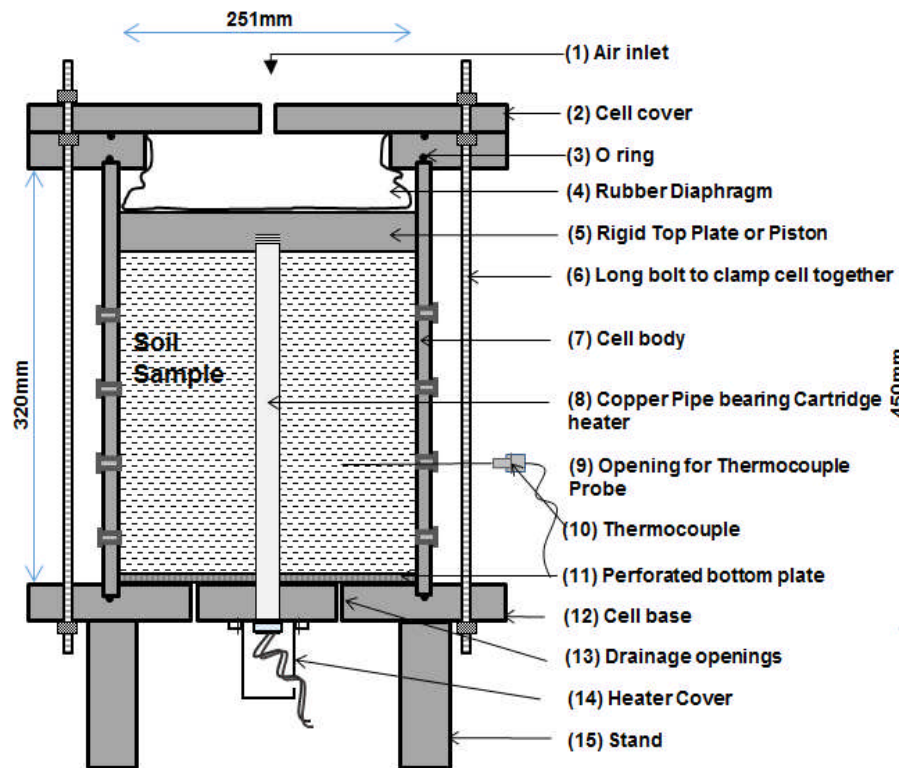


Figure 3.32: Top view of initial and modified bottom plates

## 3.7 Description of Modified Test Rig

Figure 3.33 on page 73 shows diagrams of both rig designs side by side to highlight the differences due to design change, while the modified test rig is described subsequently.

### A: INITIAL RIG DESIGN



### B: MODIFIED RIG DESIGN

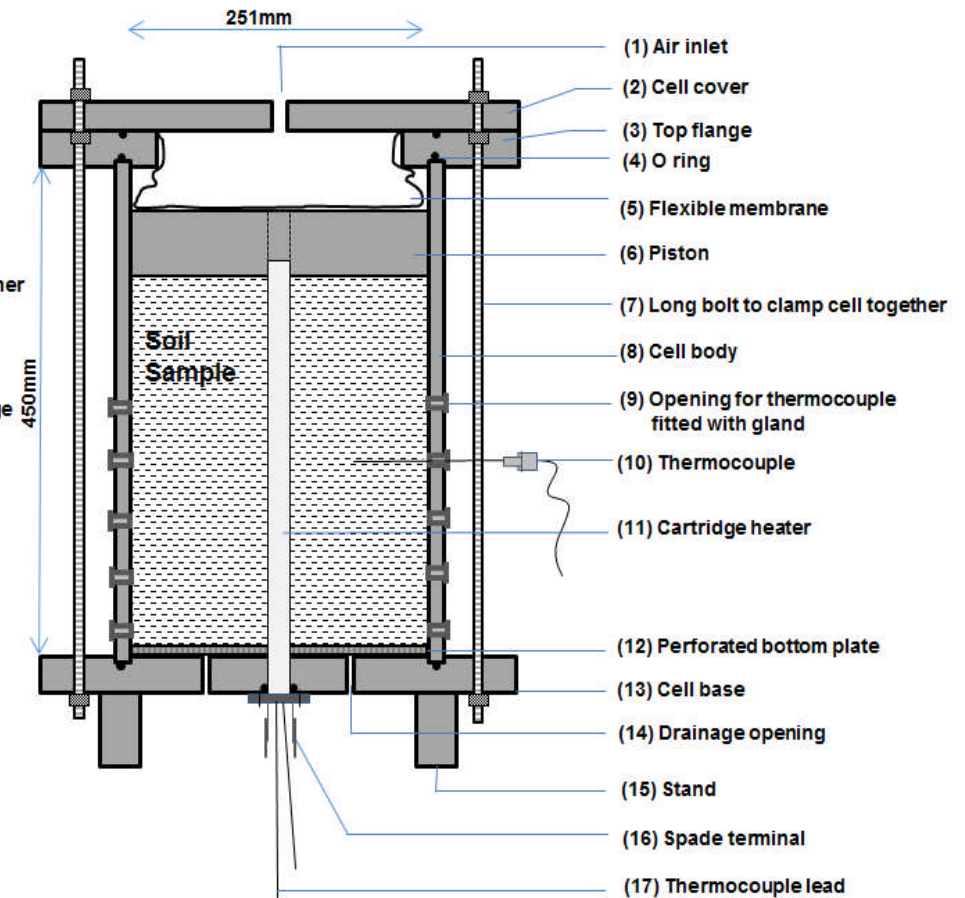


Figure 3.33: Diagrams of initial and modified rig designs

The sample of soil to be tested (Figure 3.33B) is within a cylindrical test cell also referred to as the cell body (8). This chamber is made from HDPE.

There are openings (9) fitted with glands, down the sides of the cell to enable insertion of thermocouples for monitoring temperature changes within the chamber.

A piston (6) placed on top of the sample is pressurised by introducing pressurized air through a flexible membrane (5) to simulate an element of soil at some depth below the ground surface, and operates by using a consolidation mechanism similar to the Rowe cell (Head, 2006). The piston also has a central opening through which a cartridge heater (11) can slide upwards as the piston pushes downwards on the sample. The piston is also made of HDPE and acts as an insulator to prevent heat loss from the cartridge heater.

The base of the cell (13) is fitted with a perforated plate (12) to allow excess pore water pressures to dissipate and drain out through drainage openings (14) in cell base. Both the cell base and perforated plates are made of HDPE.

The cell base also has a central opening through which the cartridge heater is fitted from the base of the cell into the test chamber. The cell cover and cell base are clamped to the cell body by long bolts (7), to provide a watertight seal by compressing the O-rings between the cell base and cell wall.

### **3.8 Assembling of the Rig**

This section explains the step by step procedures in setting up of the rig for a typical experiment. With the use of photographs to aid the descriptions, the processes involved are described in three main tasks which involve:

1. Setting up the cell base and its components
2. Setting up the cell body and its components
3. Attaching the cell cover to the test chamber

#### **3.8.1 Task 1: Setting up the cell base and its components**

The first task is to set up the cell base. Several steps are required to do this and are listed as follows:

- 1) The four stands are screwed into threaded openings in the bottom of the cell base by means of threaded bolts attached to the stands as shown in Figure 3.34 on page 75.

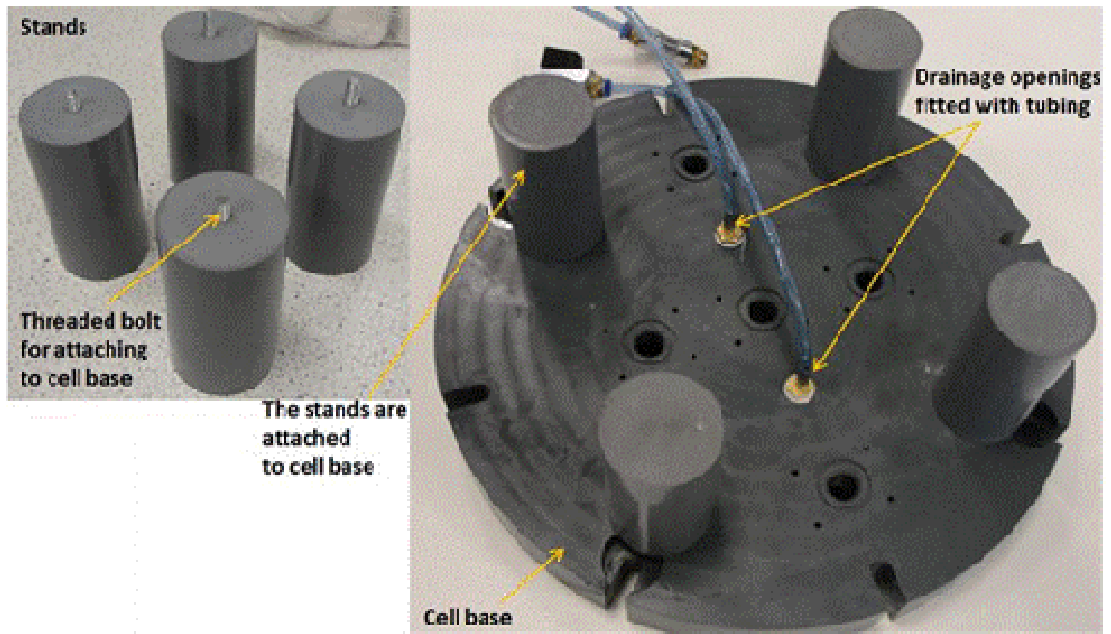


Figure 3.34: Assembling the cell base

- 2) The openings provided for drainage are fitted with drainage fittings and tubing as shown in Figure 3.34.
- 3) An O-ring of appropriate dimension is installed into the groove around the circumference of the cell base as shown in Figure 3.35.
- 4) The other openings that are not in use during the test are sealed off with blanking plugs fitted with O-rings to ensure proper sealing. The O-rings are fitted into grooves around the stem of the plug as shown in Figure 3.35.

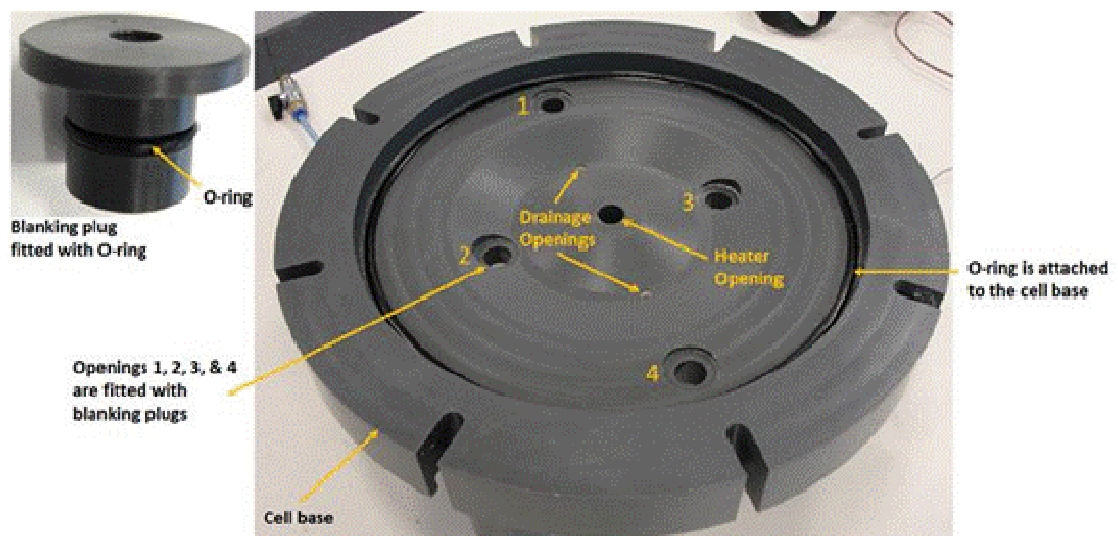


Figure 3.35: Setting up of the cell base with O-rings and plugs



- 5) In the next step, an O-ring of appropriate dimensions is fitted into the groove of the central opening and the cartridge heater is fitted through the opening.
- 6) The heater is secured in place by bolts screwed through the flange onto the cell base as shown in Figure 3.36.

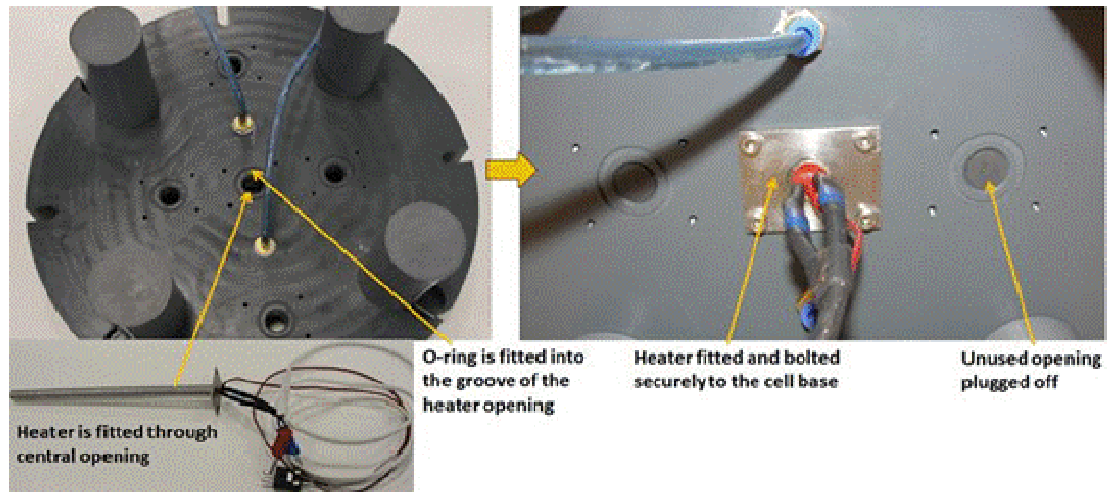


Figure 3.36: Installing the cartridge heater

- 7) The final step in this task is to slide the perforated bottom plate over the heater through its central opening, onto the surface of the cell base as shown in Figure 3.37. The plate is then lined with filter paper to keep sample in place while allowing drainage of water. The filter paper was placed over the heater by making a central opening in it.

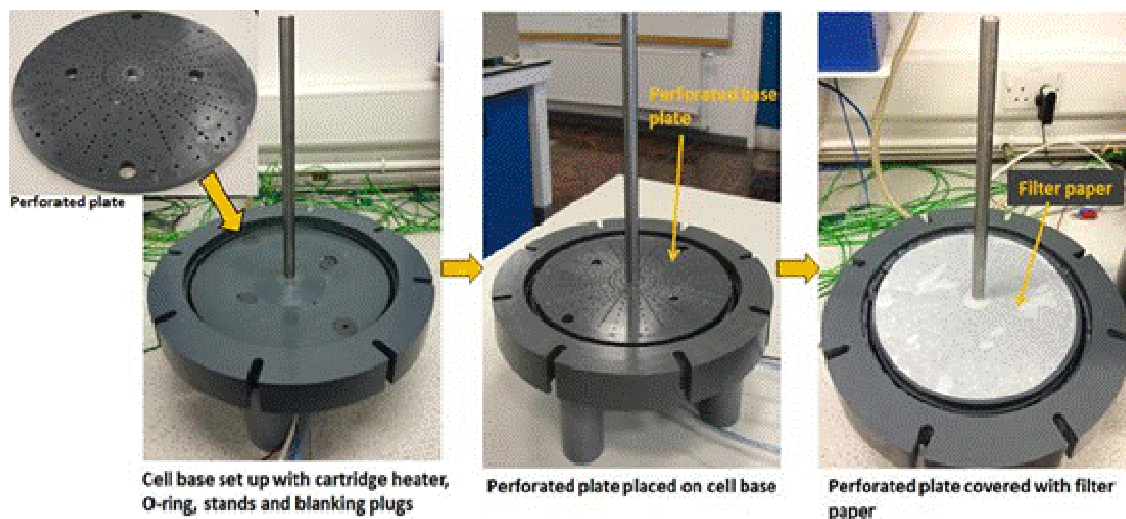


Figure 3.37: Assembling the test rig showing the base plate with the cartridge heater in place and filter paper to allow excess pore pressures to dissipate as pore fluid is drained from the sample

### 3.8.2 Task 2: Setting up the cell body and its components

Several steps are required in this task:

- 1) The openings on the cell body are threaded to enable them be sealed off with threaded blanking plugs as shown in Figure 3.38. This is to prepare the cell body to be loaded with sample and to prevent any leakage when pressure is applied to the sample in the cell. The plugs are replaced with Swagelok glands after the sample is consolidated.

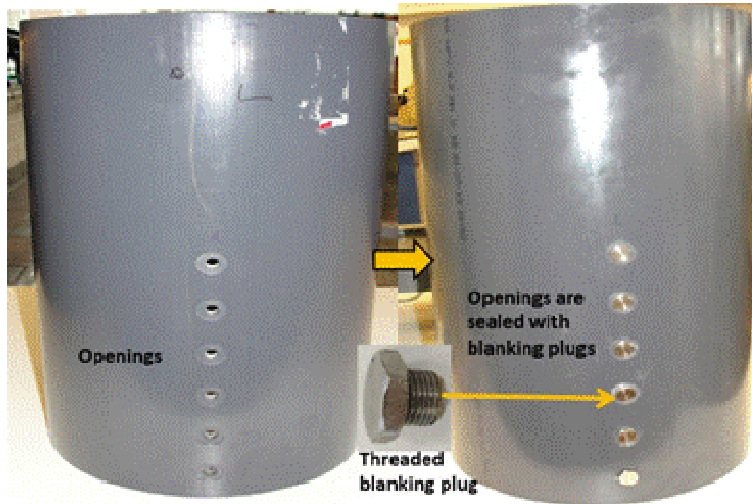


Figure 3.38: Sealing the openings on the cell body for sample loading

- 2) The cell body is then placed over the already set-up cell base as shown in Figure 3.39. It is important to ensure that the openings are accessible.

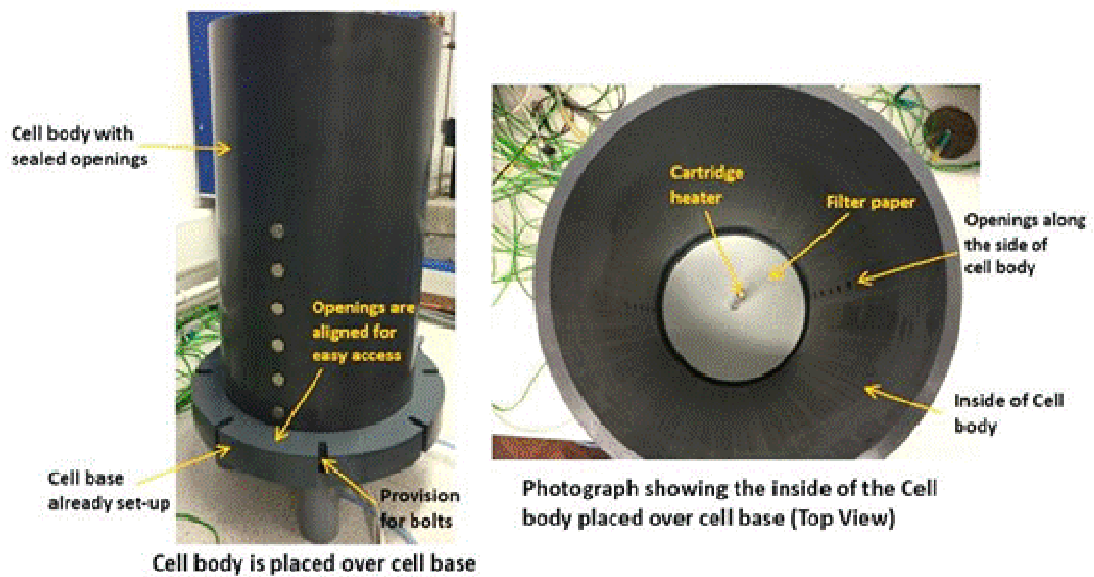


Figure 3.39: Photograph showing (a) the cell body fitted into the already set-up cell base; and (b) the inside of the test chamber from top view

- 3) An O-ring of appropriate dimension is fitted into the groove around the circumference of the top flange as shown in Figure 3.40. The top flange is then mounted onto the cell body as shown in Figure 3.40. The presence of the O-ring is to ensure air-tight sealing of the rig when in testing operation.

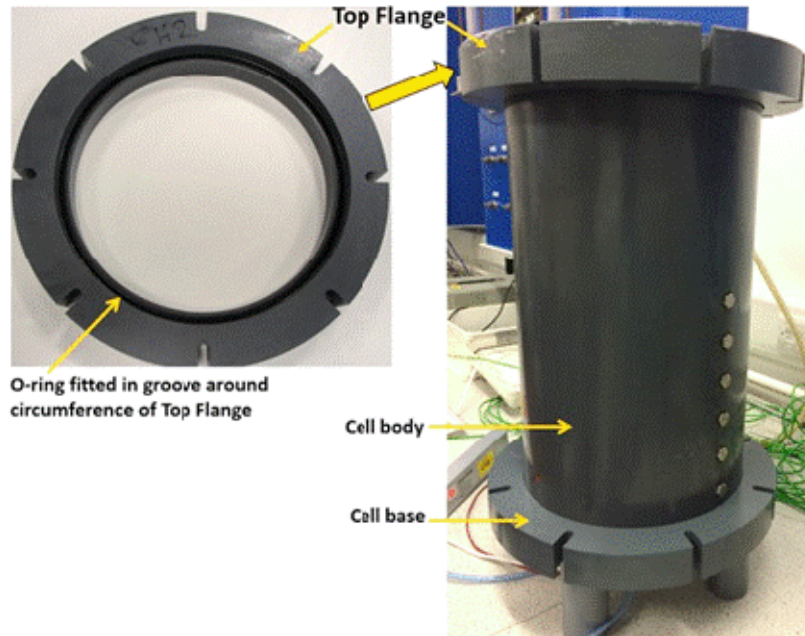


Figure 3.40: Top flange mounted on cell body

- 4) The final step in this task is to attach the cell body firmly to the cell base by clamping the top flange to the cell base using threaded iron bars, nuts and washers. This is illustrated in Figure 3.41.

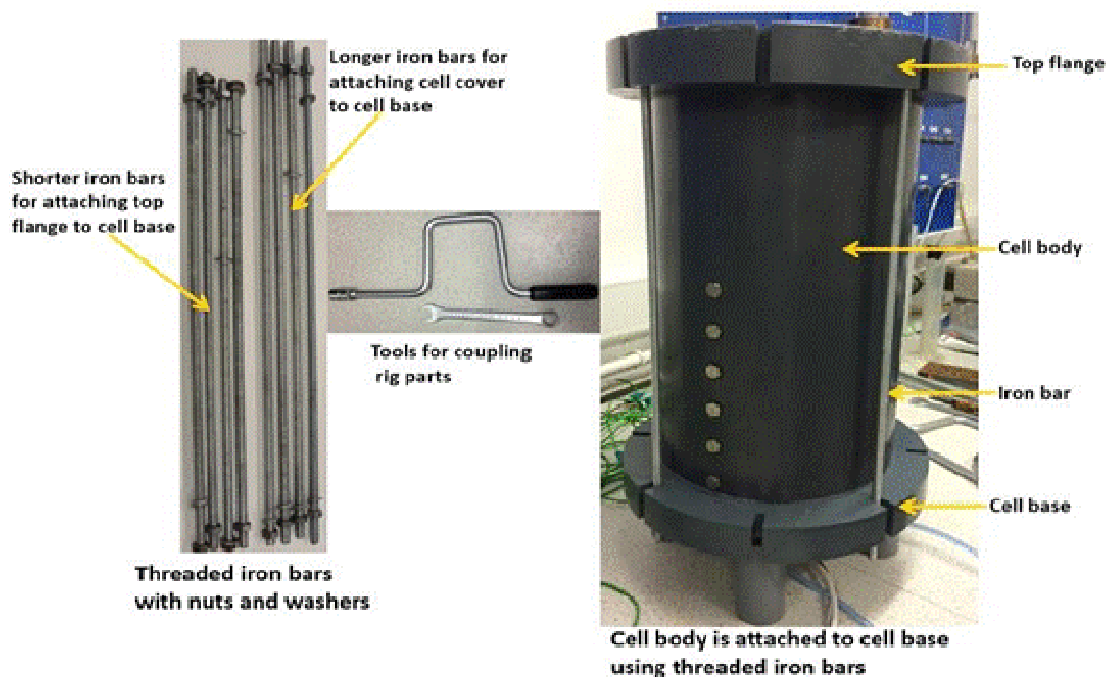


Figure 3.41: The test chamber (cell body and cell base) is bolted in place by threaded iron bars

At this stage, the cell body is ready to be loaded with the soil slurry which is described in the next subsection.

### 3.8.2.1 Loading the Rig Chamber

The soil slurry is carefully loaded by hand into the test chamber up to almost level with the cartridge heater, as shown in Figure 3.42.

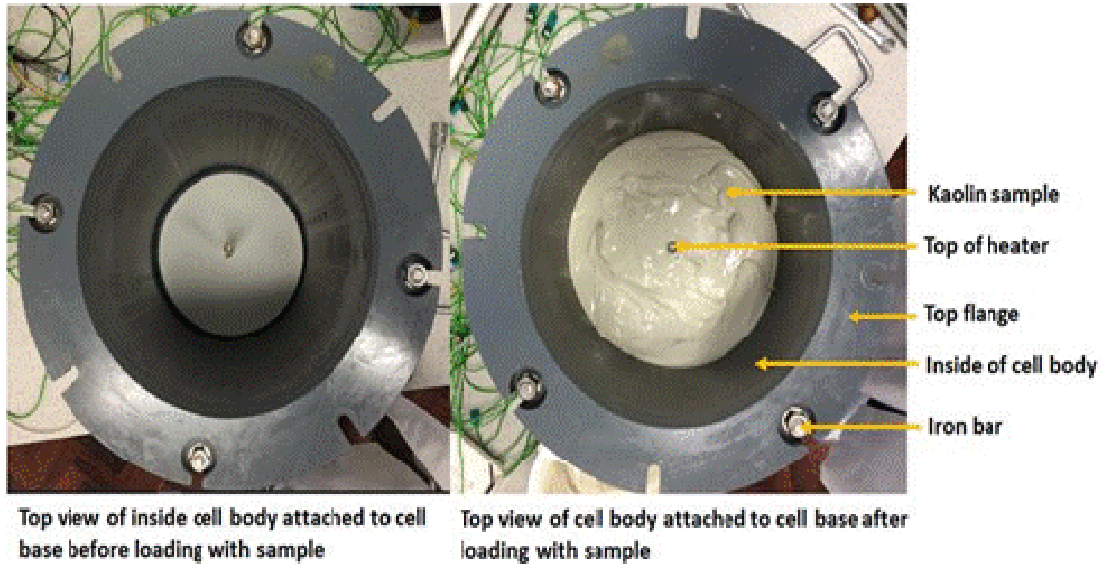


Figure 3.42: Inside the test chamber loaded with sample

The sample is placed in such a way to eliminate air that may be present in the sample. The sample in the rig is allowed to stabilize to the controlled room temperature.

The piston is then placed over the sample so that the top of the cartridge heater fits through its central opening (Figure 3.43A). This allows for free downward movement of the piston as sample consolidates. The piston accommodates the heater exposed by the settlement of the sample and also acts as an insulator to prevent heat loss.

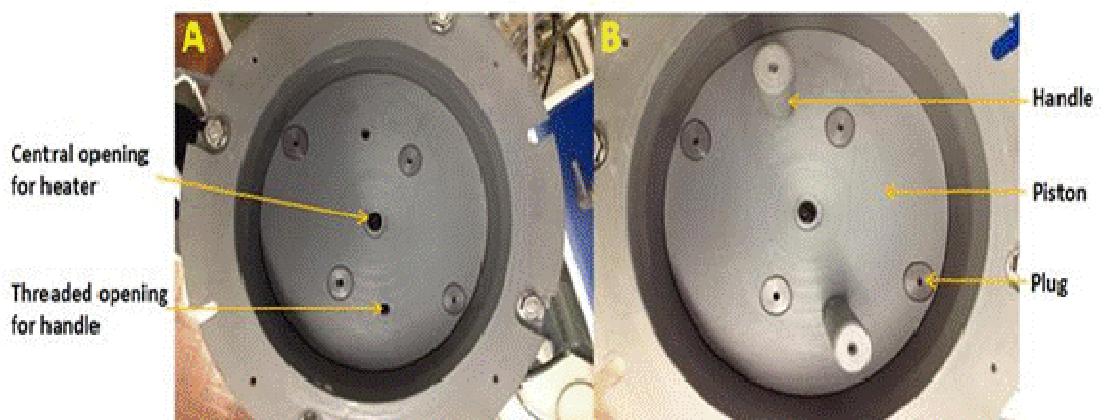


Figure 3.43: Top piston placed over sample

The piston is lowered over the sample using the handles provided for this purpose as shown in Figure 3.43B, and then removed afterwards.

The cell cover fitted with the flexible rubber diaphragm as shown in Figure 3.44, is placed over the top flange and clamped to the cell base with another set of threaded iron bars. This concludes the setting up process.

### 3.8.3 Task 3: Attaching the cell cover to the test chamber

This final task involves attaching the cell cover to the test chamber already set up in tasks one and two.

The cell cover, to which the rubber diaphragm is attached, is placed over the top flange and clamped to the cell base with the longer set of threaded iron bars which are tightened across to balance the torque. This is shown in Figure 3.44.



Figure 3.44: Attaching the cell cover to the test chamber

## 3.9 Test set up

After setting up the rig, an air pressure supply unit is connected through valves on the cell cover to introduce air pressure which is uniformly distributed over the sample by the rubber diaphragm.

When consolidation of the sample is complete, power is supplied to the cartridge heater from a laboratory direct current power supply source. Thermocouples are fitted through the Swagelok openings on the sides of the cell body at specific distances from

the heat source to measure temperature changes across the sample. The thermocouples are connected to a data logger which is set to record the temperature changes at regular intervals. The data is stored in the logger until retrieved using a laptop programmed with the appropriate data logger software. Figure 3.45 shows a test set up in operation.

Detailed drawings showing dimensions and specifications of the various parts of the rig are attached in the Appendix.

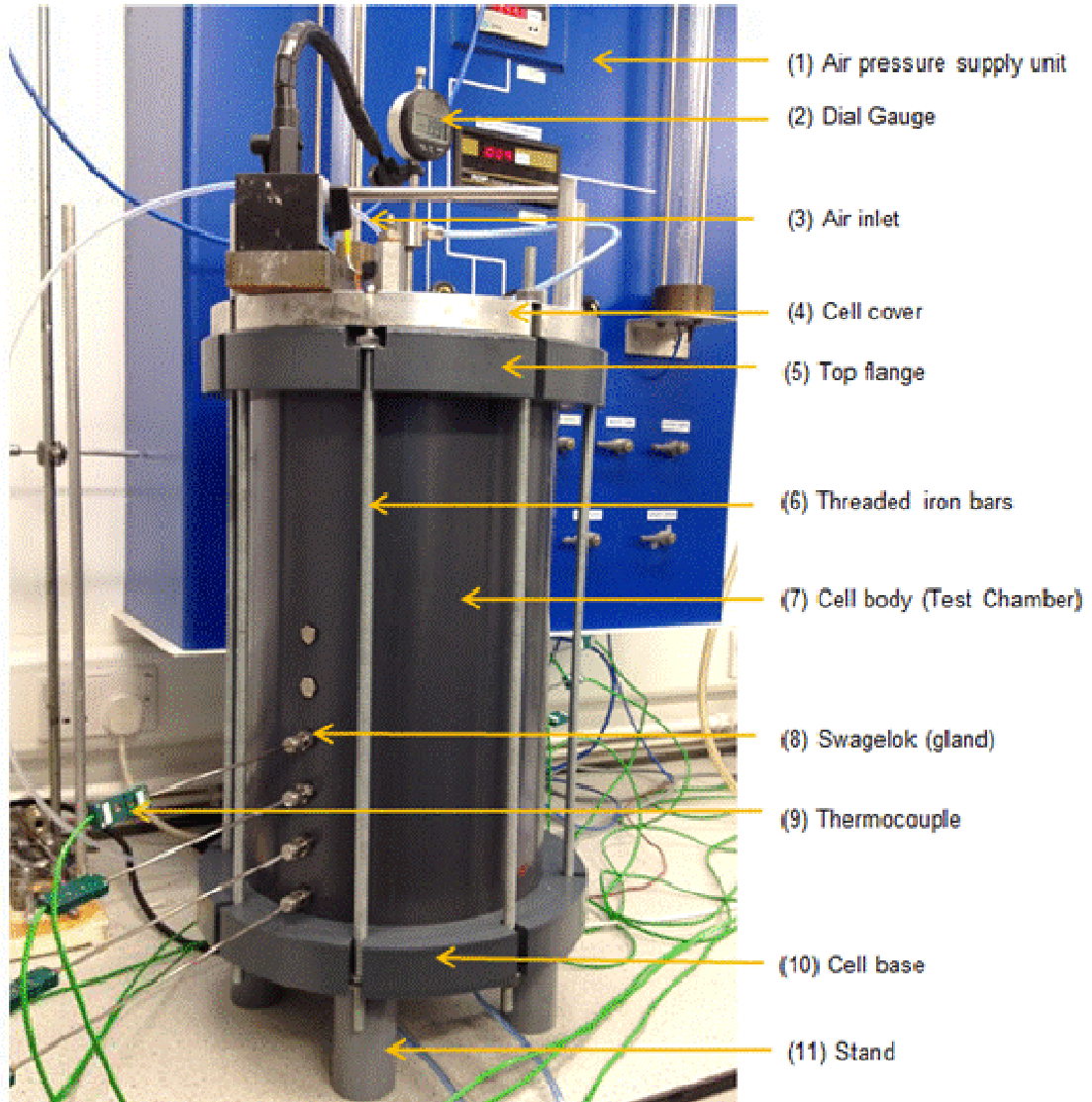


Figure 3.45: An overview of test set up in the modified rig

### 3.10 Summary of Features of the Rig that met Design Criteria

The test that was run after the modified rig was set up was observed closely to ensure that the design criteria had been met.

The increased thickness of the piston allowed for free upward movement of the cartridge heater during sample consolidation and also resolved the issues of heat loss and water leakage from the base of the heater. The use of different sizes of O-rings especially around the circumference of the base plate to which the cell body was attached, and around the base of the cartridge heater, also prevented water leakages.

The re-design of the cartridge heater and spade wiring which allowed it to be screwed directly to the base plate, eliminated the need for the copper pipe and the heat variations between the heater and pipe earlier encountered. This also ensured heat flow directly from the heat source into the sample.

Better drainage of pore fluids during sample consolidation was enhanced by the increased perforations made in the bottom plate in a radial pattern.

With the two main problems of water leakage, and temperature differences along the heater length and between the heater and copper pipe wall resolved by the modifications to the initial rig design, a graph is presented in Figure 3.46 shows the temperature variations across the sample at the top and bottom of rig, and in comparison to the theoretically predicted variation.

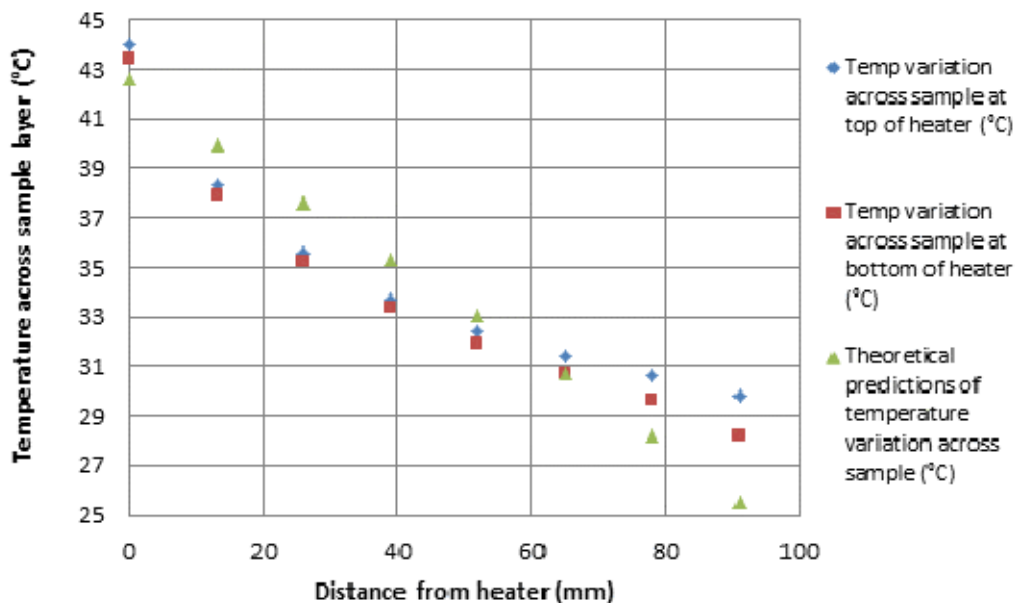


Figure 3.46: Temperature variations across the sample compared to the theoretical variation

When compared with Figure 3.25 (page 66), which shows the temperature variations across sample in the initial rig design, Figure 3.46 shows a more uniform temperature at the top and bottom of the heater and thus, improvement in heat transfer within the system. The disparities observed between actual and predicted variations are discussed in more detail in Chapter 7.

In conclusion after the set up of the modified rig, the details of the procedures involved in carrying out a test are discussed in the next chapter.

### **3.11 Conclusion**

In this chapter, the design concept, materials and testing parameters were presented and discussed. The design aspects and justifications for the parameters and materials selection for fabricating the rig were also discussed. The rig was commissioned. The problems detected and encountered during the commissioning of the rig, were presented alongside the need for modifications, which were made to the initial design to make it fit for purpose. The step by step procedures for setting up both the initial and modified rigs were described in detail. Both rig designs were then compared and the changes to the design explained.

The test procedure will be discussed in Chapter 4.



## **Chapter 4 Test Procedure and Typical Results**

### **4.1 Introduction**

Following on from chapter 3 where the test rig, its components and assembly were described, this chapter focuses on details of the test procedure which covers the following areas:

- 1) Instrumentation and leakage checks
- 2) Sample materials and preparation procedure
- 3) Tests for the purpose of studying heat dissipation through kaolin, sand and mixtures of kaolin and sand in varying proportions while controlling parameters such as water content, temperature/power, heating cycles, pressure load, and time taken in order to study their effects on the soil thermal behaviour. To achieve this, a heater was centrally placed in the sample while measuring and recording temperature changes within a sample at specified intervals and the time taken for the sample to heat up and cool down was recorded.
- 4) Analysis of soil properties after the tests
- 5) An overview of typical test results

### **4.2 Instrumentation and Leakage Testing of Rig and its Components**

Instrumentation and leakage tests were carried out on the rig to ensure it performed according to the design expectations and was compatible with other instruments and equipment required in setting up the experiment.

The leakage test consisted of setting up the rig as described in chapter 3 and then filling it with water to detect any leakages. It was successful with the modified rig design as no leakage was observed as was the case of the first rig design.

In the instrumentation test, the cartridge heater and its electrical components were tested to ensure they were in good working condition.

The heater was tested in detail with the aim of establishing its temperature response to a specific power input by connecting it to a power supply unit and adjusting the current and the voltage.

The heater was first tested in water and in kaolin samples held in a glass jar (Figure 4.1 on page 85) to test its performance which was easier to monitor in the jar, before

proceeding to use it in various tests within samples in the rig. The reason for this was to test the cartridge heater, thermocouples, power supply unit and data-logger and study how they work within a small sample of kaolin, towards gaining a better understanding of how the heating component of the rig works.

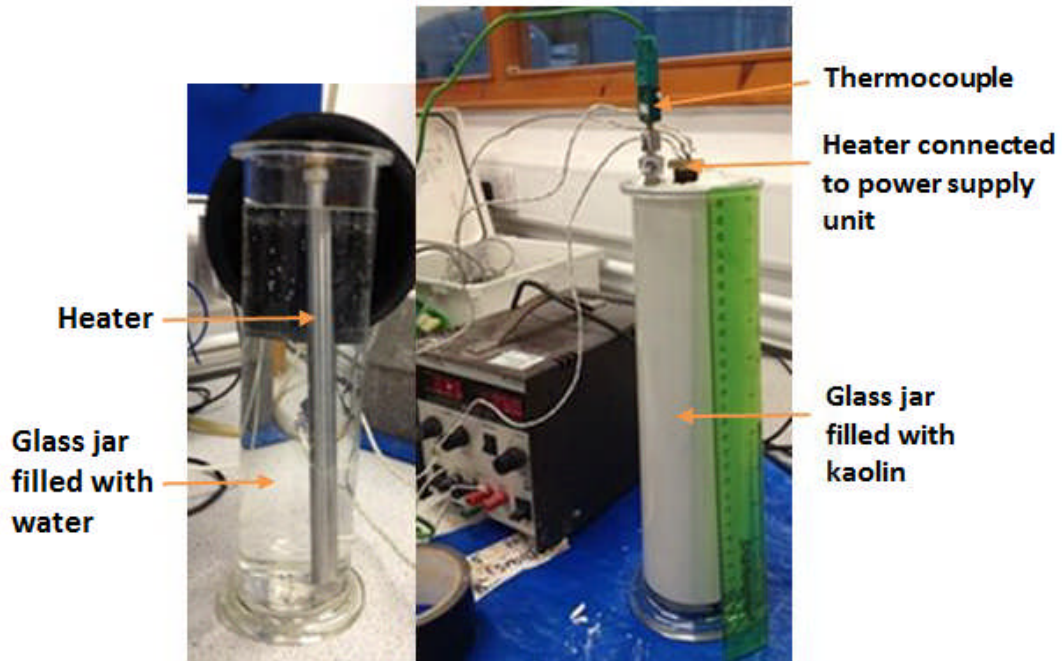


Figure 4.1: The cartridge heater being tested on a small scale to establish its temperature response to power input

### 4.3 Typical Test Procedure

This section describes a typical test procedure which consists of the following five phases:

- 1) Sample preparation
- 2) Consolidation
- 3) Equilibrium testing
- 4) Thermal Cycles
- 5) Assessing the Soil Properties

#### 4.3.1 Sample Preparation

Due to the varied composition of natural soils, soil behaviour is often studied using artificial soils (Mitchell and Soga, 2005). In order to represent the ground element of an energy pile, three types of soils were studied: clay, sand and composite soil formed of clay and sand. Kaolin and Leighton Buzzard sand were used to study the behaviour of fine grained soils and also because they are typical laboratory soils with standard

properties which can be controlled and studied. Composite soils were formed of mixtures of kaolin and sand in the proportions 75:25, 50:50 and 25:75.

#### **4.3.1.1 Materials/Equipment Required**

The materials and equipment required in the sample preparation process include:

- 1) Kaolin powder (high grade laboratory type)
- 2) Leighton Buzzard Sand (fraction size C; 600um-300um)
- 3) Leighton Buzzard Sand (fraction size D; 300um-150um)
- 4) Industrial Mixer with all its electrical components
- 5) Weighing scale
- 6) Distilled Water
- 7) Plastic buckets and scoops

#### **4.3.1.2 Sample Preparation Process**

Since the thermal properties of clay, sand, water and air are different, it follows therefore, that the thermal properties of any soil will depend on the proportion of clay, sand, water and air within a sample. The sample preparation process therefore, involved mixing kaolin powder with distilled water to achieve specific water content, and also mixing specific quantities of kaolin, sand and distilled water to form composite soil samples.

Although the samples used in each test varied from each other in terms of water content and soil type/composition, the mixing process was similar in each case. The mixing processes of the different samples are described in the following sub-sections.

#### **4.3.1.3 Kaolin Sample Mixture**

This section describes the processes involved in preparing kaolin slurry at approximately 82% water content, at which the saturation level is approximately 150% of its liquid limit in order to limit the amount of trapped air in the sample.

The weight of distilled water and kaolin powder required to produce the desired water content of slurry was first of all determined, and in the case of a kaolin slurry with 82% water content, typically 12.5kg of Kaolin powder was mixed with 10.1kg of distilled water to yield the quantity of sample required to fill the test chamber of the rig up to the level of the cartridge heater.

The sample mixing process takes place within an extraction chamber to minimize inhalation of the kaolin particles. The set-up is shown in Figure 4.2 on page 87.

The distilled water was poured into the bowl of the mixer and it was switched on, after which the kaolin powder was carefully added scoop by scoop as shown in Figure 4.3, and the mixing process was continued until the mixture turned to smooth slurry.



Figure 4.2: A mixing unit set up inside an extraction chamber for mixing samples



Figure 4.3: Photo showing kaolin sample mixing process where kaolin powder is being added to the distilled water in the mixer bowl

On completion of the mixing process, the slurry was transferred from the mixer into clean and dry plastic buckets with lids for easier movement and onward loading into the test rig (Figure 4.4A). At this stage, several samples were collected for the determination of the actual water content of the prepared mixture (Figure 4.4B) as specified in BS:1377 (Head, 2006).

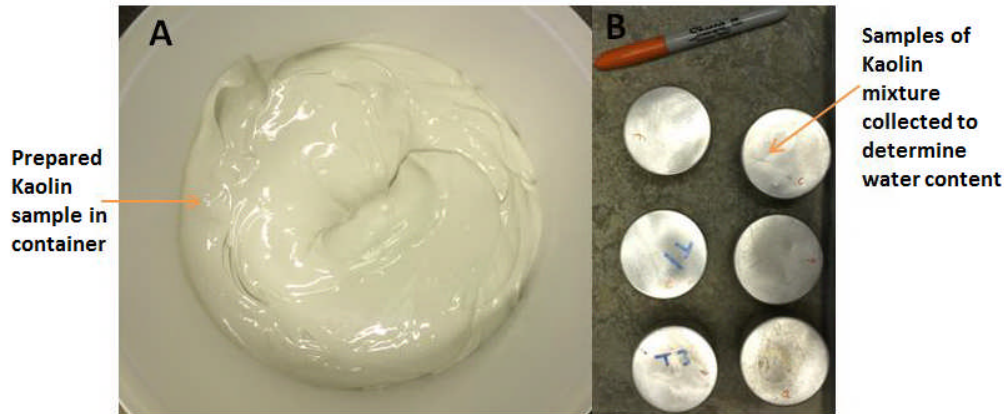


Figure 4.4: Photo showing (a) Well mixed kaolin sample ready for testing (b) Kaolin samples collected for determination of actual water content of prepared sample

Following the procedure described earlier (pages 86 & 87),, a total of five samples were prepared for both preliminary tests and subsequent tests carried out under varying overburden pressures of 25, 50, 100, & 200kPa.

#### 4.3.1.4 Kaolin Sample Mixture for Control Test

A separate sample was prepared following the procedure described earlier (pages 86 & 87), but with different proportions of kaolin powder to distilled water in order to achieve a slurry with approximate water content of 85%. 12kg Kaolin powder and 10kg distilled water was used to obtain this. The purpose of this sample was to serve as comparison with the other samples of lower water content to further study the impact of water content on thermal properties of soil, and was tested at 0, 25 and 50kPa.

#### 4.3.1.5 Kaolin Sand Sample Mixture (Kaolin to Sand ratio is 3:1)

This sample was prepared with three parts of kaolin powder to one part of sand. It required combining 11.25kg kaolin powder with 3.75kg sand. The 3.75kg of sand was comprised of 1.25kg fraction C and 2.5kg fraction D. 9kg of distilled water was used in preparing this sample. The distilled water and kaolin powder were mixed following the standard process described earlier (pages 86 & 87) and the sand was gradually mixed in until a smooth consistency was achieved as shown in Figure 4.5 on page 89. The average water content of this sample as determined by the water content test was

59%. Two sets of this sample were prepared and loaded into two separate rigs. One test was run at 25kPa while the other at 100kPa.



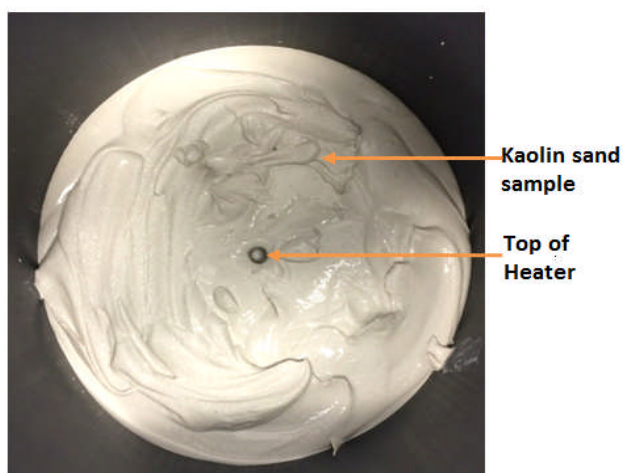
Figure 4.5: Photo showing sample mixture of three parts of kaolin to one part of sand in the test chamber

#### 4.3.1.6 Kaolin Sand Sample Mixture (Kaolin to Sand ratio is 1:1)

This sample was prepared with one part of kaolin powder to one part of sand. It required combining 9kg kaolin powder with 9kg sand. The 9kg of sand was comprised of 3kg fraction C and 6kg fraction D. 8kg of distilled water was used in preparing this sample.

The distilled water and kaolin powder were mixed following the standard process described earlier (pages 86 & 87), and the sand was gradually mixed in until a smooth consistency was obtained. The average water content of this sample as determined by the water content test was 44.4%.

The prepared sample was loaded into the rig as shown in Figure 4.6 and tested first at 25kPa, then at 50kPa and finally at 100kPa.



**Sample mixture of one part kaolin to one part sand**

Figure 4.6: Photo showing sample mixture of one part of kaolin to one part of sand in test chamber

#### 4.3.1.7 Kaolin Sand Sample Mixture (Kaolin to Sand ratio is 1:3)

This sample was prepared with one part of kaolin powder to three parts of sand. It required combining 5kg kaolin powder with 15kg sand. The 15kg of sand was comprised of 5kg fraction C and 10kg fraction D. 6.4kg of distilled water was used to prepare this sample based on the calculation that 3.9kg of distilled water was required to saturate the sand, while 2.5kg of water was required to achieve 50% water content for the weight of kaolin powder used.

The distilled water and kaolin powder were mixed following the standard process described earlier (pages 86 & 87), and the sand was gradually missed in until smooth. The average water content of this sample as determined by the water content test was 32%.

The prepared sample was loaded into the rig as shown in Figure 4.7 and tested first at 25kPa, then at 50kPa and finally at 100kPa.



**Sample mixture of one part kaolin to three parts sand**

Figure 4.7: Photo showing sample mixture of one part of kaolin to one three parts of sand in test chamber

#### 4.3.1.8 Dry Sand Sample

In the case of dry sand, 1 part of fraction C grain size sand was mixed with 2 parts of fraction D grain size sand (5.5kg fraction C: 11kg fraction D giving total mass of 16.5kg).

The sand mixture was poured carefully into the test chamber of the rig after setting up the rig for sample loading. To prevent the sand from sticking to the piston as a result of statics, a layer of filter paper was placed over the top of the sand after perforating it in

the centre to create an opening for the top of the heater. The process of loading the sand sample is shown in Figure 4.8.

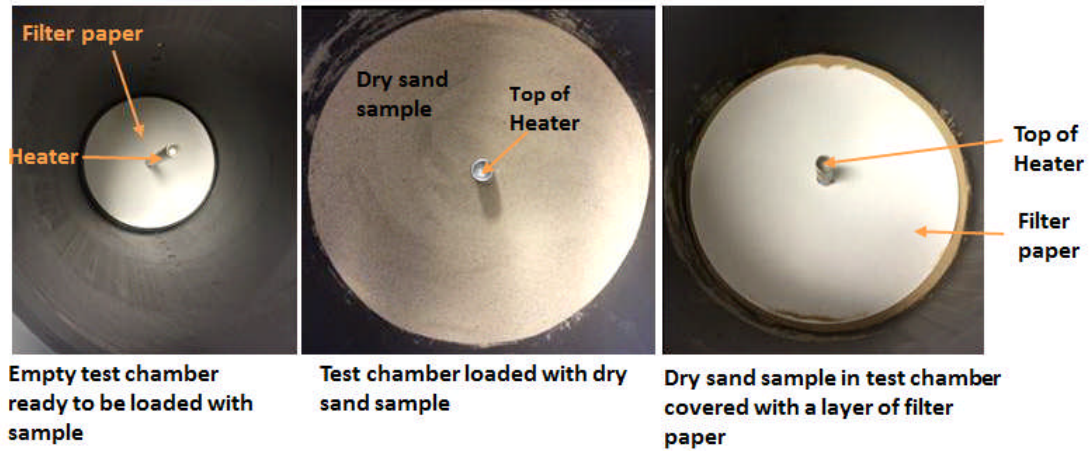


Figure 4.8: Photo showing process of loading test chamber with dry sand sample before testing

The cell cover was put in place and pressure load of 25kPa was applied in preparation for testing.

#### 4.3.1.9 Saturated Sand Sample

Dry sand of the same proportion as the previous sample was loaded into the test rig following the same process. While in the test chamber, the sample was saturated by connecting a vacuum pump to the rig to suck out air from the system so that while the air was being sucked out, water connected to the rig through the drainage openings of the test chamber was sucked up into the sand sample to replace the air and saturate the sample. 4.3kg of distilled water was required to saturate the dry sand weighing 16.5kg. Figure 4.9 on page 92, shows the vacuum pump attached to the test rig during the process of saturating the sand sample.

#### 4.3.2 Consolidation Phase

As described in Chapter 3, the prepared sample was carefully placed into the test chamber in layers to exclude as much air as possible to achieve full saturation. The top of the cell was assembled and the pressure applied to consolidate the sample.

Tests were carried out on the samples at overburden pressures of 0kPa, 25kPa, 50kPa, 100kPa and 200kPa to simulate depths below 20m.

The drainage valves were opened to release pore water pressure resulting from the applied load. The fluid was collected in cylinders via tubing connected to the drainage openings as shown in Figure 4.10 on page 93.





Figure 4.9: Photo showing the process of preparation of saturated sand sample where water is connected to the rig through the drainage tubing and the vacuum pump is connected to the rig to suck out air from the sample while drawing water into the sample

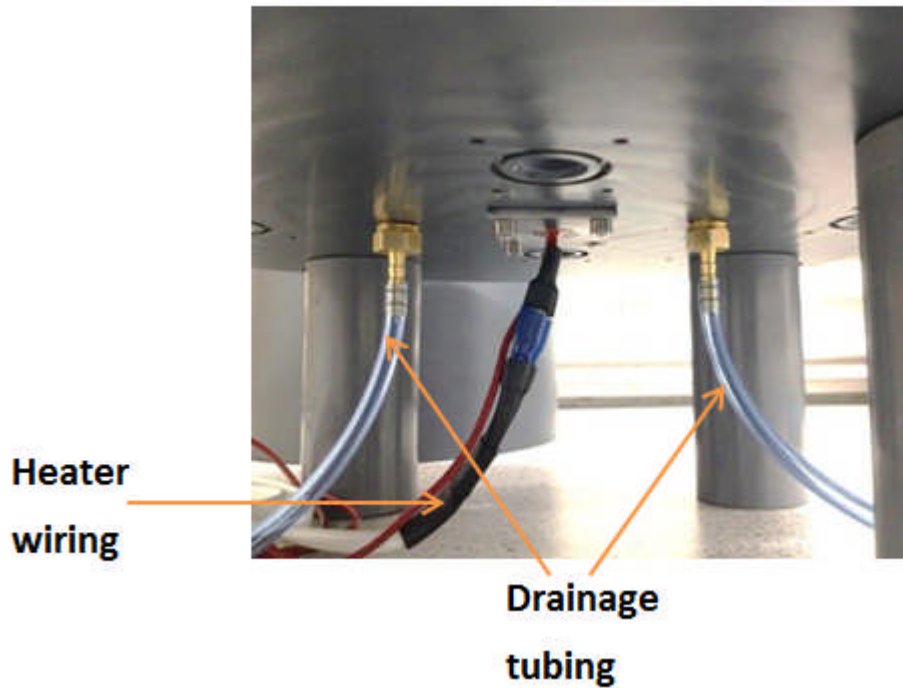


Figure 4.10: Photo showing drainage tubing connected at bottom of cell base to collect water expelled from sample during consolidation

The settlement of the piston and the volume of expelled water were measured to establish the end of consolidation and determine the consolidation characteristics of the soil. The consolidation was measured by a dial gauge set up as shown in Figure 4.11 and the total consolidation time varied from sample to sample.



Figure 4.11: Settlement dial-gauge set up to monitor progress of consolidation in sample

By the end of the consolidation phase, the soil sample had stabilized to the room temperature which was controlled to act as external constant temperature.

### 4.3.3 Heating to Equilibrium and Cooling

At the end of the consolidation phase, the test rig was prepared for the heating tests. The blanking plugs used in sealing off the openings on both sides of the cell body were replaced with Swagelok glands to enable the thermocouples to be inserted into the sample to measure temperature changes (Figure 4.12).



Figure 4.12: The blanking plugs are replaced with Swagelok gland for insertion of thermocouples

Thermocouples (probes) were inserted through openings in the chamber and positioned at specific distances between the heater and the wall of the test chamber to measure the temperature changes within the sample at various locations across the cell.

A typical layout of the thermocouples within the test chamber is shown in Figure 4.13.

The heater was powered through a laboratory Direct Current Constant voltage supply to enable control of voltage and current. This was switched on to commence the test and the heater was allowed to attain temperatures between 30°C and 40°C typical of site installations (Brandl, 2006). A few tests were run at slightly higher temperatures for comparison.

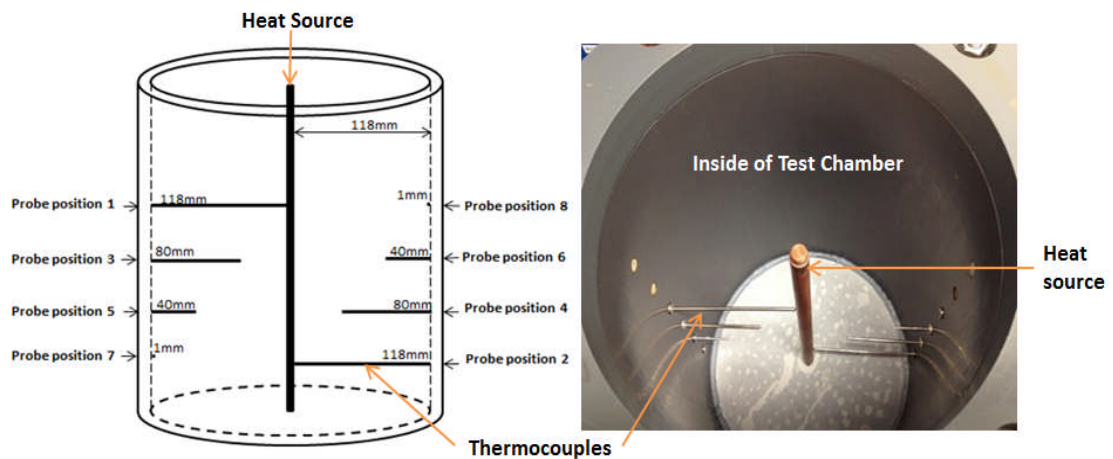


Figure 4.13: Drawing and photo of thermocouple arrangement within Test Chamber in relation to distance from heat source

The heater is powered through a laboratory Direct Current Constant voltage supply to enable control of voltage and current. This was switched on to commence the test and the heater was allowed to attain a fixed temperature between 30°C and 40°C typical of site installations (Brandl, 2006). A few tests were run at slightly higher temperatures for comparison.

The tests were carried out in a constant temperature laboratory controlled to approximately  $18^{\circ}\text{C} \pm 1.5^{\circ}\text{C}$ .

The temperature changes in the heater and within the sample were measured by the thermocouples and the readings were logged at regular intervals. The duration of heating was recorded with reference to the time it took the sample to attain equilibrium conditions.

A graph of the temperature recorded across the sample was plotted against time to give a heating curve. This represents the **heating cycle test** which is presented in Figure 4.19 (page 101).

With the sample still in heating equilibrium condition, a **temperature profile test** was carried out. This was achieved by placing the probes uniformly at specified intervals

from the cell centre to the inner edge of the cell wall as illustrated in Figure 4.14, while taking readings at these intervals.

To commence the test, the probes positioned from top to bottom on both sides of the test chamber were fully pushed into the centre of the test chamber as illustrated in Figure 4.15 on page 97.

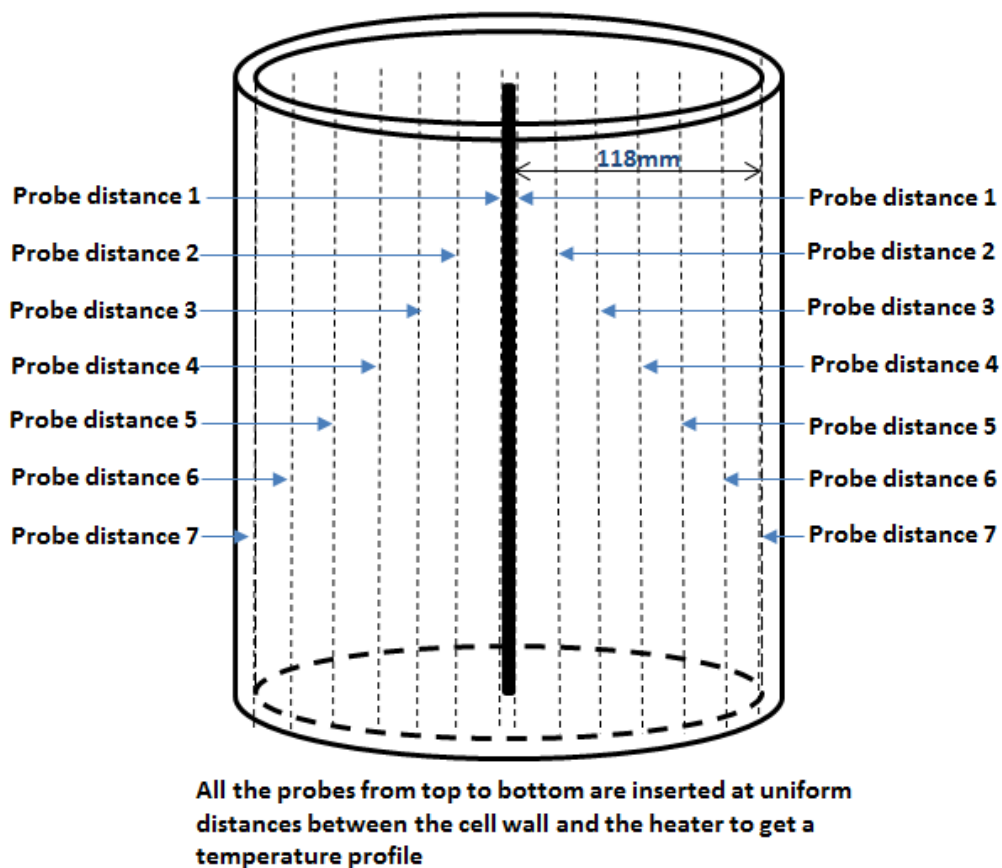


Figure 4.14: Temperature profile within the test chamber is captured by inserting all the probes at uniform radial distances from the heater to the edge of the cell wall.

In this way the temperatures along the heater from top to bottom were measured to show any temperature variations along its length. All the probes were then moved outwards at uniform radii and the temperature readings again recorded. This continued at specific intervals ending up at the inner edge of the cell wall.

The aim of this test was to capture a temperature profile at different radii and depth within the sample contained in the test chamber. This test was used in the determination of soil sample properties such as thermal conductivity and was useful in establishing temperature variations along the heater length.

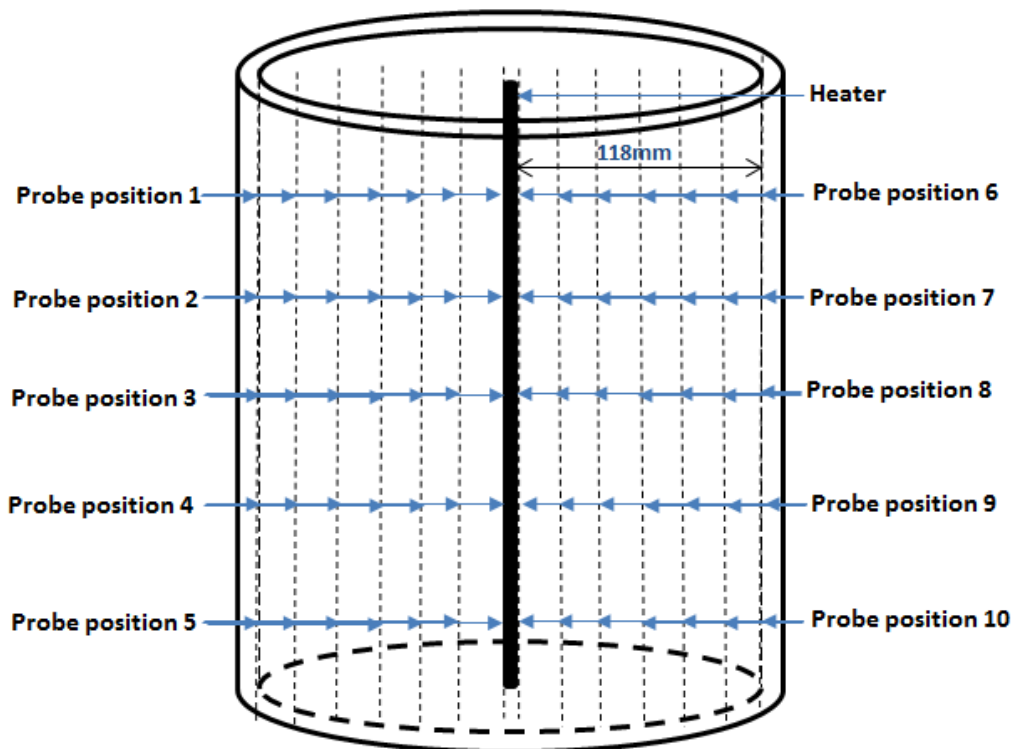


Figure 4.15: Temperature profile within the test chamber is captured by inserting all the probes from top to bottom at uniform distances from the heater to the edge of the cell wall.

The third test in this phase is the **cooling cycle**.

At the end of the profile test, the positions of the probes were changed to the initial locations used during the heating cycle and then the power supply was disconnected and sample allowed to cool back to the controlled room temperature.

The temperature changes within the cell were recorded and plotted against time to give the cooling curve. The time taken for the sample to cool back to room temperature was recorded.

#### 4.3.4 Thermal Cycles

The cyclic tests were based on a 24 hour period consisting of 8 hours heating and 16 hours cooling; a thermal load for a typical office during a normal working day.

In the preliminary tests the heating cycles were at first run two hourly from 2, 4, 6, 8, 10, 12, 14, 16, 18, 20 and 22 hours heating within a 24 hour test period in order to study the sample response to heating and cooling cycles. This process helped to establish the maximum heating periods of a sample beyond which complete cooling will not be established within a 24 hour test period. The cycles were repeated over a

number of days, up to 14 days in the preliminary tests to observe the sample thermal behaviour and if changes occurred in the heating curves with repetition over time.

When the repeated curves were compared, no significant changes were found and this pattern was then used to establish subsequent test cycles to an average of 3-5 days for cyclic tests. Further cyclic tests were then restricted to 4, 8 and 12 hours heating cycles.

#### 4.3.5 Soil Properties

At the end of the test regime, 80 to 100 representative points at specified locations across the cell were analyzed for strength parameters using the laboratory vane test, which is a method commonly used for measuring shear strength in soft to firm clays and organic deposits. Samples were then collected from the locations that were tested for shear strength, and analyzed for their water content. The aim of this was to get a clear picture of the strength and water content distribution across the sample in a real test condition and to establish a relationship between the sample strength, water content and sample distance from the heat source. These analyses were carried out on the sample after the complete series of heating tests had been run.

In order to assess the sample for strength and water content distribution, the rig was stripped open so that the sample in the test chamber became accessible for the test and sample collection. The sample was then divided into four layers and testing and collection points were marked uniformly across each sample layer at specified distances from the centre of the cell which is the heat source, to the edge of the cell wall. The layout of test and sample collection points is illustrated in Figure 4.16.

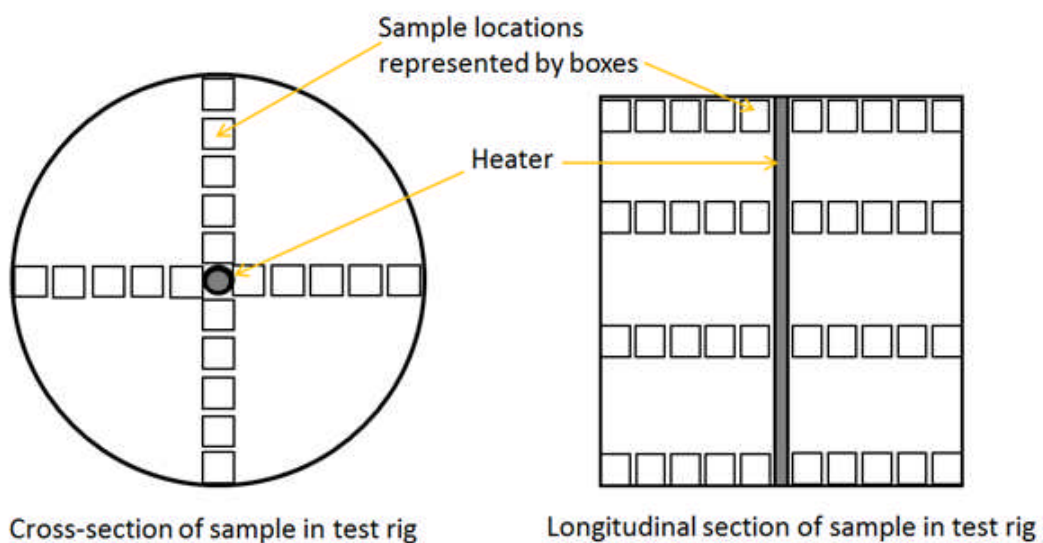


Figure 4.16: Sketch of layout for sample analysis and testing at the end of the heating tests

The laboratory vane test consists of advancing a four-bladed vane into cohesive soil (saturated clays) to the desired depth and applying a measured torque at a constant rate until the soil fails in shear along a cylindrical surface to provide its undrained shear strength (Knappett and Craig, 2012). This test was selected in the determination of the strength properties of the sample over other methods such as the triaxial test due to the need to carry out the tests in-situ in the rig with little or no disturbance at 80-100 sample locations and also the constraint presented by the overall small size of the sample. Vane dimensions (height x dia.) of 40x20mm was used in the tests.

The tests were carried out accordance with BS 1377-7:1990. Figure 4.17 depicts some of the processes involved in carrying out the vane tests and sampling.

The limitations associated with the use of the laboratory vane test include the fact that it is only suitable for testing for soft cohesive soils and may not give reliable results for clays mixed with sand or silt (Knappett and Craig, 2012).

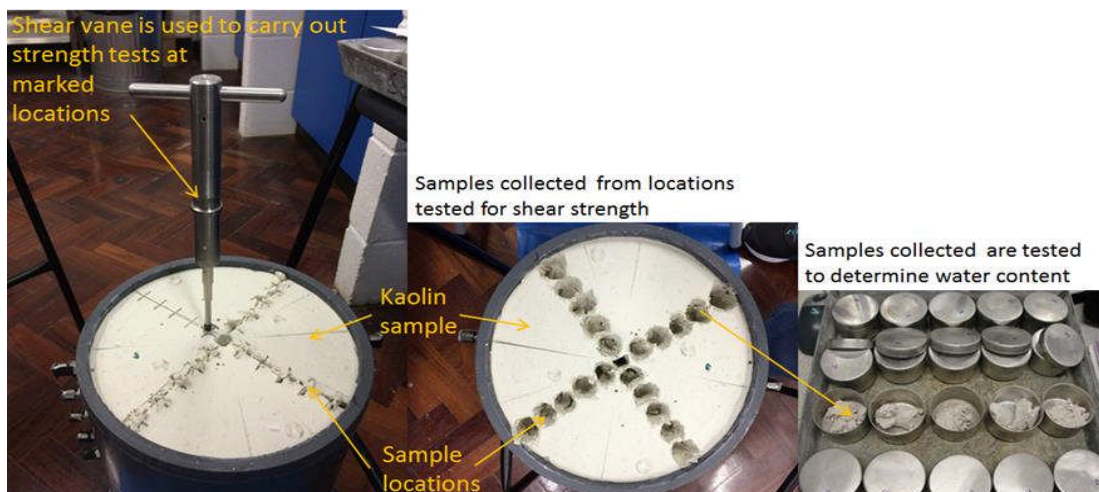


Figure 4.17: Samples were collected for water content determination after the shear strength test carried out at every sample point

#### 4.4 Preliminary Tests

As part of commissioning the equipment, preliminary tests were carried out to understand the behaviour of the rig and kaolin sample under the testing conditions. The findings from the first two tests were useful in the setting up and running of subsequent tests. One of the tests carried out is described briefly in this section.

The test was commenced with a prepared kaolin sample of 82% water content loaded into the cell following the steps described in the test procedure.



The sample was tested at an over burden pressure of 25kPa which was applied in increments of 6kPa, 12.5kPa and finally 25kPa. Each loading increment was maintained long enough to achieve full settlement. The dial gauge readings and excess pore water dissipated allowed for the end of the consolidation phase to be established. The water drained from sample was used to determine average water content of the sample.

At the end of the consolidation phase, thermocouples were fixed at specified distances across the cell in order to monitor the temperature variations at each point as shown in Figure 4.18.

The heating cycle commenced with the introduction of power to the heating element and the temperature variations across the cell were monitored with reference to the probe positions. Being a preliminary test, several heating and cooling cycles were carried out using several combinations of current and voltage (power) until the desired heater temperature within the sample of up to 40°C was established. Other tests were carried out while the sample maintained equilibrium conditions.

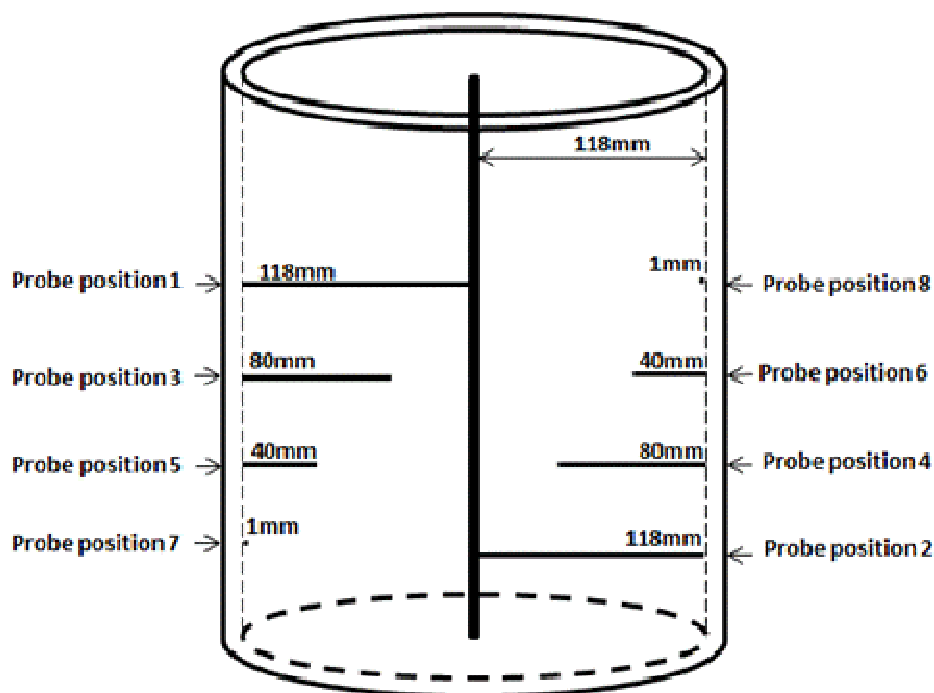


Figure 4.18: Arrangement of thermocouples within the test chamber to monitor temperature changes within the sample

At the end of the heating tests, analyses of the sample properties were carried out after dismantling the rig.

A summary of results from the tests is presented and discussed in the next section.

## 4.5 Typical Test Results

The observations and findings made from the preliminary tests carried out in the initial rig design informed the modifications applied to improve the new rig design.

The results presented in this section were obtained from preliminary tests carried out in the initial rig design alongside results obtained from similar tests carried out in the modified rig. Both sets of results are discussed and compared.

### 4.5.1 Heating to Equilibrium

The layout of the probe arrangements in Figure 4.18 (page 100), is the same for all the preliminary tests carried out in the initial rig.

Figure 4.19 show the heating curves of a kaolin sample to thermal equilibrium, with the probe positions indicated in Figure 4.18, in relation to the heater in the initial rig design.

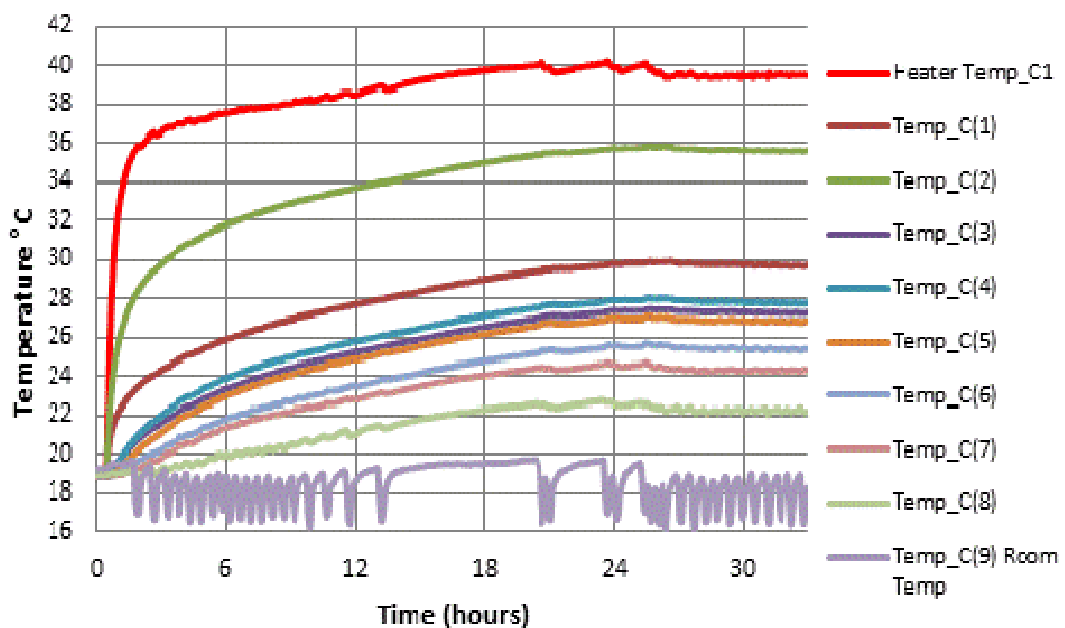


Figure 4.19: The heating curves of kaolin sample to thermal equilibrium showing the variation in temperature with time at the various probe locations in the initial rig design

The test was carried out on a sample at controlled room temperature of  $18^{\circ}\text{C} \pm 1.5^{\circ}\text{C}$ .

In Figure 4.19, the red line at the top represents the cartridge heater within the copper pipe. This line shows an increase in temperature which eventually attained an equilibrium value of between  $39.5^{\circ}\text{C}$  and  $40^{\circ}\text{C}$  in about 16 hours of heating.

The green line directly below the red line represents probe position 2 which is a point at the bottom of the copper pipe touching its outside wall. At equilibrium condition, the temperature attained is 35.5°C which gives a significant difference of approximately 4.5°C between the heater in the copper pipe and the outside wall of the copper pipe.

The third line represents probe position 1 which is a point at the top of the copper tube touching its outside wall. At equilibrium condition, the temperature attained is 29.6°C which gives a significant difference of approximately 10.3°C between the heater in the copper pipe and the outside wall of the copper pipe. It also indicates a temperature difference of about 6°C between the top and the bottom of the cartridge heater, with the bottom showing a higher temperature than the top.

The fourth line represents probe position 4 which is a point in the sample about 38mm from the heater. It shows a steady increase in temperature in response to the heat transferred radially from the heater through the sample. The same applies to the next four lines below.

The purple bottom line represents the controlled room temperature which fluctuates within an the range of  $\pm 1.5^{\circ}\text{C}$  in a constant temperature room.

The light green line directly above the room temperature line represents probe position 8 in the figure. It is at the top right side of the inner edge of the cell wall of the test chamber and shows a relatively constant temperature increase which indicates that the insulation properties of the cell wall works according to design since the external temperature was not constant.

From this test, it was observed that the cartridge heater showed significant temperature variation along its length with the bottom showing higher temperatures than the top. Another issue observed was the significant temperature difference between the cartridge heater within the copper pipe and the outside wall of the copper pipe. An attempt was made to resolve this issue in the modified rig design by eliminating the copper pipe and installing the cartridge heater directly in the sample. The issue of temperature variation along the length of the heater was also resolved during the manufacture of the new heater design.

Figure 4.20 on page 103, shows a layout of the probe arrangements for all the preliminary tests carried out in the modified rig.

Figure 4.21 also on page 103, shows the heating curves of a kaolin sample to thermal equilibrium in the modified rig, with the probe positions same as indicated in Figure 4.20, in relation to the heater. The test was also carried out on a sample at controlled room temperature of  $18^{\circ}\text{C} \pm 1.5^{\circ}\text{C}$ .

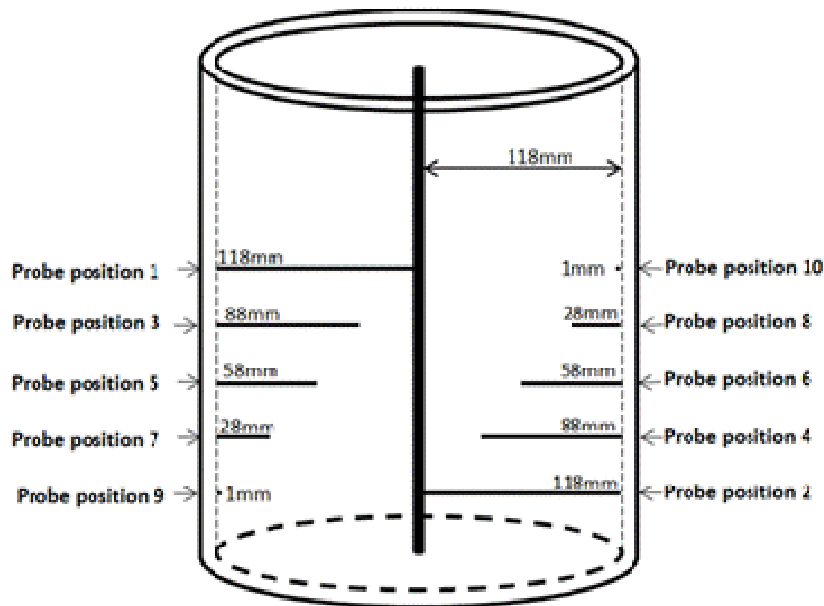


Figure 4.20: Layout of the probe arrangements for all the preliminary tests carried out in the modified rig design

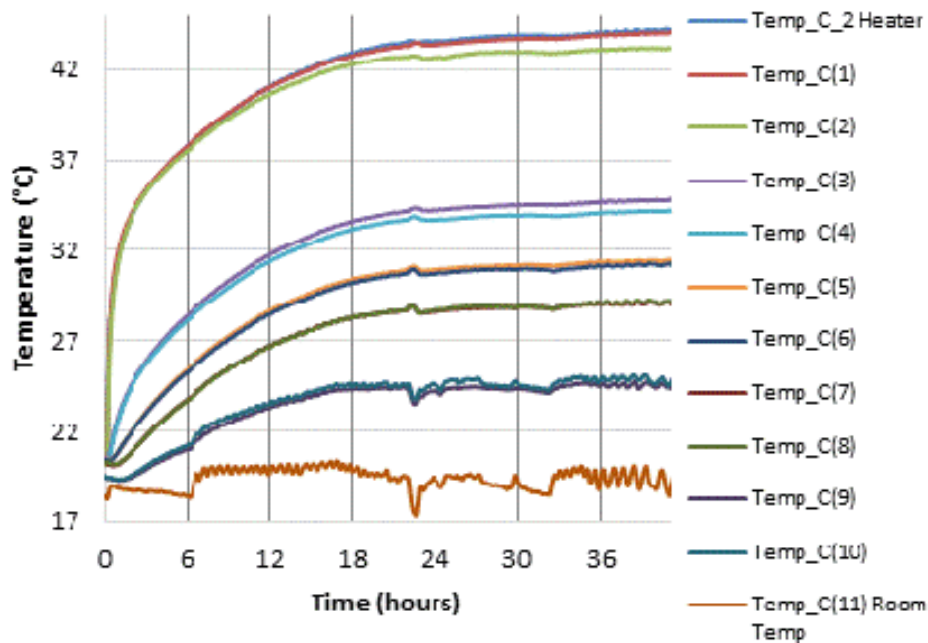


Figure 4.21: The heating curves of kaolin sample to thermal equilibrium showing the variation in temperature with time at the various probe locations in the modified rig design

The first three lines at the top represent the cartridge heater and probe positions 1 touching the top of the heater, and 2 touching the bottom. They all show very similar temperatures at equilibrium which confirms uniform heating at the top and bottom of the heater and shows that the issues identified from the preliminary results have been resolved.

The bottom line represents the controlled room temperature which fluctuates within an average of 1.5°C in a constant temperature room.

The two lines directly above the room temperature line represent probe positions 9 and 10 in the figure. They are at the inner edges at the top right and bottom left of the cell wall of the test chamber and show a relatively constant temperature increase which indicates that the insulation properties of the cell wall works according to design.

Probe positions 3, 5, 7 and 9 placed in the sample at specific distances varying with depth on the left side of the test chamber, show similar temperatures to probes 4, 6, 7 and 10 placed at corresponding distances on the right side of the test chamber. This indicates a uniform temperature along the heater which shows that the issue of temperature variation along the length of the heater was resolved in the modified rig design.

#### 4.5.2 Temperature Profile Contour plots

With the samples still in thermal equilibrium, Figures 4.22 and 4.23 (page 105), show contour plots of the temperature variations within the samples in both the initial rig design and modified rigs respectively. These contour plots represent the vertical temperature profiles at different radii across the samples.

The Figures show that there is temperature variation across the cell even while in thermal equilibrium, with each of the different colours and shades of the same colour representing different temperature ranges between 22°C and 44°C.

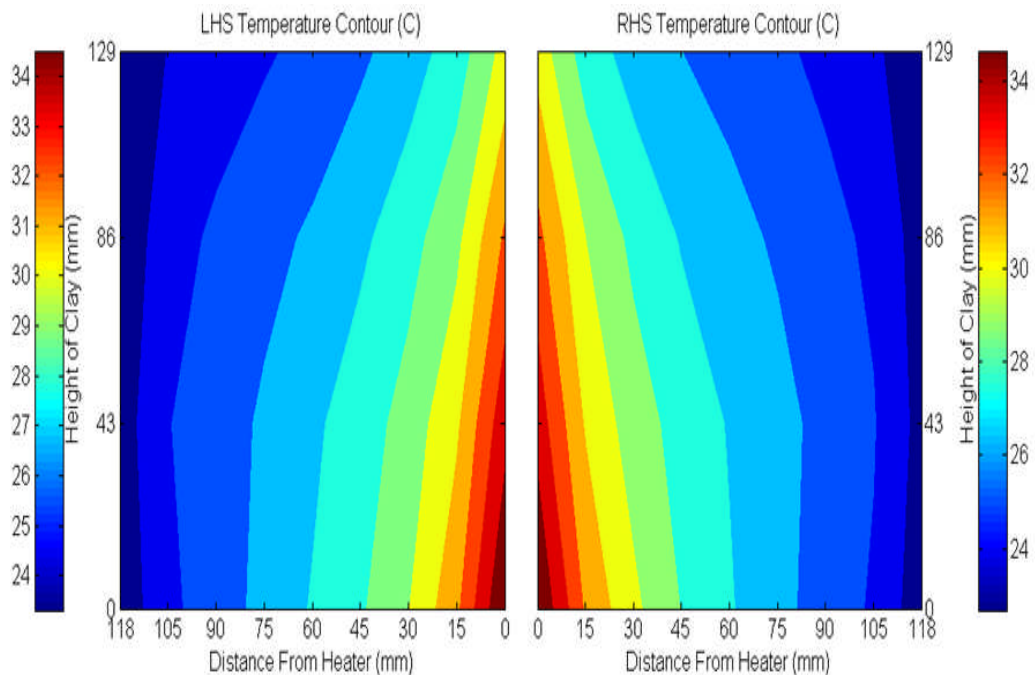


Figure 4.22: Temperature contour plot of the vertical temperature profiles at different radii across the sample in initial rig design

In Figure 4.22 (page 104), which shows the temperature profile of the sample in the initial rig design, the radial heat dissipation can be seen as the sample shows different temperature intensities between the centre and edge of the sample.

The Figure shows a clear picture of the temperature differential along the heater length as earlier observed from the heating test, with the base showing a higher temperature intensity than the top. It can be seen from the plot that the sample is cooler at the top and the temperature profile lines are not parallel.

Figure 4.23 which represents the sample in the modified rig shows a more radially uniform heat dissipation across the sample. The temperature along the length of the heater is shown to be almost uniform which is a clear improvement over the initial design.

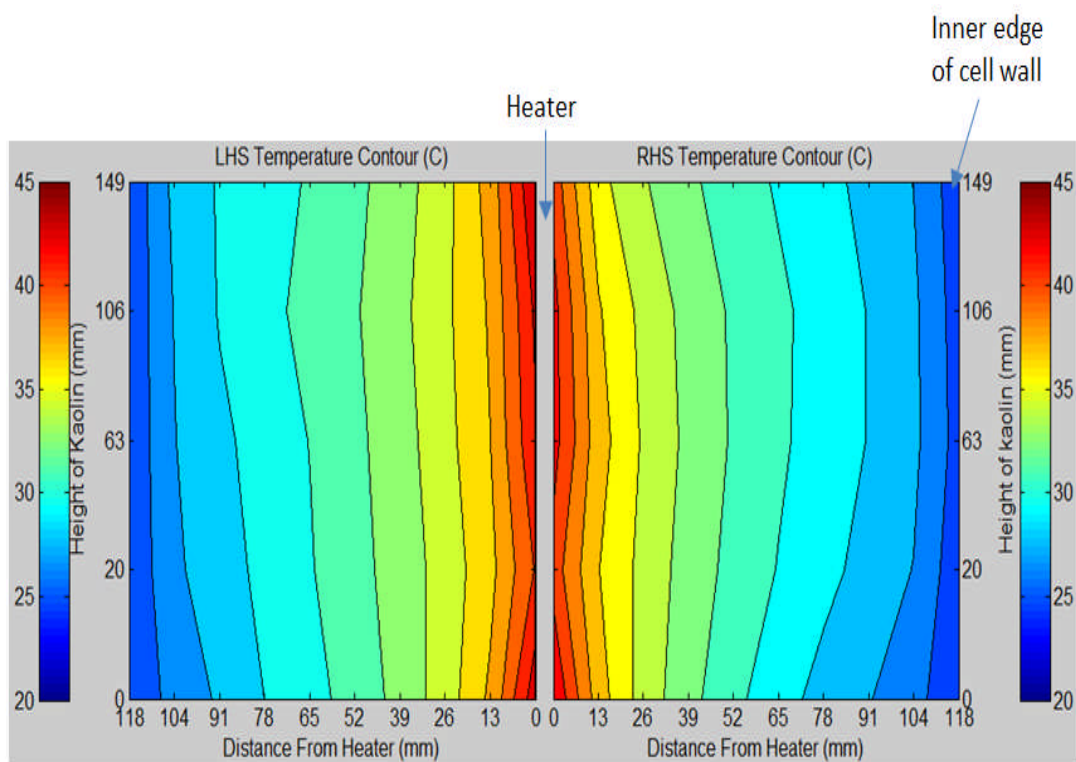


Figure 4.23: Temperature Contour plot of the vertical temperature profiles at different radii across the sample in modified rig

From both figures, the temperature variations indicate a more uniform heat distribution in the modified rig than in the initial rig design.

### 4.5.3 Variation of Temperature across layer of sample at one level

Figures 4.24 on page 106, shows a graph of temperature variations across the sample layer in the initial rig design while Figure 4.25 (page 106), shows the same graph for tests carried out in the modified rig.

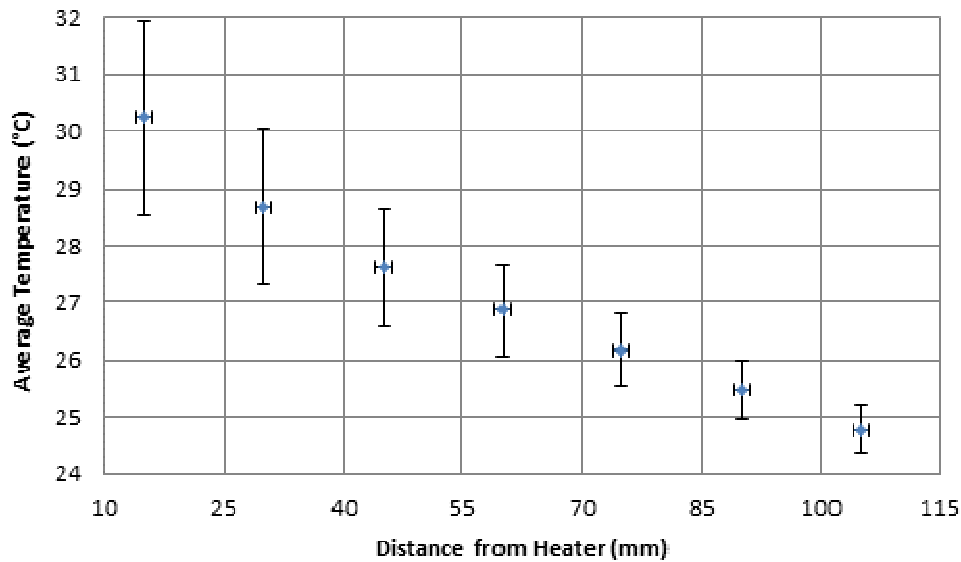


Figure 4.24: Range of average temperature measurements showing the variations from top to bottom of sample at each location across the sample layer, and also showing that the average temperature reduces with distance from the heater, in the initial rig design

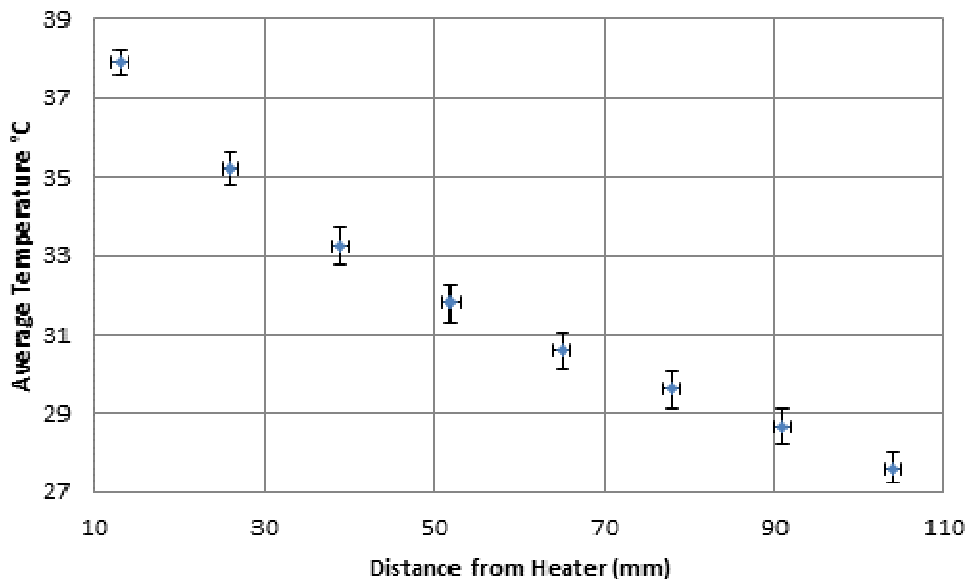


Figure 4.25: Range of average temperature measurements showing the variations from top to bottom of sample at each location across the sample layer, and also showing that the average temperature reduces with distance from the heater, in the modified rig

The graphs represent readings recorded at varying radii from the heat source to the inner edge of the cell wall. The temperature readings were obtained from two probes inserted into the test chamber from opposite sides, at the same level while the sample was in thermal equilibrium. The graphs represent temperature variations across one level or layer of the sample while in thermal equilibrium, and show the range/variation

of temperatures from top to bottom of the sample between the heat source and the inner edge of the wall of the test chamber.

The points plotted in both graphs excluded the readings from the probes located at the heater and the inner edge of the cell wall in order to have a temperature variation within the sample and devoid of the thermal effects of the heater and cell wall materials, especially as the cell wall acts as an insulator to reduce the effect of the room fluctuations on the soil.

From Figure 4.24 (page 106), representing the initial rig design, the variation from top to bottom of the sample ranged from  $\pm 0.4^{\circ}\text{C}$  near the cell wall to  $\pm 1.7^{\circ}\text{C}$  closer to the heater. This confirms the temperature differential from top to bottom of heater earlier observed, hence a less radial heat dissipation across the sample

The temperature variation in the modified rig as shown in Figure 4.25 (page 106), ranged from  $\pm 0.3^{\circ}\text{C}$  to  $\pm 0.5^{\circ}\text{C}$ , and showed a more uniform spread from top to bottom, hence a more radial dissipation across the sample.

#### 4.5.4 The Cooling Curve

Figure 4.26 shows a cooling curve for a test carried out in the initial rig design while Figure 4.27 on page 108, shows a cooling curve for a test carried out in the modified rig.

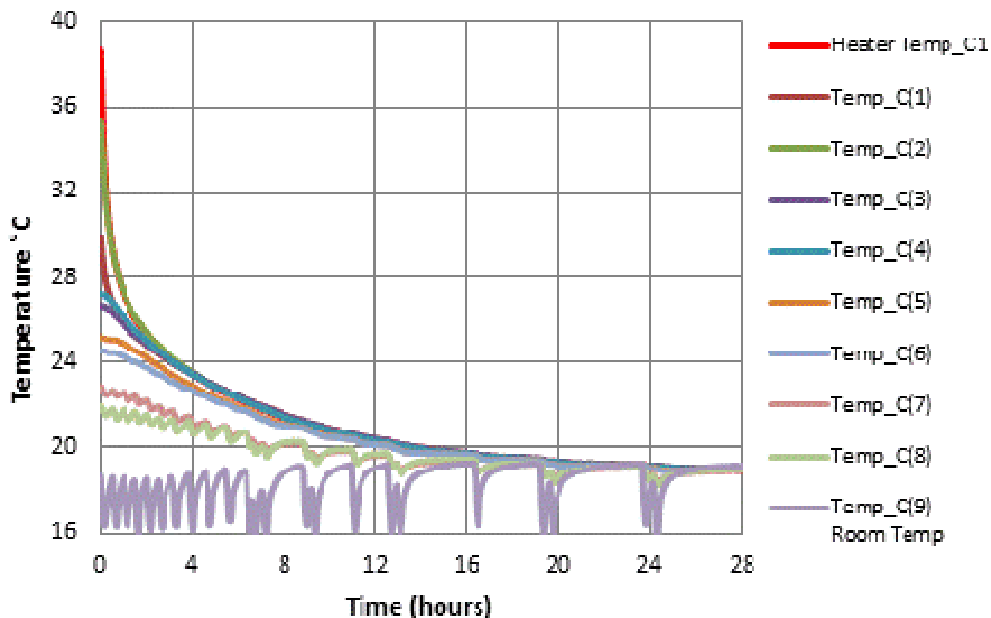


Figure 4.26: Cooling curves of kaolin sample from equilibrium heating back to controlled room temperature showing the variation in temperature with time at the various probe locations in initial rig design



Both graphs represent the cooling curves of the sample from equilibrium heating back to controlled room temperature, showing the variation in temperature with time at the various probe locations. The cooling process commences when the power supply to the heater is turned off, and continues until the sample cools down to the controlled room temperature.

It can be observed from graph in Figure 4.26 (page 107), that most of the cooling took place within the first 15 hours and within 24 hours the sample had fully cooled to the controlled room temperature.

From graph 4.27 the cooling process was slightly longer than that of the initial rig.by about 3 hours. This was expected since the sample started cooling from a higher temperature than the sample in the initial cell design.

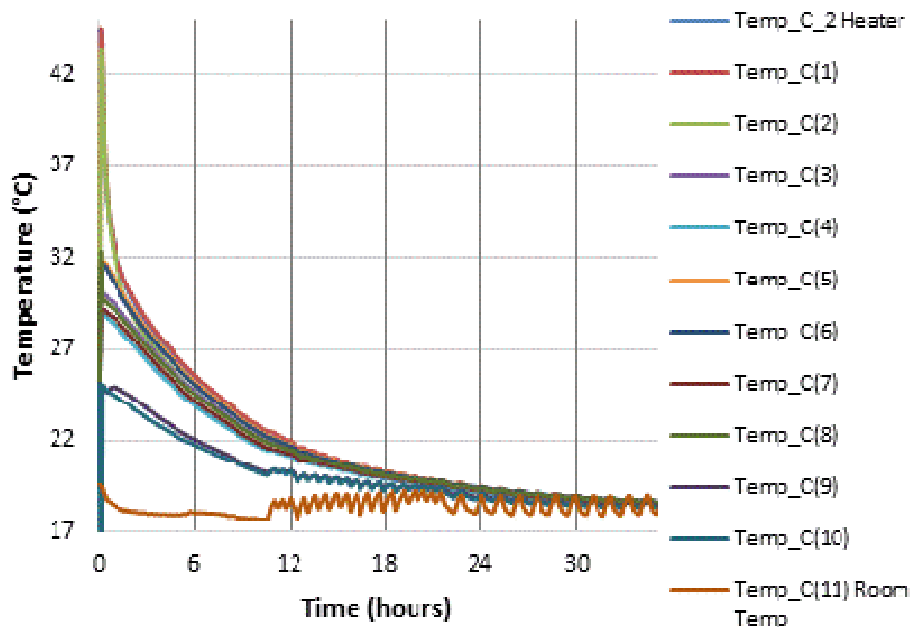


Figure 4.27: Cooling curves of kaolin sample from equilibrium heating back to controlled room temperature showing the variation in temperature with time at the various probe locations in modified rig

In both tests, the room temperature shows fluctuations which fall within the range of  $\pm 1.5^{\circ}\text{C}$  as controlled by the temperature setting installed in the laboratory. These fluctuations which were more pronounced due to prolonged human activity in the laboratory, could indicate heat movement in and out of the rig and raise concern about errors in the measurement system. This concern was resolved by the fact that only the thermocouple data recorded in the inner edge of the rig reflected fluctuations in response to the fluctuations in the room temperature and the data recorded within the

soil sample remained unaffected, hence the decision to exclude the data close to the cell wall in the analysis.

#### 4.5.5 Thermal Cycles

The thermal cycles is of particular interest as it represents the thermal loading cycles on an office building based on a daily cycle in which it reaches its heating peak within the working day and cools back during the night, all taking place within a 24 hour cycle.

Figure 4.28 shows five days of thermal loading cycles cyclic loading consisting of 8 hours heating and 16 hours cooling carried out in the initial rig design while Figure 4.29 on page 110, shows two days of thermal cyclic loading consisting of 8 hours heating and 16 hours cooling carried out in the modified rig.

The tests were carried out on the basis of 8 hours heating and 16 hours cooling cycles corresponding with the day and night heating and cooling needs of a typical office complex in 5 working days.

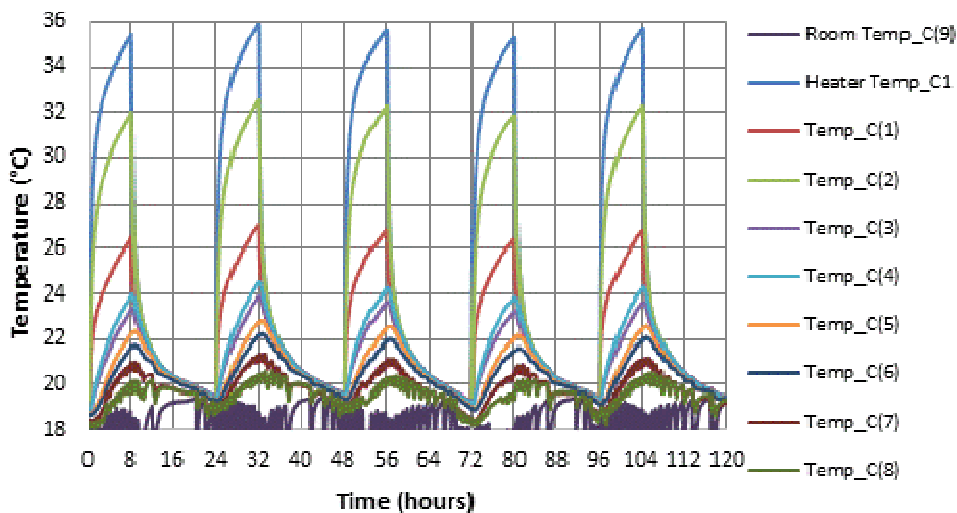


Figure 4.28: Five days thermal loading cycles consisting of 8 hours heating and 16 hours cooling in initial rig design

The graph in Figure 4.28 shows five cycles of daily variation of temperature generated over time to represent a working week which allows for cooling over the weekend. The daily heating curves are similar to the heating curves obtained when heating the sample to equilibrium which was discussed earlier, and have the same explanations. The only difference is the shorter heating duration which means that lower peak temperatures are attained. The daily cooling cycle is also similar to the cooling curve discussed earlier. Complete cooling of the sample is achieved within the 24 hour cyclic test.

Repeating the cycles over a few days allowed for comparison of the daily results in order to identify any changes in cyclic behaviour over time. The daily cycles were analysed and compared and there were no differences or changes observed, hence, further tests were reduced to fewer daily cycles.

The tests carried out in the modified rig shown in the graph in Figure 4.29, reflects fewer daily cycles. The heating and cooling curves of a daily cycle are similar to the heating and cooling curves earlier discussed in the modified rig with the only difference being that the peak temperature achieved is lower due to the shorter heating time. Complete cooling of the sample is also achieved within the 24 hour cyclic test.

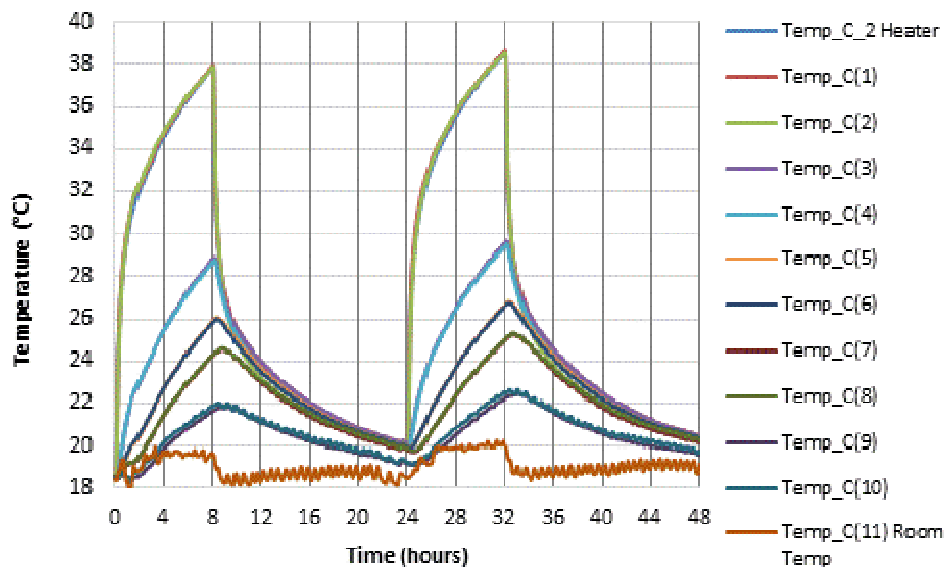


Figure 4.29: Two days of thermal loading cycles consisting of 8 hours heating and 16 hours cooling in modified rig

Figure 4.29 also showed the uniformity of the temperature readings recorded from probes placed on opposite sides of the rig at similar distances from the heat source at the centre of the rig. The temperature readings recorded at the heater, and at the probes placed at the top and bottom of the heater all correspond as depicted by the first three lines merged at the top of the graph in Figure 4.29. This also showed that the modified rig design ensured more uniform heating of the sample.

#### 4.5.6 Analysis of Soil Properties after the Heating Tests carried out in both rig designs

At the end of the heating tests, an analysis of soil properties such as strength and water content tests were carried out on the sample (Head and Epps, 2011; Head, 2006; Knappett and Craig, 2012; Aysen, 2002) The sample was divided into four layers and an average of 20 samples were collected from each layer from the specific locations where the shear strength tests had been carried out, to determine the water

content. Results from the four layers from top to bottom were analysed to provide information on each layer of the sample to determine if the total sample was homogenous or had different properties.

The results of the shear strength tests from each sample location, were plotted against the results from the water content tests at the same location to determine a relationship as shown in Figure 4.30 for the test run in the initial rig design at an overburden pressure of 25kPa, and Figure 4.31 for the test run in the modified rig at an overburden pressure of 100kPa. Both graphs were plotted from results based on the analysis carried out on the bottom layer of both tests.

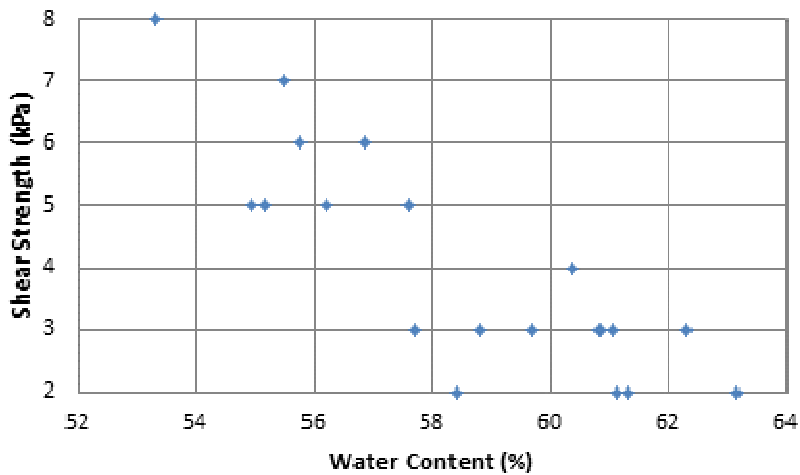


Figure 4.30: Shear strength against water content carried out on the sample at the end of the heating tests in the initial rig design at 25kPa

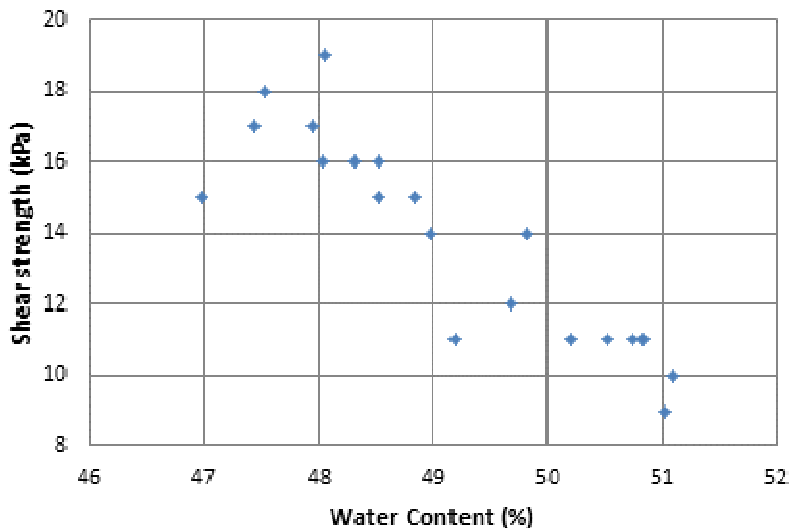


Figure 4.31: Shear strength against water content carried out on the sample at the end of the heating tests in the modified rig at 100kPa

From both graphs, a relationship was seen to exist between the shear strength and water content of the sample which showed that areas of lower water content showed corresponding higher shear strength values which was expected.

## **4.6 Chapter Summary**

This chapter covered the setting-up of the rig including instrumentation and leakage tests. Typical test procedures including sample preparation, consolidation, heating to thermal equilibrium, thermal loading cycles, determination of water content and shear strength within sample, and an overview of the analysis of soil properties were covered in detail. Typical test results were also presented and discussed. The analysis focused on the comparison of the results obtained from the tests carried out in both the initial and modified rigs, which showed that a radial and more uniform heating pattern was more achieved in the modified rig than in the initial rig design

Conclusions drawn from this chapter highlight the successful coupling of the rig and its parts, and conducting preliminary tests from which measurable and realistic data were collected. Based on the progress recorded after the stage of preliminary tests, the main tests were carried out according to plan. In the Chapter 5, data and results from the tests carried out will be presented and discussed in more detail. Other relationships to be discussed in Chapter 5 include the variation of shear strength and water content in the sample with respect to distance from the heat source.

## **Chapter 5 Results obtained from Tests in the First Rig Design**

### **5.1 Introduction**

Chapter 4 dealt with the test procedure and typical test results. In this chapter, the first rig was proof tested by carrying out tests to establish the test procedure, and the details of the tests are presented here.

Several experiments were carried out on kaolin to study its thermal behaviour under the following parameters:

- 1) The water content of the sample
- 2) The overburden pressure applied to the sample in the test chamber
- 3) The power input determining the heater temperature as controlled by the current and voltage used
- 4) Time or duration of the test
- 5) Thermal cycle loads

### **5.2 Tests Carried out in Initial Rig Design**

A total of four samples were prepared and tested in the initial rig design, to gain a better understanding of the working mechanism of the rig, its components, and of the test procedure.

Each sample underwent thermal tests lasting for between 4 and 21 weeks. Details of the tests carried out on each of the four samples are presented one after the other on the basis of the objectives behind carrying out each of them.

#### **5.2.1 Objectives of Thermal Tests Carried out on Soil Samples**

Each of the four samples were prepared and underwent a series of thermal tests to achieve the following objectives:

- 1) To determine how long it took the soil sample being tested to achieve thermal equilibrium or steady state conditions when heated from a controlled room temperature at a specific pressure, water content, and power input
- 2) To determine the time it took to cool back to the room temperature when the power supply was disconnected
- 3) To determine the distribution of temperature across the sample at thermal equilibrium

- 4) To investigate a range of thermal loading cycles from 2, 4, 6, 8 12, up to 22 hours heating and cooling within a 24 hour cycle to determine sample response to heating cycles and time required to cool down. The thermal loading cycles tested differed from test to test and were specified for each test
- 5) To determine shear strengths and water contents within the sample in relation to distance from heat source and different levels of sample height at the end of a test

A summary of the samples prepared and the conditions under which they were tested is presented in Table 5.1.

Each of the tests are described in detail, and for this purpose, are identified by their serial number in the Table 5.1, the sample soil type and the pressure applied.

Table 5.1: Summary of samples prepared and tests carried out on each sample

Samples	S/N	1	2	3	4
<b>VARIABLES / PROPERTIES / TESTS</b>	<b>Material</b>	<b>Kaolin (Preliminary)</b>	<b>Kaolin (Preliminary)</b>	<b>Kaolin</b>	<b>Kaolin</b>
	<b>Water Content before Test (%)</b>	89.5	82	82	82
	<b>Pressure Applied (kPa)</b>	50	50	50	25
	<b>Power (W)</b>	NA	4.8, 5.98	5.4, 4.84, 3.6	4.49, 7.98, 9.48, 17.05
	<b>Sample Height before Test (mm)</b>	280	280	280	280
	<b>Sample Height after Test (mm)</b>	241	183	183	215
	<b>Height Diff. (mm)</b>	39	97	97	65
	<b>Av. Shear Strength after Tests (kPa)</b>	NA	NA	7.3	5.3
	<b>Av. Water Content after Test (%)</b>	NA	52.8	47.8	56.7
	<b>Thermal Cycles within 24 hour (hours)</b>	NA	NA	8	4, 8, 12, 16, 20
	<b>Heating to steady state (hours)</b>	NA	16	30	26 - 28
	<b>Cooling duration (hours)</b>	NA	-	30	30
	<b>Whole Duration of Test (weeks)</b>	NA	4	11	37
	<b>Period of Test</b>	March 2013	March to April 2013	May to July 2013	Oct 2013 – July 2014

## **5.2.2 Other Tests**

Leakage and instrumentation tests were conducted before the actual tests in the rig were commenced. The objective of the leakage test was to find out how well sealed the rig to ensure that there was no unaccountable loss of water.

The instrumentation test was carried out by means of a small scale test with the following objectives:

- i. To test the cartridge heater, thermocouples, power supply unit and data-logger and how they work together in a small sample of kaolin
- ii. To gain better understanding of how the cartridge heater works and what power inputs would be required to achieve a certain temperature range.

### **5.2.2.1 Leakage Tests**

Before the start of the tests, the rigs were filled with water and tested for signs of leakage.

There were leakage problems identified in the first cell design which was temporarily resolved by the use of silicon grease to allow the rig to be used for tests.

A more lasting solution was achieved through the modification made to the cell design. The modified rig design passed the leakage test when it was tested as no leakage was observed.

### **5.2.2.2 Instrumentation Test**

Prior to the start of the soil thermal tests in the rig, a small scale test was carried out. A kaolin sample was prepared and loaded into a glass beaker of approximately 320mm in height and 75mm in diameter. The heater was inserted into the centre of the kaolin and connected to a power supply unit, while a thermocouple was inserted at the edge of the beaker. Both were connected to a data-logger to monitor temperature changes. The photograph showing the set-up of this test was presented as Figure 4.1 in chapter 4.

Several current and voltage combinations were tested until eventually at a power input of approximately 5.3W, a temperature of 40°C was achieved and maintained as shown in Figure 5.1.



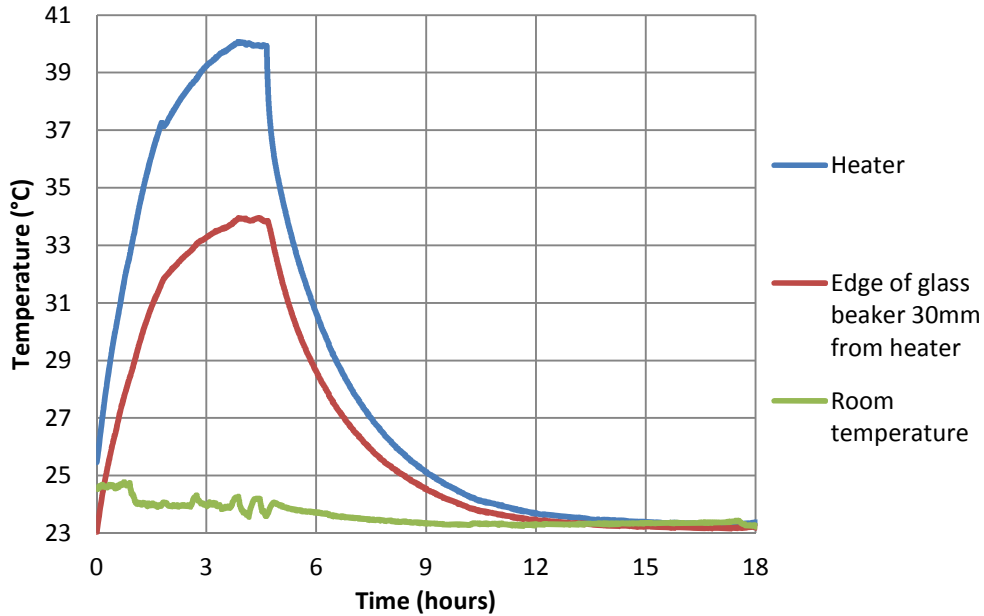


Figure 5.1: Graph showing cartridge heater, thermocouple and room temperature changes during the small scale test

The blue line at the top of the graph in Figure 5.1 represents the cartridge heater while the red line directly below it represents the temperature point about 30mm away from the heater and by the inner edge of the glass beaker. This temperature increases in response to the heater temperature and indicates heat transfer across the sample.

The green line at the bottom of the graph represents the controlled room temperature which showed some fluctuations during the test duration. It is noted that the temperature within the sample did not show fluctuations to the same extent as those for the room temperature, suggesting that the variations of less than 1°C in room temperature would not be critical.

### 5.2.3 Sample No. 1 (Preliminary Tests on Kaolin Sample)

Following the instrumentation test, a preliminary test was carried out in the initial cell design. The objectives of carrying out this test include:

- i. To gain an understanding of sample preparation and setting up of tests
- ii. To prepare samples of varying water contents and selecting the most practical range to work with
- iii. To test how the rig and its additional components work when assembled and loaded with sample
- iv. To determine the range of power input required by the cartridge heater to achieve a certain temperature within the sample

- v. To practically test the procedure for setting up and running of tests proposed during the design of the experiment with a view to improve on it where necessary
- vi. To determine appropriate temperature logging intervals for the thermal tests
- vii. To work with actual data collected from tests
- viii. To gain a practical experience of carrying out the tests with a view to identify likely errors and reduce them

#### **5.2.3.1 Procedure**

Sample No. 1 was prepared by mixing kaolin and distilled water to achieve 89.5% water content, that is 1.5 times the liquid limit to ensure saturation. The rig was assembled, the soil carefully placed in the cell and the sample loaded.

A pressure of 50kPa was immediately applied to the sample which resulted in kaolin slurry being forcefully pushed out through the drainage valves. The test was stopped.

The rig was dismantled and holes were evident in the filter paper placed on the perforated bottom plate at the base of the test cell. The holes occurred around the drainage openings and were likely caused by the sudden introduction of high pressure on a kaolin sample of such high water content.

Lessons learnt from this test include:

- i. Allow sample to settle in the rig for up to 12 hours before applying pressure
- ii. Beginning the consolidation phase with the application of lower pressures and increase incrementally
- iii. Reduce water content of kaolin sample to make it more manageable for testing while keeping it high enough to limit air in sample.

Although the first preliminary test ended abruptly without achieving all the objectives, valuable experience was gained for more successful running of subsequent tests.

#### **5.2.4 Sample No. 2 (Preliminary Tests on Kaolin Sample at 50kPa)**

In order to accomplish the objectives set out in the first preliminary test which was discontinued, another kaolin sample was prepared with a water content of 82%. This sample was tested at a pressure of 50kPa which was applied in incremental pressures of 12.5, 25 and finally 50kPa, with the consolidation phase lasting approximately two weeks. The excess pore water drained from the rig was collected and weighed.

At the end of the consolidation phase, thermocouples were inserted at different radii and levels within the sample from the centre to the edge and a heating test

commenced. After several hours of monitoring the heating process and adjusting the power input, the sample attained steady state conditions after approximately 16 hours of heating. The heater subsequently maintained a temperature of 40°C based on power input of 5.98W.

Heating and cooling tests were carried out three times over a period of 90 hours as the results in Figure 5.2 show. The blue line at the top represents the cartridge heater while the lines at the bottom represent the room temperature. Two thermocouples numbered 5 & 6 in the Figure, were set to record the room temperature for the purpose of comparison, and both recorded similar readings. The other lines in between them represent various locations within the sample from the edge of the heater to the inner edge of the cell.

The temperature difference between the heater and the thermocouple placed just outside of the heater wall was 12.9°C suggesting that the heat transfer was not adequate. This was taken note of with a view to resolve it in the following tests. Some leakage was also observed around the heater base at bottom of cell but it was less than that in the first test.

The fluctuations observed in the room temperature as shown in Figure 5.2 was due to the laboratory temperature control being fixed during this test. The test came to an end after cooling was completed.

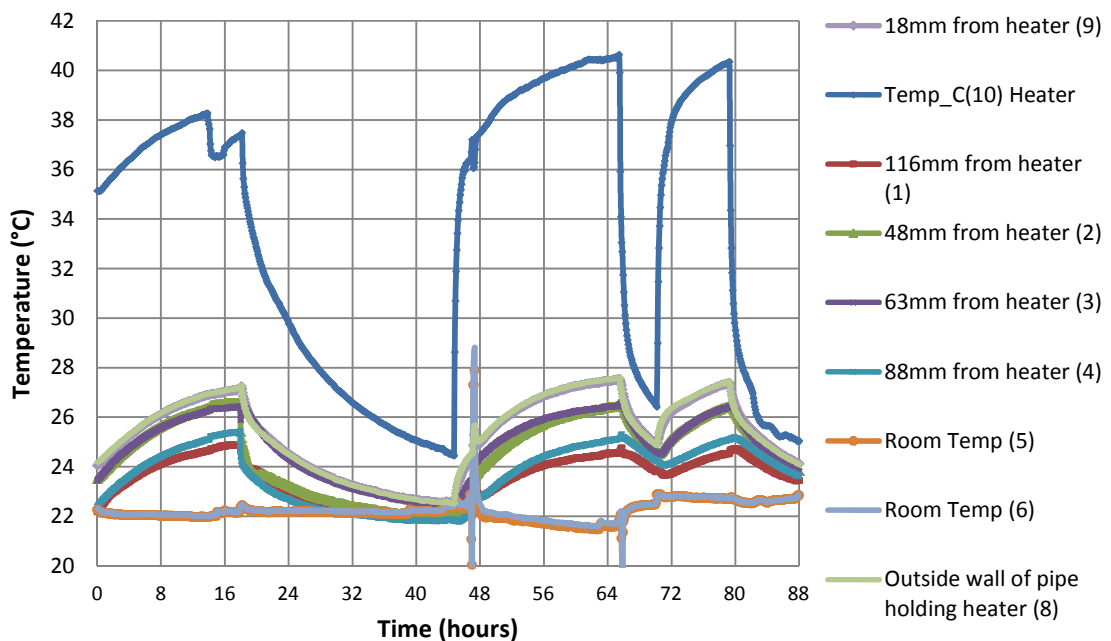


Figure 5.2: Graph of heating and cooling tests from second preliminary test

The objectives set out for the preliminary tests were achieved.

#### **5.2.4.1 Dismantling and Stripping Test For Sample Collection**

At the end of the heating and cooling tests. The cell was dismantled and samples were collected from various location to determine the water content within the sample. The average water content of the sample was 52.8%.

#### **5.2.5 Sample No. 3 (Tests carried out on kaolin sample at 50kPa)**

A kaolin sample was prepared at 82% water content and carefully loaded into the test rig following the test procedure described in the previous chapter. During the consolidation phase a pressure of 50kPa was applied in incremental loads of 12.5, 25 and finally 50kPa.

The objectives for setting up this test were in line with the objectives common to all the tests as listed in section 5.2.1. The thermal loading cycles investigated during this test was 8 hours heating and 16 hours cooling.

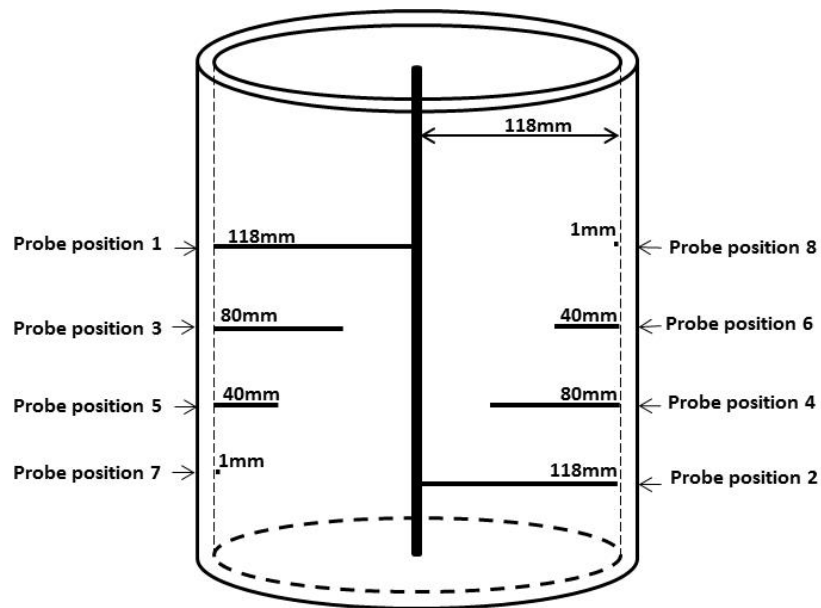
At the end of the consolidation phase, thermocouples were inserted into the test chamber from two opposite sides. Each thermocouple on the left side had a thermocouple on the right hand placed at a similar distance from the heater to build in redundancy, allow for a failure of a thermocouple and provide a means of averaging the temperature variation or measure the variation both vertically and horizontally.

Eight thermocouples were inserted into the test chamber with four on each side. They were inserted from the inner edge of the cell towards the heater at distances of 1mm, 40mm, 80mm and 118mm (touching copper pipe bearing the heater) from the inner cell wall, at four levels from bottom to top, with each on a different level of the sample height, at intervals of 40mm. The lowest probe was inserted at about 45mm above the sample base, and all other probes inserted 40mm above each other. The four on the other side were placed at the same distances and levels from top to bottom. Figure 5.3 on page 120, shows the layout of thermocouples for this test.

##### **5.2.5.1 Objective 1: Equilibrium Heating Duration**

To achieve the first objective of the test, which was to determine how long it took the soil sample being tested to achieve equilibrium or steady state conditions, the heating test was commenced by supplying power to the cartridge heater from the power supply unit.

Both the cartridge heater and all the thermocouples fixed into the test chamber were connected to the data-logger to allow the temperature changes in heater and points within the sample to be logged every five minutes.



1. Height from base of sample to bottom probe is 45mm
2. Interval between each probe is 40mm
3. Heater is probe Temp\_C10
4. Room temperature is probe 9

Figure 5.3: Layout of thermocouples within test chamber for tests carried out on sample no.3; kaolin at 50kPa

Figure 5.4 shows a graph of the increase in temperature across the sample until equilibrium with a power input of 5.4W. Note that the room temperature varied by up to 2°C even though tests were carried out in a temperature controlled room. This had little effect on the temperature across the cell suggesting the average room temperature could be used in the analysis.

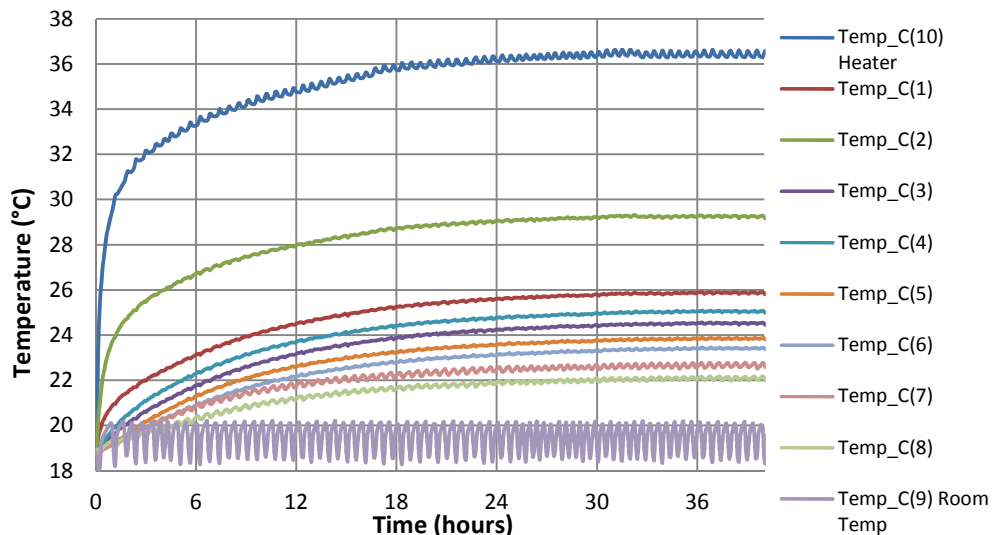


Figure 5.4: The variation of temperature with time across a sample of kaolin consolidated to 50kPa showing that thermal equilibrium was achieved after about 30hrs

Table 5.2 presents the temperature values of the sample in thermal equilibrium after 38 hours of remaining in equilibrium. The sample being able to maintain similar temperature conditions for this period confirmed that the sample had achieved steady state.

Table 5.2: Temperature values at probe locations in equilibrium heating condition for kaolin at 50kPa and 5.4W power

Probe label	Distance from Heater (mm)	Temp at Equilibrium after 30 hours (°C)	Temp at Equilibrium after 38 hours (°C)
Probe 10	Heater	36.5	36.6
Probe 1	Outer edge top of pipe	25.8	25.8
Probe 2	Outer edge bottom of pipe	29.2	29.2
Probe 3	38	24.5	24.5
Probe 4	38	24.9	25.0
Probe 5	78	23.8	23.8
Probe 6	78	23.4	23.4
Probe 7	117	22.6	22.6
Probe 8	117	22.0	22.0
Probe 9	Controlled Room Temp	18.8	18.8

### 5.2.5.2 Objective 2: Cooling Duration

The second objective was to determine the duration of cooling. This was done by disconnecting power supply to the heater and allowing the sample to return to its initial temperature (controlled room temperature).

From Figure 5.5, complete cooling of the sample from the elevated thermal equilibrium condition back to the initial, room temperature was approximately 30 hours.

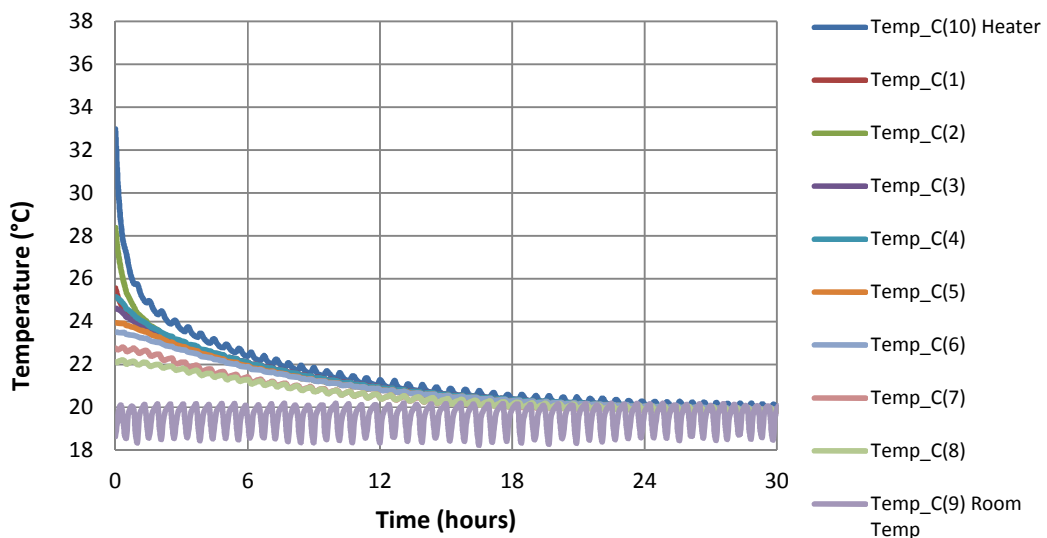


Figure 5.5: The time to return to room temperature (test at 50kPa; sample no.3)

### 5.2.5.3 Objective 3: Temperature Variations in Sample

This objective was to measure the temperature profile across the sample under thermal equilibrium to show the temperature variations between the centre and edge of sample. Observations from this test, shown by the graph in Figure 5.6, indicate that the temperature at the bottom of the cell was observed to be higher than that at the top of the cell.

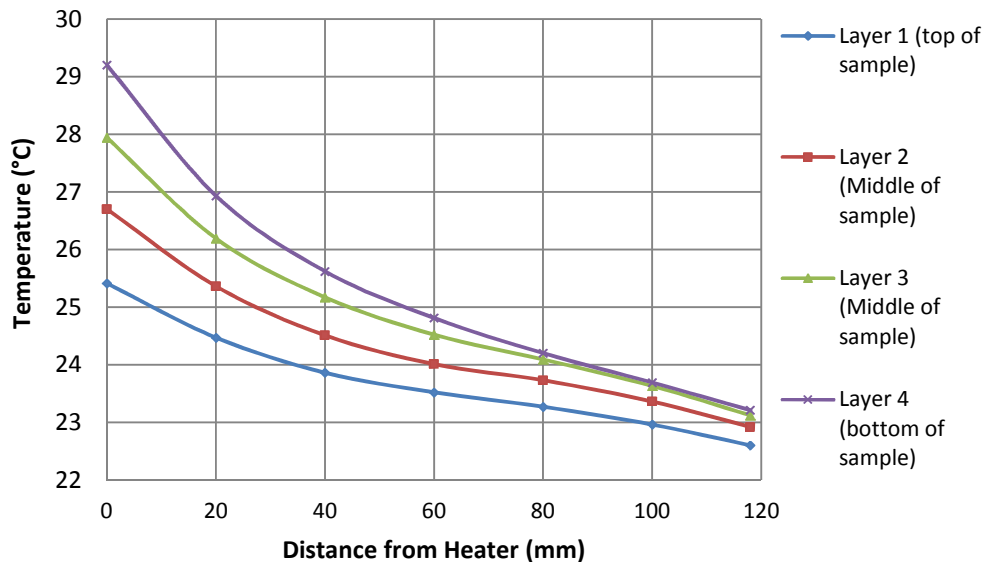


Figure 5.6: Temperature variations across sample from outer wall of pipe containing the heater to edge of test chamber and from top to bottom of sample

It is also to be noted that although a temperature reading of around 36°C was obtained in the heater, the maximum reading obtained from the outside wall of the pipe holding the heater was approximately 29°C. This is indicative of inefficient heat transfer between the heater and the pipe wall.

The temperature values at the measured locations within the sample are shown in Table 5.3.

Table 5.3: Table showing temperature variation for sample no.3

Distance from heater (mm)	Layer 1 (top of sample)	Layer 2 (Middle of sample)	Layer 3 (Middle of sample)	Layer 4 (bottom of sample)
0	25.4	26.7	27.9	29.2
20	24.5	25.4	26.2	26.9
40	23.9	24.5	25.2	25.6
60	23.5	24.0	24.5	24.8
80	23.3	23.7	24.1	24.2
100	23.0	23.4	23.6	23.7
118	22.6	22.9	23.1	23.2

#### 5.2.5.4 Objective 4: Thermal Loading Cycles

Objective 4 was to investigate a range of thermal cyclic loads from 2 to 22 hours of heating and cooling within a 24 hour cycle to determine the sample response to heating cycles and time required to cool down.

The heating cycle was run for 8 hours and then allowed to cool for 16 hours and this was repeated over a period of five days to investigate if changes will take place as the test is repeated over time. A graph of the results from this test are shown in Figure 5.7.

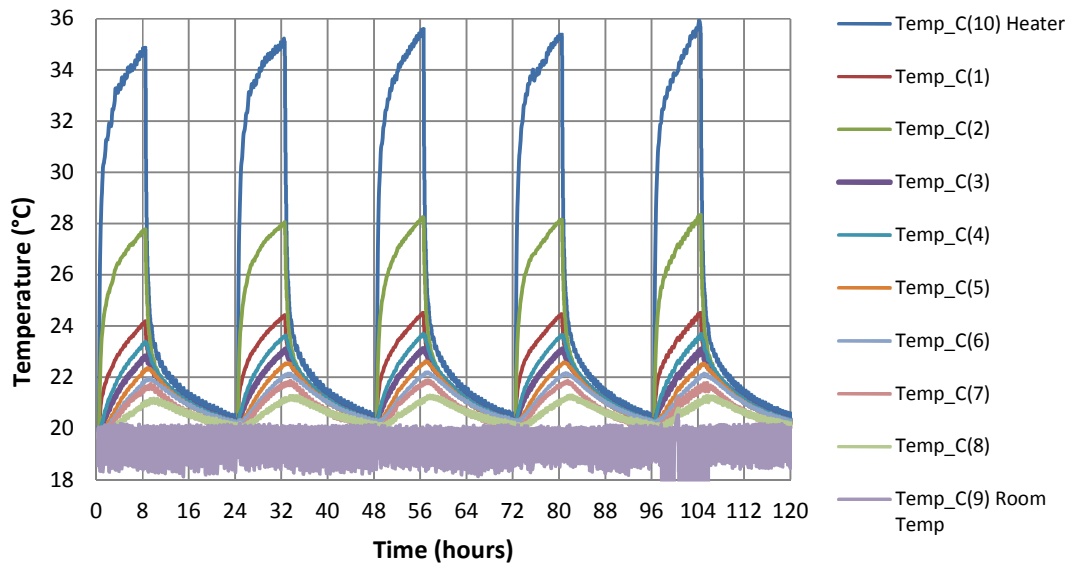


Figure 5.7: The temperature variation across the sample during 8 hours heating and 16 hours cooling for five days on a kaolin sample at 50kPa and at 5.4W

Table 5.4 presents the temperature values at points within the sample at the end of each thermal heating load and cooling after 24 hours. It shows that the cycles of thermal loading had little effect on the maximum and minimum temperatures, and the sample did not reach thermal equilibrium after 8hrs of heating.

Table 5.4: Temperature values after 8 hours thermal heating load and 16 hours cooling for day 1 and day 5 in kaolin at 50kPa and 5.4W power

Probe label	Distance from Heater (mm)	Temp after 8 hours thermal load (°C) Day 1	Temp after 16 hours cooling (°C) Day 1	Temp after 8 hours thermal load (°C) Day 5	Temp after 16 hours cooling (°C) Day 5
Probe 10	Heater	34.7	20.4	35.3	20.6
Probe 1	Outer edge top of pipe	24.1	20.3	24.2	20.8
Probe 2	Outer edge bottom of pipe	27.7	20.2	28.0	20.2
Probe 3	38	22.7	20.3	22.7	20.3
Probe 4	38	23.3	20.3	23.3	20.3



Probe label	Distance from Heater (mm)	Temp after 8 hours thermal load (°C) Day 1	Temp after 16 hours cooling (°C) Day 1	Temp after 8 hours thermal load (°C) Day 5	Temp after 16 hours cooling (°C) Day 5
Probe 5	78	22.2	20.3	22.2	20.3
Probe 6	78	21.8	20.3	21.8	20.3
Probe 7	117	21.6	20.1	21.4	20.1
Probe 8	117	21.0	20.2	20.9	20.1
Probe 9	Controlled Room Temp	18.8	18.8	20.0	18.5

**5.2.5.5 Objective 5: Shear Strength and Water Content Tests**

The objective was to determine shear strengths and water contents within the sample relative to the heat source and bottom of the sample.

At the end of the thermal tests the rig was dismantled by stopping the test, disconnecting the pressure, and removing the cell cover and top piston. The shear strength and water content tests were carried out while the sample was still in the test chamber in order to avoid disturbing the sample and altering its state.

Locations were marked on the sample with reference to distance from the heater and shear strength tests using the vane apparatus were carried out at those locations. Samples were collected from the tested points to determine their water contents. The tests were carried out layer by layer in four layers each approximately 46mm in height. A total of 96 samples were tested.

Figure 5.8 shows the variation of shear strength with distance from heater in the four layers from top to bottom of the sample.

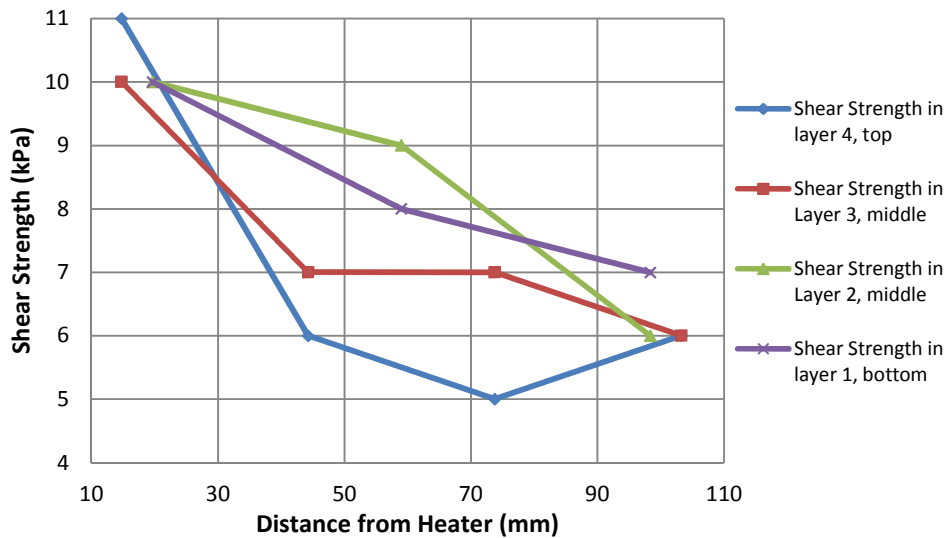


Figure 5.8: Variation of shear strength with distance from heater in the four layers from top to bottom of the sample

The plot indicates an increase in sample strength closer to the heat source which is consistent with the reduction in water content shown in Figure 5.8.

Similarly, Figure 5.9 shows the variation of water content with distance from heater in the four layers from top to bottom of the sample. The plot indicates a decrease in percentage water content closer to the heat source.

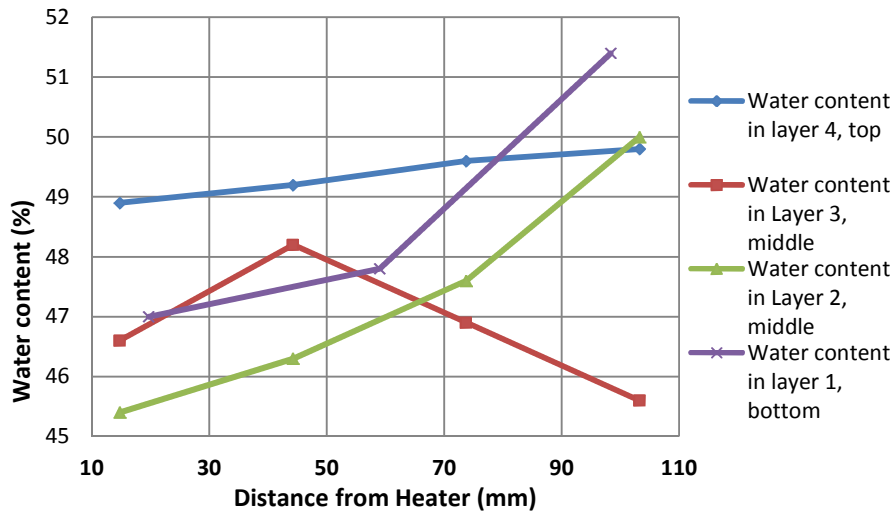


Figure 5.9: Variation of percentage water content with distance from heater in the four layers from top to bottom of the sample

Figure 5.10 shows a plot of shear strength against water content for the sample tested. Samples tested from each layer were represented differently to give an indication of how the shear strength and water content vary from top to bottom of the sample.

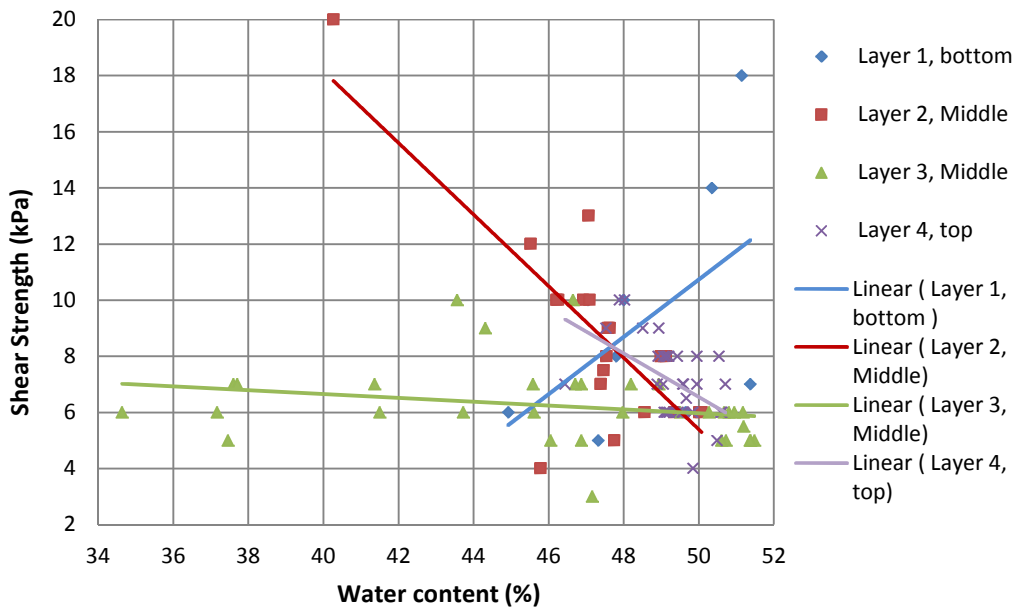


Figure 5.10: The variation of shear strength with percentage water content in Sample No.3 at the end of the heating tests

The trend lines generally do not show a clear relationship between the shear strength and water content, but show a trend of increasing shear strength with a reduction in water content which is best defined in layer 2 where the relationship can be considered strong for the water content range of 45.8-50.3% as shown in Table 5.5. The trend lines for layers 1 and 4 have similar R-squared values as shown in Table 5.5, which also shows the coefficients and regression values for the trend lines in Figure 5.10. This being a preliminary test was used as basis for improving the test procedure.

Table 5.5: The coefficients and regression values for sample No. 3

Sample layer	Equation for fit $y = mx + c$	$R^2$	Validity range of water content (%)
Layer 4 (Top)	$-0.7767x + 45.374$	0.2649	46.4 - 50.7
Layer 3 (Middle)	$-0.068x + 9.3731$	0.0559	34.6 - 51.5
Layer 2 (Middle)	$-1.2772x + 69.248$	0.6093	45.8 - 50.3
Layer 1 (Bottom)	$1.0223x - 40.369$	0.2638	44.9 - 51.4

### 5.2.5.6 Observations and Problems Encountered During Test

By the end of this test (Test No. 3), the five objectives of the tests were achieved.

Problems that arose during this test and how they were resolved are as follows:

- 1) Delay was experienced in the course of running the test due to heater failure. It stopped working as a result of damage caused by the leakage from the preliminary tests as the wiring was not adequately protected. Two heaters were ordered from the manufacturers for use with the rig, therefore there was a backup available. As a precaution, the wiring of the second heater was then protected by securing it with water proof material. In order to replace the faulty heater in the already set up rig, the test was interrupted and a forklift was used to raise the rig gently to create access to its base through which the new heater was installed. This was done successfully and the test proceeded.
- 2) To solve the problem of temperature disparity between the heater and outside the copper pipe wall as identified from the previous test, heat transfer gel was ordered to smear around the heater prior to placing it in the pipe to allow for uniform heat conduction through the pipe and also get rid of air in the pipe. Delayed supply of the heat transfer gel translated to a delay in the test.

- 3) Also during the course of this test, it was identified that a wrong thermocouple wiring in the data-logger was being used for the heater. K thermocouple wiring was used instead of J wiring meant for the heater. This was resolved as soon as it was noticed. The use of the heat transfer gel resulted in reducing the temperature difference between the heater and outer wall of pipe.
- 4) Slight leakage persisted during the test.

Due to all the problems encountered during the period of testing Sample No. 3, it was considered as a learning test and most data collected were not used in the discussion chapter because of the errors noted.

A lasting and more reliable solution to the problems identified above led to the need to modify the rig and heater design for more reliable tests and data. The process of modification was set in motion and at the end, a modified rig design was fabricated.

### **5.2.6 Sample No. 4 (Tests carried out on kaolin sample at 25kPa)**

While awaiting the fabrication of the modified rig design, another test was set-up, taking care to make improvements based on the experiences of the previous test.

A kaolin sample was prepared at 82% water content and carefully loaded into the test cell. During the consolidation phase a pressure of 25kPa was applied in incremental stages of 6, 12.5, and finally 25kPa.

The objectives for setting up this test were in line with the objectives of the tests listed in section 5.2.1.

Eight thermocouples were inserted into the test chamber with four on each side. They were inserted from the inner edge of the cell towards the heater at distances of 1mm, 40mm, 80mm and 118mm (touching the heater), and at four levels with each on a different level of the sample height, at intervals of 40mm. The lowest probe was inserted at about 45mm above the sample base, and all other probes inserted 40mm above each other.

Figure 5.11 on page 128, shows the layout of thermocouples for the thermal tests carried out on this sample.

#### **5.2.6.1 Objective 1: Equilibrium Heating Duration**

To determine how long it took the soil sample being tested to achieve equilibrium or steady state conditions, the heating test was commenced by supplying power to the cartridge heater from the power supply unit.

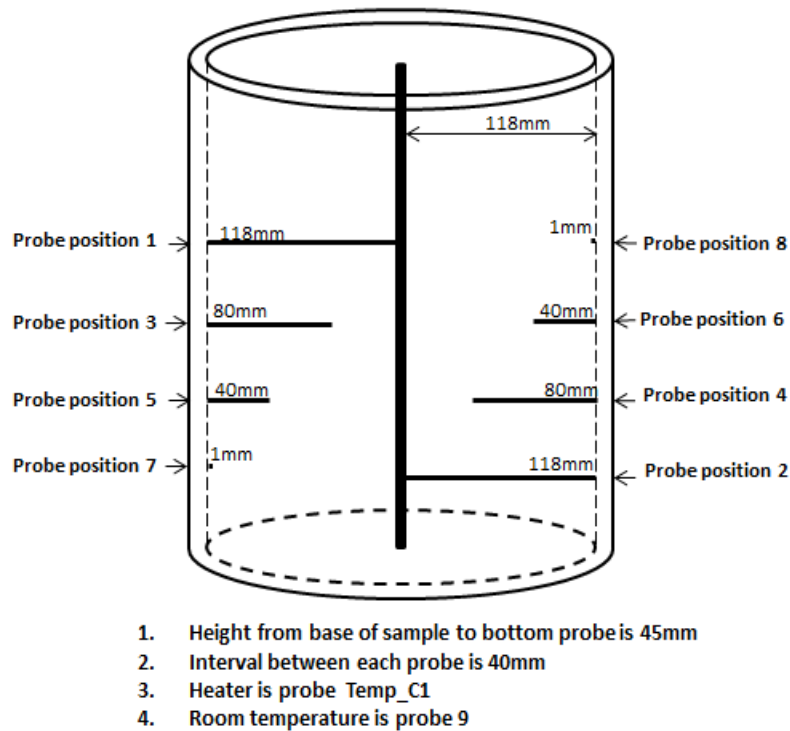


Figure 5.11: Layout of thermocouples for tests carried out on kaolin sample at 25kPa

The temperature changes in the heater and within the sample were logged during the test and the results are presented in Figures 5.12. and 5.13 (page 129) The figures present two graphs of the sample being heated to steady state condition at two different power inputs of 4.49W and 9.48W respectively

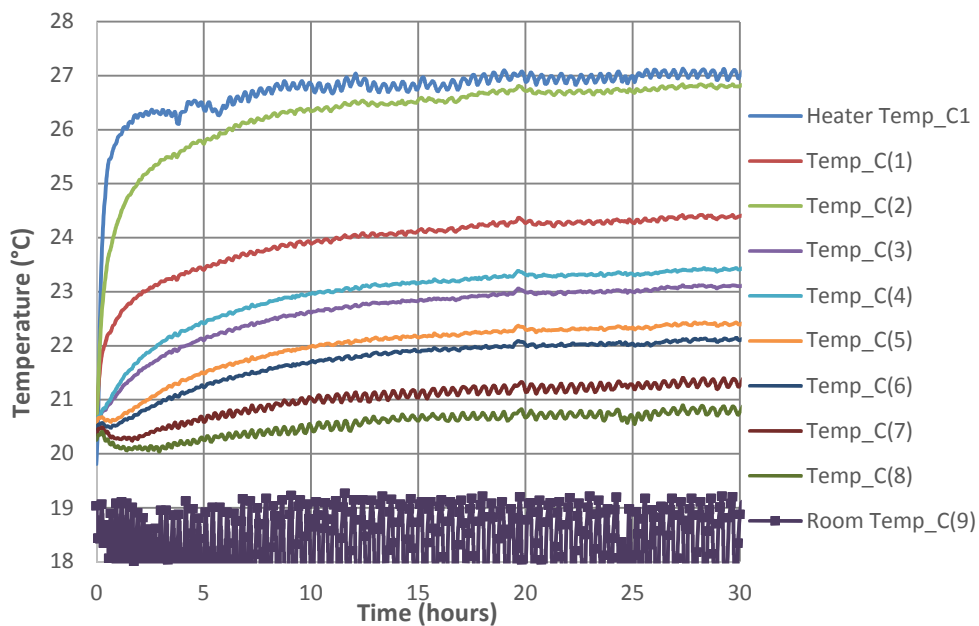


Figure 5.12: Kaolin Test at 25kPa at thermal equilibrium for power input of: 4.49W

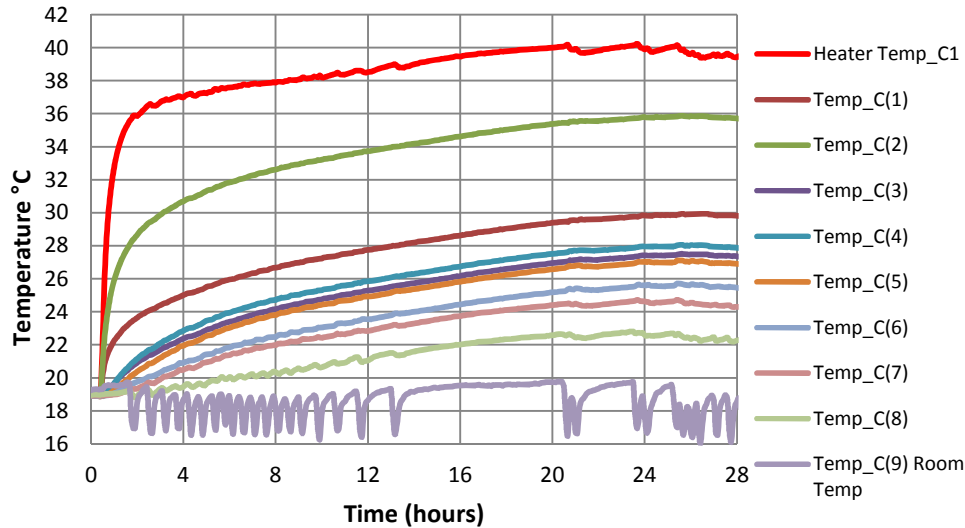


Figure 5.13: Kaolin Test at 25kPa at thermal equilibrium for power input of 9.48W

The sample was allowed ample time to cool down between the tests, and the second test was only commenced after the sample had cooled down to room temperature. The sample achieved equilibrium conditions after approximately 28 hours of heating at the lower power input and 26 hours at the higher power input. The higher power meant that the sample heated up faster.

An observation from this test is that the difference between the heater temperature and outside the pipe wall reduced considerably after the use of the heat transfer gel around the heater and also rectifying the heater wiring to the correct one.

The temperature values at fixed locations within the sample in equilibrium condition at both power inputs are presented in Table 5.6.

Table 5.6: Temperature values at probe locations for thermal equilibrium for kaolin at 25kPa and 4.49W and 9.48W power

Probe label	Distance from Heater (mm)	Temp in Equilibrium after 28 hours at power of 4.49W (°C)	Temp in Equilibrium after 26 hours at power of 9.48W (°C)
Probe 10	Heater	27.0	39.4
Probe 1	Outer edge top of pipe	24.4	29.9
Probe 2	Outer edge bottom of pipe	26.8	35.9
Probe 3	38	23.1	27.5
Probe 4	38	23.4	28.0
Probe 5	78	22.4	27.1
Probe 6	78	22.1	25.6
Probe 7	117	21.2	24.5
Probe 8	117	20.8	22.2
Probe 9	Controlled Room Temp	18.2	16.0

### 5.2.6.2 Objective 2: Cooling Duration

The second objective was to determine the duration of cooling. This was done by disconnecting power supply to the heater and allowing the sample return to initial temperature (controlled room temperature). From Figures 5.14 and 5.15, complete cooling of the sample from equilibrium condition back to initial temperature lasted approximately 30 hours in both cases of heating at different power inputs.

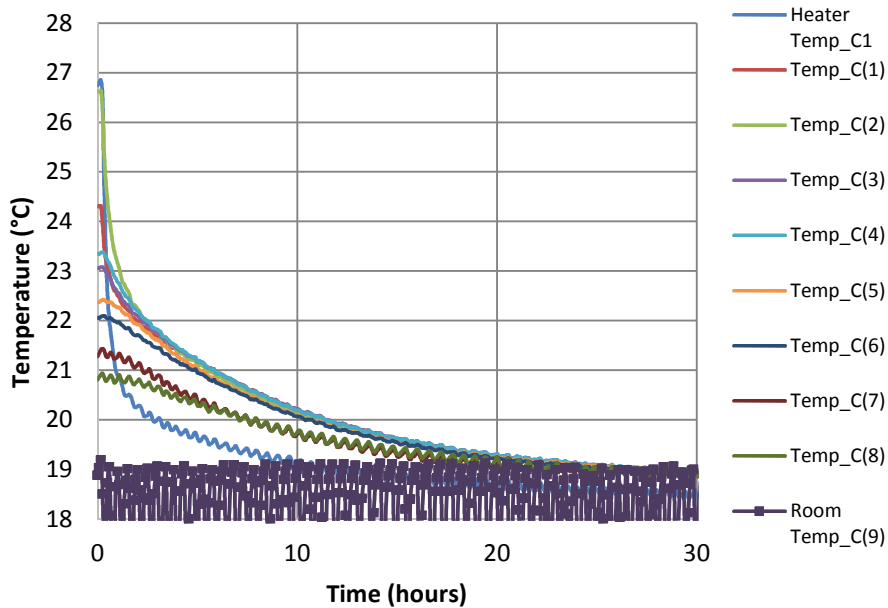


Figure 5.14: Cooling curves for kaolin test at 25kPa from thermal equilibrium achieved at power input of 4.49W

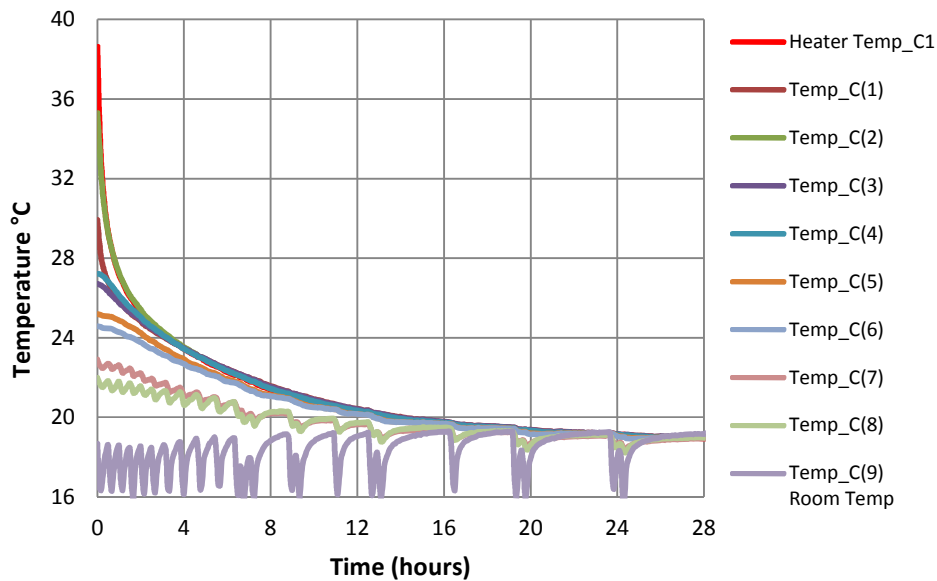


Figure 5.15: Cooling curves for kaolin test at 25kPa from thermal equilibrium achieved at power input of: 9.48W

### 5.2.6.3 Objective 3: Temperature Variations in Sample at Start of Test

The objective of this test was to measure the temperature profile across the sample when in thermal equilibrium at the start of the testing regime to show the temperature variations between the centre and edge of sample. This was carried out across the sample and at four levels along the sample height according to the procedure explained in Chapter 4. The graph of results from this test is shown in Figure 5.16. From this figure, the temperature at the bottom of the cell was observed to be higher than that at the top of the cell.

Table 5.7 presents the temperature values measured at intervals of 15mm across the sample and at four levels from top to bottom of the sample during the profile test while sample remained in thermal equilibrium.

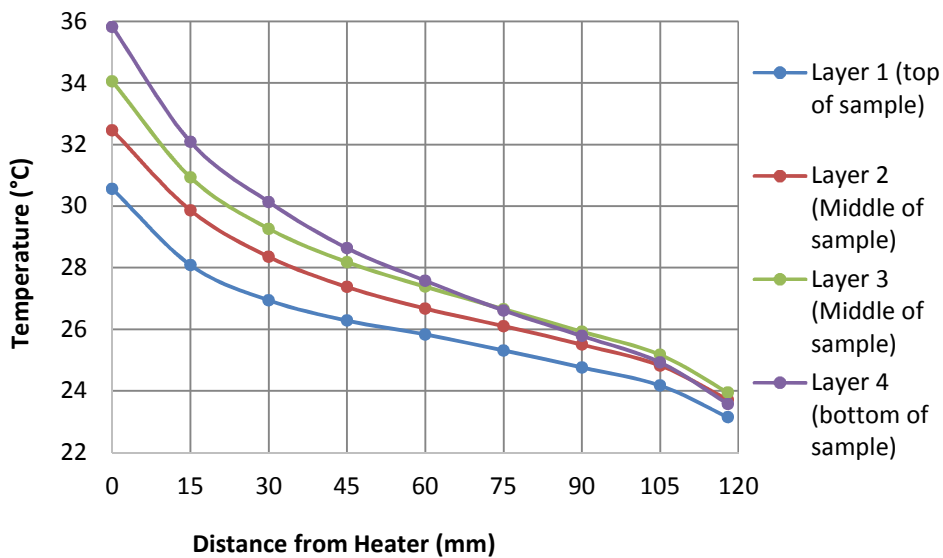


Figure 5.16: Temperature variations across sample and at four levels from top to bottom of sample at start of kaolin at 25kPa test

Table 5.7: Table showing temperature variation values at start of test on sample no.4

Distance from heater (mm)	Layer 1 (top of sample)	Layer 2 (Middle of sample)	Layer 3 (Middle of sample)	Layer 4 (bottom of sample)
0	30.6	32.5	34.1	35.8
15	28.1	29.9	30.9	32.1
30	26.9	28.4	29.3	30.1
45	26.3	27.4	28.2	28.6
60	25.8	26.7	27.4	27.6
75	25.3	26.1	26.7	26.6
90	24.8	25.5	25.9	25.8
105	24.2	24.8	25.2	24.9
118	23.1	23.7	23.9	23.6



Figure 5.17 presents a temperature contour plot of the sample in thermal equilibrium, with each of the different colours and shades of the same colour representing different temperature ranges. This figure captures the temperature variations across the sample and from top to bottom of the sample at the end of the test when a power of 17.05W was applied. This Figure shows that the temperature in the sample reduces radially as expected but there is also some temperature reduction from bottom to top of the sample which suggests some heat loss from the top of the sample. However, the most of the heat loss was radial.

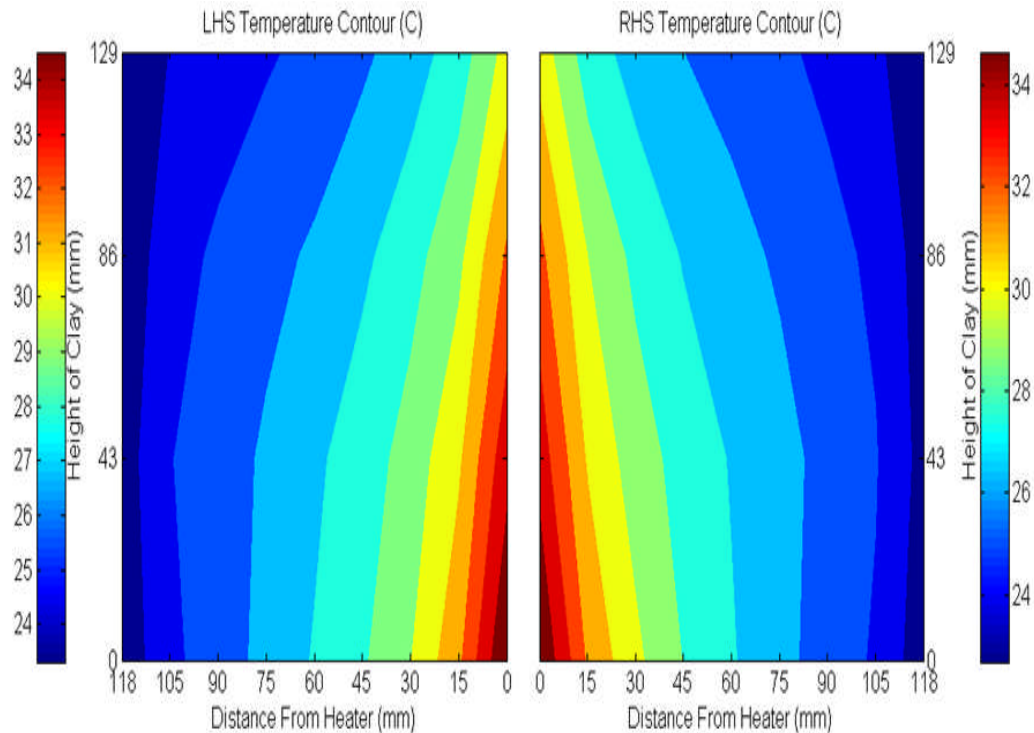


Figure 5.17: Contour plot of temperature variations across sample no.4 in heating equilibrium condition

#### 5.2.6.4 Objective 4: Thermal Loading Cycles

Another test was carried out on this sample to investigate thermal loading cycles within a 24 hour period. Thermal cyclic loads tested during this test include 4, 8, 12, 16 and 20 hours of heating within a 24 hour testing period. They were run over several days and at different power inputs.

The results from the 8 hours heating and 16 hours cooling is presented here in Figure 5.18 (page 133).

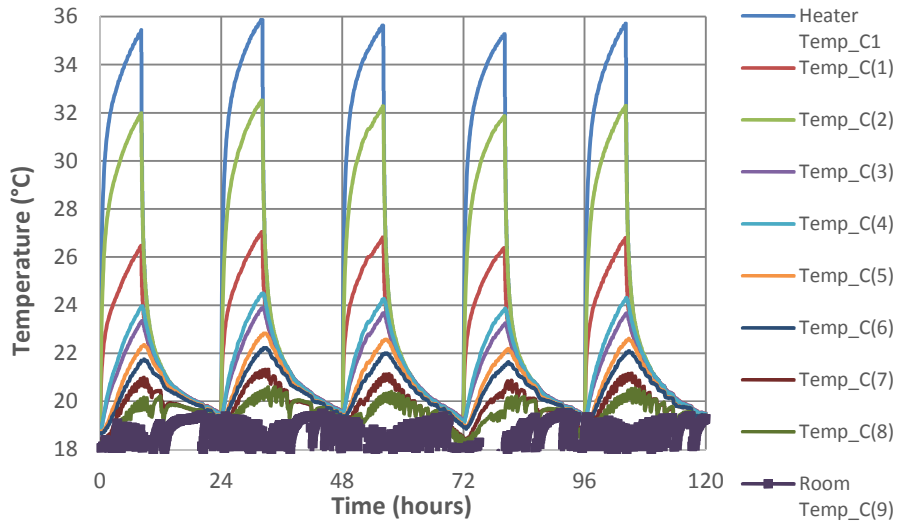


Figure 5.18: Variation in temperature with time for thermal loading cycles of 8 hours heating and 16 cooling over five days on kaolin sample at 25kPa and 9.48W

Table 5.8 presents the temperature values measured at points within the sample at the end of the thermal heating load and at cooling after 24 hours, and also the thermal load and cooling on the fifth day (that is, the last cycle of thermal loading). The temperature after 8hrs of thermal loading on the fifth day was consistently higher than that after one day. The difference varied between 0.4°C at the heater to 0.1°C at the wall of the cell .

Table 5.8: Temperature values after 8 hours thermal heating load and 16 hours cooling in kaolin at 25kPa and 9.48W power

Probe label	Distance from Heater (mm)	Temp after 8 hours thermal load (°C) Day 1	Temp after 16 hours cooling (°C) Day 1	Temp after 8 hours thermal load (°C) Day 5	Temp after 16 hours cooling (°C) Day 5
Probe 10	Heater	35.3	19.4	35.7	19.4
Probe 1	Outer edge top of pipe	26.4	19.5	26.8	19.5
Probe 2	Outer edge bottom of pipe	31.9	19.4	32.2	19.4
Probe 3	38	23.3	19.5	23.6	19.5
Probe 4	38	23.9	19.4	24.2	19.5
Probe 5	78	22.2	19.4	22.4	19.4
Probe 6	78	21.6	19.3	21.9	19.4
Probe 7	117	20.9	19.2	21.0	19.2
Probe 8	117	20.1	19.2	20.2	19.3
Probe 9	Controlled Room Temp	18.8	19.0	18.6	19.3

### 5.2.6.5 Objective 5: Shear Strength and Water Content Tests

The objective of this test was to determine shear strengths and water contents within the sample in relation to distance from heat source and different levels of sample height.

At the end of the thermal tests the rig was dismantled by stopping the test, disconnecting the pressure, and removing the cell cover and top piston. The shear strength and water content tests were carried out while the sample was still in the test chamber in order to avoid disturbing the sample and altering its state.

Locations were marked on the sample with reference to distance from the heater and shear strength tests were carried out in those locations. Samples were collected from the tested points to determine their water contents. The tests were carried out layer by layer in four layers. 20 samples were tested on each layer ranging in thickness between 50-60mm. A total of 80 samples were tested.

Figure 5.19 shows the variation of shear strength with distance from heater in the four layers from top to bottom of the sample. The plot indicates an increase in shear strength closer to the heat source.

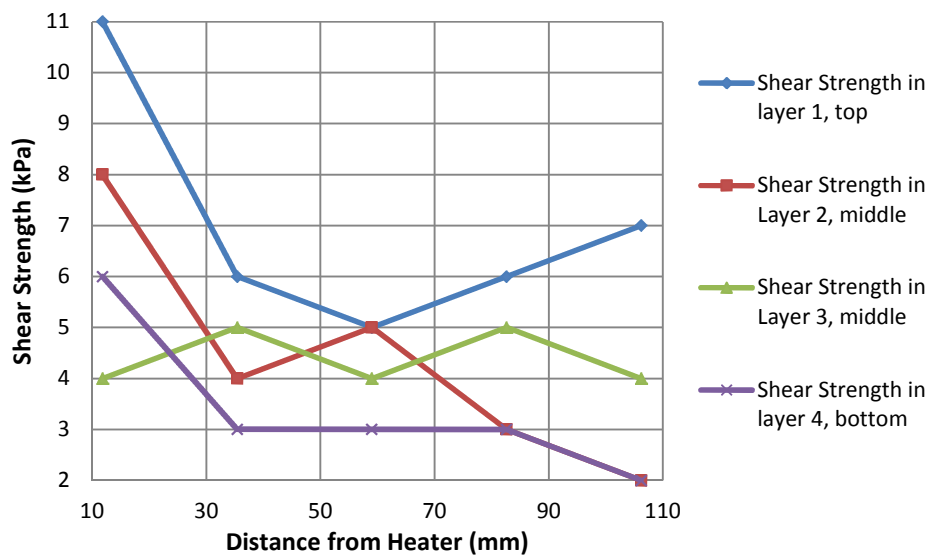


Figure 5.19: Variation of shear strength with distance from heater in the four layers from top to bottom of the sample

Figure 5.20 shows the variation of water content with distance from heater in the four layers from top to bottom of the sample. The plot indicates a decrease in percentage water content closer to the heat source.

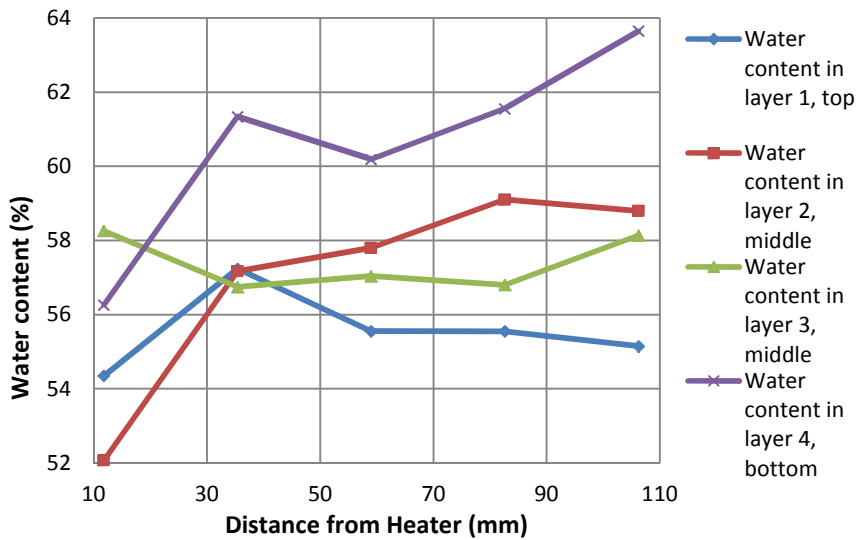


Figure 5.20; Variation of percentage water content with distance from heater in the four layers from top to bottom of the sample

Figure 5.21 shows a plot of shear strength against water content for this sample. Samples tested from each layer are represented in different colours in the graph to give an indication of how the shear strength and water content vary from top to bottom of the sample.

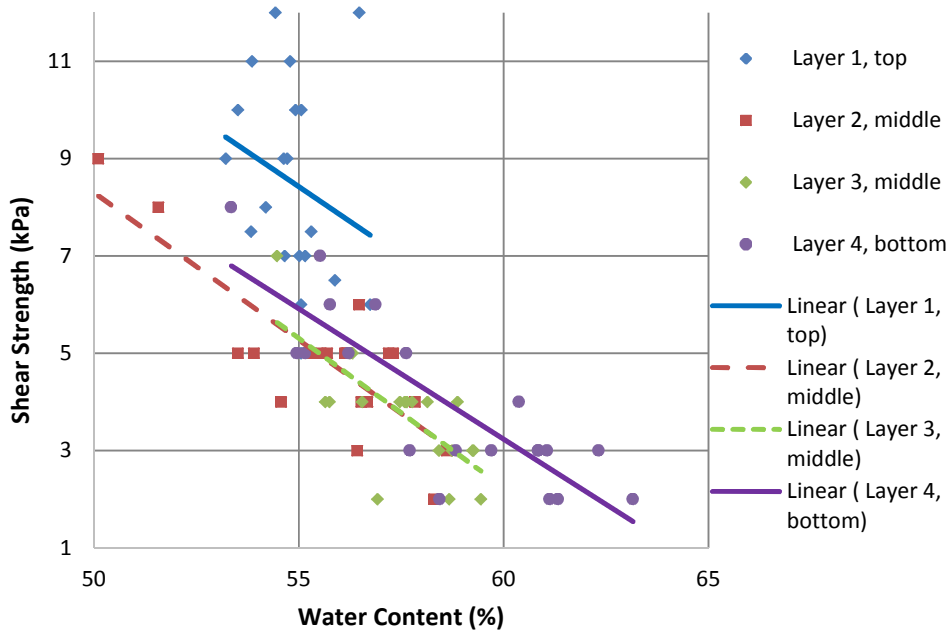


Figure 5.21: The variation of shear strength with percentage water content in kaolin sample tested at 25kPa at the end of the testing regime

The trend lines show a strong trend of increasing shear strength with a reduction in water content. The trend lines for layers 2 and 3 are the same. The trend lines for layers 2, 3 and 4 have similar R-squared values as shown in Table 5.9 which shows

the coefficients and regression values for the trend lines in Figure 5.21. The values from this Figure show a clear improvement over those in Figure 5.10 which being the first test was used as basis for improving the test procedure.

Table 5.9: The coefficients and regression values for sample No. 4

Sample layer	Equation for fit $y = mx + c$	$R^2$	Validity range of water content (%)
Layer 1 (Top)	$-0.5732x + 39.945$	0.0596	53.2 – 56.9
Layer 2 (Middle)	$-0.6044x + 38.512$	0.6732	50 – 58.5
Layer 3 (Middle)	$-0.6143x + 39.092$	0.5268	54.5 – 59.4
Layer 4 (Bottom)	$-0.5363x + 35.4$	0.7167	53.3 – 63.1

### 5.2.6.6 Conclusion

This was the last test carried out in the first rig. All subsequent tests were carried out in the modified rig to improve on the quality of results obtained.

The modifications made to the rig include changes to the cartridge heater design to allow it be placed directly within the sample and secured with O-rings and bolts to the cell base thus eliminating the need for the copper pipe, heat transfer gel and leakage from around the pipe.

The temperature differential in the heater shown by the contour profile plot was also addressed during the heater modification.

The power supply unit was replaced due to fluctuating power inputs, to a more stable unit.

Preliminary tests were carried out to develop the test procedures following the set objectives. The results obtained were analysed and used as a basis for improving on subsequent tests carried out in the modified rig, which are presented in Chapter 6.

## **Chapter 6 Results from Modified Rig Tests**

### **6.1 Introduction**

Chapter 6 is a continuation of chapter 5 in presenting the details of all the tests carried out. While chapter 5 focused on tests carried out in the first rig design, this chapter focuses on the tests carried out in the modified rig design. The results presented here will be discussed in Chapter 7.

The need for the modification was highlighted by the problems encountered during the preliminary tests as described in Chapter 5. The key issues addressed by the modifications were that of water leakage and temperature differential in the heater in order to improve on the quality of results obtained.

The samples tested in the modified rig were kaolin, sand and a mixture of both in different proportions, to study their thermal behaviour under the following parameters:

- 1) The soil type constituting the sample tested
- 2) The water content of the sample
- 3) The overburden pressure applied to the sample in the test chamber
- 4) The power input determining the heater temperature as controlled by the current and voltage used
- 5) Time or duration of the test
- 6) Thermal loading cycles

### **6.2 Tests Carried out in Modified Rig**

A total of nine samples were prepared and tested in the modified rig, with several categories of tests carried out on each sample. The samples tested and presented were numbered from 5 to 13, each varying in composition, water content, and overburden pressure at which the test was carried out. The numbering is a continuation of the numbering of the samples presented in Chapter 5.

The results will be presented in three groups according to the soil type constituting the samples. The groups are:

- 1) Tests carried out on kaolin
- 2) Tests carried out on kaolin and sand mixtures
- 3) Tests carried out on sand

Within the groups, the results of tests carried out on the samples will be presented according to the sample label for each of the 9 samples and the details of the tests carried out on each of them will be presented one after the other on the basis of the objectives behind carrying out each of them.

### **6.2.1 Objectives of Thermal Tests Carried out on Soil Samples**

Each of the nine samples was prepared and underwent series of thermal tests to achieve a set of objectives. The following objectives were common to all the samples being tested:

- 6) To determine how long it took the soil sample being tested to achieve thermal equilibrium or steady state conditions when heated from a controlled room temperature at a specific pressure, water content, and power input
- 7) To determine the time it took to cool back to the room temperature when the power supply is disconnected
- 8) To determine the distribution of temperature across the sample in thermal equilibrium
- 9) To investigate a range of thermal loading cycles from 2, 4, 6, 8 12, up to 22 hours heating and cooling within a 24 hour cycle to determine sample response to heating cycles and time required to cool down. The thermal cycles tested differ from test to test and will be specified for each test
- 10) To determine shear strengths and water contents within the sample in relation to distance from heat source and different levels of sample height at the end of each test.

A summary of the samples prepared and the conditions under which they were tested is presented in Table 6.1, and the samples will be identified by their serial number on the Table 6.1 (page 139), the sample soil type and the pressure applied.

### **6.2.2 Tests carried out on Kaolin**

Samples number 5, 6 and 7 were formed of kaolin which was tested under varying conditions of water content and overburden pressures. Tests carried out are discussed according to the sample numbers.

#### **6.2.2.1 Sample No. 5 (Tests carried out on kaolin sample at 100kPa)**

On the arrival of the modified rig design, leakage tests were carried out on it as explained earlier, and no leakage was detected.

Table 6.1: Detailed summary of samples and tests carried out on each sample

Samples S/N		5	6	7	8	9	10	11	12	13
VARIABLES / PROPERTIES / TESTS	Material	Kaolin	Kaolin	Kaolin	Kaolin Sand 75:25	Kaolin Sand 75:25	Kaolin Sand 50:50	Kaolin Sand 25:75	Sand	Sand
	Water content before Test (%)	82	82	84.5	59	59	44.4	32	Dry	26
	Pressure Applied (kPa)	100	200	0, 25, 50	25	100	25, 50, 100	25, 50, 100	25	25
	Power (W)	17.03	17.03	17.03	17.03	17.03	17.03	17.03	4.23	19.04
	Sample Height before Test (mm)	275	275	285	285	285	275	270	228	218
	Sample Height after Test (mm)	190	186.5	205	234	218	213	220	218	218
	Height Diff. (mm)	85	88.5	80	51	67	62	50	10	0
	Avg. Shear Strength after Test (kPa)	16.3	38.7	11.4	5.9	17.2	28	13	NA	NA
	Avg. Water Content after Test (%)	48	42	49.8	42.1	36.5	22.8	19.6	NA	NA
	Thermal Cycles within 24 hours (hours)	2, 4, 6, 8, 12, 14, 18, 22	4, 8, 12, 18, 22	8, 12	4, 8, 12, 20	4, 8, 12, 20	4, 8, 12	8, 12	4, 8, 12	8, 12
	Heating to Steady State (hours)	29	48	36, 40, 38	26	40	39, 42, 43	28, 28, 48	24	24.5
	Cooling Duration (hours)	26	30	24, 28, 23	30	32	20, 32, 30	27, 23, 24	18	22
Duration of whole Test (weeks)	19	21	8	7	10	15	12	8	6	

A kaolin sample was prepared at 82% water content to ensure saturation, and carefully placed in the rig cell for a series of thermal tests to be carried out at a pressure of 100kPa. The objectives of the tests carried out on this sample were common to those listed in section 6.2.1.



During the consolidation phase, pressure was applied in incremental loads of 6, 12.5, 25, 50 and finally 100kPa.

At the end of the consolidation phase, thermocouples were inserted into the test chamber from two opposite sides, at different radii and levels. Each thermocouple on the left side had a thermocouple on the right hand placed at a similar distance from the heater to build in redundancy, allow for a failure of a thermocouple and provide a means of averaging the temperature variation or measure the variation both vertically and horizontally. Figure 6.1 shows the layout of thermocouples for this test.

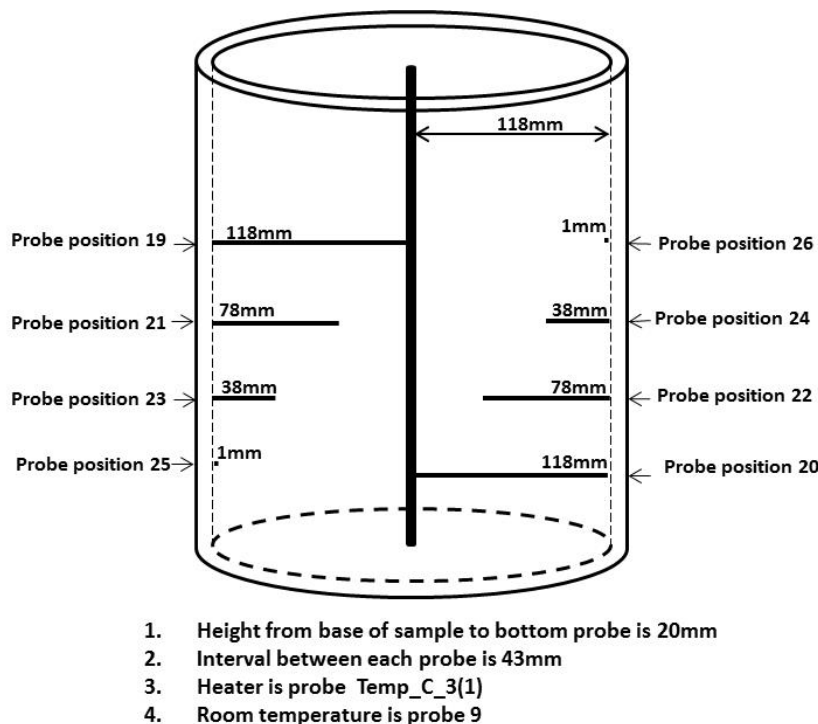


Figure 6.1: Layout of thermocouples within the test chamber for tests on kaolin at 100kPa

Eight thermocouples were inserted into the test chamber with four on each side. They were inserted from the inner edge of the cell towards the heater at distances of 1mm, 38mm, 78mm and 118mm (touching the heater), and at four levels with each on a different level of the sample. The lowest thermocouple was positioned at 20mm above the sample base, while the others were placed at intervals of 43mm above each other. Additional thermocouple numbers were assigned to subsequent tests as the previous thermocouples were still in use in sample no 4 when this test was set up.

#### 6.2.2.1.1 Objective 1: Equilibrium Heating Duration

This heating test was undertaken to determine how long it took the soil sample to achieve equilibrium or steady state conditions.

The heating test was commenced by supplying power to the cartridge heater from the power supply unit.

A power input of 17.03W was used in this test and the sample achieved equilibrium conditions after approximately 29 hours of heating. The temperature changes in the heater and within the sample were logged during the test and a graph of the results is presented in Figure 6.2. Temperature fluctuations observed in the room temperature were expected within the range of  $\pm 1.5^{\circ}\text{C}$ .

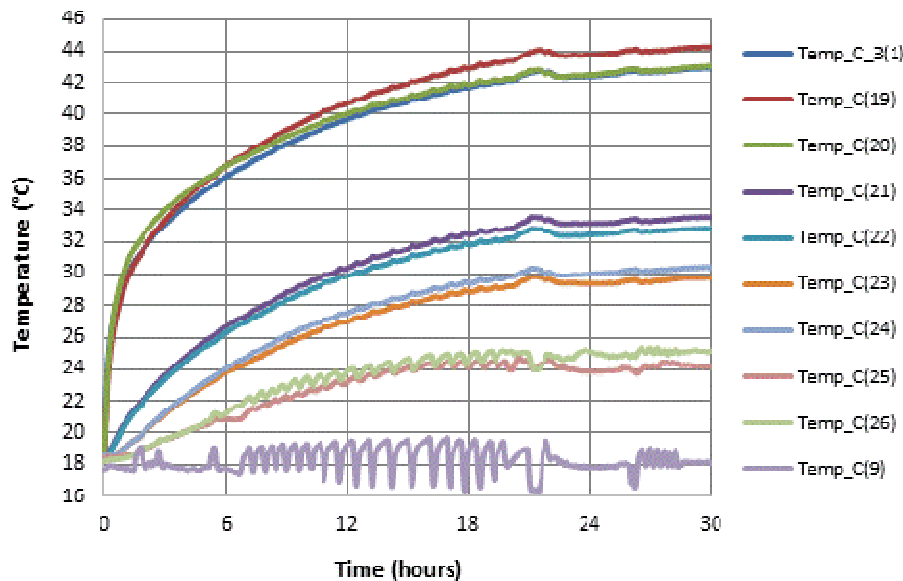


Figure 6.2: The variation of temperature with time across a sample of kaolin consolidated to 50kPa showing that thermal equilibrium was achieved after about 29 hours

The temperature values at fixed locations within the sample in equilibrium condition at the power input of 17.03W are presented in Table 6.2.

Table 6.2: Temperature values at probe locations in thermal equilibrium for kaolin test at 100kPa and power input of 17.03W

Probe label	Distance from Heater (mm)	Temp in steady state after 29 hours ( $^{\circ}\text{C}$ )
Probe 10	Heater	42.9
Probe 19	Outer edge top of heater	44.2
Probe 20	Outer edge bottom of heater	43.0
Probe 21	40	33.5
Probe 22	40	32.8
Probe 23	80	29.7
Probe 24	80	30.4
Probe 25	117	24.3
Probe 26	117	25.2
Probe 9	Controlled Room Temp	18.1

### 6.2.2.1.2 Objective 2: Cooling Duration

To determine the duration of cooling the power supply to the heater was disconnected. The sample was allowed to return to its initial temperature (controlled room temperature). From Figure 6.3, complete cooling of the sample from equilibrium condition back to initial temperature lasted approximately 26 hours.

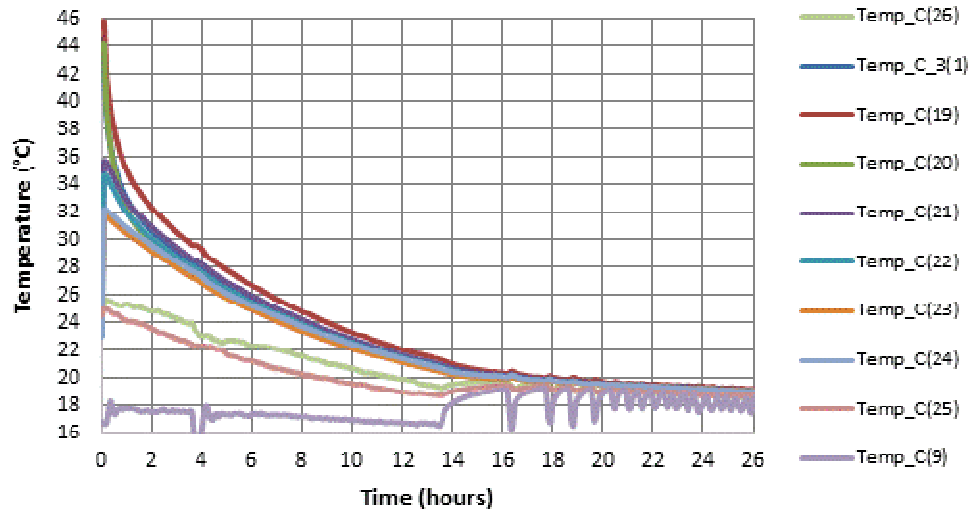


Figure 6.3: The time to return to room temperature (test at 100kPa)

### 6.2.2.1.3 Objective 3: Temperature Variations across Sample

The objective here was to measure the temperature profile across the sample under thermal equilibrium, in order to obtain the temperature variations within the sample at the start of the testing regime. Results from this test are shown in Figure 6.4.

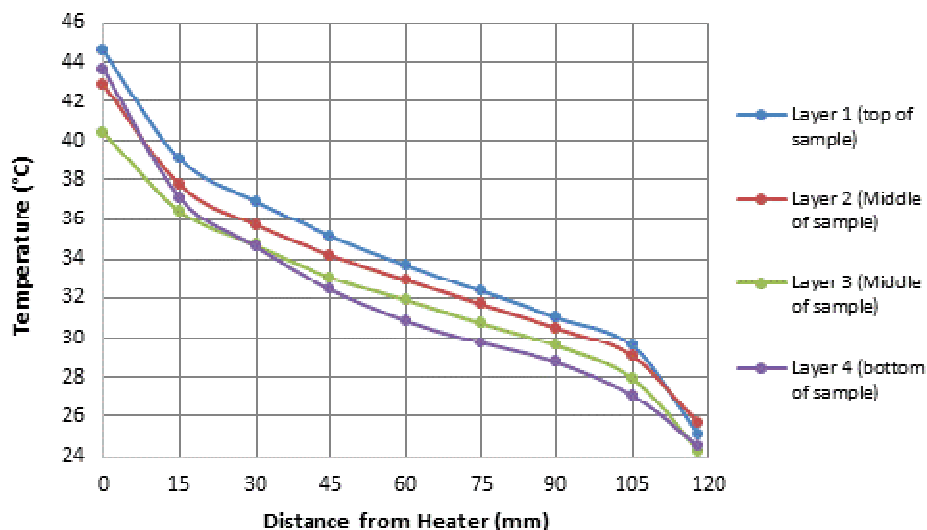


Figure 6.4: Temperature variations across sample from heater to edge of test chamber and from top to bottom of sample at start of test on kaolin sample at 100kPa

The temperature variation in the new heater design was also investigated during this test. The temperature values measured at the locations within the sample are presented in Table 6.3.

Table 6.3: Table showing temperature variation values at the start of test on kaolin at 100kPa

Distance from heater (mm)	Layer 1 (top of sample)	Layer 2 (Middle of sample)	Layer 3 (Middle of sample)	Layer 4 (bottom of sample)
0	44.5	42.8	40.4	43.6
15	39.1	37.8	36.4	37.1
30	36.9	35.7	34.7	34.6
45	35.2	34.2	33.1	32.4
60	33.7	32.9	31.9	30.9
75	32.3	31.7	30.7	29.7
90	31.0	30.5	29.6	28.7
105	29.6	29.1	27.9	27.1
118	25.1	25.6	24.3	24.5

A second temperature profile across the sample in thermal equilibrium was carried out at the end of the thermal testing on the sample to show the temperature variations within the sample. Results from this test are shown in Figure 6.5. Both tests were compared to observe changes in the sample between the start of tests and at the end. This is discussed in Chapter 7.

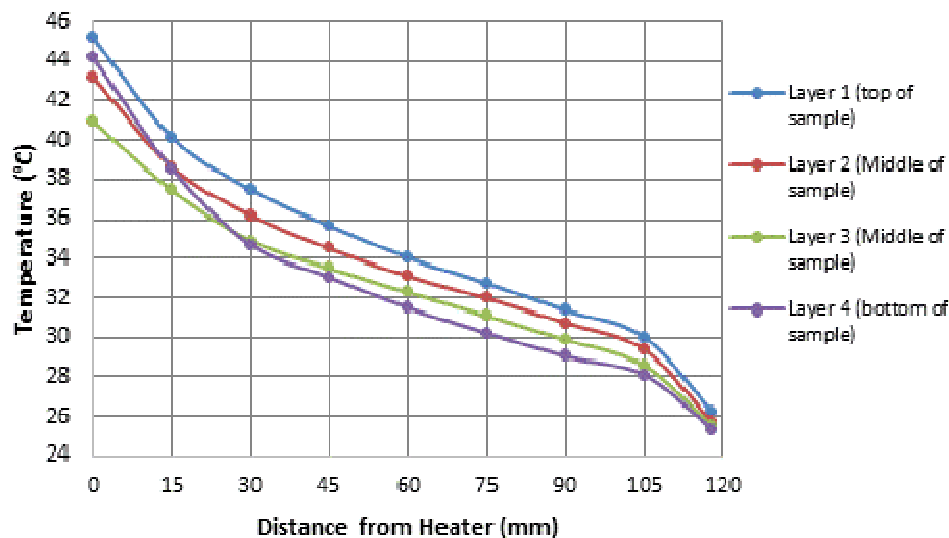


Figure 6.5: Temperature variations across sample from heater to edge of test chamber and from top to bottom of sample at end of tests on sample no. 5

The temperature contour profile plot in Figure 6.6 (page 144) shows the temperature variation in the sample No. 5 in thermal equilibrium at the end of the thermal tests carried out on sample no. 5.

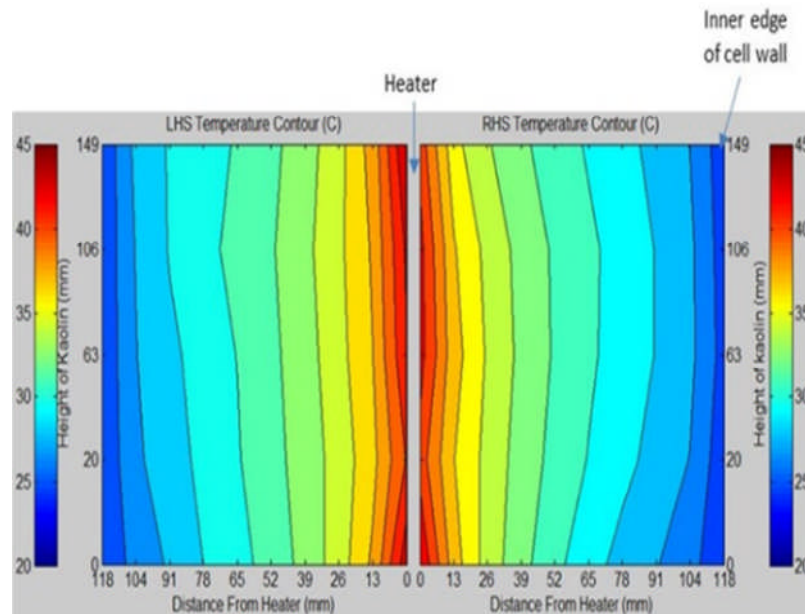


Figure 6.6: Temperature contour plot showing temperature variations in sample no. 5 at the end of the testing period

Figure 6.6 shows a more radial temperature distribution in the sample as compared with the preliminary test shown in Figure 5.17 in Chapter 5.

The temperature values measured at the locations within the sample are presented in Table 6.4

Table 6.4: Table showing temperature variation values at end of tests on sample no.5

Distance from heater (mm)	Layer 1 (top of sample)	Layer 2 (Middle of sample)	Layer 3 (Middle of sample)	Layer 4 (bottom of sample)
0	45.2	43.2	40.9	44.2
15	40.1	38.6	37.4	38.5
30	37.5	36.2	34.9	34.7
45	35.7	34.5	33.5	33.0
60	34.0	33.1	32.3	31.5
75	32.7	32.0	31.1	30.2
90	31.4	30.7	29.9	29.0
105	30.0	29.4	28.6	28.1
118	26.2	25.7	25.5	25.3

#### 6.2.2.1.4 Objective 4: Thermal Loading Cycles

Several thermal loading cycles were investigated on this sample. Thermal cyclic loads tested in kaolin sample at 100kPa within a 24 hour testing period include:

- 1) 2 hours heating cycles run for five days
- 2) 4 hours heating cycles run for two days
- 3) 6 hours heating cycles run for two days, and then repeated for 2 days later in the test
- 4) 8 hours heating cycles run for 14 days, and then repeated for 8 days later in the test
- 5) 12 hours heating cycles run for three days
- 6) 14 hours heating cycles run for five days
- 7) 18 hours heating cycles run for five days
- 8) 22 hours heating cycles run for five days

The results from the 8 hours heating and 16 hours cooling over a period of 14 days are presented here in Figure 6.7.

The 8 hours thermal cycles were repeated over two weeks to investigate any changes between the first day and the last day. The findings are presented and discussed in section 7.5.7 of Chapter 7.

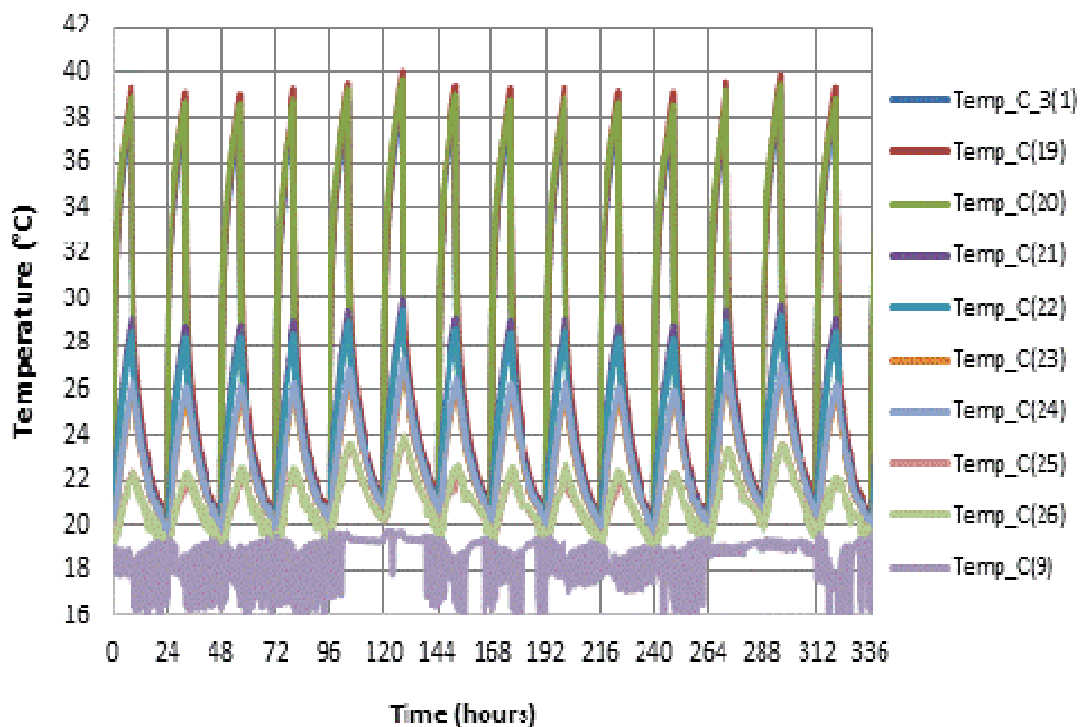


Figure 6.7: The temperature variation across the sample during 8 hours heating and 16 cooling for 14 days on kaolin sample at 100kPa and 17.03W

Table 6.5 presents the temperature values measured at points within the sample at the end of the thermal heating load and at cooling after 24 hours for all the cycles run during this test.

Table 6.5: Temperature values at probe locations after thermal cyclic loads for 2, 4, 6, 8, 12, 14, 18 and 22 hours of heating and subsequent cooling within 24 hours

Probe label	Probe 10	Probe 19	Probe 20	Probe 21	Probe 22	Probe 23	Probe 24	Probe 25	Probe 26	Probe 9
Distance from Heater (mm)	Heater	Outer edge top of heater	Outer edge bottom of heater	38	38	78	78	117	117	Room Temp
Temp after 2 hours thermal load (°C)	32.3	32.5	33.2	23.1	22.7	20.8	20.9	19.7	19.9	19.7
Temp after 22 hours cooling (°C)	18.8	18.9	18.8	18.8	18.8	18.8	18.8	18.5	18.5	17.4
Temp after 4 hours thermal load (°C)	34.5	35.0	35.2	25.2	24.7	22.4	22.5	19.3	19.6	17.0
Temp after 20 hours cooling (°C)	19.2	19.3	19.1	19.2	19.1	19.2	19.1	18.9	18.9	18.6
Temp after 6 hours thermal load (°C)	35.7	36.6	36.3	26.7	25.9	23.6	23.8	20.3	20.7	17.4
Temp after 18 hours cooling (°C)	19.3	19.4	19.3	19.3	19.2	19.2	19.2	18.7	18.7	17.1
Temp after 8 hours thermal load (°C)	38.4	39.4	38.9	29.1	28.5	25.9	26.1	22.2	22.2	18.2
Temp after 16 hours cooling (°C)	19.9	20.1	19.8	20.0	19.8	19.8	19.8	19.2	19.0	17.0
Temp after 12 hours thermal load (°C)	39.7	40.9	37.3	30.7	30.1	27.0	27.6	22.6	25.0	19.0
Temp after 12 hours cooling (°C)	21.3	21.6	21.1	21.4	21.2	20.9	21.1	19.3	20.3	17.4
Temp after 14 hours thermal load (°C)	41.2	42.4	38.7	32.3	31.6	28.6	29.1	24.0	26.1	18.4
Temp after 10 hours cooling (°C)	22.9	23.3	22.6	23.1	22.8	22.6	22.7	21.2	21.8	19.4
Temp after 18 hours thermal load (°C)	41.5	42.8	41.6	32.6	31.6	28.9	29.3	23.8	24.6	19.1
Temp after 6 hours cooling (°C)	24.8	25.6	24.3	25.1	24.6	24.3	24.4	21.7	22.1	18.5
Temp after 20 hours thermal load (°C)	42.3	43.7	42.5	33.5	32.5	29.7	30.1	24.1	25.0	16.5
Temp after 2 hours cooling (°C)	29.3	30.7	28.5	29.5	28.8	28.0	28.3	23.4	24.2	17.5

The graph in Figure 6.8 (page 147), is a summary of all the thermal cyclic tests run on this sample, and shows the peak heating temperatures of each thermal cycle across the sample.

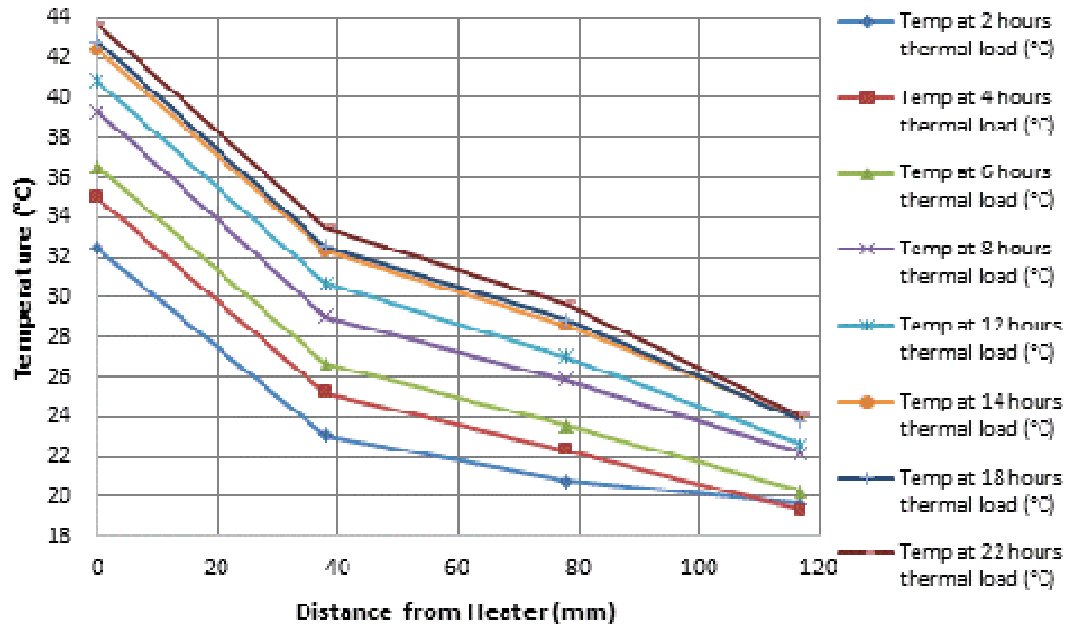


Figure 6.8: Variation of various thermal loads at peak temperatures across sample no. 5 from heater to edge of the test chamber

#### 6.2.2.1.5 Objective 5: Objective 5: Shear Strength and Water Content Tests

The objective of this test was to determine shear strengths and water contents within the sample in relation to distance from heat source and different levels of sample height. At the end of the thermal tests the rig was dismantled and the shear strength and water content tests were carried out while the sample was still in the test chamber in order to avoid disturbing the sample and altering its state.

Locations for this test were marked on the sample with reference to distance from the heater and shear strength tests were carried out in those locations. Samples were collected from the tested points to determine their water contents. The tests were carried out layer by layer in four layers with each layer ranging in thickness between 50-60mm. A total of 80 samples were tested.

Samples tested from each layer are shown separately and presented in different colours to give an indication of how the shear strength and water contents vary from top to bottom of the sample.



Figure 6.9 shows the variation of shear strength with distance from heater in the four layers from top to bottom of the sample which indicates an increase in shear strength closer to the heat source in the top and bottom layers of the sample. In the middle layers, the shear strength only changed within  $\pm 1$  kPa.

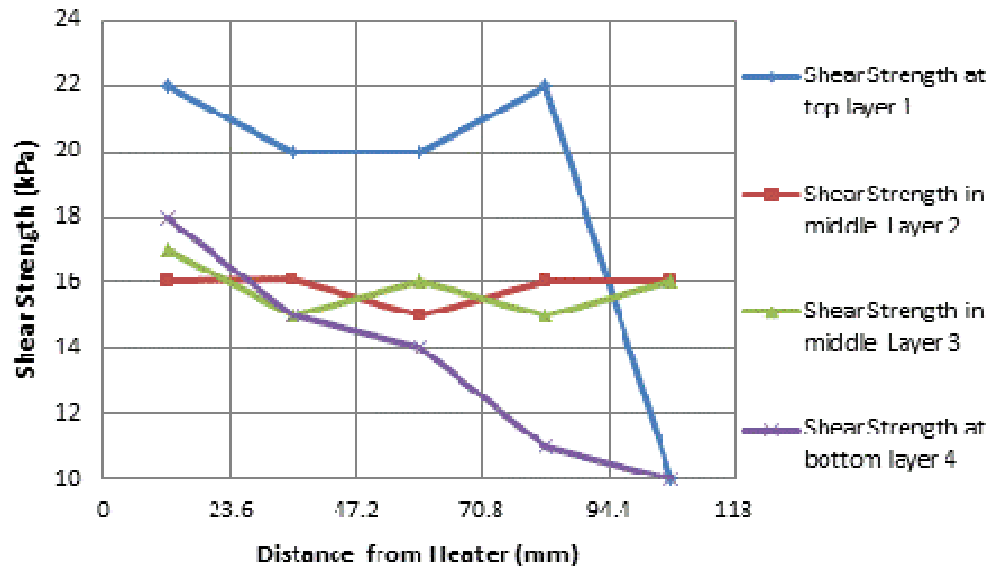


Figure 6.9: Variation of shear strength with distance from heater in the four layers from top to bottom of the sample

Figure 6.10 shows the variation of water content with distance from heater in the four layers from top to bottom of the sample which indicates a decrease in percentage water content closer to the heat source.

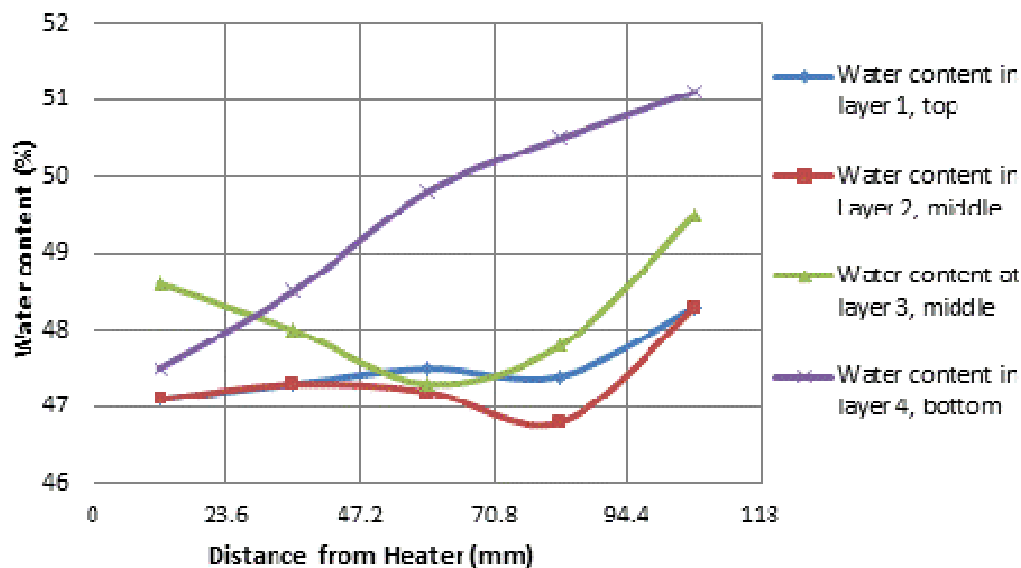


Figure 6.10: Variation of percentage water content with distance from heater in the four layers from top to bottom of the sample

Figure 6.11 on page 149, shows a plot of shear strength against water content for this sample.

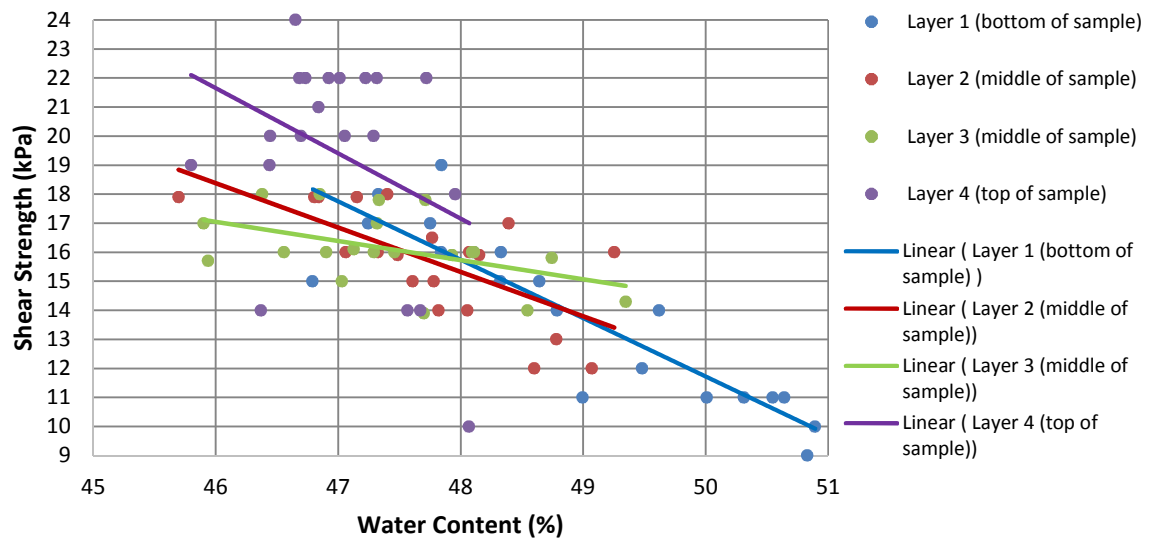


Figure 6.11: The variation of shear strength with percentage water content in kaolin sample tested at 100kPa at the end of the testing regime

The trend lines show a strong trend of increasing shear strength with a decrease in water content, with the bottom layer showing the strongest relationship. Table 6.6 shows the coefficients and regression values for the trend lines in Figure 6.11.

Table 6.6: The coefficients and regression values for sample No. 5

Sample layer	Equation for fit $y = mx + c$	$R^2$	Validity range of water content (%)
Layer 1 (Bottom)	$-2.0096x + 112.6$	0.7919	47.0 – 51.1
Layer 2 (Middle)	$-1.5303x + 89.081$	0.4668	45.9 – 49.5
Layer 3 (Middle)	$-0.6593x + 47.505$	0.2318	46.1 – 49.5
Layer 4 (Top)	$-2.2505x + 125.63$	0.1304	45.9 – 48.3

### 6.2.2.2 Sample No. 6 (Tests carried out on kaolin sample at 200kPa)

A kaolin sample was prepared at 82% water content and carefully loaded into the test rig for a series of thermal tests to be carried out at a pressure of 200kPa. The objectives of the tests carried out on this sample were in line with those of previous samples listed in section 6.2.1. The procedure for setting up this test was same as that described in section 6.2.2.1. The layout of thermocouples for this test is the same as shown in Figure 6.1 (page 140).

### 6.2.2.2.1 Objective 1: Equilibrium Heating Duration

This heating test was undertaken to determine how long it took the soil sample to achieve equilibrium or steady state conditions. A power input of 17.03W was used in this test and the sample achieved thermal equilibrium after approximately 48 hours of heating. The temperature changes in the heater and within the sample were logged during the test and a graph of the results is presented in Figure 6.12.

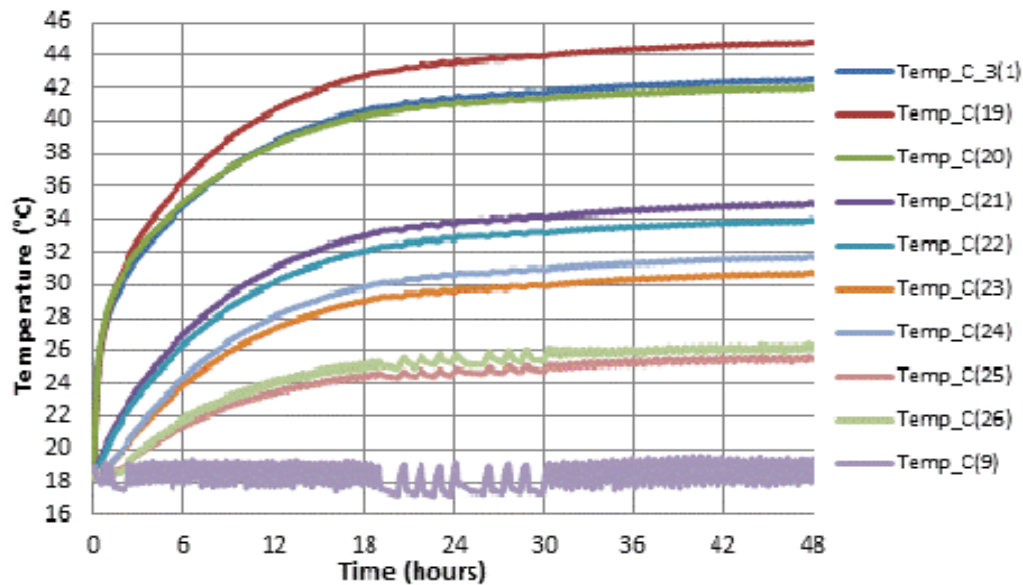


Figure 6.12: The variation of temperature with time across a kaolin sample consolidated to 200kPa showing that thermal equilibrium was achieved after about 48 hours

The temperature values at fixed locations within the sample in equilibrium condition at the power input of 17.03W are presented in Table 6.7.

Table 6.7: Temperature values at probe locations in thermal equilibrium for kaolin test at 200kPa and power input of 17.03W

Probe label	Distance from Heater (mm)	Temp in equilibrium heating condition after 48 hours (°C)
Probe 10	Heater	42.5
Probe 19	Outer edge top of heater	44.8
Probe 20	Outer edge bottom of heater	42.1
Probe 21	40	34.9
Probe 22	40	33.9
Probe 23	80	30.7
Probe 24	80	31.7
Probe 25	117	25.6
Probe 26	117	26.3
Probe 9	Controlled Room Temp	18.9

### 6.2.2.2.2 Objective 2: Cooling Duration

To determine the duration of cooling of the sample, the power supply to the heater was disconnected. The sample was allowed to return to its initial temperature or controlled room temperature.

From Figure 6.13, complete cooling of the sample from equilibrium condition back to initial temperature lasted approximately 30 hours.

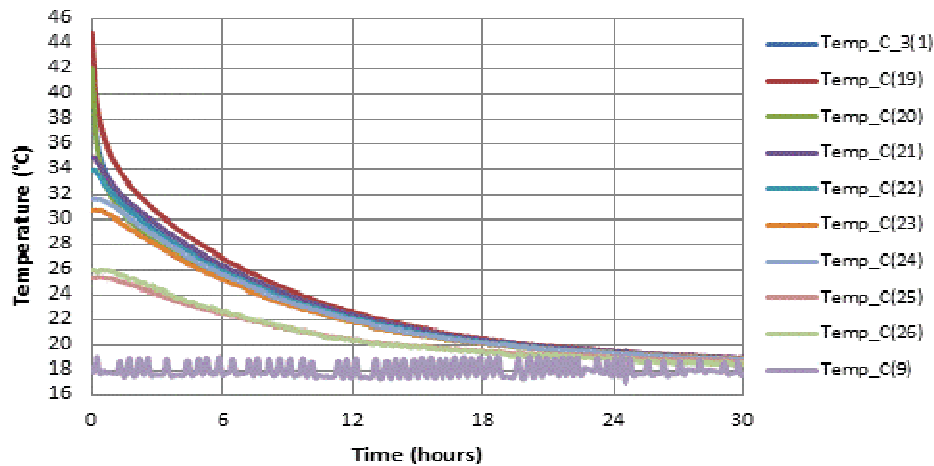


Figure 6.13: The time to return to room temperature for kaolin test at 200kPa

### 6.2.2.2.3 Objective 3: Temperature Variations across Sample

The objective of this test was to measure the temperature profile across the sample in thermal equilibrium in order to obtain the temperature variations within the sample. The graph in Figure 6.14 shows results obtained from this test, which indicate a temperature difference between the top and bottom of the sample.

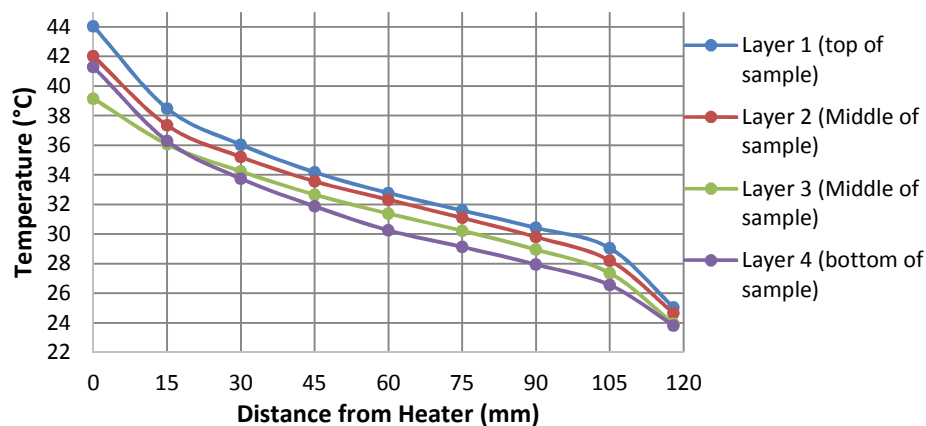


Figure 6.14: Temperature variations across sample from heater to edge of test chamber and from top to bottom of sample at start of test on kaolin sample at 200kPa

The temperature values measured at the locations within the sample are presented in Table 6.8

Table 6.8: Table showing temperature variation values at start of tests on sample no.6

Distance from heater (mm)	Layer 1 (top of sample)	Layer 2 (Middle of sample)	Layer 3 (Middle of sample)	Layer 4 (bottom of sample)
0	44.0	42.0	39.2	41.3
15	38.5	37.3	36.1	36.3
30	36.0	35.2	34.2	33.7
45	34.2	33.6	32.7	31.9
60	32.8	32.3	31.4	30.3
75	31.6	31.1	30.2	29.1
90	30.4	29.8	29.0	27.9
105	29.1	28.2	27.4	26.6
118	25.0	24.7	23.9	23.8

#### 6.2.2.2.4 Objective 4: Thermal Loading Cycles

Several thermal loading cycles tests were investigated on this sample. Thermal cyclic loads tested within a 24 hour testing period on kaolin sample at 200kPa are:

- 1) 4 hours heating cycles run for three days
- 2) 8 hours heating cycles run for three days
- 3) 12 hours heating cycles run for three days
- 4) 18 hours heating cycles run for three days
- 5) 22 hours heating cycles run for three days

All the thermal cyclic load tests were carried out on this sample for a period of three days each. The results from the 12 hours heating and 12 hours cooling for a period of three days is presented here in Figure 6.15

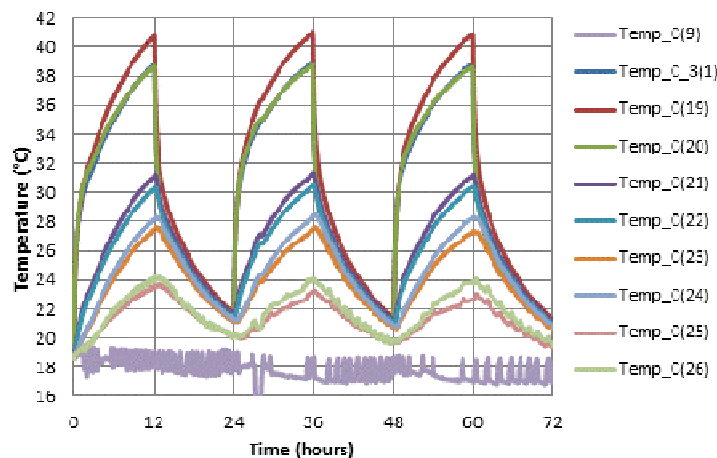


Figure 6.15: The temperature variation across the sample during thermal loading cycles of 12 hours heating and 12 cooling for three days on kaolin sample at 200kPa and 17.03W

Figure 6.16 shows a summary of four thermal cyclic tests run on this sample. The graph shows the peak heating temperatures of each thermal cycle across the sample.

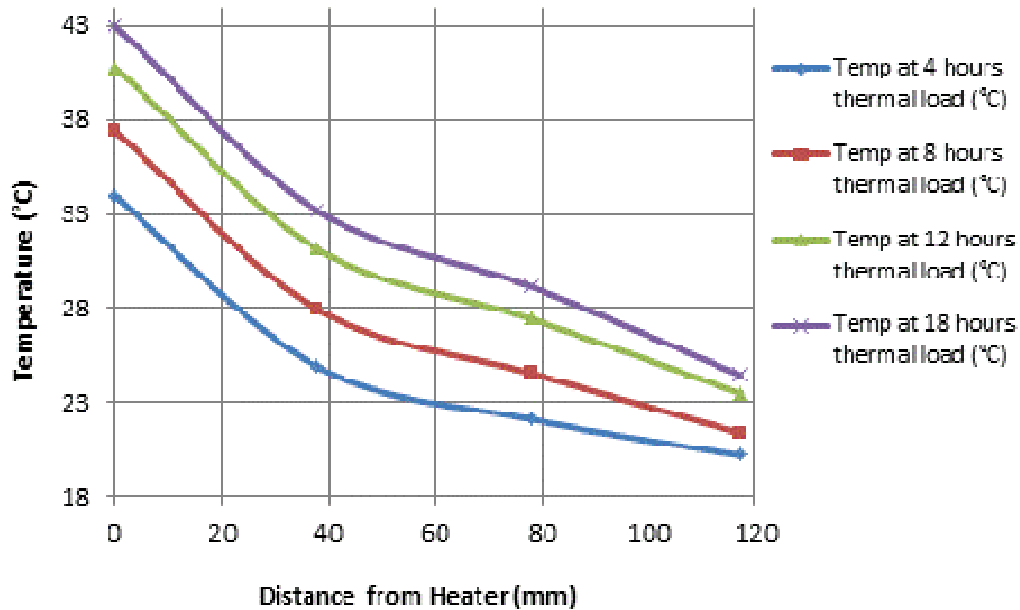


Figure 6.16: Various thermal loads at peak temperatures when in thermal equilibrium, also showing the decrease in temperature across sample no. 6 away from the heater

Table 6.9 presents the temperature values measured at points within the sample at the end of the thermal heating load and at cooling after 24 hours for thermal loading cycles run at 4, 8, 12 and 18 hours on sample no. 6.

Table 6.9: Temperature values after 4, 8, 12, and 18 hours thermal heating load and subsequent cooling in sample no. 6 at 17.03W power

Probe label	Distance from Heater (mm)	Temp after 4 hours thermal load (°C)	Temp after 20 hours cooling (°C)	Temp after 8 hours thermal load (°C)	Temp after 16 hours cooling (°C)	Temp after 12 hours thermal load (°C)	Temp after 12 hours cooling (°C)	Temp after 18 hours thermal load (°C)	Temp after 6 hours cooling (°C)
Probe 10	Heater	32.7	18.7	35.7	20.1	38.8	21.4	40.8	25.3
Probe 19	Outer edge	34.0	18.8	37.4	20.2	40.8	21.7	43.0	26.1
Probe 20	Outer edge	33.1	18.7	35.8	20.0	38.7	21.2	40.5	24.8
Probe 21	38	24.9	18.8	27.9	20.2	31.1	21.5	33.2	25.7
Probe 22	38	24.3	18.8	27.2	20.1	30.3	21.4	32.2	25.3
Probe 23	78	22.1	18.8	24.6	20.0	27.4	21.1	29.1	24.7
Probe 24	78	22.4	18.7	25.2	20.0	28.2	21.3	30.0	25.1
Probe 25	117	20.2	18.5	21.4	19.6	23.5	20.2	24.5	22.2
Probe 26	117	20.2	18.3	22.0	19.5	24.1	20.2	25.1	22.4
Probe 9	Controlled Room Temp	17.8	18.3	17.0	18.0	19.1	19.0	17.8	18.5

### 6.2.2.2.5 Objective 5: Shear Strength and Water Content Tests

The objective and procedure of this test are the same as those presented in sub-section 6.2.2.1.5 For this sample the tests were carried out layer by layer in three layers of approximately 62mm each, and a total of 60 samples were tested.

Figure 6.17 shows the variation of shear strength with distance from heater in the three layers from top to bottom of the sample. The plot indicates an increase in sample stiffness closer to the heat source in the middle and bottom layers.

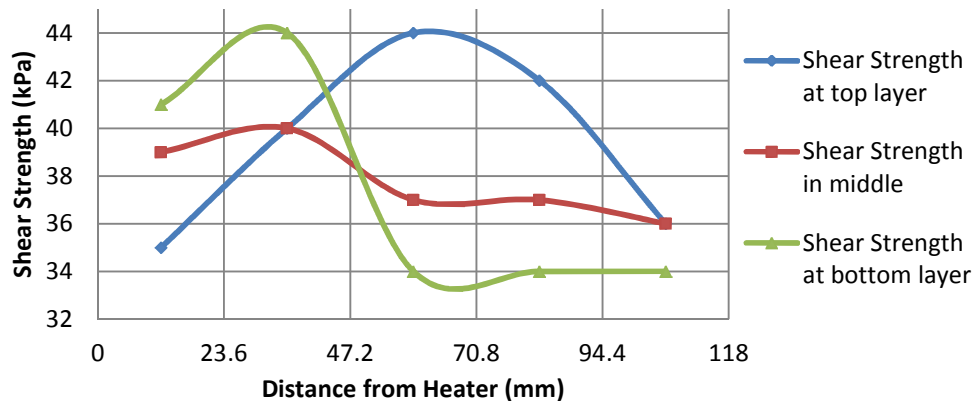


Figure 6.17: Variation of shear strength with distance from heater in the three layers from top to bottom of the sample

Similarly, Figure 6.18 shows the variation of water content with distance from heater in the three layers from top to bottom of the sample. The plot indicates a decrease in percentage water content closer to the heat source more pronounced in the middle and bottom layers.

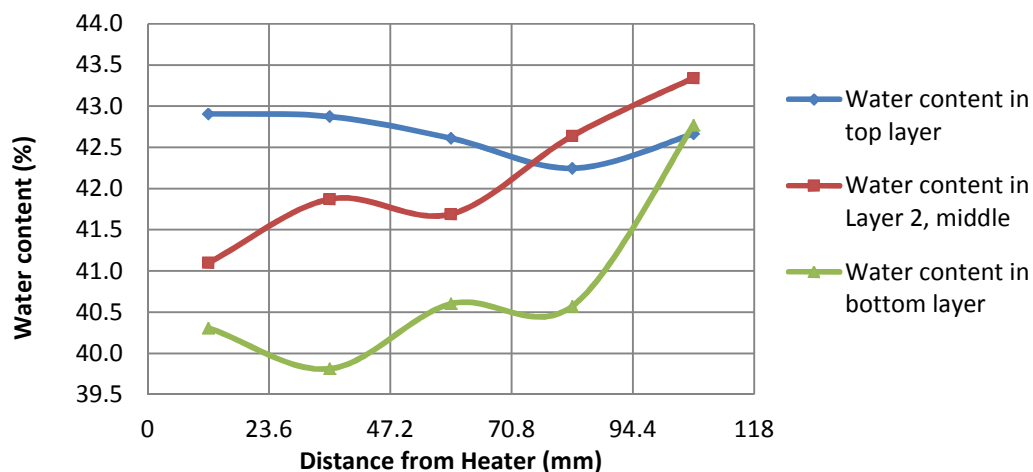


Figure 6.18: Variation of percentage water content with distance from heater in the three layers from top to bottom of the sample

Figure 6.19 presents a plot of shear strength against water content for this sample showing how the shear strength and water contents vary from top to bottom of the sample.

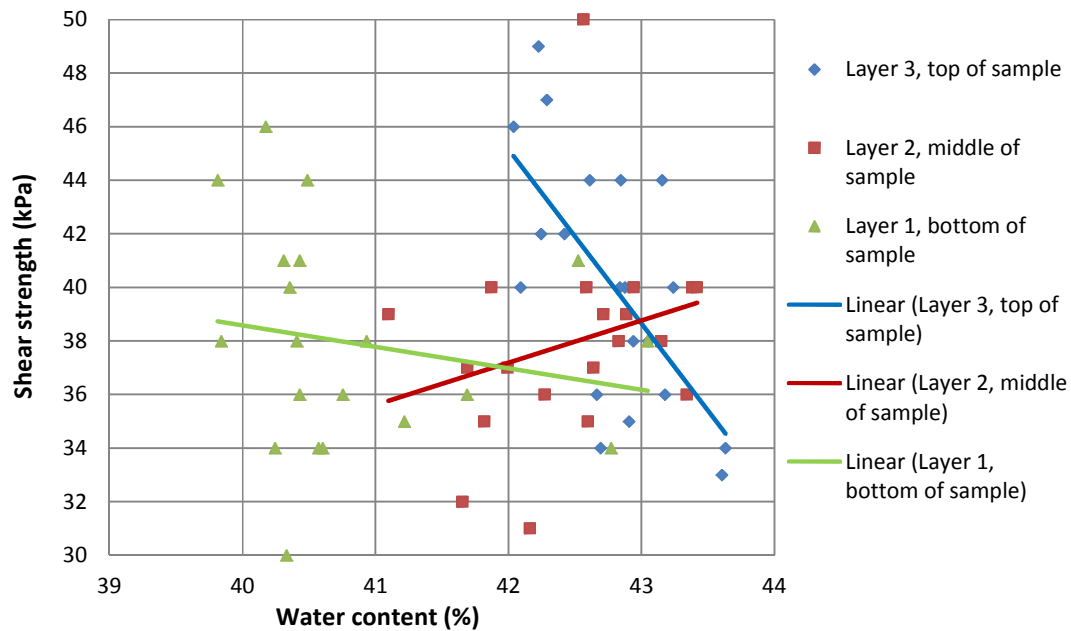


Figure 6.19: Plot of shear strength against water content carried out on kaolin sample tested at 200kPa at the end of the testing regime

The trend lines show a weak relationship between shear strength and water content. The trend lines in the bottom layer show a trend of increasing shear strength with a decrease in water content. Table 6.10 shows the coefficients and regression values for the trend lines in Figure 6.19.

Table 6.10: The coefficients and regression values for the trend lines in Figure 6.19.

Sample layer	Equation for fit $y = mx + c$	$R^2$	Validity range of water content (%)
Layer 1 (Bottom)	$-0.8029x + 70.697$	0.0341	39.8 – 43.0
Layer 2 (Middle)	$1.578x - 29.084$	0.07	41.0 – 43.4
Layer 3 (Middle)	$-6.5065x + 318.42$	0.4241	42.0 – 43.6

### 6.2.2.3 Sample No. 7 (Tests carried out on kaolin sample at 0, 25, & 50kPa)

This sample was prepared at 84.5% water content which was 2.5% higher than the other kaolin samples in order to investigate the effect of the additional water content on the test results. The soil was carefully placed in the cell of the assembled rig.



The thermal tests were carried out on this sample in three phases, with the overall objectives the same as those listed in section 6.2.1.

The three phases of tests carried out on this sample were:

- 1) Testing the sample at 0kPa
- 2) Testing the sample at a pressure of 25kPa
- 3) Testing the sample at a pressure of 50kPa

For the sample tested at 0kPa and 25kPa, only the first four objectives are presented, as the fifth objective could only be carried out after the test at 50kPa as it involved stripping the cell apart.

The arrangement of the thermocouples within the test chamber remained the same for the three phases of tests carried out on this sample and is shown in Figure 6.20.

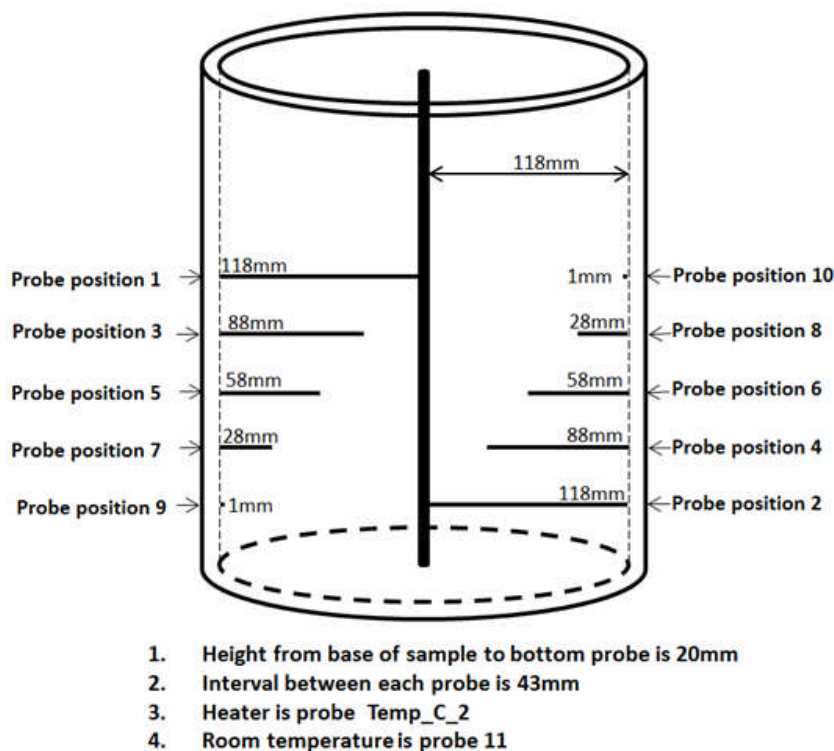


Figure 6.20: Layout of thermocouples within test chamber for tests carried out on sample no. 7

#### 6.2.2.4 Testing Sample No. 7 at 0kPa

The tests carried out on the sample with no pressure applied include heating and cooling tests, thermal cyclic loading tests and a temperature profile test across sample in equilibrium condition. These tests are described in terms of the objectives for carrying them out.

### 6.2.2.4.1 Objective 1: Equilibrium Heating Duration

This heating test was undertaken to determine how long it took the soil sample to achieve equilibrium or steady state conditions.

A power input of 17.03W was used in this test and the sample achieved equilibrium conditions after approximately 36 hours of heating. The temperature changes in the heater and within the sample were logged during the test and a graph of the results is presented in Figure 6.21.

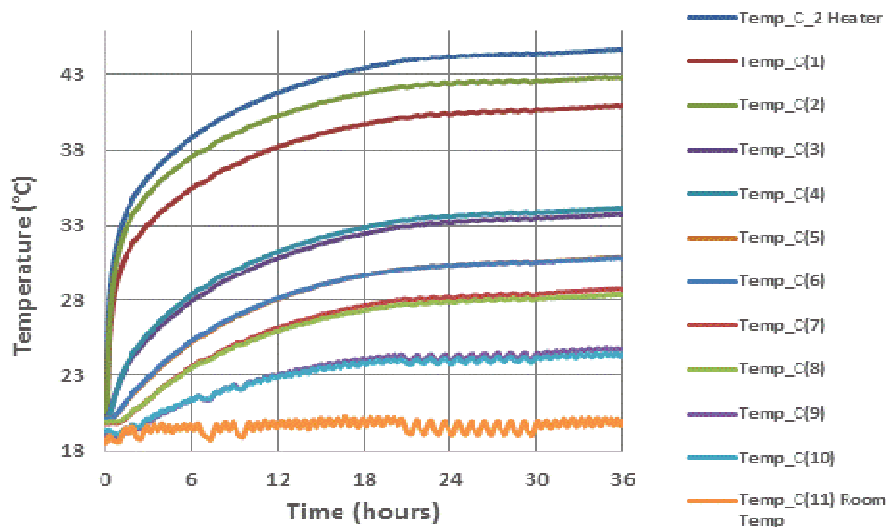


Figure 6.21: The variation of temperature with time across a sample of kaolin at 0kPa and power input of 17.03W showing thermal equilibrium was achieved after about 36 hours

The temperature values at fixed locations within the sample in equilibrium condition at the power input of 17.03W are presented in Table 6.11.

Table 6.11: Temperature values at probe locations in thermal equilibrium for sample no.7 tested at 0kPa and power input of 17.03W

Probe label	Distance from Heater (mm)	Temp in equilibrium heating condition after 36 hours (°C)
Probe C_2	Heater	44.7
Probe 1	Outer edge top of heater	40.9
Probe 2	Outer edge bottom of heater	42.8
Probe 3	30	33.8
Probe 4	30	34.1
Probe 5	60	30.9
Probe 6	60	30.9
Probe 7	90	28.7
Probe 8	90	28.3
Probe 9	117	24.7
Probe 10	117	24.3
Probe 11	Controlled Room Temp	19.8

### 6.2.2.4.2 Objective 2: Cooling Duration

To determine the duration of cooling, the power supply to the heater was disconnected. The sample was allowed to return to the controlled room temperature.

Complete cooling of the sample from equilibrium heating condition to controlled room temperature lasted approximately 24 hours as shown in Figure 6.22.

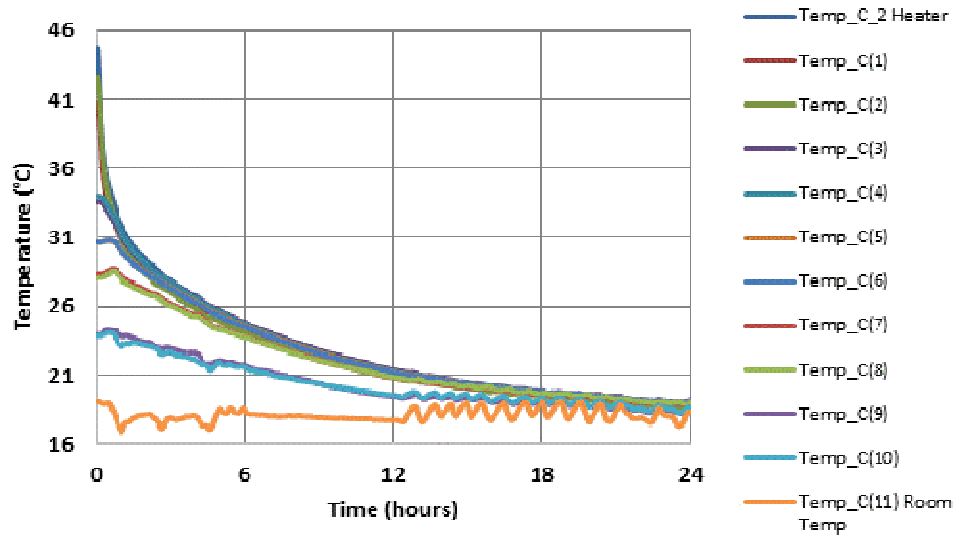


Figure 6.22: Cooling curves for sample no. 7 at 0kPa showing the time to return to room temperature

### 6.2.2.4.3 Objective 3: Temperature Variations across Sample

The objective of this test was to measure the temperature variations across the sample in thermal equilibrium. Figure 6.23 shows a graph of results obtained from this test.

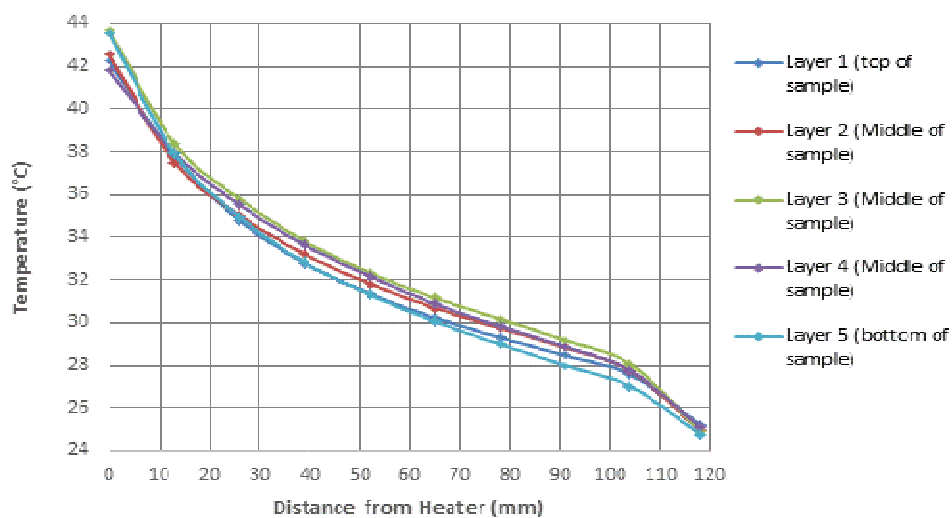


Figure 6.23: Temperature variations across sample from heater to edge of test chamber and from top to bottom of sample at start of test on sample no. 7 at 0kPa

The temperature values measured at the locations within the sample are presented in Table 6.12.

Table 6.12: Table showing temperature variation values in sample no.7 at 0kPa

Distance from heater (mm)	Layer 1 (top of sample)	Layer 2 (Middle of sample)	Layer 3 (Middle of sample)	Layer 4 (Middle of sample)	Layer 5 (bottom of sample)
0	42.2	42.5	43.7	41.8	43.6
13	37.8	37.5	38.4	37.9	37.9
26	34.8	35.0	35.8	35.5	35.0
39	32.8	33.2	33.8	33.6	32.8
52	31.3	31.8	32.3	32.2	31.3
65	30.2	30.7	31.2	30.9	30.0
78	29.3	29.7	30.2	29.8	29.0
91	28.5	28.8	29.2	28.9	28.0
104	27.6	27.7	28.1	27.7	27.0
118	25.2	24.9	24.9	25.1	24.8

#### 6.2.2.4.4 Objective 4: Thermal Loading Cycles

Thermal loading cyclic tests were carried out on this sample. Thermal cyclic loads tested within a 24 hour testing period on sample no. 7 at 0kPa are:

- 1) 8 hours heating cycle run for one day
- 2) 12 hours heating cycles run for three days

The graph of results from both the 8 and 12 hours heating and subsequent cooling within the 24 hour period for both tests is presented in Figure 6.24.

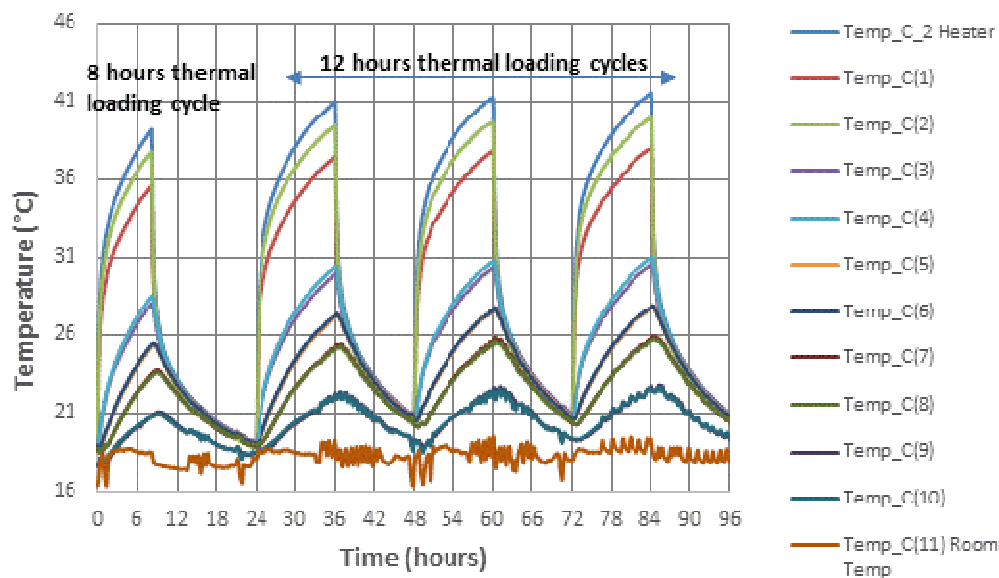


Figure 6.24: The temperature variation across sample during 8 and 12 hours heating and subsequent cooling on sample no. 7 at 0kPa and 17.03W

Table 6.13 presents the temperature values measured at points within the sample at the end of the thermal heating load and at cooling after 24 hours for thermal loading cycles run at 8 and 12 hours on sample no. 7 at 0kPa.

Table 6.13: Temperature values at probe locations after thermal cyclic loads for 8 &12 hours of heating and subsequent cooling within 24 hours

Probe label	Distance from Heater (mm)	Temp after 8 hours thermal load (°C)	Temp after 16 hours cooling (°C)	Temp after 12 hours thermal load (°C)	Temp after 12 hours cooling (°C)
Probe C_2	Heater	39.0	19.0	41.0	20.6
Probe 1	Outer edge top of heater	35.5	19.1	37.4	20.8
Probe 2	Outer edge bottom of heater	37.6	18.8	39.4	20.4
Probe 3	30	27.9	19.1	29.9	20.9
Probe 4	30	28.4	19.0	30.4	20.8
Probe 5	60	25.1	19.0	27.1	20.7
Probe 6	60	25.3	19.0	27.2	20.7
Probe 7	90	23.4	18.9	25.2	20.3
Probe 8	90	23.3	18.9	25.0	20.2
Probe 9	117	20.8	18.4	22.2	19.1
Probe 10	117	20.7	18.5	22.2	19.1
Probe 11	Controlled Room Temp	18.5	18.1	19.3	17.7

### 6.2.2.5 Testing Sample No. 7 at 25kPa

The tests carried out on sample no. 7 at pressure of 25kPa include heating and cooling tests, thermal cyclic loading tests and a temperature profile test across sample in equilibrium condition. These tests are described in terms of the objectives for carrying them out.

#### 6.2.2.5.1 Objective 1: Equilibrium Heating Duration

This heating test was undertaken to determine how long it took the soil sample to achieve equilibrium or steady state conditions.

A power input of 17.03W was used in this test and the sample achieved equilibrium conditions after approximately 40 hours of heating. A graph of the heating test is presented in Figure 6.25.

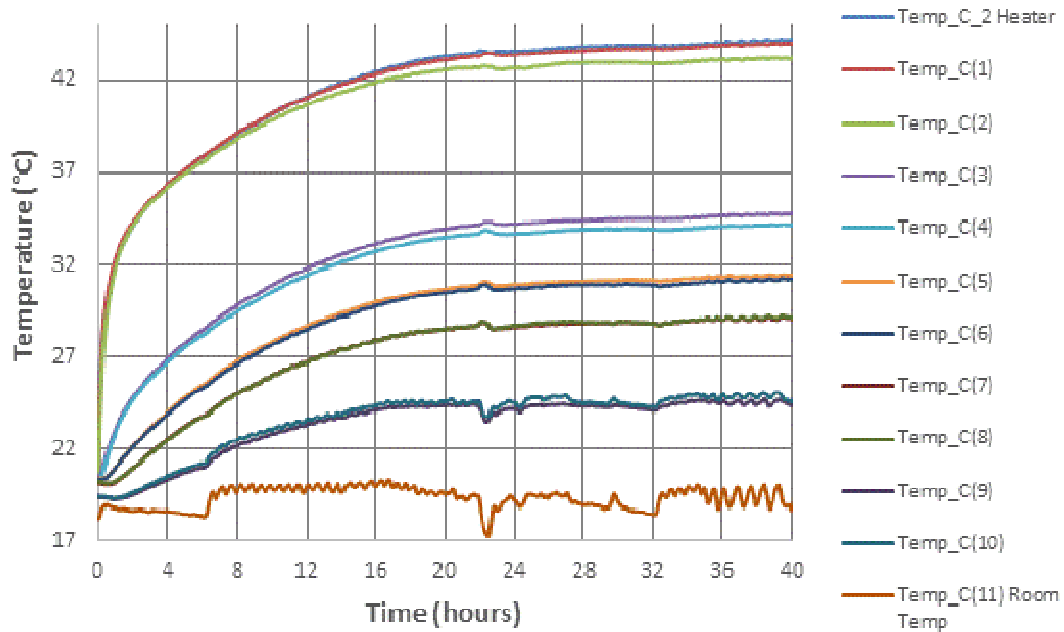


Figure 6.25: The variation of temperature with time across a sample of kaolin consolidated to 25kPa showing that thermal equilibrium was achieved after about 40hrs

#### 6.2.2.5.2 Objective 2: Cooling Duration

To determine the duration of cooling, the power supply to the heater was disconnected and the sample was allowed to return to the controlled room temperature. Complete cooling of the sample from equilibrium heating condition to controlled room temperature lasted approximately 28 hours as shown in Figure 6.26.

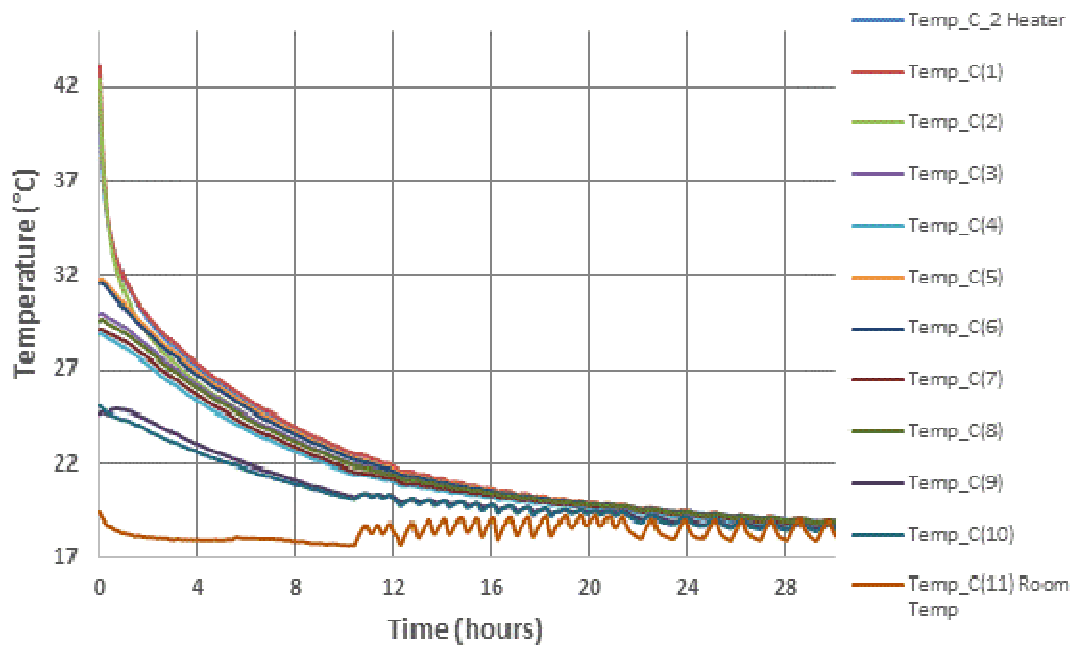


Figure 6.26: The time to return to room temperature for sample no. 7 at 25kPa

### 6.2.2.5.3 Objective 3: Temperature Variations across Sample

The objective of this test was to measure the temperature variations across the sample in thermal equilibrium. Figure 6.27 shows a graph of results obtained from this test.

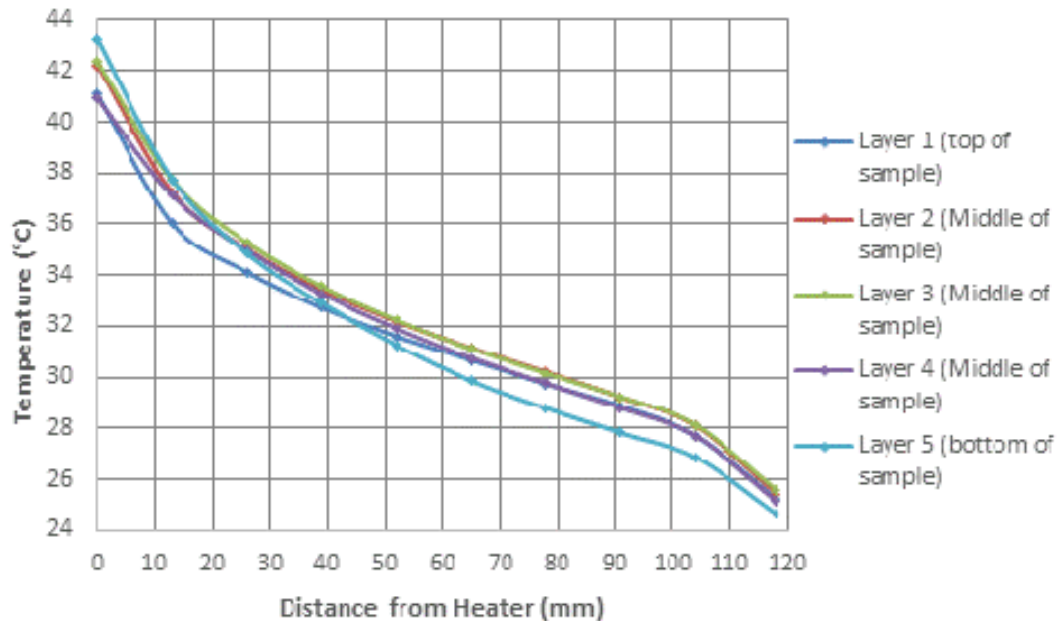


Figure 6.27: Temperature variations across sample from heater to edge of test chamber and from top to bottom of sample at start of test on sample no. 7 at 25kPa

The temperature values measured at the locations within the sample during the temperature profile test carried out to investigate temperature variations across the sample are presented in Table 6.14.

Table 6.14: Table showing temperature variation values in sample no.7 at 25kPa

Distance from heater (mm)	Layer 1 (top of sample)	Layer 2 (middle of sample)	Layer 3 (middle of sample)	Layer 4 (middle of sample)	Layer 5 (bottom of sample)
0	41.1	42.2	42.3	40.9	43.2
13	36.0	37.2	37.7	37.1	37.7
26	34.1	35.0	35.3	35.0	34.8
39	32.7	33.4	33.6	33.3	32.9
52	31.6	32.2	32.2	31.9	31.3
65	30.7	31.2	31.1	30.8	29.9
78	29.7	30.2	30.2	29.8	28.8
91	28.9	29.2	29.2	28.8	27.8
104	27.7	28.1	28.1	27.7	26.9
118	25.3	25.5	25.6	25.2	24.7

#### 6.2.2.5.4 Objective 4: Thermal Loading Cycles

Thermal loading cyclic tests were carried out on this sample. Thermal cyclic loads tested within a 24 hour testing period on sample no. 7 at 25kPa are:

- 1) 8 hours heating cycles run for two days
- 2) 11.5 hours heating cycles run for two days. This test was meant to be for 12 hours but an error in the timer resulted in 11.5 hours thermal cyclic loads being run instead.

A graph of results from both tests is presented in Figure 6.28.

The temperature values at fixed locations within the sample in thermal equilibrium at the power input of 17.03W are presented in Table 6.15 (page 164) Also shown in this table are the temperature values measured at points within the sample at the end of the thermal heating loads and at cooling after 24 hours for thermal loading cycles run at 8 and 11.5 hours on sample no. 7 at 25kPa.

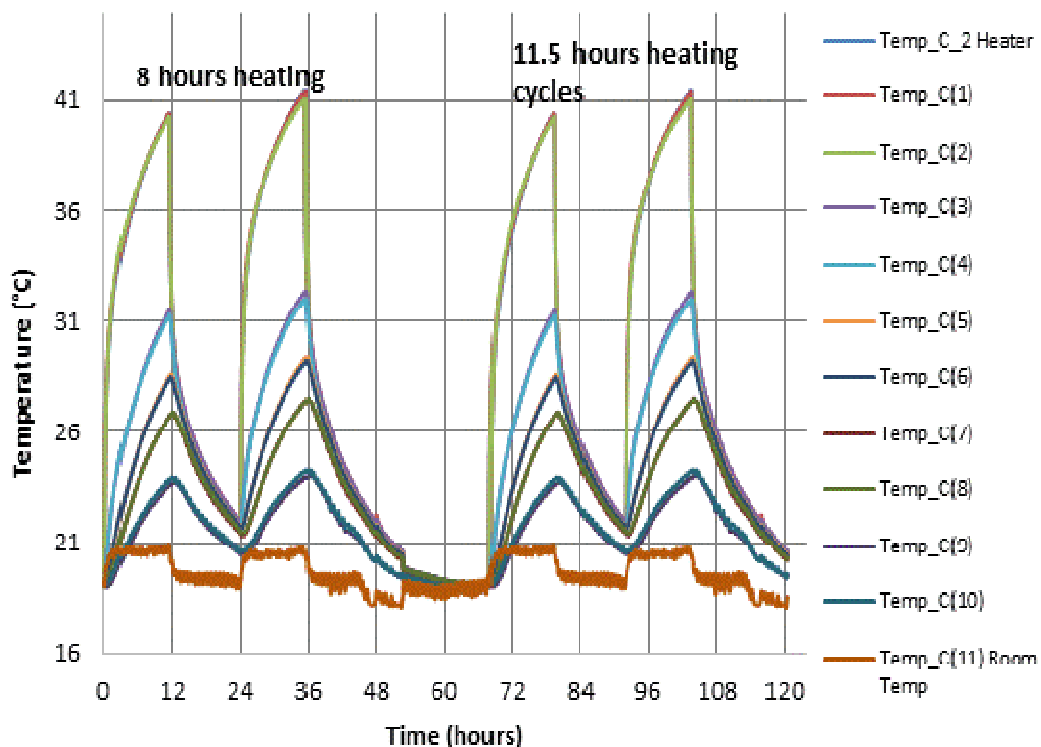


Figure 6.28: The temperature variation across sample during 8 and 11.5 hours heating and subsequent cooling in sample no. 7 at 25kPa and 17.03W



Table 6.15: Peak temperature values at thermal equilibrium and thermal cyclic loads in sample no. 7 at 25kPa

Probe label	Distance from Heater (mm)	Temp in thermal equilibrium after 36 hours (°C)	Temp after 8 hours thermal load (°C)	Temp after 16 hours cooling (°C)	Temp after 11.5 hours thermal load (°C)	Temp after 12.5 hours cooling (°C)
Probe c_2	Heater	44.2	37.9	19.9	40.2	21.7
Probe 1	Outer edge top of heater	44.0	38.0	20.1	40.4	21.9
Probe 2	Outer edge bottom of heater	43.2	37.9	19.8	40.2	21.5
Probe 3	30	34.8	28.9	20.1	31.5	21.9
Probe 4	30	34.2	28.7	19.9	31.3	21.7
Probe 5	60	31.4	25.9	20.0	28.5	21.7
Probe 6	60	31.2	25.9	19.9	28.4	21.7
Probe 7	90	29.1	24.3	19.8	26.8	21.4
Probe 8	90	29.1	24.3	19.9	26.7	21.5
Probe 9	117	24.4	21.7	19.1	23.6	20.4
Probe 10	117	24.6	21.9	19.2	23.9	20.6
Probe 11	Controlled Room Temp	18.8	19.6	18.5	20.8	19.2

#### 6.2.2.6 Testing Sample No. 7 at 50kPa

The tests carried out on sample no. 7 at pressure of 50kPa include heating and cooling tests, thermal cyclic loading tests and a temperature profile test across sample in thermal equilibrium conducted at the end of the thermal tests. The tests are described in terms of the objectives for carrying them out.

##### 6.2.2.6.1 Objective 1: Equilibrium Heating Duration

This heating test was undertaken to determine how long it took the soil sample to achieve equilibrium or steady state conditions.

A power input of 17.03W was used in this test and the sample achieved equilibrium conditions after approximately 38 hours of heating. A graph of the heating test is presented in Figure 6.29 on page 165.

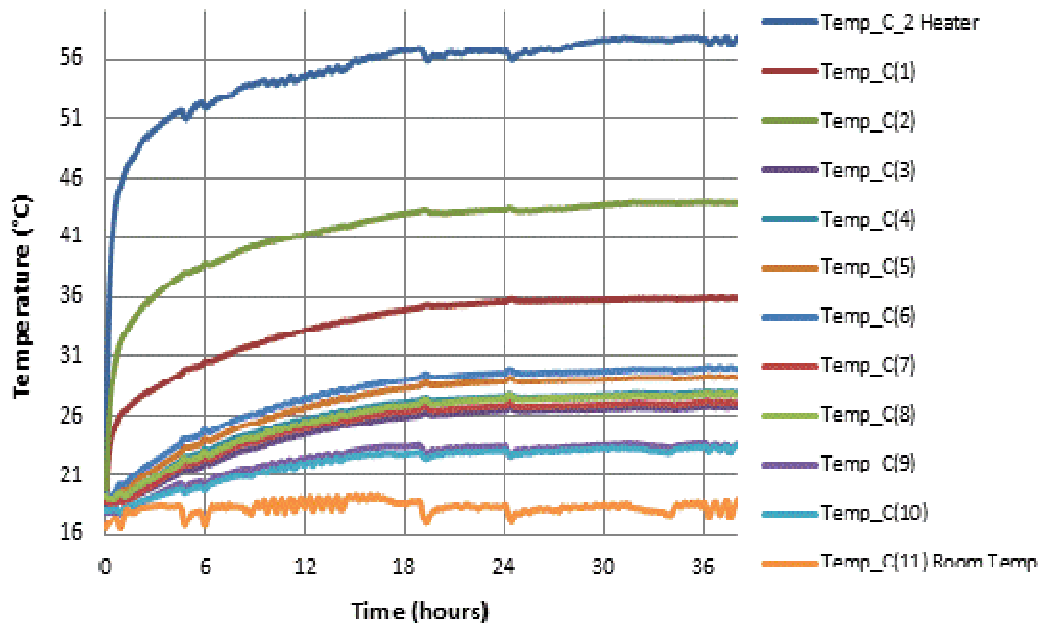


Figure 6.29: The variation of temperature with time across a sample of kaolin consolidated to 50kPa showing that thermal equilibrium was achieved after about 38hours

#### 6.2.2.6.2 Objective 2: Cooling Duration

To determine the duration of cooling, the power supply to the heater was disconnected and the sample was allowed to return to the controlled room temperature. Complete cooling of the sample from equilibrium heating condition to controlled room temperature lasted approximately 23 hours as shown in Figure 6.30.

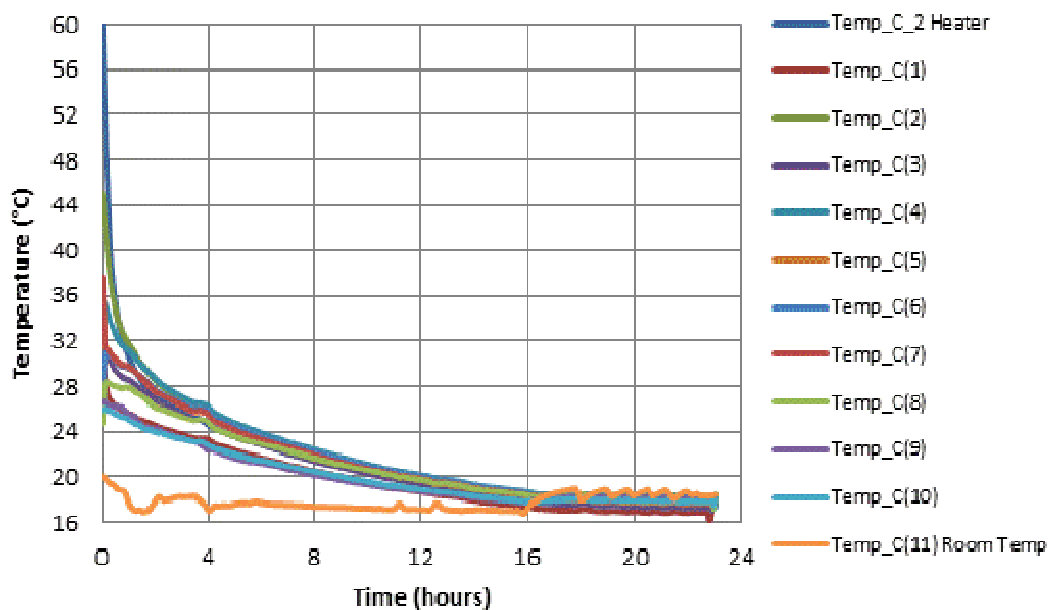


Figure 6.30: The time to return to room temperature for sample no. 7 at 50kPa

### 6.2.2.6.3 Objective 3: Temperature Variations across Sample

The objective of this test was to measure the temperature variations across the sample under equilibrium heating conditions. Figure 6.31 shows a graph of results obtained from this test.

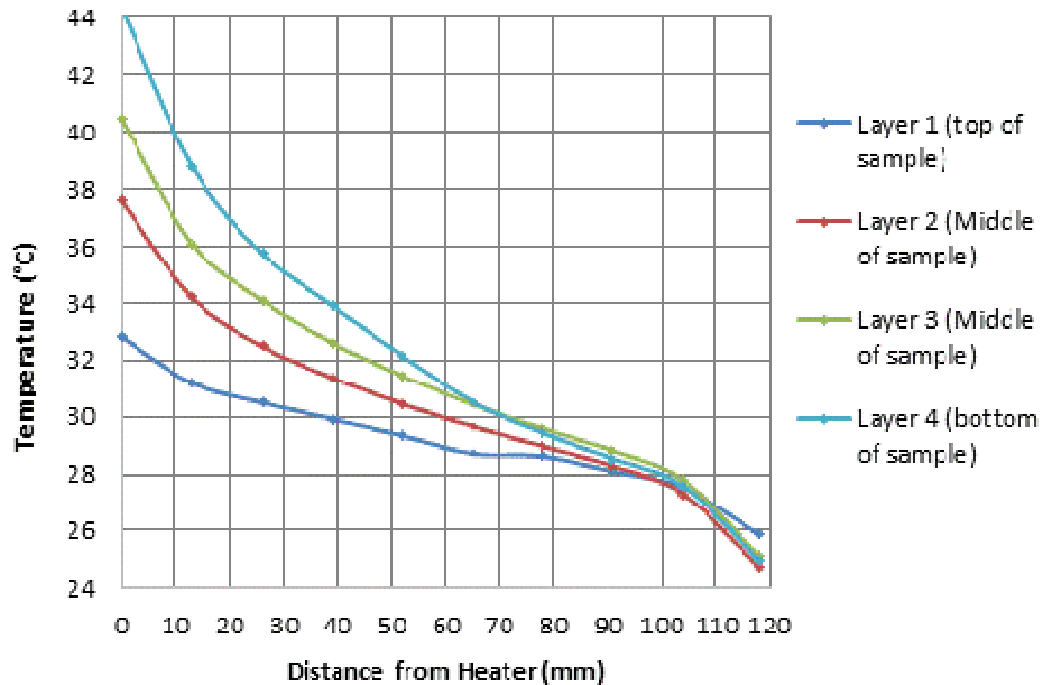


Figure 6.31: Temperature variations across sample from heater to edge of test chamber and from top to bottom of sample at start of test on sample no. 7 at 50kPa

The temperature values measured at specific locations within the sample during the temperature profile test carried out to investigate temperature variations across the sample are presented in Table 6.16.

Table 6.16: Table showing temperature variation values in sample no.7 at 50kPa

Distance from heater (mm)	Layer 1 (top of sample)	Layer 2 (Middle of sample)	Layer 3 (Middle of sample)	Layer 4 (bottom of sample)
0	32.8	37.6	40.5	44.3
13	31.2	34.2	36.1	38.8
26	30.5	32.5	34.1	35.8
39	29.9	31.4	32.6	33.9
52	29.3	30.5	31.5	32.2
65	28.7	29.7	30.4	30.5
78	28.6	29.0	29.6	29.4
91	28.1	28.3	28.8	28.5
104	27.5	27.3	27.8	27.6
118	25.9	24.7	25.1	25.0

#### 6.2.2.6.4 Objective 4: Thermal Loading Cycles

Thermal loading cyclic tests were carried out on this sample. Thermal cyclic loads tested within a 24 hour testing period on sample no. 7 at 25kPa are:

- 1) 8 hours heating cycle run for two days
- 2) 12 hours heating cycles run for three days.

A graph of results from both tests is presented in Figure 6.32.

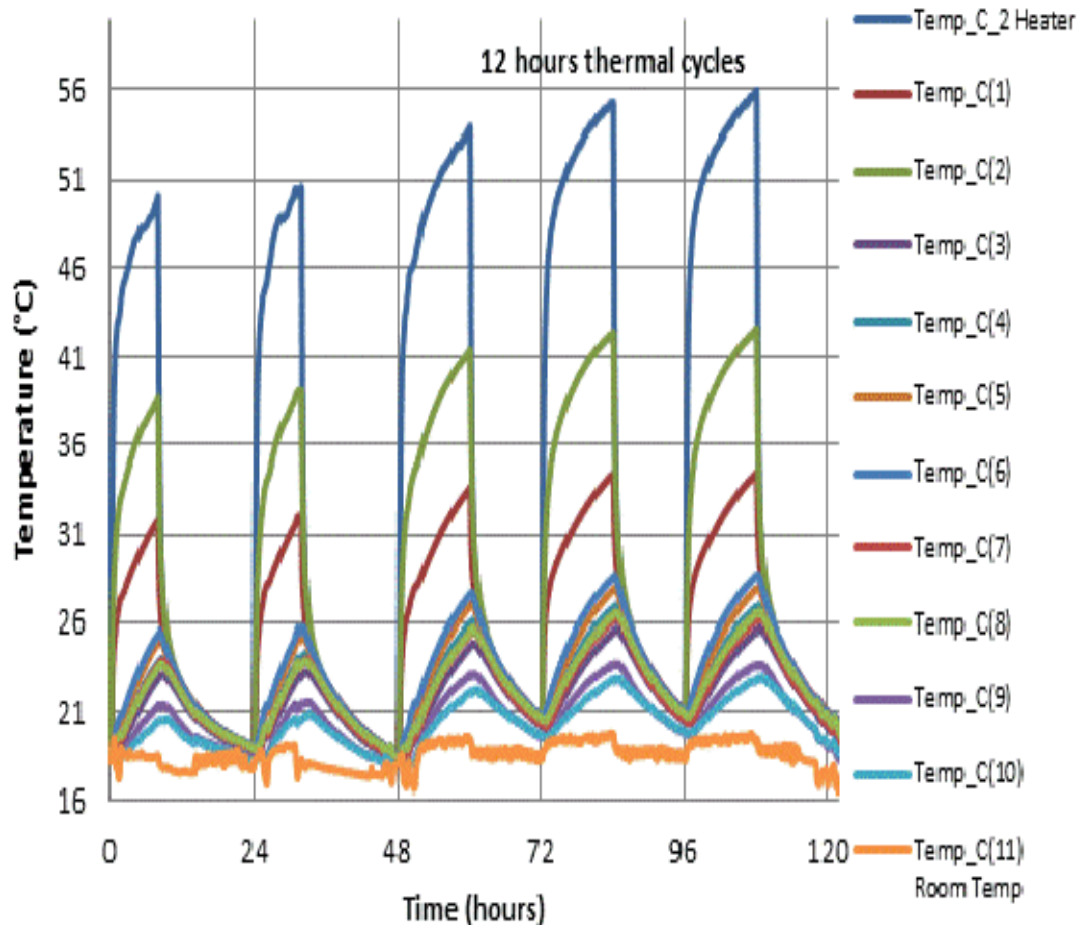


Figure 6.32: The temperature variation across sample during 8 and 12 hours heating and subsequent cooling in sample no. 7 at 50kPa and 17.03W

The temperature values at fixed locations within the sample in equilibrium condition at the power input of 17.03W are presented in Table 6.17 on page 168

Also shown in this Table are the temperature values measured at points within the sample at the end of the thermal heating loads and at cooling after 24 hours for thermal loading cycles run at 8 and 12 hours on sample no. 7 at 50kPa.

Table 6.17: Peak temperature values at equilibrium condition and thermal cyclic loads in sample no. 7 at 50kPa

Probe label	Distance from Heater (mm)	Temp in thermal equilibrium after 42 hours (°C)	Temp after 8 hours thermal load (°C)	Temp after 16 hours cooling (°C)	Temp after 11.5 hours thermal load (°C)	Temp after 12.5 hours cooling (°C)
Probe c_2	Heater	58.4	50.1	18.7	53.9	20.2
Probe 1	Outer edge top of heater	36.3	31.8	19.0	33.7	20.7
Probe 2	Outer edge bottom of heater	44.4	38.7	18.9	41.4	20.5
Probe 3	30	27.3	22.9	18.6	24.7	20.2
Probe 4	30	28.5	23.8	18.7	26.0	20.4
Probe 5	60	29.8	24.9	18.9	27.0	20.6
Probe 6	60	30.5	25.4	19.0	27.6	20.7
Probe 7	90	27.8	23.6	18.8	25.4	20.3
Probe 8	90	28.3	23.5	18.8	25.5	20.6
Probe 9	117	24.5	21.3	18.2	23.1	19.5
Probe 10	117	24.1	20.4	18.2	22.1	19.6
Probe 11	Controlled Room Temp	19.8	18.5	18.0	19.3	18.3

#### 6.2.2.6.5 Objective 5: Shear Strength and Water Content Tests

The objective and procedure of this test are same as those stated in sub-section 6.2.2.1.5. For this sample the tests were carried out layer by layer in four layers, each approximately 51mm in height. A total of 80 samples were tested.

Figure 6.33 shows the variation of shear strength with distance from heater in the four layers from top to bottom of the sample.

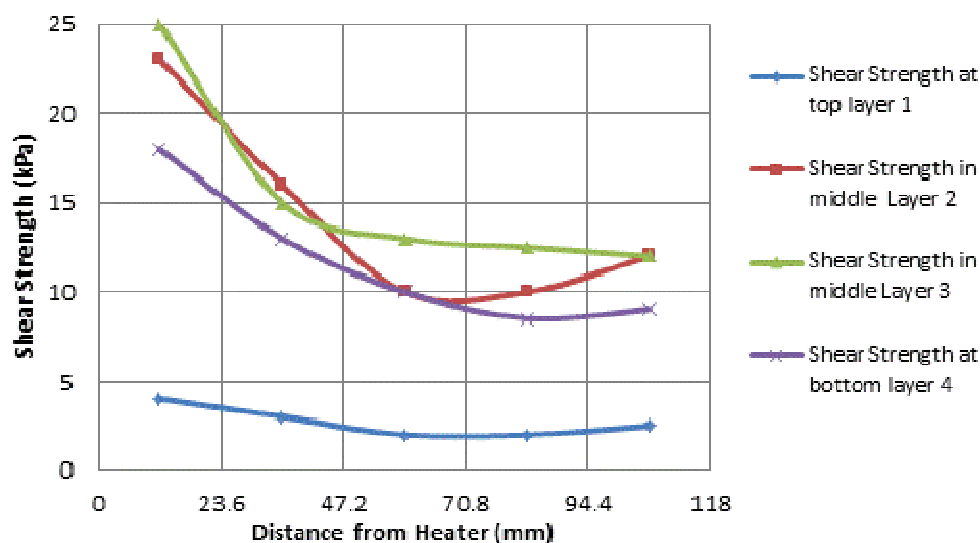


Figure 6.33: Variation of shear strength with distance from heater in the four layers from top to bottom of the sample

The plot indicates an increase in sample stiffness closer to the heat source, gradually reducing towards the cell edge.

Similarly, Figure 6.34 shows the variation of water content with distance from heater in the four layers from top to bottom of the sample. The plot indicates a decrease in percentage water content closer to the heat source, increasing towards the cell edge.

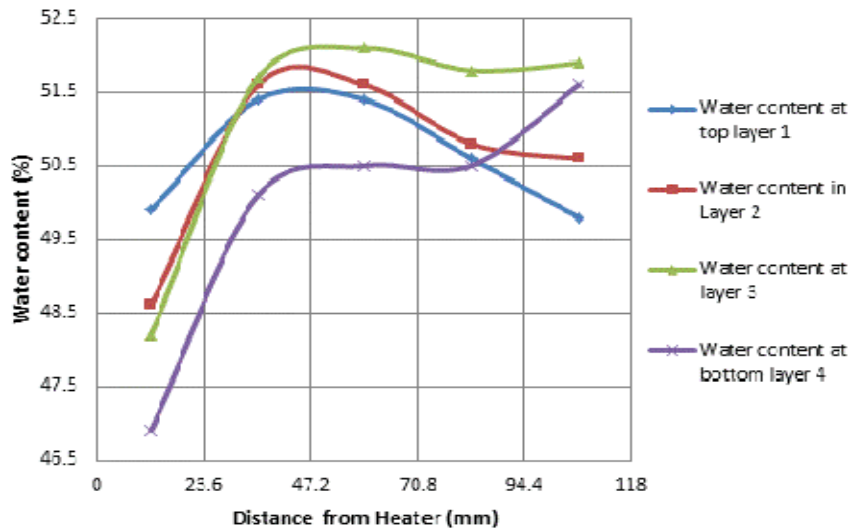


Figure 6.34: Variation of percentage water content with distance from heater in the four layers from top to bottom of the sample

Figure 6.35 shows a plot of shear strength against water content for this sample at different levels to show how the shear strength and water contents vary from top to bottom of the sample.

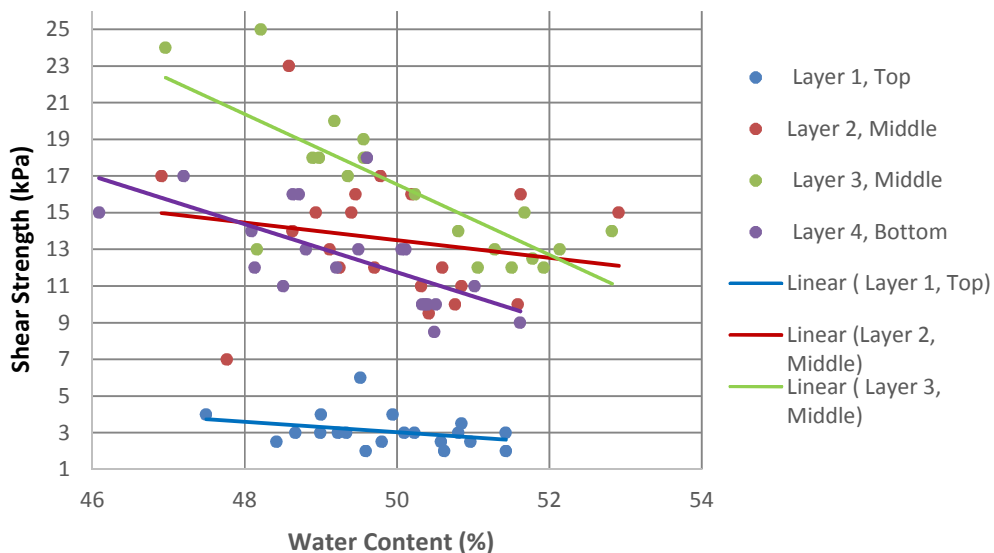


Figure 6.35: Variation of shear strength with percentage water in sample no. 7 at the end of the tests carried out at 50kPa

The trend lines show a general trend of increasing shear strength with a reduction in water content; this is more pronounced in layers 3 and 4. Table 6.18 shows the coefficients and regression values for the trend lines in Figure 6.35, and the validity range of water content.

Table 6.18: The coefficients and regression values for the trend lines in Figure 6.35 and the validity range of water content.

Sample layer	Equation for fit $y = mx + c$	$R^2$	Validity range of water content (%)
Layer 1 (Top)	$-0.2832x + 17.192$	0.1031	47.5 – 51.4
Layer 2 (Middle)	$-0.4776x + 37.378$	0.0346	46.9 – 52.9
Layer 3 (Middle)	$-1.9172x + 112.39$	0.6112	47– 52.8
Layer 4 (Bottom)	$-1.3132x + 77.406$	0.4248	46.1 – 51.6

### 6.2.3 Tests carried out on Kaolin and Sand Mixtures

After carrying out thermal tests on kaolin samples, a combination of kaolin and sand samples were also tested to investigate changes that may occur due to difference in soil type.

Samples number 8, 9, 10 and 11 were constituted of kaolin and sand combined in proportions of 75:25, 50:50 and 25:75. These samples were tested under varying conditions of water content and overburden pressures. Tests carried out are discussed according to the sample numbers.

#### 6.2.3.1 Sample No. 8 (Tests carried out on Kaolin:Sand 75:25 at 25kPa)

Sample no. 8, a combination of kaolin and sand, was prepared at a ratio of three parts of kaolin to one part of sand, at 59% water content. The sample was carefully placed in the rig cell for a series of thermal tests carried out at a pressure of 25kPa. The objectives of the tests carried out on sample no. 8 were in line with those of previous samples listed in section 6.2.1.

During the consolidation phase, pressure was applied in incremental loads of 6, 12.5, and lastly 25kPa.

At the end of the consolidation phase, thermocouples were inserted into the test chamber from two opposite sides, at different levels and specified distances from the heater. Each thermocouple on the left side had a thermocouple on the right hand placed at a similar distance from the heater to build in redundancy, allow for a failure of a

thermocouple and provide a means of averaging the temperature variation or measure the variation both vertically and horizontally. Ten thermocouples were inserted into the test chamber with 5 on each side. They were inserted from the inner edge of the cell towards the heater at distances of 1mm, 28mm, 58mm, 88mm and 118mm (touching the heater), and at five levels with each on a different level of the sample height. The lowest thermocouple was positioned at 20mm above the sample base, while the others were placed at intervals of 43mm above each other. The arrangement of the thermocouples within the test chamber is shown in Figure 6.36.

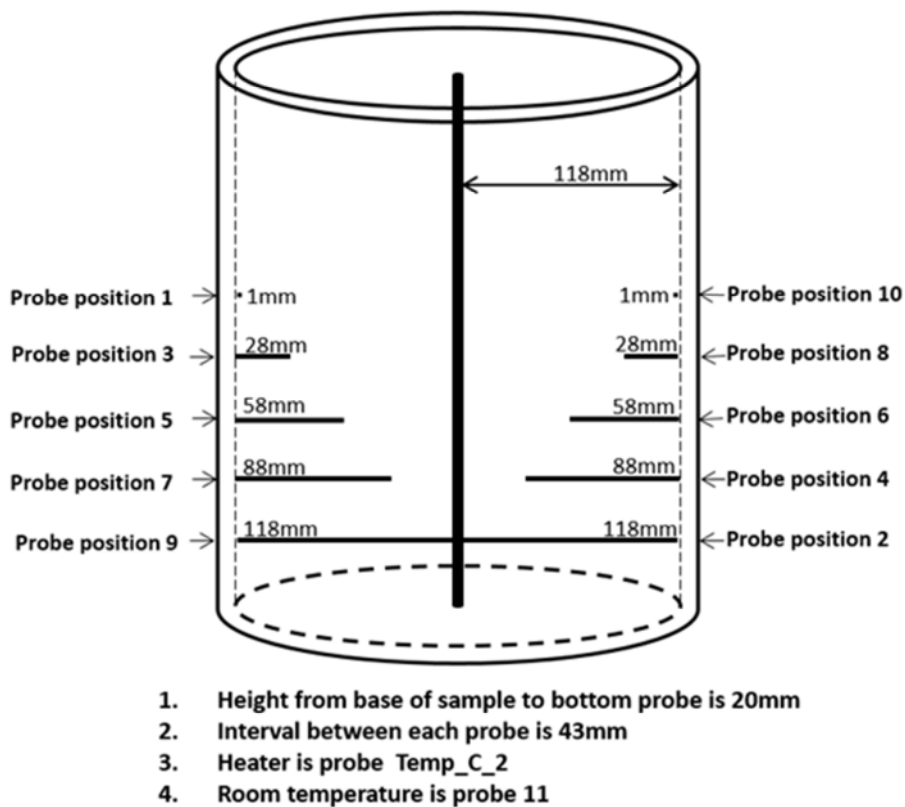


Figure 6.36: Layout of thermocouples within test chamber for tests carried out on sample no. 8

### 6.2.3.1.1 Objective 1: Equilibrium Heating Duration

A heating test was undertaken to determine how long it took the soil sample to achieve thermal equilibrium or steady state conditions.

A power input of 17.03W was used in this test and the sample achieved thermal equilibrium after approximately 26 hours of heating which is a shorter duration than the pure kaolin samples that required between 30 and 40 hours to attain thermal equilibrium. The variation of temperature with time across the sample during the steady state heating is presented in Figure 6.37.



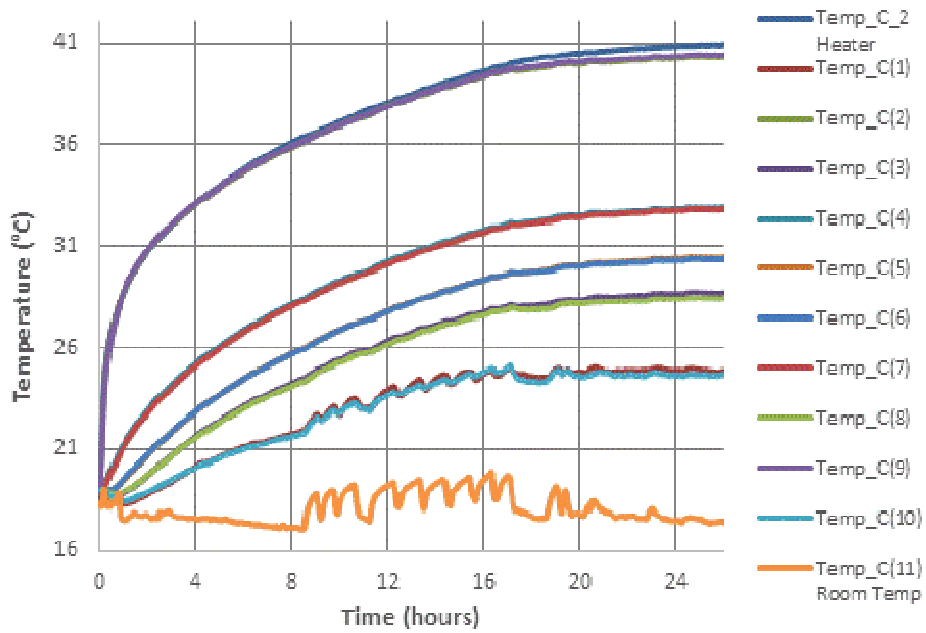


Figure 6.37: The variation of temperature with time across a sample of 75:25 Kaolin & sand consolidated to 25kPa showing that thermal equilibrium was achieved after about 26 hours

#### 6.2.3.1.2 Objective 2: Cooling Duration

To determine the duration of cooling, the power supply to the heater was disconnected and the sample was allowed to return to the controlled room temperature. Complete cooling of the sample from equilibrium heating condition to controlled room temperature lasted approximately 30 hours as shown in Figure 6.38.

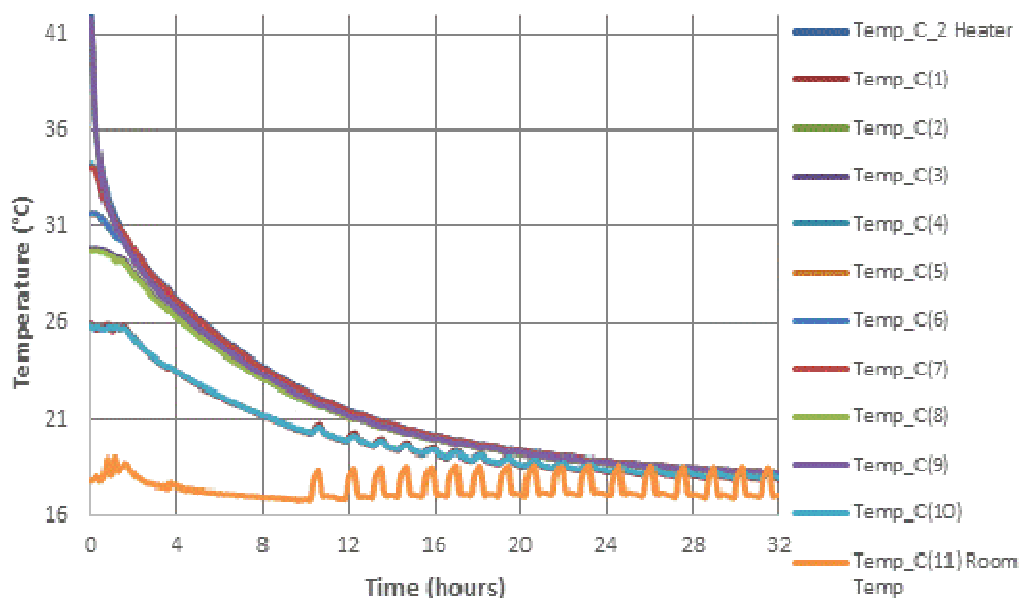


Figure 6.38: The time to return to room temperature for sample no. 8 at 25kPa

### 6.2.3.1.3 Objective 3: Temperature Variations across Sample

The objective of this test was to measure the temperature profile across the sample under thermal equilibrium in order to obtain the temperature variations within the sample. The graph in Figure 6.39 shows results from this test. It is observed that the sample shows similar temperature profiles irrespective of the level, unlike other pure kaolin samples that showed clear differences.

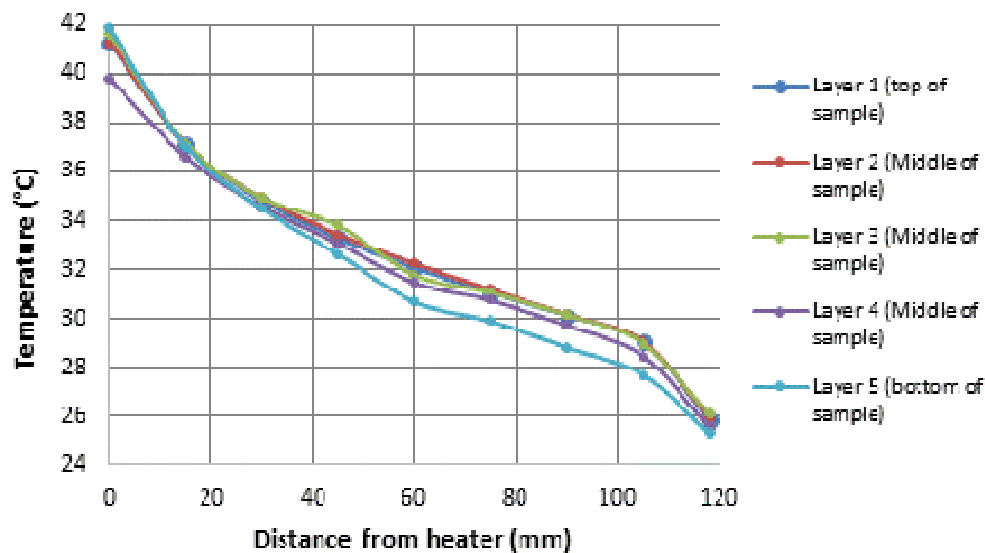


Figure 6.39: Temperature variations across sample from heater to edge of test chamber and from top to bottom of sample at end of test on sample no. 8 at 25kPa

The temperature values measured at specific locations within the sample during the temperature profile test carried out to investigate temperature variations across the sample are presented in Table 6.19.

Table 6.19: Table showing temperature variation values in sample no.8 at 25kPa

Distance from heater (mm)	Layer 1 (top of sample)	Layer 2 (Middle of sample)	Layer 3 (Middle of sample)	Layer 4 (Middle of sample)	Layer 5 (bottom of sample)
0	41.3	41.3	41.6	39.8	41.9
15	37.1	37.1	37.2	36.6	37.0
30	34.8	34.9	34.9	34.6	34.5
45	33.3	33.4	33.8	33.1	32.6
60	32.1	32.2	31.8	31.5	30.7
75	31.1	31.2	31.1	30.8	29.9
90	30.1	30.2	30.2	29.7	28.8
105	29.0	29.1	29.0	28.5	27.7
118	25.9	26.0	26.1	25.6	25.3

#### 6.2.3.1.4 Objective 4: Thermal Loading Cycles

Several thermal loading cycles were investigated on this sample. Thermal cyclic loads tested within a 24 hour testing period on sample no. 8 at 25kPa were:

- 1) 4 hours heating cycles run for five days
- 2) 8 hours heating cycles run for five days
- 3) 12 hours heating cycles run for five days.
- 4) 20 hours heating cycles run for five days

The results from the 8 hours heating and 16 hours cooling for a period of five days are presented here in Figure 6.40.

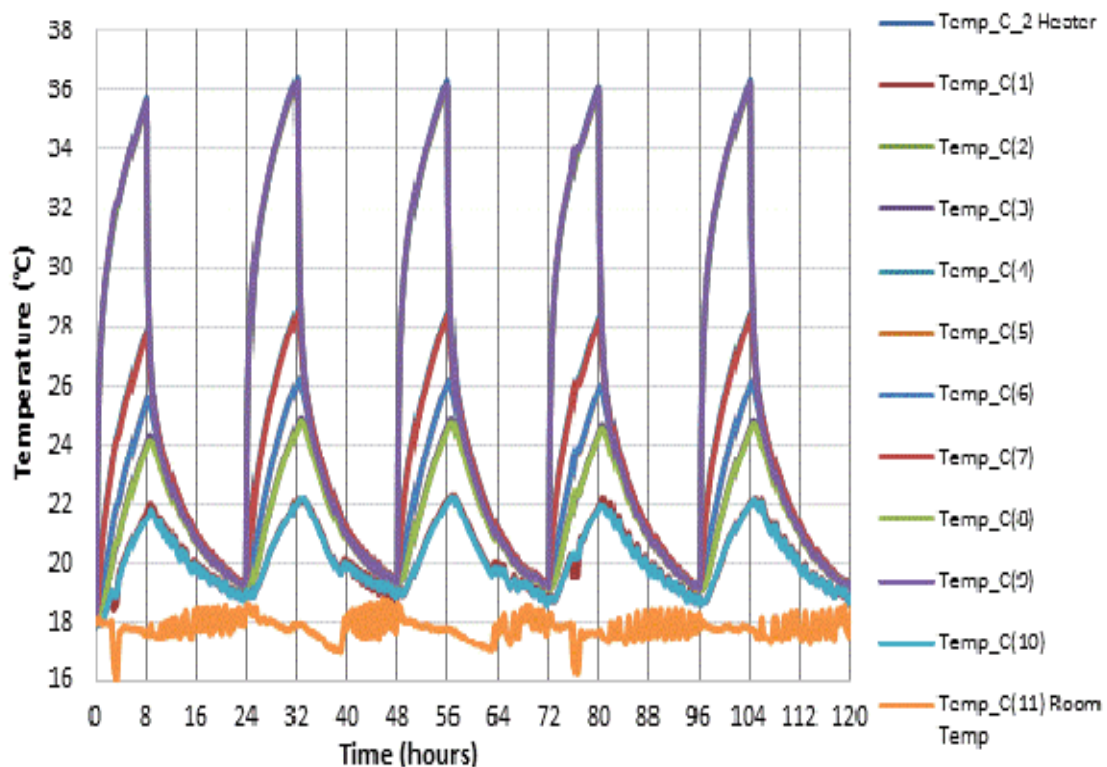


Figure 6.40: Temperature variation across the sample during 8 hours heating and 16 hours cooling in sample no. 8 at 25kPa and 17.03W

The temperature values at fixed locations within the sample in equilibrium condition at the power input of 17.03W are presented in Table 6.20.

Also shown in this table are the temperature values measured at points within the sample at the end of the thermal heating loads and at cooling after 24 hours for thermal loading cycles run at 4, 8, 12 and 20 hours on sample no. 8 at 25kPa.

Table 6.20: Peak temperature values at equilibrium condition and thermal cyclic loads in sample no. 8 at 25kPa

Probe label	Distance from Heater (mm)	Temp in thermal equilibrium after 43 hours (°C)	Temp after 4 hours thermal load (°C)	Temp after 20 hours cooling (°C)	Temp after 8 hours thermal load (°C)	Temp after 16 hours cooling (°C)	Temp after 12 hours thermal load (°C)	Temp after 12 hours cooling (°C)	Temp after 20 hours thermal load (°C)	Temp after 4 hours cooling (°C)
Probe C_2	Heater	41.9	32.5	17.9	35.7	19.3	37.4	22.0	40.2	26.1
Probe 1	117	25.7	19.8	17.6	21.6	19.0	23.1	19.9	24.7	22.7
Probe 2	Outer edge bottom of heater	41.3	32.6	17.8	35.5	19.4	37.2	21.1	40.0	25.6
Probe 3	90	29.6	21.1	17.9	24.0	19.4	25.7	20.5	28.3	25.3
Probe 4	30	33.9	24.7	17.9	27.8	19.5	29.6	20.7	32.4	26.0
Probe 5	60	31.4	22.3	17.9	25.4	19.5	27.2	20.7	29.9	25.9
Probe 6	60	31.4	22.3	17.9	25.4	19.5	27.2	20.6	29.9	25.8
Probe 7	30	33.8	24.5	17.9	27.7	19.5	29.5	20.7	32.3	26.1
Probe 8	90	29.5	21.1	17.8	23.9	19.4	25.6	20.4	28.2	25.2
Probe 9	Outer edge bottom of heater	41.4	32.6	17.9	35.6	19.4	37.2	21.0	40.0	25.7
Probe 10	117	25.6	19.7	17.6	21.5	18.9	23.2	19.8	25.0	22.6
Probe 11	Controlled Room Temp	18.0	17.6	16.9	17.7	18.4	18.3	18.4	18.8	17.6

#### 6.2.3.1.5 Objective 5: Shear Strength and Water Content Tests

The objective and procedure of this test are same as those presented in sub-section 6.2.2.1.5 For this sample the tests were carried out layer by layer in four layers of approximately 58.5mm in height, and a total of 80 samples were tested.

Figure 6.41 shows the variation of shear strength with distance from heater in the four layers from top to bottom of the sample which indicates an increase in shear strength closer to the heat source.

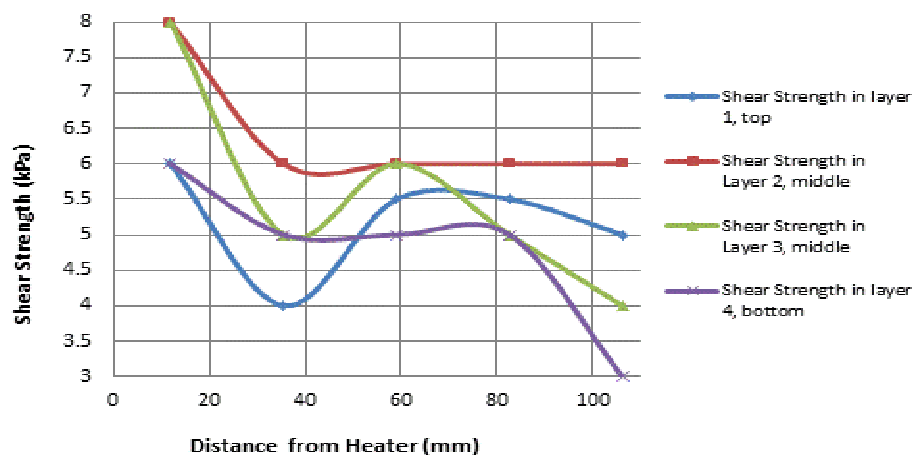


Figure 6.41: Variation of shear strength with distance from heater in the four layers from top to bottom of the sample

Figure 6.42 shows the variation of water content with distance from heater in the four layers from top to bottom of the sample which indicates a decrease in percentage water content closer to the heat source.

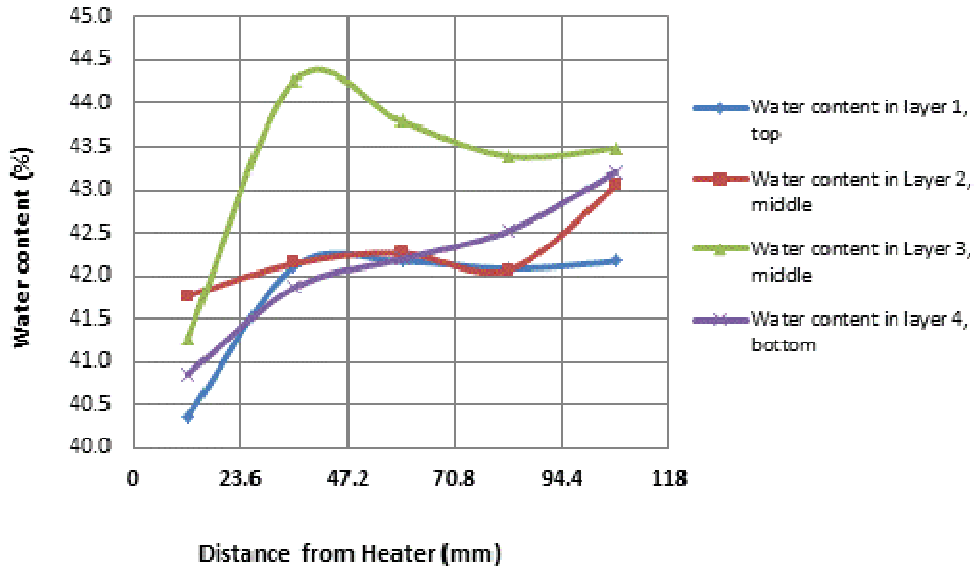


Figure 6.42: Variation of percentage water content with distance from heater in the four layers from top to bottom of the sample

Figure 6.43 shows the variation of shear strength with percentage water content for this sample at different levels to show how the shear strength and water contents vary from top to bottom of the sample.

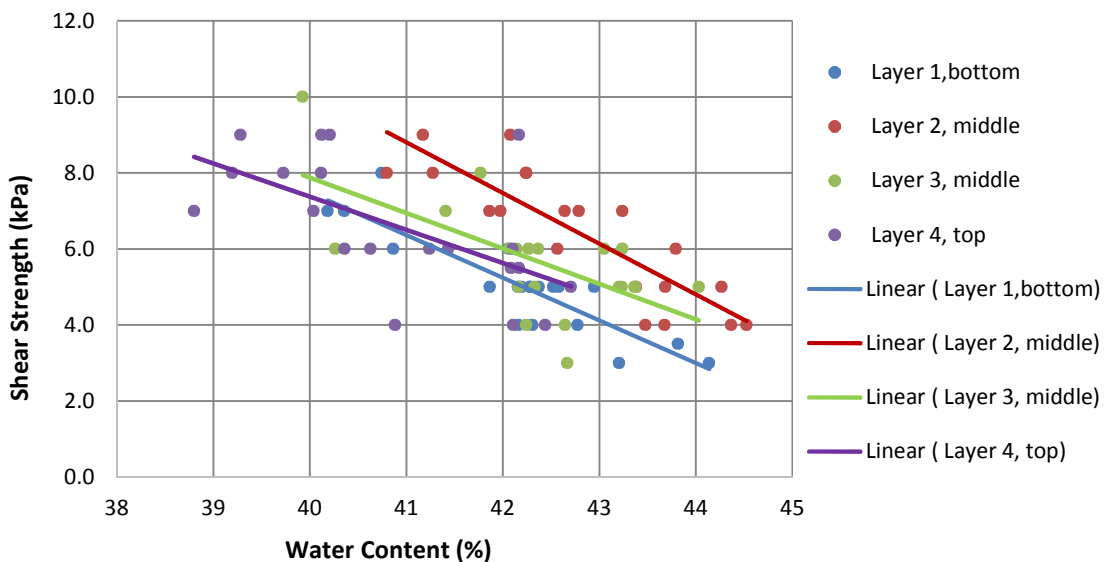


Figure 6.43: The variation of shear strength with percentage water content in sample no. 8 consolidated to 25kPa at the end of the testing regime

The trend lines show a good trend of increasing shear strength with a reduction in water content. The trend lines in layers 1 and 2 show a strong relationship between the shear strength and water content. Table 6.21 shows the coefficients and regression values for the trend lines in Figure 6.43, and the validity range of water content.

Table 6.21: The coefficients and regression values for the trend lines in Figure 6.43 and the validity range of water content

Sample layer	Equation for fit $y = mx + c$	$R^2$	Validity range of water content (%)
Layer 1 (Bottom)	$-1.1216x + 52.347$	0.7833	40.2 – 44.1
Layer 2 (Middle)	$-1.3322x + 63.423$	0.741	40.8 – 44.5
Layer 3 (Middle)	$-0.9299x + 45.064$	0.396	39.9– 44
Layer 4 (Top)	$-0.8722x + 42.265$	0.3741	38.8 – 42.7

### 6.2.3.2 Sample No. 9 (Tests carried out on Kaolin:Sand 75:25 at 100kPa)

Sample no. 9 was prepared in a similar manner to sample no. 8 with the same proportion of kaolin to sand and at the same water content of 59%. The only difference being that sample no. 9 was tested at a pressure of 100kPa which was applied incrementally.

The objectives of the tests carried out on sample no. 9 were in line with those of previous samples as listed in section 6.2.1.

The arrangement of the thermocouples within this test chamber is shown in Figure 6.44 on page 178.

#### 6.2.3.2.1 Objective 1: Equilibrium Heating Duration

A heating test was undertaken to determine how long it took the soil sample to achieve thermal equilibrium or steady state conditions. At a power input of 17.03W the sample achieved equilibrium conditions after approximately 40 hours of heating. The temperature changes in the heater and within the sample during the steady state heating is presented in Figure 6.45.

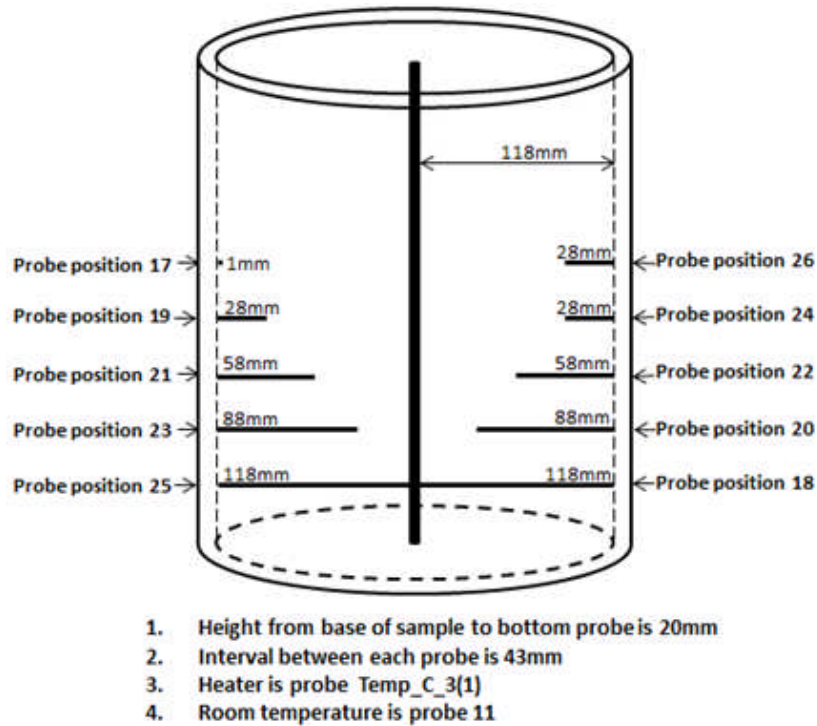


Figure 6.44: Layout of thermocouples within test chamber for tests carried out on sample no. 9

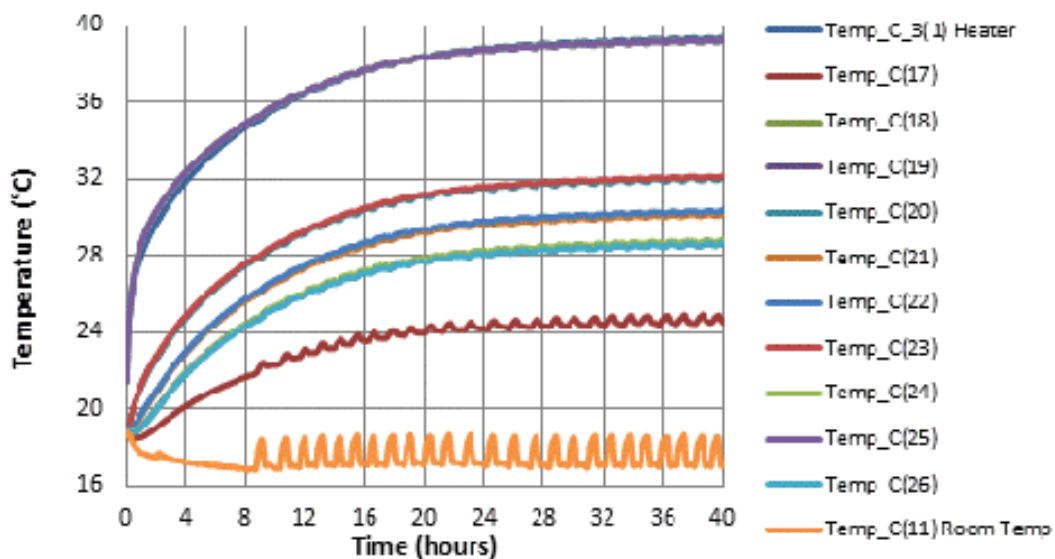


Figure 6.45: of the variation of temperature with time across sample no. 9 consolidated to 100kPa showing that thermal equilibrium was achieved after about 40 hours

#### 6.2.3.2.2 Objective 2: Cooling Duration

To determine the duration of cooling, the sample was allowed to return to the controlled room temperature. Complete cooling of the sample from equilibrium heating condition to controlled room temperature lasted approximately 32 hours as shown in Figure 6.46.

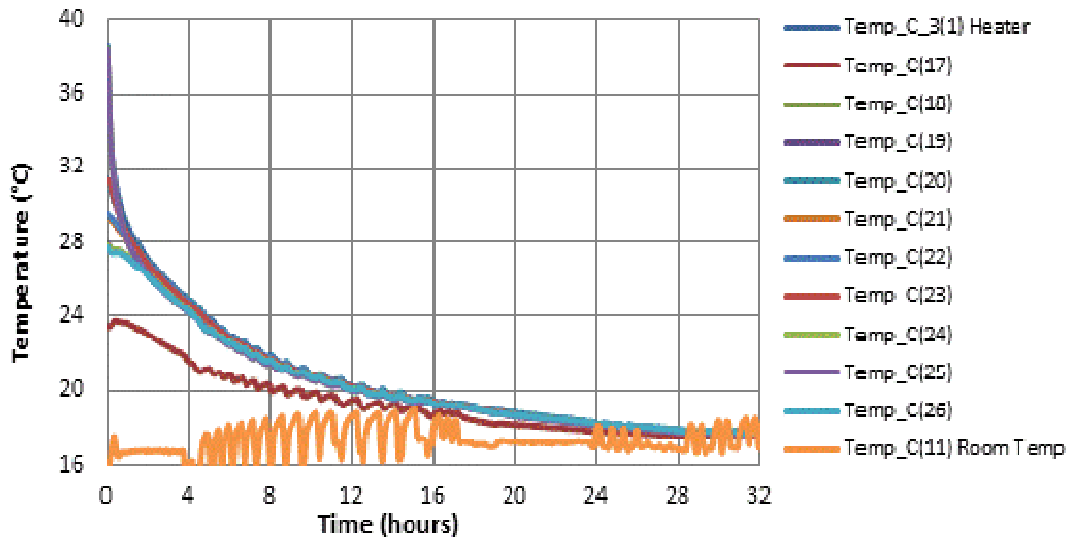


Figure 6.46: The time to return to room temperature for sample no. 9 at 100kPa

### 6.2.3.2.3 Objective 3: Temperature Variations across Sample

The objective of this test was to measure the temperature profile across the sample when in thermal equilibrium in order to obtain the temperature variations within the sample. The graph in Figure 6.47 shows results obtained from this test.

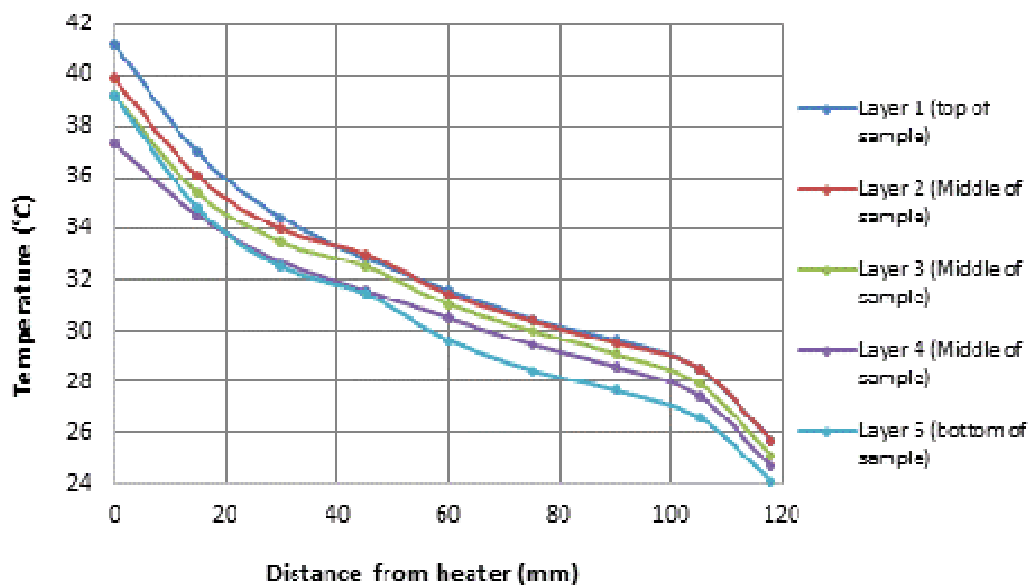


Figure 6.47: Temperature variations across sample from heater to edge of test chamber and from top to bottom of sample at end of test on sample no. 9 at 100kPa

The temperature values measured at specific locations within the sample during the temperature profile test carried out to investigate temperature variations across the sample are presented in Table 6.22.



Table 6.22: Temperature variation values in sample no.9 at 100kPa

Distance from heater (mm)	Layer 1 (top of sample)	Layer 2 (Middle of sample)	Layer 3 (Middle of sample)	Layer 4 (Middle of sample)	Layer 5 (bottom of sample)
0	41.2	39.9	39.2	37.3	39.2
15	37.0	36.0	35.4	34.5	34.8
30	34.4	34.0	33.5	32.7	32.5
45	32.9	33.0	32.5	31.6	31.5
60	31.6	31.4	31.0	30.5	29.6
75	30.5	30.4	30.0	29.4	28.5
90	29.6	29.5	29.1	28.6	27.7
105	28.5	28.5	27.9	27.5	26.6
118	25.7	25.7	25.1	24.7	24.1

#### 6.2.3.2.4 Objective 4: Thermal Loading Cycles

Several thermal loading cycles were investigated on this sample. Thermal cyclic loads tested within a 24 hour testing period on sample no. 8 at 25kPa are:

- 1) 4 hours heating cycles run for five days
- 2) 8 hours heating cycles run for five days
- 3) 12 hours heating cycles run for five days.
- 4) 20 hours heating cycles run for four days

The results from the 8 hours heating and 16 hours cooling for a period of five days is presented here in Figure 6.48

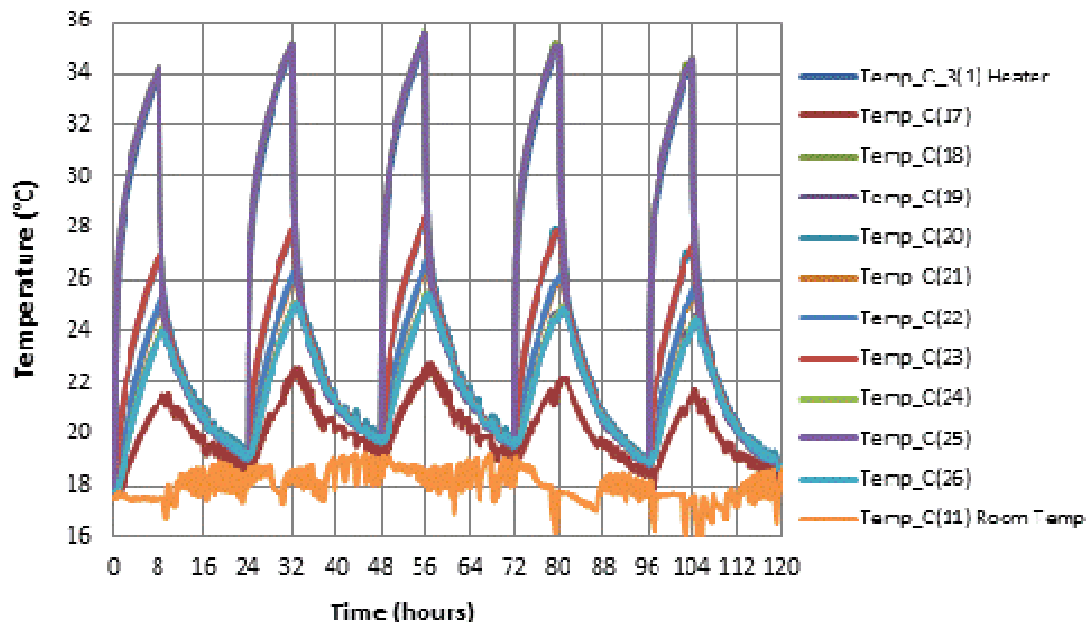


Figure 6.48: The temperature variation across the sample during 8 hours heating and 16 hours cooling in sample no. 9 at 100kPa and 17.03W

The temperature values at fixed locations within the sample in thermal equilibrium at the power input of 17.03W are presented in Table 6.23.

Also shown in this table are the temperature values measured at points within the sample at the end of the thermal heating loads and at cooling after 24 hours for thermal loading cycles run at 4, 8, 12 and 20 hours on sample no. 9 at 100kPa.

Table 6.23: Peak temperature values at equilibrium condition and thermal cyclic loads in sample no. 9 at 100kPa

Probe label	Distance from Heater (mm)	Temp in equilibrium heating condition after 40 hours (°C)	Temp after 4 hours thermal load (°C)	Temp after 20 hours cooling (°C)	Temp after 8 hours thermal load (°C)	Temp after 16 hours cooling (°C)	Temp after 12 hours thermal load (°C)	Temp after 12 hours cooling (°C)	Temp after 20 hours thermal load (°C)	Temp after 4 hours cooling (°C)
Probe C_3(1)	Heater	39.4	31.1	18.5	34.0	19.1	36.4	20.5	39.2	26.2
Probe 17	117	24.6	19.6	18.3	21.2	18.8	22.5	19.1	24.7	23.0
Probe 18	Outer edge bottom of heater	39.3	31.5	18.5	34.2	19.0	36.5	20.3	39.1	25.6
Probe 19	90	28.7	21.1	18.5	23.8	19.0	25.9	20.2	28.6	25.6
Probe 20	30	32.1	24.0	18.5	26.9	19.1	29.2	20.5	31.9	26.2
Probe 21	60	30.2	22.1	18.5	25.0	19.1	27.2	20.3	29.9	25.9
Probe 22	60	30.4	22.2	18.5	25.1	19.2	27.4	20.4	30.1	26.1
Probe 23	30	32.1	24.1	18.5	26.9	19.1	29.2	20.3	31.9	26.0
Probe 24	90	28.8	21.2	18.5	23.9	19.1	26.0	20.2	28.7	25.6
Probe 25	Outer edge bottom of heater	39.2	31.5	18.4	34.2	19.0	36.4	20.2	39.1	25.6
Probe 26	90	28.6	21.1	18.5	23.8	19.1	25.8	20.2	28.5	25.6
Probe 11	Controlled Room Temp	17.1	17.7	18.4	17.5	18.5	17.3	17.6	19.1	19.0

#### 6.2.3.2.5 Objective 5: Shear Strength and Water Content Tests

The objective and procedure of this test are the same as those stated in sub-section 6.2.2.1.5 For this sample the tests were carried out layer by layer in four layers of approximately 54.5mm each, and a total of 80 samples were tested.

Figure 6.49 on page 182, shows the variation of shear strength with distance from heater in the four layers from top to bottom of the sample which indicates a decrease in shear strength away from the heat source.

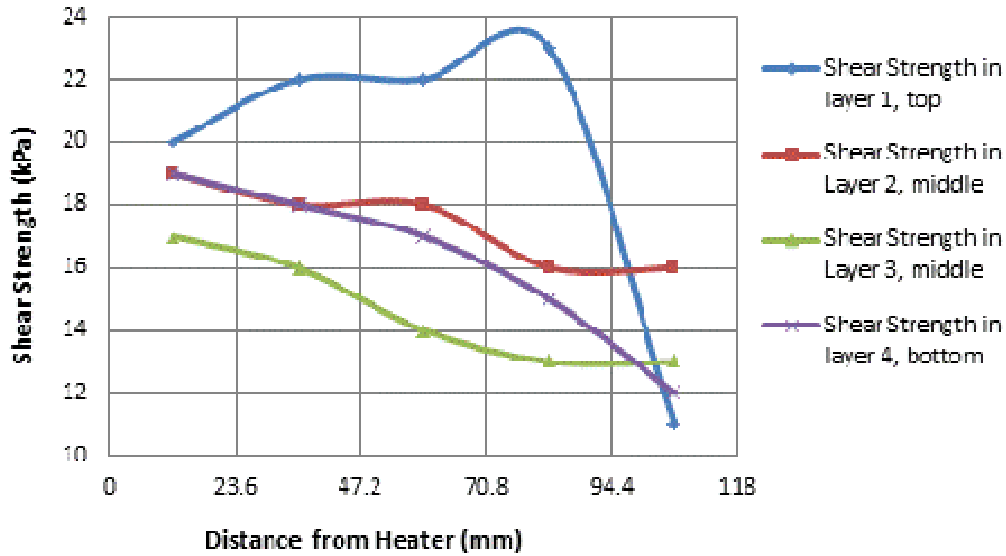


Figure 6.49: Variation of shear strength with distance from heater in the four layers from top to bottom of the sample

Figure 6.50 shows the variation of water content with distance from heater in the four layers from top to bottom of the sample which indicates an increase in percentage water content closer to the cell edge.

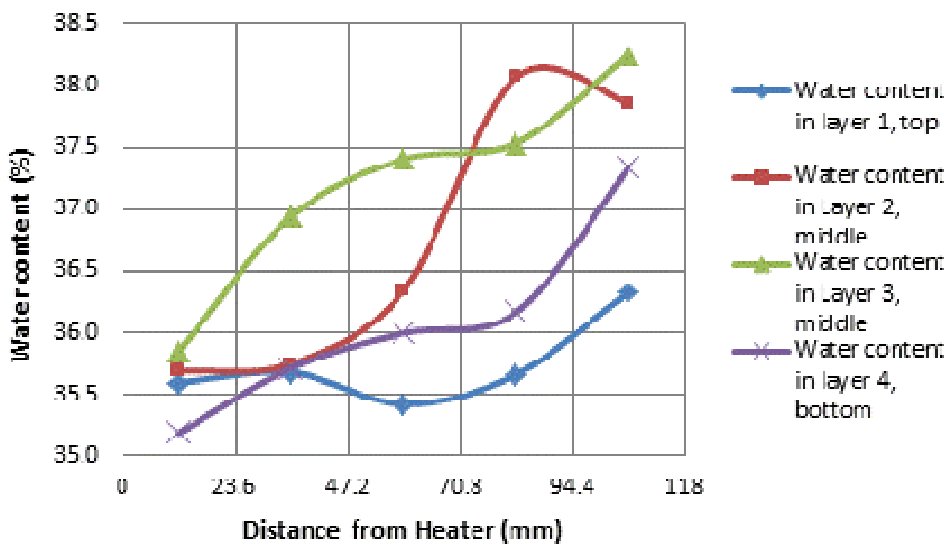


Figure 6.50: Variation of percentage water content with distance from heater in the four layers from top to bottom of the sample

Figure 6.51 on page 183, shows a plot of shear strength against water content for this sample at different levels to show how the shear strength and water contents vary from top to bottom of the sample.

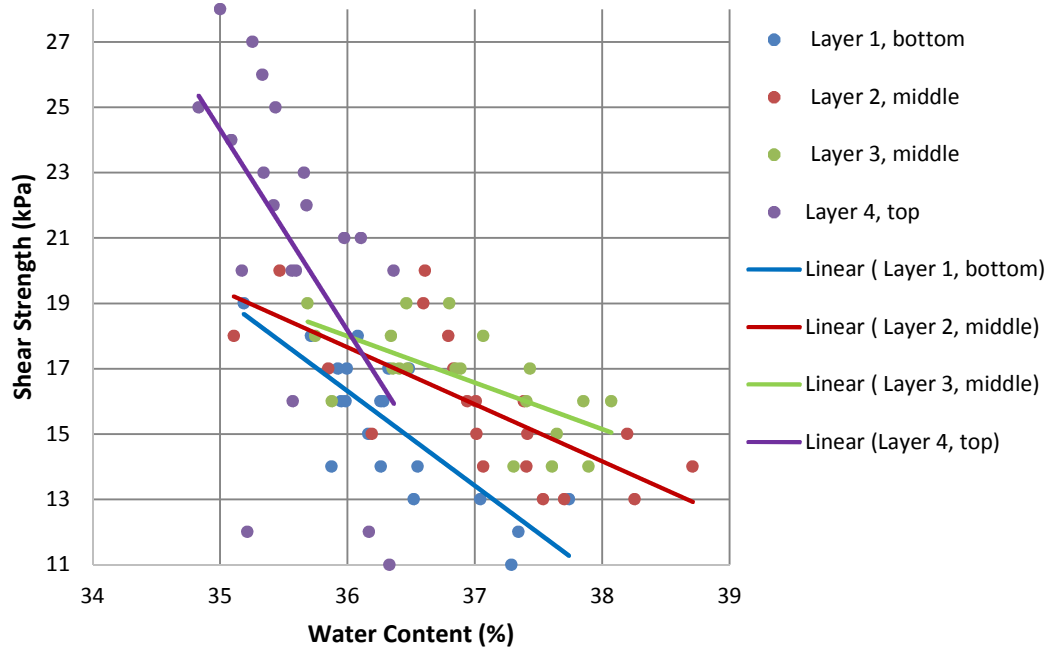


Figure 6.51: Variation of shear strength with percentage water content carried out on 75:25 kaolin:sand sample tested at 100kPa at the end of the testing regime.

The trend lines show a strong trend of increasing shear strength with a reduction in water content. Table 6.24 shows the coefficients and regression values for the trend lines in Figure 6.43, and the validity range of water content.

Table 6.24: The coefficients and regression values for the trend lines in Figure 6.51 and the validity range of water content

Sample layer	Equation for fit $y = mx + c$	$R^2$	Validity range of water content (%)
Layer 1 (Bottom)	$-2.899x + 120.67$	0.6443	35.2 – 37.3
Layer 2 (Middle)	$-1.7479x + 80.582$	0.5042	35.1 – 38.7
Layer 3 (Middle)	$-1.4212x + 69.155$	0.4245	35.7– 38.1
Layer 4 (Top)	$-6.1543x + 239.72$	0.3074	34.8 – 36.4

### 6.2.3.3 Sample No. 10 (Tests carried out on Kaolin:Sand 50:50 at 25, 50, 100kPa)

Sample no. 10 which is another combination of kaolin and sand was prepared at a ratio of one part of kaolin to one part of sand, at 44.4% water content. The sample was

carefully placed in the test rig for a series of thermal tests carried out in three phases of consolidation, with the overall objectives as those listed in section 6.2.1 except for the last objective of shear strength which will not be accurate for this sample constituted of 50% sand because the laboratory vane shear test is only suitable for testing for soft cohesive soils and may not give dependable results for clays mixed with sand or silt (Knappett and Craig, 2012).

The three phases of tests carried out on this sample were:

- 1) Testing the sample at a pressure of 25kPa
- 2) Testing the sample at a pressure of 50kPa
- 3) Testing the sample at a pressure of 100kPa

The arrangement of the thermocouples within the test chamber remained the same for the three phases of tests carried out on this sample and is shown in Figure 6.52.

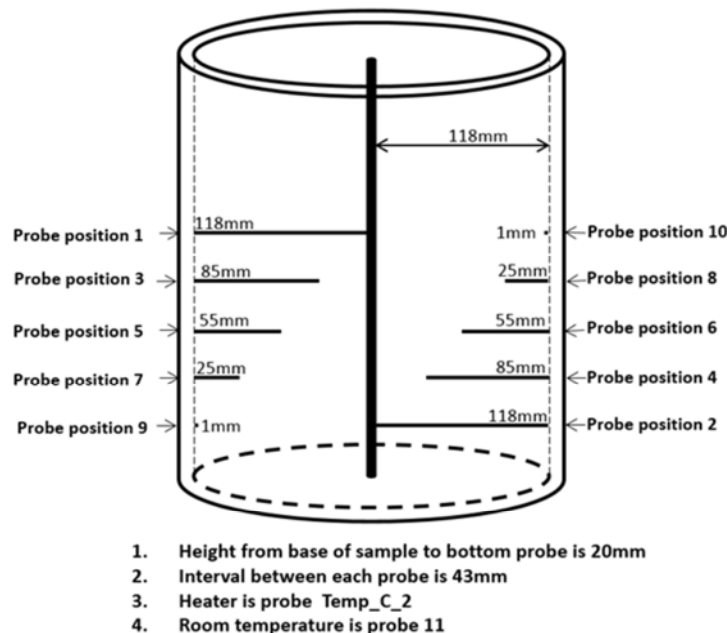


Figure 6.52: Layout of thermocouples within test chamber for tests carried out on sample no. 10

#### 6.2.3.4 Testing Sample No. 10 at 25kPa

The tests carried out on the sample at 25kPa pressure include heating and cooling tests, thermal cyclic loading tests and a temperature profile test across sample in thermal equilibrium. These tests are described in terms of the objectives for carrying them out.

##### 6.2.3.4.1 Objective 1: Equilibrium Heating Duration

A heating test was undertaken to determine how long it took the soil sample to achieve thermal equilibrium or steady state conditions.

At a power input of 17.03W the sample achieved equilibrium conditions after approximately 39 hours of heating. The variation of temperature with time in the heater and within the sample during the steady state heating is presented in Figure 6.53.

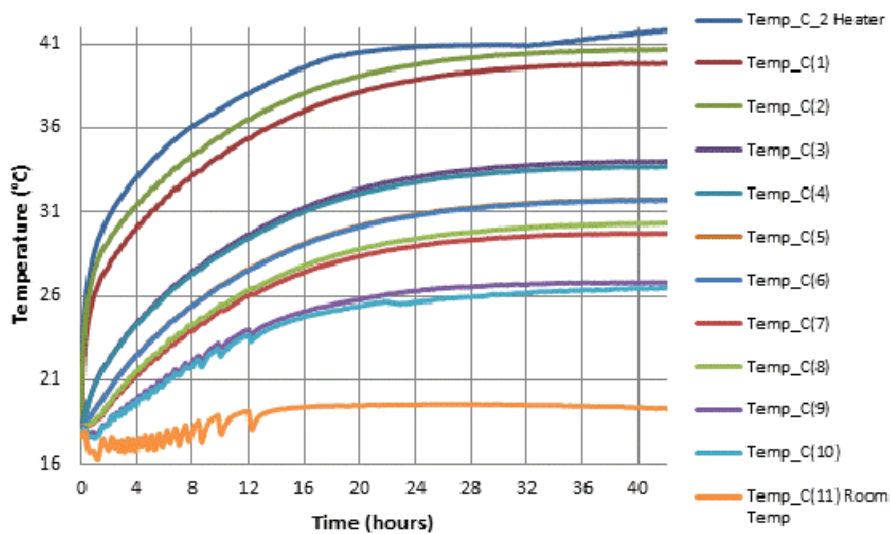


Figure 6.53: The variation of temperature with time across sample no. 10 at 25kPa and power input of 17.03W showing thermal equilibrium was achieved after about 39 hours

#### 6.2.3.4.2 Objective 2: Cooling Duration

To determine the duration of cooling, the power supply to the heater was disconnected and the sample was allowed to return to the controlled room temperature. Complete cooling of the sample from equilibrium heating condition to controlled room temperature lasted approximately 20 hours as shown in Figure 6.54.

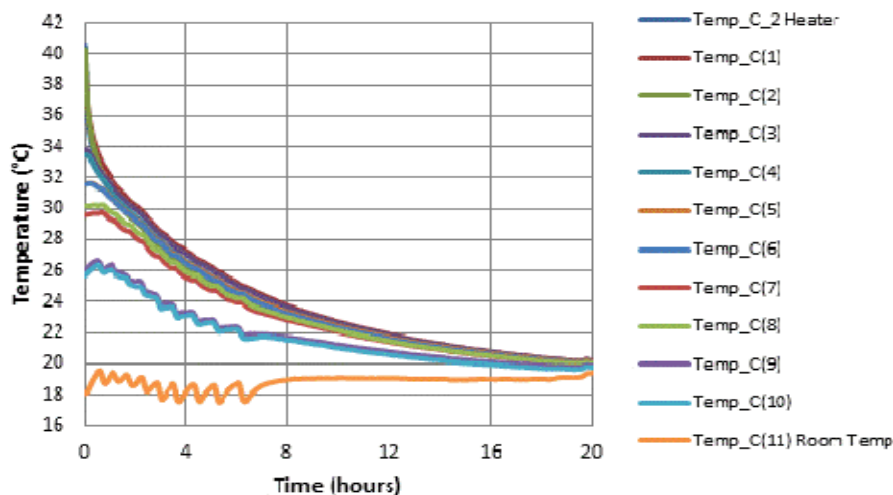


Figure 6.54: Cooling curves for sample no. 10 at 25kPa showing the time to return to room temperature

### 6.2.3.4.3 Objective 3: Temperature Variations across Sample

The objective of this test was to measure the temperature profile across the sample in thermal equilibrium in order to obtain the temperature variations within the sample. The graph in Figure 6.55 shows results from this test.

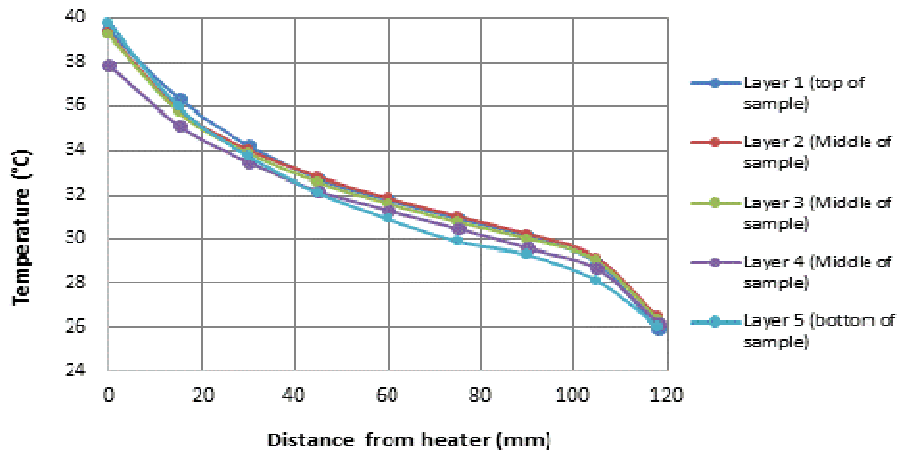


Figure 6.55: Temperature variations across sample from heater to edge of test chamber and from top to bottom of sample at end of test on sample no. 10 at 25kPa

The temperature values measured at specific locations within the sample during the temperature profile test carried out to investigate temperature variations across the sample are presented in Table 6.25.

Table 6.25: Table showing temperature variation values in sample no.10 at 25kPa

Distance from heater (mm)	Layer 1 (top of sample)	Layer 2 (Middle of sample)	Layer 3 (Middle of sample)	Layer 4 (Middle of sample)	Layer 5 (bottom of sample)
0	39.5	39.3	39.3	37.9	39.8
15	36.4	35.9	35.7	35.1	36.0
30	34.3	34.0	33.9	33.5	33.8
45	32.7	32.8	32.6	32.2	32.1
60	31.8	31.9	31.6	31.3	30.9
75	30.9	31.0	30.8	30.5	29.9
90	30.1	30.2	30.0	29.6	29.3
105	29.0	29.2	29.1	28.7	28.1
118	25.9	26.5	26.3	26.2	26.0

### 6.2.3.4.4 Objective 4: Thermal Loading Cycles

Thermal loading cycles were investigated on this sample. Thermal loading cycles tested within a 24 hour testing period on sample no. 10 at 25kPa were:

- 1) 4 hours heating cycle
- 2) 8 hours heating cycles run for two days
- 3) 12 hours heating cycles run for two days.

A graph of results from the 4 and 8 hours heating and 20 and 16 hours cooling respectively, is presented in Figure 6.56.

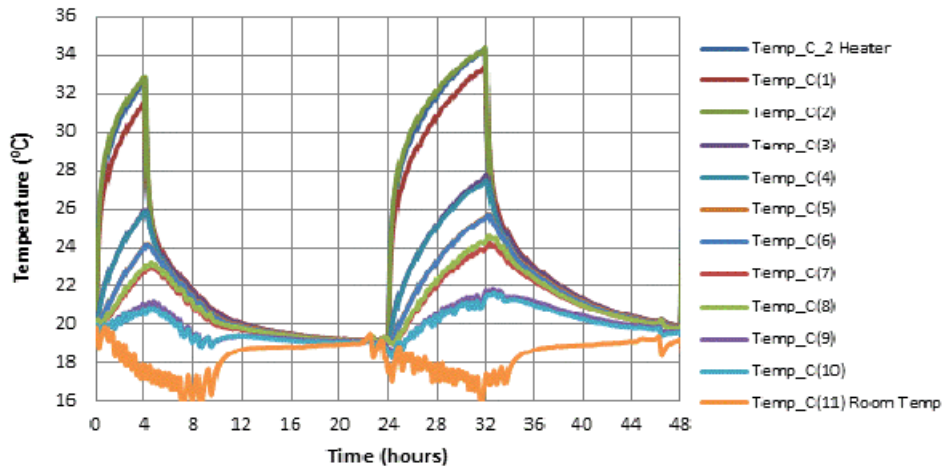


Figure 6.56: The temperature variation across the sample during thermal loading cycles of 8 hours heating and 16 hours cooling in sample no. 10 at 25kPa and 17.03W

The temperature values at fixed locations within the sample in equilibrium condition at the power input of 17.03W are presented in Table 6.26. Also shown in this table are the temperature values measured at points within the sample at the end of the thermal heating loads and at cooling after 24 hours for thermal loading cycles run at 4, 8, and 12 hours on sample no. 10 at 25kPa.

Table 6.26: Peak temperature values at equilibrium condition and thermal cyclic loads in sample no. 10 at 25kPa

Probe label	Distance from Heater (mm)	Temp in equilibrium heating condition after 39 hours (°C)	Temp after 4 hours thermal load (°C)	Temp after 24 hours cooling (°C)	Temp after 8 hours thermal load (°C)	Temp after 16 hours cooling (°C)	Temp after 12 hours thermal load (°C)	Temp after 12 hours cooling (°C)
Probe C_2	Heater	41.6	32.7	19.1	34.1	19.9	35.8	20.8
Probe 1	Outer edge top of heater	39.8	31.5	19.2	33.1	20.0	35.1	21.0
Probe 2	Outer edge bottom of heater	40.6	32.8	19.2	34.1	19.9	36.0	20.8
Probe 3	30	34.0	25.9	19.3	27.4	20.0	29.4	21.0
Probe 4	30	33.7	25.8	19.3	27.2	19.9	29.1	20.8
Probe 5	60	31.7	24.0	19.3	25.4	19.9	27.3	20.9
Probe 6	60	31.7	24.0	19.3	25.4	19.9	27.2	20.8
Probe 7	90	29.7	22.8	19.2	23.9	19.8	25.7	20.7
Probe 8	90	30.3	23.0	19.2	24.2	19.8	26.1	20.7
Probe 9	117	26.8	21.0	18.7	21.3	19.7	23.5	20.3
Probe 10	117	26.4	20.7	18.6	21.1	19.6	23.3	20.2
Probe 11	Controlled Room Temp	19.4	17.8	17.5	16.8	19.1	18.9	19.2



### 6.2.3.5 Testing Sample No. 10 at 50kPa

The tests carried out on the sample at a pressure of 50kPa include heating and cooling tests, thermal cyclic loading tests and a temperature profile test across sample in equilibrium condition. These tests are described in terms of the objectives for carrying them out.

#### 6.2.3.5.1 Objective 1: Equilibrium Heating Duration

A heating test was undertaken to determine how long it took the soil sample to achieve thermal equilibrium or steady state conditions.

At a power input of 17.03W the sample achieved equilibrium conditions after approximately 42 hours of heating. The variation of temperature with time in the heater and within the sample during the steady state heating is presented in Figure 6.57.

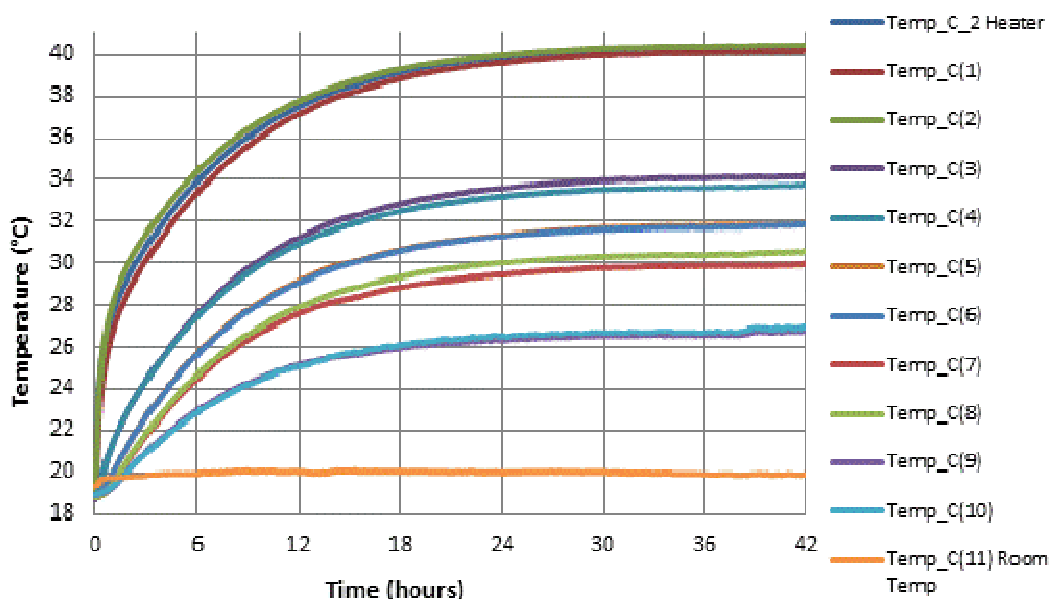


Figure 6.57: Temperature variation with time across sample no. 10 consolidated to 50kPa showing that thermal equilibrium was achieved after about 42 hours

#### 6.2.3.5.2 Objective 2: Cooling Duration

To determine the duration of cooling, the power supply to the heater was disconnected and the sample was allowed to return to the controlled room temperature. Complete cooling of the sample from equilibrium heating condition to controlled room temperature lasted approximately 32 hours as shown in Figure 6.58.

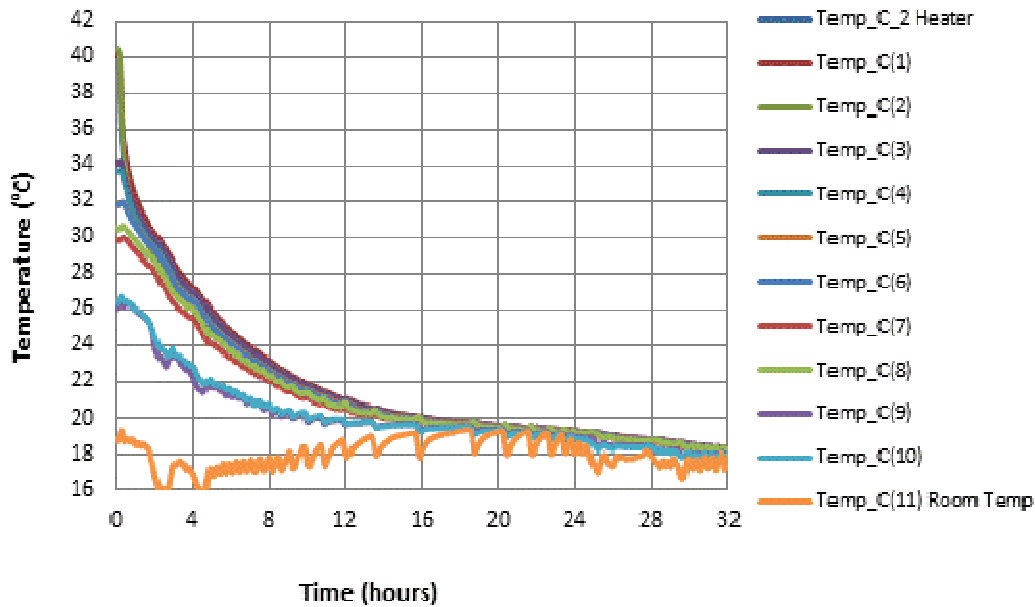


Figure 6.58: Time to return to room temperature for sample no. 10 at 50kPa

### 6.2.3.5.3 Objective 3: Temperature Variations across Sample

The objective of this test was to measure the temperature profile across the sample while in thermal equilibrium in order to obtain the temperature variations within the sample. The graph in Figure 6.59 shows results from this test.

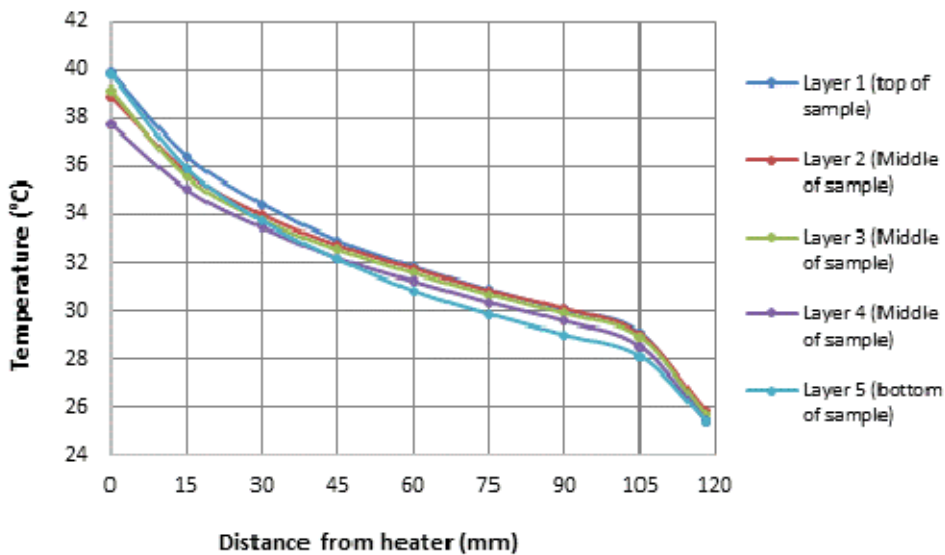


Figure 6.59: Temperature variations across sample from heater to edge of test chamber and from top to bottom of sample at end of test on sample no. 10 at 50kPa

The temperature values measured at specific locations within the sample during the temperature profile test carried out to investigate temperature variations across the sample are presented in Table 6.27.

Table 6.27: Table showing temperature variation values in sample no.10 at 50kPa

Distance from heater (mm)	Layer 1 (top of sample)	Layer 2 (Middle of sample)	Layer 3 (Middle of sample)	Layer 4 (Middle of sample)	Layer 5 (bottom of sample)
0	39.9	38.9	39.2	37.8	39.8
15	36.4	35.8	35.6	35.1	35.9
30	34.5	34.0	33.8	33.5	33.7
45	32.9	32.7	32.6	32.2	32.2
60	31.8	31.8	31.6	31.2	30.9
75	30.9	30.9	30.7	30.4	29.9
90	30.1	30.1	29.9	29.6	29.0
105	29.1	29.1	28.9	28.5	28.1
118	25.4	25.8	25.7	25.4	25.4

#### 6.2.3.5.4 Objective 4: Thermal Loading Cycles

Thermal loading cycles were investigated on this sample. Thermal loading cycles investigated within a 24 hour testing period on sample no. 10 at 50kPa were:

- 1) 8 hours heating cycles run for two days
- 2) 12 hours heating cycles run for several days in separate tests.

A graph of results from the 8 hours heating and 16 hours cooling for a period of two days is presented in Figure 6.60.

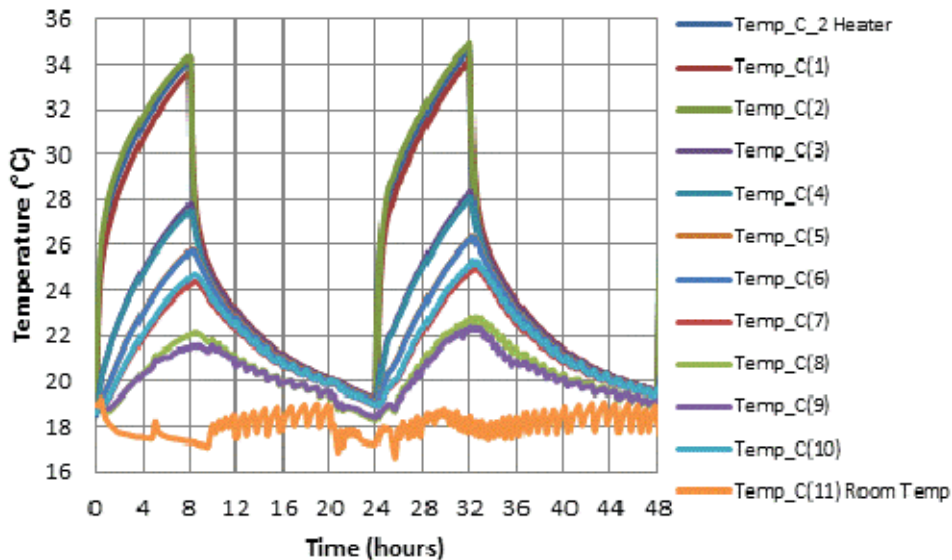


Figure 6.60: The temperature variation across the sample during thermal loading cycles of 8 hours heating and 16 hours cooling in sample no. 10 at 50kPa and 17.03W

The temperature values at fixed locations within the sample in thermal equilibrium at the power input of 17.03W are presented in Table 6.28. Note that during the steady state heating test, probes 8 and 10 swapped positions.

Also shown in Table 6.28 are the temperature values measured at points within the sample at the end of the thermal heating loads and at cooling after 24 hours for thermal loading cycles run at 8 and 12 hours on sample no. 10 at 50kPa.

Table 6.28: Peak temperature values at equilibrium condition and thermal cyclic loads in sample no. 10 at 50kPa

Probe label	Distance from Heater (mm)	Temp in equilibrium heating condition after 42 hours (°C)	Temp after 8 hours thermal load (°C)	Temp after 16 hours cooling (°C)	Temp after 12 hours thermal load (°C)	Temp after 12 hours cooling (°C)
Probe C_2	Heater	40.4	34.1	19.1	36.5	21.2
Probe 1	Outer edge top of heater	40.2	33.6	19.2	36.2	21.4
Probe 2	Outer edge bottom of heater	40.5	34.3	19.0	36.8	21.1
Probe 3	30	34.2	27.8	19.2	30.3	21.3
Probe 4	30	33.8	27.5	19.1	30.0	21.2
Probe 5	60	31.9	25.7	19.1	28.2	21.2
Probe 6	60	31.9	25.7	19.0	28.2	21.2
Probe 7	90	30.0	24.2	18.9	26.6	21.0
Probe 8	90	30.6	22.0	18.3	24.5	20.2
Probe 9	117	26.8	21.5	18.4	23.7	20.2
Probe 10	117	27.0	24.6	18.9	27.0	21.1
Probe 11	Controlled Room Temp	19.9	17.3	17.3	19.3	18.5

### 6.2.3.6 Testing Sample No. 10 at 100kPa

The tests carried out on the sample at 100kPa pressure include heating and cooling tests, thermal cyclic loading tests and a temperature profile test across sample in equilibrium condition. These tests are described in terms of the objectives for carrying them out.

#### 6.2.3.6.1 Objective 1: Equilibrium Heating Duration

A heating test was undertaken to determine how long it took the soil sample to achieve thermal equilibrium or steady state conditions. At a power input of 17.03W the sample achieved equilibrium conditions after approximately 43 hours of heating. The variation of temperature with time in the heater and within the sample during the steady state heating is presented in Figure 6.61.

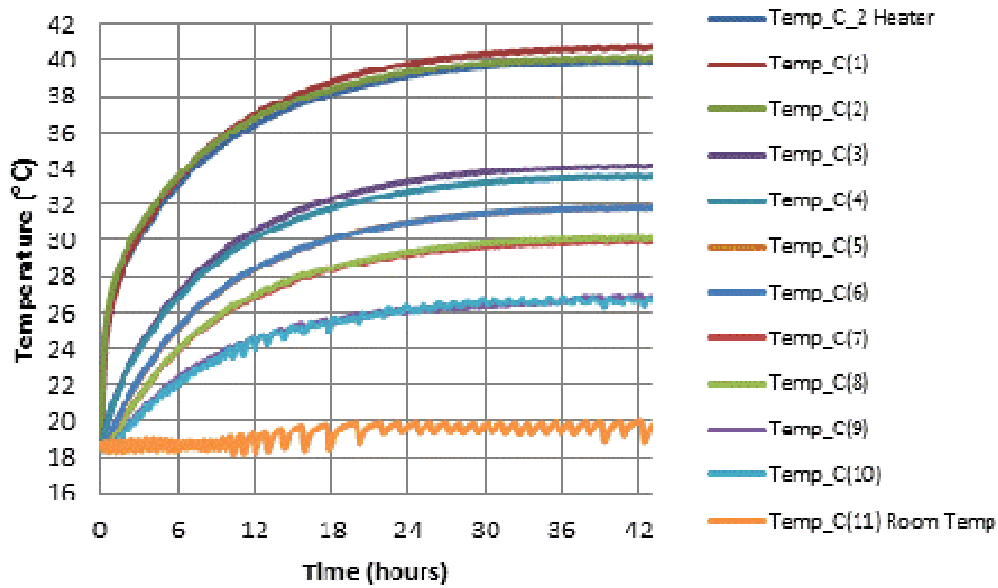


Figure 6.61: Variation of temperature with time across sample no. 10 consolidated to 100kPa showing that thermal equilibrium was achieved after about 43 hours

#### 6.2.3.6.2 Objective 2: Cooling Duration

To determine the duration of cooling of the sample, the power supply to the heater was disconnected and the sample was allowed to return to the controlled room temperature. Complete cooling of the sample from equilibrium heating condition to controlled room temperature lasted approximately 30 hours as shown in Figure 6.62.

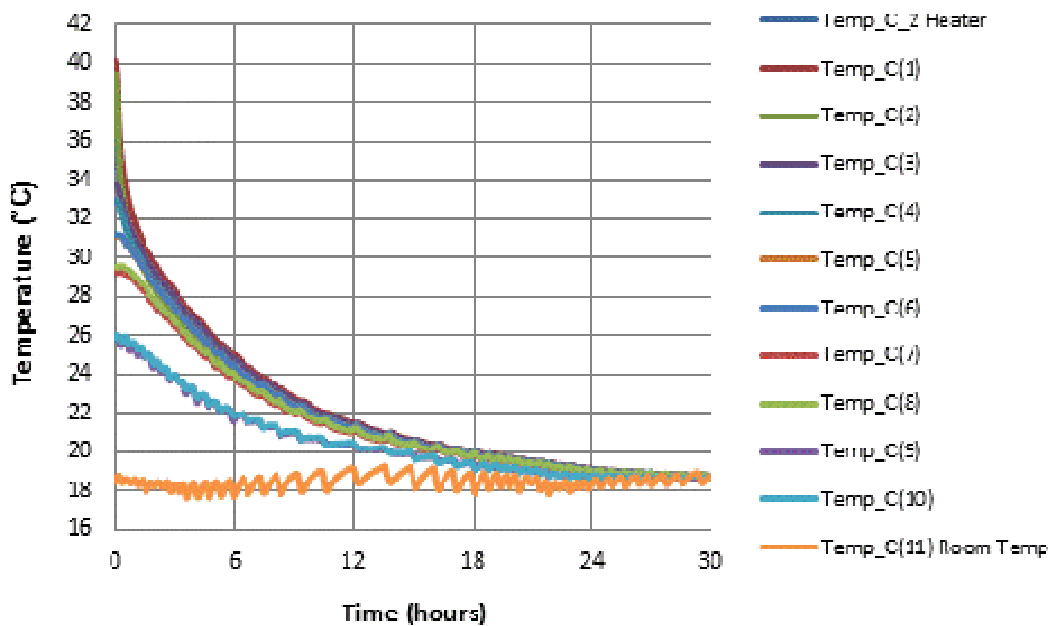


Figure 6.62: The time to return to room temperature for sample no. 10 at 100kPa

### 6.2.3.6.3 Objective 3: Temperature Variations across Sample

The objective of this test was to measure the temperature profile across the sample while in thermal equilibrium, in order to obtain the temperature variations within the sample. The graph in Figure 6.63 shows results from this test.

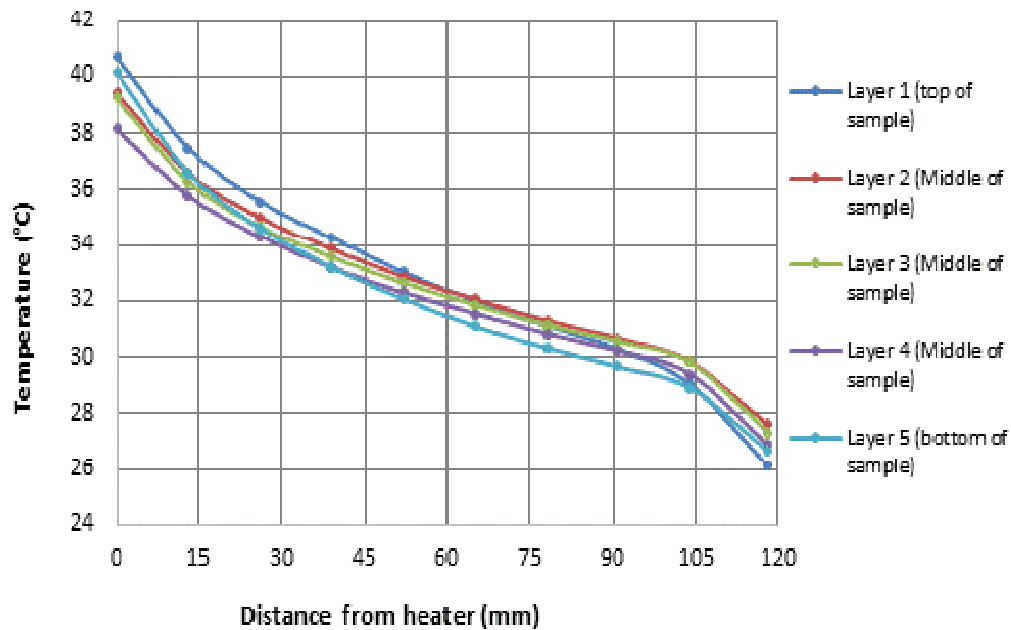


Figure 6.63: Temperature variations across sample from heater to edge of test chamber and from top to bottom of sample at end of test on sample no. 10 at 100kPa

The temperature values measured at specific locations within the sample during the temperature profile test carried out to investigate temperature variations across the sample are presented in Table 6.29.

Table 6.29: Table showing temperature variation values in sample no.10 at 100kPa

Distance from heater (mm)	Layer 1 (top of sample)	Layer 2 (Middle of sample)	Layer 3 (Middle of sample)	Layer 4 (Middle of sample)	Layer 5 (bottom of sample)
0	40.7	39.4	39.3	38.2	40.2
13	37.5	36.6	36.3	35.8	36.6
26	35.6	35.0	34.7	34.3	34.6
39	34.3	33.9	33.6	33.2	33.2
52	33.0	32.9	32.6	32.3	32.1
65	32.0	32.1	31.9	31.6	31.1
78	31.1	31.3	31.1	30.8	30.3
91	30.3	30.7	30.6	30.2	29.7
104	29.0	29.8	29.8	29.4	28.9
118	26.1	27.6	27.3	26.9	26.7

#### 6.2.3.6.4 Objective 4: Thermal Loading Cycles

Thermal loading cycles were investigated on this sample. Thermal loading cycles tested within a 24 hour testing period on sample no. 10 at 100kPa were:

- 1) 8 hours heating cycles run for two days
- 2) 12 hours heating cycles run for three days at first and later on repeated for four days

A graph of results from the 8 hours heating and 16 hours cooling for a period of two days is presented here in Figure 6.64.

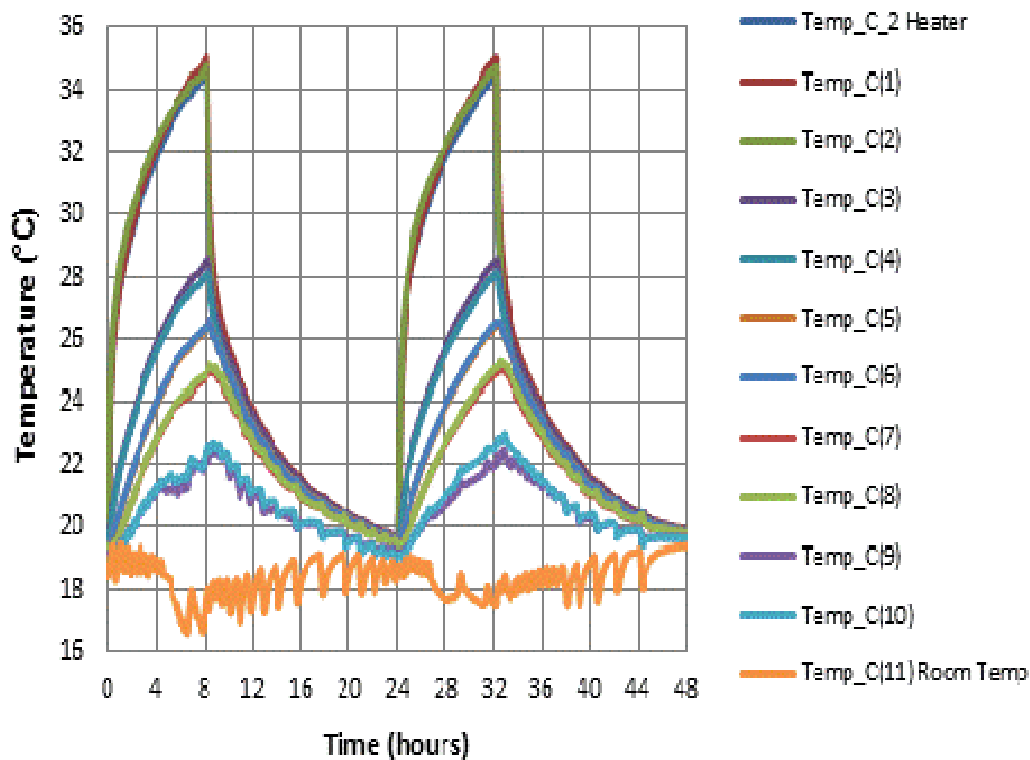


Figure 6.64: The temperature variation across the sample during thermal loading cycles of 8 hours heating and 16 hours cooling in sample no. 10 at 100kPa and 17.03W

The temperature values at fixed locations within the sample in equilibrium condition at the power input of 17.03W are presented in Table 6.30.

Also shown in the Table are the temperature values measured at points within the sample at the end of the thermal heating loads and at cooling after 24 hours for thermal loading cycles run at 8 and 12 hours on sample no. 10 at 100kPa.

Table 6.30: Peak temperature values at equilibrium condition and thermal cyclic loads in sample no. 10 at 100kPa

Probe label	Distance from Heater (mm)	Temp in equilibrium heating condition after 43 hours (°C)	Temp after 8 hours thermal load (°C)	Temp after 16 hours cooling (°C)	Temp after 12 hours thermal load (°C)	Temp after 12 hours cooling (°C)
Probe C_2	Heater	40.0	34.4	19.5	36.2	21.0
Probe 1	Outer edge top of heater	40.7	35.0	19.7	36.9	21.2
Probe 2	Outer edge bottom of heater	40.2	34.7	19.5	36.6	21.0
Probe 3	30	34.2	28.5	19.7	30.4	21.2
Probe 4	30	33.5	28.1	19.6	30.0	21.1
Probe 5	60	31.8	26.3	19.6	28.2	21.1
Probe 6	60	31.8	26.4	19.6	28.3	21.1
Probe 7	90	30.0	24.8	19.5	26.6	21.0
Probe 8	90	30.1	24.9	19.5	26.8	20.9
Probe 9	117	26.9	22.2	19.2	24.0	20.3
Probe 10	117	26.7	22.3	19.1	24.3	19.9
Probe 11	Controlled Room Temp	19.7	17.4	18.6	19.0	18.2

### 6.2.3.7 Sample No. 11 (Tests carried out on Kaolin:Sand 25:75 Test at 25, 50, 100kPa)

Sample no. 11 which is another combination of kaolin and sand was prepared at a ratio of one part of kaolin to three parts of sand, at approximately 32.1% water content. The sample was carefully placed in the test rig for a series of thermal tests carried out in three phases with the overall objectives the same as those listed in section 6.2.1.

The three phases of tests carried out on this sample were:

- 1) Testing the sample at a pressure of 25kPa
- 2) Testing the sample at a pressure of 50kPa
- 3) Testing the sample at a pressure of 100kPa

The arrangement of the thermocouples within the test chamber remained the same for the three phases of tests carried out on this sample and is shown in Figure 6.65.



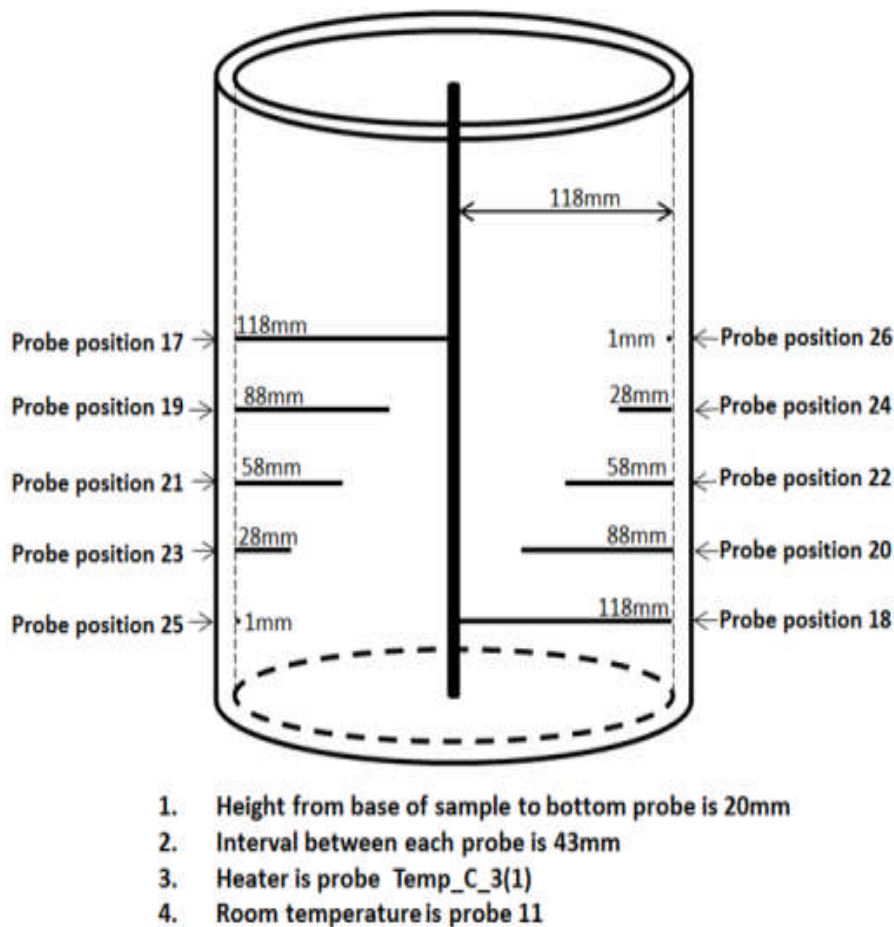


Figure 6.65: Layout of thermocouples within test chamber for tests carried out on sample no. 11

### 6.2.3.8 Testing Sample No. 11 at 25kPa

The tests carried out on the sample at 25kPa pressure include heating and cooling tests, thermal loading cycles and a temperature profile test across sample in thermal equilibrium condition. These tests are described in terms of the objectives for carrying them out.

#### 6.2.3.8.1 Objective 1: Equilibrium Heating Duration

A heating test was undertaken to determine how long it took the soil sample to achieve thermal equilibrium or steady state conditions.

At a power input of 17.03W the sample achieved equilibrium conditions after approximately 28 hours of heating. The variation of temperature with time in the heater and within the sample during the steady state heating is presented in Figure 6.66 on page 197.

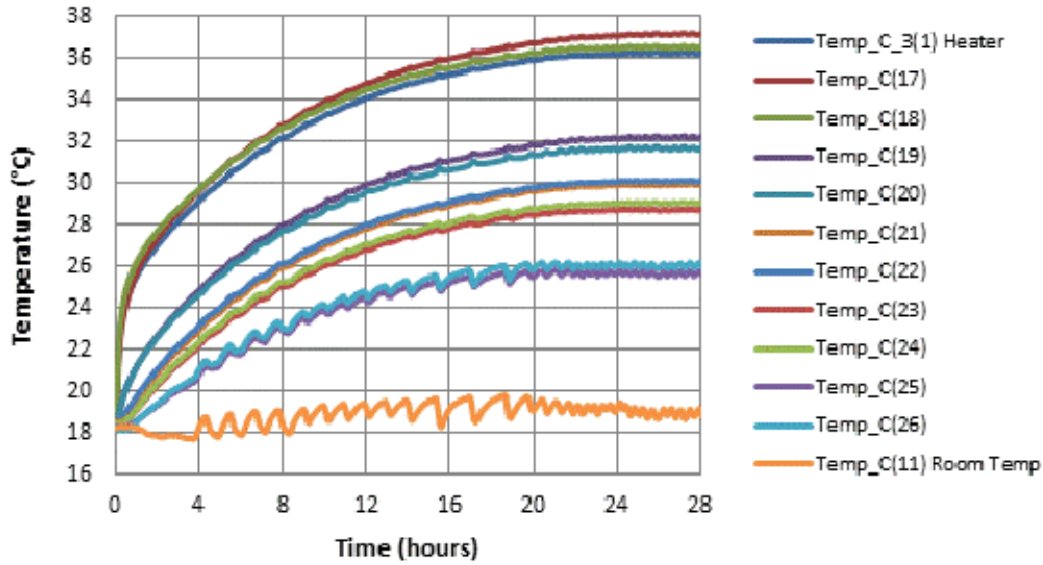


Figure 6.66: The variation of temperature with time across sample no. 11 consolidated to 25kPa and power input of 17.03W showing thermal equilibrium was achieved after about 28 hours

#### 6.2.3.8.2 Objective 2: Cooling Duration

To determine the duration of cooling, the power supply to the heater was disconnected and the sample was allowed to return to the controlled room temperature. Complete cooling of the sample from thermal equilibrium to controlled room temperature lasted approximately 27 hours as shown in Figure 6.67.

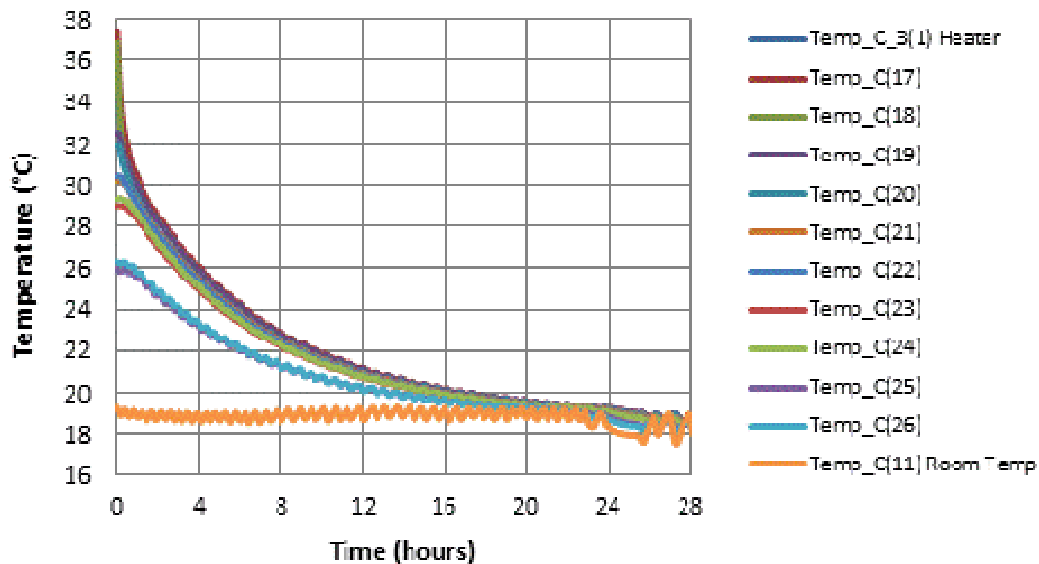


Figure 6.67: Cooling curves for sample no. 11 consolidated to 25kPa showing the time to return to room temperature

### 6.2.3.8.3 Objective 3: Temperature Variations across Sample

The objective of this test was to obtain the temperature variations within the sample when in thermal equilibrium. The graph in Figure 6.68 shows results from this test.

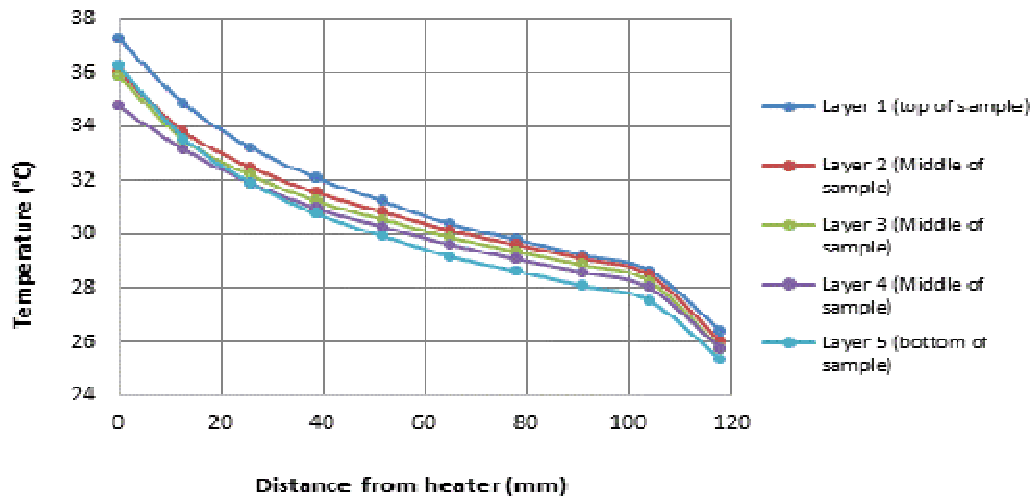


Figure 6.68: Temperature variations across sample from heater to edge of test chamber and from top to bottom of sample at end of test on sample no. 11 at 25kPa

The temperature values measured at specific locations within the sample during the temperature profile test carried out to investigate temperature variations across the sample are presented in Table 6.31.

Table 6.31: Table showing temperature variation values in sample no.11 at 25kPa

Distance from heater (mm)	Layer 1 (top of sample)	Layer 2 (Middle of sample)	Layer 3 (Middle of sample)	Layer 4 (Middle of sample)	Layer 5 (bottom of sample)
0	37.3	36.0	35.9	34.8	36.3
13	34.8	33.8	33.5	33.2	33.6
26	33.2	32.5	32.2	31.9	31.9
39	32.1	31.5	31.2	31.0	30.8
52	31.2	30.8	30.6	30.3	29.9
65	30.4	30.1	29.9	29.6	29.2
78	29.8	29.6	29.4	29.1	28.6
91	29.2	29.1	28.9	28.6	28.1
104	28.7	28.5	28.3	28.0	27.5
118	26.4	26.0	25.7	25.7	25.3

### 6.2.3.8.4 Objective 4: Thermal Loading Cycles

Thermal loading cycles were investigated on this sample. Thermal cycles tested within a 24 hour testing period on sample no. 11 at 25kPa were:

- 1) 8 hours heating cycles run for three days
- 2) 12 hours heating cycles run for two days.

The results from the 8 hours heating and 16 hours cooling for a period of three days are presented here in Figure 6.69.

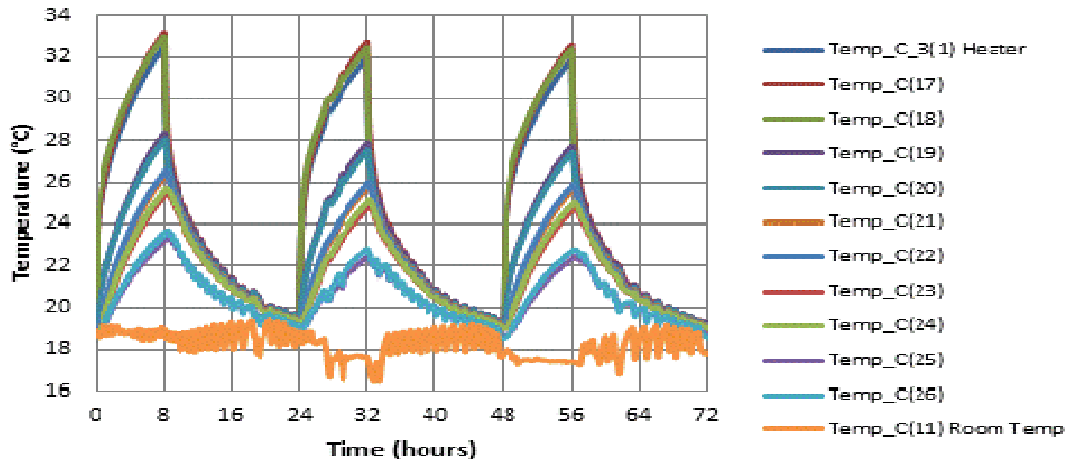


Figure 6.69: of the temperature variation across sample during 8 hours heating and 16 hours cooling in sample no. 11 at 25kPa and 17.03W

The temperature values at fixed locations within the sample in equilibrium condition at the power input of 17.03W are presented in Table 6.32. Also shown in this table are the temperature values measured at points within the sample at the end of the thermal heating loads and at cooling after 24 hours for thermal loading cycles run at 8 and 12 hours on sample no. 11 at 25kPa.

Table 6.32: Peak temperature values at equilibrium condition and thermal cyclic loads in sample no. 11 at 25kPa

Probe label	Distance from Heater (mm)	Temp in thermal equilibrium after 36.5 hours (°C)	Temp after 8 hours thermal load (°C)	Temp after 16 hours cooling (°C)	Temp after 12 hours thermal load (°C)	Temp after 12 hours cooling (°C)
Probe C_3(1)	Heater	36.4	32.5	19.4	33.6	20.0
Probe 17	Outer edge top of heater	37.2	33.2	19.5	34.3	20.3
Probe 18	Outer edge bottom of heater	36.6	33.0	19.3	34.0	19.9
Probe 19	30	32.3	28.3	19.5	29.4	20.2
Probe 20	30	31.8	28.0	19.4	29.0	20.0
Probe 21	60	30.1	26.3	19.4	27.4	20.0
Probe 22	60	30.2	26.5	19.3	27.6	19.9
Probe 23	90	28.9	25.4	19.3	26.4	19.8
Probe 24	90	29.2	25.6	19.3	26.6	19.8
Probe 25	117	26.0	23.3	19.1	24.2	19.2
Probe 26	117	26.4	23.6	19.0	24.5	19.2
Probe 11	Controlled Room Temp	19.5	18.9	18.5	19.1	17.7

### 6.2.3.9 Testing Sample No. 11 at 50kPa

The tests carried out on the sample at 50kPa pressure include heating and cooling tests, thermal cyclic loading tests and a temperature profile test across sample in thermal equilibrium. These tests are described in terms of the objectives for carrying them out.

#### 6.2.3.9.1 Objective 1: Equilibrium Heating Duration

A heating test was undertaken to determine how long it took the soil sample to achieve thermal equilibrium or steady state conditions.

At a power input of 17.03W the sample achieved thermal equilibrium after approximately 28 hours of heating. The variation of temperature with time in the heater and within the sample during the steady state heating is presented in Figure 6.70.

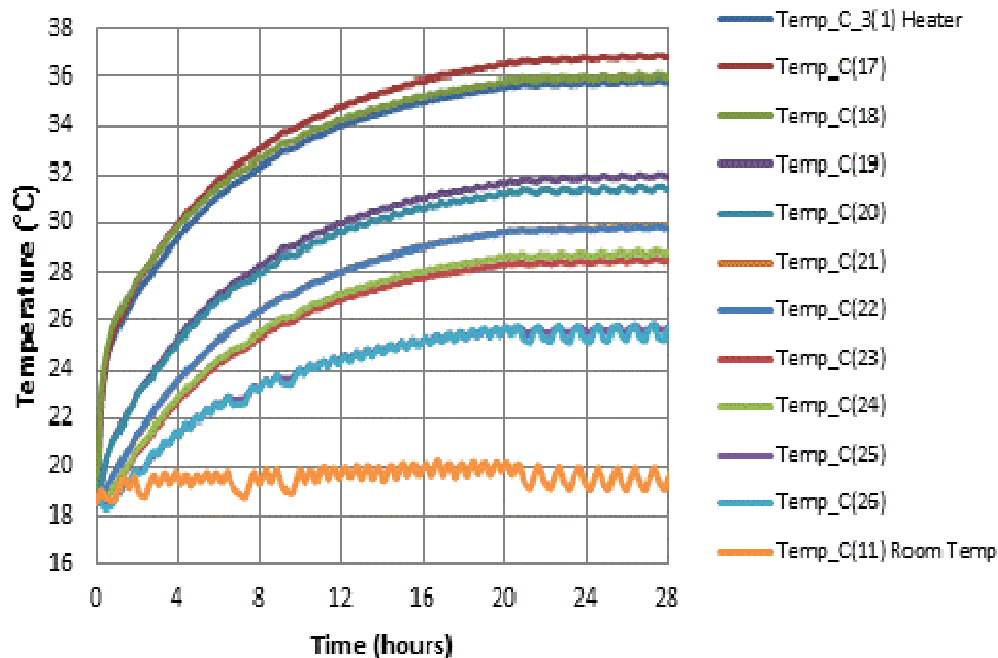


Figure 6.70: Temperature variation with time across sample no. 11 consolidated to 50kPa showing that thermal equilibrium was achieved after about 28 hours

#### 6.2.3.9.2 Objective 2: Cooling Duration

To determine the duration of cooling, the power supply to the heater was disconnected and the sample was allowed to return to the controlled room temperature. Complete cooling of the sample from equilibrium heating condition to controlled room temperature lasted approximately 23 hours as shown in Figure 6.71 on page 201

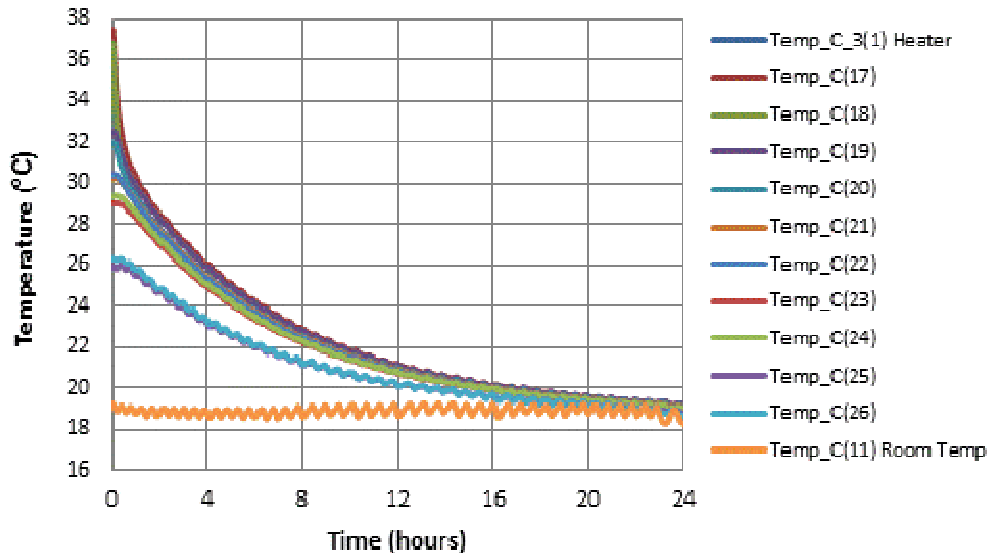


Figure 6.71: Cooling curves for sample no. 11 at 50kPa showing time to return to room temperature

### 6.2.3.9.3 Objective 3: Temperature Variations across Sample

The objective of this test was to measure the temperature profile across the sample when in thermal equilibrium in order to obtain the temperature variations within the sample. The graph in Figure 6.72 shows results from this test.

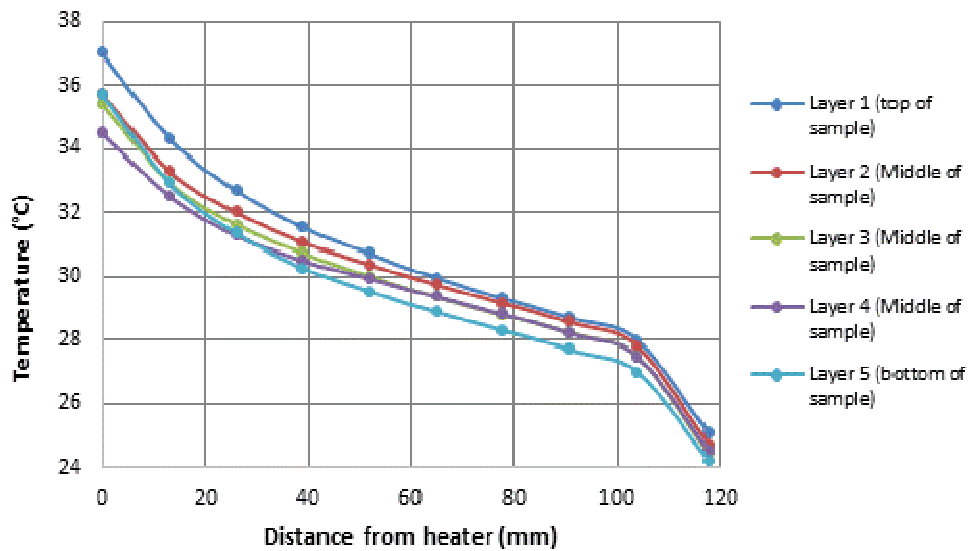


Figure 6.72: Temperature variations across sample from heater to edge of test chamber and from top to bottom of sample at end of test on sample no. 11 at 50kPa

The temperature values measured at specific locations within the sample during the temperature profile test carried out to investigate temperature variations across the sample are presented in Table 6.33.

Table 6.33: Table showing temperature variation values in sample no.11 at 50kPa

Distance from heater (mm)	Layer 1 (top of sample)	Layer 2 (Middle of sample)	Layer 3 (Middle of sample)	Layer 4 (Middle of sample)	Layer 5 (bottom of sample)
0	37.0	35.7	35.4	34.5	35.7
13	34.3	33.3	33.0	32.5	32.9
26	32.7	32.0	31.6	31.3	31.3
39	31.5	31.1	30.7	30.5	30.3
52	30.7	30.4	30.0	29.9	29.5
65	30.0	29.7	29.4	29.4	28.9
78	29.3	29.2	28.8	28.8	28.3
91	28.7	28.6	28.2	28.2	27.7
104	28.0	27.8	27.5	27.5	27.0
118	25.1	24.7	24.4	24.5	24.2

#### 6.2.3.9.4 Objective 4: Thermal Loading Cycles

Thermal loading cyclic tests were carried out on this sample. Thermal cyclic loads tested within a 24 hour testing period on sample no. 11 at 50kPa were:

- 1) 8 hours heating cycles run for one day
- 2) 12 hours heating cycles run for three days.

A graph of results from the 12 hours heating and 12 hours cooling for a period of three days is presented in Figure 6.73.

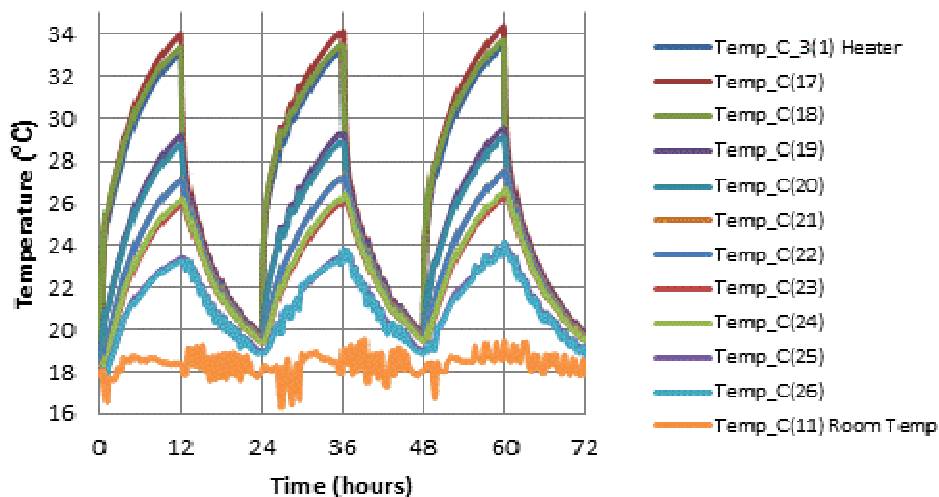


Figure 6.73: Temperature variation across sample during 12 hours heating and 12 hours cooling in sample no. 11 at 50kPa and 17.03W

The temperature values at fixed locations within the sample in equilibrium condition at the power input of 17.03W are presented in Table 6.34. Also shown in this table are the temperature values measured at points within the sample at the end of the thermal heating loads and at cooling after 24 hours for thermal loading cycles run at 8 and 12 hours on sample no. 11 at 50kPa.

Table 6.34: Peak temperature values at equilibrium condition and thermal cyclic loads in sample no. 11 at 50kPa

Probe label	Distance from Heater (mm)	Temp in thermal equilibrium after 37 hours (°C)	Temp after 8 hours thermal load (°C)	Temp after 16 hours cooling (°C)	Temp after 12 hours thermal load (°C)	Temp after 12 hours cooling (°C)
Probe C_3(1)	Heater	36.2	31.4	18.2	33.1	19.5
Probe 17	Outer edge top of heater	37.2	32.2	18.3	34.0	19.7
Probe 18	Outer edge bottom of heater	36.4	31.7	18.2	33.4	19.5
Probe 19	30	32.3	27.3	18.3	29.2	19.7
Probe 20	30	31.8	27.0	18.2	28.8	19.5
Probe 21	60	30.2	25.4	18.2	27.2	19.6
Probe 22	60	30.1	25.4	18.2	27.1	19.5
Probe 23	90	28.8	24.3	18.2	26.0	19.4
Probe 24	90	29.1	24.6	18.1	26.2	19.4
Probe 25	117	25.8	22.2	18.0	23.4	19.0
Probe 26	117	25.8	22.2	17.8	23.3	18.9
Probe 11	Controlled Room Temp	19.7	18.7	17.7	18.3	18.0

### 6.2.3.10 Testing Sample No. 11 at 100kPa

The tests carried out on the sample when consolidated to 100kPa include heating and cooling tests, thermal loading cycles and a temperature profile test across sample in equilibrium condition. These tests are described in terms of the objectives for carrying them out.

#### 6.2.3.10.1 Objective 1: Equilibrium Heating Duration

A heating test was undertaken to determine how long it took the soil sample to achieve thermal equilibrium or steady state conditions.

At a power input of 17.03W the sample achieved equilibrium conditions after approximately 48 hours of heating.



The temperature variations with time in the heater and within the sample during the steady state heating are presented in Figure 6.74 on page 204.

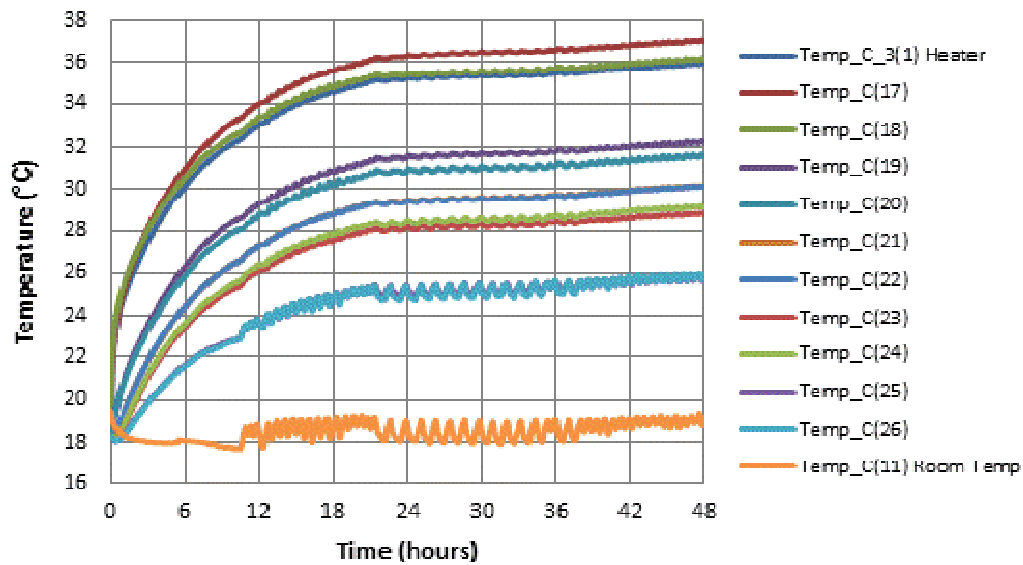


Figure 6.74: Variation of temperature with time across sample no. 11 at 100kPa in showing that thermal equilibrium was achieved after about 48 hours

### 6.2.3.10.2 Objective 2: Cooling Duration

To determine the duration of cooling, the sample was allowed to return to the controlled room temperature. Complete cooling of the sample from equilibrium heating condition to controlled room temperature lasted approximately 24 hours as shown in Figure 6.75.

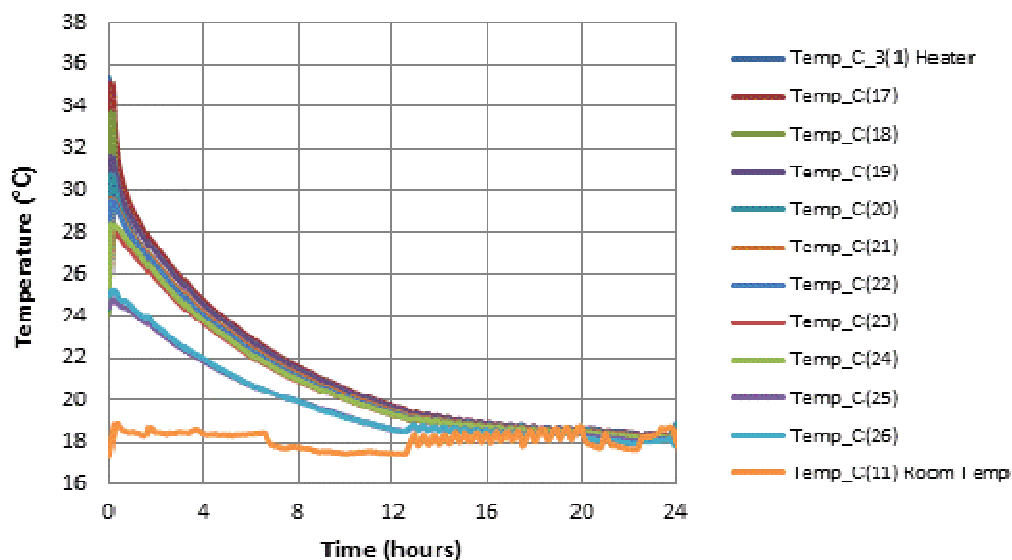


Figure 6.75: Cooling curves for sample no. 11 at 100kPa showing the time to return to room temperature

### 6.2.3.10.3 Objective 3: Temperature Variations across Sample

The objective of this test was to obtain the temperature variations within the sample when in thermal equilibrium. The graph in Figure 6.76 shows results from this test.

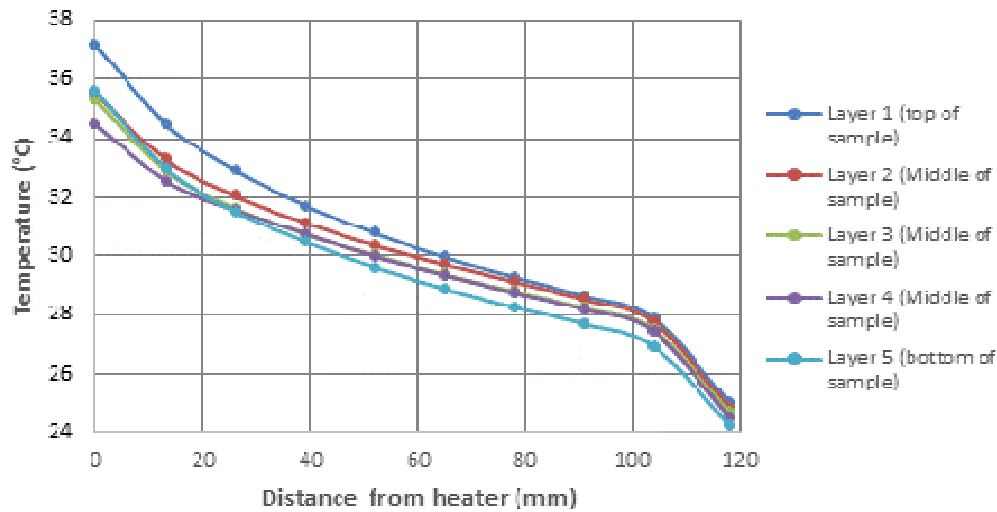


Figure 6.76: Temperature variations across sample from heater to edge of test chamber and from top to bottom of sample at end of test on sample no. 11 at 100kPa

The temperature values measured at specific locations within the sample during the temperature profile test carried out to investigate temperature variations across the sample are presented in Table 6.35

Table 6.35: Table showing temperature variation values in sample no.11 at 100kPa

Distance from heater (mm)	Layer 1 (top of sample)	Layer 2 (Middle of sample)	Layer 3 (Middle of sample)	Layer 4 (Middle of sample)	Layer 5 (bottom of sample)
0	37.2	35.5	35.3	34.5	35.6
13	34.5	33.3	32.9	32.5	33.0
26	32.9	32.0	31.6	31.6	31.5
39	31.7	31.1	30.7	30.8	30.5
52	30.8	30.3	30.0	30.0	29.6
65	29.9	29.7	29.4	29.3	28.9
78	29.3	29.1	28.8	28.7	28.3
91	28.6	28.5	28.2	28.2	27.7
104	27.9	27.7	27.5	27.4	26.9
118	25.0	24.8	24.6	24.5	24.2

### 6.2.3.10.4 Objective 4: Thermal Loading Cycles

Thermal loading cyclic tests were carried out on this sample. Thermal cyclic loads tested within a 24 hour testing period on sample no. 11 at 100kPa were:

- 1) 8 hours heating cycles run for two days

2) 12 hours heating cycles run for three days.

A graph of results from the 8 hours heating and 16 hours cooling for a period of two days is presented in Figure 6.77.

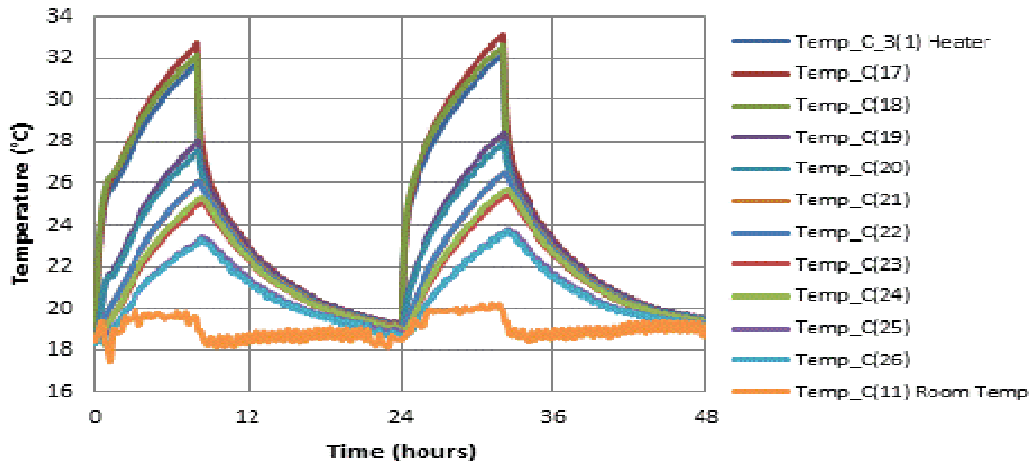


Figure 6.77: Temperature variation across sample during 8 hours heating and 16 hours cooling in sample no. 11 at 100kPa and 17.03W

The temperature values at fixed locations within the sample in equilibrium condition at the power input of 17.03W are presented in Table 6.36. Also shown in this table are the temperature values measured at points within the sample at the end of the thermal heating loads and at cooling after 24 hours for thermal loading cycles run at 8 and 12 hours on sample no. 11 at 100kPa.

Table 6.36: Peak temperature values at equilibrium condition and thermal cyclic loads in sample no. 11 at 100kPa

Probe label	Distance from Heater (mm)	Temp in thermal equilibrium after 48 hours (°C)	Temp after 8 hours thermal load (°C)	Temp after 16 hours cooling (°C)	Temp after 12 hours thermal load (°C)	Temp after 12 hours cooling (°C)
Probe C_3(1)	Heater	36.0	31.8	19.1	34.3	20.6
Probe 17	Outer edge top of heater	37.1	32.7	19.2	35.3	20.8
Probe 18	Outer edge bottom of heater	36.2	32.2	19.1	34.6	20.6
Probe 19	30	32.2	28.0	19.2	30.5	20.7
Probe 20	30	31.6	27.5	19.1	30.0	20.6
Probe 21	60	30.2	26.0	19.1	28.5	20.6
Probe 22	60	30.1	26.0	19.0	28.5	20.6
Probe 23	90	28.8	24.9	19.0	27.3	20.5
Probe 24	90	29.1	25.2	19.0	27.7	20.5
Probe 25	117	25.9	23.2	18.9	25.4	20.2
Probe 26	117	25.9	23.1	18.7	25.3	20.1
Probe 11	Controlled Room Temp	19.1	19.4	18.5	20.2	19.2

## 6.2.4 Tests carried out on Sand

After carrying out thermal tests on samples of kaolin and combinations of kaolin and sand, also tested, were dry and saturated sand samples to investigate changes that may occur due to difference in soil type.

Sample number 12 was dry sand while sample number 13 saturated sand. These samples were tested and described according to the sample numbers as follows.

### 6.2.4.1 Sample No. 12 (Tests carried out on Dry Sand at 25kPa)

Sample no. 12 which comprised of 1 part of C grain size sand to 2 parts of D grain size sand was carefully poured into the test rig to eliminate air before commencing a series of thermal tests carried out at a pressure of 25kPa. The objectives of the tests carried out on sample no. 12 were in line with those of previous samples listed in section 6.2.1., except for the last objective of determination of shear strength and water content relative to distance from the heater, which is not applicable to this sample due to its non-cohesive nature.

The arrangement of the thermocouples within the test chamber for this test is shown in Figure 6.78.

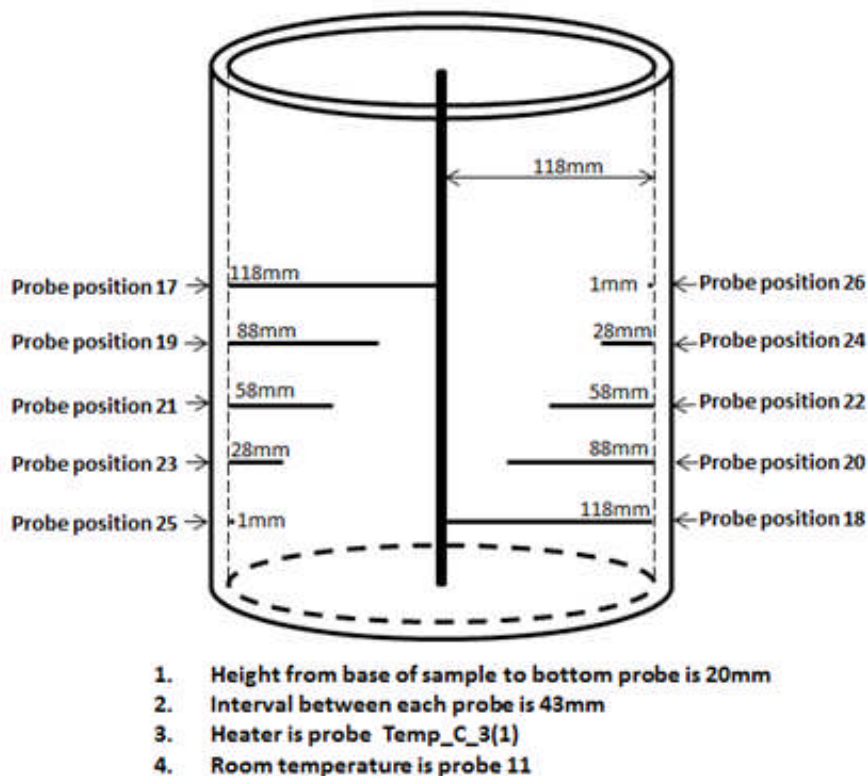


Figure 6.78: Layout of thermocouples within test chamber for tests carried out on sample no. 12

### 6.2.4.1.1 Objective 1: Equilibrium Heating Duration

A heating test was undertaken to determine how long it took the soil sample to achieve thermal equilibrium or steady state conditions. An initial power input of 17.03W was used and the sample heated up to very high temperatures and was discontinued. The power input was adjusted until a suitable temperature range was attained at an input of 4.23W. The sample achieved thermal equilibrium after approximately 24 hours of heating as shown by the temperature-time graph presented in Figure 6.79.

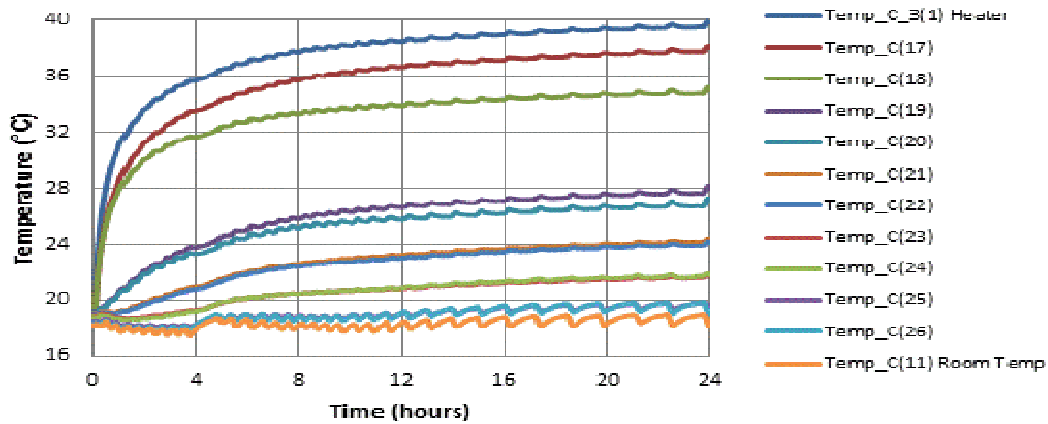


Figure 6.79: Variation of temperature with time in sample no. 12 at 25kPa showing that thermal equilibrium was achieved after about 24 hours

### 6.2.4.1.2 Objective 2: Cooling Duration

To determine the duration of cooling, the power supply to the heater was disconnected and the sample was allowed to return to the controlled room temperature. Complete cooling of the sample from thermal equilibrium to controlled room temperature lasted approximately 18 hours as shown in Figure 6.80.

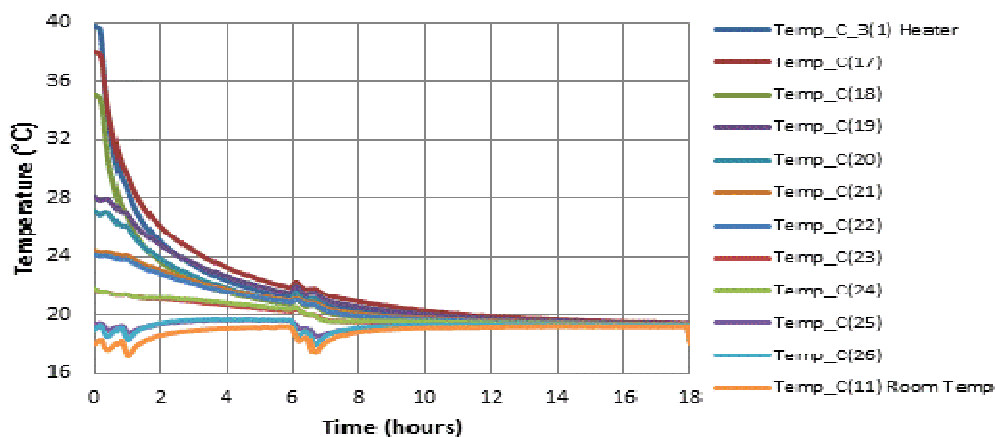


Figure 6.80: Cooling curves for sample no. 12 at 25kPa showing time to return to room temperature

### 6.2.4.1.3 Objective 3: Temperature Variations across Sample

The objective of this test was to obtain the temperature variations within the sample when in thermal equilibrium. The graph in Figure 6.83 shows results from this test.

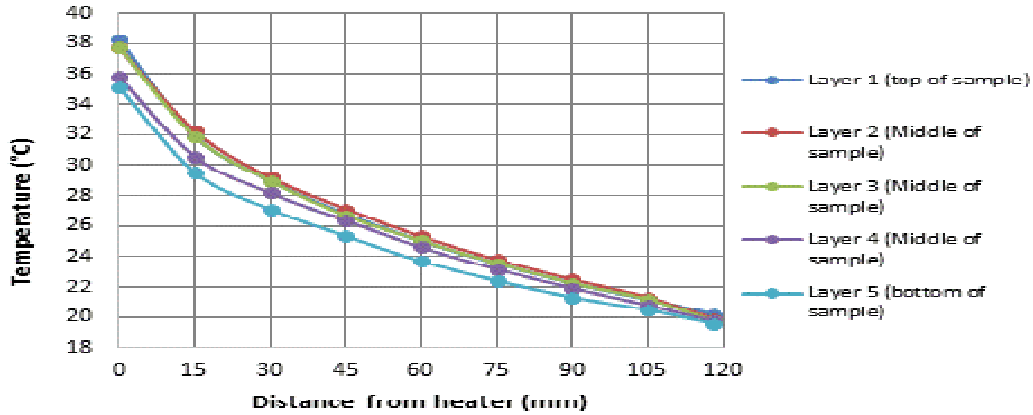


Figure 6.81: Temperature variations across sample from heater to edge of test chamber and from top to bottom of sample at end of test on sample no. 12 at 25kPa

The temperature values measured at specific locations within the sample during the temperature profile test carried out to investigate temperature variations across the sample are presented in Table 6.37.

Table 6.37: Table showing temperature variation values in sample no.12 at 25kPa

Distance from heater (mm)	Layer 1 (top of sample)	Layer 2 (Middle of sample)	Layer 3 (Middle of sample)	Layer 4 (Middle of sample)	Layer 5 (bottom of sample)
0	38.3	37.8	37.8	35.8	35.1
15	31.9	32.3	31.9	30.6	29.5
30	29.0	29.2	29.0	28.2	27.1
45	26.8	27.1	26.7	26.4	25.4
60	25.0	25.3	25.0	24.6	23.7
75	23.5	23.8	23.6	23.2	22.4
90	22.3	22.5	22.3	21.9	21.3
105	21.2	21.3	21.2	20.8	20.5
118	20.2	19.9	19.8	19.7	19.6

### 6.2.4.1.4 Objective 4: Thermal Loading Cycles

Thermal loading cycles tests were investigated on this sample. Thermal cycles investigated within a 24 hour testing period on sample no. 12 at 25kPa were:

- 1) 4 hours heating cycles run for two days
- 2) 8 hours heating cycles run for three days
- 3) 12 hours heating cycles run for three days

A chart showing the 8 hours heating and 16 hours cooling for a period of two days is presented in Figure 6.82.

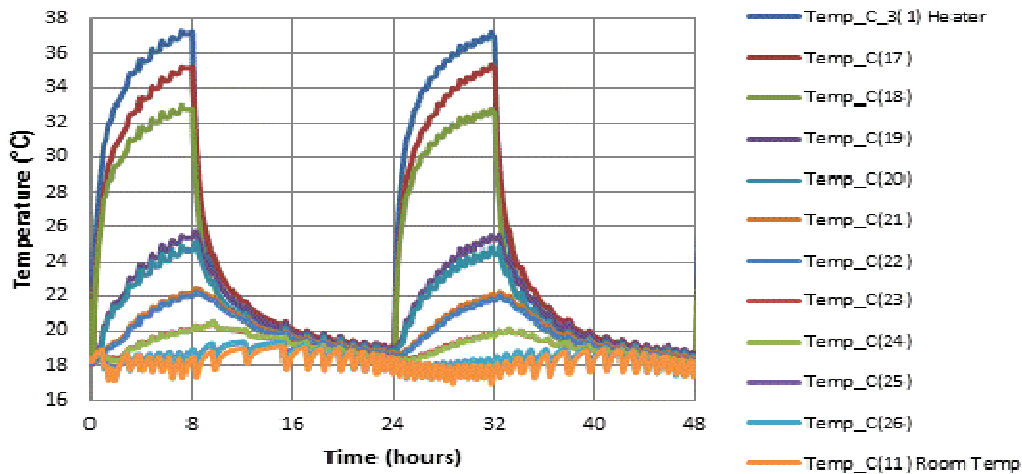


Figure 6.82: Temperature variation across sample during thermal loading cycles of 8 hours heating and 16 hours cooling in sample no. 12 at 25kPa

The temperature values at fixed locations within the sample in equilibrium condition at the power input of 4.23W are presented in Table 6.38. Also shown in this table are the temperature values measured at points within the sample at the end of the thermal heating loads and at cooling after 24 hours for thermal loading cycles run at 4, 8 and 12 hours on sample no. 12 at 25kPa.

Table 6.38: Peak temperature values at equilibrium condition and thermal cyclic loads in sample no. 12 at 25kPa

Probe label	Distance from Heater (mm)	Temp in thermal equilibrium after 24 hours (°C)	Temp after 4 hours thermal load (°C)	Temp after 20 hours cooling (°C)	Temp after 8 hours thermal load (°C)	Temp after 16 hours cooling (°C)	Temp after 12 hours thermal load (°C)	Temp after 12 hours cooling (°C)
Probe C_3(1)	Heater	39.9	35.2	19.5	37.2	18.8	37.9	19.4
Probe 17	Outer edge top of heater	38.2	33.1	19.2	35.2	19.1	36.0	19.6
Probe 18	Outer edge bottom of heater	35.2	31.2	19.1	32.9	18.6	33.5	19.3
Probe 19	30	28.2	23.4	19.0	25.4	19.0	26.2	19.5
Probe 20	30	27.3	22.9	18.9	24.7	18.8	25.4	19.3
Probe 21	60	24.4	20.4	18.8	22.2	18.7	23.0	19.4
Probe 22	60	24.2	20.2	18.7	22.0	18.6	22.8	19.3
Probe 23	90	21.8	18.8	18.6	20.2	18.5	20.8	19.2
Probe 24	90	21.9	18.6	18.5	20.1	18.4	20.9	19.3
Probe 25	117	19.6	17.4	18.0	18.9	18.0	19.4	19.2
Probe 26	117	19.2	17.2	17.5	18.9	17.7	19.4	19.2
Probe 11	Controlled Room Temp	18.3	16.8	17.4	18.5	17.6	18.7	19.1

### 6.2.4.2 Sample No. 13 (Tests carried out on Saturated Sand at 25kPa)

Sample no. 13 which is a mixture of 1 part of C grain size sand to 2 parts of D grain size sand was saturated before carrying out thermal tests at a pressure of 25kPa. The objectives of the tests carried out on sample no. 13 were in line with those of previous samples listed in section 6.2.1.

The arrangement of the thermocouples within the test chamber is shown in Figure 6.83.

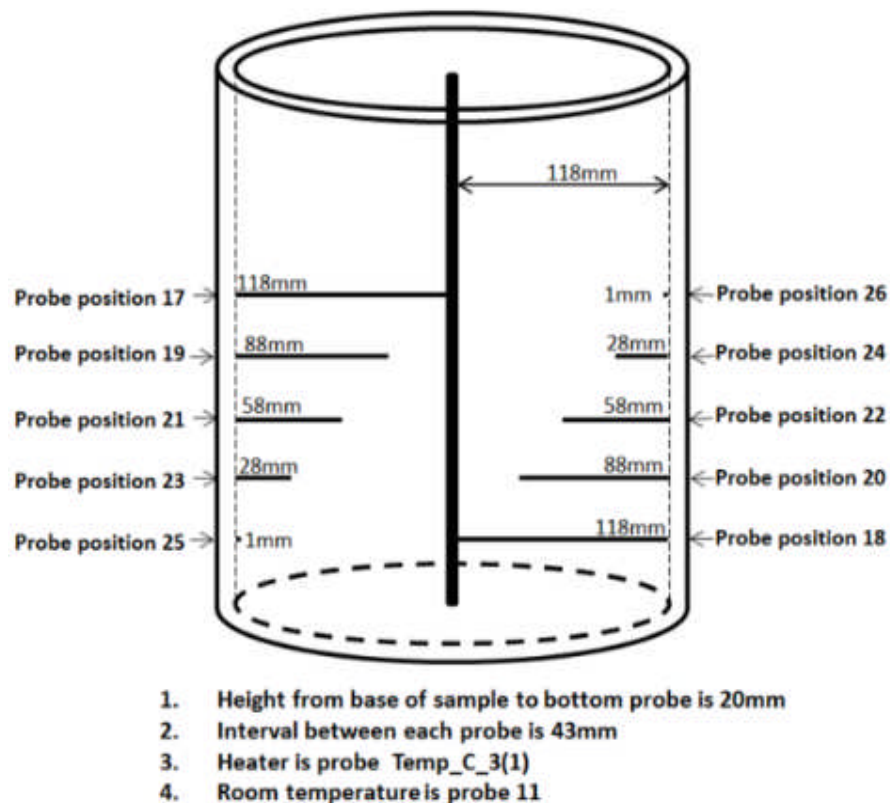


Figure 6.83: Layout of thermocouples within test chamber for tests carried out on sample no13

#### 6.2.4.2.1 Objective 1: Equilibrium Heating Duration

Several heating tests were undertaken to determine how long it took the soil sample to achieve thermal equilibrium or steady state conditions. An initial power input of 17.03W was found to be insufficient in raising the sample to the expected temperature range. The power input was adjusted until a suitable temperature range was attained at an input of 19.04W.

The sample achieved equilibrium conditions after approximately 24.5 hours of heating as shown by the temperature-time graph presented in Figure 6.84.



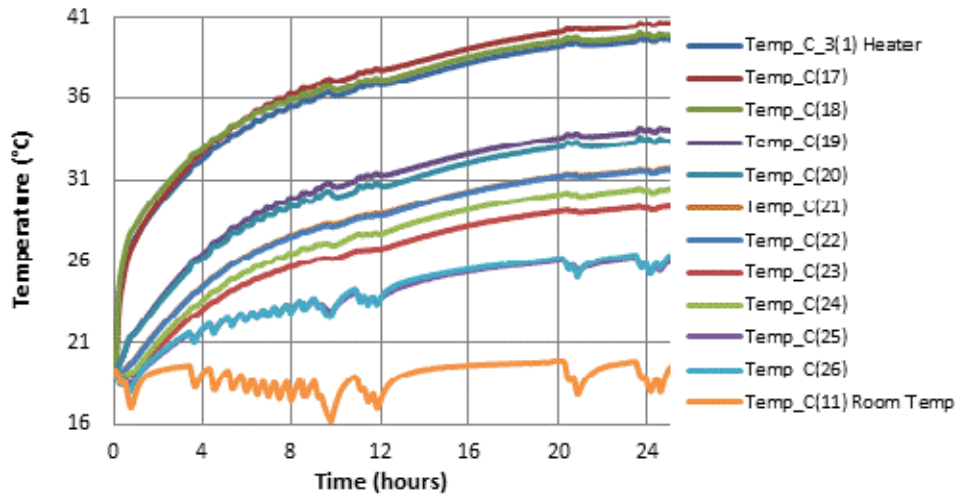


Figure 6.84: Variation of temperature with time in sample no. 13 at 25kPa showing that thermal equilibrium was achieved after about 24.5 hours

#### 6.2.4.2.2 Objective 2: Cooling Duration

To determine the duration of cooling, the power supply to the heater was disconnected and the sample was allowed to return to the controlled room temperature. Complete cooling of the sample from thermal equilibrium to controlled room temperature lasted approximately 22 hours as shown in Figure 6.85.

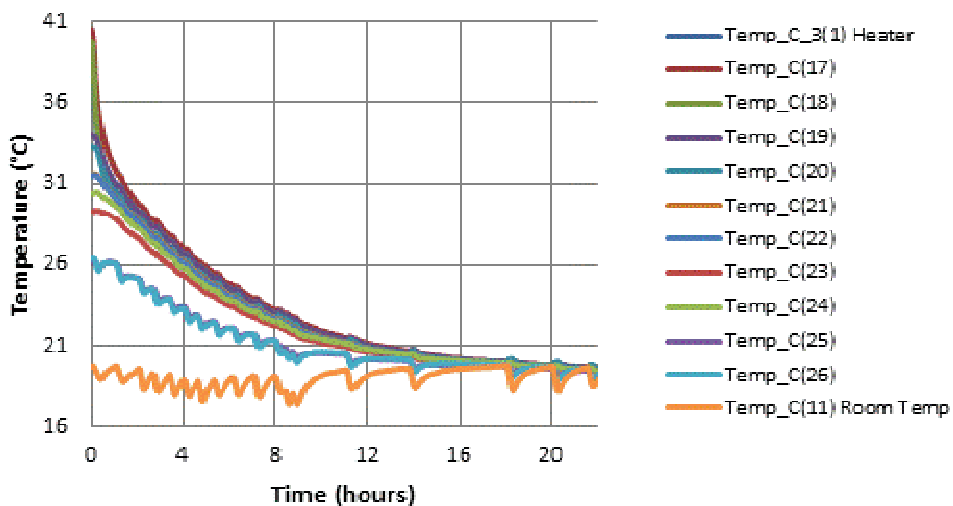


Figure 6.85: Cooling curves for sample no. 13 at 25kPa showing time to return to room temperature

#### 6.2.4.2.3 Objective 3: Temperature Variations across Sample

The objective of this test was to obtain the temperature variations within the sample when in thermal equilibrium. The graph in Figure 6.86 shows results from this test.

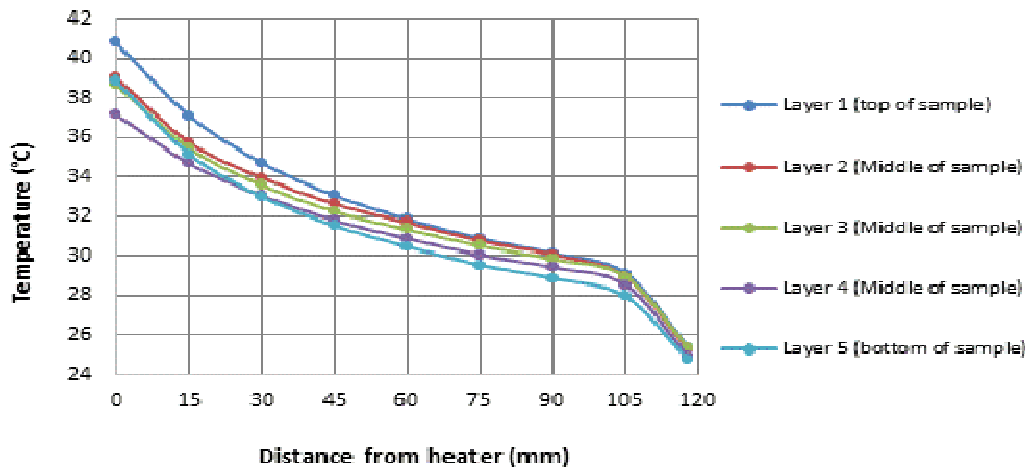


Figure 6.86: Temperature variations across sample from heater to edge of test chamber and from top to bottom of sample at end of test on sample no. 13 at 25kPa

The temperature values measured at specific locations within the sample during the temperature profile test carried out to investigate temperature variations across the sample are presented in Table 6.39.

Table 6.39: Table showing temperature variation values in sample no.13 at 25kPa

Distance from heater (mm)	Layer 1 (top of sample)	Layer 2 (Middle of sample)	Layer 3 (Middle of sample)	Layer 4 (Middle of sample)	Layer 5 (bottom of sample)
0	40.8	39.0	38.7	37.2	38.9
15	37.1	35.8	35.5	34.7	35.2
30	34.7	34.0	33.6	33.1	33.0
45	33.1	32.6	32.3	31.8	31.6
60	31.9	31.7	31.4	30.9	30.5
75	30.9	30.8	30.5	30.1	29.6
90	30.2	30.1	29.8	29.4	28.9
105	29.1	29.0	29.0	28.5	28.0
118	25.4	25.3	25.3	24.9	24.7

The tests carried out on both the dry and saturated sand samples lasted for shorter durations compared to the tests carried out on the other samples because they took less time to achieve thermal equilibrium and to cool back to the controlled room temperature.

#### 6.2.4.2.4 Objective 4: Thermal Loading Cycles

Thermal loading cycles were investigated on this sample. Thermal loading cycles investigated within a 24 hour testing period on sample no. 13 at 25kPa were:

- 1) 8 hours heating cycles run for three days
- 2) 12 hours heating cycles run for three days

The chart showing 8 hours heating and 16 hours cooling for one day is presented in Figure 6.87.

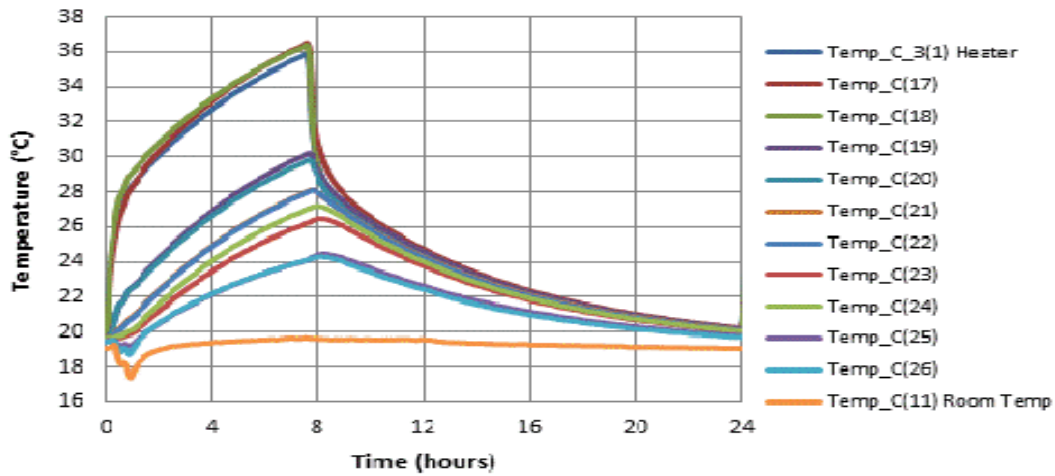


Figure 6.87: Temperature variation across sample during thermal loading cycles of 12 hours heating and 12 hours cooling in sample no. 13 at 25kPa

The temperature values at fixed locations within the sample when in thermal equilibrium at the power input of 19.04W are presented in Table 6.40. Also shown in this table are the temperature values measured at points within the sample at the end of the thermal heating loads and at cooling after 24 hours for thermal loading cycles run at 8 and 12 hours on sample no. 13 at 25kPa.

Table 6.40: Peak temperature values at equilibrium condition and thermal cyclic loads in sample no. 13 at 25kPa

thermal data	Distance from Heater (mm)	Temp in thermal equilibrium after 24.5 hours (°C)	Temp after 8 hours thermal load (°C)	Temp after 16 hours cooling (°C)	Temp after 12 hours thermal load (°C)	Temp after 12 hours cooling (°C)
Probe C_3(1)	Heater	39.6	29.6	20.1	30.6	20.8
Probe 17	Outer edge top of heater	40.6	30.8	20.2	32.2	21.0
Probe 18	Outer edge bottom of heater	39.9	29.5	20.1	30.4	20.7
Probe 19	30	34.1	29.2	20.2	30.3	20.9
Probe 20	30	33.5	28.8	20.1	29.7	20.8
Probe 21	60	31.6	27.9	20.1	28.8	20.7
Probe 22	60	31.5	28.0	20.1	28.7	20.6
Probe 23	90	29.3	26.5	20.0	27.0	20.4
Probe 24	90	30.4	27.2	20.0	27.8	20.5
Probe 25	117	25.5	24.4	19.8	24.2	19.6
Probe 26	117	25.7	24.3	19.7	24.3	19.5
Probe 11	Controlled Room Temp	18.6	19.6	19.1	18.1	17.9

### **6.3 Conclusion**

The tests described in this chapter were successfully carried out in the modified rig without encountering any of the problems identified with the initial rig design. The spade terminals attached to the new heater design worked as expected without any damage. Therefore the modification to the rig, its parts and the heater proved to be a lasting and more reliable solution to the problems encountered at the beginning of the tests as was the goal.

Tests were carried out on three groups of samples consisting of kaolin, combinations of kaolin and sand, and saturated and dry sand.

The results obtained from the tests carried out were described briefly in this chapter. Detailed analyses and discussion of results will be carried out in Chapter 7.

## Chapter 7 Discussion

### 7.1 Introduction

Chapters 3 to 6 described how a test rig was developed and utilized in undertaking experiments based on a linear heat source to model an energy pile. This was achieved through the use of heat transfer equations from theory and the assumptions they were based on.

This Chapter deals with the interpretation and discussion of the results of the tests undertaken to show how soil water content, temperature, pressure, the power input to the system and thermal loading cycles affected the behaviour and performance of the simulated energy pile, and the validation of the results against theory.

### 7.2 Errors Associated with the Experimental Process

Random and systematic errors are normally associated with measurement procedures (Lyons, 1991). Errors were likely to have occurred during the process of sample preparation and testing, from the equipment used such as cartridge heater, data logger, thermocouples, power supply unit, pressure unit, as well as from human errors during sample preparation, reading of data, setting up and carrying out of the tests. The manufacturer's notes on error margins for each equipment were taken into consideration during testing and data compilation (Taylor, 1997).

The errors could be grouped and discussed in relation to soil type, water content determination, temperature measurements, consolidation pressure and time or duration of test. In this section, the possible errors to have occurred are presented and discussed according to the groups of variables, as well the measures that were taken to reduce their impact on the final results.

#### 7.2.1 Sample Preparation

Errors associated with the soil type could arise from the sample preparation process which consisted of:

- 1) The weighing of soil samples and distilled water could lead to measurement errors within the margin of  $\pm 0.1$  gram.
- 2) Sample loss during mixing process due to spills. This was minimal due to researcher taking extreme care during the mixing process and could be estimated in the region of 1g per kilogram of sample.

## 7.2.2 Water Content Determination

In order to ensure that the actual water content of a sample after the preparation was the same as estimated, freshly mixed samples were collected and their water content determined. Measurement errors within the range of  $\pm 0.1$  gram could have occurred during the water content determination. In the calculation of water content values an error of  $\pm 1\%$  was taken into consideration.

For the water content determination tests carried out on the sample after the thermal tests, 60 to 80 samples were collected from the main sample in the test rig to ensure an average representation, thus reducing the overall impact of errors on the results obtained.

## 7.2.3 Temperature Measurements

Errors associated with temperature measurements arose mainly from the equipment used which included: the cartridge heater, thermocouples, data-logger and power supply unit. They operate within error margins which are presented in Table 7.1.

Table 7.1: Error margins for equipment used

Equipment	Accuracy
Cartridge heater	Measured by data-logger as a thermocouple
Data-logger	$\pm 0.06\%$ of reading + offset For thermocouple measurements $\pm 0.3^\circ\text{C}$
Power supply unit	$\pm 0.1\text{V}$ (Voltage 0.1% of reading + 1 digit) $\pm 0.01\text{A}$ (Current 0.3% of reading + 1 digit)
Thermocouples	Measured and recorded by data-logger in $^\circ\text{C}$

The room temperature was controlled and operated within a temperature range of  $18^\circ\text{C} \pm 1.5^\circ\text{C}$ .

Thermocouples which are formed by joining two dissimilar metals at the tip or junction, produce a voltage based on temperature difference. The k-type thermocouple was used to measure the temperature, and typically consists of alumel and chromel wires. The thermocouples were fitted into their connectors which were wired and plugged into a data-logger that was programmed to convert the resistance into temperature, which was recorded and stored for retrieval.

Figure 7.1 on page 218, is a plot of temperature with time for measurements taken from two sides of a sample as backup against data loss and error impact.

Figure 7.2 expresses the relationship between the temperature measurements. The probe positions 5 and 6 used in the plot are shown in Figure 7.3.

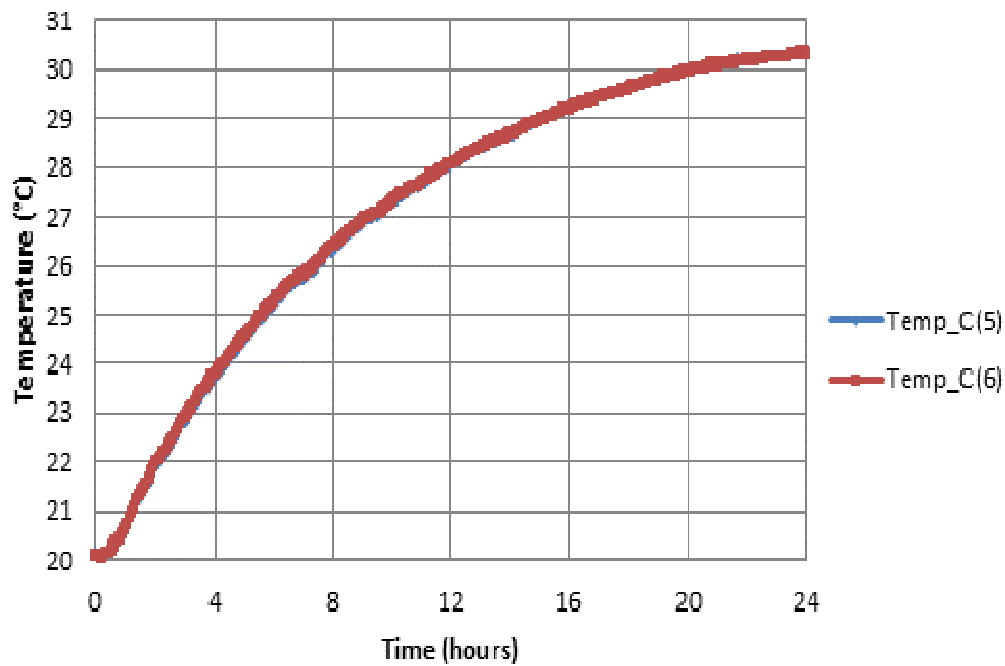


Figure 7.1: Variation of temperature with time from probes placed at two opposite sides of the test rig showing the similarity between the measurements

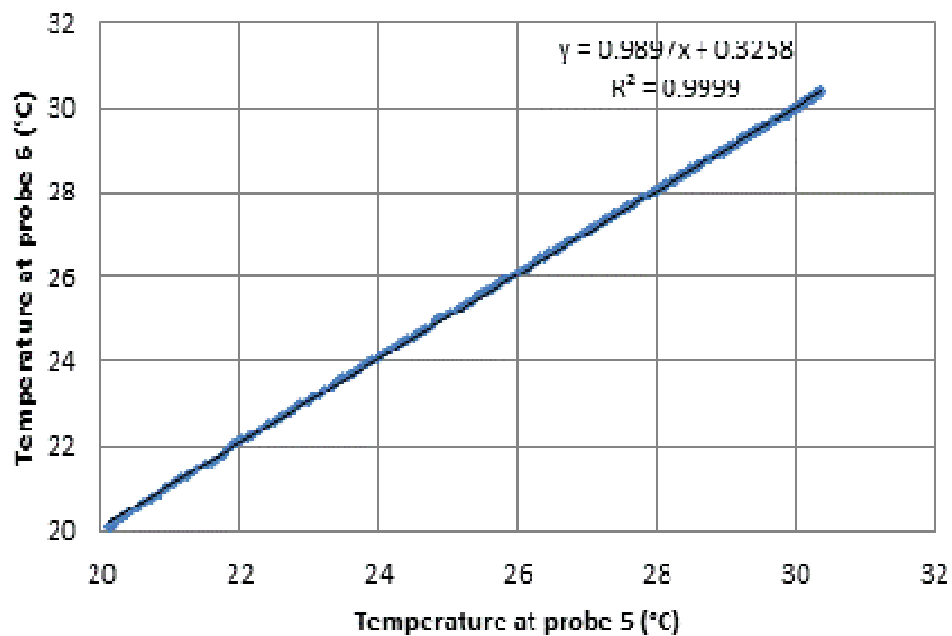


Figure 7.2: The fit of temperature measurements from opposite sides of the test rig

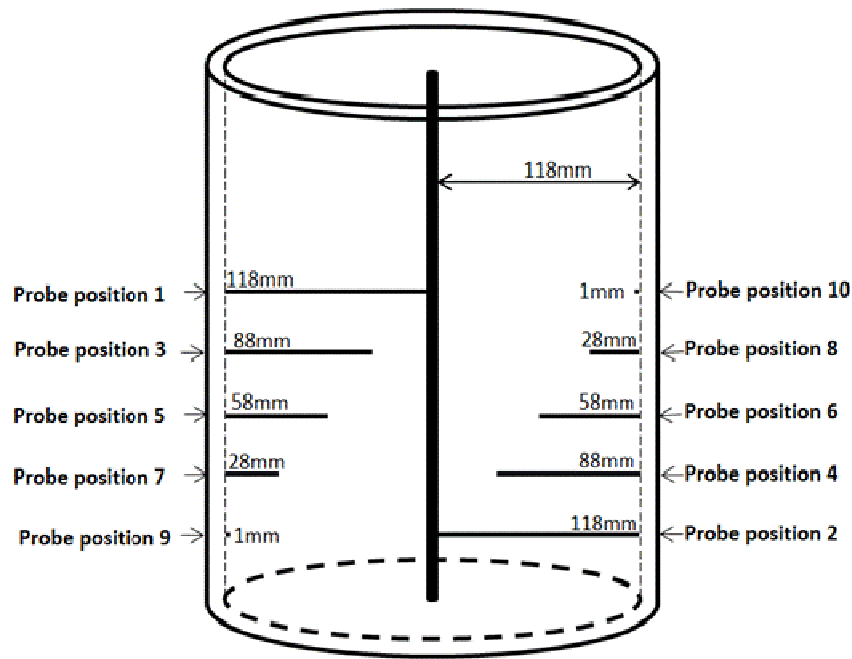


Figure 7.3: Test rig showing probe positions

#### 7.2.4 Consolidation Pressure

Errors associated with this group could occur from the power supply unit used in loading air pressure on the sample. The error margin for this is  $\pm 0.1\text{kPa}$ .

#### 7.2.5 Time / Duration of Test

Errors occurring due to time could stem from the timing device used in timing the duration of the test. A built in error margin of approximately  $\pm 5$ seconds was taken into consideration.

#### 7.2.6 Strength Tests

Just as in the case of the water content determination carried out at the end of the thermal tests, the in-situ strength tests were carried out at 60 to 80 locations per sample in the test rig to ensure accuracy. The blades of the vanes were carefully cleaned in between the tests to further limit errors. As noted in Chapter 3 section 4.3.5, a hand vane was used and the torque measurement from which the shear strength was calculated, was recorded. An error margin of  $\pm 1\text{kPa}$  was taken into consideration for the shear strength measurements.

#### 7.2.7 Impact of Errors on Results

Other instruments used included the dial gauge used in measuring the consolidation which had an error margin of  $\pm 0.1\text{mm}$ .



The measuring tape and metal metre rule used in measuring sample height and distances had an error margin of  $\pm 0.5\text{mm}$ .

Additional errors in measuring the temperature at the probe locations could also be due to temperature fluctuations in the heater. The impact of fluctuations on the results was considered low because they usually occurred for brief periods not long enough to reflect changes in the soil temperature at the time of measurement.

As all the experiments were carried out by only the researcher, human errors arising from measurements and taking of readings were likely to re-occur in all the tests and will therefore, be common to all the results.

### 7.3 Repeatability/Reproducibility of Tests

The impact of errors can be reduced by the repeatability of the tests (Bevington and Robinson, 1992; Lyons, 1991). The reproducibility of a test is “the ability of a researcher to duplicate the results of a prior study using the same materials as were used by the original investigator” (Goodman et al., 2016). To check repeatability during experiments with a view to observe the impact of errors, a four hour heating test was initially carried out on a kaolin sample and then a repeat test was conducted under the same conditions. Figure 7.4 shows a graph comparing the results of the two tests. Comparing both test results in Figure 7.5, a strong relationship is indicated by the fit of the regression line giving R-squared value of almost one, which thus confirms the repeatability of the tests.

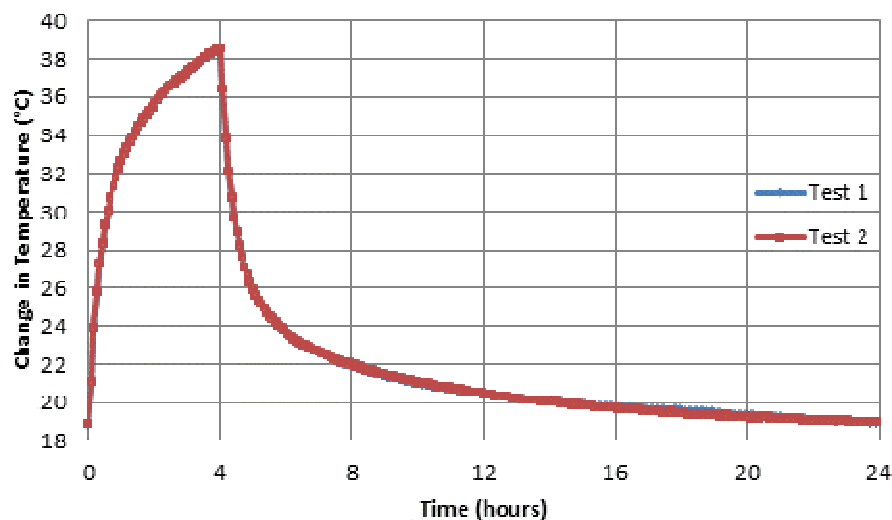


Figure 7.4: Comparison between two tests on a kaolin sample subjected to 4 hours of heating and 20 hours of cooling

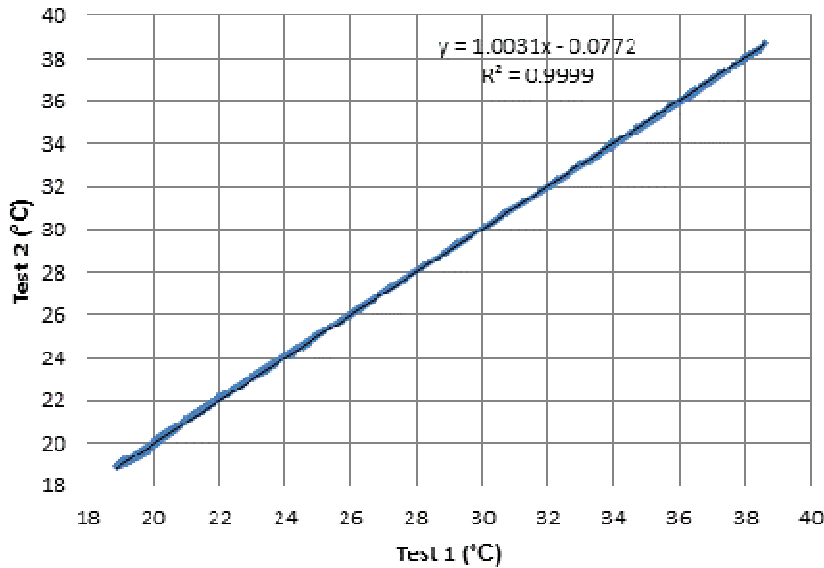


Figure 7.5: The fit of two tests carried out on a kaolin sample subjected to 4 hours of heating and 20 hours of cooling

## 7.4 Validation of Experiment Results against Theory

Before the discussion of the results obtained from tests carried out on prepared samples in the test rig, a brief recap of the principles behind the design of the experimental model designed to dissipate heat radially by conduction from a line source by optimising the radial distribution of temperature is given below.

The design principles and assumptions used in the experimental model were based on:

- 1) An axisymmetric problem similar to an installed energy pile was developed to simulate the ground element of heat transfer by conduction.
- 2) To ensure constant temperature boundaries and avoid external influence, the cell wall was designed to contain but not restrict heat flow, and the rig size was of sufficient diameter to control the experiment.
- 3) The top and bottom of the rig were insulated to try to ensure that heat flow was radial and could be monitored across the sample in order to record temperature changes and study the thermal behaviour of the soil
- 4) It was designed to be able to model elements of the pile at different depths to study thermal behaviour changes with depth.

The calculations used for purpose of this research involved the use of conduction heat transfer equations and were based on the following assumptions which were necessary for the model to be treated as a one-dimensional heat conduction case.

- 1) A single geological layer with constant properties
- 2) Fixed boundaries with constant temperatures at both the internal and external boundaries
- 3) Single cylindrical heat source

#### 7.4.1 Determination of Thermal Conductivity of Tested Samples

The results obtained during the experiments were validated against theory by calculating the actual thermal conductivity of each sample tested and comparing with accepted values in existing literature.

From data obtained during tests carried out to investigate the temperature variations in the samples in equilibrium condition, it was observed that although the heat dissipation took place in a mostly radial direction as was expected, there were slight axial temperature variations within the sample. The variations are shown in the temperature contour profile plot in Figure 7.6. This was taken into consideration during the determination of the thermal conductivity values of the samples and so the average values of the temperature measured radially across the sample and in four layers from the top to the bottom of the sample, were used to calculate the average thermal conductivity of the sample.

In a separate column are the thermal conductivity values obtained from calculations based on the temperature values recorded radially across the middle layer of the sample to compare with the average values in order to find out how much they differ from the average values.

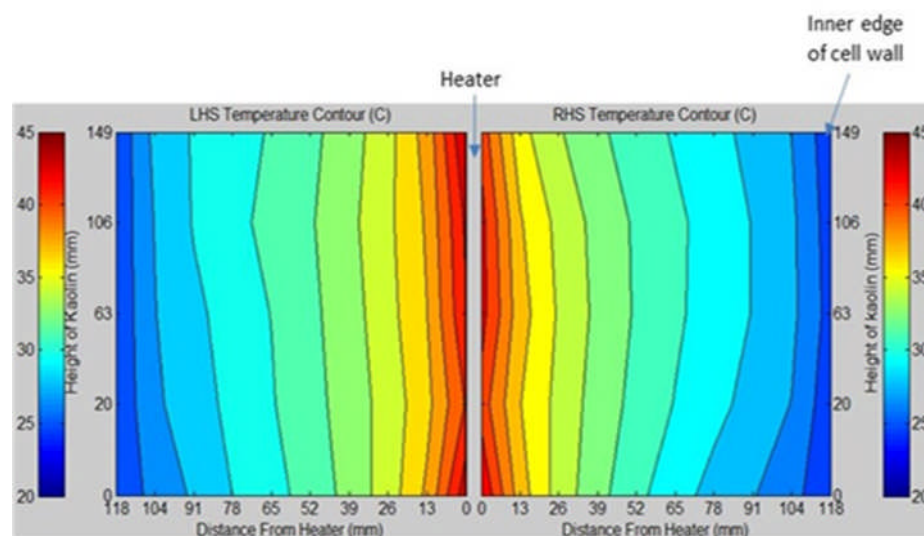


Figure 7.6: Temperature contour profile of sample in equilibrium condition showing both radial and axial variations

The temperature values across the middle layer were considered as this layer showed a more radial temperature distribution from across the sample. The temperature readings were obtained from the temperature test run while the sample was in steady state as shown in Figure 7.7. This procedure is described in Chapter 4 section 4.3.3.

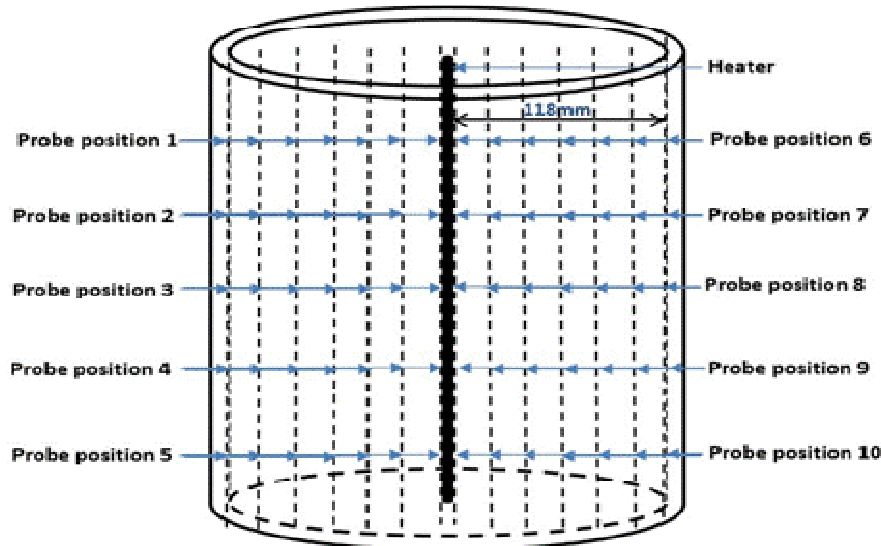


Figure 7.7: Temperature profile measurements of sample within the test chamber at specified locations from top to bottom and at uniform distances from the heater to the edge of the cell wall while sample is in steady state

The temperature readings in the sample at the edge of the cell wall were disregarded while calculating the thermal conductivity to avoid external influences on the result due to room temperature fluctuations or interference with the thermocouple.

Figure 7.8 shows the radial and axial temperature variations within the sample while Figure 7.9 shows the average temperature variations of the same sample.

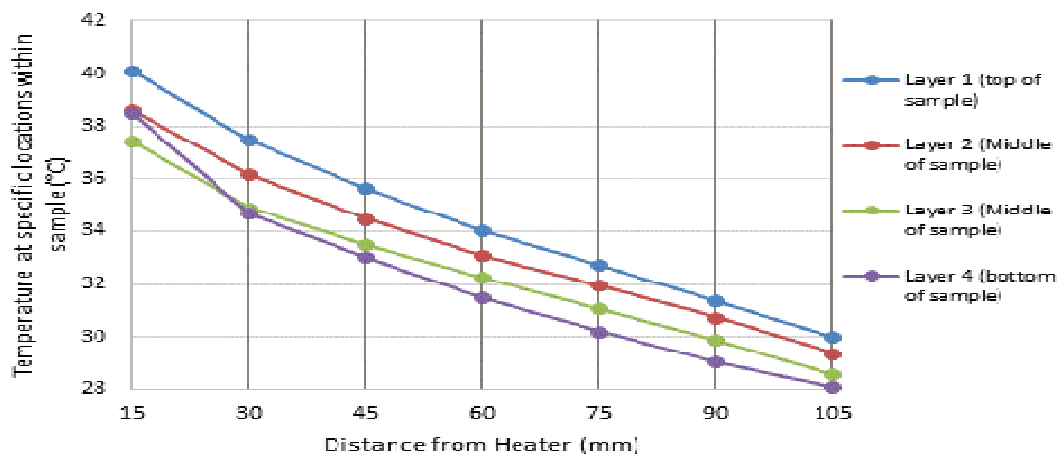


Figure 7.8: Radial and axial temperature variations within the sample in Fig 7.6

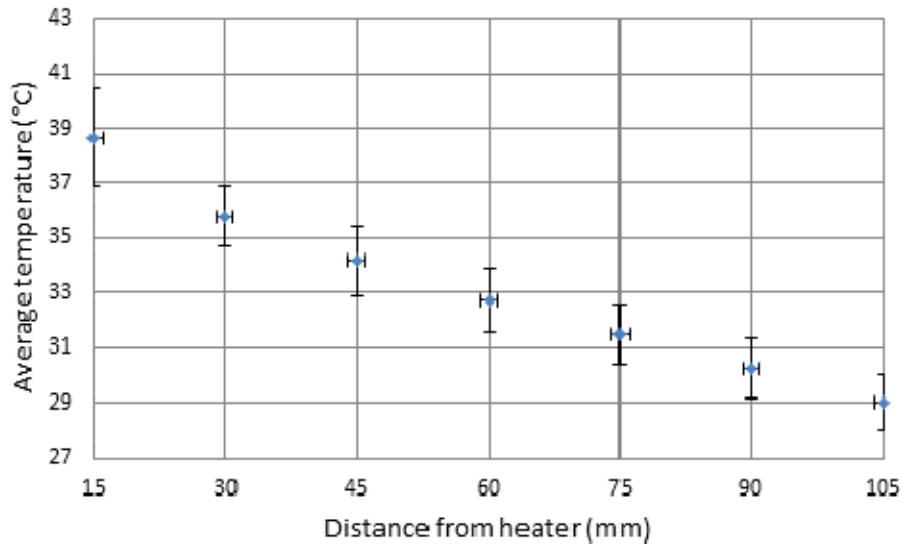


Figure 7.9: Range of average temperature measurements showing the variations from top to bottom of sample at each location and also showing that the average temperature reduces with distance from the heater, in the sample shown in Figure 7.6

The axial temperature variations may be influenced by the variations in water content within the sample due to consolidation which may allow the sample to be wetter towards the base. This is because there will be some transfer of the load to the walls of the cell. Figure 7.10 shows the variation of water content within the sample. The Figure shows the sample to be wetter at the bottom and towards the cell wall away from the heat source.

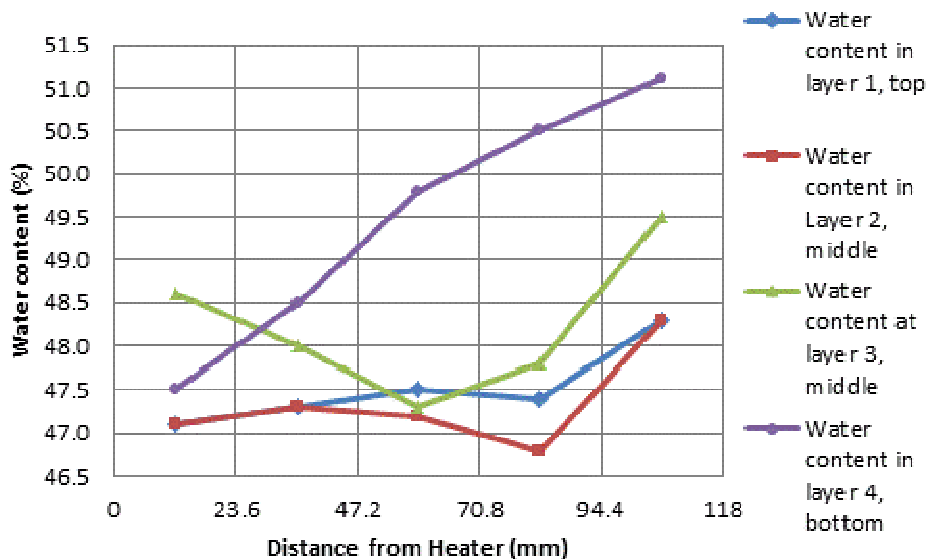


Figure 7.10: Water content variation from top to bottom and across sample in Figure 7.6, with respect to distance from heat source

The thermal conductivity values will vary within the sample due to the variation of water content within the sample, and for that reason, the thermal conductivity values for the samples at the top and bottom layers were also calculated for the purpose of comparison. The values are also shown in Table 7.2.

Using data obtained from the tests, Equation 7.1 was used in the determination of thermal conductivity values in the various samples tested while in steady state conditions. The results obtained are presented in Table 7.2.

$$Q = \frac{2\pi Lk\Delta T}{\ln(R_2/R_1)} \quad (7.1)$$

Table 7.2: Summary of calculated values of thermal conductivity for the samples tested

SN	SAMPLE TYPE	PRESSURE APPLIED (kPa)	WATER CONTENT BEFORE TEST (%)	WATER CONTENT AFTER TEST (%)	THERMAL COND. TOP LAYER (W/m.K)	THERMAL COND. MIDDLE LAYER (W/m.K)	THERMAL COND. BOTTOM LAYER (W/m.K)	AV. THERMAL COND. WHOLE SAMPLE (W/m.K)
1	KAOLIN	0	84.5	NA	1.58	1.56	1.48	1.57
2	KAOLIN	25	82	56.7	2.47	1.89	1.46	1.86
3	KAOLIN	100	82	48	2.31	2.58	2.24	2.41
4	KAOLIN	200	82	42	2.48	2.62	2.40	2.53
5	KAOLIN:SAND (75:25)	25	59	42.1	2.32	2.28	2.00	2.24
6	KAOLIN:SAND (75:25)	100	59	36.5	2.37	2.69	2.45	2.59
7	KAOLIN:SAND (50:50)	100	44.4	22.8	2.55	3.33	2.80	3.01
8	KAOLIN:SAND (25:75)	100	32.1	19.6	3.16	3.50	3.81	3.64
9	SAND	25	26	26	2.84	3.49	3.15	3.27
10	SAND	25	DRY	NA	0.45	0.46	0.54	0.48

The thermal conductivity values obtained for the kaolin samples under steady state conditions range from 1.46W/m.K to 2.62W/m.K and fall within the range of expected values from 0.9W/m.K to 2.93W/m.K for kaolin samples of varying levels of saturation Banks (2008); (Clarke et al., 2008; Abuel-Naga, H. et al., 2015b; Thomas and Rees, 2009).

Thermal conductivity values given for sand by (Clarke et al., 2008) range from 0.15W/m.K to 3.34W/m.K for fine to medium sand in dry and saturated conditions. The

values obtained from the experiments are 0.45-0.54W/m.K for dry sand and 2.84-3.49W/m.K for saturated sand. The values therefore, agree with those in the literature.

The various combinations of kaolin and sand samples gave thermal conductivity values ranging from 2.0W/m.K to 2.81W/m.K. The values fall within the expected range for kaolin and quartz (Hamdhan and Clarke, 2010; Yu, X.B. et al., 2016). This is a validation of the experiments.

From the values of thermal conductivity obtained and presented in Table 7.2, a relationship was observed between the thermal conductivity values and water content of the samples which is shown in Figure 7.11 for kaolin samples. The samples higher in water content showed lower thermal conductivity values. This was consistent for kaolin samples of water content ranging from 48-85% with thermal conductivity values of 2.41-1.57W/m.K. In the case of the kaolin sample with 42% water content, the thermal conductivity value reduced to 1.85W/m.K. The lower thermal conductivity values in the samples higher in water content is due to the much lower thermal conductivity values of water which is given as 0.57W/m.K (Thomas and Rees, 2009) and 0.6W/m.K (Abuel-Naga, H. et al., 2015b).

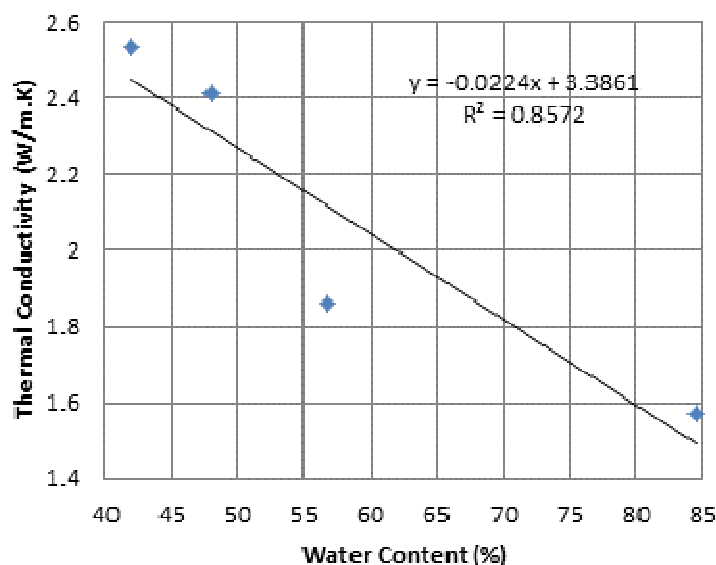


Figure 7.11: The variation of thermal conductivity with percentage water content in kaolin samples

The thermal conductivity value of the dry sand sample was much lower than that of the saturated sand. Quartz has a high thermal conductivity value of 7.8W/m.K (Abuel-Naga, H. et al., 2015b), 8.79 W/m.K (Thomas and Rees, 2009) while air has a very low thermal conductivity value of 0.024W/m.K (Banks, 2008). It follows therefore, that the presence of air in the dry sand is responsible for the low thermal conductivity value of 0.53W/m.K

obtained from the experiment because the majority of the heat flow would have been through the particle contacts; whereas in the saturated sand, heat would have flowed through the water as well.

It was observed that the average thermal conductivity values and those obtained based on layers at the top, middle and bottom of the sample were close in value and did not differ much as shown in Figure 7.12, suggesting that the loss of heat at the ends of the sample did not affect the results much.

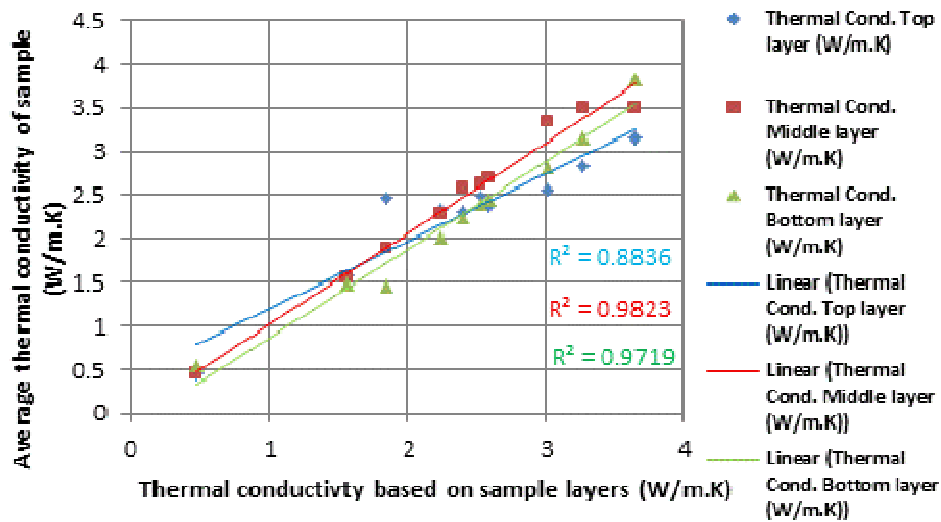


Figure 7.12: Comparing thermal conductivity values obtained from top, middle and bottom of sample with the average values.

## 7.4.2 Comparing Measured Temperature Distribution Within Sample With Values Predicted From Theory

The radial temperature variations across the different samples recorded while the samples were in thermal equilibrium, were compared against temperature variation values predicted from theory.

Thermal conductivity values determined from the samples were used in the prediction of the temperature distribution using Equation 1. The predicted values were plotted alongside the measured values in the graphs presented in Figures 7.13 to 7.22, where the red dotted lines represent the predicted values based on theory while the blue broken lines represent the measured values. Measured temperature values were plotted against the predicted temperature values.



It was observed from the graphs, that both the predicted temperatures and the measured temperatures have similar trends and show a strong relationship as indicated by the fit between them shown in the same Figures.

The differences between the predicted and the measured data groups could be due to the partially insulating behaviour of the wall of the test chamber as the predicted values are lower in temperature than the measured values for all the samples. It is noted that the measured values in all tests exceeded the predicted values even though there may have been some heat loss from the top and bottom of the sample.

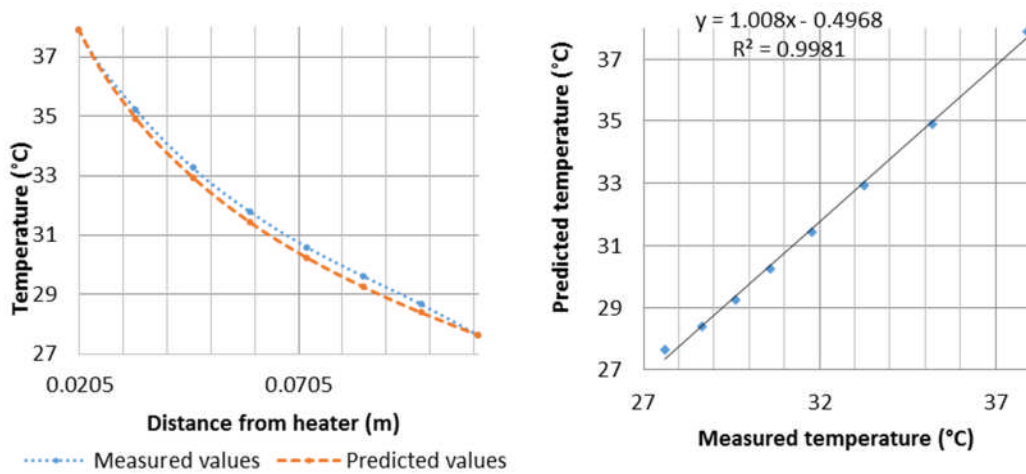


Figure 7.13: The fit of predicted and measured temperature distribution within kaolin sample with 84.5% water content, tested at 0kPa

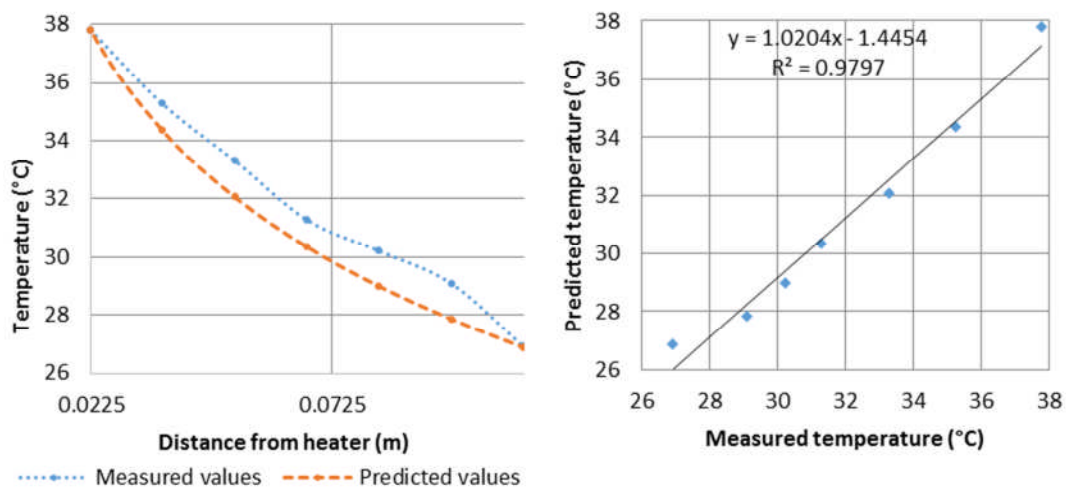


Figure 7.14: The fit of predicted and measured temperature distribution within kaolin sample tested at 25kPa; 56.7% water content

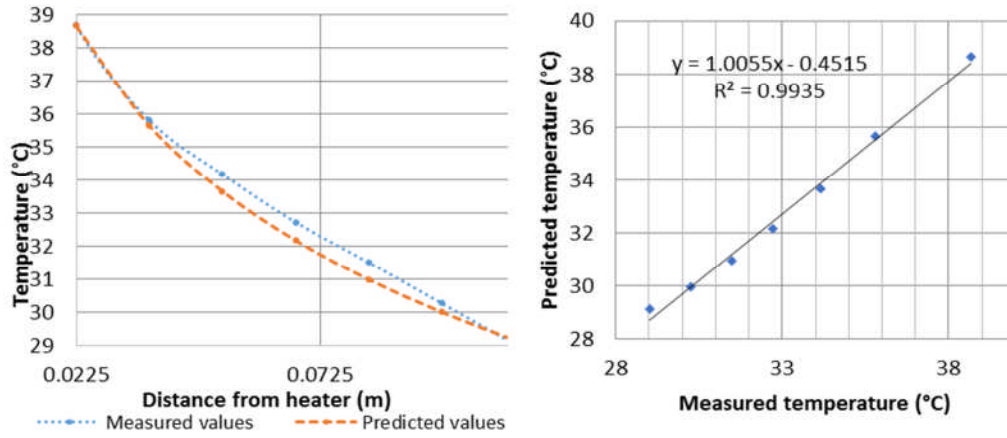


Figure 7.15: The fit of predicted and measured temperature distribution within kaolin sample tested at 100kPa and 48% water content

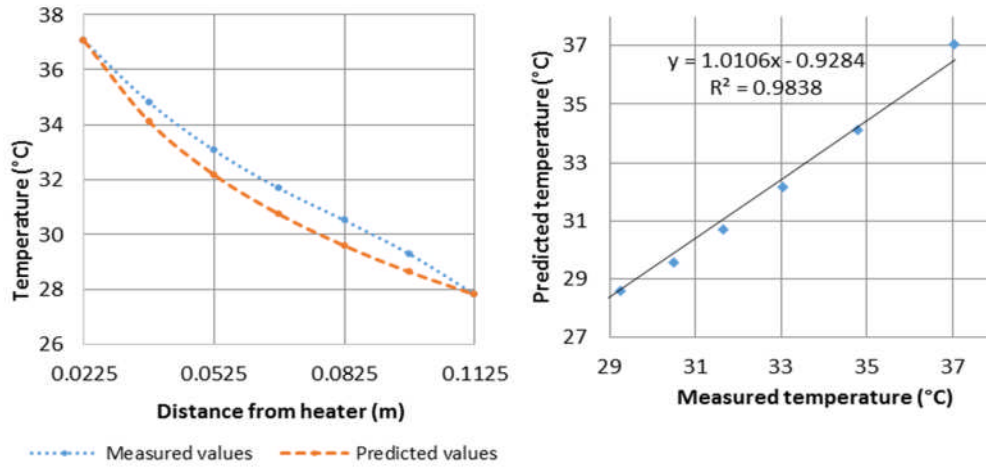


Figure 7.16: The fit of predicted and measured temperature distribution within kaolin sample tested at 200kPa; 42% water content

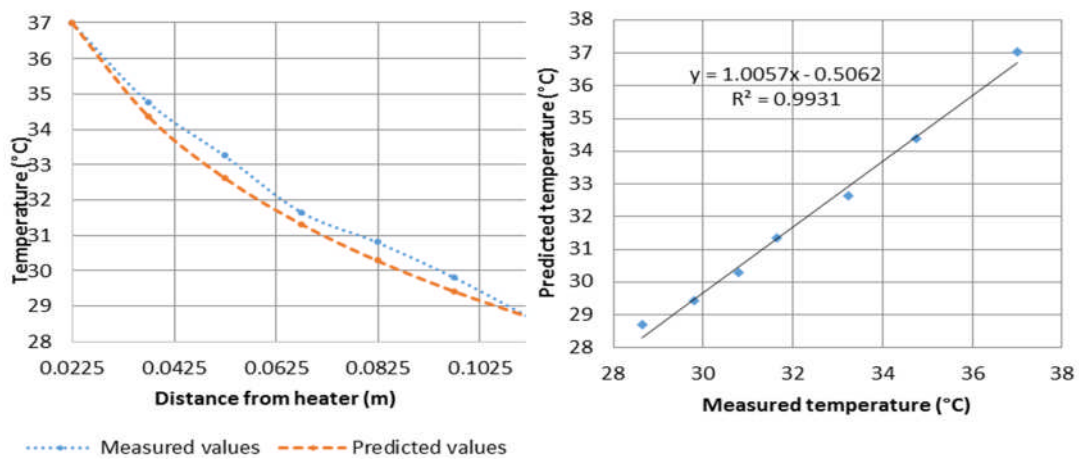


Figure 7.17: The fit of predicted and measured temperature distribution within 75:25 kaolin:sand samples tested at 25kPa; 42.1% water content

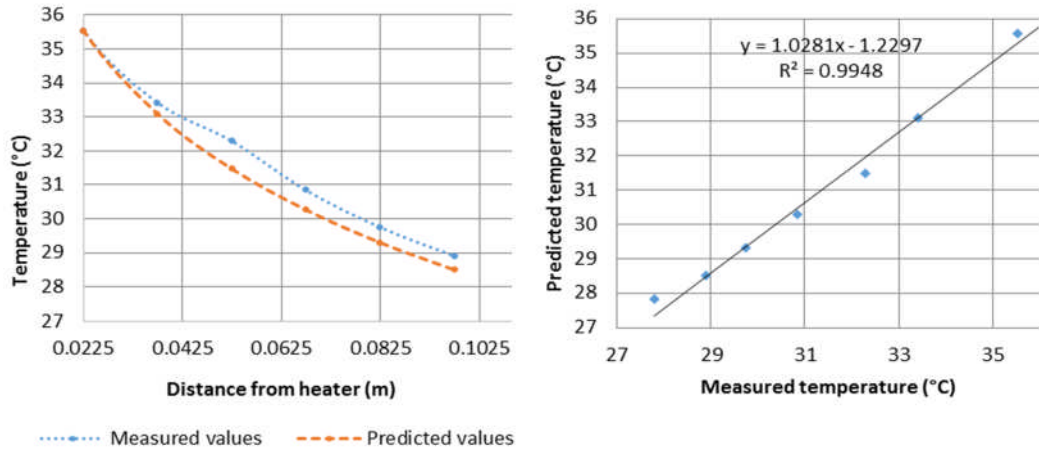


Figure 7.18: The fit of predicted and measured temperature distribution within 75:25 kaolin:sand sample tested at 100kPa; 36.5% water content

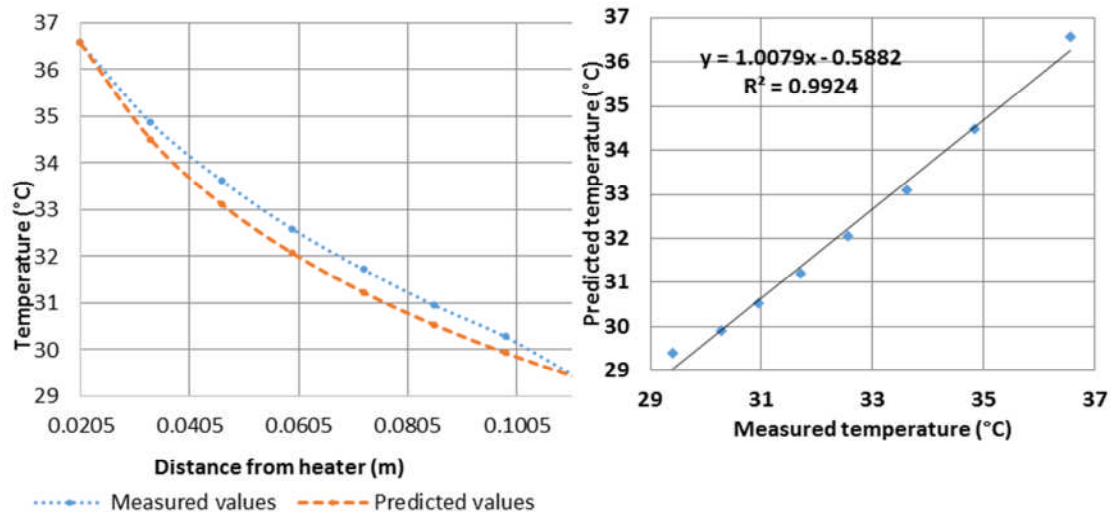


Figure 7.19: The fit of predicted and measured temperature distribution within 50:50 kaolin:sand sample tested at 100kPa; 28% water content

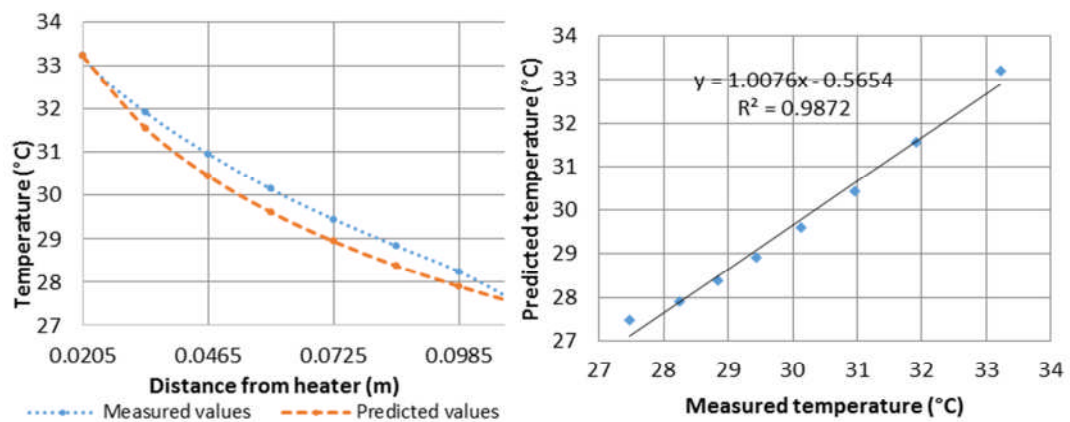


Figure 7.20: The fit of predicted and measured temperature distribution within 25:75 kaolin:sand sample tested at 100kPa; 19.6% water content

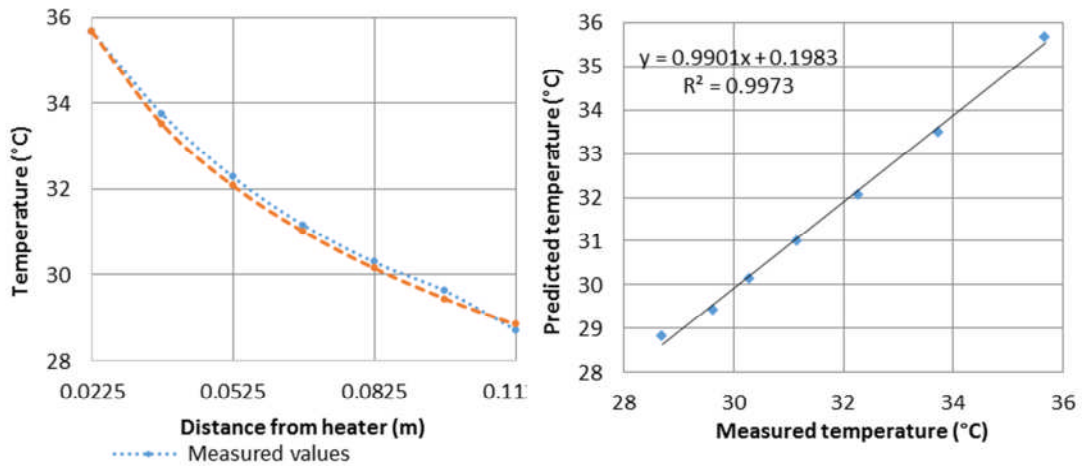


Figure 7.21: The fit of predicted and measured temperature distribution within saturated sand sample tested at 25kPa

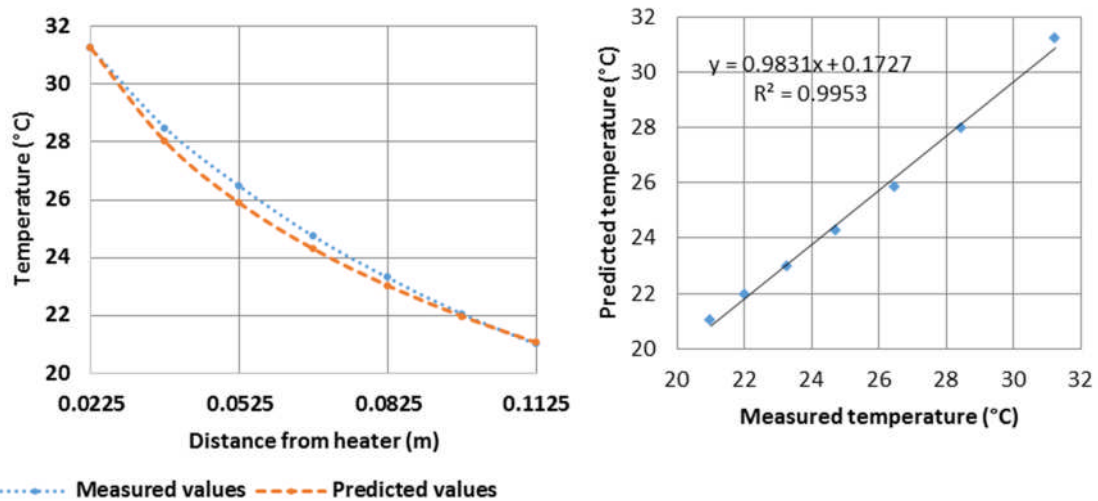


Figure 7.22: The fit of predicted and measured temperature distribution within dry sand sample tested at 25kPa

## 7.5 Discussion of Kaolin Sample at 100kPa

The kaolin sample prepared at a water content of 82% and consolidated at 100kPa, with power input of 17.03W is discussed in detail in this section. Subsequently tests carried out on the other samples will be discussed in relation to this sample.

The discussion is in line with the objectives of the tests conducted on the sample as described in Chapter 6 on the basis of soil type, water content, temperature/power input, pressure, thermal cycles and time.

### 7.5.1 Heating To Steady State / Thermal Equilibrium

A heating test was carried out on the kaolin sample at controlled room temperature of  $18^{\circ}\text{C} \pm 1.5^{\circ}\text{C}$ . The probe arrangements within the sample during the heating test is shown in Figure 7.23.

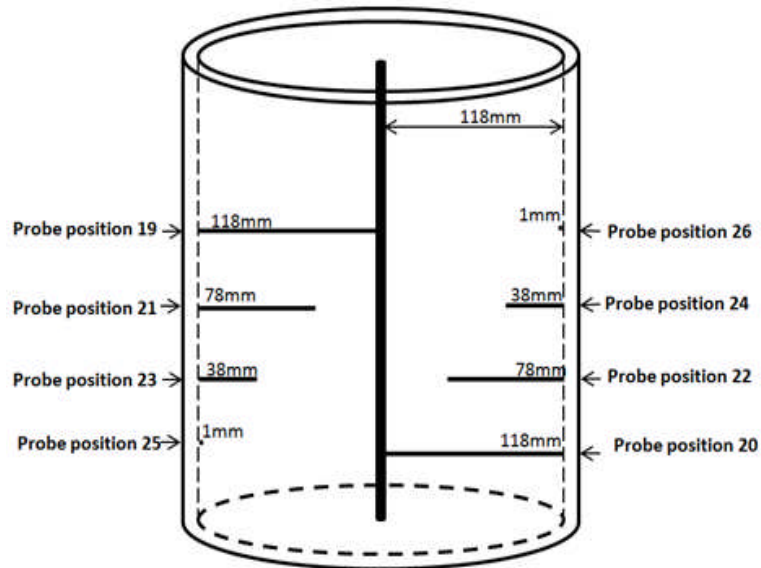


Figure 7.23: Layout of probes within kaolin sample during the heating test

Figure 7.24 shows the variation of temperature with time within the sample being heated to steady state conditions.

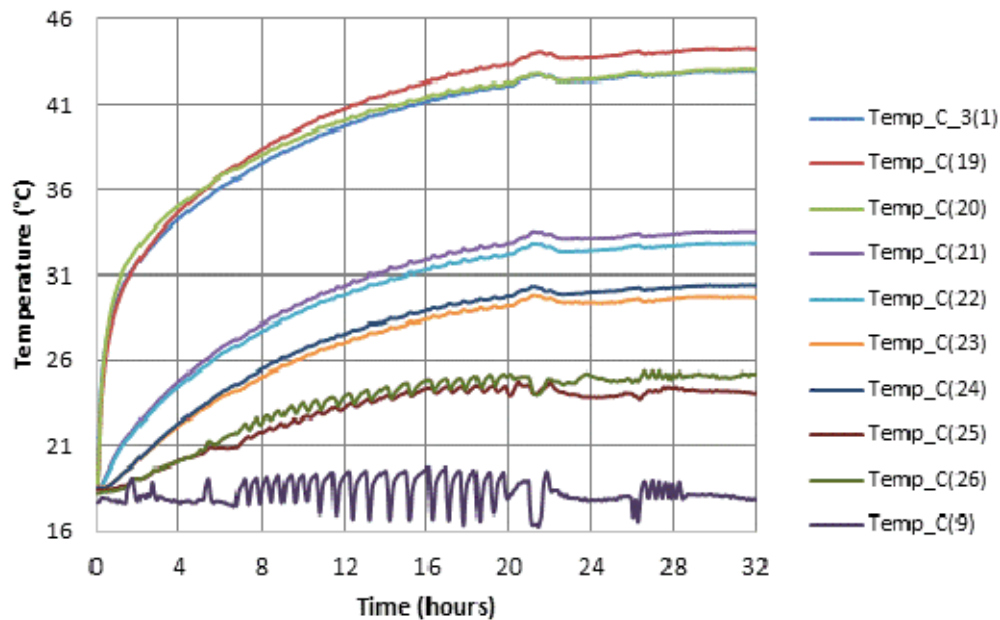


Figure 7.24: Variation of temperature with time across kaolin sample consolidated at 100kPa being heated to steady state

The three lines at the top of the graph represent the heater and probe positions 19 and 20 both touching the top and bottom of the heater respectively within the sample. They attained temperatures between 43°C and 44°C after about 32 hours of heating.

The next two lines below them are represented by probe positions 21 and 22 which are located within the sample at approximately 40mm from the heater. When in thermal equilibrium, the temperatures attained were 33.5°C and 32.9°C respectively. The probes were positioned at different levels within the sample and at opposite sides of the test chamber. This is true of all the other probes and explains why there is a slight difference in temperatures recorded by both sets of probes even though they were placed at the same distances from the heater.

At 40mm from the heater, the sample temperature is about 10°C lower than the temperature at the heater.

The next set of lines below are represented by probe positions 23 and 24 which were located within the sample at approximately 80mm from the heater. At thermal equilibrium, the temperatures attained were 29.7°C and 30.5°C respectively.

At 80mm from the heater, the sample temperature was about 13°C lower than the temperature at the heater. It is also only at 3°C lower than the temperature in the sample at about 40mm away and towards the heater.

The purple line at the bottom represents the controlled room temperature which was controlled at 18°C and fluctuated within an average of  $\pm 1.5^\circ\text{C}$  in a constant temperature room.

The dark red and green lines directly above the room temperature line represent probe positions 25 and 26 in the Figure. They were located at the bottom left and top right side of the inner edge of the cell wall of the test chamber respectively.

They showed temperatures of 24°C and 25°C respectively. They also showed a relatively constant increase which indicated that the insulation properties of the cell wall worked according to design. This point was further buttressed by the constant temperature profile retained in the sample in spite of the fluctuating room temperature.

Looking at probe 22 which was located in the sample at about 40mm away from the heater, like the rest of the probes, it recorded an equilibrium temperature after about 32 hours of heating. Although approximately 32.9°C was recorded at this location after 32 hours of heating, a temperature of 27.7°C was achieved after 8 hours of heating,. This translates to almost 65% of the equilibrium temperature.

By 12 hours of heating, a temperature of 29.9°C translating to almost 80% of the equilibrium temperature had been achieved.

By 16 hours of heating, a temperature of 31.3°C which is about 89% of the equilibrium temperature had been achieved.

By 20 hours of heating, a temperature of 32.2°C which is about 95% of the equilibrium temperature had been achieved.

By 24 hours of heating, a temperature of 32.4°C which is about 97% of the equilibrium temperature had been achieved, even though the sample finally reached equilibrium after approximately 32 hours of heating.

This is depicted by Figure 7.25, which shows that 24 hours was sufficient duration to allow for the sample to achieve most of its full heating potential while a minimum heating duration of 16 hours was required to reach almost 90% of this potential.

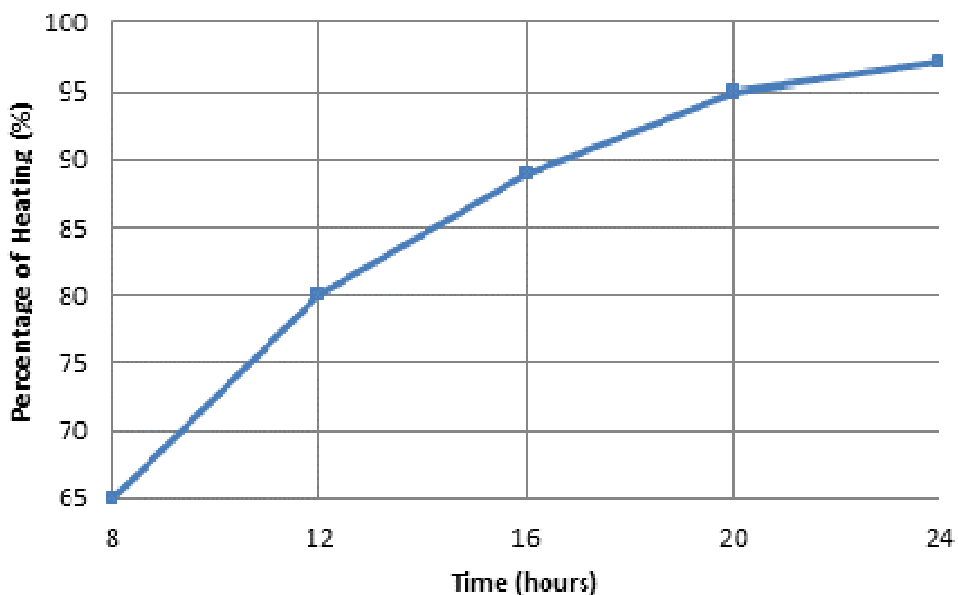


Figure 7.25: Percentage of maximum temperature attained by sample against time of heating

### 7.5.2 Cooling Of Sample

During the cooling test, the power to the heater was disconnected and the sample was allowed to return to its initial or controlled room temperature. From the graph in Figure 7.26, the cooling duration lasted approximately 27 hours to fully return to the controlled room temperature of 19°C.

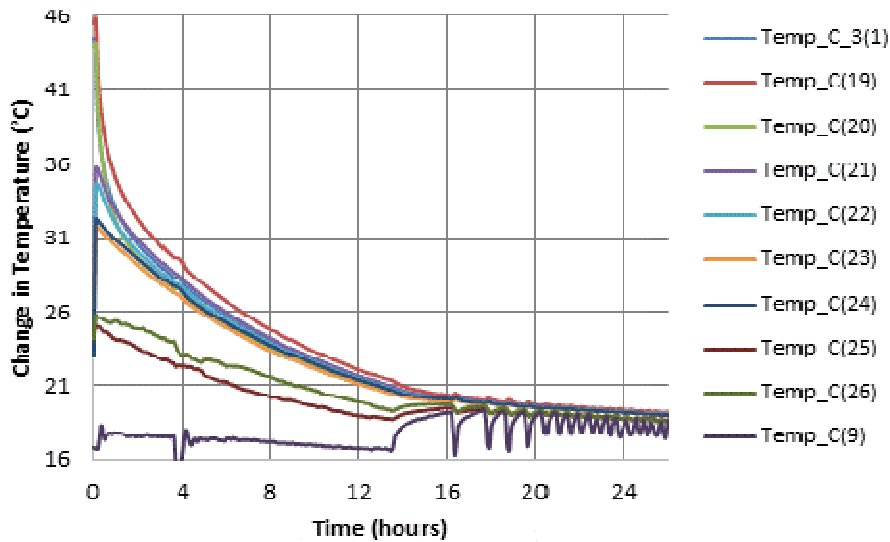


Figure 7.26: Time for kaolin sample consolidated at 100kPa to cool back to controlled room temperature

Looking at the sample location where the temperature was recorded by probe 22, within 8 hours of cooling, at a temperature of 23.9°C, about 79% of cooling had been achieved.

By 12 hours of cooling the temperature was 21.5°C which meant 88% of cooling had been achieved.

By 16 hours of cooling, the temperature had dropped to 20.1°C indicating that 94% of cooling had been achieved. This is depicted by Figure 7.27. These data show that a duration of 12 to 16 hours was required for significant cooling to take place in this sample.

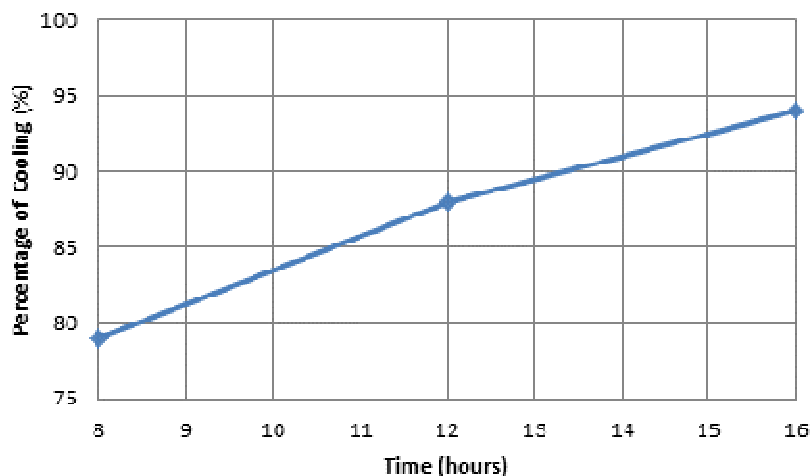


Figure 7.27: Percentage of maximum temperature against time of cooling



### 7.5.3 Temperature Variations within Sample in Thermal Equilibrium

While the sample was in thermal equilibrium, a temperature profile test was carried out to determine the temperature variations within the sample. This was done at the beginning of the thermal tests carried out on the sample, and was repeated on the sample after several weeks of being subjected various thermal tests. Both temperature variations were compared to investigate if any changes occurred in the sample over the period of being subjected to thermal tests lasting up to 19 weeks.

Figure 7.28 is a chart of both tests showing the average temperature variations across the sample when in thermal equilibrium, at the beginning, and after sample was subjected to weeks of thermal tests. Both results appeared similar, but to further compare them, they were plotted against each other as shown in Figure 7.29.

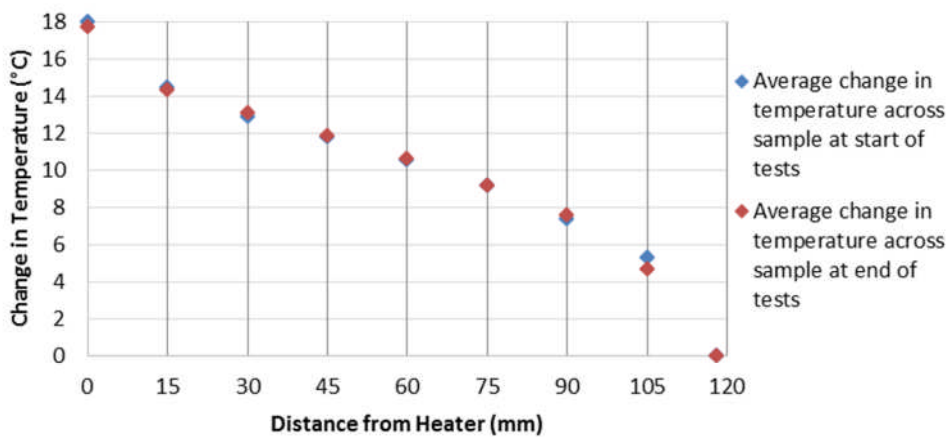


Figure 7.28: Variations in average change in temperature at locations across sample of kaolin at 100kPa at both the start and end of thermal tests

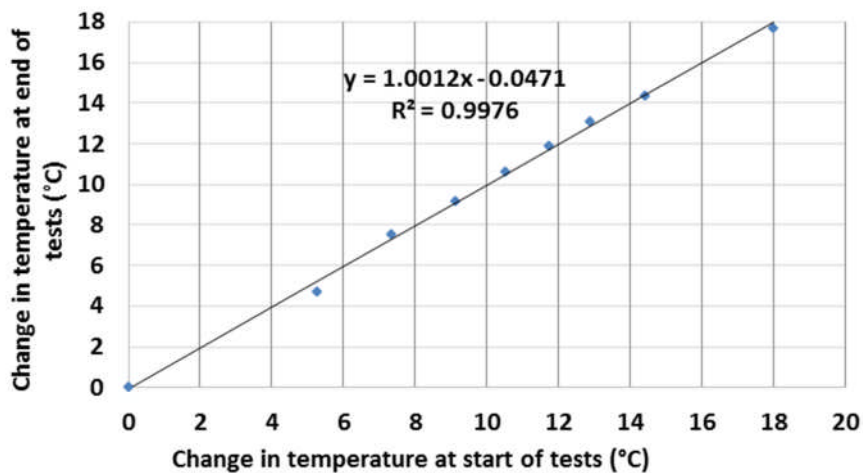


Figure 7.29: Fit of variations in average change in temperature across sample at start and end of tests

From Figure 7.29, the results show the changes in temperature at the end of the tests to be higher within a range of 0.3°C to 1.1°C than those measured at the start of the test. This indicated that the thermal properties of the sample still remained relatively the same even after undergoing series of long-term heating and cooling tests lasting a duration of about 19 weeks, suggesting that the properties of the soil did not change between tests. The increased temperature at the end of the test was likely caused by migration of water due to the increase in temperature in the first cycle which was permanent.

#### 7.5.4 Temperature and Thermal Conductivity

A relationship was observed between thermal conductivity values and temperature across the sample in thermal equilibrium as shown in Figure 7.30. The thermal conductivity values were found to be higher in parts of the sample with higher temperatures and closer to the heat source, which is also consistent with the fact that the water content was lower nearer the heater.

The thermal conductivity values ranged from 1.85W/m.K to 2.98W/m.K over a temperature range of approximately 8°C

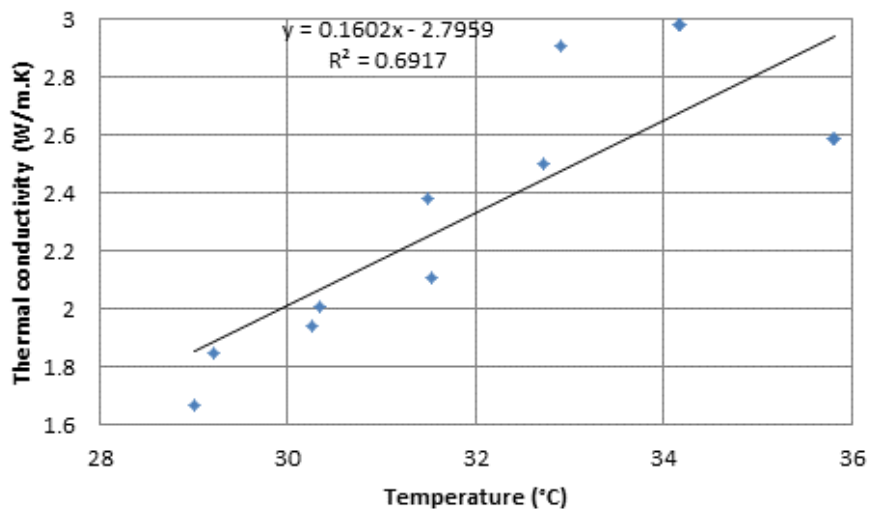


Figure 7.30: Thermal conductivity values plotted against corresponding temperature values across the sample to show relationship

#### 7.5.5 Water Content and Thermal Conductivity

A relationship was observed between the thermal conductivity values and the water content across the sample as shown in Figure 7.31.

The thermal conductivity values differed by 0.6W/m.K over water content values ranging within 2% of each other. The parts of the sample that showed higher water contents also showed lower thermal conductivity values and lower temperatures and vice versa (Lee et

al., 2011). This was explained earlier as likely resulting from the influence of the lower thermal conductivity values of water in samples higher in water content.

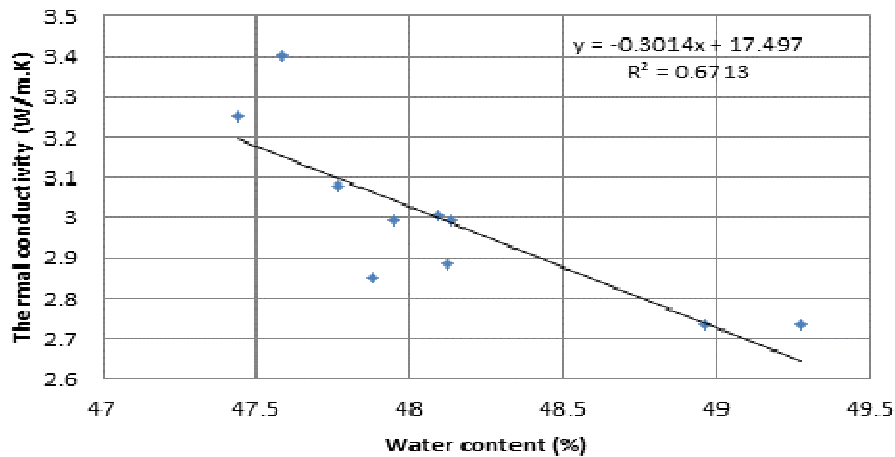


Figure 7.31: Thermal conductivity values plotted against corresponding water content values across the sample to show relationship

### 7.5.6 Water Content and shear strength across sample

The water content at the end of the test was found to vary across and along the sample as shown by the graph in Figure 7.32. From the graph, the sample showed less water content towards the centre of the sample closer to the heat source. The water content also varied from the top to the bottom of the sample, with the bottom showing a higher percentage than the top, possibly due to some load transfer to the cell wall during consolidation of the sample. Towards the outer edge of the cell, the water content was also found to be higher. This suggests that the water migrated from the soil around the heat source.

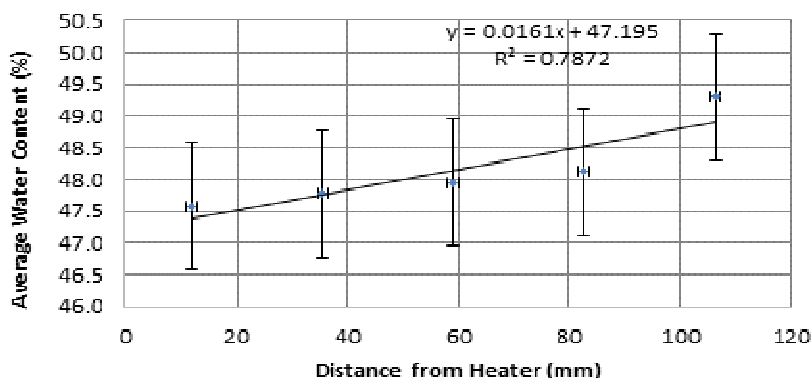


Figure 7.32: Variation in water content across the sample with respect to distance from the heater the range of average water content at each location indicating that the water content increases with distance from the heater

Another relationship was also found to exist between the sample shear strength in relation to distance from the heat source as shown in Figures 7.33 and 7.34. The graph shows that the sample had higher shear strength values closer to the heat source and lower values towards the edge of the sample, and also higher values at the top of the sample relative to the bottom. The middle of the sample showed fairly uniform values.

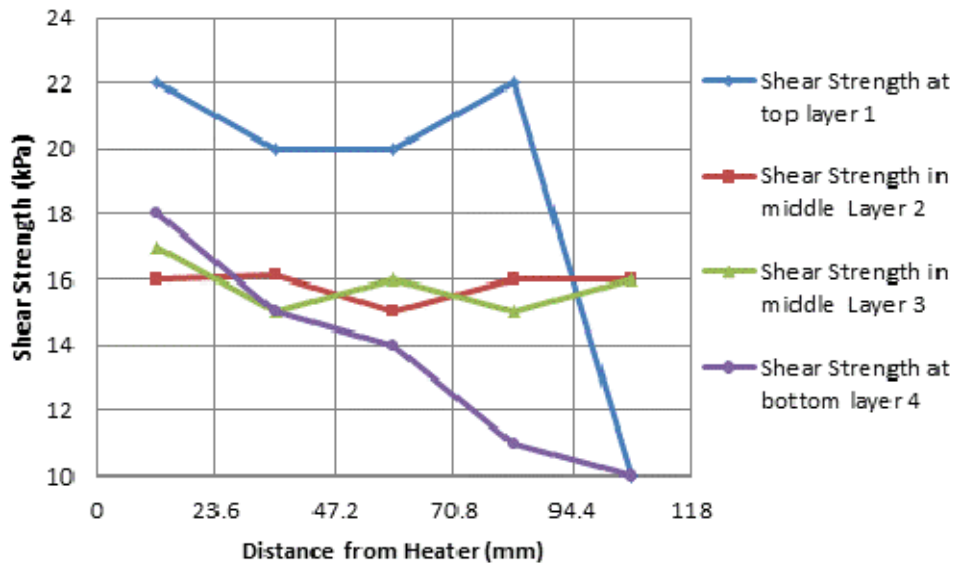


Figure 7.33: Variation of shear strength values with the sample

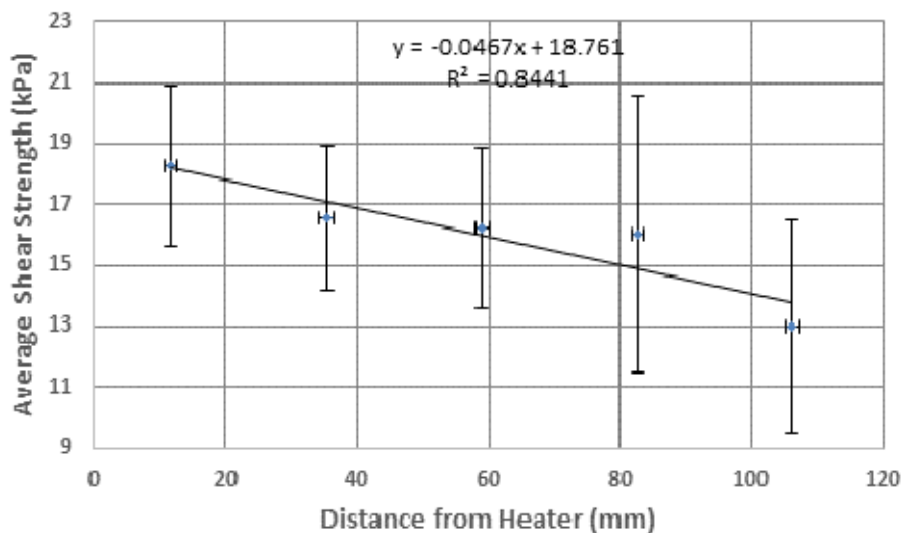


Figure 7.34: Range of variation in average shear strength values at each location showing that the average shear strength reduces with distance from the heat source

The shear strength values which were measured in relation to distance from the heat source were plotted against the water content of samples taken from the same locations tested. Their relationship is shown in Figure 7.35.

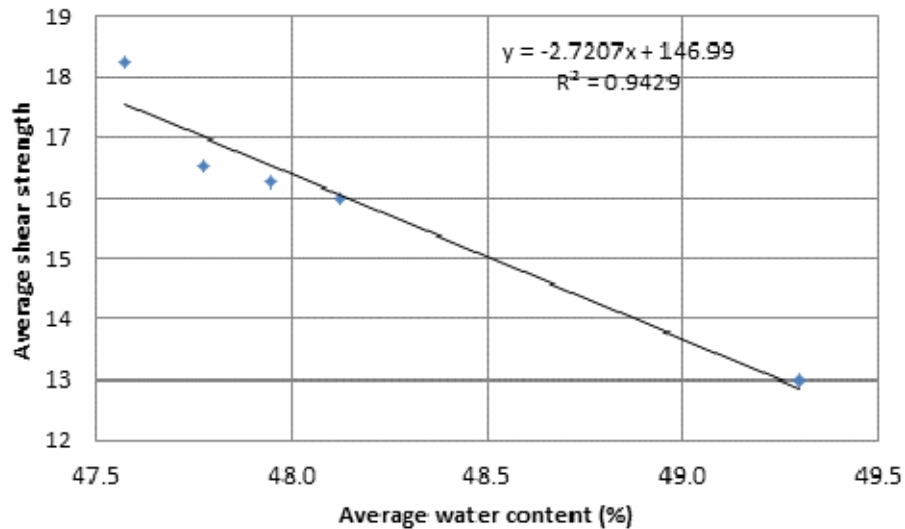


Figure 7.35: Relationship between the average shear strength values and corresponding water content values with respect to distance from the heat source

Figure 7.36 shows the relationship between the shear strength values and corresponding water content values in the top, middle and bottom layers of the sample.

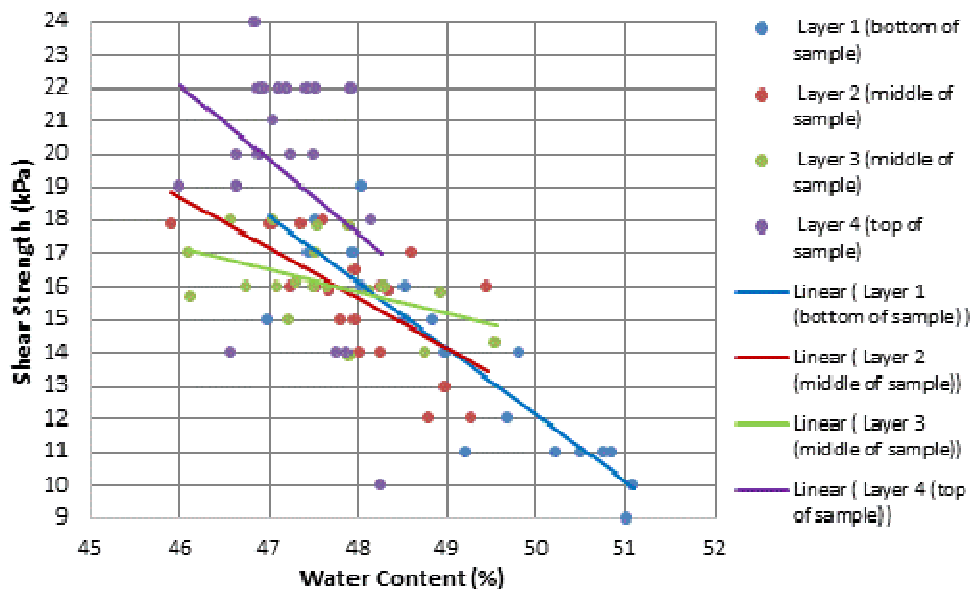


Figure 7.36: Shear strength values against corresponding water content values in top, middle and bottom of kaolin sample at 100kPa

The trend lines show a strong trend of increasing shear strength with a decrease in water content. The bottom layer shows the strongest relationship. The differences in the trend

lines are likely due to spatial variations in the properties of the soil, the errors in measuring strength ( $\pm 1\text{kPa}$ ) and water content, ( $\pm 1\%$ ) as well as the variation in water content due to consolidation. They all show that a reduction in water content near to the heater is associated with an increase in shear strength.

Table 7.3 shows the coefficients and regression values for the trend lines in Figure 7.36 and their water content validity range.

Table 7.3: The coefficients and regression values for the trend lines in Figure 7.36 and the validity range of water content

Sample layer	Equation for fit $y = mx + c$	$R^2$	Validity range of water content (%)
Layer 1 (Bottom)	$-2.0096x + 112.6$	0.7919	47.0 – 51.1
Layer 2 (Middle)	$-1.5303x + 89.081$	0.4668	45.9 – 49.5
Layer 3 (Middle)	$-0.6593x + 47.505$	0.2318	46.1 – 49.5
Layer 4 (Top)	$-2.2505x + 125.63$	0.1304	45.9 – 48.3

### 7.5.7 Thermal Cyclic Loads

Several thermal loading cycles consisting of periods of heating and cooling over a 24 hour period were investigated on this sample. Thermal loading cycles investigated include 2, 4, 6, 8, 12, 14, 18 and 22 hours of heating loads with corresponding periods of cooling within a duration of 24 hours. The cycles were repeated over several days to investigate any difference in sample behaviour over time of repeating the cycles.

The results obtained from comparing data from the first and last days of the 8 hours heating cycle carried out over a period of 14 days are presented in Figure 7.37.

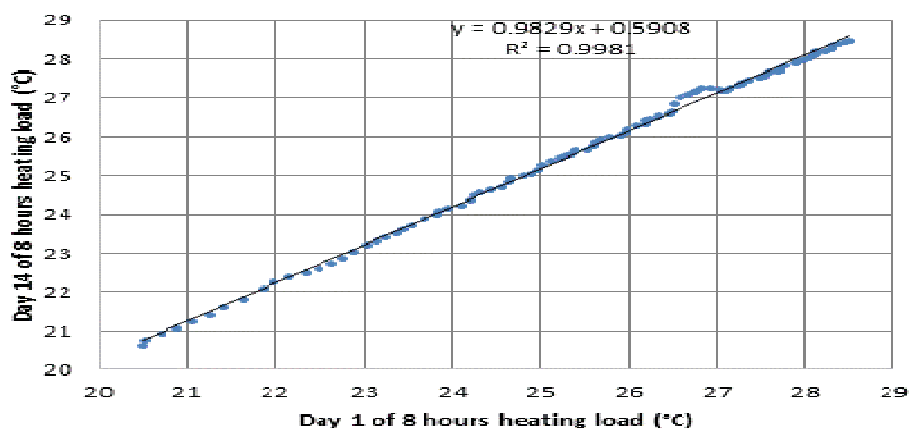


Figure 7.37: Comparing temperature values from day 1 of 8 hours thermal load cycle with day 14 of the same thermal load

Similarly, the results obtained by comparing data from the first and last days of the 16 hours cooling after the 8 hours thermal load over a period of 14 days is presented in Figure 7.38.

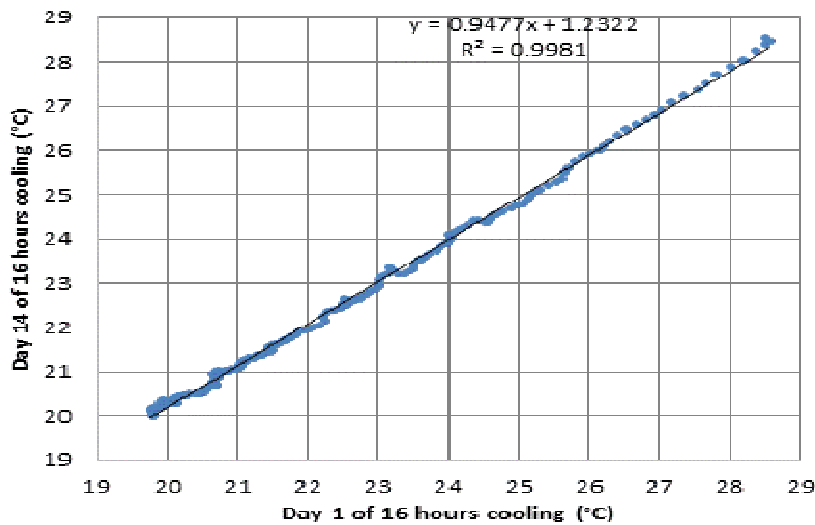


Figure 7.38: Comparing temperature values from day 1 of 16 hours cooling cycle with day 14 of the same cooling cycle

Results from the graphs comparing both the heating and cooling curves in Figures 7.37 and 7.38 show that no difference occurs in the sample after several heating cycles. This indicates that the repeated cycles did not affect the thermal properties of the sample.

The maximum or peak temperatures reached at specific hours of heating (thermal loads), and the corresponding temperatures upon cooling within a 24 hour period, were investigated and plotted against time to obtain the graph shown in Figure 7.39.

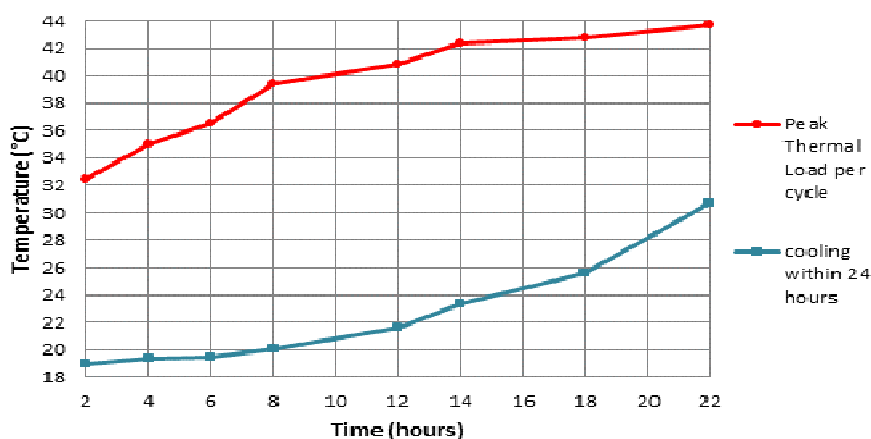


Figure 7.39: Thermal cyclic loading showing peak temperatures reached and corresponding cooling temperatures within a 24 hour period.

Findings from the detailed investigations of the individual thermal cycles show that , the thermal cyclic loads of 2, 4, 6, 8 hours of heating, with subsequent cooling within 24 hours, were well within the heating and cooling capacity of the sample.

For the cycles run at 12 and 14 hours of heating with subsequent cooling for 12 and 10 hours, the sample was still able to achieve a high percentage of cooling.

The cycles run at 18 and 22 hours of heating did not allow the sample sufficient cooling period and resulted in residual heat being built up in the sample. This is in agreement with sections 7.5.1 and 7.5.2 discussing the cooling duration of this sample where 12 to 16 hours were found to be the time required for the sample to cool properly after being subjected to heating loads.

## 7.6 Effect of Soil Type/Composition on duration of heating to thermal equilibrium

Heat transfer is determined by the thermal properties of the material to be tested. For this reason, standard soil types such as kaolin, sand and a mixture of both kaolin and sand in different proportions were tested to study the effect of soil types on thermal behaviour of sample. All the tests carried out were based on five groups of soil types and combinations which constituted the samples and are presented in Table 7.4.

Table 7.4: The composition of the samples

Sample composition	Kaolin	Kaolin:sand mixture	Kaolin:sand mixture	Kaolin:sand mixture	Sand
Proportions by percentage	100	75:25	50:50	25:75	100

The effect of soil composition on thermal behaviour in soils was investigated by carrying out tests on the different soil types under similar conditions.

Figure 7.40 shows heating curves of the time to equilibrium from tests carried out on five different soil types including combinations of kaolin and sand under similar conditions of power input, pressure and time (duration) of testing. The curves obtained for each sample type indicate a different heating response from each of the soil samples tested. The results presented in the graph are from samples of kaolin, sand and combinations of kaolin and sand in proportions of 75:25, 50:50 and 25:75 representing a predominantly kaolin sample, a sample of equal kaolin and sand proportions and a predominantly sandy sample respectively.



The temperatures recorded at same location within the five different sample types were compared in terms of time to equilibrium. Due to the soil types being different, the water content varied between the samples. They were tested at the same pressure of 25kPa and the same power input of 17.03W.

The soil types with the highest sand composition reached its equilibrium temperature the fastest at approximately 24 hours of heating, and had the lowest maximum temperature of about 31.8°C.

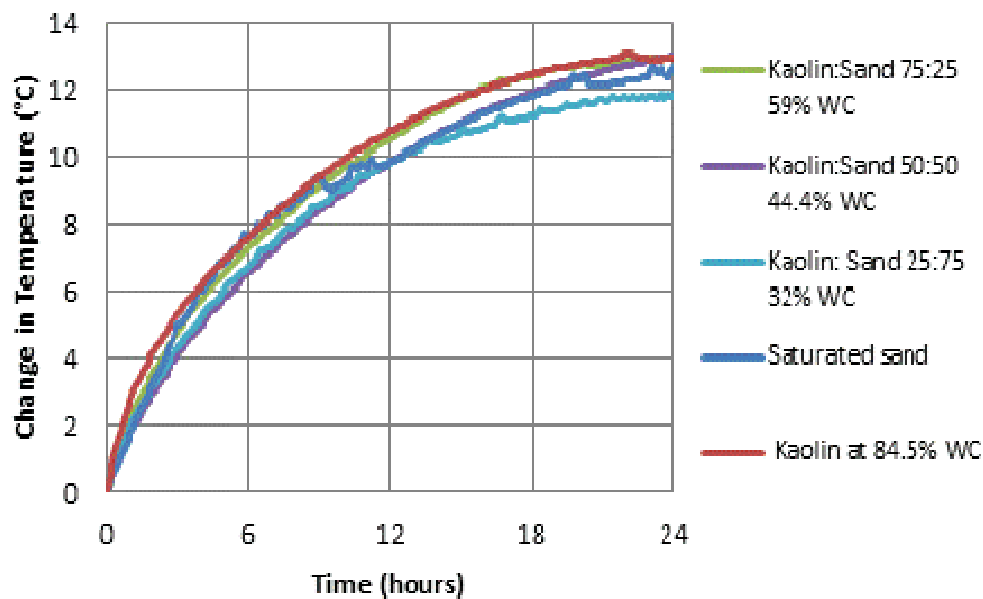


Figure 7.40: Heating curves of the different soils compositions with varying water contents, tested at same power input of 17.03W. The sample made up of just kaolin with no sand content took the longest time to reach equilibrium temperature and also had the highest equilibrium temperature of about 34°C.

Figure 7.41 on page 245, shows a graph of time to equilibrium against sand content of sample.

It shows that the combination samples higher in sand content generally attained thermal equilibrium temperature faster than samples with lower sand content, although other factors such as water content also influence time to equilibrium. This is mostly as a result of the higher thermal conductivity value of the sand content, enhanced by the kaolin particles filling the voids between the sand particles and replacing the water between the sand particles. This results in an increase in mass of solids and decrease in mass of water, thereby leading to a higher thermal conductivity in the sample and shorter time to

equilibrium than in the predominantly kaolin samples. The samples were tested at the same power input.

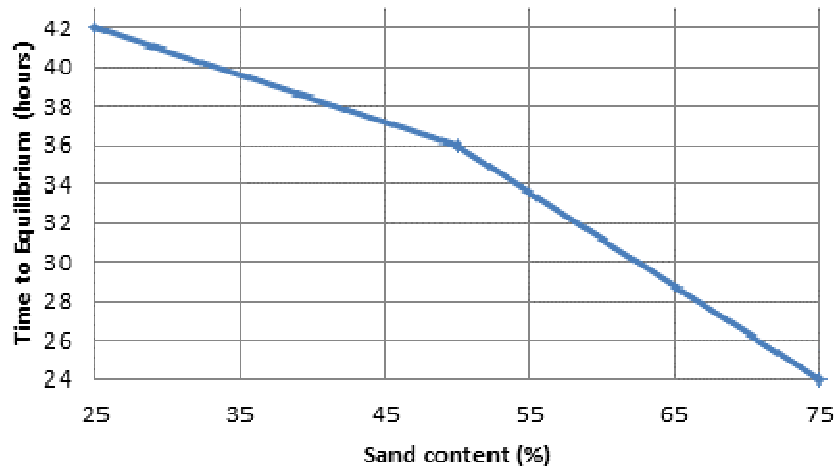


Figure 7.41: Time to equilibrium of combination samples of kaolin and sand with respect to the percentage sand content

Figure 7.42 shows a plot of maximum temperature attained versus sand content of sample. It shows that samples with higher sand content attained lower equilibrium temperatures for tests carried out at the same power input, which could be due to the lower specific heat capacity of wet sand ( $1632\text{J/Kg.K}$ ) relative to that of wet kaolin ( $2362\text{J/Kg.K}$ ).

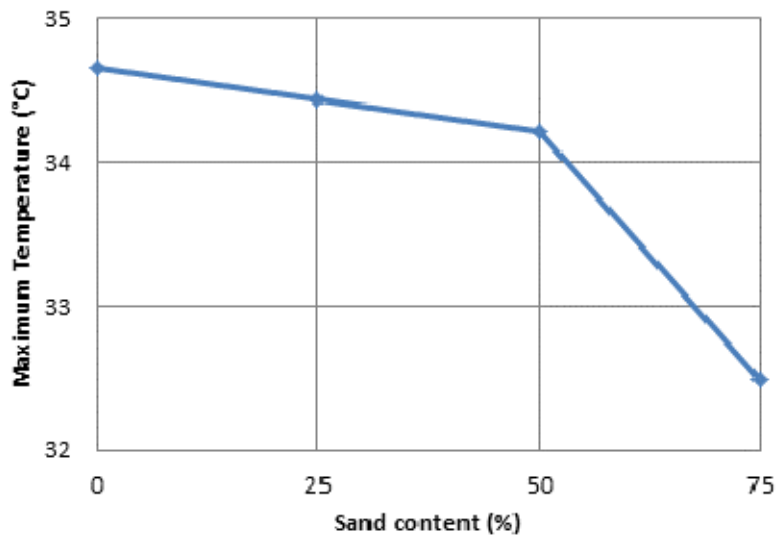


Figure 7.42: Maximum temperature attained relative to the percentage sand content of sample after 42 hours of heating

Figure 7.43 shows a graph of the cooling curves of the samples which shows that the samples cooled at a similar rate compared to the heating rate, although the combination

sample with 75% sand content cooled fastest due to its lower heat capacity. The saturated sand sample did not cool as fast which is due to the higher specific heat capacity of water (4187J/Kg.K).

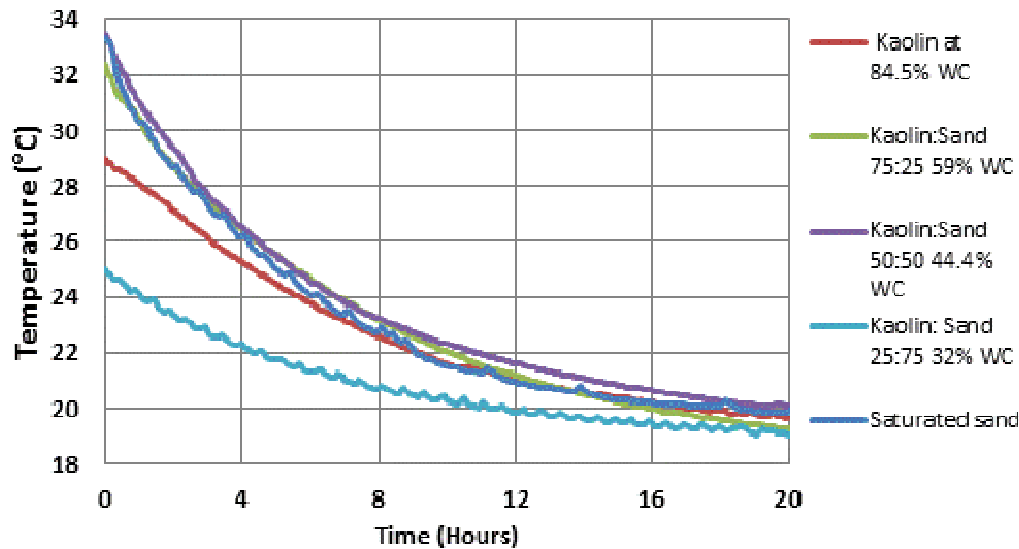


Figure 7.43: Cooling curves for the different soils compositions with varying water contents, after being heated at power input of 17.03W

Therefore, time to equilibrium and cooling, differ from sample to sample and although is influenced by factors such as water content, soil composition, thermal conductivity, temperature and pressure, soil composition plays the most dominant role.

## 7.7 Effect of Consolidation Pressure and Water Content on heat dissipation

Thermal diffusivity is defined by Shiozawa and Campbell (1990) as “the ratio of thermal conductivity to volumetric heat capacity, and is a measure of the rate of transmission of temperature change into soil, when the surface temperature changes with time”.

The time required for the sample to attain thermal equilibrium is therefore, influenced by both the soil thermal conductivity and diffusivity, which in turn rely on soil composition, bulk density, particle shape, and water content (Shiozawa and Campbell, 1990; Mitchell and Soga, 2005).

Prior to testing, the samples were prepared by mixing the dry kaolin or sand with distilled water to achieve specific water contents. Apart from sand which was tested in both dry and saturated forms, all the other samples were tested within controlled ranges of water

content and were assumed to be saturated because of the method of sample preparation. On the basis of the soil types and the proportions used in constituting the samples, the water content levels at the start of the tests varied from sample to sample.

The effect of water content on the heating tests was investigated in relation to the effect of pressure applied to the sample, this is because the water content of the sample in the test chamber changed after the consolidation phase and so differed from that at the start of the test. Therefore, the effect of water content on thermal behaviour is being discussed with reference to the effect of the consolidation pressure applied to the test.

The test rig was built to allow for pressure to be applied to the top of the sample to simulate overburden pressure as samples were tested to simulate underground conditions. The pressure applied also determined the water content of the sample during the test.

All the tests were carried out within 5 groups of pressure ranging from 0kPa to 200kPa. These are presented in Table 7.5.

Table 7.5: The pressure applied during the tests

<b>PRESSURE (kPa)</b>	<b>0</b>	<b>25</b>	<b>50</b>	<b>100</b>	<b>200</b>
<b>SAMPLE GROUPS TESTED</b>	<b>KAOLIN</b>	<b>KAOLIN</b>	<b>KAOLIN</b>	<b>KAOLIN</b>	<b>KAOLIN</b>
		<b>SAND</b>			
		<b>KAOLIN:SAND (75:25)</b>	<b>KAOLIN:SAND (50:50)</b>	<b>KAOLIN:SAND (75:25)</b>	
		<b>KAOLIN:SAND (50:50)</b>		<b>KAOLIN:SAND (50:50)</b>	
		<b>KAOLIN:SAND (25:75)</b>		<b>KAOLIN:SAND (25:75)</b>	

To investigate the influence of water content of sample and pressure applied, on heat dissipation and time to equilibrium, the same soil type (kaolin) having the same water content of 82% at the start of tests, was tested at the same power input of 17.03W but at different consolidation pressures of 25kPa, 100kPa and 200kPa. The kaolin sample of 84.5% water content at 0kPa was tested alongside for comparison. The samples had different thermal conductivity values due to their varying water contents.

Heating curves from the results of this test the are presented in Figure 7.44. The graph shows that within the first 24 hours of the heating test, the samples at different pressures had very similar curves and dissipated heat at similar rates, within 1.5°C of each other

under the different pressure loads. The samples at pressures of 25kPa and 200kPa with different water contents both behaved similarly.

The sample tested at the lowest pressure of 0kPa and with highest water content achieved equilibrium temperature before the other samples. In conclusion all the samples behaved similarly even though the water content and consolidation pressures were different, and the time to equilibrium was not directly influenced by the water content in the case of kaolin samples, suggesting that the soil composition had more influence on its thermal behaviour.

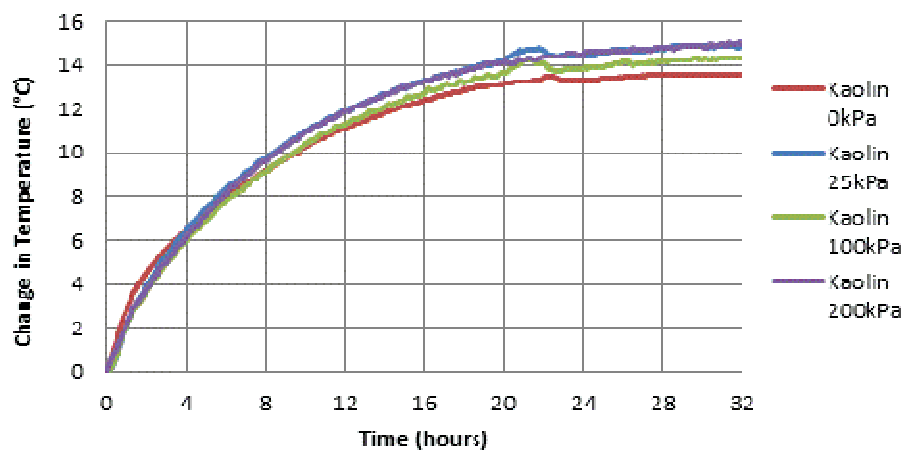


Figure 7.44: Heating curves for kaolin samples at 84.5% water content at 0kPa, and 82% water content at start of test, and tested at the same power input of 17.03W but different consolidation pressures of 25, 100 and 200kPa

When all four samples were allowed to cool back to their initial temperatures, they still behaved in a similar way and had cooled to the same temperature after approximately 26 hours as shown in Figure 7.45.

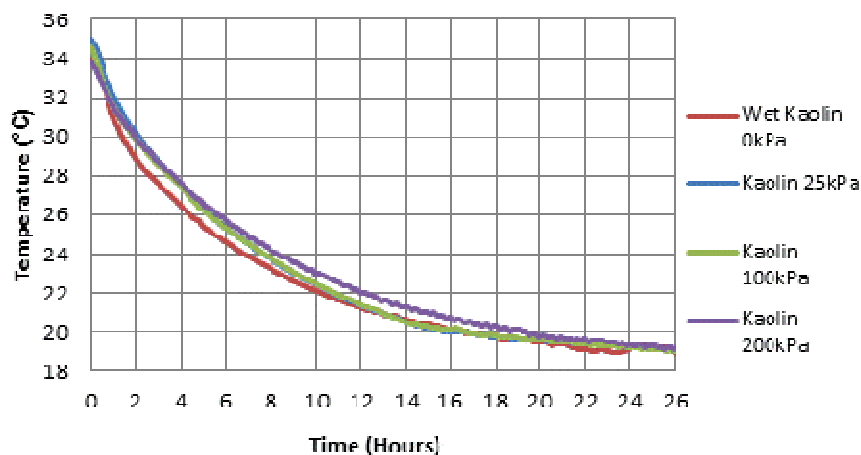


Figure 7.45: Cooling curves for the kaolin samples in Figure 7.44

As the influence of water content and consolidation pressures were not clearly defined in the kaolin samples tested, another soil type was tested under similar conditions for comparison.

Figure 7.46 shows the heating curves of kaolin and sand samples combined in a proportion of 75% kaolin to 25% sand. This soil combination both had the same initial water content and was tested at the same power input of 17.03W but at different consolidation pressures of 25kPa and 100kPa.

Both samples behaved differently, as that tested at 100kPa with resultant lower water content reached equilibrium by 30 hours of heating at a maximum temperature of approximately 32°C, while the sample tested at 25kPa with resultant higher water content reached equilibrium after 42 hours of heating, at a maximum temperature of approximately 34°C.

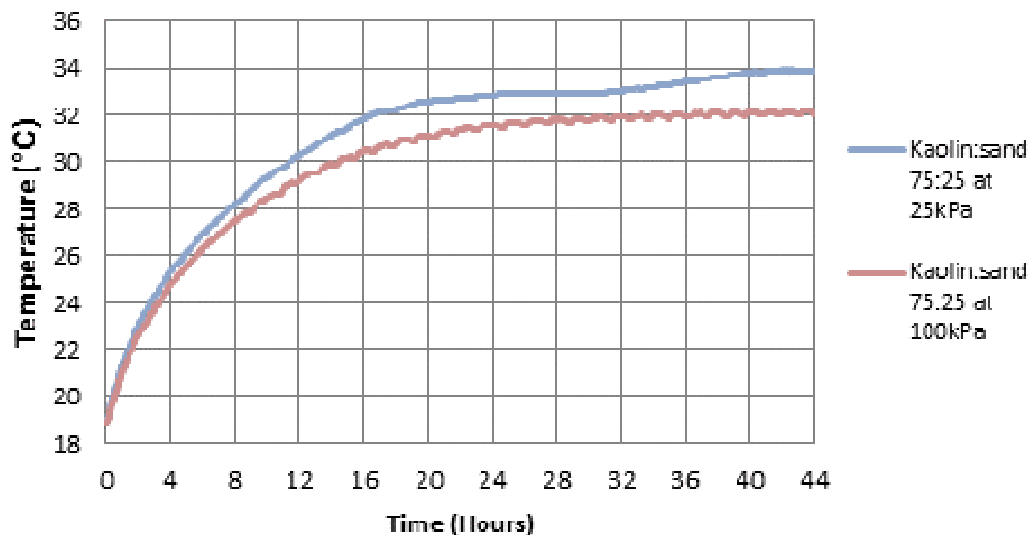


Figure 7.46: heating curves for kaolin:sand (75:25) samples with same water content at start of test, same power input of 17.03W but at different consolidation pressures of 25kPa and 100kPa

When the same samples were allowed to cool, the sample tested at 25kPa with higher water content took an additional 6 hours to cool to the same temperature as the sample tested at 100kPa.

The graph of the cooling curves is shown in Figure 7.47 on page 250. In this case, where the samples were composed of both kaolin and sand, the water content seemed to have influenced the heating and cooling of sample. This is likely due to the higher specific heat capacity of water relative to that of kaolin and sand.

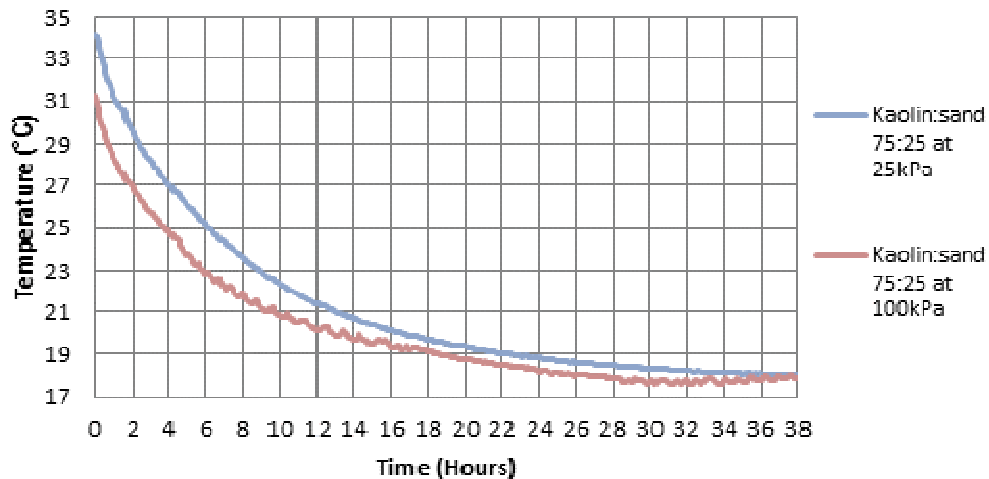


Figure 7.47: Cooling curves for the kaolin:sand (75:25) samples in Figure 7.46

Another soil type consisting of a combination of 50% kaolin and 50% sand was further tested to investigate the influence of water content and consolidation pressure. The graph of the result is shown in Figure 7.48. This sample was tested at the same power input of 17.03W, with the same water content at the start of the test. The consolidation pressures applied were 25kPa, 50kPa and 100kPa.

From Figure 7.48, it can be seen that although the samples started to heat up at different temperatures, all within 1°C of each other, they all reached equilibrium temperature at approximately the same time in 35 hours. They achieved the same maximum temperature of 33.6°C in the samples tested at 25kPa and 50kPa while that tested at 100kPa was very close at 33.4°C. Unlike the previous sample with 25% sand content where the influence of water content was noticeable, the sand content of 50% in the sample is seen to have overridden the influence of water content in this test.

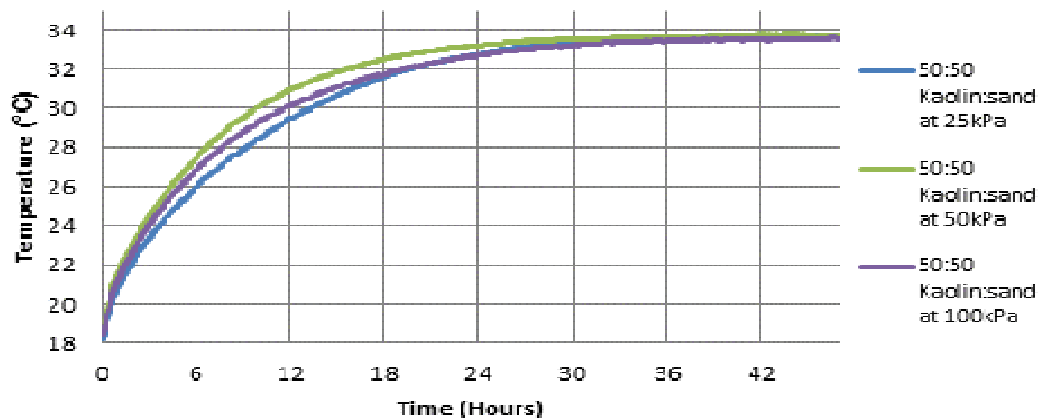


Figure 7.48: Heating curves for kaolin:sand (50:50) samples with same water content at start of test, same power input of 17.03W but different consolidation pressures of 25, 50 and 100kPa

When the samples were allowed to cool, they behaved similarly as by 22 hours, the samples tested at 50kPa and 100kPa had reached the same cooling temperature, while the sample tested at 25kPa remained about 0.5°C higher in temperature as shown in Figure 7.49.

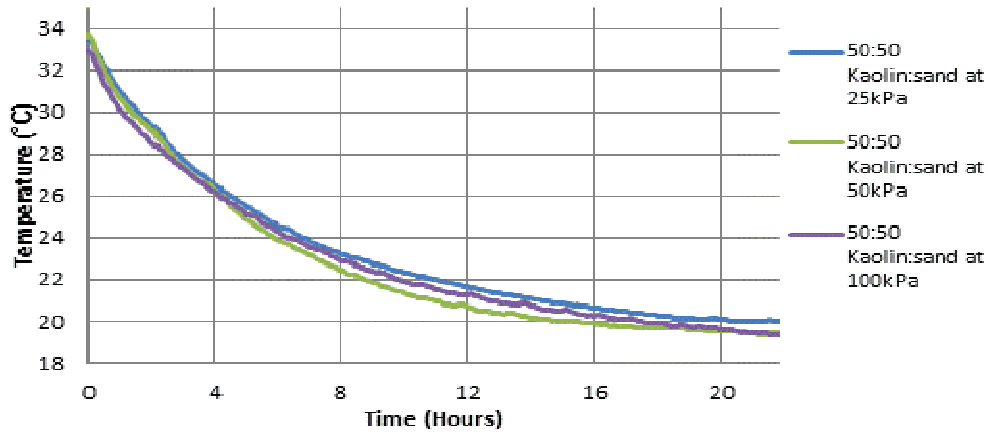


Figure 7.49: Cooling curves for the kaolin:sand (50:50) samples in Figure 7.48

Another soil type consisting of a combination of 25% kaolin and 75% sand was further tested to investigate the influence of water content and consolidation pressure. The graph of the result is shown in Figure 7.50. This sample was tested at the same power input of 17.03W, with the same water content at the start of the test. The consolidation pressures applied were 25kPa, 50kPa and 100kPa.

From Figure 7.50, the samples behaved in a similar way during the heating, and they all reached equilibrium temperature at about the same time in 24 hours, and achieved the same maximum temperature within 0.5°C of each other with the sample tested at 100kPa having the lower temperature.

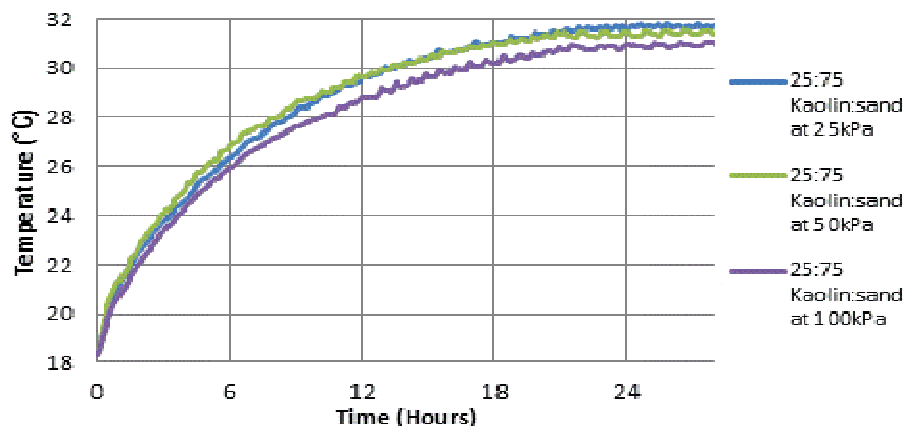


Figure 7.50: Heating curves for kaolin:sand (25:75) samples with same water content at start of test, same power input of 17.03W but different consolidation pressures of 25, 50 and 100kPa



The graph of the samples cooling is shown in Figure 7.51. The samples had cooled by 26 hours, with the sample tested at 25kPa approximately 0.5°C higher than those tested at 50kPa and 100kPa. This is also likely to be influenced by the higher specific heat capacity of water relative to kaolin and sand.

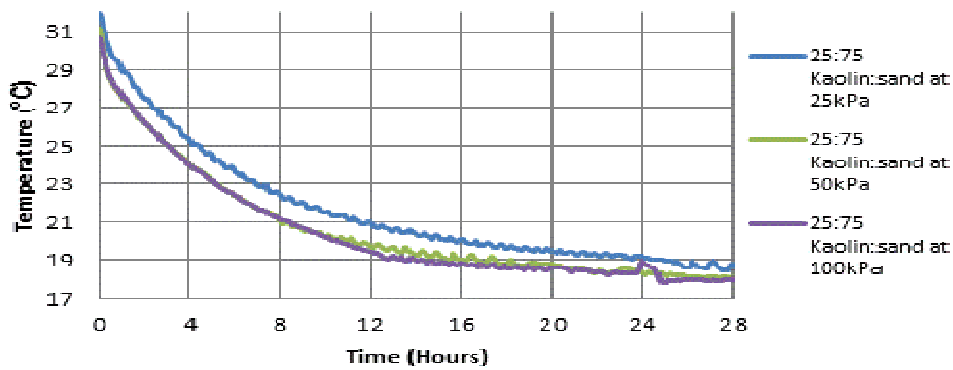


Figure 7.51: Cooling curves for the kaolin:sand (25:75) samples in Figure 7.50

The dry sand and saturated sand samples were not compared as both required different power inputs for heating, with the saturated sample requiring up to five times the power requirement of the dry sample, which could still be attributed to the higher specific heat capacity of water relative to sand.

Therefore, while both the water content and soil composition influence the thermal conductivity as shown in Figure 7.52, which in turn influences the heat dissipation in the soil, the thermal diffusivity is more influenced by the soil composition.

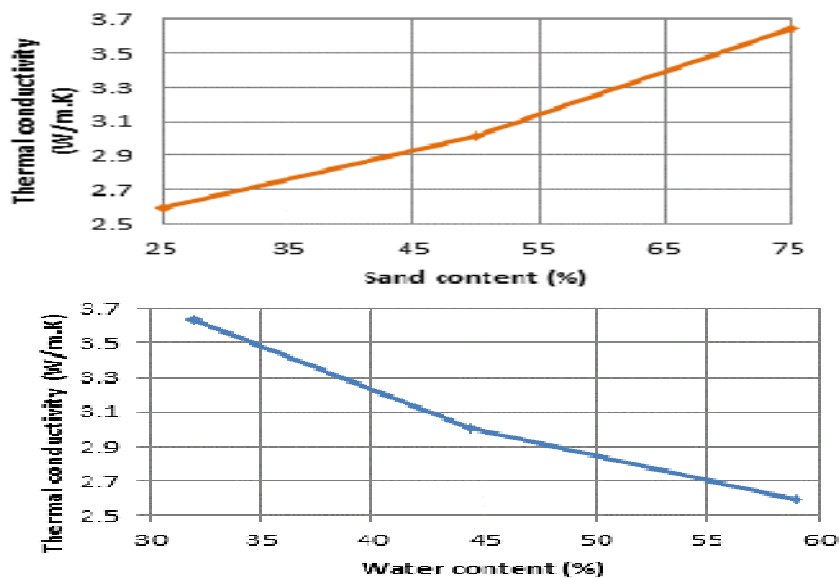


Figure 7.52: Thermal conductivity of sample as a function of both percentage sand content and percentage water content

In conclusion, while both water content and consolidation pressure influenced the heat dissipation in the various samples, the influence of the soil composition was seen to be more dominant.

## 7.8 Discussion of the Determination and Prediction of Thermal Conductivity of the Samples and the influence of Water Content and Sample Composition on the Thermal Conductivity

The thermal conductivity values for the soil samples tested were predicted using equation 7.1 (Fourier's law of heat conduction) and the results presented in Table 7.6, which shows that the thermal conductivity of the soil samples is determined by the water and sand contents. In the case of the kaolin samples, the thermal conductivity of the soil sample generally increases as the consolidation pressure increases, this is because the void ratio, and consequently the water content, reduces. This is expected since the thermal conductivity of water is less than that of clay.

In the case of the samples of kaolin and sand combinations, the thermal conductivity increases as the sand content increases because the thermal conductivity of sand is higher than that of kaolin.

Table 7.6: Thermal conductivity of samples based on Fourier's Law of heat conduction

SN	SAMPLE	PRESSURE APPLIED (kPa)	WATER CONTENT BEFORE TEST (%)	WATER CONTENT AFTER TEST (%)	AV. THERMAL COND. WHOLE SAMPLE ( $k_{t\text{mass}}$ ) (W/m.K)
1	KAOLIN	0	84.5	NA	1.57
2	KAOLIN	25	82	56.7	1.86
3	KAOLIN	100	82	48	2.41
4	KAOLIN	200	82	42	2.53
5	KAOLIN:SAND (75:25)	25	59	42.1	2.24
6	KAOLIN:SAND (75:25)	100	59	36.5	2.59
7	KAOLIN:SAND (50:50)	100	44.4	22.8	3.01
8	KAOLIN:SAND (25:75)	100	32.1	19.6	3.64
9	SAND	25	26	26	3.27

Numerous models have been developed to predict the thermal conductivity of soils based on the properties of the constituents, from the model proposed by de Vries, which is based on the volume fractions of the continuous medium (water in this case) and the soil particles and the thermal conductivity of these two fractions (Lee et al., 2011; Tian et al., 2016);

Assuming that the thermal conductivity is a function of the volume fractions of the kaolin, sand and water, then a simple assumption is the thermal conductivity of the sample mass,  $k_{t\text{mass}}$ , is given by equation 7.2

$$k_{t\text{mass}}V_{\text{mass}} = k_{t\text{water}}V_{\text{water}} + k_{t\text{kaolin}}V_{\text{kaolin}} + k_{t\text{sand}}V_{\text{sand}} \quad (7.2)$$

Since tests were carried out on saturated kaolin samples and saturated sand samples, and the thermal conductivity of water well known from literature as (0.6W/m.K), the effective  $k_{t\text{kaolin}}$  and  $k_{t\text{sand}}$  can be calculated from this equation.

The results obtained are presented in Table 7.7. The average effective  $k_{t\text{kaolin}}$  is 2.34W/m.K and the effective  $k_{t\text{sand}}$  is 3.71W/m.K. A typical thermal conductivity for solid clay minerals is 1.93W/m.K and that for quartz, 3W/m.K. Hence these values correspond in magnitude as the effective thermal conductivity of the constituents of the soil used in the tests.

Table 7.7: Effective thermal conductivity values of kaolin and sand based on Equation 7.2

SN	SAMPLE	PRESSURE APPLIED (kPa)	WATER CONTENT BEFORE TEST (%)	WATER CONTENT AFTER TEST (%)	AV. THERMAL COND. WHOLE SAMPLE ( $k_{t\text{mass}}$ ) (W/m.K)	EFFECTIVE THERMAL COND OF SOIL. ( $k_{t\text{soil}}$ ) (W/m.K)
1	KAOLIN	0	84.5	NA	1.57	1.55
2	KAOLIN	25	82	56.7	1.86	2.03
3	KAOLIN	100	82	48	2.41	2.80
4	KAOLIN	200	82	42	2.53	2.97
5	SATURATED SAND	25	26	26	3.27	3.71

Using the effective thermal conductivities of the solid constituents (kaolin and sand), it is also possible to predict the mass thermal conductivity of the kaolin/sand samples using this equation.

The results obtained are presented in Table 7.8 (page 255), and in Figure 7.53 (page 256), in which the predicted thermal conductivity of each sample is compared with the water content.

Figure 7.53 shows that an increase in sand content shows an increase in the mass thermal conductivity of the sample, and an increase in water content shows a decrease in the thermal conductivity. It is noted that there is an increase in thermal conductivity with sand but the increase between 75% and 100% sand exceeds that between 0% and 25%, 25% and 50%, 50% and 75%. This could be due to the fact that with a sand content less than about 75%, the engineering behaviour of soil is similar to that of pure

kaolin since the voids between the sand particles are filled with kaolin and water (Al-Moadhen Muataz et al., 2017).

Table 7.8: Predicted mass thermal conductivity values of kaolin/sand samples based on Equation 7.2

Sample	Water content (%)	Mass Thermal Conductivity (W/m.K)	Sand content (%)
Kaolin	84.5	1.06	0
	82	1.07	
	68	1.12	
	61.8	1.16	
	52.7	1.21	
	46.8	1.26	
Kaolin:sand (75:25)	60	1.36	25
	41.9	1.53	
	36.3	1.60	
Kaolin:sand (50:50)	44.4	1.68	50
	31.9	1.87	
	30.4	1.90	
	27.4	1.96	
Kaolin:sand (25:75)	32	2.08	75
	21.5	2.34	
	20.9	2.36	
	18.8	2.42	
Sand	26.1	3.71	100

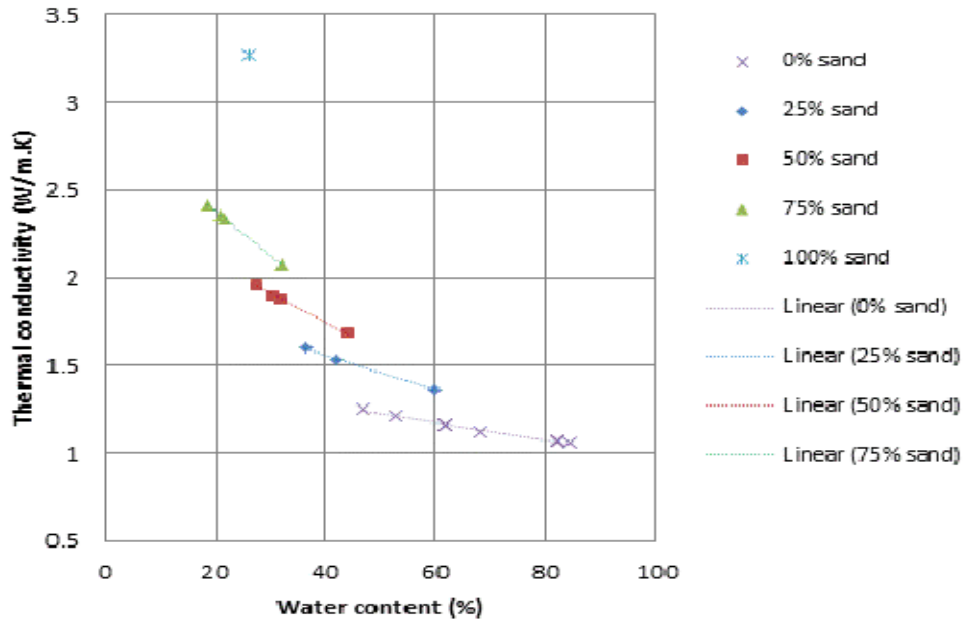


Figure 7.53: Thermal conductivity in kaolin/sand samples showing an increase with increased sand content and a decrease with increased water content based on volume

The trend lines for the data in Figure 7.53 for the different sand contents suggests that there is a linear relationship between the thermal conductivity and water content. These relationships were used to calculate the thermal conductivity at 50%, 100%, 150% and 200% of the liquid limit. The results, as presented in Figure 7.54, show that for water content below the liquid limit, when the soil is considered a solid, there is a linear relationship between thermal conductivity and sand content

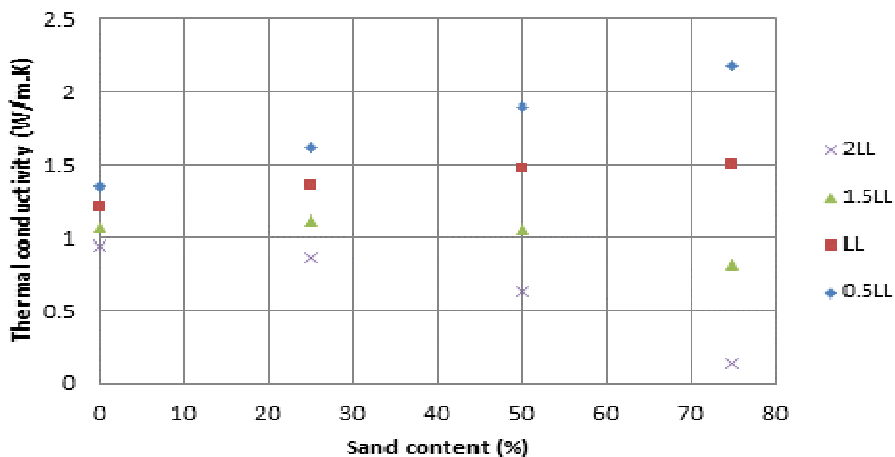


Figure 7.54: Relationship between thermal conductivity and sand content at various levels of saturation based on volume

If the water content is 26%, the same as the water content of the saturated sand used in this study, then the predicted  $k_{\text{mass}}$  is 2.51W/m.K, which is less than that determined from

the heat transfer equation (3.71W/m.K). Further, the thermal conductivity of a sand with a water content of 107%, would be less than that of water, which is not possible. This suggests that this proposal to base the predicted thermal conductivity on the volume of a soil's constituents may not be appropriate.

Another option was to consider that the thermal conductivity of the soil depends on the mass of the soil, which is based on the assumption that heat is transferred by conduction. In that case,  $k_{t_{mass}}$  is:

$$k_{t_{mass}}W_{mass} = k_{t_{water}}W_{water} + k_{t_{kaolin}}W_{kaolin} + k_{t_{sand}}W_{sand} \quad (7.3)$$

The effective thermal conductivities of kaolin and sand based on mass are 3.14W/m.K and 3.97W/m.K respectively as shown in Table 7.9. While these values exceed typical values for clay minerals and quartz, they are of the same order of magnitude.

Table 7.9: Effective thermal conductivity values of kaolin and sand based on Equation 7.3

SN	SAMPLE	PRESSURE APPLIED (kPa)	WATER CONTENT BEFORE TEST (%)	WATER CONTENT AFTER TEST (%)	AV. THERMAL COND. WHOLE SAMPLE ( $k_{t_{mass}}$ ) (W/m.K)	EFFECTIVE THERMAL COND. OF SOIL ( $k_{t_{soil}}$ ) (W/m.K)
1	KAOLIN	0	84.5	NA	1.57	2.39
2	KAOLIN	25	82	56.7	1.86	2.57
3	KAOLIN	100	82	48	2.41	3.23
4	KAOLIN	200	82	42	2.53	3.34
5	SATURATED SAND	25	26	26	3.27	3.97

Figure 7.55 shows predicted values of thermal conductivity of the kaolin/sand samples using mass of the constituents and the effective thermal conductivity of the kaolin and sand. They show that an increase in sand content increases the thermal conductivity and an increase in water content reduces the thermal conductivity.

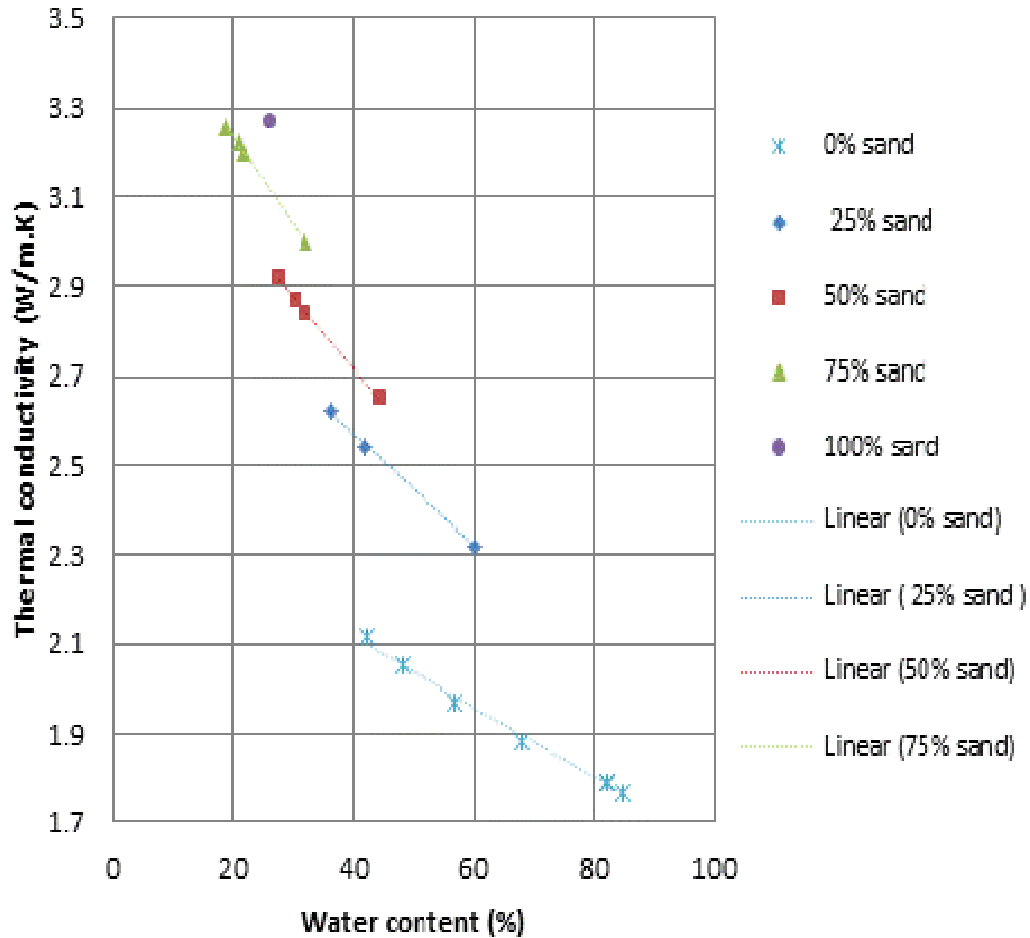


Figure 7.55: Thermal conductivity in kaolin/sand samples showing an increase with increased sand content and a decrease with increased water content based on mass

Figure 7.56 on page 259, shows the thermal conductivity at 50%, 100%, 150% and 200% of the liquid limit. The results show that for water content below the liquid limit, when the soil is considered a solid, there is a linear relationship between thermal conductivity and sand content. If the water content is 26%, the same as the water content of the saturated sand used in this study, then the predicted  $k_{\text{mass}}$  for saturated sand is 3.47W/m.K, which is less than that determined from the heat transfer equation (3.79W/m.K but this is closer in value than that based on the volumes of the constituents. However, the thermal conductivity of a sand with a water content of 107% is tending towards that of water which suggests that this may be a better method to produce the thermal conductivity of sand/clay soils.

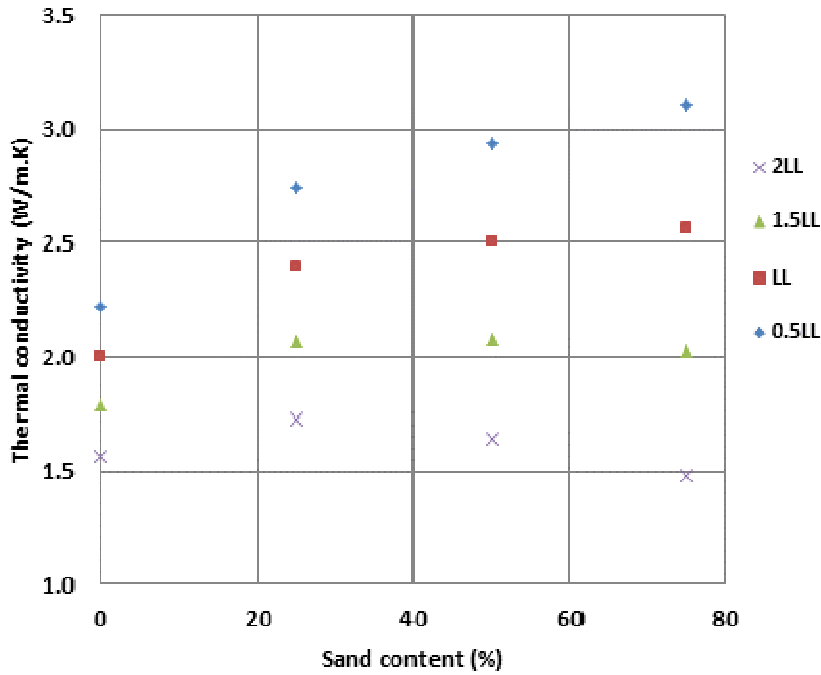


Figure 7.56: Relationship between thermal conductivity and sand content at various levels of saturation based on mass

Figure 7.57 shows a comparison between the predicted values of thermal conductivity using Equation 7.3, and those determined directly using the heat transfer equation (Equation 7.1). It shows that the predicted values based on mass are closer to the values determined from the heat transfer equation than those predicted from the volume. This is not absolute as more data is required to validate this proposal.

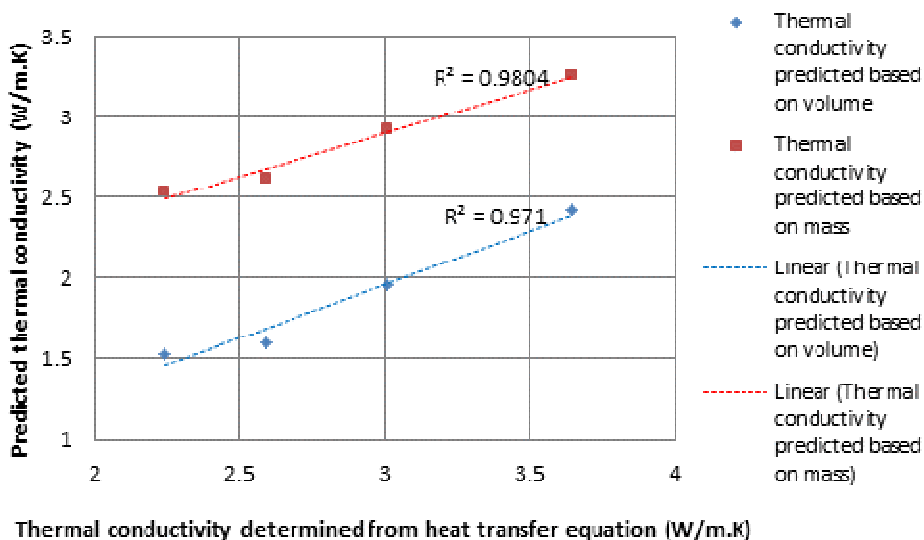


Figure 7.57: Comparison of thermal conductivity values of determined from the heat transfer equation and those predicted based on the mass and volume of the sample constituents



## 7.9 Effect of Temperature (Power input)

The sample temperature was controlled by the current and voltage (power) input introduced into the test through the cartridge heater within the test chamber. Tests were carried out at different power inputs to study the influence of temperature/power input on heat dissipation in the soil samples tested.

Samples were tested with power inputs ranging from 4.23W to 19.04W as presented in Table 7.10.

Table 7.10: Table showing the power inputs used in carrying out the tests

<b>POWER (W)</b>	RANGING FROM 4.49 TO 17.05	17.03	RANGING FROM 4.23 TO 19.04
<b>SAMPLE GROUPS TESTED</b>	KAOLIN	KAOLIN:SAND (75:25 )	SAND
		KAOLIN:SAND (50:50)	
		KAOLIN:SAND (25:75)	

The heater temperature was determined by the power input which meant that lower power inputs yielded lower heater temperatures and higher power inputs yielded higher temperatures.

The different sample types also had different power requirements to achieve the same temperature, which was also the case with the same sample type at different water contents or different consolidation pressure.

To show how the same sample responded to different power inputs, a kaolin sample at 82% water content and consolidation pressure of 25kPa, was tested at different power inputs and the results obtained are presented in Figure 7.58 on page 261.

The graph shows the different responses of the sample to the different power inputs. The main difference noted was the time to equilibrium and the maximum temperatures attained.

At a power input of 4.49W, the sample reached equilibrium in approximately 20 hours at a maximum temperature of 23.3°C. At a power input of 9.48W, the same sample reached equilibrium after 25 hours at a maximum temperature of 28°C. And at a power input of 17.05W, it reached equilibrium after 42 hours, at a maximum temperature of 34°C.

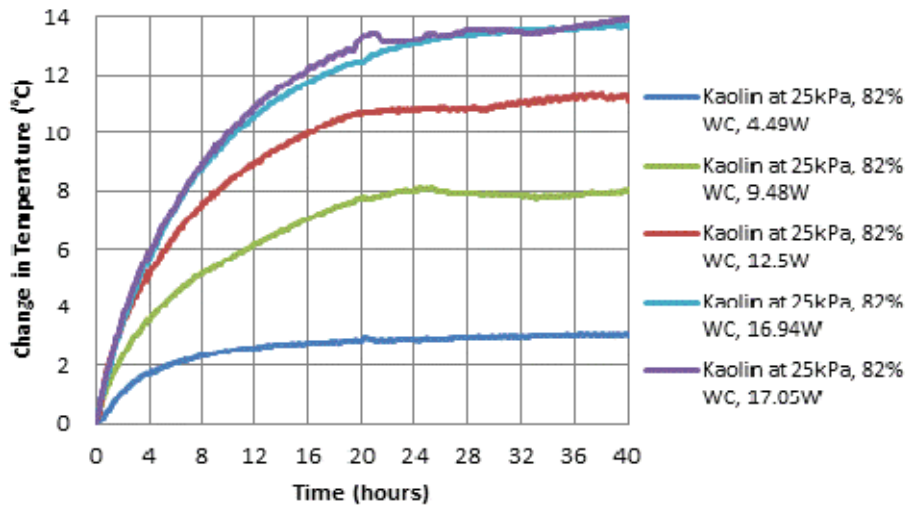


Figure 7.58: Heating curves of the same soil type, kaolin at 82% water content and consolidation pressure but at different power inputs ranging from 4.49-17.05W

It therefore, suggests that a higher power input or higher temperature in the energy pile could result in longer time to equilibrium and a higher temperature attained in the soil composed of kaolin. A different outcome may be observed with a different soil composition.

Figure 7.59 shows variations in temperature across a sample in equilibrium condition for two different power inputs in kaolin sample at 82% water content and tested at 25kPa consolidation pressure.

The temperature variations due to both power inputs, vary from almost 3°C at the inner edge of the cell wall to approximately 10°C closer the heater.

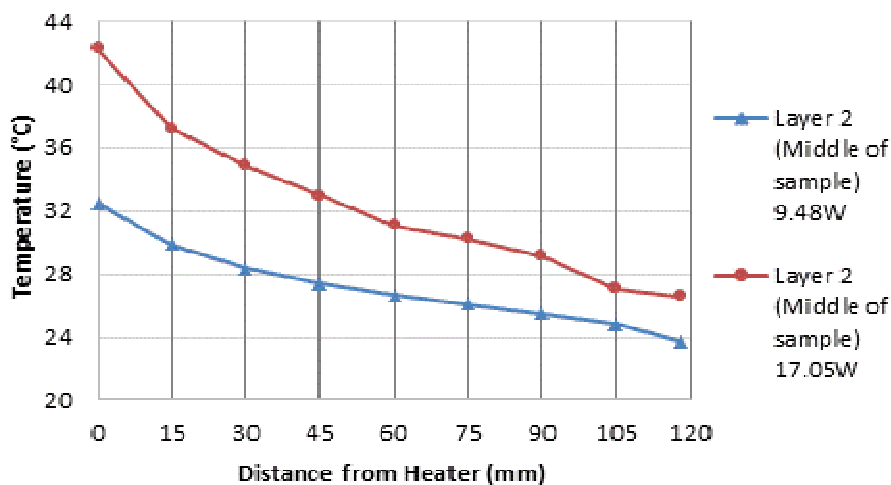


Figure 7.59: Spatial variation in temperature across the same kaolin sample at two different power inputs

## 7.10 Thermal Cycles

The samples were subjected to heating and cooling cycles to reflect heating load from a building. The thermal cycles were typically based on a 24 hour period of 8 hours heating and 16 hours cooling to reflect a typical office during a working day generating heat while cooling down overnight.

In the kaolin sample of 82% initial water content, tested at 100kPa the heating cycles were first run two hourly from 2, 4, 6, 8, 10, 12, 16, 18 20 and 22 hours heating in order to study the soil response to heating and cooling cycles. This process helped to establish the maximum heating time of the sample above which complete cooling cannot be established within a 24 hour test period. It was found that the 8 hours heating and 16 hours cooling cycles allowed the sample recover back to its initial temperature.

In the same sample, the 8 hours thermal cycles were repeated over a period of 14 days, to observe the sample thermal behaviour and if changes in behaviour would occur over time. The curves were compared and the findings which indicated no significant change, was used to establish subsequent test cycles to an average of 3-5 days cyclic tests. Further tests were then restricted to 4, 8 and 12 hours heating cycles.

For the purpose of an office building, the 8 hours thermal cycles run for five days to represent a working week was explored in the various sample types to investigate their cooling capacity over the 24 hour period. In all the samples the 8 hours thermal loading proved to allow for adequate cooling.

Figure 7.60 on page 263, shows a typical graph of 8 hours thermal cycles run for a period of five days in a kaolin:sand sample.

Thermal loads of 4, 8, 12 and 18 hours were carried out on a kaolin sample and the results of the one day cycles are presented in Figure 7.61 (page 263), to show how the sample responded to the thermal loads and to what extent it cooled down within the 24 hour period.

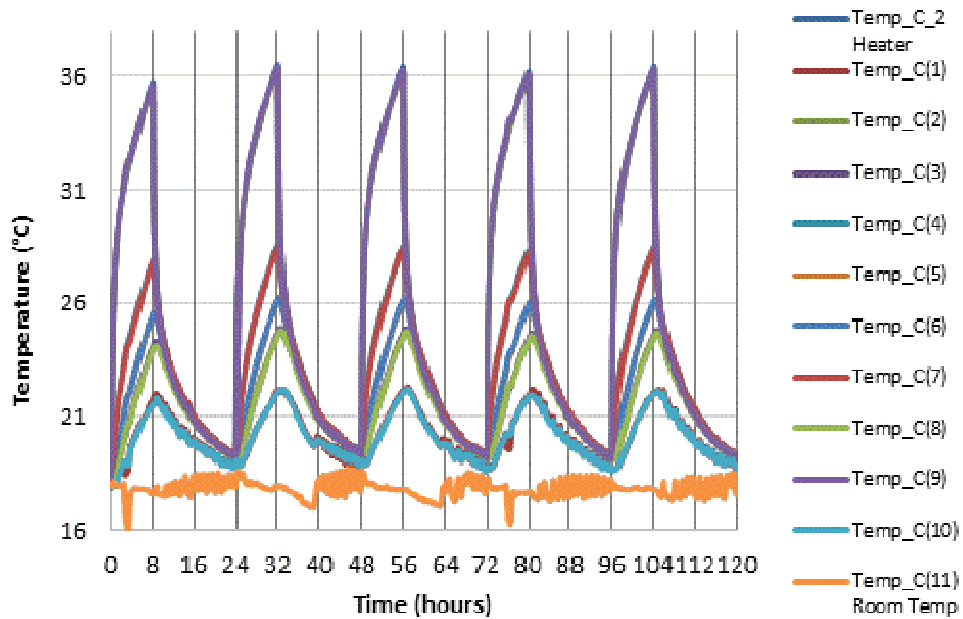


Figure 7.60: Thermal loading cycles of 8 hours heating and 16 hours cooling in 75:25 kaolin:sand sample at 25kPa and 17.03W

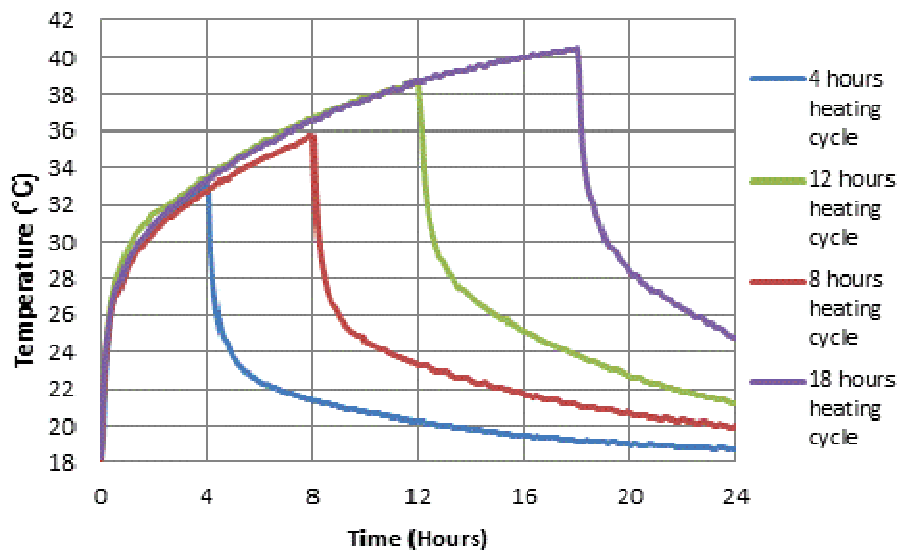


Figure 7.61: 4, 8, 12 and 18 hours heating cycles on a kaolin sample tested over a 24 hour period to study to what degree cooling was established within time

The samples were subjected to thermal cyclic tests to investigate the effect of 8 hours thermal loads on the soil thermal behaviour. The maximum temperature reached when in thermal equilibrium was compared with the maximum temperature reached during an 8 hour thermal load.

A kaolin sample at 84.5% water content, heated with a power input of 17.03W and at zero consolidation pressure, reached a maximum temperature of 28.4°C after 8 hours thermal load, and a maximum of 34.1°C when it reached equilibrium at 36 hours of heating.

Running the 8 hours thermal load on this sample, required the use of approximately 63% of its maximum equilibrium capacity.

Similarly, a kaolin sample of about 48% water content, heated with a power input of 17.03W, reached a maximum temperature of 28.5°C after 8 hours thermal load, and a maximum temperature of 32.9°C when it reached equilibrium at 32 hours of heating.

Running the 8 hours thermal load on this sample, required the use of almost 70% of its maximum equilibrium capacity.

The same kaolin sample at about 42% water content, heated at a power input of 17.03W, reached a maximum temperature of 27.2°C after 8 hours thermal load, and a maximum of 33.9°C when it reached equilibrium at 48 hours of heating.

Running the 8 hours thermal load on this sample, required the use of about 57% of the sample maximum equilibrium capacity.

Figure 7.62 shows the peak temperatures attained by the three kaolin samples with respect to the duration of heating they were subjected to.

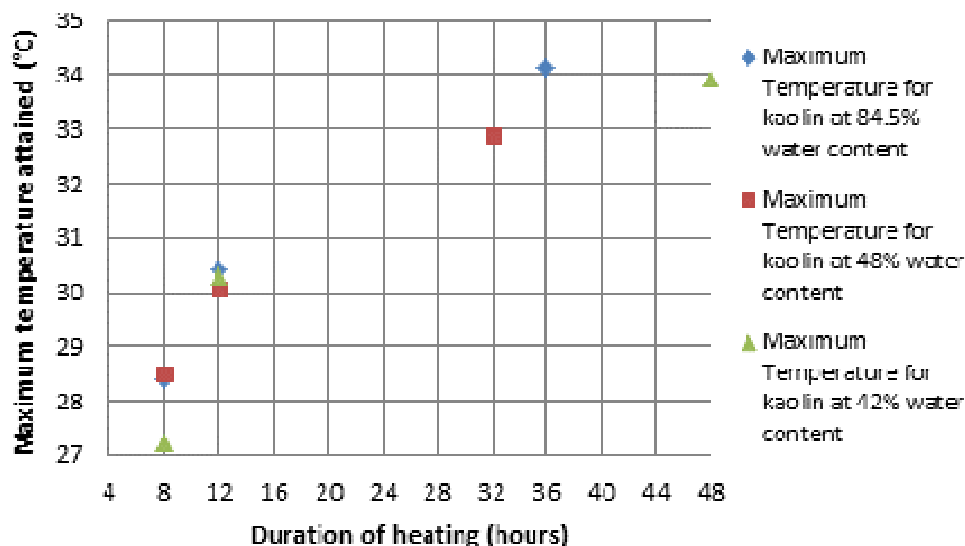


Figure 7.62: Peak temperatures attained in kaolin samples of varying water contents with respect to duration of heating

A 75:25 kaolin:sand sample at 42.1% water content, heated at a power input of 17.03W , reached a maximum temperature of 27.82°C after 8 hours thermal load, and a maximum of 33.9°C when it reached equilibrium at 43 hours of heating.

Running the 8 hours thermal load on this sample, required the use of about 61% of the sample maximum equilibrium capacity.

While the same sample 75:25 kaolin:sand sample at a different water content of about 36.5%, heated at a power input of 17.03W, reached a maximum temperature of 26.9°C after 8 hours thermal load, and a maximum temperature of 32.1°C when it reached equilibrium at 40 hours of heating.

Running the 8 hours thermal load on this sample, required the use of about 62% of the sample maximum equilibrium capacity.

Figure 7.63 shows the peak temperatures attained by both 75:25 kaolin:sand samples of varying water contents with respect to their duration of heating.

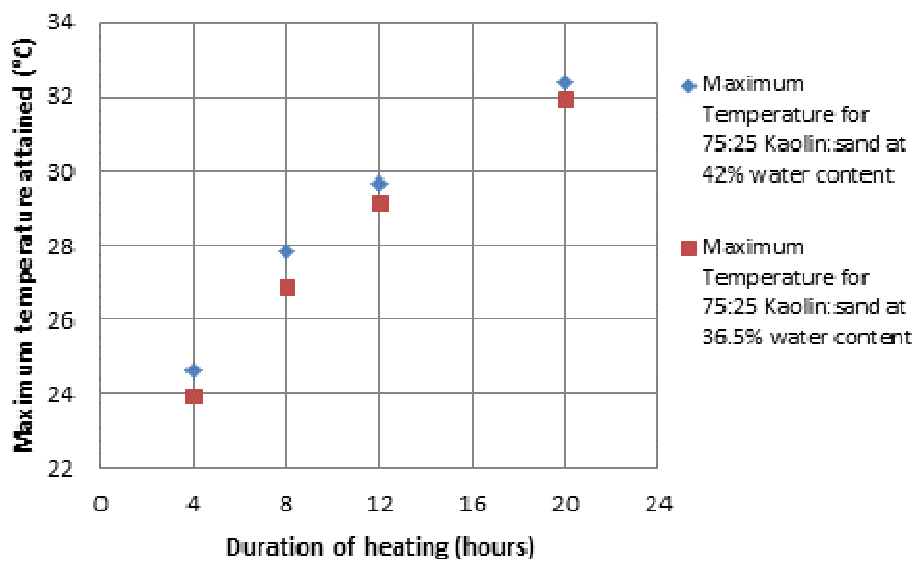


Figure 7.63: Peak temperatures attained in 75:25 kaolin:sand samples of varying water contents with respect to duration of heating

Heating a 50:50 kaolin:sand sample at 31.9% water content, at a power input of 17.03W, resulted in a maximum temperature of 27.2°C reached after 8 hours thermal load, and a maximum of 33.7°C reached at thermal equilibrium after 39 hours.

Running the 8 hours thermal load on this sample, required the use of about 58% of the sample maximum equilibrium capacity.

Similarly, a 50:50 kaolin:sand sample at 30.4% water content, heated at a power input of 17.03W, reached a maximum temperature of 27.5°C after 8 hours thermal load, and a maximum of 33.8°C when it reached equilibrium at 42 hours of heating.

Running the 8 hours thermal load on this sample, required the use of 59% of the sample maximum equilibrium capacity.

The same 50:50 kaolin:sand sample at 22.8% water content, heated at a power input of 17.03W, reached a maximum temperature of 28 °C after 8 hours thermal load, and a maximum of 33.5°C when it reached equilibrium at 43 hours of heating.

Running the 8 hours thermal load on this sample, required the use of about 64% of the sample maximum equilibrium capacity.

Figure 7.64 presents the peak thermal temperatures attained by the three samples of 50:50 kaolin:sand at varying water contents with respect to their duration of heating.

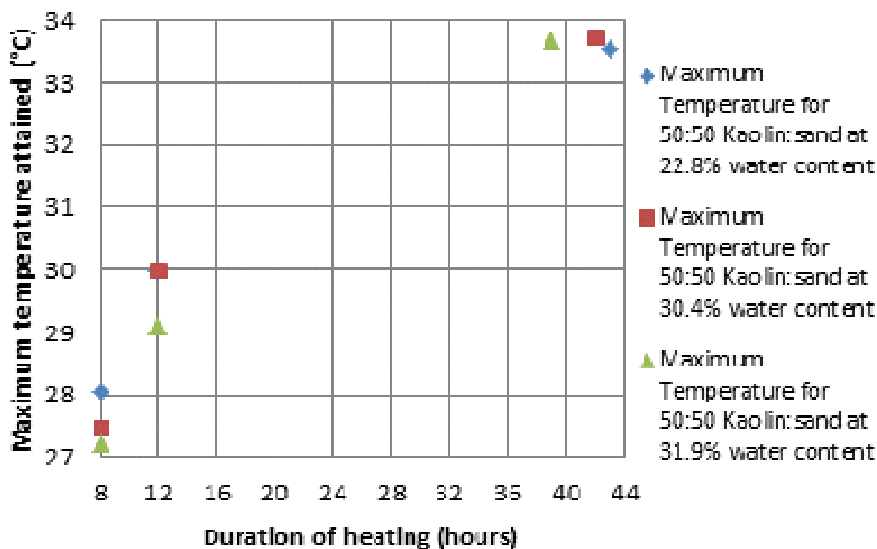


Figure 7.64: Peak temperatures attained in 50:50 kaolin:sand samples of varying water contents with respect to duration of heating

A 25:75 kaolin:sand sample at 21.5% water content, heated at a power input of 17.03W, reached a maximum temperature of 28°C after 8 hours thermal load, and a maximum of 31.8°C when it reached equilibrium at 36.5 hours of heating.

Running the 8 hours thermal load on this sample, required the use of about 72% of the sample maximum equilibrium capacity.

The same 25:75 kaolin:sand sample at 20.9% water content, heated at a power input of 17.03W, reached a maximum temperature of 27 °C after 8 hours thermal load, and a maximum of 31.8°C when it reached equilibrium at 37 hours of heating.

Running the 8 hours thermal load on this sample, requires the use of about 64% of the sample maximum equilibrium capacity.

The same sample of 25:75 kaolin:sand sample at 19.6% water content, heated at a power input of 17.03W, reached a maximum temperature of 27.5°C after 8 hours thermal load, and a maximum of 31.6°C when it reached equilibrium at 48 hours of heating.

Running the 8 hours thermal load on this sample, required the use of 69 % of the sample maximum equilibrium capacity.

Figure 7.65 shows the peak thermal temperatures attained by the three samples of 25:75 kaolin:sand at varying water contents with respect to their duration of heating

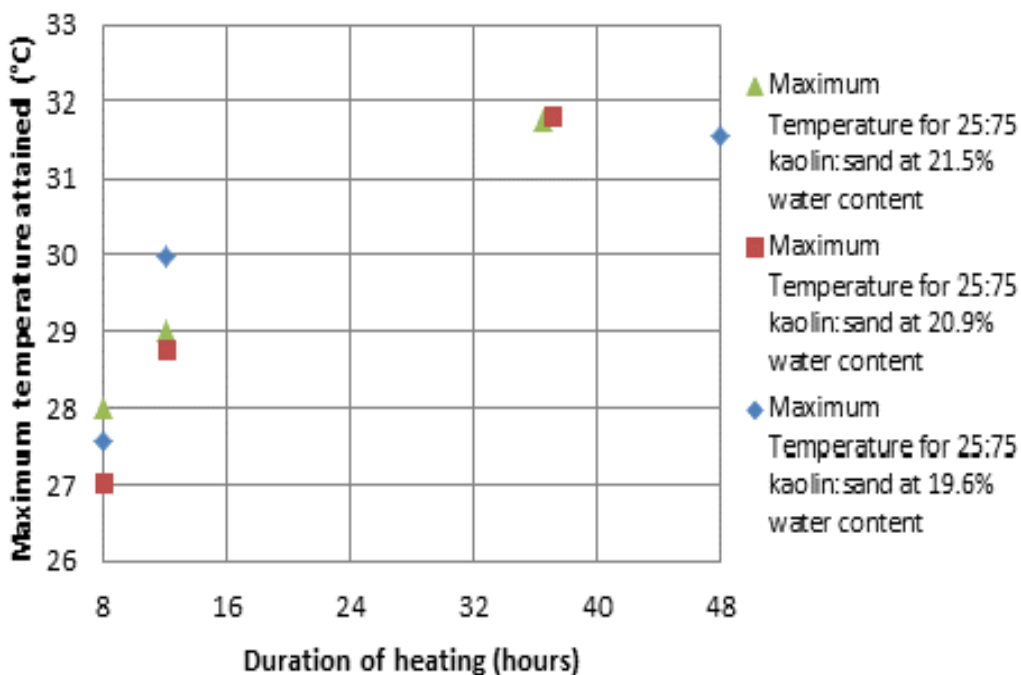


Figure 7.65: Peak temperatures attained in kaolin samples of varying water contents with respect to duration of heating

A saturated sand sample at 26% water content, heated at a power input of 19.04W and tested at 25kPa consolidation pressure, reached a maximum temperature of 28.8°C after 8 hours thermal load, and a maximum of 33.5°C when it reached equilibrium at 24.5 hours of heating.

Running the 8 hours thermal load on this sample, requires the use of about 69% of the sample maximum equilibrium capacity.



Dry sand sample heated at a power input of 4.23W and tested at 25kPa consolidation pressure, reached a maximum temperature of 24.7°C after 8 hours thermal load, and a maximum of 27.3°C when it reached equilibrium at 23.9 hours of heating.

Running the 8 hours thermal load on this sample, required the use of about 70% of the sample maximum equilibrium capacity.

Figure 7.66 shows the peak thermal temperatures attained by the dry and saturated sand samples with respect to their duration of heating.

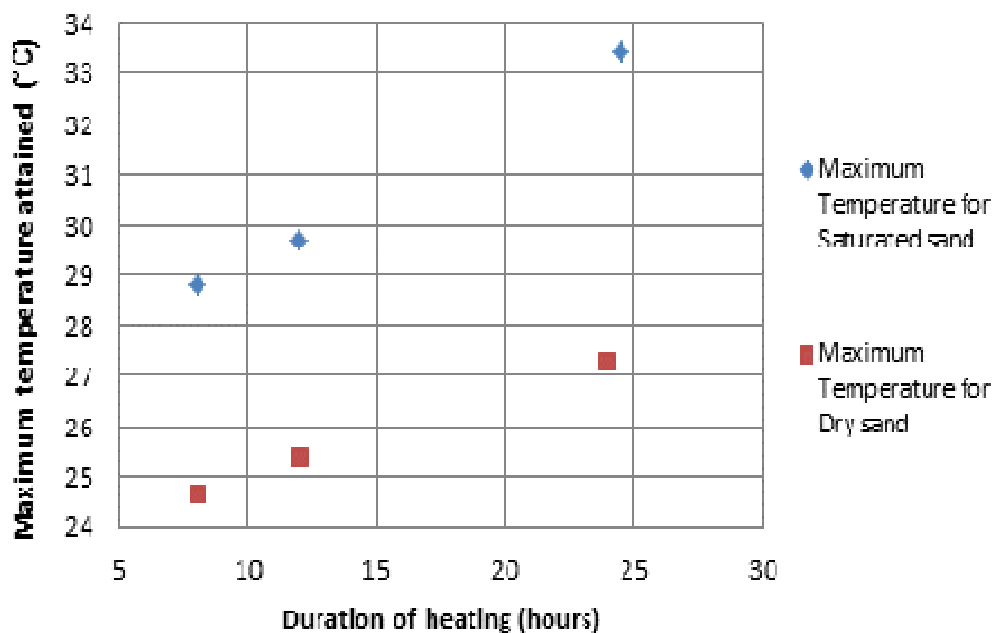


Figure 7.66: Peak temperatures attained in dry sand and saturated sand samples with respect to duration of heating

Table 7.11 on page 269, presents the maximum temperature values recorded during the thermal loading cycles and the heating of sample to equilibrium condition. Also shown in the Table are the time to equilibrium of the samples as well as a percentage value for the 8 hours thermal cyclic peak temperatures in relation to the peak equilibrium temperatures attained by the samples.

The calculated percentages range between 56% and 72% of the peak equilibrium temperatures which suggests that all the soil types tested under the varying levels of saturation and consolidation pressure will perform suitably for 8 hours thermal loading and still cool back to its initial temperature within the 24 period.

## 7.11 Sample Properties Analyzed after Thermal Tests

At the end of a test, analyses of soil properties was carried out on all the samples that had undergone thermal tests except for the sand tests. Due to the nature of sandy soils, neither direct shear strength nor water content tests would give useful data for analyses.

From all the samples tested, a total of 729 samples were collected for water content determination after direct shear tests were carried out at the same locations tested.

Table 7.11: Summary of maximum temperatures at 8 hours thermal load and at equilibrium, also showing percentage temperature of sample equilibrium is required for 8 hours thermal cycles

Sample	Water content (%)	Consolidation Pressure (kPa)	Maximum Temperature at 8 hours thermal load (°C)	Maximum Temperature at equilibrium (°C)	Time to equilibrium (hours)	8 hours peak thermal load percentage temperature of equilibrium peak load (%)
Kaolin	84.5	0	28.4	34.1	36	63
Kaolin	48	100	28.5	32.9	29	70
Kaolin	42	200	27.2	33.9	48	57
75:25 kaolin:sand	42.1	25	27.8	33.9	26	61
75:25 kaolin:sand	36.5	100	26.9	32.1	40	62
50:50 kaolin:sand	31.9	25	27.2	33.7	39	58
50:50 kaolin:sand	30.4	50	27.5	33.8	42	59
50:50 kaolin:sand	22.8	100	28.1	33.5	43	64
25:75 kaolin:sand	21.5	25	28	31.8	28	72
25:75 kaolin:sand	20.9	50	27	31.8	28	64
25:75 kaolin:sand	19.6	100	27.5	31.6	48	69
Saturated sand	26	25	28.8	33.6	24.5	69
Dry sand	NA	25	24.7	27.3	24	70

To establish a relationship between the shear strength and water contents in the sample, results from both tests at the same sample location were plotted against each other.

Figure 7.67 shows the spatial variation of shear strength and water content from results gathered from the analyses of all the kaolin samples tested at different consolidation pressures, thus resulting in different post-test water contents and shear strengths.

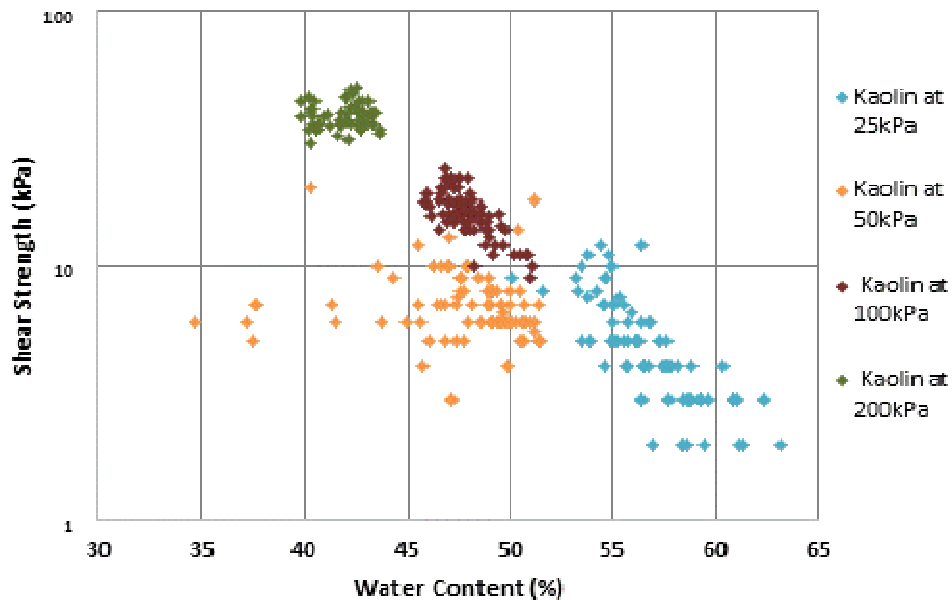


Figure 7.67: Spatial variation of shear strength and water content of four kaolin samples tested at 25, 50, 100 and 200kPa

A summary of the details of the shear strength and water content tests carried out on samples at the end of the thermal tests, is presented in Table 7.12.

Table 7.12: Table showing details of soil properties analysed after thermal tests

Sample Type	kaolin	kaolin	kaolin	kaolin	kaolin	kaolin:sand (75:25)	kaolin:sand (75:25)	kaolin:sand (50:50)	kaolin:sand (25:75)
Pressure Applied (kPa)	50	25	0 25 50	100	200	25	100	25 50 100	25 50 100
Water Content at start of Test (%)	82	82	84.5	82	82	59	59	44.4	32
No. of samples tested	109	80	80	80	60	80	80	80	80
Av. Water content at end of tests (%)	47.5	56.7	49.8	48	42	42.1	36.5	22.8	19.6
Av. Shear strength at end of tests (kPa)	7.7	5.3	11.4	16.3	38.7	5.9	17.2	28	13

The relationship between the shear strength and water content in relation to distance from the heat source indicates that the sample is stiffer and lower in water content closer to the heat source. This suggests that the soil around the energy pile is likely to be stiffer than soil further away from it.

Figure 7.68 shows a graph of the distribution of average water content in samples in relation to normal load to which they were subjected during testing.

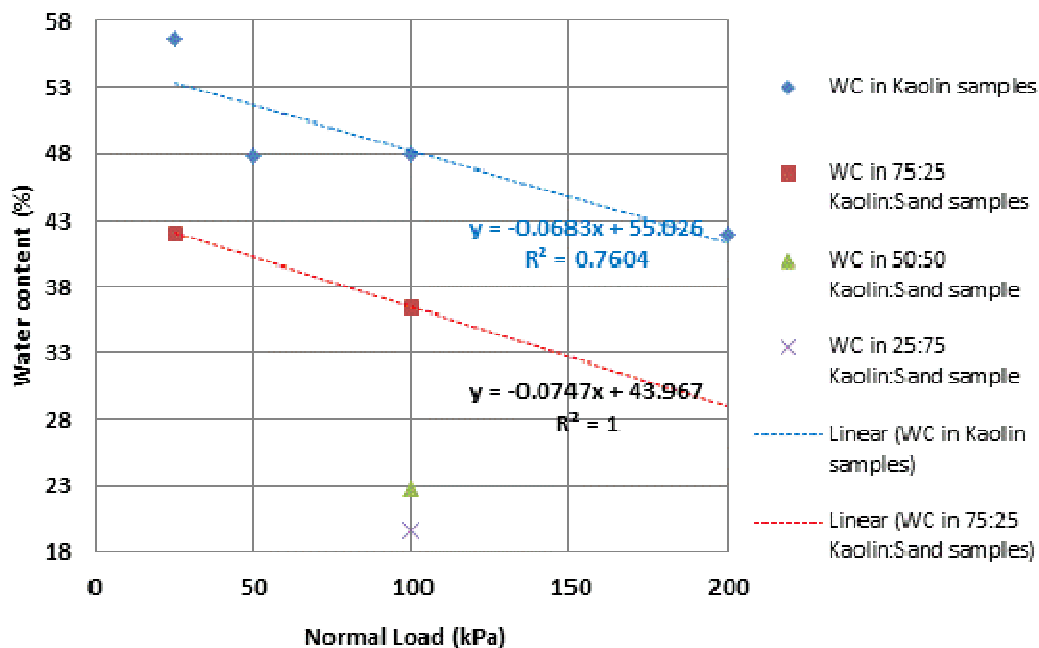


Figure 7.68: Average water content in samples at end of tests plotted against normal load applied to samples during tests

## 7.12 Chapter Summary

This Chapter dealt with the analysis, interpretation and discussion of the results obtained from the tests undertaken to show how soil water content, temperature, pressure, power input and thermal loading cycles, affected the thermal behaviour of soil with regards to heat dissipation from a simulated energy pile.

The results were successfully validated against theoretical predictions by determining the thermal conductivity values of the samples by use of heat transfer equation,, and comparing with values found in literature to show agreement.

Thermal conductivity values were also predicted by using the mass fractions of the sample constituents and thermal conductivity of the fractions. Although this was shown to be a possible basis for thermal conductivity determination, more data is required to validate this. Results obtained from this prediction, compares well with results obtained

in literature. Possible errors were identified and discussed with a view to minimize their impacts on the results obtained.

The tests were shown to be repeatable

Water content and soil composition were seen to play a very key role in influencing the thermal conductivity of the soil and hence the heat dissipation and consequently the performance of an energy pile.

Thermal conductivity was observed to increase with increased sand content of sample, and to decrease with increased water content. Temperature increase in sample also corresponded with an increase in thermal conductivity in sample.

The thermal cycles investigated within a 24 hour period (8 hours heating and 16 hours cooling) on the various sample compositions at different water contents, consolidation pressure and durations of thermal loading, suggest that they will perform suitably for cooling an office building where it is typically required for 8 hours thermal loading.

This is because the thermal cycles showed that all the sample types tested at heating cycles of up to 14 hours were able to cool back adequately to be suited to the typical heating and cooling needs of a office building

The strength of the soil was shown to increase with proximity to the heat source, while the water content of the sample on the other hand increased with distance away from the heat source.

The relationship between the shear strength and water content in relation to distance from the heat source indicates that the sample is stiffer and lower in water content closer to the heat source. This suggests that the soil around the energy pile is likely to be stiffer than soil further away from it.

Thermal equilibrium was achieved within samples tested and the time to equilibrium was shown to be determined by chiefly by sample composition, while water content and power input also influenced it, amongst other factors

Sandy samples tended to achieve thermal equilibrium faster and also cooled faster which could be both as a result of the higher thermal conductivity value of the sand content, and a possible decrease in water content due to the kaolin particles filling the voids between the sand particles and replacing the water. Hence resulting in a higher thermal conductivity in the sample and shorter time to equilibrium than in the predominantly kaolin samples.

Sandy samples also attained lower equilibrium temperatures compared to samples higher in kaolin content possibly due to the lower specific heat capacity of wet sand (1632J/Kg.K) relative to wet kaolin (2362J/Kg.K).

The samples higher in water content took longer to cool possibly due to the higher specific capacity of water relative to those of sand and kaolin.

The thermal behaviour of the soil samples tested was shown to be unaffected after being subjected to series of tests over a prolonged period of up to 19 weeks.

## **Chapter 8 Overall Conclusions and Recommendation for Further Work**

### **8.1 Introduction**

This research was undertaken to investigate the thermal behaviour of the soil around a simulated energy pile as influenced by soil type, water content, temperature, pressure, time and thermal cycles. Investigations were carried out which sought to identify the parameters that had the most influence on thermal behaviour, so as to recommend the factors to be considered when designing an energy pile system, especially as a means of cooling an office building, and to make original contribution to knowledge while adding to existing data. This target was achieved as presented in this Chapter.

A novel experimental test rig and laboratory procedures for operating it, were designed and developed to study heat dissipation radially by conduction from a linear heat source within a soil mass, modelled to depict a scenario typical to that of an energy pile exchanging heat with the surrounding soil while being subjected to overburden pressure.

In a bid to establish a relationship between specific soil properties and the performance of an energy pile, a series of tests were carried out on prepared soil samples in the fabricated test rig to investigate their thermal behaviour and to record changes in heat dissipation influenced by controlling and varying the soil composition, water content, overburden pressure, temperature, time and thermal cycles.

### **8.2 Research Conclusions**

In the course of the research, data on subsurface heat transfer were generated and analyzed from which key findings were made. On the basis of these findings and the original contributions made through this research, some conclusions were reached at the end of the research. They are presented below under the objectives for carrying them out.

#### **8.2.1 Establishing the use of the ground as a low grade energy source**

The use of the GSHPs of which an energy pile constitutes a closed system, was identified as a method primarily used to abstract heat from the ground by relying on heat transfer by conduction from the surrounding soil. The technology converts the low

grade energy of the ground into usable form. Energy is stored in the ground, and in soils the most important means of heat transfer between the building and the ground is through conduction. Factors that affect heat flow and thermal behaviour of the ground such as soil type, water content, overburden pressure, temperature and thermal cycles were identified for investigation.

### **8.2.2 Designing and developing of test rig to investigate the thermal behaviour of soil around a model energy pile**

A test rig was developed using classic predictions of thermal behaviour that allowed for the investigation of thermal behaviour of soil around an energy pile. Ground conditions were simulated by creating an axisymmetric problem similar to an installed energy pile. The characteristics of the tests to be undertaken in terms of dimensions of the test rig, materials to be used for its fabrication, variables to be controlled, and parameters to be measured were determined from an analysis of the laboratory scale test.

The test rig was designed and successfully fabricated which allowed a range of tests to be undertaken to simulate an energy pile under cyclic thermal loading based on a 24hour cycle to simulate an office environment.

### **8.2.3 Developing of test procedure for carrying out experiments to study heat dissipation in soil and the effects of cooling of buildings over a typical diurnal cycle, and the Validation of results**

A test procedure was developed for running the experiments. The soil types tested were selected as 100% kaolin, 100% sand and various combinations of both in the proportions of 75:25, 50:50 and 25:75, which allowed for the influence of sand content to be investigated. The sample preparation method was established by carrying out preliminary tests in the laboratory, and the test procedure which was also developed through carrying out preliminary tests, allowed for changes in heat flow influenced by soil water content, temperature, overburden pressure, thermal cycles and the power input to the system to be monitored.

A protocol was developed for measuring and recording heat distribution within the soil sample subject to varying cycles of thermal loading and unloading to simulate practical use of energy piles in an office environment. This was done by setting up the test rig and placing thermocouples at specific distances within the soil sample in the test rig through the openings along the sides of the test chamber. The thermocouples were connected to a data-logger which was programmed to record the temperature changes



within the soil samples. The recorded data were retrieved through the use of a computer with relevant software installed for the purpose. This allowed for the thermal properties of samples in terms of temperature variations within the soil, time taken to achieve equilibrium conditions and time taken to cool back to controlled room temperature to be determined.

The results of the tests conducted during this research were presented in chapters 5 and 6, and several findings were made based on these results in line with the research objectives.

Adequate consideration was given to possible errors identified with the experimental procedure, with a view to minimize their impacts on the results obtained.

The experiments showed repeatability which will enable other researchers carry out experiments using the test rig with consistent results. The results were successfully validated against theoretical predictions. Variations in temperature of different soil compositions were determined to be mostly radial, and the data obtained was used to calculate thermal conductivity values of the different soil samples using the heat transfer equation. The values obtained from the experimental data for the different soil compositions (sand, kaolin and their combination in different proportions) at different water contents varying from about 20% to 85%, ranged from 0.45W/m.K to 3.81W/m.K and are similar to values given in literature as ranging between 0.15W/m.K and 7.8W/m.K for similar soil types at similar water contents. Kaolin samples ranging from 42% - 85% water content showed thermal conductivity values of 1.46W/m.K - 2.58W/m.K. The samples composed of sand and kaolin combinations in proportions of 75:25, 50:50 and 25:75, gave thermal conductivity values ranging from 2.0W/m.K – 3.81W/m.K, for water contents ranging from 19% – 42%. The thermal conductivity values obtained for dry sand were between 0.45W/m.K and 0.54W/m.K, and for saturated sand, 2.84W/m.K – 3.49W/m.K.

A relationship was established between the values of thermal conductivity obtained from the kaolin samples, and the water content of the samples. The samples higher in water content showed lower thermal conductivity values which was expected due to the influence of the lower thermal conductivity value of water given as 0.6W/m.K from literature.

Water content and soil composition were observed to play an important role in influencing the thermal conductivity of the soil and hence heat dissipation and therefore, the performance of an energy pile

Thermal conductivity was seen to increase with increased sand content of sample, and to decrease with increased water content. An increase in sample temperature also corresponded with an increase in thermal conductivity of sample.

The thermal conductivity value of the dry sand sample was much lower than that of the saturated sand, because, although quartz has a high thermal conductivity value of 7.8-8.79W/m.K, air has a very low thermal conductivity value of 0.025 W/m.K. It follows therefore, that the possible presence of air in the dry sand sample, is responsible for the low thermal conductivity value of 0.54 W/m.K obtained.

Thermal conductivity predicted by using the mass fractions of the sample constituents and thermal conductivity of the fractions, were shown to be a possible basis for thermal conductivity determination, but requires more data to validate. However, the results obtained from this prediction, were close in value to the results obtained from the use of the heat transfer equation

Measured and predicted temperature variations within the tested samples, with respect to distance from the heater were compared. The fit of both data showed strong relationships between them.

With the validation of the experiment and test procedure, this laboratory based test rig developed could be used to test site specific samples for their extensive thermal behaviour while at the same time determine their thermal conductivity values with reference to their intended use.

#### **8.2.4 Determining the effects of soil type, water content, temperature, overburden pressure, time and thermal cycles on the thermal performance of an energy pile**

Thermal equilibrium was successfully achieved within samples tested although the time to equilibrium in almost all the samples exceeded the diurnal cycle.

The time to equilibrium was shown to be mainly influenced by sample composition, followed by water content and magnitude of temperature amongst other factors.

With regards to how quickly the different soil types tested reached equilibrium temperatures at a constant power supply, and how quickly they cooled back to their initial temperatures, the samples higher in sand composition reached thermal equilibrium faster than the other samples lower in sand content, while at the same time, having the lowest maximum temperature compared to the other samples higher in kaolin content. This is likely due to the lower specific heat capacity of wet sand (1632J/Kg.K) relative to wet kaolin (2362J/Kg.K).

The sandy samples also cooled faster which could be both as a result of the higher thermal conductivity of the sand content, and a likely decrease in water content due to the kaolin particles replacing water while filling the voids between the sand particles. This will result in a higher thermal conductivity in the sample and shorter time to equilibrium than in the predominantly kaolin samples.

The samples higher in water content took a longer time to cool, possibly due to the higher specific capacity of water relative to those of sand and kaolin.

The influence of water content and consolidation pressure on the duration of reaching equilibrium in the various samples was observed to increase significantly in samples tested at higher pressures and thus lower water content.

It can therefore, be concluded that although the influence of water content and consolidation pressure on the duration of heating was observed to increase with an increase in pressure (lower water content), but at the same time the increase in the duration was observed to be dependent on the soil type. The soil type therefore, had greater influence on the soil thermal behaviour than water content or overburden pressure. The higher the thermal load or temperature the sample is subjected to, the longer it takes to reach thermal equilibrium and vice versa.

### **8.2.5 Studying the effects of thermal cyclic loading on an energy pile to determine what impact the thermal cycles have on the soil properties**

Although the time to reach equilibrium varied between the soil types, it was observed that after 12 hours of heating, up to 80% of the equilibrium temperature is reached, and after 16 hours of heating in most of the samples, up to 89% of the equilibrium temperatures are achieved. By the end of 24 hours, up to 97% of the equilibrium temperatures are reached. Therefore, while most samples vary in their heating duration, by the end of 24 hours, almost all the samples are very close to their equilibrium temperatures. Thus an average duration of 24 hours thermal load would get most samples close to their equilibrium capacity. In cooling capacity for the soil to return to its initial state, a minimum duration of 16 hours is required to reach 94% of its initial temperature which is adequate for cooling an office building.

Thermal cyclic tests carried out for 8 hours to represent the heating load from an office building, and 16 hours to cool back was repeated over a period of 14 days. A comparison of the experimental data obtained from both the first and last days of the cyclic tests showed no noticeable difference in the soil thermal properties. Therefore, when the soil around an energy pile in an office building is subjected to 8 hours

thermal cyclic loading, the 16 hours overnight period is adequate for the soil to cool back to its initial state and so is not affected in the long-term by residual temperatures. To buttress this, temperature variation test measurements were carried out on a kaolin sample tested at 100kPa both at the beginning of the tests, and after approximately 19 weeks of being subjected to heating and cooling tests. Results from both tests when compared, showed no noticeable difference in the soil thermal properties, as they remained unchanged even after being subjected to series of tests over the prolonged period.

All the soil types when subjected to 8 hours thermal loading cycle were able to cool back to the initial temperature within a 24 hour period that is, after 16 hours of cooling. Therefore, it is possible to operate a heating and cooling cycle in a 24 hour period. This is because the time to attain thermal equilibrium in the samples far exceeds 8 hours. For example, the sample made up of 50:50 kaolin:sand combination, when subjected to the 8 hours thermal loading cycle, attained a maximum temperature of 27.2°C, as against its peak temperature of 33.7°C when thermal equilibrium is attained after 39 hours.

For the thermal cycles run at 12 and 14 hours of heating with subsequent cooling for 12 and 10 hours (i.e. the 24hr cycle), a sample was still able to achieve some percentage of cooling but in the long-term there was a build up of residual heat in the soil. Thermal cycles run beyond 14 hours within a 24 hour period are not recommended as the case of cycles run at 18 and 22 hours of heating did not allow the sample sufficient cooling period and resulted in residual heat in the sample.

It can be concluded that the thermal cycles investigated within a 24 hour period (8 hours heating and 16 hours cooling) on the various sample compositions investigated at different water contents, consolidation pressure and durations of thermal loading, suggest that they will perform suitably for cooling an office building where it is typically required for 8 hours thermal loading.

The variation in shear strength and water content within samples, measured in relation to distance from heat source and different levels of sample height showed the shear strength of the soil to increase towards the heat source, while the water content of the sample increased with distance away from the heat source. This means lower water contents, and higher shear strength values around the heat source, and higher water contents and lower shear strength values further away from the heat source. This may have implications on the axial capacity of an energy pile.

### **8.3 Recommendations for Further Work**

In the course of this research, certain areas were identified, which if investigated further, promises to be of interest while also broadening the scope of the research already carried out. It is recommended therefore, that further work be carried out in the areas highlighted below.

Further work could be carried out to investigate arrangements of energy piles to assess the interaction of the thermal behaviour of individual piles so that the efficiency of an energy piled foundation could be determined. The test rig was designed with provisions made for these interactions to be investigated.

The water content and strength of the samples varied as a result of the transfer of heat from the energy pile to the ground. This means the load carrying capacity of the energy pile will change over time and is worth investigating further. The rig can be adapted to assess this effect.

Tests were carried out on sand, kaolin and mixtures of sand and kaolin at different water contents and overburden pressures. This can be extended to a wider range of soil compositions in order to investigate the relationship between soil type, water content and thermal conductivity and the effect they have on the performance of energy piles.

Studying a larger sample size which will mean that these laboratory scale tests can be scaled up to pilot tests to establish whether the behaviour observed in the laboratory is representative of the field.

With the exception of the dry sand, all other samples tested were fully saturated to begin with. Of interest will be the investigation of partially saturated samples. This will enable other soil properties to be investigated in more detail.

This research focused on cooling of buildings by sending heat to the ground. A similar study could be carried out in the case of the reverse, which is abstracting heat from the soil by cooling it.

In the area of predicting thermal conductivity by using the mass fractions of the sample constituents and thermal conductivity of the fractions, further research is required to provide more data to aid in validating this proposal.

## References

- Abdelaziz, S.L. and Ozudogru, T.Y. 2016. Selection of the design temperature change for energy piles. *Applied Thermal Engineering*. **107**, pp.1036-1045.
- Abuel-Naga, H., Raouf, M.I.N., Raouf, A.M.I. and G., N.A. 2015a. Energy piles: current state of knowledge and design challenges. *Environmental Geotechnics*. **2**(4), pp.195-210.
- Abuel-Naga, H., Raouf, M.I.N., Raouf, A.M.I. and Nasser, A.G. 2015b. Energy piles: current state of knowledge and design challenges. *Environmental Geotechnics*. **2**(4), pp.195-210.
- Abuel-Naga, H.M., Bouazza, B.A. and Ramana, G. 2007. Volume change behaviour of saturated clays under drained heating conditions: experimental results and constitutive modeling. *Canadian Geotechnical Journal*. **44**(8), pp.942-956.
- Adam, D. and Markiewicz, R. 2009. Energy from earth-coupled structures, foundations, tunnels and sewers. *Geotechnique*. **59**(3), pp.229-236.
- Al-Moadhen Muataz, Clarke Barry G. and Chen Xiaohui 2017. Hydraulic conductivity of composite soils. *Proceedings of the 2nd Symposium on Coupled Phenomena in Environmental Geotechnics (CPEG2), Leeds, UK 2017*.
- Arkhangelskaya, T. and Lukyashchenko, K. 2018. Estimating soil thermal diffusivity at different water contents from easily available data on soil texture, bulk density, and organic carbon content. *Biosystems Engineering*. **168**, pp.83-95.
- Aysen, A. 2002. *Soil mechanics: basic concepts and engineering applications*. Lisse, The Netherlands: A.A. Balkema Pub.
- Badescu, V., Laaser, N. and Crutescu, R. 2010. Warm season cooling requirements for passive buildings in Southeastern Europe (Romania). *Energy*. **35**(8), pp.3284-3300.
- Banks, D. 2008. *An introduction to thermogeology : ground source heating and cooling*. Oxford: Blackwell.
- Bayer, P., Saner, D., Bolay, S., Rybach, L. and Blum, P. 2012. Greenhouse gas emission savings of ground source heat pump systems in Europe: A review. *Renewable and Sustainable Energy Reviews*. **16**(2), pp.1256-1267.
- Bevington, P.R. and Robinson, D.K. 1992. *Data reduction and error analysis for the physical sciences*. New York: WCB/McGraw-Hill.
- Blum, P., Campillo, G., Münch, W. and Kölbl, T. 2010. CO<sub>2</sub> savings of ground source heat pump systems - A regional analysis. *Renewable Energy*. **35**(1), pp.122-127.

- Bourne-Webb, P.J., Amatya, B.L., SOGA, K., AMIS, T., Davidson, C. and Payne, P. 2009. Energy pile test at Lambeth College, London: geotechnical and thermodynamic aspects of pile response to heat cycles. *Géotechnique*. **59**(3), pp.237-248.
- Bourne-Webb, P.J., Freitas, T.M.B. and Assuncao, R.M.F. 2016. Soil-pile thermal interactions in energy foundations. *GEOTECHNIQUE*. **66**(2), pp.167-171.
- Boyle, G. 2004. *Renewable energy / editor, Godfrey Boyle*. 2nd ed. ed. Oxford :: Oxford University Press in Association with The Open University.
- Brandl, H. 2006. Energy foundations and other thermo-active ground structures. *Geotechnique*. **56**(2), pp.81-122.
- Bristow, K.L., Kluitenberg, G.J., Goding, C.J. and Fitzgerald, T.S. 2001. A small multi-needle probe for measuring soil thermal properties, water content and electrical conductivity. *Computers and Electronics in Agriculture*. **31**(3), pp.265-280.
- British Petroleum. 2012. *World Energy Review* [Online]. [Accessed 11 December 2012]. Available from:  
[http://www.bp.com/assets/bp\\_internet/globalbp/globalbp\\_uk\\_english/reports\\_and\\_publications/statistical\\_energy\\_review\\_2011/STAGING/local\\_assets/pdf/statistical\\_review\\_of\\_world\\_energy\\_full\\_report\\_2012.pdf](http://www.bp.com/assets/bp_internet/globalbp/globalbp_uk_english/reports_and_publications/statistical_energy_review_2011/STAGING/local_assets/pdf/statistical_review_of_world_energy_full_report_2012.pdf)
- Britto, A.M., Savvidou, C., Maddocks, D.V., Gunn, M.J. and Booker, J.R. 1989. Numerical And Centrifuge Modeling Of Coupled Heat-Flow And Consolidation Around Hot Cylinders Buried In Clay. *Geotechnique*. **39**(1), pp.13-25.
- Brook, B.W., Edney, K., Hillerbrand, R., Karlsson, R. and Symons, J. 2016. Energy research within the UNFCCC: a proposal to guard against ongoing climate-deadlock. *Climate Policy*. **16**(6), pp.803-813.
- Burghignoli, A., Desideri, A. and Miliziano, S. 2000. A laboratory study on the thermomechanical behaviour of clayey soils. *Canadian Geotechnical Journal*. **37**(4), pp.764-780.
- Busby, J. 2016. Thermal conductivity and diffusivity estimations for shallow geothermal systems. *Quarterly Journal of Engineering Geology and Hydrogeology*. **49**(2), pp.138-146.
- Busby, J., Lewis, M., Reeves, H. and Lawley, R. 2009. Initial geological considerations before installing ground source heat pump systems. *Quarterly Journal of Engineering Geology and Hydrogeology*. **42**, pp.295-306.
- Çengel, Y.A. 2005. *Fundamentals of thermal-fluid sciences*. 2nd , international edition. ed. Boston ; London: McGraw-Hill.
- CIBSE. 2004. *Energy efficiency in buildings : CIBSE guide F*. London: Chartered Institution of Building Services Engineers.

CIBSE. 2005. *Heating, ventilating, air conditioning and refrigeration : CIBSE guide B*. London: Chartered Institution of Building Services Engineers.

Clarke, B.G., Agab, A. and Nicholson, D. 2008. Model specification to determine thermal conductivity of soils. *Proceedings of the Institution of Civil Engineers-Geotechnical Engineering*. **161**(3), pp.161-168.

Committee on Climate Change. 2018. *The Climate Change Act*. [Online]. [Accessed 2018]. Available from: <https://www.theccc.org.uk/tackling-climate-change/the-legal-landscape/the-climate-change-act/>

Cui, Y.J., Le, T.T., Tang, A.M., Delage, P. and Li, X.L. 2009. Investigating the time-dependent behaviour of Boom clay under thermomechanical loading. *Geotechnique*. **59**(4), pp.319-329.

Darkwa, J., Su, W. and Chow, D.H.C. 2013. Heat dissipation effect on a borehole heat exchanger coupled with a heat pump. *Applied Thermal Engineering*. **60**(1–2), pp.234-241.

Demirbas, A. 2005. Potential applications of renewable energy sources, biomass combustion problems in boiler power systems and combustion related environmental issues. *Progress in Energy and Combustion Science*. **31**(2), pp.171-192.

Di Donna, A. and Laloui, L. 2015. Response of soil subjected to thermal cyclic loading: Experimental and constitutive study. *Engineering Geology*. **190**(0), pp.65-76.

Ellabban, O., Abu-Rub, H. and Blaabjerg, F. 2014. Renewable energy resources: Current status, future prospects and their enabling technology. *Renewable and Sustainable Energy Reviews*. **39**, pp.748-764.

Elliott, D. 2013. *Renewables: a review of sustainable energy supply options*. Bristol England (Temple Circus, Temple Way, Bristol BS1 6HG, UK): IOP Publishing.

ETSU. 1994. *An Assessment of Renewable Energy for the UK*. London: HMSO.

European Commission. 2018. *Energy Efficiency*. [Online]. [Accessed April]. Available from: <https://ec.europa.eu/energy/en/topics/energy-efficiency/buildings>

Faizal, M., Bouazza, A. and Singh, R.M. 2016. Heat transfer enhancement of geothermal energy piles. *Renewable and Sustainable Energy Reviews*. **57**, pp.16-33.

Fan, D., Rees, S. and Spitler, J. 2013. A dynamic thermal network approach to the modelling of Foundation Heat Exchangers. *Journal of Building Performance Simulation*. **6**(2), pp.81-97.

Field, C.B., Barros, V.R. and Intergovernmental Panel on Climate Change. Working, G., II. 2014. *Climate change 2014: impacts, adaptation, and vulnerability*. New York: Cambridge University Press.



- Florides, G. and Kalogirou, S. 2007. Ground heat exchangers - A review of systems, models and applications. *Renewable Energy*. **32**(15), pp.2461-2478.
- Gabrielsson, A., Bergdahl, U. and Moritz, L. 2000. Thermal energy storage in soils at temperatures reaching 90 degrees C. *Journal of Solar Energy Engineering-Transactions of the Asme*. **122**(1), pp.3-8.
- Glassley, W.E. 2010. *Geothermal energy renewable energy and the environment*. [Online]. Boca Raton: CRC Press,. Available from: <http://0-marc.crcnetbase.com.wam.leeds.ac.uk/isbn/9781420075717>
- Glassley, W.E. 2015. *Geothermal energy: renewable energy and the environment*. Boca Raton, FL: CRC Press.
- Goodman, S.N., Fanelli, D. and Ioannidis, J.P.A. 2016. What does research reproducibility mean? *Science Translational Medicine*. **8**(341), pp.341ps312-341ps312.
- Hamdhan, I.N. and Clarke, B.G. 2010. Determination of thermal conductivity of coarse and fine sand soils. In: *Proceedings of World Geothermal Congress*.
- Head, K.H. 2006. *Manual of soil laboratory testing: Vol. 1, Soil classification and compaction tests*. 3rd ed. Boca Raton, FL;Dunbeath, Scotland;: Whittles.
- Head, K.H. and Epps, R. 2011. *Manual of soil laboratory testing: Volume 2, Permeability, shear strength and compressibility tests*. Third ed. Caithness, Scotland;Boca Raton, FL;: Whittles Pub.
- Hemmingway, P. and Long, M. 2012. Design and development of a low-cost thermal response rig. *Proceedings of the Institution of Civil Engineers - Energy*. **165**(3), pp.137-148.
- Incropera, F.P. 2007a. *Fundamentals of heat and mass transfer*. 6th ed. Hoboken, N.J.: Wiley.
- Incropera, F.P. 2007b. *Introduction to heat transfer*. Hoboken NJ: Wiley.
- International Energy Agency. 2018. *Global Energy & CO2 Status Report*. [Online]. [Accessed April]. Available from: <https://www.iea.org/geco/>
- International Workshop on Effects of Expected Climate Change on Soil Processes in the T. and Sub, t. 1990. *Soils on a warmer earth*. Amsterdam ; Oxford: Elsevier.
- Janna, W.S. 1988. *Engineering heat transfer*. SI ed. London: Van Nostrand Reinhold International.
- Kalantidou, A., Pereira, J.M., Tang, A.M. and Hassen, G. 2012. Preliminary study on the mechanical behaviour of heat exchanger pile in physical model. *Geotechnique*. **62**(11), pp.1047-1051.

- Kharseh, M., Al-Khawaja, M. and Suleiman, M.T. 2015. Potential of ground source heat pump systems in cooling-dominated environments: Residential buildings. *Geothermics*. **57**(0), pp.104-110.
- Knappett, J. and Craig, R.F. 2012. *Craig's soil mechanics*. 8th ed. London: Spon Press.
- Laloui, L. and Di Donna, A. 2011. Understanding the behaviour of energy geo-structures. *Proceedings of the Institution of Civil Engineers-Civil Engineering*. **164**(4), pp.184-191.
- Laloui, L., Nuth, M. and Vulliet, L. 2006. Experimental and numerical investigations of the behaviour of a heat exchanger pile. *International Journal for Numerical and Analytical Methods in Geomechanics*. **30**(8), pp.763-781.
- Lee, J., Kim, Y.S., Kim, H.S., Kang, J.M. and Bae, G.J. 2011. Evaluation of Methods For Predicting Thermal Conductivity of Saturated Unfrozen Kaolinite. In: *The Twenty-first International Offshore and Polar Engineering Conference, 2011/1/1/, Maui, Hawaii, USA*. ISOPE: International Society of Offshore and Polar Engineers.
- Li, S., Yang, W. and Zhang, X. 2009. Soil temperature distribution around a U-tube heat exchanger in a multi-function ground source heat pump system. *Applied Thermal Engineering*. **29**(17–18), pp.3679-3686.
- Lim, T.H., De Kleine, R.D. and Keoleian, G.A. 2016. Energy use and carbon reduction potentials from residential ground source heat pumps considering spatial and economic barriers. *Energy and Buildings*. **128**, pp.287-304.
- Liu, G. and Si, B.C. 2011. Single- and Dual-Probe Heat Pulse Probe for Determining Thermal Properties of Dry Soils. *Soil Science Society of America Journal*. **75**(3), pp.787-794.
- Loveridge, F., Low, J. and Powrie, W. 2017. Site investigation for energy geostructures. *Quarterly Journal of Engineering Geology and Hydrogeology*. **50**(2), pp.158-168.
- Loveridge, F. and Powrie, W. 2012. Pile heat exchangers: thermal behaviour and interactions. *Proceedings of the ICE - Geotechnical Engineering*. pp.1-19.
- Lyons, L. 1991. *A practical guide to data analysis for physical science students*. Cambridge: Cambridge University Press.
- Mensah, K., Jang, Y.-S. and Choi, J.M. 2017. Assessment of design strategies in a ground source heat pump system. *Energy and Buildings*. **138**, pp.301-308.
- Mills, A.F. 1999. *Basic heat and mass transfer*. Upper Saddle River, N.J.: Prentice Hall.
- Mitchell, J.K. and Soga, K. 2005. *Fundamentals of Soil Behavior (3rd Edition)*. John Wiley & Sons. Available from:  
<http://app.knovel.com/hotlink/toc/id:kpFSBE0002/fundamentals-soil-behavior/fundamentals-soil-behavior>

- Nathanail, J. and Banks, V. 2009. Climate change: implications for engineering geology practice. *Geological Society, London, Engineering Geology Special Publications*. **22**(1), pp.65-82.
- Omer, A.M. 2008. Ground-source heat pumps systems and applications. *Renewable & Sustainable Energy Reviews*. **12**(2), pp.344-371.
- Preene, M. and Powrie, W. 2009a. Ground energy systems: delivering the potential. *Proceedings of the ICE - Energy*. **162**(2), pp.77-84.
- Preene, M. and Powrie, W. 2009b. Ground energy systems: from analysis to geotechnical design. *Geotechnique*. **59**(3), pp.261-271.
- Rees, S.J. 2015. An extended two-dimensional borehole heat exchanger model for simulation of short and medium timescale thermal response. *Renewable Energy*. **83**, pp.518-526.
- Rees, S.W., Adjali, M.H., Zhou, Z., Davies, M. and Thomas, H.R. 2000. Ground heat transfer effects on the thermal performance of earth-contact structures. *Renewable & Sustainable Energy Reviews*. **4**(3), pp.213-265.
- Rybach, L. 2012. 7.06 - Shallow Systems: Geothermal Heat Pumps A2 - Sayigh, Ali. *Comprehensive Renewable Energy*. Oxford: Elsevier, pp.189-207.
- Saggu, R. and Chakraborty, T. 2015. Thermal analysis of energy piles in sand. *Geomechanics and Geoengineering*. **10**(1), pp.10-29.
- Sanner, B., Karytsas, C., Mendrinou, D. and Rybach, L. 2003. Current status of ground source heat pumps and underground thermal energy storage in Europe  
*Geothermics*. **32**(4-6), pp.579-588.
- Sanner, B., Mands, E., Sauer, M.K. and Grundmann, E. 2008. Thermal response test: A routine method to determine thermal ground properties for GSHP design. In: *Proceedings 9th International Energy Agency Heat Pump Conference*, pp.20-22.
- Shiozawa, S. and Campbell, G.S. 1990. Soil thermal conductivity. *Remote Sensing Reviews*. **5**(1), pp.301-310.
- Snape, J.R., Boait, P.J. and Rylatt, R.M. 2016. Performance comparison of UK domestic renewable incentives. *Proceedings of the Institution of Civil Engineers - Energy*. **169**(3), pp.126-139.
- Spitler, J.D., Liu, X., Rees, S.J. and Yavuzturk, C. 2005. Simulation and Optimization of Ground Source Heat Pump Systems. *8th International Energy Agency Heat Pump Conference, Las Vegas*.

Suryatriyastuti, M.E., Mroueh, H. and Burlon, S. 2012. Understanding the temperature-induced mechanical behaviour of energy pile foundations. *Renewable & Sustainable Energy Reviews*. **16**(5), pp.3344-3354.

Tang, A.M., Cui, Y.J. and Barnel, N. 2008. Thermo-mechanical behaviour of a compacted swelling clay. *Geotechnique*. **58**(1), pp.45-54.

Taylor, J.R. 1997. *An introduction to error analysis: the study of uncertainties in physical measurements*. Sausalito, Calif: University Science Books.

The Institute of Refrigeration. 2012. *Ground source heat pumps*. [Online]. [Accessed 12 October 2012]. Available from: [www.ior.org.uk/ground-source-heat-pumps-in-the-u](http://www.ior.org.uk/ground-source-heat-pumps-in-the-u)

Thomas, H.R. and Rees, S.W. 2009. Measured and simulated heat transfer to foundation soils. *Geotechnique*. **59**(4), pp.365-375.

Tian, Z., Lu, Y., Horton, R. and Ren, T. 2016. A simplified de Vries-based model to estimate thermal conductivity of unfrozen and frozen soil. *European Journal of Soil Science*. **67**(5), pp.564-572.

United Nations Framework Convention on Climate Change. 2018. *Kyoto Protocol*. [Online]. [Accessed April]. Available from: [http://unfccc.int/kyoto\\_protocol/items/2830.php](http://unfccc.int/kyoto_protocol/items/2830.php)

Vieira, A., Maranha, J., Christodoulides, P., Alberdi-Pagola, M., Loveridge, F., Nguyen, F., Florides, G., Radioti, G., Cecinato, F., Prodan, I., Ramalho, E., Georgiev, A., Rosin-Paumier, S., Lenart, S., Erbs Poulsen, S., Popov, R., Lenart, S., Erbs Poulsen, S., Radioti, G., Javed, S., Van Lysebetten, G. and Salciarini, D. 2017. Characterisation of Ground Thermal and Thermo-Mechanical Behaviour for Shallow Geothermal Energy Applications. *Energies*. **10**(12), p2044.

Westaway, R. 2016. Repurposing of disused shale gas wells for subsurface heat storage: preliminary analysis concerning UK issues. *Quarterly Journal of Engineering Geology and Hydrogeology*. **49**(3), pp.213-227.

Wood, C.J., Liu, H. and Riffat, S.B. 2009. Use of energy piles in a residential building, and effects on ground temperature and heat pump efficiency. *Geotechnique*. **59**(3), pp.287-290.

Yu, X., Wang, R.Z. and Zhai, X.Q. 2011. Year round experimental study on a constant temperature and humidity air-conditioning system driven by ground source heat pump. *Energy*. **36**(2), pp.1309-1318.

Yu, X.B., Zhang, N., Pradhan, A. and Puppala, A.J. 2016. Thermal conductivity of sand-kaolin clay mixtures. *Environmental Geotechnics-Journal*. **3**(4), pp.190-202.

Zhang, C., Wang, Y., Liu, Y., Kong, X. and Wang, Q. 2018. Computational methods for ground thermal response of multiple borehole heat exchangers: A review. *Renewable Energy*. **127**, pp.461-473.

## Bibliography

- Abdelaziz, S. and Ozudogru, T.Y. Non-uniform thermal strains and stresses in energy piles. *Environmental Geotechnics*. **0**(0), pnull.
- Abdelaziz, S.L. and Ozudogru, T.Y. 2016. Selection of the design temperature change for energy piles. *Applied Thermal Engineering*. **107**, pp.1036-1045.
- Abuel-Naga, H., Bergado, D. and Bouazza, A. 2008. Thermal conductivity evolution of saturated clay under consolidation process. *International Journal of Geomechanics*. **8**(2), pp.114-122.
- Abuel-Naga, H., Raouf, M.I.N., Raouf, A.M.I. and G., N.A. 2015. Energy piles: current state of knowledge and design challenges. *Environmental Geotechnics*. **2**(4), pp.195-210.
- Abuel-Naga, H.M., Bouazza, B.A. and Ramana, G. 2007. Volume change behaviour of saturated clays under drained heating conditions: experimental results and constitutive modeling. *Canadian Geotechnical Journal*. **44**(8), pp.942-956.
- Adam, D. and Markiewicz, R. 2009. Energy from earth-coupled structures, foundations, tunnels and sewers. *Geotechnique*. **59**(3), pp.229-236.
- Akrouch, G.A., Sánchez, M. and Briaud, J.-L. Effect of the Unsaturated Soil Condition on the Thermal Efficiency of Energy Piles. pp.1618-1627.
- Akrouch, G.A., Sánchez, M. and Briaud, J.-L. 2016. An experimental, analytical and numerical study on the thermal efficiency of energy piles in unsaturated soils. *Computers and Geotechnics*. **71**, pp.207-220.
- Al-Ajmi, F., Loveday, D.L. and Hanby, V.I. 2006. The cooling potential of earth-air heat exchangers for domestic buildings in a desert climate. *Building and Environment*. **41**(3), pp.235-244.
- Al-Moadhen Muataz, Clarke Barry G. and Chen Xiaohui 2017. Hydraulic conductivity of composite soils. *Proceedings of the 2nd Symposium on Coupled Phenomena in Environmental Geotechnics (CPEG2), Leeds, UK 2017*.
- Altenergymag.com. 2018. *Geothermal Energy*. [Online]. [Accessed April]. Available from: <https://www.altenergymag.com/article/2013/12/geothermal-energy-a-resource-waiting-to-be-more-fully-tapped/1342>
- Amara, S., Nordell, B. and Benyoucef, B. 2011. Using Fougara for Heating and Cooling Buildings in Sahara. In: Salame, C., et al. eds. *Impact of Integrated Clean Energy on the Future of the Mediterranean Environment*. pp.55-64.
- Amatya, B.L., Soga, K., Bourne-Webb, P.J., Amis, T. and Laloui, L. 2012. Thermo-mechanical behaviour of energy piles. *Géotechnique*. **62**(6), pp.503-519.
- Arkhangelskaya, T. and Lukyashchenko, K. 2018. Estimating soil thermal diffusivity at different water contents from easily available data on soil texture, bulk density, and organic carbon content. *Biosystems Engineering*. **168**, pp.83-95.
- Ascione, F., Bellia, L. and Minichiello, F. 2011. Earth-to-air heat exchangers for Italian climates. *Renewable Energy*. **36**(8), pp.2177-2188.
- Aysen, A. 2002. *Soil mechanics: basic concepts and engineering applications*. Lisse, The Netherlands: A.A. Balkema Pub.
- Badescu, V., Laaser, N. and Crutescu, R. 2010. Warm season cooling requirements for passive buildings in Southeastern Europe (Romania). *Energy*. **35**(8), pp.3284-3300.

- Bai, B. and Su, Z.Q. 2012. Thermal Responses of Saturated Silty Clay During Repeated Heating-Cooling Processes. *Transport in Porous Media*. **93**(1), pp.1-11.
- Banks, D. 2008. *An introduction to thermogeology : ground source heating and cooling*. Oxford: Blackwell.
- Banks, D. 2009. An introduction to 'thermogeology' and the exploitation of ground source heat. *Quarterly Journal of Engineering Geology and Hydrogeology*. **42**, pp.283-293.
- Banks, D. 2015. William Thomson – father of thermogeology. *Scottish Journal of Geology*. **51**(1), pp.95-99.
- Banks, D., Withers, J.G., Cashmore, G. and Dimelow, C. 2013. An overview of the results of 61 *in situ* thermal response tests in the UK. *Quarterly Journal of Engineering Geology and Hydrogeology*. **46**(3), pp.281-291.
- Barry-Macaulay, D., Bouazza, A., Singh, R.M., Wang, B. and Ranjith, P.G. 2013. Thermal conductivity of soils and rocks from the Melbourne (Australia) region. *Engineering Geology*. **164**, pp.131-138.
- Bartlett, J.W. and Frost, C. 2008. Reliability, repeatability and reproducibility: analysis of measurement errors in continuous variables. *Ultrasound in Obstetrics and Gynecology*. **31**(4), pp.466-475.
- Bauer, N., Mouratiadou, I., Luderer, G., Baumstark, L., Brecha, R.J., Edenhofer, O. and Kriegler, E. 2016. Global fossil energy markets and climate change mitigation – an analysis with REMIND. *Climatic Change*. **136**(1), pp.69-82.
- Bayer, P., Saner, D., Bolay, S., Rybach, L. and Blum, P. 2012. Greenhouse gas emission savings of ground source heat pump systems in Europe: A review. *Renewable and Sustainable Energy Reviews*. **16**(2), pp.1256-1267.
- Bevington, P.R. 1969. *Data reduction and error analysis for the physical sciences*. New York McGraw-Hill.
- Bevington, P.R. and Robinson, D.K. 1992. *Data reduction and error analysis for the physical sciences*. New York: WCB/McGraw-Hill.
- Bevington, P.R. and Robinson, D.K. 2003. *Data reduction and error analysis for the physical sciences*. Boston;London;: McGraw-Hill.
- Blum, P., Campillo, G., Münch, W. and Kölbl, T. 2010. CO<sub>2</sub> savings of ground source heat pump systems - A regional analysis. *Renewable Energy*. **35**(1), pp.122-127.
- Boominathan, A. and Ayothiraman, R. 2006. Dynamic response of laterally loaded piles in clay. *Proceedings of the Institution of Civil Engineers - Geotechnical Engineering*. **159**(3), pp.233-241.
- Bourne-Webb, P.J., Amatya, B. and Soga, K. 2013. A framework for understanding energy pile behaviour. *Proceedings of the Institution of Civil Engineers - Geotechnical Engineering*. **166**(2), pp.170-177.
- Bourne-Webb, P.J., Amatya, B.L., SOGA, K., AMIS, T., Davidson, C. and Payne, P. 2009. Energy pile test at Lambeth College, London: geotechnical and thermodynamic aspects of pile response to heat cycles. *Géotechnique*. **59**(3), pp.237-248.
- Bourne-Webb, P.J., Bodas Freitas, T.M. and Freitas Assunção, R.M. 2016. Soil–pile thermal interactions in energy foundations. *Géotechnique*. **66**(2), pp.167-171.
- Boyle, G. 2004. *Renewable energy / editor, Godfrey Boyle*. 2nd ed. ed. Oxford :: Oxford University Press in Association with The Open University.
- Brandl, H. 2006. Energy foundations and other thermo-active ground structures.

*Geotechnique*. **56**(2), pp.81-122.

Brigaud, F. and Vasseur, G. 1989. Mineralogy, porosity and fluid control on thermal conductivity of sedimentary rocks. *Geophysical Journal International*. **98**(3), pp.525-542.

Bristow, K.L., Kluitenberg, G.J., Goding, C.J. and Fitzgerald, T.S. 2001. A small multi-needle probe for measuring soil thermal properties, water content and electrical conductivity. *Computers and Electronics in Agriculture*. **31**(3), pp.265-280.

British Petroleum. 2012. *World Energy Review* [Online]. [Accessed 11 December 2012]. Available from:  
[http://www.bp.com/assets/bp\\_internet/globalbp/globalbp\\_uk\\_english/reports\\_and\\_publications/statistical\\_energy\\_review\\_2011/STAGING/local\\_assets/pdf/statistical\\_review\\_of\\_world\\_energy\\_full\\_report\\_2012.pdf](http://www.bp.com/assets/bp_internet/globalbp/globalbp_uk_english/reports_and_publications/statistical_energy_review_2011/STAGING/local_assets/pdf/statistical_review_of_world_energy_full_report_2012.pdf)

Britto, A.M., Savvidou, C., Maddocks, D.V., Gunn, M.J. and Booker, J.R. 1989. Numerical And Centrifuge Modeling Of Coupled Heat-Flow And Consolidation Around Hot Cylinders Buried In Clay. *Geotechnique*. **39**(1), pp.13-25.

Brook, B.W., Edney, K., Hillerbrand, R., Karlsson, R. and Symons, J. 2016. Energy research within the UNFCCC: a proposal to guard against ongoing climate-deadlock. *Climate Policy*. **16**(6), pp.803-813.

Bulusan. 2013. *Renewable Energy*. [Online]. [Accessed 2nd January,]. Available from:  
<http://bulusangeothermal.com/renewable-energy/>

Buonaccorsi, J.P. 2010. *Measurement error: models, methods, and applications*. Boca Raton: CRC Press.

Burghignoli, A., Desideri, A. and Miliziano, S. 2000. A laboratory study on the thermomechanical behaviour of clayey soils. *Canadian Geotechnical Journal*. **37**(4), pp.764-780.

Busby, J. 2016. Thermal conductivity and diffusivity estimations for shallow geothermal systems. *Quarterly Journal of Engineering Geology and Hydrogeology*. **49**(2), pp.138-146.

Busby, J., Lewis, M., Reeves, H. and Lawley, R. 2009. Initial geological considerations before installing ground source heat pump systems. *Quarterly Journal of Engineering Geology and Hydrogeology*. **42**, pp.295-306.

Casas, W. and Schmitz, G. 2005. Experiences with a gas driven, desiccant assisted air conditioning system with geothermal energy for an office building. *Energy and Buildings*. **37**(5), pp.493-501.

Cecinato, F. and Loveridge, F.A. 2015. Influences on the thermal efficiency of energy piles.

Cekerevac, C. and Laloui, L. 2004. Experimental study of thermal effects on the mechanical behaviour of a clay. *International Journal for Numerical and Analytical Methods in Geomechanics*. **28**(3), pp.209-228.

Çengel, Y.A. 2005. *Fundamentals of thermal-fluid sciences*. 2nd , international edition. ed. Boston ; London: McGraw-Hill.

Change, I.P.C. 2014. *Climate Change 2014 – Impacts, Adaptation and Vulnerability: Part B: Regional Aspects: Volume 2, Regional Aspects: Working Group II Contribution to the IPCC Fifth Assessment Report*. Cambridge University Press.

Chen, S.X. 2008. Thermal conductivity of sands. *Heat and Mass Transfer*. **44**(10), p1241.

Cheng-long, W., Han-long, L., Gang-qiang, K., W., N.C.W. and Di, W. 2016. Model tests

- of energy piles with and without a vertical load. *Environmental Geotechnics*. **3**(4), pp.203-213.
- Chiasson, A.D., Yavuzturk, C. and Ashrae. 2009. A Design Tool for Hybrid Geothermal Heat Pump Systems in Cooling-Dominated Buildings. *Ashrae Transactions 2009, Vol 115, Pt 2*. pp.74-87.
- CIBSE. 2004. *Energy efficiency in buildings : CIBSE guide F*. London: Chartered Institution of Building Services Engineers.
- CIBSE. 2005. *Heating, ventilating, air conditioning and refrigeration : CIBSE guide B*. London: Chartered Institution of Building Services Engineers.
- Civan, F. *Reservoir Formation Damage - Fundamentals, Modelling, Assessment, and Mitigation*. Elsevier. Available from:  
<http://app.knovel.com/hotlink/toc/id:kpRFDFMAM2/reservoir-formation-damage/reservoir-formation-damage>
- Claesson, J. and Eskilson, P. 1988. Conductive heat extraction to a deep borehole: Thermal analyses and dimensioning rules. *Energy*. **13**(6), pp.509-527.
- Clarke, B.G., Agab, A. and Nicholson, D. 2008. Model specification to determine thermal conductivity of soils. *Proceedings of the Institution of Civil Engineers-Geotechnical Engineering*. **161**(3), pp.161-168.
- Cohen, E.R. 1998. An Introduction to Error Analysis: The Study of Uncertainties in Physical Measurements. *Measurement Science and Technology*. **9**(6).
- Committee on Climate Change. 2018. *The Climate Change Act*. [Online]. [Accessed 2018]. Available from: <https://www.theccc.org.uk/tackling-climate-change/the-legal-landscape/the-climate-change-act/>
- Craig, R.F. 2004. *Craig's soil mechanics*. New York;London;: Spon Press.
- Cui, Y.J., Le, T.T., Tang, A.M., Delage, P. and Li, X.L. 2009. Investigating the time-dependent behaviour of Boom clay under thermomechanical loading. *Geotechnique*. **59**(4), pp.319-329.
- da Rosa, A. 2013. Chapter 12 - Solar Radiation. *Fundamentals of Renewable Energy Processes (Third Edition)*. Boston: Academic Press, pp.485-532.
- da Rosa, A. 2013. Chapter 13 - Biomass. *Fundamentals of Renewable Energy Processes (Third Edition)*. Boston: Academic Press, pp.533-590.
- da Rosa, A. 2013. Chapter 14 - Photovoltaic Converters. *Fundamentals of Renewable Energy Processes (Third Edition)*. Boston: Academic Press, pp.591-681.
- da Rosa, A. 2013. Chapter 15 - Wind Energy. *Fundamentals of Renewable Energy Processes (Third Edition)*. Boston: Academic Press, pp.685-763.
- da Rosa, A. 2013. Chapter 16 - Ocean Engines. *Fundamentals of Renewable Energy Processes (Third Edition)*. Boston: Academic Press, pp.765-792.
- da Rosa, A. 2013. Chapter 18 - Storage of Energy. *Fundamentals of Renewable Energy Processes (Third Edition)*. Boston: Academic Press, pp.821-862.
- Darkwa, J., Su, W. and Chow, D.H.C. 2013. Heat dissipation effect on a borehole heat exchanger coupled with a heat pump. *Applied Thermal Engineering*. **60**(1-2), pp.234-241.
- Davidsdottir, B. 2012. 7.10 - Sustainable Energy Development: The Role of Geothermal Power A2 - Sayigh, Ali. *Comprehensive Renewable Energy*. Oxford: Elsevier, pp.273-297.



- De Paepe, M. and Janssens, A. 2003. Thermo-hydraulic design of earth-air heat exchangers. *Energy and Buildings*. **35**(4), pp.389-397.
- Dehkordi, S.E. and Schincariol, R.A. 2014. Effect of thermal-hydrogeological and borehole heat exchanger properties on performance and impact of vertical closed-loop geothermal heat pump systems. *Hydrogeology Journal*. **22**(1), pp.189-203.
- Demirbas, A. 2005. Potential applications of renewable energy sources, biomass combustion problems in boiler power systems and combustion related environmental issues. *Progress in Energy and Combustion Science*. **31**(2), pp.171-192.
- Dhillon, B.S. 2013. *Safety and human error in engineering systems*. Boca Raton, FL: CRC Press.
- Di Donna, A. and Laloui, L. 2015. Response of soil subjected to thermal cyclic loading: Experimental and constitutive study. *Engineering Geology*. **190**(0), pp.65-76.
- Dou, H. and Byrne, P.M. 1996. Dynamic response of single piles and soil–pile interaction. *Canadian Geotechnical Journal*. **33**(1), pp.80-96.
- Eckert, E.R.G. 1976. The ground used as energy source, energy sink, or for energy storage. *Energy*. **1**(3), pp.315-323.
- Edenhofer, O. 2014. *Mitigation of climate change*. Cambridge University Press.
- Eicker, U. and Thumm, F. 2012. Energy efficiency and cost effectiveness of low depth geothermal heating and cooling for non-residential buildings. *Bauphysik*. **34**(1), pp.11-18.
- Ellabban, O., Abu-Rub, H. and Blaabjerg, F. 2014. Renewable energy resources: Current status, future prospects and their enabling technology. *Renewable and Sustainable Energy Reviews*. **39**, pp.748-764.
- Elliott, D. 2013. *Renewables: a review of sustainable energy supply options*. Bristol England (Temple Circus, Temple Way, Bristol BS1 6HG, UK): IOP Publishing.
- ETSU. 1994. *An Assessment of Renewable Energy for the UK*. London: HMSO.
- European Commission. 2018. *Energy Efficiency*. [Online]. [Accessed April]. Available from: <https://ec.europa.eu/energy/en/topics/energy-efficiency/buildings>
- Faizal, M., Bouazza, A. and Singh, R.M. 2016. Heat transfer enhancement of geothermal energy piles. *Renewable and Sustainable Energy Reviews*. **57**, pp.16-33.
- Fan, D., Rees, S. and Spitler, J. 2013. A dynamic thermal network approach to the modelling of Foundation Heat Exchangers. *Journal of Building Performance Simulation*. **6**(2), pp.81-97.
- FAO. 2005. *Mechanisms Of Energy Transfer*. [Online]. [Accessed 20th February]. Available from: <http://www.fao.org/docrep/008/y7223e/y7223e00.htm>
- Farouki, O.T. 1981. *Thermal properties of soils*. DTIC Document.
- Field, C.B., Barros, V.R. and Intergovernmental Panel on Climate Change. Working, G., II. 2014. *Climate change 2014: impacts, adaptation, and vulnerability*. New York: Cambridge University Press.
- Florides, G. and Kalogirou, S. 2007. Ground heat exchangers - A review of systems, models and applications. *Renewable Energy*. **32**(15), pp.2461-2478.
- Florides, G.A., Pouloupatis, P.D., Kalogirou, S., Messaritis, V., Panayides, I., Zomeni, Z., Partasides, G., Lizides, A., Sophocleous, E. and Koutsoumpas, K. 2011. The geothermal characteristics of the ground and the potential of using ground coupled heat pumps in Cyprus. *Energy*. **36**(8), pp.5027-5036.

- Flóvenz, Ó.G., Hersir, G.P., Sæmundsson, K., Ármannsson, H. and Friðriksson, Þ. 2012. 7.03 - Geothermal Energy Exploration Techniques A2 - Sayigh, Ali. *Comprehensive Renewable Energy*. Oxford: Elsevier, pp.51-95.
- Focaccia, S. 2013. Thermal response test numerical modeling using a dynamic simulator. *Geothermal Energy*. **1**(1), p3.
- Frame, D.J., Macey, A.H. and Allen, M.R. 2014. Cumulative emissions and climate policy. *Nature Geosci.* **7**(10), pp.692-693.
- Gabrielsson, A., Bergdahl, U. and Moritz, L. 2000. Thermal energy storage in soils at temperatures reaching 90 degrees C. *Journal of Solar Energy Engineering-Transactions of the Asme*. **122**(1), pp.3-8.
- Gao, J., Zhang, X., Liu, J., Li, K. and Yang, J. 2008. Numerical and experimental assessment of thermal performance of vertical energy piles: An application. *Applied Energy*. **85**(10), pp.901-910.
- Gao, J., Zhang, X., Liu, J., Li, K.S. and Yang, J. 2008. Thermal performance and ground temperature of vertical pile-foundation heat exchangers: A case study. *Applied Thermal Engineering*. **28**(17-18), pp.2295-2304.
- Gao, Q., Li, M., Yu, M., Spitler, J.D. and Yan, Y.Y. 2009. Review of development from GSHP to UTES in China and other countries. *Renewable & Sustainable Energy Reviews*. **13**(6-7), pp.1383-1394.
- Gao, Z., Wang, L. and Horton, R. 2009. Comparison of six algorithms to determine the soil thermal diffusivity at a site in the Loess Plateau of China. *Hydrology and Earth System Sciences Discussions*. **6**(2), pp.2247-2274.
- Glassley, W.E. 2010. *Geothermal energy renewable energy and the environment*. [Online]. Boca Raton: CRC Press,. Available from: <http://0-marc.crcnetbase.com.wam.leeds.ac.uk/isbn/9781420075717>
- Glassley, W.E. 2015. *Geothermal energy: renewable energy and the environment*. Boca Raton, FL: CRC Press.
- Golubev, É.A. and Fatkudinova, S.R. 2006. ISO 5725 standard and reference laboratories: Error requirements. *Measurement Techniques*. **49**(2), pp.133-137.
- Gonzalez, R.G., Verhoef, A., Vidale, P.L., Main, B., Gan, G.G. and Wu, Y.P. 2012. Interactions between the physical soil environment and a horizontal ground coupled heat pump, for a domestic site in the UK. *Renewable Energy*. **44**, pp.141-153.
- Goodman, S.N., Fanelli, D. and Ioannidis, J.P.A. 2016. What does research reproducibility mean? *Science Translational Medicine*. **8**(341), pp.341ps312-341ps312.
- Haigh, S. 2012. *Thermal conductivity of sands*.
- Hamdhan, I.N. and Clarke, B.G. 2010. Determination of thermal conductivity of coarse and fine sand soils. In: *Proceedings of World Geothermal Congress*.
- Head, K.H. 2006. *Manual of soil laboratory testing: Vol. 1, Soil classification and compaction tests*. 3rd ed. Boca Raton, FL;Dunbeath, Scotland;: Whittles.
- Head, K.H. and Epps, R. 2011. *Manual of soil laboratory testing: Volume 2, Permeability, shear strength and compressibility tests*. Third ed. Caithness, Scotland;Boca Raton, FL;: Whittles Pub.
- Head, K.H. and Epps, R.J. 2014. *Manual of soil laboratory testing: Volume 3, Effective stress tests*. Third ed. Caithness, Scotland: Whittles Publishing.
- Hemmingway, P. and Long, M. 2011. Geothermal energy: settlement and water

- chemistry in Cork, Ireland. *Proceedings of the Institution of Civil Engineers - Engineering Sustainability*. **164**(3), pp.213-224.
- Hemmingway, P. and Long, M. 2012. Design and development of a low-cost thermal response rig. *Proceedings of the Institution of Civil Engineers - Energy*. **165**(3), pp.137-148.
- Hillel, D. 1982. Soil temperature and heat flow. *Fundamentals of soil physics, Chapt. 12*, pp.287-317.
- Hoffschmidt, B., Alexopoulos, S., Rau, C., Sattler, J., Anthrakidis, A., Boura, C., O'Connor, B. and Hilger, P. 2012. 3.18 - Concentrating Solar Power A2 - Sayigh, Ali. *Comprehensive Renewable Energy*. Oxford: Elsevier, pp.595-636.
- Horton, R., Wierenga, P. and Nielsen, D. 1983. Evaluation of Methods for Determining the Apparent Thermal Diffusivity of Soil Near the Surface 1. *Soil Science Society of America Journal*. **47**(1), pp.25-32.
- Hueckel, T., Francois, B. and Laloui, L. 2009. Explaining thermal failure in saturated clays. *Geotechnique*. **59**(3), pp.197-212.
- Incropera, F.P. 2002. *Fundamentals of heat and mass transfer*. 5th ed. New York ; Chichester: Wiley.
- Incropera, F.P. 2002. *Introduction to heat transfer*. 4th ed. New York ; Chichester: Wiley.
- Incropera, F.P. 2007. *Fundamentals of heat and mass transfer*. 6th ed. Hoboken, N.J.: Wiley.
- Incropera, F.P. 2007. *Introduction to heat transfer*. Hoboken NJ: Wiley.
- Institution of Civil Engineers. 2012. *Ground Storage Energy Systems*. [Online]. [Accessed 12 October 2012]. Available from: [www.ice.org.uk/Information-resources/](http://www.ice.org.uk/Information-resources/)
- Intergovernmental Panel on Climate, C. 2015. *Climate change 2014: impacts, adaptation and vulnerability. Part B, Regional aspects, working group II contribution to the IPCC fifth assessment report*. Cambridge: Cambridge University Press.
- International Energy Agency. 2018. *Global Energy & CO2 Status Report*. [Online]. [Accessed April]. Available from: <https://www.iea.org/geco/>
- International Workshop on Effects of Expected Climate Change on Soil Processes in the, T. and Sub, t. 1990. *Soils on a warmer earth*. Amsterdam ; Oxford: Elsevier.
- Jadi, M.H. and Prakash, F.S. 2003. Lateral dynamic response of single vertical piles. *BGA International Conference on Foundations: Innovations, observations, design and practice*. pp.351-360.
- Janna, W.S. 1988. *Engineering heat transfer*. SI ed. London: Van Nostrand Reinhold International.
- Jastrzebska, M. and Wawrzynczyk, B. 2016. The Analysis Of The Direct Foundation With Energy Foundations On The Basis Of The Office Building "A4 Business Park" In Katowice At Francuska Street. *Architecture Civil Engineering Environment*. **9**(2), pp.65-76.
- Jefferson, I. and Rogers, C.D.F. 1998. Liquid limit and the temperature sensitivity of clays. *Engineering geology*. **49**(2), pp.95-109.
- Jeffer, E.J. 2010. *Green energy : sustainable electricity supply with low environmental impact*. Boca Raton, FL: CRC Press.
- Kalantidou, A., Pereira, J.M., Tang, A.M. and Hassen, G. 2012. Preliminary study on the mechanical behaviour of heat exchanger pile in physical model. *Geotechnique*. **62**(11),

pp.1047-1051.

Kalogirou, S.A. 2012. 3.01 - Solar Thermal Systems: Components and Applications – Introduction A2 - Sayigh, Ali. *Comprehensive Renewable Energy*. Oxford: Elsevier, pp.1-25.

Kambezidis, H.D. 2012. 3.02 - The Solar Resource A2 - Sayigh, Ali. *Comprehensive Renewable Energy*. Oxford: Elsevier, pp.27-84.

Kawata, S., Kanoh, H. and Masubuchi, M. 1989. A Correlation Between Steady-State and Dynamic Response of a Counterflow Heat Exchanger. *Journal of Dynamic Systems, Measurement, and Control*. **111**(1), pp.115-118.

Kharseh, M., Al-Khawaja, M. and Suleiman, M.T. 2015. Potential of ground source heat pump systems in cooling-dominated environments: Residential buildings. *Geothermics*. **57**(0), pp.104-110.

Knappett, J. and Craig, R.F. 2012. *Craig's soil mechanics*. 8th ed. London: Spon Press.

Knellwolf, C., Peron, H. and Laloui, L. 2011. Geotechnical Analysis of Heat Exchanger Piles. *Journal of Geotechnical and Geoenvironmental Engineering*. **137**(10), pp.890-902.

Koumoto, T. and Houlsby, G.T. 2001. Theory and practice of the fall cone test. *Geotechnique*. **51**(8), pp.701-712.

Kurevija, T. and Vulin, D. 2010. Determining Undisturbed Ground Temperature As Part Of Shallow Geothermal Resources Assessment/Određvanje Statice Temperature Tla Kao Dijela Vrijednovanja Plitkih Geotermalnih Potencijala. *Rudarsko - Geolosko - Naftni Zbornik*. **22**(1), pp.27-36.

Laloui, L. and Di Donna, A. 2011. Understanding the behaviour of energy geo-structures. *Proceedings of the Institution of Civil Engineers-Civil Engineering*. **164**(4), pp.184-191.

Laloui, L., Nuth, M. and Vulliet, L. 2006. Experimental and numerical investigations of the behaviour of a heat exchanger pile. *International Journal for Numerical and Analytical Methods in Geomechanics*. **30**(8), pp.763-781.

Lazzarin, R.M. 2012. Dual source heat pump systems: Operation and performance. *Energy and Buildings*. **52**, pp.77-85.

Lee, C.K. and Lam, H.N. 2013. A simplified model of energy pile for ground-source heat pump systems. *Energy*. **55**, pp.838-845.

Lee, J., Kim, Y.S., Kim, H.S., Kang, J.M. and Bae, G.J. 2011. Evaluation of Methods For Predicting Thermal Conductivity of Saturated Unfrozen Kaolinite. In: *The Twenty-first International Offshore and Polar Engineering Conference, 2011/1/1/, Maui, Hawaii, USA*. ISOPE: International Society of Offshore and Polar Engineers.

Li, M. and Lai, A.C.K. 2012. Heat-source solutions to heat conduction in anisotropic media with application to pile and borehole ground heat exchangers. *Applied Energy*. **96**, pp.451-458.

Li, S.H., Yang, W.H. and Zhang, X.S. 2009. Soil temperature distribution around a U-tube heat exchanger in a multi-function ground source heat pump system. *Applied Thermal Engineering*. **29**(17-18), pp.3679-3686.

Liao, S.T. and Roesset, J.M. 1997. Dynamic response of intact piles to impulse loads *International Journal for Numerical and Analytical Methods in Geomechanics*. **21**(4), pp.255-275.

Liebel, H.T., Huber, K., Frengstad, B.S., Ramstad, R.K. and Brattli, B. 2012. Thermal response testing of a fractured hard rock aquifer with and without induced groundwater flow. *Bulletin of Engineering Geology and the Environment*. **71**(3), pp.435-445.

- Lienhard, J.H. 2000. *A heat transfer textbook*. 3rd edition. ed. London: s.n.
- Lim, T.H., De Kleine, R.D. and Keoleian, G.A. 2016. Energy use and carbon reduction potentials from residential ground source heat pumps considering spatial and economic barriers. *Energy and Buildings*. **128**, pp.287-304.
- Liu, G. and Si, B.C. 2011. Single- and Dual-Probe Heat Pulse Probe for Determining Thermal Properties of Dry Soils. *Soil Science Society of America Journal*. **75**(3), pp.787-794.
- Loria, A.F.R. and Laloui, L. 2017. Thermally induced group effects among energy piles. *Géotechnique*. **67**(5), pp.374-393.
- Loveridge, F., Low, J. and Powrie, W. 2017. Site investigation for energy geostructures. *Quarterly Journal of Engineering Geology and Hydrogeology*. **50**(2), pp.158-168.
- Loveridge, F. and Powrie, W. 2012. Pile heat exchangers: thermal behaviour and interactions. *Proceedings of the ICE - Geotechnical Engineering*. pp.1-19.
- Loveridge, F. and Powrie, W. 2013. Pile heat exchangers: thermal behaviour and interactions. *Proceedings of the Institution of Civil Engineers - Geotechnical Engineering*. **166**(2), pp.178-196.
- Low, J.E., Loveridge, F.A., Powrie, W. and Nicholson, D. 2015. A comparison of laboratory and in situ methods to determine soil thermal conductivity for energy foundations and other ground heat exchanger applications. *Acta Geotechnica*. **10**(2), pp.209-218.
- Lu, J. and Chen, M. 2010. The Analysis and Simulation on Operating Characteristics of GSHP in Summer. *Journal of Superconductivity and Novel Magnetism*. **23**(6), pp.1091-1093.
- Lu, S., Ren, T., Gong, Y. and Horton, R. 2007. An Improved Model for Predicting Soil Thermal Conductivity from Water Content at Room Temperature This research was supported by the Natural Science Foundation of China under Grant no. 40471061, the Program for Changjiang Scholars and Innovative Research Team in University (IRT0412), and the U.S. National Science Foundation under Grant no. 0337553. *Soil Science Society of America Journal*. **71**, pp.8-14.
- Lund, J.W., Freeston, D.H. and Boyd, T.L. 2011. Direct utilization of geothermal energy 2010 worldwide review. *Geothermics*. **40**(3), pp.159-180.
- Lund, P. 1984. Studies On Solar Heating-Systems With Long-Term Heat-Storage For Northern High-Latitudes. *Acta Polytechnica Scandinavica-Applied Physics Series*. (147), pp.1-48.
- Lund, P.D. 1984. Optimization Of A Community Solar Heating-System With A Heat-Pump And Seasonal Storage. *Solar Energy*. **33**(3-4), pp.353-361.
- Lund, P.D. 2010. Exploring past energy changes and their implications for the pace of penetration of new energy technologies. *Energy*. **35**(2), pp.647-656.
- Lund, P.D. and Routti, J.T. 1984. Feasibility Of Solar Pond Heating For Northern Cold Climates. *Solar Energy*. **33**(2), pp.209-215.
- Lyons, L. 1991. *A practical guide to data analysis for physical science students*. Cambridge: Cambridge University Press.
- Man, Y., Yang, H.X., Diao, N.R., Liu, J.H. and Fang, Z.H. 2010. A new model and analytical solutions for borehole and pile ground heat exchangers. *International Journal of Heat and Mass Transfer*. **53**(13-14), pp.2593-2601.
- Marcotte, D. and Pasquier, P. 2008. Fast fluid and ground temperature computation for

- geothermal ground-loop heat exchanger systems. *Geothermics*. **37**(6), pp.651-665.
- McConnell, J., Nunnally, B.K. and McGarvey, B. 2009. Blame the Laboratory- Understanding Analytical Error. *Journal of Validation Technology*. **15**(3), pp.23-28.
- McKendry, P. 2002. Energy production from biomass (part 1): overview of biomass. *Bioresource Technology*. **83**(1), pp.37-46.
- Mensah, K., Jang, Y.-S. and Choi, J.M. 2017. Assessment of design strategies in a ground source heat pump system. *Energy and Buildings*. **138**, pp.301-308.
- Mihalakakou, G., Lewis, J.O. and Santamouris, M. 1996. On the heating potential of buried pipes techniques - Application in Ireland. *Energy and Buildings*. **24**(1), pp.19-25.
- Mihalakakou, G., Santamouris, M. and Asimakopoulos, D. 1994. Use Of The Ground For Heat Dissipation. *Energy*. **19**(1), pp.17-25.
- Mills, A.F. 1999. *Basic heat and mass transfer*. Upper Saddle River, N.J.: Prentice Hall.
- Mitchell, J.K. 1991. Conduction phenomena: from theory to geotechnical practice. *Géotechnique*. **41**(3), pp.299-340.
- Mitchell, J.K. and Soga, K. 2005. *Fundamentals of Soil Behavior (3rd Edition)*. John Wiley & Sons. Available from: <http://app.knovel.com/hotlink/toc/id:kpFSBE0002/fundamentals-soil-behavior/fundamentals-soil-behavior>
- Mochtar, I.B. and Edil, T.B. 1988. Shaft Resistance Of Model Pile In Clay. *Journal of Geotechnical Engineering-Asce*. **114**(11), pp.1227-1244.
- Molloy, E. 1941. *Pumps and pumping : a practical manual on the operation, installation, and maintenance of reciprocating, centrifugal, and rotary pumps*. London: Newnes.
- Nam, Y., Ooka, R. and Hwang, S. 2008. Development of a numerical model to predict heat exchange rates for a ground-source heat pump system. *Energy and Buildings*. **40**(12), pp.2133-2140.
- Nathanail, J. and Banks, V. 2009. Climate change: implications for engineering geology practice. *Geological Society, London, Engineering Geology Special Publications*. **22**(1), pp.65-82.
- Nenmore. 2010. *Geothermal Heat Pumps*. [Online]. [Accessed 2nd January,]. Available from: <http://nenmore.blogspot.co.uk/2010/09/geothermal-heat-pumps-yes.html>
- Ng, C.W.W., Ma, Q.J. and Gunawan, A. 2016. Horizontal stress change of energy piles subjected to thermal cycles in sand. *Computers and Geotechnics*. **78**, pp.54-61.
- Niemi, R., Mikkola, J. and Lund, P.D. 2012. Urban energy systems with smart multi-carrier energy networks and renewable energy generation. *Renewable Energy*. **48**, pp.524-536.
- Omer, A.M. 2008. Ground-source heat pumps systems and applications. *Renewable & Sustainable Energy Reviews*. **12**(2), pp.344-371.
- Panwar, N.L., Kaushik, S.C. and Kothari, S. 2011. Role of renewable energy sources in environmental protection: A review. *Renewable and Sustainable Energy Reviews*. **15**(3), pp.1513-1524.
- Porges, F. 2001. 4 - Heat and thermal properties of materials. *HVAC Engineer's Handbook (Eleventh Edition)*. Oxford: Butterworth-Heinemann, pp.45-68.
- Porges, F. 2001. 6 - Heat losses. *HVAC Engineer's Handbook (Eleventh Edition)*. Oxford: Butterworth-Heinemann, pp.90-112.

- Porges, F. 2001. 7 - Cooling loads. *HVAC Engineer's Handbook (Eleventh Edition)*. Oxford: Butterworth-Heinemann, pp.113-118.
- Prakash, S. 1990. *Pile foundations in engineering practice*. New York ; Chichester: Wiley.
- Prasad, M.S., Reid, K.J. and Murray, H.H. 1991. Kaolin: processing, properties and applications. *Applied Clay Science*. **6**(2), pp.87-119.
- Preene, M. 2008. Sustainable groundwater-source cooling systems for buildings. *Proceedings of the Institution of Civil Engineers-Engineering Sustainability*. **161**(2), pp.123-133.
- Preene, M. 2010. Discussion: Sustainable groundwater-source cooling systems for buildings. *Proceedings of the Institution of Civil Engineers-Engineering Sustainability*. **163**(3), pp.175-176.
- Preene, M. and Powrie, W. 2009. Ground energy systems: delivering the potential. *Proceedings of the ICE - Energy*. **162**(2), pp.77-84.
- Preene, M. and Powrie, W. 2009. Ground energy systems: from analysis to geotechnical design. *Geotechnique*. **59**(3), pp.261-271.
- Pretech. 2010. *Geothermal Energy*. [Online]. [Accessed 2nd January,]. Available from: <http://www.pretech.qc.ca/en/geothermal.html>
- Putkonen, J. 1998. Soil thermal properties and heat transfer processes near Ny-Alesund, northwestern Spitsbergen, Svalbard. *Polar research*. **17**(2), pp.165-179.
- R., D. and V., A. 2009. *Fundamentals of renewable energy processes*. [Online]. 2nd ed. Amsterdam ; Boston: Academic Press/Elsevier.
- Rajeev, P. and Kodikara, J. 2016. Estimating apparent thermal diffusivity of soil using field temperature time series. *Geomechanics and Geoengineering*. **11**(1), pp.28-46.
- Raupach, M.R., Marland, G., Ciais, P., Le Quéré, C., Canadell, J.G., Klepper, G. and Field, C.B. 2007. Global and regional drivers of accelerating CO<sub>2</sub> emissions. *Proceedings of the National Academy of Sciences*. **104**(24), pp.10288-10293.
- RedOrbit. 2013. *CO<sub>2</sub> Emissions Soaked Up By CSIRO 'Solar Sponge'*. [Online]. [Accessed 2nd January,]. Available from: <http://www.redorbit.com/news/science/1112787244/co2-carbon-dioxide-emissions-csiro-solar-sponge-021913/>
- Rees, S.J. 2015. An extended two-dimensional borehole heat exchanger model for simulation of short and medium timescale thermal response. *Renewable Energy*. **83**, pp.518-526.
- Rees, S.J. 2016. 1 - An introduction to ground-source heat pump technology. *Advances in Ground-Source Heat Pump Systems*. Woodhead Publishing, pp.1-25.
- Rees, S.J., Spitler, J.D., Deng, Z., Orio, C.D. and Johnson, C.N. 2004. A Study of Geothermal Heat Pump And Standing Column Well Performance. *ASHRAE Transactions*. **109**(Part 1), pp.3-13.
- Rees, S.W., Adjali, M.H., Zhou, Z., Davies, M. and Thomas, H.R. 2000. Ground heat transfer effects on the thermal performance of earth-contact structures. *Renewable & Sustainable Energy Reviews*. **4**(3), pp.213-265.
- Rees, S.W., Zhou, Z. and Thomas, H.R. 2007. Ground heat transfer: A numerical simulation of a full-scale experiment. *Building and Environment*. **42**(3), pp.1478-1488.
- Reuss, M., Beck, M. and Muller, J.P. 1997. Design of a seasonal thermal energy storage

in the ground. *Solar Energy*. **59**(4-6), pp.247-257.

Rybach, L. 2012. 7.06 - Shallow Systems: Geothermal Heat Pumps A2 - Sayigh, Ali. *Comprehensive Renewable Energy*. Oxford: Elsevier, pp.189-207.

Saadi, L. 2011. *System Innovation for Sustainability 4*. Sheffield: Greenleaf Publishing Limited.

Saggu, R. and Chakraborty, T. 2015. Thermal analysis of energy piles in sand. *Geomechanics and Geoengineering*. **10**(1), pp.10-29.

Sahdi, F., Gaudin, C. and White, D.J. 2014. Strength properties of ultra-soft kaolin. *Canadian Geotechnical Journal*. **51**(4), pp.420-431.

Sanner, B., Hellström, G., Spitler, J. and Gehlin, S. 2005. Thermal response test—current status and world-wide application. In: *Proceedings world geothermal congress: International Geothermal Association*, pp.24-29.

Sanner, B., Karytsas, C., Mendrinou, D. and Rybach, L. 2003. Current status of ground source heat pumps and underground thermal energy storage in Europe *Geothermics*. **32**(4-6), pp.579-588.

Sanner, B., Mands, E., Sauer, M.K. and Grundmann, E. 2008. Thermal response test: A routine method to determine thermal ground properties for GSHP design. In: *Proceedings 9th International Energy Agency Heat Pump Conference*, pp.20-22.

Self, S.J., Reddy, B.V. and Rosen, M.A. 2013. Geothermal heat pump systems: Status review and comparison with other heating options. *Applied Energy*. **101**, pp.341-348.

Sharqawy, M.H., Said, S.A., Mokheimer, E.M., Habib, M.A., Badr, H.M. and Al-Shayea, N.A. 2009. First in situ determination of the ground thermal conductivity for borehole heat exchanger applications in Saudi Arabia. *Renewable Energy*. **34**(10), pp.2218-2223.

Shiozawa, S. and Campbell, G.S. 1990. Soil thermal conductivity. *Remote Sensing Reviews*. **5**(1), pp.301-310.

Sigfusson, T.I. 2012. 7.01 - Geothermal Energy – Introduction A2 - Sayigh, Ali. *Comprehensive Renewable Energy*. Oxford: Elsevier, pp.1-2.

Singh, Rao M., Bouazza, A. and Wang, B. 2015. Near-field ground thermal response to heating of a geothermal energy pile: Observations from a field test. *Soils and Foundations*. **55**(6), pp.1412-1426.

Sivakumar, V., Boyd, J.L., Black, J.A., McNeill, J.A., Serridge, C.J., Slocombe, B.C. and Bell, A.L. 2012. Discussion: Effects of granular columns in compacted fills. *Proceedings of the Institution of Civil Engineers-Geotechnical Engineering*. **165**(4), pp.267-270.

Smith, P.L. 2011. Sampling Errors in Validation. *Journal of Validation Technology*. **17**(1), pp.81-88.

Snape, J.R., Boait, P.J. and Rylatt, R.M. 2016. Performance comparison of UK domestic renewable incentives. *Proceedings of the Institution of Civil Engineers - Energy*. **169**(3), pp.126-139.

Spitler, J.D., Liu, X., Rees, S.J. and Yavuzturk, C. 2005. Simulation and Optimization of Ground Source Heat Pump Systems. *8th International Energy Agency Heat Pump Conference, Las Vegas*.

Stephansson, O. and Shen, B. 1991. Modelling of faulted rock mass response to glaciation, thermal loading and seismicity. *Quarterly Journal of Engineering Geology and Hydrogeology*. **24**(4), pp.355-362.

Suryatriyastuti, M.E., Mroueh, H. and Burlon, S. 2012. Understanding the temperature-



induced mechanical behaviour of energy pile foundations. *Renewable & Sustainable Energy Reviews*. **16**(5), pp.3344-3354.

Tang, A.M., Cui, Y.J. and Barnel, N. 2008. Thermo-mechanical behaviour of a compacted swelling clay. *Geotechnique*. **58**(1), pp.45-54.

Taylor, J.R. 1997. *An introduction to error analysis: the study of uncertainties in physical measurements*. Sausalito, Calif: University Science Books.

The Institute of Refrigeration. 2007. *Ground Source Heat Pumps in the UK*. [Online]. [Accessed 25 May 2012]. Available from: <http://www.ior.org.uk/ground-source-heat-pumps-in-the-u>

The Institute of Refrigeration. 2012. *Ground source heat pumps*. [Online]. [Accessed 12 October 2012]. Available from: [www.ior.org.uk/ground-source-heat-pumps-in-the-u](http://www.ior.org.uk/ground-source-heat-pumps-in-the-u)

Thomas, H.R. and Rees, S.W. 1998. The thermal performance of ground floor slabs—a full scale in-situ experiment. *Building and Environment*. **34**(2), pp.139-164.

Thomas, H.R. and Rees, S.W. 1999. The thermal performance of ground floor slabs - a full scale in-situ experiment. *Building and Environment*. **34**(2), pp.139-164.

Thomas, H.R. and Rees, S.W. 2009. Measured and simulated heat transfer to foundation soils. *Geotechnique*. **59**(4), pp.365-375.

Tian, Z., Lu, Y., Horton, R. and Ren, T. 2016. A simplified de Vries-based model to estimate thermal conductivity of unfrozen and frozen soil. *European Journal of Soil Science*. **67**(5), pp.564-572.

Tiki. 2013. *Energy Guide for Kids*. [Online]. [Accessed 2nd January,]. Available from: <http://tiki.oneworld.net/energy/energy3.html>

Twidell, J. and Weir, T. 2006. *Renewable energy resources*. 2nd ed. London: Taylor and Francis.

United Nations Framework Convention on Climate Change. 2018. *Kyoto Protocol*. [Online]. [Accessed April]. Available from: [http://unfccc.int/kyoto\\_protocol/items/2830.php](http://unfccc.int/kyoto_protocol/items/2830.php)

Vieira, A., Maranha, J., Christodoulides, P., Alberdi-Pagola, M., Loveridge, F., Nguyen, F., Florides, G., Radioti, G., Cecinato, F., Prodan, I., Ramalho, E., Georgiev, A., Rosin-Paumier, S., Lenart, S., Erbs Poulsen, S., Popov, R., Lenart, S., Erbs Poulsen, S., Radioti, G., Javed, S., Van Lysebetten, G. and Salciarini, D. 2017. Characterisation of Ground Thermal and Thermo-Mechanical Behaviour for Shallow Geothermal Energy Applications. *Energies*. **10**(12), p2044.

Voss, K., Herkel, S., Pfafferott, J., Lohnert, G. and Wagner, A. 2007. Energy efficient office buildings with passive cooling - Results and experiences from a research and demonstration programme. *Solar Energy*. **81**(3), pp.424-434.

Wang, C.-I., Liu, H.-I., Kong, G.-q. and Ng, C.W.W. 2017. Different types of energy piles with heating–cooling cycles. *Proceedings of the Institution of Civil Engineers - Geotechnical Engineering*. **170**(3), pp.220-231.

Westaway, R. 2016. Repurposing of disused shale gas wells for subsurface heat storage: preliminary analysis concerning UK issues. *Quarterly Journal of Engineering Geology and Hydrogeology*. **49**(3), pp.213-227.

Whittaker, P.B., Wang, X., Regenauer-Lieb, K., Blair, D. and Tong Chua, H. 2014. Geothermal air conditioning: typical applications using deep-warm and shallow-cool reservoirs for cooling in Perth, Western Australia. *Int. J. Simul. Multidisci. Des. Optim.* **5**, pA10.

Wood, C.J., Liu, H. and Riffat, S.B. 2009. Use of energy piles in a residential building,

and effects on ground temperature and heat pump efficiency. *Geotechnique*. **59**(3), pp.287-290.

Xie, Y., Gilmour, M.S., Yuan, Y., Jin, H. and Wu, H. 2017. A review on house design with energy saving system in the UK. *Renewable & Sustainable Energy Reviews*. **71**, pp.29-52.

Yang, W., Lu, P. and Chen, Y. 2016. Laboratory investigations of the thermal performance of an energy pile with spiral coil ground heat exchanger. *Energy and Buildings*. **128**, pp.491-502.

Yang, W., Zhou, J., Xu, W. and Zhang, G.Q. 2010. Current status of ground-source heat pumps in China. *Energy Policy*. **38**(1), pp.323-332.

Yang, W.J., Clark, J.A. and Arpaci, V.S. 1961. Dynamic Response of Heat Exchangers Having Internal Heat Sources—Part IV. *Journal of Heat Transfer*. **83**(3), pp.321-336.

Yavari, N., Tang, A.M., Pereira, J.M. and Hassen, G. 2016. Mechanical behaviour of a small-scale energy pile in saturated clay. *Géotechnique*. **66**(11), pp.878-887.

Younger, P. 2015. Geothermal Energy: Delivering on the Global Potential. *Energies*. **8**(10), p11737.

Yu, X., Wang, R.Z. and Zhai, X.Q. 2011. Year round experimental study on a constant temperature and humidity air-conditioning system driven by ground source heat pump. *Energy*. **36**(2), pp.1309-1318.

Yu, X., Zhai, X.Q. and Wang, R.Z. 2010. Design and performance of a constant temperature and humidity air-conditioning system driven by ground source heat pumps in winter. *Energy Conversion and Management*. **51**(11), pp.2162-2168.

Yu, X.B., Zhang, N., Pradhan, A. and Puppala, A.J. 2016. Thermal conductivity of sand-kaolin clay mixtures. *Environmental Geotechnics-Journal*. **3**(4), pp.190-202.

Zeng, H.Y., Diao, N.R. and Fang, Z.H. 2002. A finite line-source model for boreholes in geothermal heat exchangers. *Heat Transfer—Asian Research*. **31**(7), pp.558-567.

Zhang, C., Wang, Y., Liu, Y., Kong, X. and Wang, Q. 2018. Computational methods for ground thermal response of multiple borehole heat exchangers: A review. *Renewable Energy*. **127**, pp.461-473.

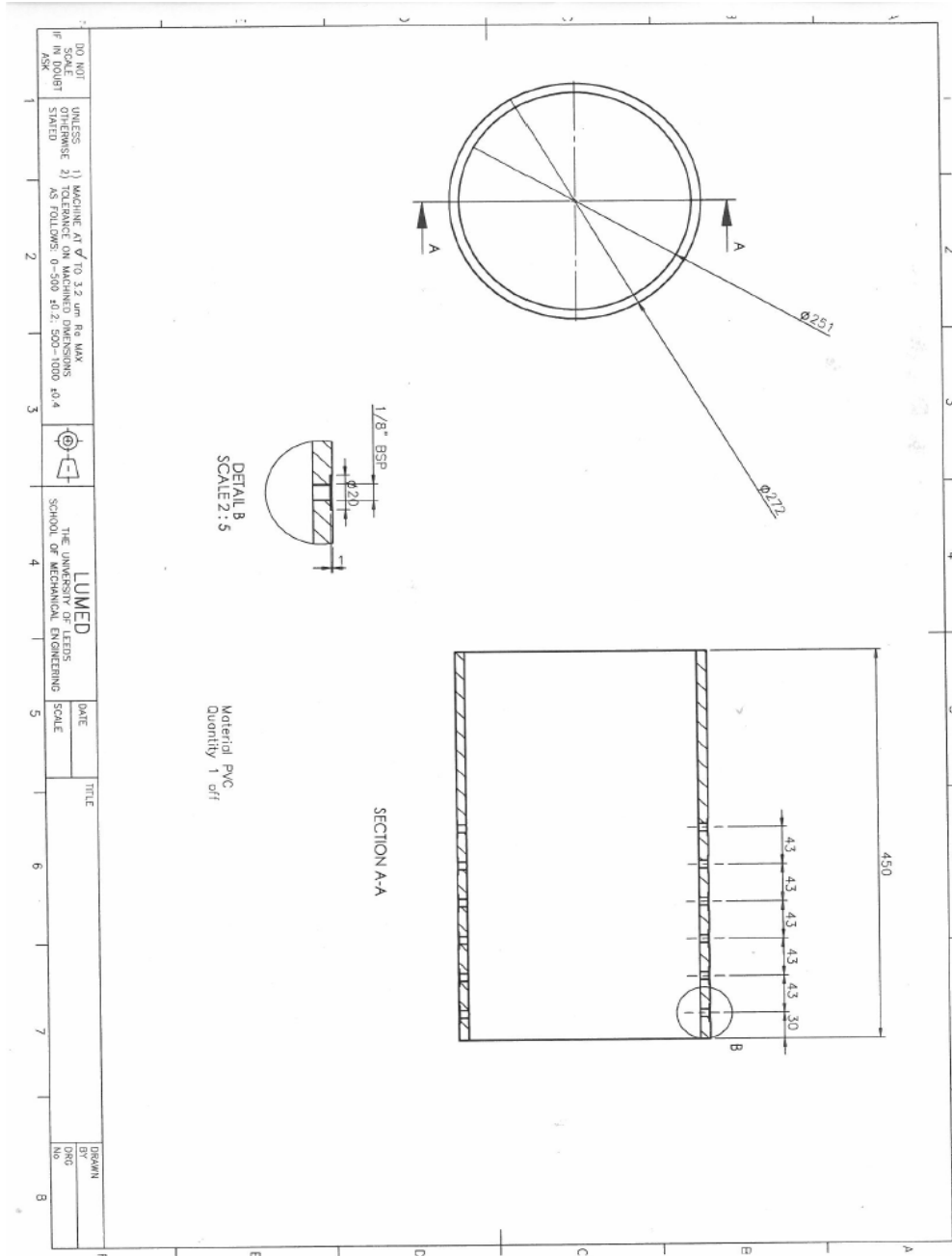
Zhang, W.K., Yang, H.X., Lu, L. and Fang, Z.H. 2012. Investigation on heat transfer around buried coils of pile foundation heat exchangers for ground-coupled heat pump applications. *International Journal of Heat and Mass Transfer*. **55**(21-22), pp.6023-6031.

Zhou, Z., Rees, S.W. and Thomas, H.R. 2002. A numerical and experimental investigation of ground heat transfer including edge insulation effects. *Building and Environment*. **37**(1), pp.67-78.

Zohuri, B. 2011. *Heat pipe design and technology : a practical approach*. Boca Raton, Fla.: CRC press.

## **Appendix**

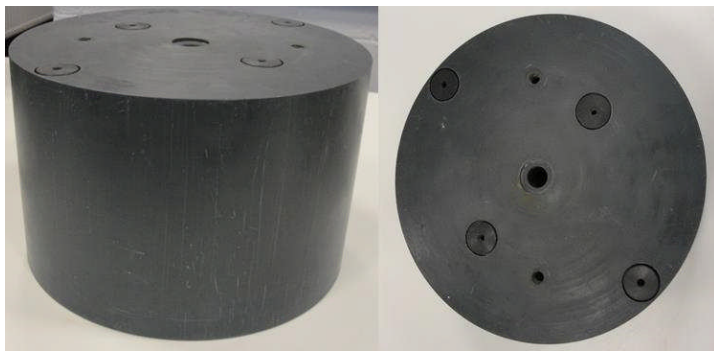
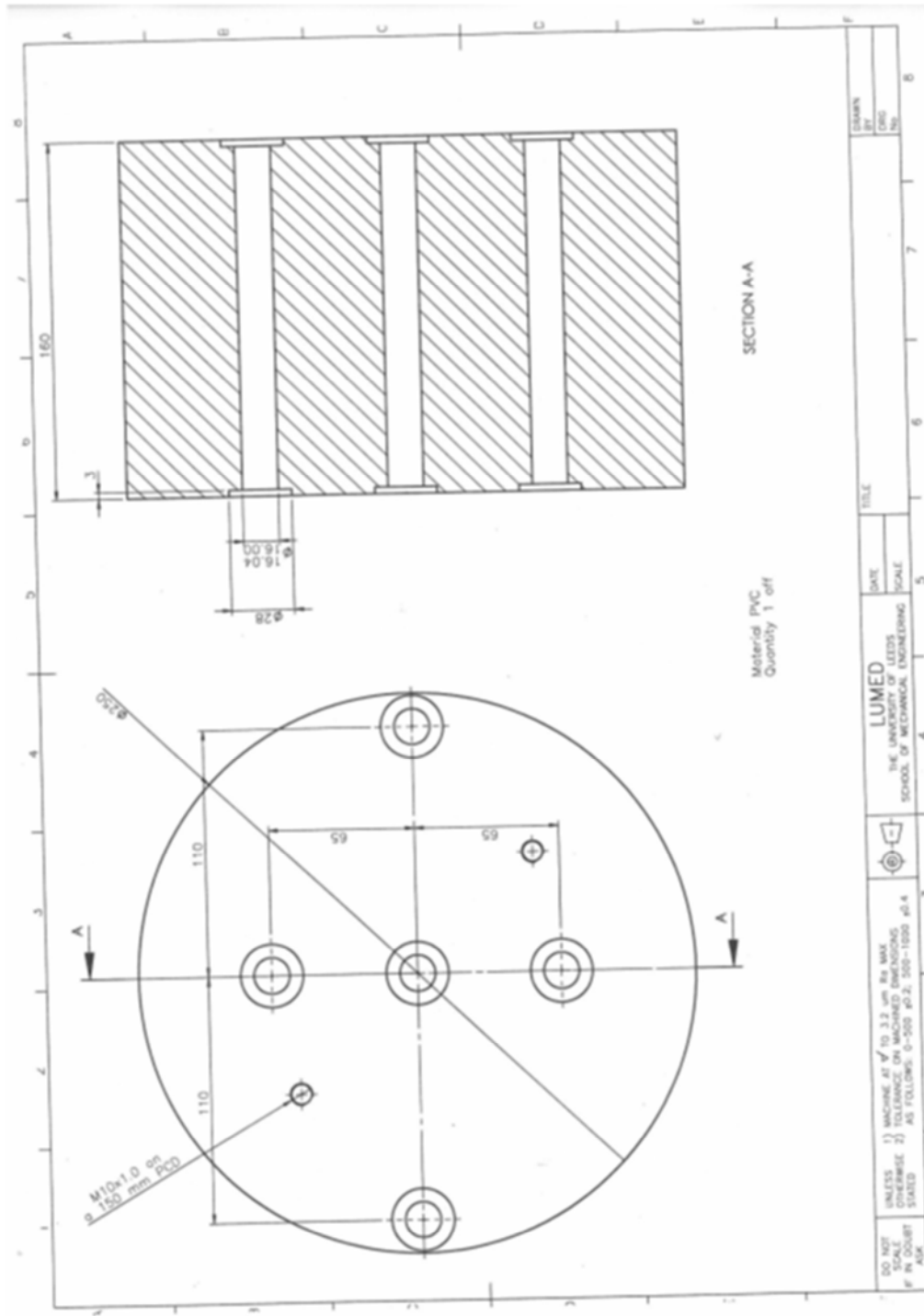
### **Drawings and Photos of Test Rig and Parts**



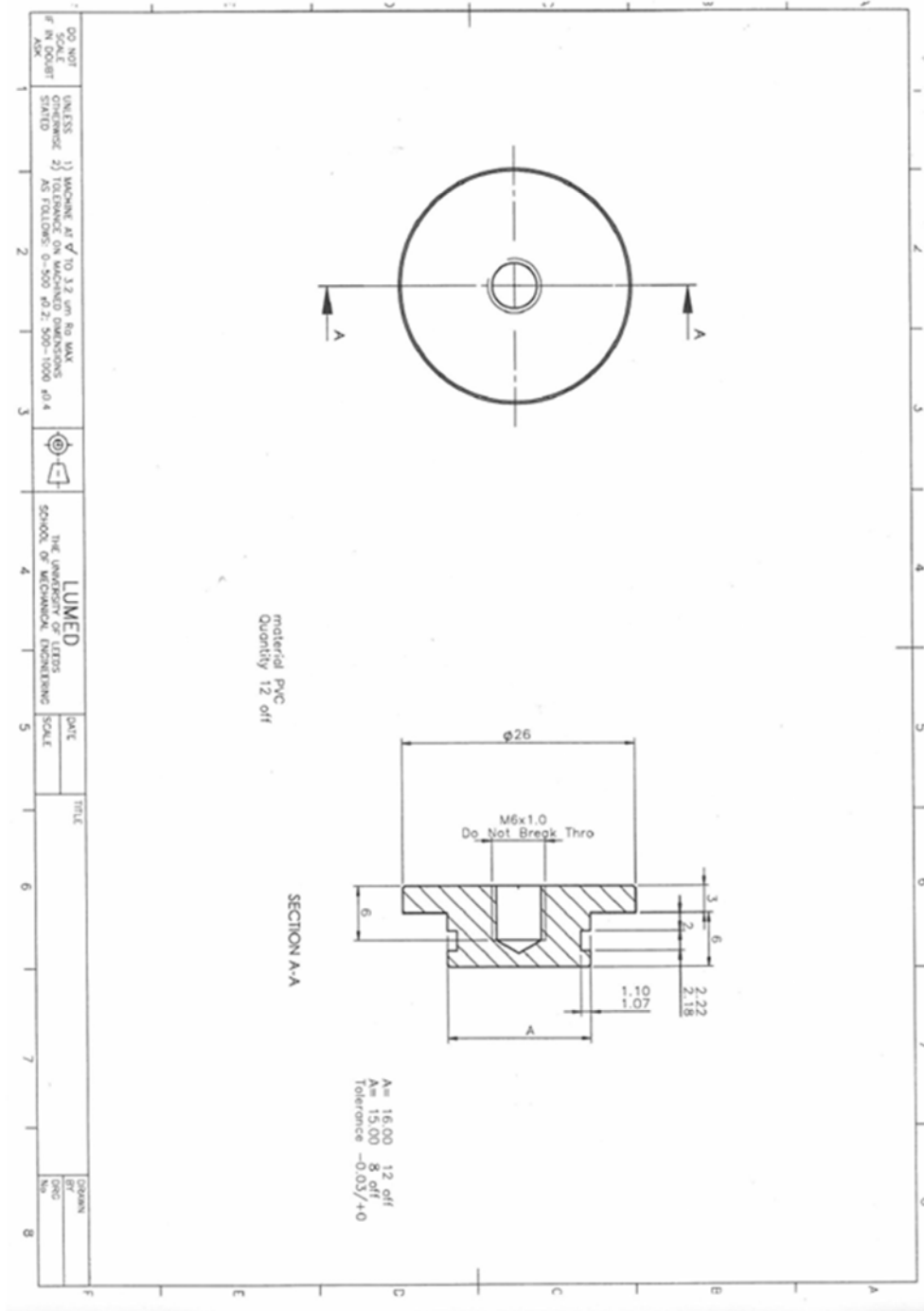
Drawing and photos of Test Chamber/Cell body

DO NOT SCALE UNLESS STATED OTHERWISE	UNLESS 1) MACHINING AT $\sqrt{10}$ TO 3.3 $\mu\text{m}$ Ra MAX. 2) AS FOLLOWS: 0-500 $\pm 0.2$ ; 500-1000 $\pm 0.4$	LUMED THE UNIVERSITY OF LEEDS SCHOOL OF MECHANICAL ENGINEERING	DATE	TITLE	DESIGNER
IF IN DOUBT ASK			SCALE		DRG NO.

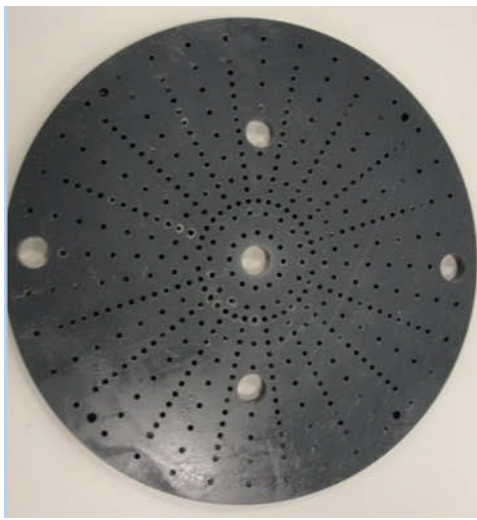
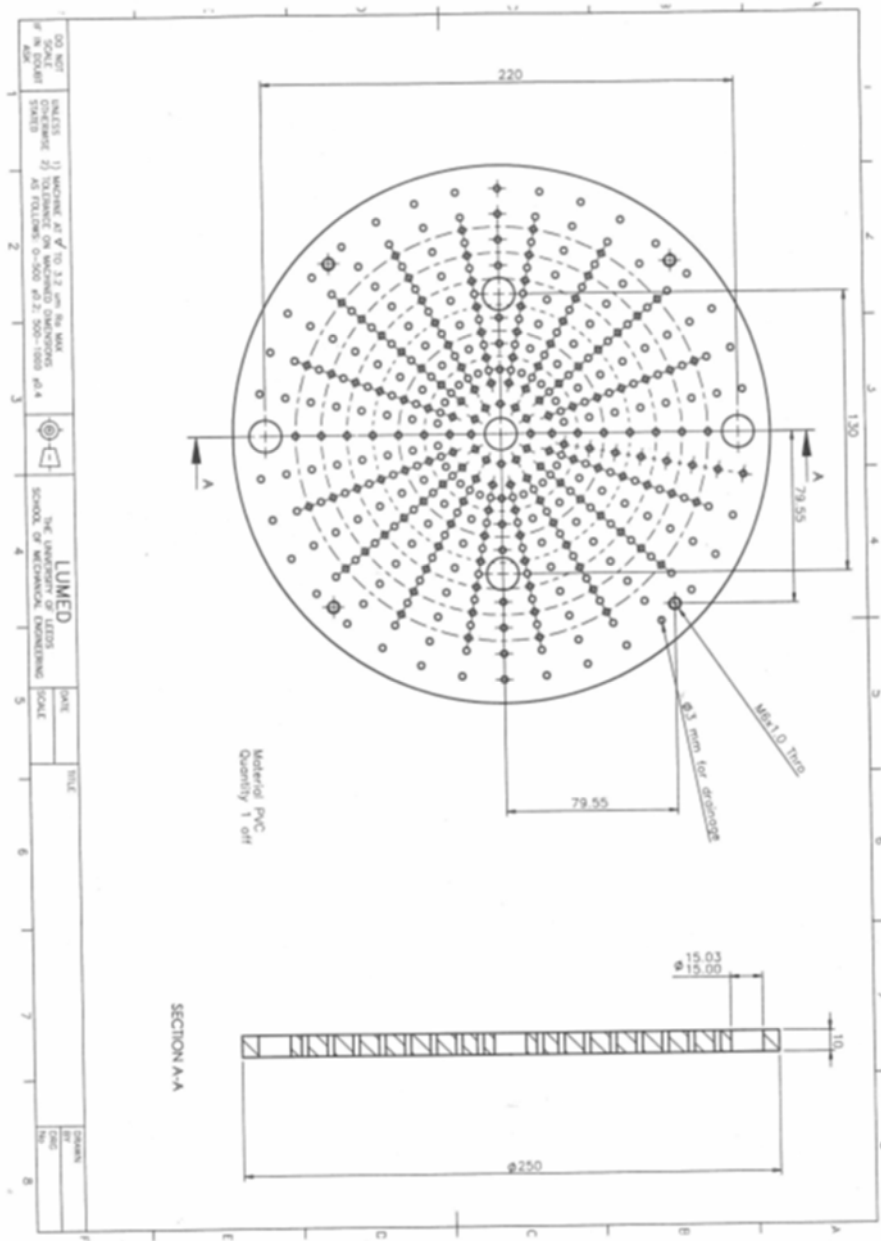
DETAIL B  
SCALE 2:5  
Material PVC  
Quantity 1 off



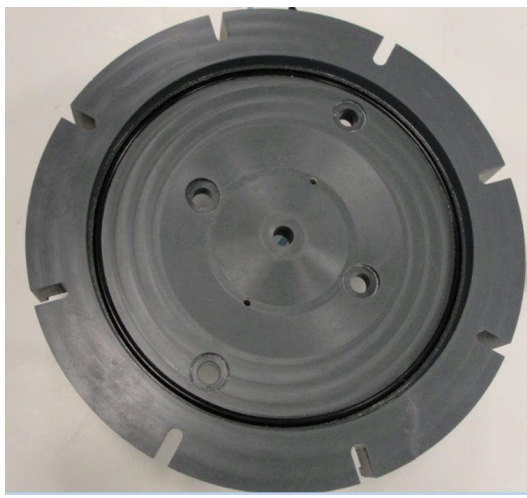
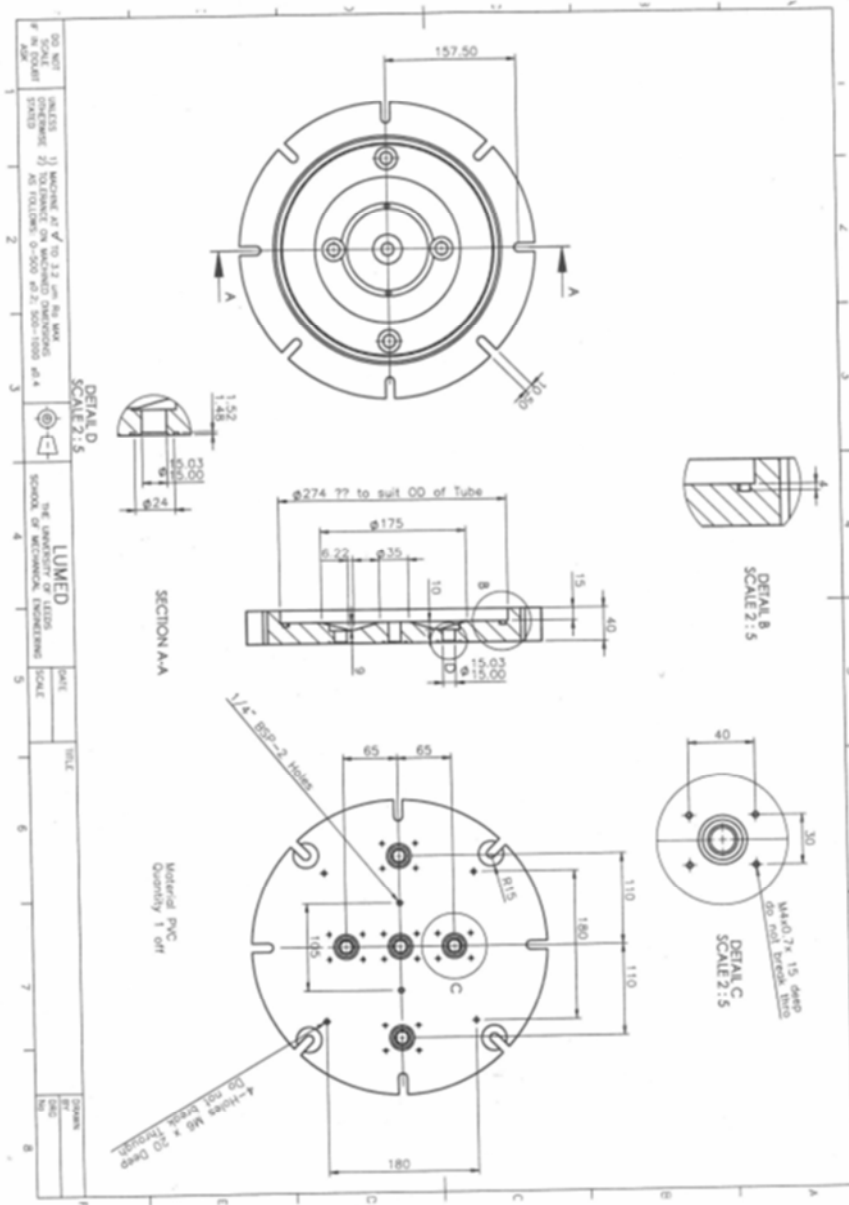
Drawing and photos of Piston



Drawing and Photo of Blanking Plug for sealing openings in piston

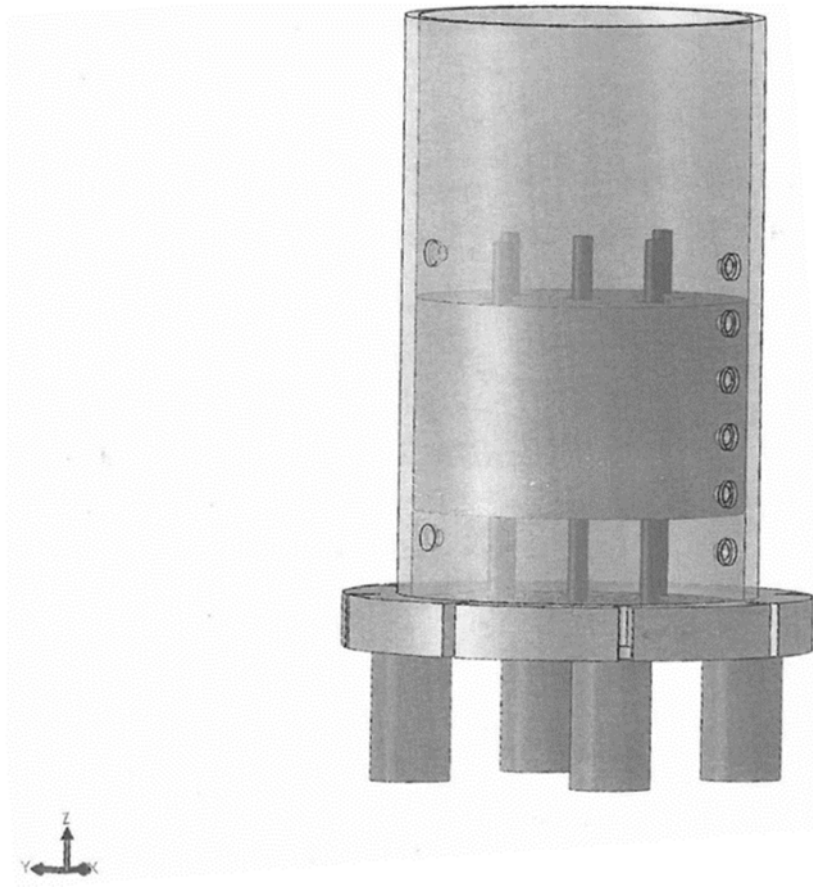


Drawing and photos of Perforated Bottom Plate



Drawing and photos of Cell Base





Model of inside of Test Chamber mounted on cell base, showing heaters in proposed positions passing through piston



Test Chamber mounted on cell base and inside view showing centrally placed heater

